The tumor microenvironment in liver metastases from colorectal cancer in the context of histologic growth patterns

Gemma Garcia Vicién

TESI DOCTORAL

THE TUMOR MICROENVIRONMENT IN LIVER METASTASES FROM COLORECTAL CANCER IN THE CONTEXT OF HISTOLOGIC GROWTH PATTERNS

GEMMA GARCIA VICIÉN

UNIVERSITAT DE BARCELONA

DESEMBRE 2022, BARCELONA

UNIVERSITAT DE BARCELONA

FACULTAT DE MEDICINA I CIÈNCIES DE LA SALUT

PROGRAMA DE DOCTORAT EN BIOMEDICINA

THE TUMOR MICROENVIRONMENT IN LIVER METASTASES FROM COLORECTAL CANCER IN THE CONTEXT OF HISTOLOGIC GROWTH PATTERNS

Memòria presentada per Gemma Garcia Vicién per optar al grau de Doctor per la Universitat de Barcelona

Dr. David García Molleví
Director

Dr. Artur Mezheyeuski
Director

Dr. Francesc Viñals Canals
Tutor

TABLE OF CONTENTS

GLOSSARY OF ABBREVIATIONS

®	Trademark
°C	degrees Celsius
µg	micrograms
µL	microliter
µm	micrometer
µM	micromolar
ACTA2	Actin alpha 2, smooth muscle
ACTG2	Actin gamma 2, smooth muscle
AJCC	American Joint Committee on Cancer
AKT	Protein kinase B
ANGPT2	Angiopoietin 2
APC	Adenomatous polyposis coli
AR	Antigen retrieval
ATCC	American Type Culture Collection
BAX	BCL2 associated X
bFGF	Basic fibroblast growth factor
BMP	Bone morphogenetic proteins
BRAF	B-Raf proto-oncogene
BSA	Bovine serum albumin
CAF	Cancer Associated Fibroblasts
CALD1	Caldesmon 1
CCL11	C-C motif chemokine ligand 11
CCL25	C-C motif chemokine ligand 25
CCL5	C-C motif chemokine ligand 5
CCR3	C-C motif chemokine receptor 3
CCR4	C-C motif chemokine receptor 4
CCR4	C-C motif chemokine receptor 4
CD5L	CD5 molecule like
$CD90^{hi}$	CD90 high expression
$CD90^{lo}$	CD90 low expression
cDNA	Complementary DNA
CFSE	Carboxyfluorescein succinimidyl ester
CI	mean+95% CI
CIMP	CpG island methylation phenotype
CIN	Chromosomal Instability
CM	Conditioned medium
CMSs	Consensus Molecular Subtypes
CNAG	Centre Nacional d'Anàlisi Genòmic
CO_2	Carbon dioxide
COL1A1	Collagen type I alpha 1 chain
COL1A2	Collagen type I alpha 2 chain
CRC	Colorectal Cancer
CRCSC	CRC Subtyping Consortium
CRLM	Colorectal Cancer Liver Metastases

CXCL10	C-X-C motif chemokine ligand 10
CXCL8	C-X-C motif chemokine ligand 8
CYGB	Cytoglobin
DAPI	4',6-diamidino-2-phenylindole
DC	Dendritic Cells
DDR1	Discoidin Domain Receptor 1
DEG	Differential expressed genes
DES	Desmin
DFS	Disease-free survival
dH_2O	Distilled water
dHGP	desmoplastic Histologic Growth Pattern
D-IHF	double immunofluorescence
DMEM	Dulbecco's modified eagle medium
dMMR	deficient-DNA-mismatch repair
DMSO	Dimethyl Sulfoxide
DNA	Deoxyribonucleic acid
ECM	Extracellular matrix
EDTA	etheylenediaminetetraacetic acid
EGF	Epidermal growth factor
EGFR	Epidermal growth factor receptor
ELN	Elastin
EMT	Epithelial-mesenchymal transition
EpCAM (CD326)	Epithelial cell adhesion molecule
F2R	Coagulation factor II thrombin receptor
FACS	Fluorescence-activated cell sorting
FADD	Apoptosis mediated FADD
FAPα	Fibroblast activation protein alpha
FBLN1	Fibulin 1
FBS	Fetal Bovine Serum
FDA	Food and Drug Administration
FFC	Fluorescence flow cytometry
FFPE	Formalin-fixed paraffin embedded
FoxP3	Forkhead box P3
gDNA	Genomic DNA
GLUT1	Glucose transporter 1
G-MDSC	Granulocyte-like myeloid derived suppressor cells
GREM1	Gremlin 1
GSEA	Gene Set Enrichment Analysis
h	hour
H&E	Hematoxylin and eosin
H_2O_2	Hydrogen peroxide
HGF	Histologic Growth Pattern
HGP	Histologic Growth Pattern
HiPathia	High throughput pathway interpretation and analysis
HNF4A	Hepatocyte nuclear factor 4 alpha
HNPCC	Hereditary non-polyposis colorectal cancer

HSA	Hepatic Specific Antigen
HSC	Hepatic Stellate Cells
HSCc	HSCs cocultured with tumoral cells
HSC-GFP	Hepatic Stellate Cells - Green Fluorescent Protein
HSCm	Monoculture of HSCs
hTERT	Human telomerase reverse transcriptase
iCAF	Inflammatory CAFs
IDIBELL	Institut d'Investigació Biomèdica de Bellvitge
IF	Immunofluorescence
IGF2	Insulin like growth factor 2
IGF2R	Insulin like growth factor 2 receptor
IGFBP-3	Insulin-like growth factor binding protein-3
IHC	Immunohistochemistry
IL-10	Interleukin 10
IL12B	Interleukin 12B
IL18R1	Interleukin 18 receptor 1
IL1β	Interleukin 1 beta
IL6	Interleukin 6
ILC	Innate lymphoid cells
IRS2	Insulin receptor substrate 2
ITGAM	Integrin subunit alpha M
ITH	Intratumoral Heterogeneity
KCs	Kupffer Cells
KDR (VEGFR2)	Kinase insert domain receptor
LLG	Lower grade glioma
LOH	Loose of heterozygosity
LSECs	Liver sinusoid endothelial cells
M	Molar
MAIT	Mucosal-associated invariant T cells
MAPK	Mitogen-activated protein kinase
MARCO	Macrophage receptor with collagenous structure
mCRC	metastatic Colorectal Cancer
MDSC	Myeloid Derived Suppressor Cells
MFAP5	Microfibril associated protein 5
mg	milligrams
MGMT	O (6)-Methylguanine-DNA-methyltransferase
MIF	Macrophage migration inhibitory factor
mIHC	Multiplex Immunohistochemistry
min	minute
mL	milliliter
MLH1	MutL homolog 1
mm	millimeter
M-MDSC	Monocytic-like myeloid derived suppressor cells
MME	Membrane metalloendopeptidase
MMR	Mismatch repair
mRNA	Messenger RNA

MSI	Microsatellite instability
MSI-H	High microsatellite instability
myc	MYC proto-oncogene
myCAFs	Miofybroblastic CAFs
MYH11	Myosin heavy chain 11
NFKB1	Nuclear factor kappa B subunit 1
NF-κB	Nuclear factor kappa B
NGFR	Nerve growth factor receptor
NK	Natural Killer
NKT	Natural Killer T cell
non-dHGP	Non-desmoplastic Histologic Growth Pattern
NPPB	Natriuretic peptide B
NPY	Neuropeptide Y
NSCL	Non-small cell lung cancer
ON	Overnight
OS	Overall Survival
P/S	Penicillin/Streptomycin
PBMC	Peripheral blood mononuclear cell
PBS	Phosphate-buffered saline
PC	Principal Component
PCA	Principal component analysis
PDAC	Pancreatic ductal adenocarcinoma
pDC	Plasmacytoid dendritic cell
PDCD4	Programmed cell death 4
PDGF	Platelet derived growth factor
PDLIM3	PDZ and LIM domain 3
PDPN	Podoplanin
PF	Portal Fibroblasts
PFc / CCPFs	PF cocultured with tumoral cells
PFm	Monoculture of PFs
PI	Propidium iodide
PI3K	Phosphatidylinositol-4,5-Bisphosphate 3-Kinase
PMN-MDSCs	Polymorphonuclear myeloid derived suppressor cells
POSTN	Periostin
PPARG	Peroxisome proliferator activated receptor gamma
pSMAD2	phosphorylated SMAD family member 2
qPCR	quantitative polymerase chain reaction
RCF	Relative centrifugal force
RNA	Ribonucleic acid
RNA seq	Ribonucleic acid sequencing
rpm	Revolutions per minute
RPMI	Roswell Park Memorial Institute medium
RT	Room temperature
S100A4	S100 calcium binding protein A4
S100A8/A9	S100 calcium binding protein A8 and A9
SCNA	DNA somatic copy number alterations

SDS-PAGE	sodium dodecyl sulfatepolyacrylamide
SERPINE1	Serpin family E member 2 (PAI1)
SSA	Sessile serrated adenoma
SULF1	Sulfatase 1
TBS	Tris buffered saline
TC	Tumoral Cells
Tfh	Follicular T helper
TGFβ1	Transforming growth factor beta 1
TGFβR2	Transforming growth factor beta receptor 2
Th2	T helper 2
THY1	Thy-1 cell surface antigen (CD90)
TIL	Tumor Infiltrating Lymphocyte
TMA	Tissue Microarray
TNF	Tumor necrosis factor
TP53	Tumor protein p53
TRADD	Apoptosis mediated TRADD
Treg	Regulatory T cells
U	Units
VEGF	Vascular endothelial growth factor
WB	Western Blot
αSMA	Actin alpha 2, smooth muscle
β-ACT	Actin beta

LIST OF FIGURES

LIST OF TABLES

SUMMARY

Colorectal cancer (CRC) is the third most frequent cancer type in the world and the second cause of death because of cancer. Nowadays, 25% of cases are diagnosed at the metastatic stage (mCRC), and 20-25% of the remaining patients develop metastases during the disease course. Patients with mCRC have a poor prognosis, as the 5-year survival rate for mCRC is less than 20%. Most CRC metastases appear in the liver (CRLM), for which the only curative treatment is surgery. However, only 30% of patients are suitable for resection. The remaining 70% can only be treated with chemotherapy in combination or not with immunotherapy. This last one has shown discouraging results in the last clinical trials. In view of all this, there is a need for further research in the biology and in new therapeutic strategies focused on CRC liver.

CRLMs are characterized by their way of growing in the host organ, as they show three histologic growth patterns (HGPs): desmoplastic, replacement and pushing. The desmoplastic pattern shows a fibrotic rim that separates tumor glands from liver parenchyma. On contrary, in replacement HGP, tumoral cells are in direct contact with hepatocytes. As the pushing pattern is the less common, the classification is usually simplified in desmoplastic (dHGP) and non-desmoplastic (non-dHGP) HGPs. These patterns have different biological aspects. However, their value is due to their utility as a prognostic and predictive marker, as dHGP has been associated with better patient outcomes, as well as a better response to anti-angiogenic treatments.

In our study, we aimed to further characterize the biology of CRLM HGPs. As no features of primary tumoral cells have been associated with the appearance of each HGP, we postulated that tumor microenvironment factors may be underlying the observed differences in prognoses. Because of that, in our project, we focused on immune infiltrates and cancer associated fibroblasts present in each HGP.

Concerning immune infiltrates, multiplex immunofluorescence (mIHC) let us investigate both lymphoid and myeloid cell subsets in a tissue microarray of 100 CRLM patients. Our results revealed an immunologically active anti-tumoral environment in dHGP, constituted by higher densities of cytotoxic T cells interacting with tumoral cells. On the other hand, higher levels of macrophages, both M1 and M2 polarized, as well as other pro-tumoral cell

subsets like Th2 lymphoid cells, non-macrophage $CD163^{+}$ cells and $Calprotectin^{+}$ cells, were at higher densities in non-dHGP, suggesting a pro-tumoral immune environment in this HGP.

Through mIHC we also investigated several cancer associated fibroblasts (CAFs) subpopulations. Our results showed an enrichment of several COL1A1 expressing CAF subsets in dHGP. This protein from the extracellular matrix is associated with tumor growth restraining and an immune-active environment.

Through *in vitro* experiments, we investigated the two main precursor cells that can give rise to activated fibroblasts in the liver: hepatic stellate cells (HSCs) and portal fibroblasts (PFs). We studied the changes at RNA level of both HSCs and PFs when activated by their co-culture with tumoral cells. The RNAseq results obtained showed differences between i) mesenchymal cells when co-cultured with tumoral cells ii) and the co-cultured conditions when compared when the corresponding monocultures. Moreover, we identified two useful markers to distinguish PF-derived CAFs, MFAP5, and HSC-derived CAFs, F2R. At functional level, PFs showed a higher capacity for recruiting Th2 cells and induce higher proliferation rates in tumor cells. We also assessed *in vitro* the function of CD90 marker through two subpopulations of CAFs isolated from the same patient, $CD90^{hi}$ and $CD90^{lo}$, that had shown differences in their secretome. $CD90^{hi}$ cells showed higher expression of Podoplanin, which is associated to macrophage recruiting and M2 polarization. Our assays showed higher capacity of $CD90^{hi}$ cells to recruit monocytes, as well as to polarize them to an M2 phenotype.

Altogether, the results of this thesis describe an immune active environment in dHGP and a pro-tumoral immune environment in non-dHGP, which could explain the failure of immunotherapy. This conclusion suggests a need for patient segregation according to HGP and proposes new targets for CRLM treatment. Moreover, both the results obtained about immune infiltrates and cancer associated fibroblasts open doors for interesting new research lines that could lead to understanding the biology underlying the prognostic value of HGPs as well as proposing new therapeutic targets for these patients.

RESUM

El càncer colorectal (CRC) és el tercer mes freqüent al món, així com el segon causant de morts per càncer. Actualment, el 25% dels pacients tenen metàstasi en el moment del diagnòstic (mCRC) i el 20-25% de la resta en desenvolupen durant el curs de la malaltia. Els pacients de mCRC tenen mal pronòstic, la supervivència als 5 anys és menor de 20%. La majoria de les metàstasis apareixen en el fetge (CRLM) i l'únic tractament disponible amb objectiu curatiu és la cirurgia, només viable per al 30% dels pacients. El 70% restant poden ser tractats amb quimioteràpia en combinació, o no, amb immunoteràpia. Aquesta última ha mostrat resultats desesperançadors en els darrers assajos clínics. Aquestes dades evidencien la necessitat d'investigar la biologia de les metàstasis hepàtiques de càncer colorectal per tal de trobar-ne noves estratègies terapèutiques.

Les mCRC es caracteritzen per la manera en la que creixen en l'òrgan hoste, ja que ho fan seguin tres patrons de creixement histològics (HGPs): el patró *desmoplastic*, el *replacement* i el *pushing*. El patró *desmoplastic* mostra una càpsula fibrosa que separa físicament les glàndules tumorals del parènquima hepàtic. Per altra banda, en el patró *replacement*, les cèl·lules tumorals es troben en contacte directe amb el parènquima. Degut a que el patró *pushing* és el menys comú, la classificació dels HGP sol simplificar-se en *desmoplastic* (dHGP) i *non-desmoplastic* (non-dHGP). Aquests patrons mostren diferències a nivell biològic, però la seva rellevància recau en el seu valor com a factor pronòstic i predictiu de resposta a fàrmacs.

El nostre projecte tenia com a objectiu caracteritzar la biologia d'aquests HGP que apareixen en les CRLM. Ja que no hi ha cap aspecte de les cèl·lules del tumor primari que s'hagin associat a l'aparició d'un patró histològic o d'un altre, vam hipotetitzar que les característiques del microambient tumoral podrien estar explicant les diferències en pronòstic observades entre els HGPs. Per aquesta raó, vam decidir centrar-nos en l'estudi dels infiltrats inflamatoris i dels fibroblasts associats a càncer (CAFs).

Respecte els infiltrats inflamatoris, la tècnica d'immunofluorescència multiplex ens va permetre investigar diferents poblacions cel·lulars tant del llinatge limfoide com mieloide, en un microarray de teixit format per mostres provinents de 100 pacients. Els resultats obtinguts mostraren un ambient immunològicament actiu i anti-tumoral en el patró dHGP, constituït per alts nivells de limfòcits T citotòxics interactuant amb les cèl·lules tumorals. Per

altra banda, en el patró non-dHGP es va observar una densitat alta de macròfags, tant polaritzats a M1 com M2, així com d'altres poblacions pro-tumorals com limfòcits Th2, cèl·lules $CD163^{+}$ $CD68^{-}$ i cèl·lules $Calprotectin^{+}$, suggerint la presència d'un ambient immunològic pro-tumoral en aquest HGP. Aquesta tècnica també va permetre estudiar els fibroblasts associats a càncer (CAFs): el patró dHGP estava enriquit en subpoblacions de CAFs que expressen COL1A1. Està descrit que aquesta proteïna de la matriu extracel·lular té un efecte restrictiu sobre el creixement tumoral i promou l'activació de les cèl·lules del sistema immune vers el tumor.

Mitjançant experiments *in vitro*, vam estudiar els dos precursors principals de CAFs en el fetge: les cèl·lules hepàtiques estrellades (HSCs) i els fibroblasts portals (PFs). Vam analitzar els canvis en RNA de HSCs i PFs quan eren co-cultivades amb cèl·lules tumorals. Els resultats obtinguts van mostrar diferències entre i) poblacions mesenquimals quan es cultivaven amb cèl·lules tumorals ii) cada població mesenquimal co-cultivada en comparació amb el seu corresponent monocultiu. També vam identificar dos marcadors que ens permeten distingir entre CAFs derivats de PFs, MFAP5, i CAFs derivats de HSCs, F2R. A nivell funcional, els PFs van mostrar una major capacitat per reclutar cèl·lules Th2 i induir un augment de la proliferació en les cèl·lules tumorals. També vam investigar a nivell *in vitro* la funció del marcador CD90 estudiant dues subpoblacions de CAFs aïllades del mateix pacient, $CD90^{hi}$ i $CD90^{lo}$, que mostraven diferències en el seu secretoma. Els $CD90^{hi}$ expressaven alts nivells de Podoplanina, una proteïna associada al reclutament i polarització de macròfags. En els assajos funcionals *in vitro* vam observar que els $CD90^{hi}$ reclutaven mes monòcits i que eren capaços d'induir la seva polarització cap a M2.

En conjunt, els resultats d'aquesta tesi descriuen un ambient immunològicament actiu en el dHGP i un de pro-tumoral en el non-dHGP, fet que podria explicar el fracàs de la immunoteràpia en aquests pacients. Aquesta conclusió suggereix una necessitat de segregar els pacients tenint en compte el HGP que mostren, al mateix temps que proposa noves dianes terapèutiques per al tractament de CRLM. A més, els resultats obtinguts tant respecte els infiltrats inflamatoris com respecte els CAFs obren portes per a noves línies de recerca. Aquestes podrien portar a entendre millor els mecanismes biològics que expliquen les diferències de pronòstic entre HGPs, així com proposar noves estratègies terapèutiques per a aquests pacients.

INTRODUCTION

1. CANCER

Cancer is a term used to refer to a large group of diseases that have one common feature: abnormal and uncontrolled cell division and growth uncontrollably. In physiological conditions, old or damaged cells are programmed to self-destroy. Then, healthy cells grow and divide to replace those destroyed cells following a highly regulated process. However, when this process is altered, abnormal or damaged cells can survive and divide indefinitely, giving rise to a solid tumor or a non-solid one, as it happens in blood cancers. These tumors can appear in almost any organ of the body, are able to invade the whole tissue in which they appear and can spread to other organs causing metastases. The latter one is the primary cause of death from cancer (1–3).

Also called neoplasm or malignant tumor, cancer is the second leading cause of death worldwide and the first one in most of the countries if we consider the population before the age of 70. In 2020, it caused nearly 10 million deaths, which means that one of six deaths was due to cancer, a ratio that is rapidly growing worldwide (4,5).

The most common types of cancer vary depending on the gender. Lung, prostate, colorectal, stomach and liver are the most common in men; while breast, colorectal, lung, cervical and thyroid cancer, the ones among women (4,5).

The process of tumor formation consists of different stages and normally begins with a pre-cancerous lesion. These stages take place due to a combination of a person's genetic makeup and ambient factors to which an individual is exposed during its life. Ambient factors include physical (e.g., ultraviolet radiation), chemical (e.g., tobacco components or food contaminants) and biological carcinogens (e.g., certain viruses and bacteria infections); what makes the lifestyle play a decisive role in cancer development. Another aspect to have in mind is that cancer incidences dramatically increase with age, as cellular control mechanism become less effective and augment the probability of tumoral cell transformation (4,5).

In conclusion, it is especially important to prevent the appearance of cancer with our daily actions. However, as cancer can affect everyone and particularly those with altered correction mechanisms, focusing research on its early detection and the appropriate treatment for each cancer type is extremely needed.

Apart from the disruption in normal cell proliferation that make these cells divide indefinitely (6), tumoral cells acquire a set of capabilities that favour further tumor development. These abilities are responsible for the huge variability among different cancer types. They were firstly described by Hanahan and Weinberg, in 2000, and were named the hallmarks of cancer (7). Initially, six hallmarks were described, including sustaining proliferative signaling, evading growth suppressors, resisting cell death, enabling replicative immortality, inducing angiogenesis, and activating invasion and metastasis. A decade after these hallmarks were revised and new emerging hallmarks were added (8). Nowadays, these hallmarks of cancer keep under revision, as knowledge of cancer mechanisms is constantly progressing. For this reason, in 2022, new hallmarks have been added (9); all of them are summarized in Figure 1.

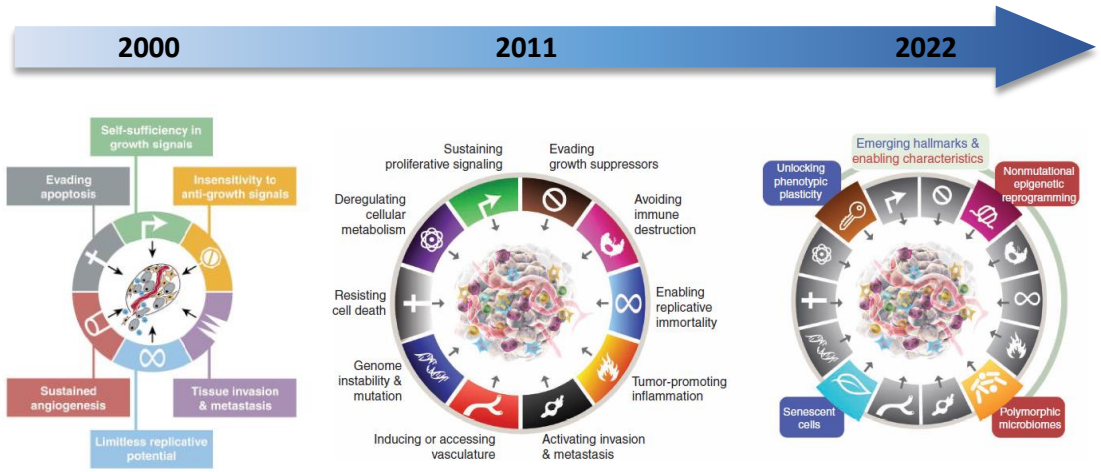

Figure 1. Illustration showing the progression of hallmarks of cancer's knowledge*. Adapted from Hanahan D. and R. Weinberg* (7–9)*.*

As previously mentioned, tumors arise from normal tissues and must hence be understood as a complex organization, composed by the inner tumor mass and multiple distinct cell types that are recruited from the surrounding environment, also called the tumor associated stroma. These cells interact between them and with tumoral cells and actively contribute to the process of tumorigenesis. Hence, when studying the biology of cancer, it is crucial to not only focus on tumoral cells, but also on the different contributors of the tumor microenvironment.

2. COLORECTAL CANCER

2.1. Epidemiology

Colorectal cancer (CRC) is the third most frequent cancer type in the world and the second cause of death because of cancer. In 2020, over 1.9 milion new cases arose, which means that one of ten new cases of cancer are CRC, according to World Health Organization (4,5). Concerning gender, it is the second most common cancer in women and the third one in men. The annual number of deaths is approximately half of the incidence, but this mortality is 25% lower in women than in men. The incidence increases by 2% each year, although it varies depending on the country, as it is four times higher in developed countries (10).

In the last decades, the screening programs applied at the national level, the standardization of pre- and post-operatory attention, the improvements in surgical techniques and the availability of more effective therapies, have estabilized and reduced the mortality of CRC, both in early and advanced stages (3,11,12). However, all the mentioned improvements are not enough, as around 25% of the patients are diagnosed at the metastatic stage, and 20-25% of the remaining patients develop metastases later during the disease. This is relevant, as the metastatic stage is associated with a notably higher mortality rate: the 5-year disease free survival for CRC is of 64%, it decays to 12% in metastatic CRC (mCRC) (13,14). Therefore, tackling this disease is one of the highest priority challenges in healthcare.

2.2. Risk factors

Concerning the risk factors for developing CRC, both ambient and hereditary factors play important roles. Familiar antecedents have shown to interfere in 10-20% of the patients (15–17). These include CRC patients affected by hereditary colorectal cancer syndromes, which conform 5-10% of the total CRC diagnosed patients. The most common inherited syndromes are Lynch syndrome (hereditary non-polyposis colorectal cancer or HNPCC) and familial adenomatous polyposis (FAP). HNPCC is characterized by low number or adenomas, which are morphologically similar to sporadic lesions, this is why sometimes they can be missed. On the other hand, FAP cases are easier to recognize, as they show high number of polyps. This last syndrome is caused by mutations in adenomatous polyposis coli (*APC*) gene, that is regulating the Wnt signalling pathway. About ambient factors, a sedentary lifestyle has the

biggest impact, but excessive alcohol intake, tobacco, red meat, and processed food consumption are also associated to CRC (18).

2.3. TNM Staging

Once diagnosed, CRC patients are stratified in different stages, depending on how advanced the disease is. The stages go from I to IV and determine the treatment strategy that will be followed. These stages are based on the American Joint Committee on Cancer's (AJCC) TNM (Tumor/Nodule/Metastases), which evaluates the depth of the tumor (T), its propagation of to the proximal lymph nodes (N) and the appearance of metastases in distant organs (M). This staging is summarized in Table 1.

STAGE	T	N	M	DESCRIPTION
0	Tis	N0	M0	Carcinoma *in situ*. Tumoral cells are kept at the most superficial part of the mucosa. No lymph nodes affected.
I	T1-2	N0	M0	The tumor has spread to the colon or rectum wall but has not gone through the muscle layer. No lymph nodes affected.
IIA	T3	N0	M0	The tumor has infiltrated all colon or rectum layers but their lymph nodes are still not affected.
IIB	T4	N0	M0	
IIIA	T1-2	N1	M0	The tumor has invaded the most proximal organs and is affecting lymph nodes.
IIIB	T3-4	N1	M0	
IIIC	T1-4	N2	M0	
IV	T1-4	N0-2	M1	Tumoral cells have disseminated through the body affecting distant organs like the liver, the lung, or the bones.

***Table 1**. **CRC TNM staging**. T, tumor; N, lymph node; M, metastasis; Tis, in situ tumor.*

It should be mentioned that CRC is a heterogenous tumor at the molecular level, an aspect that this staging does not consider. Thus, TNM staging is limited and not the only tool used

to take therapeutic decisions. Therefore, CRC is also classified into different subtypes according to their specific molecular and morphological alterations that will be explained in the following sections (19).

2.4. Molecular biology and carcinogenesis of CRC

The most characteristic feature of CRC is its genetic instability, which can arise by different mechanisms. The most common is chromosomal instability (CIN), that appears in 70-80% of CRC cases, and implies changes in chromosome number and structure including aneuploidies, chromosomal rearrangements and/or loss of heterozygosity (LOH). CIN is usually detected as a high frequency of DNA somatic copy number alterations (SCNA) and has been associated with inactivating mutations in the *APC* tumor suppressor gene, that is described as an early event in colorectum neoplasia development (20). The second most frequent genetic instability mechanism is microsatellite instability (MSI), that is associated with defective DNA mismatch repair (MMR) and the wild-type *TP53* gene. This MSI instability mechanism appears in around 13-16% of CRC patients (21). Moreover, CRC can also be triggered by epigenetic instability, that is mediated by CpG island methylation, giving rise to what is known as CIMP, or CpG island methylation phenotype. CIMP promotes hypermethylation and silencing of a range of tumor suppressor genes (22). Thus, with these genetic and epigenetic instabilities, colon cancer tumor cells acquire the genomic instability and other cancer hallmarks, which are observed in most early neoplastic lesions as the event of initiation and formation of colorectal cancer (23,24). The characteristics that may define these groups are not unique. Although the CIN and MSI pathways are often mutually exclusive, the CIMP pathway overlaps substantially with the MSI pathway.

The accumulation of mutations and epigenetic alterations in tumor suppressor genes and oncogenes drives the malignant transformation of colon cells that will lead benign adenomas to carcinomas. Such a malignant transformation, which was first described by Fearon and Vogelstein in 1989 (25), requires up to 10-15 years to develop and is called colorectal carcinogenesis. This process can follow two distinct morphological pathways: the conventional adenoma-carcinoma sequence or the less abundant alternative serrated polyps-carcinoma. Each sequence in turn has different possible pathways. The described sequences are summarized in Figure 2 (26). All of them suggest that genetic and epigenetic

changes are accumulating during time with a preferential order, which is not invariable, but which is associated with colon tumors (27). Moreover, less than five mutations are needed for inducing a malignant neoplasia, as these mutations affect oncogenes (activation) and tumor suppressor genes (inactivation). However, due to the heterogeneity that exists between individual tumors, it is now believed that the accumulation of alterations is more relevant in triggering carcinogenesis than the order in which they appear (28).

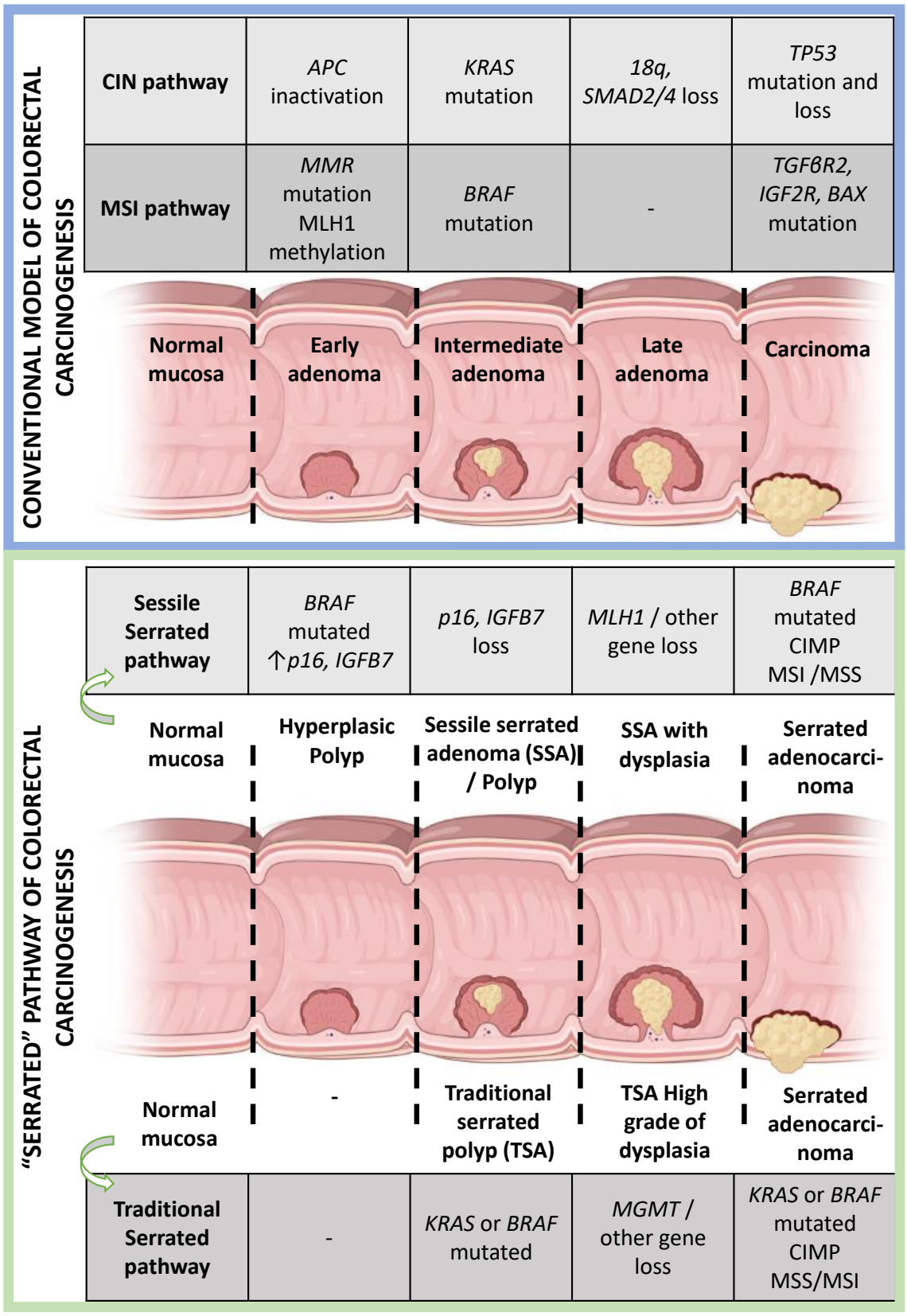

Figure 2. Conventional and serrated sequences of carcinogenesis *showing the most frequent gene loss and gain of functions. CIMP is involved in all the sequences, especially in MSI pathway, through its epigenetic regulation.*

2.5. CMS Classification of CRC

As the information TNM provides is limited, a new classification system based on molecular characteristics was generated for CRC in 2014: Consensus Molecular Subtypes (CMSs). It was elaborated by the CRC Subtyping Consortium (CRCSC) with the aim to integrate the gene expression patterns present in the different CRC subtypes, as well as their clinical behaviour and their key biological features (11,29). This new classification defines four subgroups that differ both at clinical and molecular level and that are useful to develop new biomarkers: CMS1, that is characterized by MSI and consist of the 14% of all CRC patients; and CMS2 (the canonical or conventional, present in 37% of patients), CMS3 (also called the metabolic, present in 13% of patients) and CMS4 (the mesenchymal, present in 23% of patients), all of them show genetic instability mechanism in form of CIN.

CMS1 contains most CRC patients that exhibit MSI. Patients of this group can also show hypermethylation (CIMP). These tumors usually present a mucinous histology, are more common in women, and predominantly appear at the proximal colon. This subgroup also shows the highest level of immune infiltration, especially by Th1 and T cytotoxic cells, and isthus having an immunologically active environment. This activation of the immune system is the result of a high number of *de novo* peptic sequences generated by the hypermutated phenotype, which act as immunogenic epitopes (30). This characteristic makes CMS1 CRC tumors good candidates for treatment strategies based on immunotherapy. Moreover, only TNM stages II and III are enriched in this CMS1 group, suggesting that these tumors are less aggressive, as they appear mostly localized in colon cancer than metastatic. However, CMS1 tumors are associated with a higher risk of progression and death after chemotherapy. Moreover, it should be mentioned that most of *BRAF-V600E* mutated CRCs fall into the CMS1 subgroup (31).

CMS2 is characterized by an epithelial genetic expression profile and an upregulation of Wnt and Myc pathways, which are the ones driving CRC carcinogenesis in this case. They also overexpress *EGFR*, *HER2*, *IGF2*, *IRS2* and *HNF4A*. These tumors are usually detected in distal colon and rectum. Although they show high levels of CIN, their survival rates after relapse are elevated. In fact, they have the best prognosis in a metastatic setting (11,29,32).

CMS3 shows, in comparison to the other CIN subgroups, a lower number of alterations. In fact, CMS3 has the closest resemblance to normal colon tissue regarding gene expression levels and is enriched on localized colon cancers (mainly stage II and III). On the other hand, 30% of CMS3 tumors show MSI, hypermutated phenotype and CIMP hypermethylation epigenetic alterations. In addition, this group is enriched in *KRAS* activating mutations. These *KRAS* alterations are linked to *GLUT1* upregulation, which increases the uptake of glucose as well as the glycolytic process, thereby promoting the Warburg effect in these metabolically dysregulated tumors (31,33).

CMS4 is characterized by an upregulation of epithelial-mesenchymal transition (EMT) related pathways. They show high levels of TGFβ1, integrins and proteins involved in extracellular matrix remodelling and angiogenesis. Moreover, these tumors have a high infiltration of stromal cells like cancer associated fibroblasts (CAFs). This group is associated with a poorer prognosis, as it usually diagnosed at advanced stages and is more frequent in metastatic settings (represents 40% of metastatic CRC patients) (11,29,31,32).

This CMS classification is based on primary tumors but has also been confirmed in metastatic settings. However, in the last ones there is an enrichment in CMS4 mesenchymal tumors, with fewer cases of CMS1 and CMS3, compared with stage II and III CRC.

In conclusion, this new classification method considerably improved the understanding of CRC biology through the integration of "omics" data and new treatments.

2.6. Histopathologic aspects of CRC

CRC is an example of cancer where patients benefit from the co-operation of specialists from different areas, including clinicians, surgeons, and pathologists. In the case of these last ones, their role is not only providing accurate histopathologic diagnosis, but also to assess pathologic stage, surgical margins as well as other prognostic parameters. Thus, histopathologic aspects of CRC must be considered to perform an accurate diagnosis and to properly determine the best therapeutic strategy.

On a macroscopic level, colorectal tumors have a polypoid or fungating appearance, usually with a depressed ulcer at the center. However, on a microscopic level, different histologic variants are described. Such examples are adenocarcinoma, mucinous adenocarcinoma,

signet ring cell carcinoma, squamous cell carcinoma, medullary carcinoma, and undifferentiated carcinoma, among others. Moreover, CRC tumors are also classified according to the level of differentiation of tumoral cells: well differentiated, moderated differentiated and poorly differentiated adenocarcinoma. 70% of patients show a moderated grade of differentiation, while well and poorly differentiated account for 10% and 20% respectively (34,35).

Considering histologic variants, adenocarcinoma is the most frequent. Its level of differentiation is usually moderate and lack specific histological features. Another histologic variant worth mentioning is the mucinous, which is defined by taking up >50% of the tumor volume with extracellular mucin. In this variant, tumor cells are considered mucinous differentiated. Although only 10-20% of CRC patients show this histologic variant (36), many adenocarcinomas have less than 50% of tumor volume composed by mucin and are termed adenocarcinomas with mucinous features. Mucinous adenocarcinomas are characterized by being associated to MSI and, in that case, are expected to behave in a low-grade fashion. On the other hand, when mucinous variant is found in MSS, tumors act more aggressively. The signet ring cell adenocarcinoma variant appears only in 1% of cases, is poorly differentiated and, thus, carries a worse outcome. Finally, the medullary carcinoma variant, although extremely rare, is worth mentioning because it is strongly associated with MSI, has marked lymphocyte infiltration, and shows a pushing border, which is a way of tumor growing pattern in which tumoral cells “push” the parenchymal ones. This histologic variant usually has favourable prognosis despite being poorly differentiated (34,35).

Finally, the most important aspect of pathologist’s microscopic examination is looking for evidence of invasion. In short terms, it consists of determining if muscularis mucosae is disrupted by neoplastic cells. An important feature of invasion is that it is linked to a desmoplastic reaction. This reaction implies a type of fibrous proliferation surrounding tumor cells that leads to what is called desmoplasia. Another characteristic feature of invasive colorectal carcinoma is that it frequently shows necrotic debris in the lumina of its aberrant glands. This necrosis is called “dirty necrosis” and is a unique feature that is used to identify a colorectal primary tumor when a metastasis of unknown origin is found (34,35).

2.7. CRC Treatment

Although the molecular drivers of CRC have been described, it is crucial to know where in the gut the tumor has occurred regarding possible treatments. For instance, colon cancer and rectal cancer will require different approaches, also depending on their stage. Moreover, cancer registries from different countries show differences in disease outcomes following treatment. Because of that, increasing attention is paid to improve the therapeutic strategies for these patients (37).

Concerning non-metastasized CRC, surgery is the mainstay curative treatment, but its success is strongly related to the quality of the surgery, of the pre-operative staging and treatment selection. About systemic treatments for primary disease, there is no accepted neoadjuvant treatment for colon cancer. However, in the case of rectal cancer, depending on the stage of the patient, short-course radiotherapy, neoadjuvant radiotherapy or neoadjuvant chemoradiotherapy can be applied before surgery. Concerning adjuvant treatment, as the curative rate of surgery alone is high in those patients with no invasion of lymph nodes or metastases, very few patients can benefit from it. It is only recommended in high-risk cases, like poorly differentiated tumors. By contrast, adjuvant chemotherapy based on the combination of 5-fluorouracil or capecitabine plus oxaliplatin or irinotecan, generally improves survival in stage III patients after tumor resection, while its role in stage II disease remains debated (37). Targeted therapy is often used in combination with chemotherapy in advanced stages of CRC, such as anti-VEGF (bevacizumab, aflibercept and ramucirumab) or anti-EGFR (cetuximab and panitumumab) antibodies. These second- or third-line treatments have shown to increase PFS in patients with metastatic CRC in combination with 5-Fluouracil plus oxaliplatin or irinotecan (38–40).

About metastatic CRC, it is normally limited to a few metastatic foci, typically in the liver or lung. When both primary tumor and all metastases are amenable to complete surgical removal, mCRC is termed “resectable”. With this surgery, long-term cure is achieved for less than 20% of the patients, as nodal infiltration or occult micrometastatic dissemination is common. When patients are not resectable, systemic chemotherapy is the primary treatment option, for which there is a large list of Food and Drug Administration (FDA)-

approved indications, which will be administrated depending on the molecular tumor profiling of each case. However, mCRC remains incurable for most of the patients (41).

3. COLORECTAL CANCER LIVER METASTASES (CRLM)

Among patients diagnosed with colon cancer, 20% have mCRC at the moment of the diagnosis (synchronous, stage IV) (3) and 40% of the patients diagnosed by local disease (metachronous, stages II and III) present recurrence within 5-years after surgical treatment (42). Most of these relapses occur as metastases originated by residual tumor cells that have spread out of the primary tumor prior to surgery (43). mCRC patients have a poor prognosis, as the 5-year survival rate for mCRC is less than 20% (3). mCRC consists of tumors present at a distant site of the primary colorectal tumor mass. CRC sites of metastases are lymph nodes, liver, lung, and peritoneum (44); but most of them occur in the liver (43).

For liver metastases from CRC (CRLM) the only curative treatment is surgery. However, at the moment of the diagnosis, only 15% of the patients are suitable for resection. Thanks to neoadjuvant chemotherapy, some of the patients are rescued for resection and this percentage increases to 30%, but there is still the 70% of remaining patients that can only be treated with chemotherapy in combination or not with immunotherapy. Moreover, despite the curative intent, there is a high rate of intrahepatic recurrence among the patients that have undergone resection. With all of this, when the disease is diagnosed at that advanced stage, the 5-year survival rates are less than 10%. Many retrospective studies have shown that factors like tumor size or number of lesions are associated to poor prognosis. However, any of them provide enough information to help taking surgical decisions (45,46). Thus, it is needed to stablish new prognostic factors in order to select the best therapeutic strategies for each patient.

On the one hand, important preclinical discoveries have been made in CRC stage I-III disease, describing aberrant biological pathways associated with the development and progression of the primary tumor. On the other hand, relevant pathological aspects of the formation of liver metastases in CRLM are still unknown. Thus, few advances in preclinical research have contributed into significant benefits for CRLM patients, either in clinics or to

the quality of life, highlighting the need for more research efforts for this advanced stage of CRC.

When comparing the primary tumor and the metastatic lesions, great similarities were observed at genomic level between both tumors (47). However, at the transcriptional level there are relevant differences. These changes are due to the different microenvironment that surrounds tumoral cells in both cases. Specifically, the liver has a particular microenvironment conformed of exclusive stromal cells, like Kupffer cells, hepatic stellate cells and portal fibroblasts. This environment plays an important role in both the tumor biology and the response to therapies.

In addition, CRLM lesions also differ from the primary tumor when looking at histological characteristics. In this line, CRLM show a remarkable presence of cancer-associated fibroblasts (CAFs) that constitute the main stromal cell type and reach 75-80% of the tumor mass. We must bear in mind that fibroblasts demonstrate topographic differentiation (48). Thus, CAFs from the primary tumor, which would be colonic CAFs, may present different characteristics and play different functions than those of the liver lesion (49,50). It is important to take this into account when considering therapeutic strategies focused on stromal cells, as in the same patient therapies designed against colonic CAFs may not be efficient for hepatic CAFs. Moreover, CAFs are not the only microenvironment element that changes in the liver and that can play an important role in disease development and treatment response. Another example would be the immune cells, as the liver has a unique and highly active immune environment that acts as a barrier to gut-draining pathogens and toxins, but at the same time is also immunoregulatory as it has to promote tolerance to frequently encountered antigens (46,51). Thus, studying the liver metastases microenvironment should have a determining impact on the clinical management of CRLM patients.

Concerning the morphological differences between primary and metastatic lesions, it is important to highlight a particular histologic feature that CRLM show: they grow following three different histologic growth patterns (HGP) (52,53), that will be deeply explained in the following sections. These HGP differ on many aspects, which include the fibrosis distribution, the vascularization strategy, and the presence of immune infiltrates (52–54). In addition,

HGPs are of special interest because of their prognostic and predictive value (55,56), which suggests that the microenvironment elements that differ between them are promoting or impairing tumor growth and survival (46).

To sum up, the tumor microenvironment of liver lesions is unique and presents particularities that are highly relevant for treatment selection.

3.1. Histology of CRLM

As it has already been mentioned, the main particularity of CRLM is that they grow and infiltrate liver parenchyma following three **histological growth patterns** (HGP): "pushing", "replacement" and "desmoplastic". These HGPs were first described in 1996 by Terayama *et al.* (57), who also used to include a fourth type called "sinusoidal". The terminology that is used nowadays was coined in 2001 (58), an describes the three HGP as follows.

The "**desmoplastic**" pattern, also named "encapsulated" because its most characteristic feature is that tumoral glands are enclosed by a fibrotic stromal capsule, which is impairing any contact between tumoral cells and hepatocytes. Often, this HGP shows a dense rim of immune cells infiltration located at the transition between the liver parenchyma and the fibrotic capsule. Moreover, desmoplastic CRLM also present glandular differentiation (when they derive from an adenocarcinoma) and their strategy of vascularization is based on angiogenesis (Figure 3A and B) (53,59,60).

Conversely, the "**replacement**" pattern is defined by showing a direct contact between hepatocytes and tumoral cells. In this HGP, which is also called "invasive", "replacing", "trabecular" or "infiltrative", tumor cells infiltrate liver parenchyma while literally replacing the hepatocytes following the hepatic sinusoidal structure. In this process, tumoral cells also use the sinusoidal blood vessels of the liver, a vascularization strategy that is termed vessel co-option. Thus, in this HGP, the metastatic lesion tissue architecture is mimicking the "hepatic cell plates" present between hepatic sinusoidal blood vessels in normal liver tissue. This way of invasion makes it difficult in some occasions to distinguish where the tumor ends and begins the liver parenchyma. This HGP typically shows few immune cells at the tumor-liver interface and in the tumor center; but this is not a scoring criterion. Usually,

replacement adenocarcinoma metastases are poorly differentiated, as they do not show glandular structures (Figure 3C and D) (53,61,62).

Finally, "**pushing**" or "expansive" HGP is characterized by literally pushing away hepatocytes, which become flattened in consequence, although hepatocytes and tumor cells do not reach to touch each other. Thus, in this HGP, the tumor border is clearly demarcated, like in desmoplastic HGP, but in this case, there is no fibrotic tissue involved (Figure 3E and F) (53).

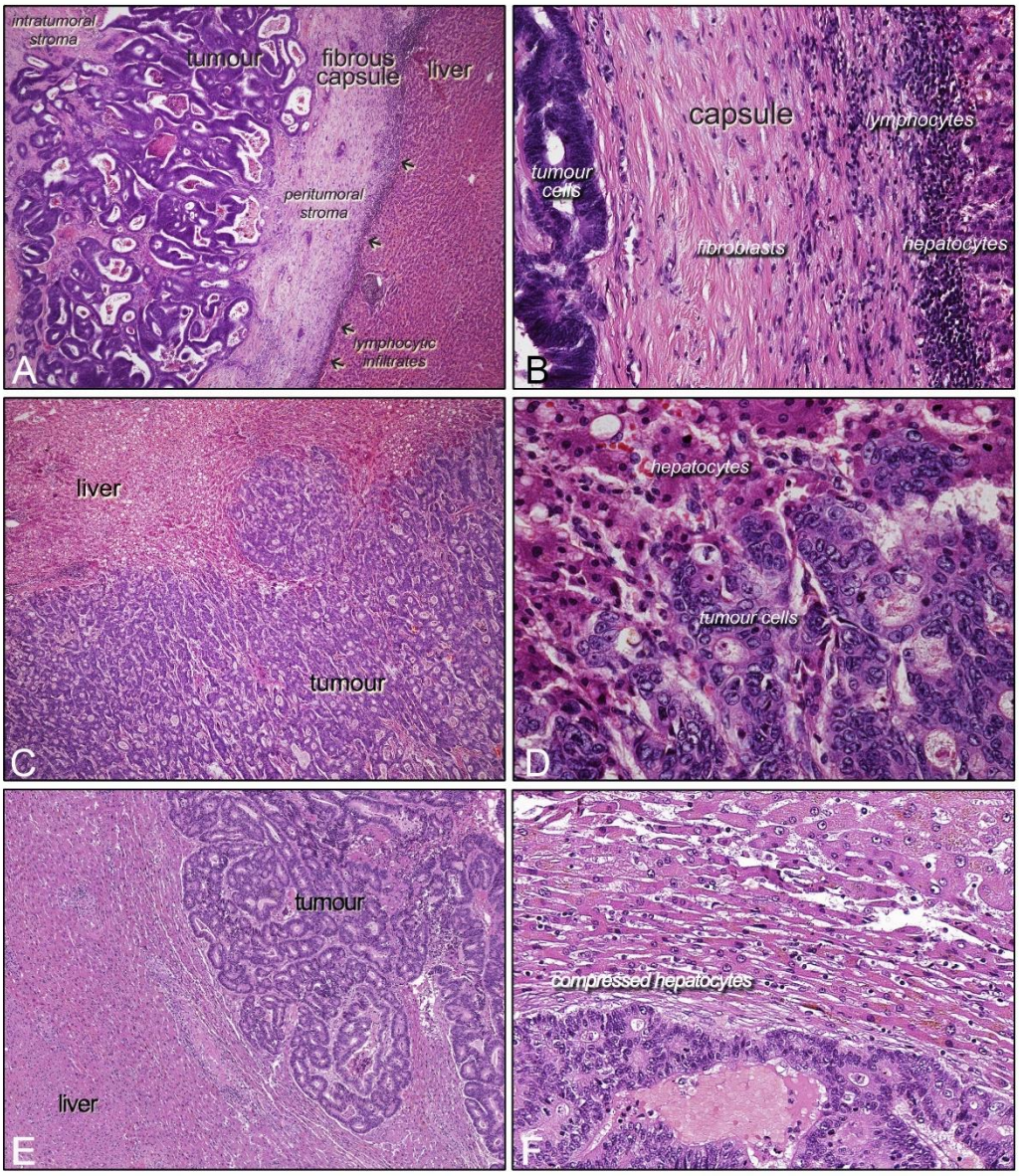

Figure 3. Haematoxylin and eosin staining of histologic growth patterns (HGPs) of liver metastases from colorectal cancer (LM-CRC). *(A, B) encapsulating/desmoplastic, (C, D) invasive/replacement, and (E, F) expansive/pushing, the different HGPs at low magnification. In the right column, same patterns at detailed magnification.*

The fourth HGP described in 1996, the sinusoidal HGP, is not considered for prognoses because it appears exclusively in patients with aggressive disease and is mainly encountered in autopsy specimens. This suggests that sinusoidal phenotype is a feature of the end-stage disease. This HGP is characterized by cancer cells that fill the sinusoidal vascular spaces and has been mainly observed in liver metastases from non-small cell lung cancer and breast cancer, rather than from CRC (63–65).

Moreover, liver metastases can also grow inside portal tracts, invading the fibrous stroma, fill the lumen of portal vein branches or lymph vessels, or even along nerves (neurotropism) and blood vessels (angiotropism). Furthermore, tumor cells can proliferate inside biliary ducts by replacing their normal epithelial cells (53).

Finally, in some replacement cases the presence of single cancer cells in the liver parenchyma distant to the tumor-liver interface have been observed. However, this has mostly been the case in melanoma liver metastases rather than in CRLM or other carcinomas (53).

3.1.1. HGPs as prognostic and predictive tool

These HGPs, have been shown to be a good **prognostic** and **predictive tool**: they have been associated with tumor recurrence and overall survival as well as good predictors for anti-angiogenic therapies. In order to homogenize how these HGP were assessed and to properly study HGP and clinical data association, an international **consensus guideline** was created in 2017 (52). These 2017's guidelines categorized those patients with <50% desmoplastic as predominant desmoplastic HGP, those ones with <50% of pushing pattern as predominant pushing HGP, and those with <50% replacement as predominant replacement. In the case where no predominant HGP was found, patients were categorized as mixed HGP. What was observed is that those patients with a predominantly desmoplastic HGP showed superior survival. However, posterior studies that have used 2017 consensus guidelines have elucidated that desmoplastic and replacement are the most common patterns; while pushing HGP is uncommon, only present in 2,5% of the tumor-liver interface of CRLM (54). Moreover, results of a study by Galjart *et al*. (54), from the Erasmus Medical Centre in Rotterdam, gave strong reasons for revising this 2017 stablished cut-off for scoring HGP as, when comparing different cut-offs, they observed that the prognosis of patients with CRLM

is primarily determined by the presence of any percentage of replacement and/or pushing growth pattern. In this study, favorable survival rates were only observed in patients with CRLM with complete desmoplastic growth, which occurred in 24% of all patients. Meanwhile, any fraction of non-desmoplastic growth reduced the 5-year OS from 78% (considering CRLM 100% desmoplastic) to 37% in the case of non-pre-surgery systemic treated patients. Considering patients that received pre-surgery systemic treatment, this percentage was reduced from 53 to 40%. Thus, they proposed to consider desmoplastic only those patients that show desmoplastic HGP in 100% of tumor-liver interface (dHGP); and non-desmoplastic those patients with any percentage of replacement or pushing HGP (non-dHGP). This proposed cut-off was subsequently referred as "**Rotterdam cut-off**" and externally validated in a large multicenter study (66). Finally, another comprehensive clinical evaluation of a large international multicenter cohort of 1931 patients was presented in 2022, updating the HGP liver metastases consensus guidelines (53). In that study, "Rotterdam cut-off" was compared to the previously stablished "**predominant HGP cut-off**" of 2017. By applying the Rotterdam cut-off, 79% of patients were classified as non-dHGP, and 21% as dHGP. Among the non-dHGP patients, 10% showed a 100% tumor-liver interface with non-desmoplastic HGP; 28% showed between 67,1-99% of non-dHGP; 16% showed between 33,1-67% of non-dHGP; and 24% showed between 0,1 and 33% of non-dHGP.

On the other hand, using predominant HGP cut-off, 43% of patients were categorized as predominant replacement; 1% as predominant pushing; 53% as predominant desmoplastic; and 2% as mixed HGP. By doing so, they observed that patient with exclusively desmoplastic HGP (dHGP) have a clear survival advantage over all other patients, confirming Galjart's results. Moreover, no differences were observed when looking at the percentage of non-desmoplastic HGP present in tumor-liver interface, suggesting an explanation of why the survival advantage of desmoplastic HGP is less pronounced when applying the predominant HGP cut-off. Finally, the learnability and accuracy of HGP scoring was better using Rotterdam cut-off approach, as the scoring method is simpler, does not require quantification and, is therefore more reproducible (53).

As the pushing pattern only appears in a low number of cases and that the most relevant feature in prognoses is the presence or not of any non-desmoplastic HGP, this project will

simplify the HGP classification in **desmoplastic HGP** (**dHGP**) and **non-desmoplastic** ones (**non-dHGP**).

Apart from the presence or not of non-dHGP at tumor-liver interface, prognosis has also been related to the thickness of the capsule: the thicker it is, the better the prognoses (67).

The differences observed in survival and recurrence between dHGP and non-dHGP could be explained by the fact that in dHGP there is a band of stroma enriched in collagen with a dense crown of lymphocytic infiltration that may act as physical obstacle for tumor expansion. Specifically, collagen type IV and integrin blockades are able to reduce the infiltration capacity of tumoral cells through liver parenchyma (58,68).

Another aspect that could be relevant for survival and recurrence are HGP **surgical implications**. For CRLM, surgical resection is the gold standard therapy with a curative aim, after which a positive resection margin is associated with poor prognoses. It has been described that patients with non-dHGP have a higher risk of positive resection margins, while dHGP patients have an increased rate of R0 (tumor-cell-clean resection margins) although R1 resection margins are observed, too. Moreover, higher number of CRLM is also associated with higher risk of an R1 resection. All of this is suggesting that both technical aspects of the liver (number of lesions) as well as the biology of the metastases (HGP) play a role in the obtainment of a clean resection margin (69,70).

3.1.2. HGP of non-CRC liver metastases

Interestingly, HGPs are also found in liver metastases from broad range of primary solid tumors, mostly carcinomas. They have been shown in liver metastases from primary lung, pancreatic, stomach (71), gallbladder/bile duct and breast carcinoma (72), as well as in skin and uveal melanoma (73,74). Recently, HGPs have also been identified in sarcoma-derived liver metastases. This fact adds more interest in both the use of HGP as a prognostic tool, as well as in understanding the biological mechanisms underlying these HGPs (53).

However, surgical resection of liver metastases from the mentioned cancer types is less common, which makes the knowledge of HGP less explored in their context (70). For this reason, the prognostic, and predictive role of HGP has been mainly studied in CRC patients. Nevertheless, there are recent studies that evaluate the impact of the HGPs on outcome in

hepatic metastases from melanoma, breast carcinoma and pancreatic primary tumors. In skin melanoma, it has been described that the presence of any replacement HGP is associated with worse overall survival (75). When considering uveal melanoma, non-dHGP also predicts diminished overall survival (74). Regarding breast cancer, very low number of patients go through surgical removal, therefore there is only one study assessing the prognostic value of HGPs. It included 36 patients and adapted the scoring categories as follows: “100% replacement” vs. “any desmoplastic” HGP, as desmoplastic HGP is rarer in breast cancer derived liver metastases compared to CRC ones. By doing so, they confirmed the association of replacement HGP with poor outcome (76). A large international study is currently being performed to further address the impact of HGPs in this context.

In conclusion, distinct HGPs can be found in liver metastases independently of the primary solid tumor type. Moreover, dHGP is always the favorable prognostic HGP. These observations suggest that the formation of an HGP is tumor-type-independent and, are liver-specific biological programs that determine which growth pattern will emerge (77).

3.1.3. Non-liver CRC metastatic places

The lung is the second most common place where CRC metastasizes (78). In fact, three different HGPs have also been described in CRC lung metastases. First, a pushing pattern, where tumoral cells compress pulmonary parenchyma. Second, a desmoplastic pattern, which also shows a desmoplastic rim containing immune infiltrates. Third and last, an aerogenous pattern that can be considered as the analogue to the replacement pattern in liver as tumor cells spread in the pulmonary air spaces without disrupting the lung architecture (62). These HGPs observed in lung metastases also have a clinical meaning, and the aerogenous pattern displays a poor prognosis, which concurs with liver replacement HGP as well. The brain is another organ where three metastatic patterns have been reported: a well-demarcated pattern, vascular co-option and diffuse infiltration; however, their impact on overall survival could not be assessed in autopsy studies (79). This suggests that host organs react when affected by metastatic lesions, in a tumor-type-independent manner. Therefore, HGPs could have a role in guiding therapeutic decisions in many different contexts apart from CRLM.

3.1.4. The HGP and treatment response

As previously mentioned, although the only curative treatment for CRLM patients is surgery, most of the patients are not suitable for it. These non-resectable patients receive different systemic treatments which include chemotherapy (different chemotherapeutic agents), immunotherapy or anti-angiogenic treatment. Thus, the effect of these treatments in HGP has been the focal point of many studies.

In this line, some studies suggest that chemotherapy induces a conversion to a desmoplastic growth pattern in patients with replacement-type CRLM (54,80). Specifically, in the case of Nierp *et al.* (80), three cohorts were taken from randomized studies in which perioperative chemotherapy treated patients were compared to chemo-naive ones. This study showed that the average presence of desmoplastic HGP at the tumor-liver interface of pre-treated patients was around 64%, while this average was around 38% in the chemo-naive group. These results would be in line with a proposed hypothesis of encapsulating fibrosis formation proposed in pancreatic cancer, called the "necrosis" hypothesis. This theory proposes that cell damage caused by chemotherapy has as a result the generation of necrotic areas that are recognized as a wound by the host organ. In response to this wound, fibrosis would be induced resulting in an encapsulated lesion, which would have the same properties as desmoplastic HGP from liver metastases (81). However, concerning the results of these studies, it remains to be determined if chemotherapy induces the HGP transformation or if pre-existing desmoplastic lesions are more resistant to chemotherapy (53).

On the other hand, there are studies that found associations between systemic treatment for CRLM and histological features typical of the replacement HGP (82,83). Concretely, these studies have described what they term the "dangerous halo", which consists of an irregular tumor-liver interface observed through RMN and TC only in patients that have received neoadjuvant chemotherapy. This "dangerous halo" shows areas of replacement growth. In contrast, lesions that do not show this "halo" have a desmoplastic HGP.

Moreover, in line with the previous studies that relate treatment with replacement HGP, Frentzas *et al.* (56) described that the growth pattern of the recurrent CRLM lesions, defined as the ones that were not detectable by imaging before treatment but appear during it, show

more often a replacement HGP than lesions that were visible since the beginning. In this case, the systemic treatment that these patients received was bevacizumab and, thus, these results are supported by several preclinical studies that have demonstrated a switch from an angiogenic to a vessel co-opting growth pattern as a response to the anti-VEGF drug treatment (84–87).

In addition, it has been reported that some features, such as the expression of a plasminogen receptor or the presence of $CD68^+$ macrophages, differ between desmoplastic and non-desmoplastic HGPs but not in neoadjuvant treated patients (88). Thus, neoadjuvant chemotherapy is altering tumor growth in many different aspects, the study of which could be crucial for the development of better treatment strategies.

Taken together, we can conclude that systemic treatment modulates HGP in many aspects. Despite this, the most reliable way to assess how different treatments affect HGP is having tools like non-invasive imaging or markers assessed in blood analyses to assess the HGPs at several time points during treatment. However, these tools are still in development (46,53).

3.1.5. Stablished standard method for assessment of HGPs in CRLM

The consensus guidelines first stablished in 2017 (52) and updated in 2022 (53) have set a standard method for assessing HGPs in CRLM context, which are resumed in **Table 2**. Considering presumed treatment-induced transition, an “escape” phenotype term is proposed to refers to liver metastases resected after preoperative systemic treatment that combines signs of a pathological response in the center of the lesions while also showing at least a partly preserved desmoplastic HGP or replacement-type “halo”.

Sampling of resection specimens:

- Complete sampling (tumor–liver interface and center) of metastases up to 2 cm.
- Sampling of a complete central section (tumor–liver interface and center) of metastases larger than 2 cm.
- If an alternative sampling method is applied, for example, a tumor-type-specific approach, this should be reported.

HGPs are assessed by **light microscopic imaging of H&E sections of FFPE tissue of resection specimens** of liver metastases. Tissue cores from needle biopsy procedures are not suitable. Resection specimen tissue sections with only a limited part of the tumor–liver interface is considered insufficient to assess HGP. Also, if no viable tumor tissue is present in the metastasis, HGP cannot be assessed. Delayed fixation artifacts may lead to insufficient quality for scoring HGP.

CRLM HGPs can be evaluated by a **pathologist** or by any other **investigator trained by a pathologist**.

The **center** of the metastasis **does not contribute** to the classification of a growth pattern.

The three common growth patterns are: **desmoplastic, pushing** and **replacement**.

The sinusoidal growth pattern is rare. In addition, metastases can grow in portal tracts and inside biliary ducts.

When more than one HGP is present: **estimate the relative fraction of each HGP**. Although when the HGPs are assessed to obtain prognostic information, it is sufficient to look for areas of replacement HGP to distinguish a non-desmoplastic from a desmoplastic status, specific scoring and reporting rules may apply to certain tumor types and settings.

In case of **multiple metastases/patient**: assess HGPs in **every individual** liver metastasis.

Reporting of the HGPs per patient:

- For each metastasis report the proportion of replacement, desmoplastic and pushing HGP.
- Small areas with a distinct HGP covering less than 5% of the interface should still be reported.
- The presence of intrabiliary, portal and sinusoidal growth should be reported as a separate remark.
- 'Escape' should be reported as being absent or present in metastases resected after chemotherapy.

The categorisation of a patient according to liver metastases HGP will depend on the **primary tumor type** and the **aim of the growth pattern assessment**.

Caveats and practical tips:

- Portal tracts at the tumor–liver interface and growth near the liver capsule should not be considered.
- Metastatic growth inside portal tracts or biliary ducts should not be regarded as desmoplastic growth.
- The presence of intrabiliary tumor growth can be underestimated, as the biliary epithelium is often replaced by cancer cells.
- Reactive proliferation of bile ducts (ductular reaction) in the desmoplastic rim can simulate a replacement growth pattern. In addition, cancer cells can build common structures with reactive bile ductuli.
- In case of severe inflammation and associated tissue changes it may be difficult to identify the growth patterns.
- Pushing type of growth should not be overestimated: only when there is no cancer cell-hepatocyte contact, the pushing HGP can be considered.

Table 2. 2022 updated standard method for histopathological growth pattern assessment of liver metastases. *Adapted from Latacz et al.* (53).

Finally, although the assessment of HGPs in the liver is exclusively done on H&E staining, there are some IHCs that could help. Doble staining of hepatocytes and cancer cells would help to distinguish HGP when a dense crown of immune infiltrates is present or to discern between replacement and pushing. Moreover, doble staining of cholangiocytes and cancer cells would be useful in cases with prominent ductular reaction, in which it is difficult to distinguish between biliary ducts, small tumor glands or cancer intrabilliary growth (53).

3.1.6. Primary CRC characteristics and CRLM HGPs

Höppener *et al.* (89) performed a study with the aim to evaluate the relationship between the HGP observed n CRLM and the histopathology of CRC primary tumors. They observed higher preoperative serum carcinoembryonic antigen levels in non-dHGP, as well as more positive surgical margins upon CRLM resection. Moreover, they equally see that in both HGP the great majority were adenocarcinomas, and that mucinous adenocarcinomas were distributed the same way between dHGP and non-dHGP.

Then they looked at primary CRC histopathology markers. In case of classical markers, such as poorly differentiated primary CRC, right sided, pT4-stage, positive lymph nodes, and presence of tumor deposits (focal aggregates of cancer nodules located in the pericolic

region or in perirectal fat) no significant differences between HGP were detected. When they looked at invasion markers, like lymphovascular, extramural venous or perineural invasion, no significant differences were observed either. When looking at tumor interface markers, peritumoral budding, known as small clusters of detached cancer cells at the invasive border, neither showed significant differences. On the contrary, two previous studies that also assessed this primary CRC feature, which used "predominant HGP cut-off" instead of "Rotterdam cut-off", observed a significant relationship between predominant replacement HGP and primary peritumoral budding (90,91). In the Höppener study, all mentioned primary CRC histopathological features were more common, although not significantly, in patients with corresponding non-dHGP in CRLM. On the other hand, non-mature stroma was significantly more often observed in primary CRC tumors of corresponding non-dHGP CRLMs. Moreover, immunological markers like the Crohn's like lymphoid reaction (a peritumoral lymphocytes aggregation that occurs in colon cancer being a major component of the host immune response to cancer) was more common in dHGP, in which TIL density was significantly lower in non-dHGP.

In conclusion, unfavorable CRC histopathology markers were more prevalent in non-dHGP. Although many of them differed in a non-statistically significant way, the cumulative prevalence of unfavorable CRC histopathology was significantly higher in non-dHGP. In brief, their results suggest an increased host-immune response in primary tumors of dHGP, and histological evidence of epithelial-mesenchymal transition in the non-dHGP corresponding ones.

Concerning the molecular characteristics, like KRAS and BRAF mutational status or CMS classification, the few studies that have been performed did not find an association between them and CRLM HGP. Thus, they found the HGP prognostic impact to be independent of genetic alterations (66,92). However, in-depth genetic association studies are still lacking. In addition, the concordance in molecular subtypes of primary colorectal tumors and their matched liver metastases has been investigated, although not associated with CRLM HGPs (93,94). These studies have shown that, despite the genomic alterations from liver metastasis being highly similar to its matched primary tumors, the gene expression levels did change between primary and metastatic lesions from the same patient, being EMT and myogenesis was enriched in primary tumors, and angiogenesis and inflammatory response

enriched in metastases (93). Moreover, when looking at the concordance of the primary tumor classification, as mentioned, usually high concordance with liver metastases was observed, in exception of mesenchymal profile (CMS2), which showed a significantly shift to CMS2 when assessing the metastases (94).

Considering all this information, we can conclude that nowadays it is not possible to predict the HGP that would arise in CRLM through the molecular or histopathological characteristics observed in its primary tumor. For that, further research with higher number of patients is needed. Furthermore, although the information exposed has a relevant impact in understanding the biology underlying metastases formation and HGPs, it also proposes that the appearance of one HGP or another relies on multiple factors, including tumoral cells and the microenvironment in which they are encountered.

3.2. Biology of CRLM

From a biological perspective, the mode through which metastases grow in the liver has awaked high interest as it should conceal the mechanisms underlying the previously described differences in prognosis.

First, if we consider how the process of liver metastases occur, it takes place following four phases, proposed for the first time by Vidal-Vanaclocha in 2011 (95), in which the hepatic microenvironment can play opposing roles (59). The first, called the **microvascular phase**, occurs in sinusoidal vessels when circulating tumor cells arrive (59,61). At this timepoint, cancer cells need to be able to attach and adhere to the endothelial cell layer and, eventually, transmigrate through the vascular endothelium. This complex process is called extravasation and leads to the following second phase: **pre-angiogenic** or **intra-lobular micrometastatic phase**. In this phase, stromal cells from liver and immune cells are recruited, but the micrometastases still do not show vascularization. In the **third angiogenic** or **panlobular phase**, the hypoxic microenvironment induces the recruitment of endothelial cells and formation of blood vessels. Finally, in the fourth **lobar growth phase**, the new tumor can be clinically detectable. The progression of these phases and the following growth of the metastasis depend on the interactions that occur between **malignant cells** and the **liver microenvironment** (59,61).

3.2.1. Colorectal cancer cells and their role in CRLM

Concerning **malignant cells**, none of the typical genetic alterations have been associated with the process of metastases in CRC. Instead, the regeneration of the tumor in a host organ, the liver in this case, seems to be linked to the acquisition of a stemlike phenotype by cancer cells. In line with this, metastatic stem cells would be able to adopt different phenotypes and behaviors depending on their interaction with the microenvironment, which would allow them to survive along all the phases of the metastatic process (43).

In CRC carcinogenesis, the mutations acquired regulate intestinal stem cells to become cancer cells with self-renewal and growth capacity in a crypt niche independent manner (96). Moreover, it has been described that acquisition of mutations in the four linear progression model pathways is sufficient for tumor cells to survive in unfavorable conditions like circulation or foreign tissues (97,98). Although most CRCs carry genetic alterations in these four driver pathways, the number of patients that develop metastases is not high. Thus, there must be additional selection factors that limit the extent of tumor spreading that remain to be elucidated.

In CRC liver metastases, when disseminating cells from primary CRC reach portal circulation, they are transported to liver sinusoids and can stablish into liver parenchyma as they can extravasate through vessel fenestration. On the other hand, to arrive to the lungs and generate CRC lung metastases, primary CRC cancer cells first have to reach general circulation to infiltrate lung parenchyma, for what active killing of capillary cells is needed (99). Experimental models have shown that the limiting step in the metastatic process is the capacity of circulating tumor cells to colonize the foreign organ (100). Most tumor cells that can survive in circulation and infiltrate a distant organ die for reasons that are not fully understood, but that may include being recognized and killed by innate and adaptive immune system (101). In case cells are not killed by the immune system cells, and neither died for other reasons, it can also happen that, rather to thrive a colony, they stay latent for months to years before resuming growth (102). In the case of CRC, there are different aspects that facilitate its metastatic colonization.

First, it is important to have in mind that any tumor is uniform, but consists of multiple cell populations, which vary phenotypically and genetically. This knocks into shape what is

known as intratumoral heterogeneity (ITH). There are three factors that contribute to ITH: organization of cell lineages, clonal diversification, and the microenvironment.

Organization of cell lineages refers to the fact that there is hierarchy of cells with distinct tumorigenic potential into a tumor: the "tumor-initiating cells", which have stem properties; and the differentiated cells, that arise from the previous ones. This differentiation would coincide with the loss of tumorigenic potential (103,104). As it happens in normal tissues, in CRC there is a balance of tumor-initiating / stem cells and the differentiated ones, which is mainly regulated by WNT, BMP and NOTCH signaling. The fact that some of the signals involved in these pathways are provided by stromal cells, suggests that the microenvironment could be crucial in tumor cell survival, in addition to the genetic alterations in the four linear progression model pathways already mentioned (43).

It is worth mentioning that there is a difference between stem cells from primary CRC and the ones present in metastases, as the first ones can grow tumors into mice but are not competent to generate metastases. This last capacity only occurs when cancer cells interact with adjacent tissues and tumor stroma, thus highlighting again the important role that the tumor microenvironment is playing, not only in stem cell maintenance, but also in enabling migration and extravasation of tumor cells (105).

Finally, an interesting feature of CRC is the presence of tumor buds in the primary tumor. Cells that possess these characteristics have a higher invasive and migratory phenotype as they express genes involved in extracellular matrix degradation and epithelial-mesenchymal transition. Moreover, these cells also accumulate nuclear beta-catenin, which suggests that they also have stem cell properties. This tumor budding has been linked to poor survival and is considered a high-risk marker for metastases (43). However, as it has been mentioned before, it is not associated with the appearance of dHGP or non-dHGP in the corresponding CRLMs (89).

3.2.2. The metastases host organ: the liver

The liver is the biggest solid organ in the body and performs crucial biological functions like help supporting the metabolism, immunity, digestion, detoxification, vitamin storage and protein production among other functions. Moreover, this organ has a dual blood supply: it

receives blood from the portal vein (75% of the total blood volume received), which is rich in nutrients but poor in O_2, and from the hepatic artery (25% of blood volume), poor in nutrients and rich in O_2. Blood coming through the portal vein originates from the blood vessels of the gut carrying all the substances that have been absorbed in it, including pathogens and toxins. Because of this, the liver has to act as a systemic barrier for all the potentially dangerous elements present in it. All this blood flows along the liver go through hepatic sinusoids and leaves the liver through the hepatic vein, a conversion of all the liver central veins. This high irrigation makes it the major metastasis-susceptible site and most of the patients affected by hepatic metastases die in the absence of effective treatment (51,95,106,107).

3.2.2.1. *Liver functional organization and cellular anatomy*

The functional unit of the liver is the **lobule**, which is always described as a hexagonal structure although in humans this hexagonal shape is not as defined as it is in pig´s liver. In each corner of this lobule there are branches of the portal vein, the hepatic artery, and the bile duct, conforming what is known as **portal triad**. This portal triad is surrounded by a fibrotic support, conformed by extracellular matrix and portal fibroblasts, forming the **portal space**. But the parenchymal cells that conform the foundation of the lobule are the hepatocytes. Blood reaches them through hepatic sinusoids, which lead into the last element of the lobule: the **central vein**. Sinusoidal capillaries significantly slow down the blood in the liver, which contributes to effective immunosurveillance and clearance of toxics from the blood. Moreover, the function of hepatocytes changes depending on the region of the lobule in which they are located. This lobule feature is termed "**zonation**", and three different zones are described: Zone 1 is the located at the periportal region. It is the best perfused, thus, it has higher levels of oxygen and nutrients, what makes it the first to regenerate when needed. Due to its high perfusion, zone 1 is highly involved in oxidative metabolism, like beta-oxidation, gluconeogenesis, amino acid catabolism and cholesterol and bile formation. Zone 2 is a transition zone comprised between zone 1 and 3. Zone 3 is defined as the pericentral vein region, has the lowest perfusion due to its distance from the portal triad and plays the largest role in detoxification, biotransformation of drugs,

ketogenesis, glycolysis, lipogenesis, glycogen synthesis and glutamine formation (Figure 4) (51,106,107).

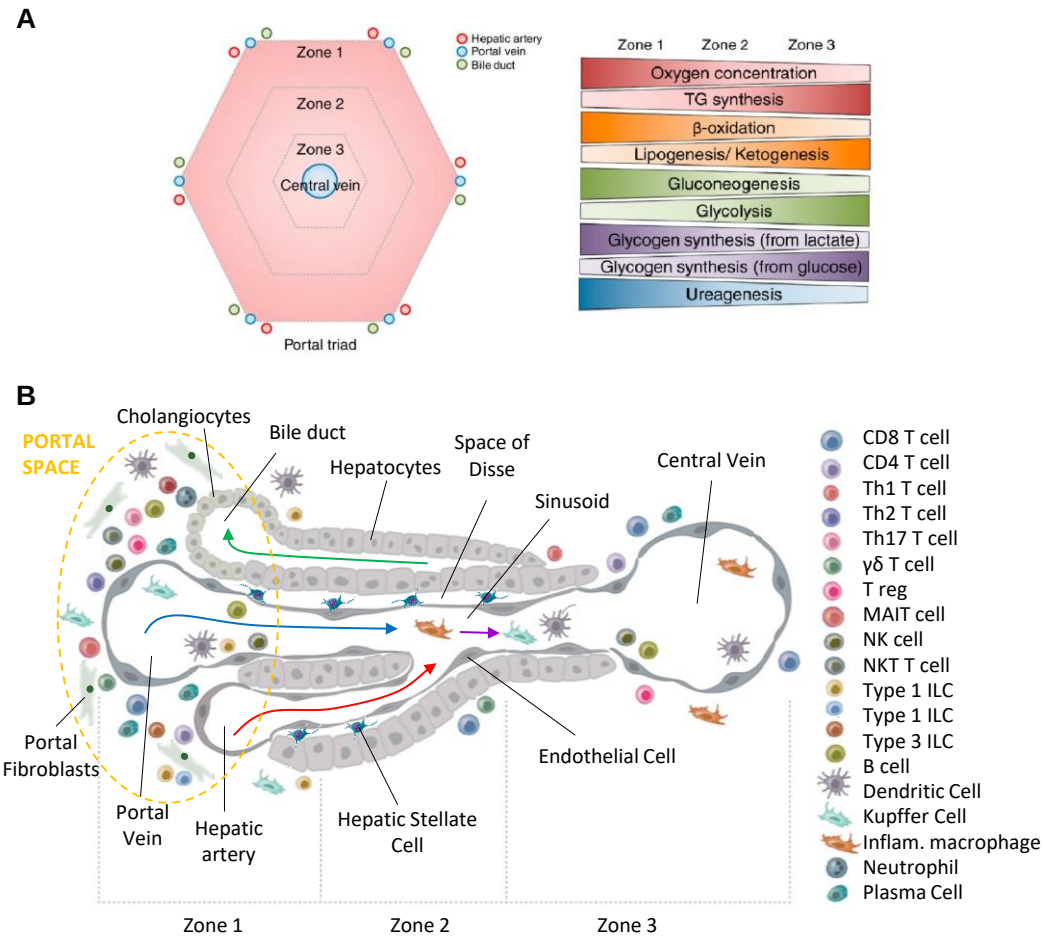

Figure 4. Liver functional organization and cellular anatomy. *(A) Geometric representation of a hepatic lobule at the left side. At the right side, a schematic representation of the gradients of both essential molecules (oxygen) and metabolic processes that occur along the sinusoid. Adapted from Trefts et al.* (107). *(B) Schematic representation of a sinusoid within the liver with the corresponding zonation and the immunological players. Adapted from Cheng et al.* (51).

But blood is not the only liquid that flows through the sinusoids. Bile moves along bile canaliculi, which is formed by apical membranes of neighboring hepatocytes and flows in the opposite direction while leaving the organ (106).

Moreover, another structural feature of the hepatic lobule is the **space of Disse**, which corresponds to the space between the sinusoidal lumen and the surrounding basolateral membrane of hepatocytes. In this space the extended microvilli form the hepatocytes' basolateral membrane, that communicates with the sinusoid to reach its' blood supply. The space of Disse is formed by an extracellular matrix composed of a variety of collagens,

proteoglycans and other proteins that serve as a of scaffold for the hepatocytes, as they do not contain a basement membrane. The space of Disse there also contains the tissue resident macrophages, also known as Kupffer cells, filtering the unnecessary or pathologic material from the circulation. Moreover, hepatic stellate cells, which serve as fat and vitamin A storage in homeostasis and become myofibroblasts in liver regeneration conditions, are also located in this space (106).

3.2.2.2. *The immune niche of the liver*

The liver is also a highly immune active organ due to its function as systemic barrier to gut-draining pathogens and toxins. However, foreign food-derived antigens and bacterial products also reach this organ through the portal vein. Thus, the liver must maintain a local immunologically tolerant environment, allowing reactions against gut-coming pathogens, but also a regulated tolerance to frequently encountered antigens like food-derived ones. In physiological conditions, this liver's tolerogenic and immune-rich environment promotes local and systemic homeostasis, in addition to enabling the potential for hepatic regeneration. However, the persistent presence of a pathological antigen like viral infection or a tumor result in an induced tolerance to it, which is a key feature of the liver. In this tolerance-inducing process, adaptive immune cells promote effector cell death and "educate" regulatory cells. These tolerance mechanisms present in every persistent antigen are believed to be responsible of almost all liver diseases. Thus, to understand and properly treat hepatic diseases, we need to completely understand the constitution and function of all the cells that compose the organ (51,108). In this line, Figure 4b summarizes the different cell types, including immune cells, that have been described in the human liver and their putative locations in hepatic lobule.

Liver has both innate and adaptive immune system cells. Adaptive immune cells that are to be found there include T cells, such as regulatory T cells (Tregs), cytotoxic T lymphocytes ($CD8^+$ T cells) and $CD4^+$ helper T cells Th1, Th2 and Th17. It also includes B and plasma cell populations (109–111).

Among **T cells**, $CD8^+$ and $CD4^+$ T cells are found all along the parenchyma and portal tracts. **$CD4^+$ T** cells are a key component of the immune system, as they are orchestrating adaptive immune responses. Five major CD4 T helper cells have been described: Th1, Th2, Th17, T

regulatory (Tregs) and follicular T helper cells (Tfh), but the last ones are not present in the liver. **Th1** cells induce immune type 1 responses to protect intracellular pathogens. **Th2** lymphocytes are involved in type 2 responses, which are the ones fighting infections of parasites. **Th17** cells mediate type 3 responses, which are in charge of extracellular bacteria and fungi clearance. Finally, in the liver we find **Tregs**, which are recognized as the primary mediators of peripheral tolerance, as they mediate immune suppression when needed (112). On the other hand, **CD8$^+$** or **cytotoxic T** cells are the major killers of pathogens and neoplastic cells (113).

Regarding **B cells**, they express **CD20$^+$** surface marker and are the responsible of producing antibodies to fight bacteria, viruses, or cancer cells. These antibodies are specific for each pathogen, lock onto the surface of an affected cell and mark it for destruction (114). The terminal differentiation step of mature B cells is known as **plasma cells**, which have an extended lifespan and could secrete large amounts of antibodies (115).

The innate immune system consists of macrophages, natural killer (NK) cells, natural killer T (NKT) cells, mucosal-associated invariant T (MAIT) cells, dendritic cells (DCs), γδ T cells, and innate lymphoid cells (ILC). Injury also results in the recruitment of peripheral immune cells like neutrophils and infiltrating monocytes (110,111).

Macrophages, which are **CD68$^+$**, are the most abundant liver immune cells and play an essential role in the maintenance of hepatic homeostasis. In the liver one can find resident macrophages, also called **Kupffer cells** (KCs), and **monocyte-derived macrophages** (116). Moreover, a single-cell study of the liver found two types of resident macrophages: an anti-inflammatory, with tolerance properties and positive for **CD163**, **MARCO** and **CD5L**; and a pro-inflammatory, negative for the previous markers but positive for **S100A8/A9** (117).

In the liver, **natural killers** are a major population of lymphocytes. In humans, they are classified as **CD56$^+$** cells, with the expressing ones having cytolytic activities, and the high expressing releasing immunomodulatory cytokines. These cells are described to have only limited constitutive interaction with the healthy liver, but they play an important role during liver inflammation (118).

Natural killer T cells are a subset of T cells that are specially enriched in the liver and that regulates immune responses in the context of autoimmunity, cancer, and microbial

infection. They generally recognize lipid antigens. Moreover, two subsets with opposing roles, pro-inflammatory and anti-inflammatory, are described (118,119).

MAIT cells are a novel innate-like T cell population that can recognize highly conserved antigens and that seem to play an important role in the first line of defense of the liver (120).

Dendritic cells are a specialized population of antigen presenting cells that play a critical role in linking the innate and adaptive immune system branches. The liver contains a heterogeneous population of these cells that contribute to both liver inflammation and fibrosis (121).

γδ T cells are a subpopulation of non-conventional T cells that express γδ TCR instead of αβ, that is expressed by conventional $CD4^+$ and $CD8^+$ T cells. They link the innate and adaptive immunity as they share features of cells from both immune system branches. When these cells leave the thymus, their potential is already defined and are in a pre-activated status that allows them to respond much faster than conventional T cells. γδ T cells can kill target cells in a similar way that conventional T cells do. Moreover, they can express different cytokines depending on the subtype to which they belong (122).

Innate lymphoid cells (ILC) conform a heterogeneous group of immune cells that is similar to T cells but do not express clonally distributed antigen receptors. These cells have a similar expression pattern as T helper cells Th1, Th2 and Th17; and are therefore referred to ILC1, ILC2 and ILC3, respectively. They are abundant at barrier sites such as the skin, liver, airways, lymph nodes and gastrointestinal tract. Their role is related to their capacity to respond rapidly to pathogens through the production of cytokines (123).

All these immune cells are in crosstalk with hepatocytes, cholangiocytes, liver sinusoid endothelial cells (LSECs) and hepatic stellate cells (HSCs) in a complex network of interactions that mediate the immunoregulatory and anti-inflammatory environment needed for liver functionality (51).

As mentioned before, there is a metabolic sub specialization of hepatocytes that depends on the zone they occupy in hepatic lobule. In line with this, immune cells also follow a specific localization inside of the lobule that is determined by interactions between surface receptors and the gradients of their chemokine ligands. Commensal bacteria induce LSECs to promote an enrichment of KCs and NKT cells in the periportal region. As for tissue-

resident macrophages, they have been identified to be throughout the hepatic sinusoid, with the ones in the periportal regions being more phagocytic and immunoregulatory, and the ones closer to the central venous more inflammatory (117,124). $CD8^+$ cells, in mice, are described to participate in hepatic immunosurveillance, but their function is not known in humans. Although the role of B cells is not well-documented in humans or mice, it is known that in humans they are localized together with plasma cells, within hepatic sinusoids close to the portal spaces, in the connective tissue conforming them (125–127). On the other hand, DCs are in the subcapsular region of the liver, between hepatocytes and concentrated in periportal areas, together with resident ILCs (128). However, the full spectrum of the cell populations subsets, its localization, function, and phenotype need further investigation.

Although the liver has mechanisms to avoid an inappropriate inflammatory response that can induce damage, an improperly eliminated pathogen can still break the homeostasis and lead to liver inflammation. Then, many circulating immune cells are recruited to create an immunogenic state (129,130). After a process of inflammation, the liver initiates self-rescue mechanisms to limit its damage. Among these mechanisms there are autophagy, increased numbers of Tregs and compensatory anti-inflammatory response by resident macrophages (131–133). Moreover, once the inflammation has been restored, the liver can go through two different processes to re-establish its structure: liver regeneration or fibrosis. It has been described that the immune microenvironment plays an important role in directing the process to one side or the other. Specially macrophages are involved in this decision, as depending on their polarization they will coordinate cells to be more pro-regenerative or pro-fibrotic. Moreover, IL-6 (as hepatocyte mitogen), Wnt signaling, HGF, EGF, TGFβ and nitric oxide synthase have also been shown to be involved in liver regeneration (134–136).

Overall, the tolerogenic environment that characterizes the liver is the result of a complex web of interactions between parenchymal and non-parenchymal liver-resident cells. Disturbance of this tolerogenic environment homeostasis can lead to inflammation derived damage as well as to induced tolerance to pathological antigens like the ones from cancer cells.

3.2.3. Tumor microenvironment in CRLM

The local microenvironment can be considered the major determinant of the host reaction on the tumor progression. Thus, in the case of CRLM, it is highly probable that it is playing a determinant role on the development of a certain HGP. Therefore, the tumor microenvironment could be key in explaining worse or better outcome of each pattern. As mentioned before, the liver harbors different non-parenchymal cells that can participate in conforming the tumor stroma in CRLM context. Among these cells we find host macrophages, host mesenchymal cells (hepatic stellate cells and portal fibroblasts), liver sinusoid endothelial cells, and all previously listed the immune cells of the liver (61,137). Moreover, there are also circulating and bone marrow-derived immune cells that are recruited in response to the malignant growth. These host cells, as well as the recruited cells of the immune system, interact in a complex interplay of cytokines and chemokines that conform to the microenvironment in which the metastatic tumor growth takes place (46).

3.2.3.1. Liver sinusoidal endothelial cells

The liver sinusoidal endothelial cells (LSEC) are the first host cells to be in direct contact with tumoral cells. LSEC are part of the liver first line of defense, also accompanied by Kupffer cells and hepatic natural killers, which may destroy tumor cells through the release of pro-apoptotic signals prior to extravasation (137,138). However, LSEC can also promote attachment and adherence of cancer cells by expressing cell surface adhesion molecules, thereby facilitating metastasis formation (137). Moreover, LSEC secrete Fibronectin, which can induce an epithelial–mesenchymal transition in cancer cells, and macrophage migration inhibitory factor (139,140). In addition, considering that HGP have different tumor vascularization strategies, LSEC can be a key player for their development, as they are closely related to the metastasis vascularization pattern (137,141–143). Finally, LSEC are endocytic cells that scavenge molecules from the bloodstream and present them to hepatic lymphocytes, which leads to a physiological immune regulation towards tolerance preventing liver parenchymal damage. However, during hepatic metastasis development, tumor-activated LSEC become highly inflamed which fosters their immune suppressive effect, especially in the replacement HGP (144). As shown in an experimental model of

hepatic CRC metastasis, the mechanism is amplified by IL-1-induced LSEC mannose receptors (46,145).

3.2.3.2. *Cancer Associated Fibroblasts (CAFs)*

As it happens in CRC primary tumors (50), CRLMs are characterized by showing desmoplasia, which is defined by having a high amount of stroma among the malignant cells. This reactive stroma contributes to create the proper environment for tumor development and is mainly composed of CAFs. In physiological conditions, fibroblasts are quiescent cells that become activated in response to a stimuli, usually tissue damage. In the case of CAFs, they have classically been described as fibroblasts that have been activated by the interaction with tumor cells. However, given the diversity of precursor cells from which they can arose, nowadays CAFs definition is the following: morphologically spindle-like cells and functionally activated fibroblastic cells present in the TME of solid cancers that have a phenotype distinct from the quiescent fibroblasts found in normal tissue (146). Studies of different cancer types have shown that, the quantity of CAFs is associated with bad prognosis (147–149). Further investigation focusing on these cells demonstrated that, in a desmoplastic tumor microenvironment, CAFs interact with the rest of stroma components and mediate processes that favor tumor cells: promoting tumor cell proliferation and migration, supporting stem cell niche generation, regulating immune suppression, and influencing chemoresistance Moreover, CAFs also seem to play an important role in the process of chemoresistance (150), as they can create a physical barrier that hinders drugs to reach the tumor cells or alter the drugs' function through factors production (151–153).

For all these reasons, CAFs were considered a potential therapeutic target for desmoplastic tumors. Therefore, many research groups focused on developing therapeutic strategies for the elimination of CAFs, which surprisingly showed opposite effects. The inhibition of CAFs' functions had some positive effect on sensitizing tumoral cells to treatments (154–157). However, other studies showed that CAF depletion could also result in a pro-tumoral effect (155,158). These observations suggested the existence of different CAF subpopulations, with pro-tumoral or anti-tumoral functions, a theory that by now has already been demonstrated in many different contexts (159,160).

3.2.3.2.1. CAF subpopulations

When fibroblasts from a healthy tissue become activated by tumoral cells, it implies morphological and gene expression changes. At morphological level, CAFs adopt a spindle-shaped morphology but with multiple branches of cytoplasm, bigger nuclei, plentiful ribosomes, increased rough endoplasmic reticulum, and well-developed Golgi apparatus. Functionally, activated CAFs exhibit an enhanced secretory phenotype and a high capacity for ECM synthesis, through which they communicate with surrounding cells (161). Among the repertoire of CAF upregulated proteins, we find the smooth muscle actin (αSMA), which is the marker that has been classically used to identify CAFs. But we can also find many other markers, like Periostin (POSTN) and fibroblast activating protein (FAP). In fact, different **marker expression patterns** have been associated to subpopulations of CAFs in many diseases, although none of them is considered valid for all the contexts and could serve as a single definitive marker for CAFs' definition.

The most accepted and used CAF classification is the one described in pancreatic cancer, by Öhlund *et al.* (162). This study differs two major types of CAFs. On the one hand, the CAFs expressing FAP and high levels of αSMA, which were termed **myofibroblastic CAFs** (myCAFs). MyCAFs need cell-cell contact to differentiate into this state and have functions mainly related to extracellular matrix production. On the other hand, CAFs that expressed low levels of FAP and αSMA but secreted high levels of cytokines and other pro-inflammatory molecules, were named **inflammatory CAFs** (iCAFs). This classification has been considered in many posterior studies and currently αSMA and FAP are the two most used CAF markers. Nonetheless, the expression of FAP is still controversial, as some papers affirm that it does not colocalize with αSMA and/or that it is a marker of iCAFs instead of myCAFs (158).

Another example of CAF subpopulations classification is the one done by (163) in breast cancer. This paper describes four different CAF subsets, but only the one that attracts T-cells and contribute to immunosuppression expressed FAP. Breast cancer CAF heterogeneity was also addressed through RNA sequencing. Finally, four subpopulations were described, termed as vascular, matrix, cell cycle and developmental CAFs. Each of them seemed to originate from different precursor cells: perivascular compartment, resident fibroblasts or malignant epithelial cells that had undergone EMT (164). But none of them differed in FAP

or αSMA expression, suggesting that these markers do not define CAF populations in breast cancer (163). Thus, the pattern of CAF markers changes depending on the tissue were the tumoral lesion is located (165). CAF subtypes have also been assessed in lung cancer, in which cell lineage tracing have elucidated other populations that differ depending on the type of lung cancer studied (166–170).

Another interesting insight of Ölund *et al.* is that the CAFs of the primary tumor had a different cytokine secretion repertoire compared to the ones from the metastatic site, suggesting a difference between the CAF population originating from the metastatic microenvironment ant the ones from the primary tumor. This highlights the importance of focusing on the TME of each organ.

At last, it has been observed that CAF marker expression also changes depending on the **CAFs' location** inside the tumor itself. These changes happen due to the proximity to cancer cells: if CAFs are at the surrounding area of the tumor or inside of it, and if they are in direct touch or not with them. For this reason, there are studies that, apart from biomarker expression patterns, classify CAFs according to their location. It is the case of Nielsen *et al.* work (171), that classified CAFs regarding their location into lobular, septal, peripheral or juxtatumoral stroma, thereby observing a particular transcriptional signature at each place (171). However, more research is needed to elucidate the most accurate classification and association of particular subsets with functionality and spatial location.

In conclusion, this data supports the assumption that there may be coexisting subpopulations of CAFs performing both, tumor-supportive and tumor-suppressive functions. These multiple subsets of CAFs arise from different precursor cells and can be identified through marker expression patterns and/or through their location inside of the tumor. Moreover, CAF subpopulations differ depending on the affected organ, as well as the fibrosis causing disease (50,154,155,162,172).

3.2.3.2.2. Cancer-promoting or cancer-restraining CAF

Many populations of CAFs have been described in different contexts according to their marker expression pattern. But, as previously mentioned, CAF effects on cancer development are also heterogeneous. There are studies that have clearly defined CAFs

promoting cancer progression through numerous mechanisms like ECM remodeling and production of cytokines, chemokines, and growth factors. Thus, they would be directly or indirectly promoting cancer progression, metabolism switch or angiogenesis (173). On the other hand, it has also become clear that there are CAFs that have inhibitory roles in cancer progression. These cancer-restraining CAFs carry out functions like acting as a barrier against cancer cell invasion and seeding, promoting anticancer immunity, proinflammatory secretome, and signaling for tumor suppressors (174–178).

Specifically, CAFs have been shown to play an important role in regulating tumor-infiltrating immune cells, both recruiting and promoting their activity (179–181) or inhibiting their antitumor immune responses (182,183).

Moreover, it has also been hypothesized that CAFs can undergo a conversion from cancer-promoting to cancer-restraining or the other way around, depending on the context, as they are very plastic and dynamic cells. Thus, CAFs have a dual role in tumorigenesis and understanding their behavior as well as associating their functions to their marker expression is needed to improve and identify new therapeutic targets (146).

3.2.3.2.3. CAFs in CRLM

In previous sections the phenotypical and functional heterogeneity of CAFs have been highlighted. This heterogeneity may be partially explained by the diverse **origins of CAFs**. Defining the origin of activated myofibroblasts is one of the major challenges in fibrosis-research, as those cells might be potential therapeutic targets against this remodeling process. Several fibroblastic cells have been defined in the human liver (184). In animal models, many more origins of fibroblast have also been identified. Fibrocyte invasion, endogenous resident fibroblasts, pericytes and gli1-positive mesenchymal stem cells would be some examples. In the context of cancer, it is also a recurrent aspect to focus on, especially in desmoplastic kind of tumors. This is the case of pancreatic cancer, where the two major stromal sources are resident pancreatic fibroblasts and stellate cells. In breast cancer, CAFs are thought to derive from pericytes, resident fibroblasts and even from the transformed epithelial cells via EMT. Consequently, the origin of CAFs, as well as the origin of myofibroblasts in fibrosis, varies depending on the disease and the tissue (163,185).

Regarding CRLM CAFs precursor cells, much can be learned from the research carried out on fibrotic liver diseases, which have processes like liver tumoral malignancies. In liver, two potential stromal sources of myofibroblasts or CAFs are described: **portal fibroblasts** (PF), and **hepatic stellate cells** (HSC) (186). However, we cannot exclude other cells that have undergone EMT (hepatocytes, cholangiocytes and endothelial cells), bone-marrow derived cells, consisting of fibrocytes and circulating mesenchymal cells, and fibroblasts surrounding the centrilobular vein, the so-called second-layer cells (187). Nevertheless, the origin of myofibroblasts may be different depending on the liver disease that causes the fibrosis (188).

Among the many cell types that can contribute to liver fibrosis reaction, it is widely assumed that hepatic stellate cells are the major source of them. This fact is demonstrated in studies using genetic fate-mapping technique (189,190), and have been further confirmed in recent scRNA-seq studies in which the majority of liver metastasis-associated CAFs showed abundant expression of HSCs signature (191,192). However, these tracing studies have been performed in mice. The mouse liver is quite similar to the human one but differs in some aspects like the amount of connective tissue (193), which could possibly influence the amount of CAFs arising from other cells present in this tissue. This highlights the need of solid markers to define HSCs and PFs and their respective activated forms, in order to assess the origin of CAFs in human liver metastases or other liver fibrotic diseases.

HSC are in the space of Disse, around the sinusoidal LSEC, and represent 5% to 8% of the cellular population in the liver. In normal conditions, they are characterized for being in a quiescent state and contain lipid droplets with vitamin A (187). Once activated, HSC acquire myofibroblast features such as αSMA expression and extracellular matrix deposition and become the orchestrating cells of the liver injury response (194). *In vitro*, these cells have been reported to undergo myofibroblastic transdifferentiation (195), although cell culture conditions may affect this feature. In hepatic metastases, HSCs release growth factors and metalloproteinases and deposit type I and IV collagens and laminin (137). They are also involved in endothelial cell recruitment and neoangiogenesis (196), as well as in tumor cell invasion and proliferation (137).

Additionally, PF can also be the origin of CAFs. It is believed that it specially happens when cancer cells are located in portal tracts, but it is not clearly demonstrated yet.

It has been observed in experimental models of fibrosis that there is a differential activation of both HSCs, depending on the cause of the fibrotic reaction. For example, HSCs are the main source of myofibroblasts in lesions induced by tetrachloromethane, whereas PFs are the main myofibrobalsts precursor cells in lesions induced through bile duct occlusion (197).

The differences between HSC and PF have been assessed, and some characteristic biomarkers of each cell type have been proposed. In the literature, PF are described to express high levels of CD90, while activated HSC would be negative for this marker (198). On the contrary, cytoglobin, desmin and NGFR, have been described as good markers for HSC, which are not expressed in PF (199). Described markers of PFs and HSCs are summarized in Table 3. Nonetheless, most of these studies describe markers of the non-activated mesenchymal cells and/or are assessed in mice. This leads to controversy around the characteristic markers of HSCs and PFs. Therefore, good markers defining human active HSCs and PFs are still lacking.

PFs	aPFs	HSCs	abscess
CD90 (THY-1) Col15a1 Elastin ENTPD2	CD90 (THY-1) GREM1 FIBULIN2 Col1A1 Elastin NTPD-2 Asporin Mucin-16 αSMA TIMP-1 TGFβ1 Col15a1 MSLN PAI-1 Fibronectin CD73	Desmin Synemin Cytoglobin NGFR (p75) L-rat GFAP PPAR RELN	Desmin Synemin Cytoglobin NGFR (p75) L-rat αSMA Col1A1 PDGF TIMP-1 RELN

***Table 3**. **Specific markers of portal fibroblasts (PFs), activated portal fibroblasts (aPFs), hepatic stellate cells (HSCs) and activated hepatic stellate cells (aHSCs)** according to the bibliography* (200–202)

In CRLM, it seems very plausible that CAFs from different origins coexist. Still, we cannot rule out that the generation of the capsule is due to intrinsic properties of the tumor cell. In any case, these are important aspects that must be considered as they could lead the path for future therapeutic strategies.

Apart from marker expression patterns, CAF subpopulations have also been described in many tissues according to their location inside of the tumor. In the case of CRLM, these lesions can grow following three HGP that can be simplified in two according to prognostic factors, as mentioned in previous sections, but also according to the presence of a fibrotic rim (dHGP) or not (non-dHGP). In this context, three **topographic locations of CAFs** can be distinguished. First, CAFs present in the fibrotic rim of the dHGP, in peritumoral stromal areas. Second, CAFs located at the invasive margin in non-dHGP. As the prognoses differ drastically in metastases that show 100% of dHGP, it may be plausible that peritumoral and intratumoral fibroblasts near to the host–tumor interface are different subsets playing different functions, or that particular juxtracrine and paracrine crosstalk with tumor cells

might induce phenotypic differences with functional consequences. Third, intratumoral CAFs located in central tumoral regions, which would be common for the different HGPs (Figure 5).

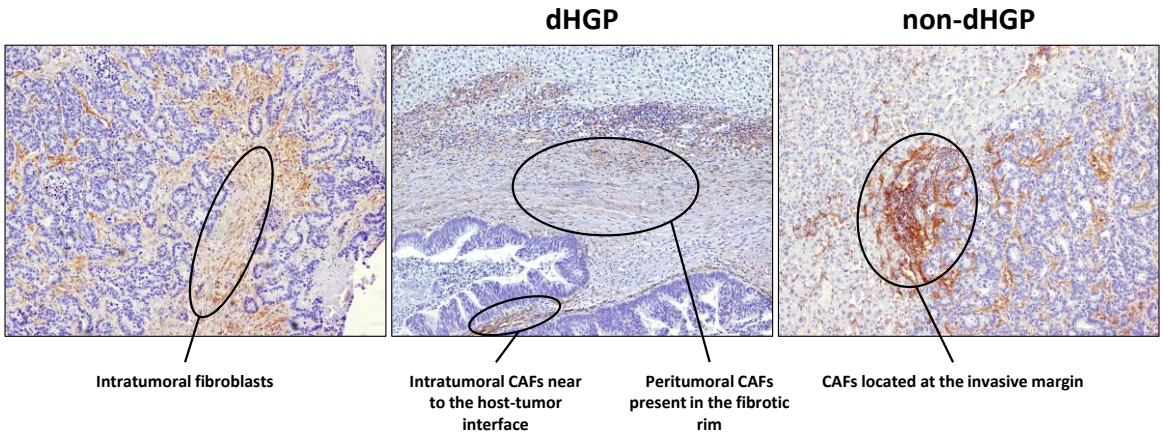

Figure 5. CAFs topographic location*. 10x magnification CD90 IHC images showing the different possible topographic locations of CAFs in CRLM.*

The fibrotic rim of the dHGP is considered by many authors as a response to the inflammation and damage in the host tissue due to the growing tumor. Moreover, the link between the presence of the desmoplastic capsule and a considerable better prognosis makes it possible to hypothesize that these CAFs play a tumor suppressor role, limiting physically and chemically the tumor growth and attracting immune infiltrates to act against malignant cells.

Overall, in the context of HGP, the concept of CAF subpopulations leads to the question of which cell type is the precursor of CRLM CAFs. If there is one precursor cell associated to each HGP or if is it a mixture of the cell types described above and, thus, how they are distributed inside the tumor. Therefore, it is crucial to know in detail the differences between HSC and PF, especially in the context of the activation of both cell types.

3.2.3.3. *Tumor vascularization*

The different HGPs that appear in CRLM have also been associated with different types of tumor vascularization. In fact, another way to classify HGPs only considers two patterns: the angiogenic, which includes desmoplastic and pushing HGPs, and the non-angiogenic pattern that refers to the replacement HGP (62).

In the replacement HGP, the tumoral cells benefit from the hepatic architecture: they progressively "replace" the hepatocyte plates and use the already existing connective tissue and blood vessels. Hence, tumor vascularization is carried out by a non-angiogenic process called vessel "co-option" (58,72,203).

On the other hand, in desmoplastic and pushing HGPs, the tumor completely disturbs the hepatic architecture, creating its own supporting stroma, new blood vessels through an angiogenic process and, in the dHGP, forming the desmoplastic rim that separates the tumor from parenchyma. As an effect of vascular endothelial growth factor (VEGF), these new angiogenic blood vessels are composed by proliferating endothelial cells and form what is called "vascular hot spots". Moreover, as they are not covered by pericytes, VEGF also induces the deposition of fibrin in a perivascular space (72,204).

Some studies have suggested that these different tumor vascularization types can be related to the route that tumoral cells take during the extravasation phase. In this line, a study performed with a murine model found that, if the cancer cells had invaded between LSEC in the space of Disse (205), the metastases with a co-option sinusoidal system developed. On contrary, as showed in the other study, if tumoral cells were injected via the portal route, near the portal tracts, they demonstrated the development of an angiogenic pattern (206). However, at the moment, further investigation is needed to prove this fact.

Overall, the exposed information might explain why the patients with a replacement (presumably non-angiogenic) HGP obtain less clinical benefit from bevacizumab-chemo treatment, which is a VEGF inhibitor, compared to patients with desmoplastic (angiogenic) metastases (62). This concept may explain the failure of anti-angiogenic therapy in breast cancer liver metastases, which predominantly show the replacement HGP (203).

In conclusion, the tumor vascularization strategy used by each HGP is another feature to consider to further understand their biological processes and finally select the best treatment option in each case.

3.2.3.4. *Immune microenvironment*

As mentioned before, liver immunity has evolved to maintain a state of unresponsiveness to the food-derived and microbial antigens. Nevertheless, the liver tolerogenic homeostasis

can be disturbed by an antigenic event like the entry of metastatic cancer cells. Once in the liver, these metastatic cancer cells encounter a cellular landscape composed by resident and recruited cells that will perform both pro and anti-immunogenic responses. Resident cells include LSEC, HSCs and immune cells among which we find Kupffer cells, NK cells and dendritic cells. On the other hand, among the immune recruited cells there are macrophages, myeloid-derived suppressor cells (MDSCs), neutrophils and T cells. These immune cell types can play opposing roles during the process of metastasis depending on their state of polarization, phenotypes, and phase of metastasis (207–211). Moreover, they can be classified as myeloid or lymphoid cells according to their lineage (Figure 6).

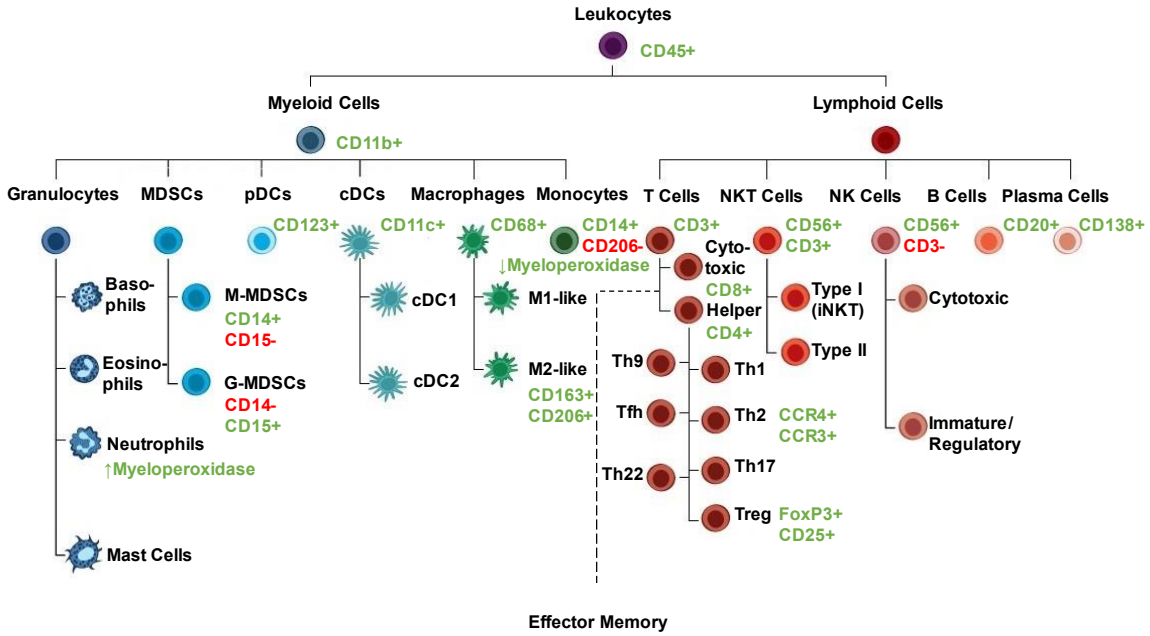

***Figure 6. Human Immune Cell Guide**. Adapted from www.cst-science.com/humanmarkers.*

3.2.3.4.1. Lymphoid immune cells

In the context of a liver metastases, some lymphoid immune cells are to be found in the liver. First, there are the **resident NK cells**. These cells account for 50% of the liver lymphocyte population and usually play anti-tumor function through the release of cytotoxic granules and apoptosis induction mechanism (212). NK cells can also modulate the innate an adaptive immunity through their secretory phenotype and are believed to play a pivotal role in controlling cancer metastasis (213–215). Clinically, NK cell infiltration combined with $CD8^+$ T cells is associated with better prognosis in CRC patients (216). However, it has also

been described that NK cells have a complex crosstalk with CRC liver metastases which can lead to mitochondrial stress and apoptosis of resident NK cells.

NKT cells are also innate-like lymphocytes that can be found in CRC liver metastases. These cells are recruited by LSECs and, similar to NK cells, they also play anti-tumoral functions like modulating tumor killers or the immune response modulation by secreting cytokines (217). But, as in NK cells, anti-tumor hepatic NKT cells can be suppressed by MDSCs in the context of CRLM (218). On the other hand, there are some controversial studies done on melanoma liver metastases claiming that NKT cells could have pro-tumoral effects by inactivating liver NK cells (219).

Concerning **T cells**, the presence of metastatic cancer cells in the liver induces the recruitment and activation of T cell mediated immune responses. These immune responses may impair the metastatic expansion through cytolytic mechanisms mediated by **$CD8^+$ T cells**. However, there are many more mechanisms that contribute to the unresponsiveness of these cells. First, although LSEC can present the antigen to incoming T cells, they also express PDL-1, and this combination leads to immune cell exhaustion. Moreover, LESC also promote the **$CD4^+$ Th2 T cells** phenotype instead of Th1 (220). Th2 differentiated T cells are described to favor tumor growth, both by promoting angiogenesis and by inhibiting cell-mediated immunity and subsequent tumor cell killing (221). On the other hand, **$CD4^+$ Th1 T cells** mediate cellular immune response against the tumor (222–224). Thus, the balance between Th1/Th2 responses is determining the pro or anti tumoral direction of the immune response (225). Other players in this immune landscape are **$CD4^+$ Th17 T cells**, which are pro-inflammatory cells that serve as an effector lymphocyte population and are also involved in recruiting Th1 cells. However, whether these cells promote or inhibit cancer development depends on the phenotype of the tumor (226). Other recruited T cell population are **$CD4^+$ $FoxP3^+$ $CD25^+$ Tregs**, which are immunosuppressive cells that suppress the function of effector T cells. High Tregs infiltration is predicted with poor clinical outcome in CRLM, suggesting that they are supporting the tumor growth of these lesions (227). Finally, γδ T cells can also be present in the liver during CRLM metastases. These cells directly recognize and kill cancer cells via an HLA-antigen presentation independent way. However, not all **γδ T cells** subtypes are effector cells. In fact, among the γδ T cells that infiltrate tumors there is also a regulatory subset with tumor-promoting potential (228).

In the case of **CD20$^+$ B cells**, their role in the context of cancer is not extensively assessed. However, recent studies have shown that intratumoral or peritumoral B cells are associated with better prognoses and response to immunotherapy in different tumor types including CRLM (229,230).

3.2.3.4.2. Myeloid immune cells

An increased number of macrophages can be found among myeloid lineage immune cells of liver metastases, specially when compared to the normal liver (231). Macrophages are cells that can change their phenotype in response to a variety of factors. This process is usually divided in two categories, **M1** and **M2 polarization**. Both are related to inflammatory responses, but while M1 is mainly involved in pro-inflammatory responses, M2 mediates anti-inflammatory ones (232). Thus, M2 polarized macrophages have been associated to tumor induced tolerance resulting in poor clinical prognoses. However, total number of macrophages, without considering their polarization, is already associated with a worse outcome (233).

Macrophages found in CRLM can be liver resident macrophages, termed **Kupffer cells** (KC), but could also be recruited due to the presence of the metastases. Concerning Kupffer cells, it is currently accepted that they originate from yolk-sac erythromyeloid progenitors, which reside in the fetal liver during embryogenesis. But there is experimental evidence supporting that they also emerge from circulating macrophage precursors that latterly migrate to the nascent fetal liver. In any case, in adult liver KC can self-renew in a bone-marrow independent way. KCs are characterized by **CD68$^+$**, **MARCO$^+$**, and **CD5L** surface markers. These cells play opposing roles in metastatic progression. During the initial stages of CRCLM, Kupffer cells exert tumoricidal activity and contribute to metastases control (234–236). On the other hand, they induce the expression of a cell adhesion molecule on LESCs, which helps the dissemination of tumoral cells, and produce factors that promote tumoral invasion, proliferation, and angiogenesis. Moreover, KCs have an enriched expression of genes involved in maintaining immune tolerance and suppressing inflammation, which turns them in a M2-like polarized phenotype. Subsequently, they release inhibitory cytokine IL-10, induce Tregs and express PD-L1 that can induce immune tolerance in front of the tumor, in the context of CRLM (237).

Monocytes and **macrophages** are recruited in the liver by CCL2 tumor cells secretion. Monocytes usually migrate to the metastatic site and there they differentiate into metastases associated macrophages (238). Macrophages generally enhance the growth of liver metastases by involving immune cells, or not. They promote angiogenesis (239), activate HSCs (240) and alter the phenotype of cancer cells (241,242). Moreover, they facilitate metastatic development by inducing liver fibrosis and mediate immunosuppression (243). As macrophages, they are plastic and can be polarized to M1 or M2 although both phenotypes promote liver metastatic growth (244).

Neutrophils are among the first myeloid cells to be recruited to the vicinity of cancer cell just before they exit from vascular channels, as these cells are recruited to sites of inflammation. Neutrophils can have pro-metastatic and anti-metastatic functions, as they also have multiple polarization states. These functional states, like in macrophages, are termed N1 and N2, and are regulated by factors from the tumor microenvironment (130,245,246). **N1 polarized** neutrophils are associated with anti-tumor activity, as they enhance the tumor cytotoxicity and attenuate immune suppression. Meanwhile, **N2 polarized** neutrophils have pro-tumoral functions like promoting tumor migration and metastases (247). The extent of neutrophil polarization in human liver metastases is largely unknown, although a study in breast cancer liver metastases has shown it to be of predominantly N2 type (248). Specifically, in CRLM, the involvement of neutrophils is reported to have mainly pro-tumoral effects and to be associated with worse prognoses (249–251).

Myeloid derived suppressor cells (MDSCs) conform a heterogeneous population of granulocytic (G-MDSCs) and monocytic (M-MDSCs) precursors. MDSCs are recruited from the bone marrow in response to chemokines, released by LESCs, KCs and. There are factors in the tumor microenvironment inhibiting their myeloid cell maturation into neutrophils or macrophages. However, these factors are not fully understood (252). Moreover, there is a lack of specific markers to differ between G-MDSCs and M-MDSCs from tumor associated neutrophiles and macrophages, respectively. Thus, it impairs the full characterization of these populations (253). Nowadays, it is believed that MDSCs promote metastatic growth by mediating immune unresponsiveness: inhibiting NK cells activity and adaptive T cells

response (254–256). However, a detailed understanding of MDSCs contribution to metastatic expansion is still lacking.

Finally, **dendritic cells** (DCs) are known as the classical antigen presenting cells of the lymphatic system. Two subtypes of these cells have been identified: myeloid dendritic cells and plasmacytoid dendritic cells. Dendritic cells have shown to play opposite roles during CRC disease progression. On the one hand, in primary CRC, myeloid DCs stimulate naïve $CD4^+$ T cells to acquire a Th1 phenotype and are then found in increased frequency at the invasive front of the tumor. However, when the disease arrives at advanced stages, CRC tumors have a lower density of these cells (257). On the other hand, DCs can be suppressed by cancer cells and as a consequence they can have an impaired antigen-presenting capacity. These suppressed DCs secrete increased levels of IL-10, hence, acquired an immunosuppressive phenotype. Moreover, they enhance invasiveness through not well-elucidated mechanism and to promote tumor cell migration, cancer cell stemness, and EMT (258–260).

3.2.3.4.3. Spatial context of the immune response

As it has been exposed in previous sections, the immune system plays a crucial role in controlling tumor growth and dissemination. However, the immune microenvironment of CRLM is not yet fully understood. Higher levels of $CD3^+$ T cells, $CD8^+$ T cells and CD45RO lymphocytes, and lower levels of $CD20^+$ B cells have been observed in liver metastases when compared to CRC primary tumors. No difference concerning FoxP3 positive cells was observed. However, these studies analyzed the whole slide average immune cell count, without considering the spatial context of the populations evaluated. Usually, the average infiltration is higher in small metastases while larger ones often have “hot spots” with a high density of lymphocytes. Moreover, although the average lymphocyte density does not differ between cases with different metastatic burdens, the individual lesions in patients with multiple metastases show significant heterogeneity when it comes to immune density (46,261,262). Immune infiltration is not homogenously distributed in liver metastases: in peripheral regions there are higher levels of CD3, CD8, CD45ROeri and CD20 lymphocytes compared to central regions and with distant peritumoral liver parenchyma (248,262). Thus, all these observations lead to the conclusion that the spatial context is an important factor to consider.

What is even more important in the context of our project is that the studies mentioned did not adjust the scoring technique according to the different HGPs observed in CRLMs, as most of the reports never considered them. However, the evaluation of inflammatory infiltrates in the context of HGPs is of crucial importance, since they topographically delimit structures that become physical and chemical barriers to infiltration. The few studies that have investigated peritumoral tissue in HGP context reported that CD4, CD8 and CD45RO were associated with the dHGP (262). Digital image analysis on an independent tissue set confirmed the results for CD8 cells. Moreover, even in individual metastases with a combination of HGPS, a high density of CD8 cells was seen in the area of dHGP while being very low in non-dHGP regions. However, flow cytometry assay demonstrated a relative increase in $CD4^+$ cells in the non-dHGP, which was not due to an increase of Tregs because $CD4^+$ $FoxP3^+$ cells did not show differences (62). Overall, further efforts are needed to fully describe the immune response in desmoplastic and non-desmoplastic HGP.

The spatial patterns of the immune response are not only assessed in the context of CRLM HGPs. In fact, this concept has been developed in recent years. Thus, tumors that show high lymphocyte infiltration are designated "**inflamed**" or "**hot**", while tumors with a low immune cell content are termed "**desert**" or "**cold**" tumors (263). But there is also a third category, which is characterized by high abundance of immune cells that are not able to penetrate cancer cell nests and keep retained in the stroma. This phenotype is called "**immune-excluded**" (**Figure 7**). In this last phenotype, immune cells can be limited to peritumoral stroma or capsule (if present) but may also infiltrate intratumoral stromal bulks (263). This would be defining two types of immune-exclusion that may have qualitative differences regarding the antitumor response.

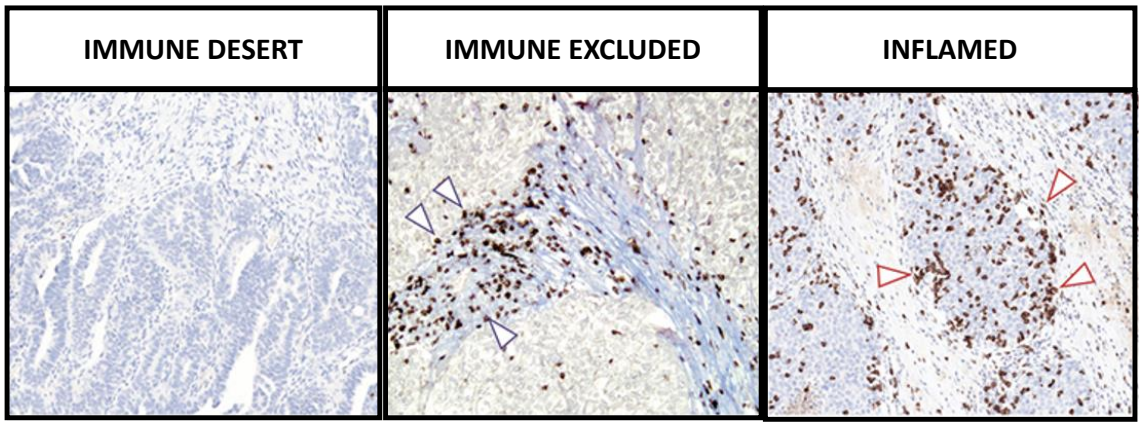

Figure 7. Categories according to the distribution of immune infiltrates*. Adapted from Roche Research Cancer immunotherapy.*

Concerning HGPs, in dHGP the majority of lymphocytes accumulate at the interface between the outer part of the desmoplastic rim and the adjacent liver parenchyma (62). Thus, these immune cells are kept relatively far from malignant tissue and makes dHGP lesions considered as "immune-excluded" tumors by some authors (62,264). In some cases, they have also been considered as "inflamed" tumors, because of the high numbers of immune cell infiltrates (265). In the case of non-dHGP, immune infiltrates are present at lower numbers but directly approach malignant cells. Thus, it highlights the need of further research to completely understand each immune response and properly classify these HGPs.

3.2.4. HGP from CRLM formation hypothesis

Why a liver metastasis develops a desmoplastic rim in one patient while in other patient it evolves in a replacement pattern-type? The answer to this question relies on the biological mechanisms that underlie the different growth patterns, which remain elusive. However, there are plausible hypothesis that try to explain these distinct HGP phenotypes. These hypotheses, which are set out below, are derived from histopathological insights, preclinical animal models and the comparison of the embryonic development.

The "**site of implantation**" hypothesis affirms that the site of cancer cell implantation in the liver determines the HGP. This theory is supported by liver metastases observations in animal models. In these models, cancer cells are introduced either via arterial route or portal route. When cells are implanted through arterial route, they give rise to a significantly higher proportion of desmoplastic metastases, which originate from portal tracts. On the other

hand, when cancer cells are introduced via the vena portae, the metastases usually arise in a replacement-type (205,207).

Moreover, in line with the previous hypothesis but with minor differences, there is a concept proposed by Fernando Vidal-Vanaclocha (207) that distinguishes at least three different "**entry points**" for cancer cells and thus three different metastatic niches which shape up the tumor–host interaction and drive the evolution of the tumor: periportal, perisinusoidal and intrasinusoidal. According to this concept, cancer cells which enter periportal and perisinusoidal spaces develop according to the "classical" process, following four phases, as described below. During the intra-lobular and pan-lobular phases, malignant cells invade parenchymal cell plates (perisinusoidal location) or the portal space (periportal location) and develop a pushing–desmoplastic phenotype, while intrasinusoidal metastases start proliferating in the intravascular space, avoiding the extravasation phase. These metastases develop in a very distinct microenvironment, surrounded by liver sinusoidal endothelial cells (LSEC) and elements of the blood, which require different surviving mechanisms. During further growth, intrasinusoidal micrometastasis disrupts the sinusoid and develops a replacement HGP. However, these processes have not been experimentally demonstrated so far.

In addition, the activation of HSCs or PFs can also be affected by the route of entrance of tumor cells. On the one hand, if tumoral cells extravasate in a portal tract, they would first interact with PF and those would mediate the stromal reaction. On the other hand, if they reach hepatic sinusoids, they will be able to activate HSC and the process of fibrosis. Therefore, this leads us to speculate that each HGP contains CAFs coming from distinct origins (95).

The "**revertant *in situ* growth**" hypothesis says that the replacement HGP is a reversion to the *in-situ* growth of cancer cells, which refers to the growing within the boundaries of a basement membrane. In brief, in a replacement growth pattern, cancer cells take the place of hepatocytes as well as of cholangiocytes from ductular structures. In this kind of growth, tumoral cells replace the cells of the host organ while keeping its structure and co-opting its vasculature (266).

The hypothesis of "**coagulation and inflammation**" is focused on the presence (desmoplastic) or absence (replacement) of coagulation and inflammation, which determines the HGP. Angiogenesis, coagulation, inflammation, and fibrosis are processes that take place during wound healing. This hypothesis suggests that these processes are also driving the desmoplastic growth pattern. Thus, when cancer cells avoid the activation of any of these processes, liver metastases grow following a replacement pattern. This is supported by the lack of angiogenesis, coagulation, fibrosis, and poor immune infiltration that characterize the replacement HGP.

The "**response to liver injury**" hypothesis propose that HGPs reflect the response of the liver after an injury, as it can mediate a fibrotic response, that would correspond to the dHGP, or a liver regeneration response, that would give rise to the replacement HGP. In the dHGP there is a desmoplastic rim containing portal-type stroma and proliferating bile ducts, which resembles the fibrotic response. In the replacement HGP, cancer cells adopt the morphologically of the replacing parenchymal hepatocytes that appear in the regeneration process mediated by progenitor cells, while preserving vascular architecture (267–269).

The "**transcriptional reprogramming**" theory postulates that HGPs are the result of transcriptional reprogramming that would be determined in the HGP-specific epigenetic landscape. CRC cells lose colon-specific genes and start expressing liver-specific ones when growing in a hepatic metastasis. In the replacement HGP, tumoral tissue mimics liver tissue at histological level, which supports this hypothesis. On the other hand, the dHGP histologically resemble the primary colorectal tumor.

The "**cancer cell motility**" hypothesis propose that the feature that determines HGPs is the cancer cell's ability to move and migrate. This theory is supported by a study in which a necessary gene for cell motility is knocked down in an animal model of liver metastasis. In consequence, a switch from a replacement to a desmoplastic pattern is observed (203,270).

The "**angiotropic extravascular migration and pericyte mimicry**" hypothesizes that the replacement HGP relies on this process as they would share embryogenesis programs (271).

Finally, the hypothesis of "**replacement is the default**" claims that the original pattern is always replacement and that the desmoplastic HGP originates from it. It is based on the remnants of co-opted portal triads that are found in the center of liver metastases,

independently of the HGP. This suggests that the dHGP comes from replacement-type metastases in a second step, as co-option of portal triads is not observed at the liver-tumor interface in dHGP. Moreover, cancer cells replace normal epithelial cells also within a bile duct, which is called ductular reaction and supports the idea of cancer cells having a natural tendency to mimic normal cells. Results from Fernández Moro C. *et al*. are in line with these hypotheses (272). In this study, high resolution scoring reveals that the prognostic outcome of patients is dependent on growth pattern proportions, being increased fractions of desmoplastic pattern associated with improved survival. Moreover, they observed a connection between tumor viability and fibrotic encapsulation, suggesting it to be a **response of the host organ**. They describe that the fibrotic rim is heterogeneous and represent a zonal evolution of distinct histological features that starts at the liver-rim interface and extends to the rim-tumor border. The outer region (perihepatic) is conformed by fibrosis that resembles the one from portal stroma. Moreover, it contains well-preserved liver parenchymal remnants conformed by hepatic artery branches and biliary ducts. On the other hand, the inner part of the rim, which is adjacent to the tumor, has lost these parenchymal remnants and is progressively adopting a more intra-metastatic stromal expression profile. Furthermore, portal tracts observed in the center of desmoplastic metastases reveals previous spread into hepatocyte compartments, which implies a process of incorporation or co-option of the portal tract architecture. Thus, it supports the idea that the desmoplastic rim firstly develops without the influence of tumor cells in a liver fibrotic mechanism, and the replacement pattern is the default HGP and represents the situation where the “tumor wins” in front of a host response. Thus, the desmoplastic growth pattern would appear later, when tumor cells fail in their replacement-type growth, as a response of this failure combined with the already active liver injury response (273).

These hypotheses are not exclusive with each other and elements from every one of them contribute to the specific growth patterns of CRLM.

3.2.5. CRLM clinical opportunities

CRLM have the particularity of recruiting a large number of cells with an immune suppressive capacity. This mediates resistance to a multitude of antitumor drugs (274). However, the particular pathological and histological characteristics HGPs are aspects that could be

exploited clinically. We have already commented that HGPs have prognostic and predictive value. Thus, knowing the HGP prior to surgery could contribute to the better selection of patients for the treatment form which they could benefit the most. For example, knowing the HGP at the pre-operative stage could improve patient selection for neoadjuvant treatment, minimizing the toxicity effects and surgery-related risks. This could be approached by the use of modern medical imaging techniques or radiomics (275–277). Thus, in a retrospective study, Cheng *et al.* managed to predict the HGP with remarkable accuracy using contrast phase imaging (278).

Another important feature of CRLMs is the type of vascularization that the tumor develops. As previously described, two vascularization strategies, vessel co-option (non-dHGP) and angiogenesis (dHGP), can be clearly distinguished. In this regard, patients with the dHGP would be candidates for receiving anti-angiogenic drugs in neoadjuvant settings. Thus, non-invasive imaging for the classification of the HGPs would be especially useful in such therapeutic approach.

Another aspect to consider is that, without taking into account HGP, it is widely described that CRLMs are characterized by some degree of immune suppression. Anti-angiogenic and anti-fibrotic therapies could be interesting strategies to re-stablish the anti-tumoral immunity and, thus, could be direct immunotherapeutic targets. However, these strategies can be counterproductive and have been reports of opposite observations. Thus, a detailed knowledge of the mechanisms of immune suppression in each HGP is needed to properly apply these strategies. Moreover, immunotherapy has shown to be ineffective in most of the patients (279–281), in exception of patients with MSI (282,283), probably because of the described immune suppression. However, these studies do not segregate the patients according to their HGP, which could be masking the effect of these therapies in the dHGP or non-dHGP subset of patients.

The counterproductive results obtained using the deletion of mesenchymal cells highlights the importance of studying the different CAF subsets. This fact is especially relevant in the context of HGPs and considering different potential precursors of CAFs in the liver. It could be hypothesized that the fibroblasts that form the capsule are different from those that are located in the central regions of the tumor. For example, fibroblasts that form the fibrotic

rim may exert a protective role by enveloping the tumor and hindering the invasion into the liver tissue. As mentioned above, the capsule in the dHGP may have certain similarities to the peritumoral host reaction against benign tumors or abscesses. On the other hand, intratumoral CAFs are found in large numbers in both d-HGP and non-dHGP and would probably have different functions to the ones found in the non-dHGP invasive front. Thus, once a detailed description of CRLM CAF subsets and their functions would be stablished, reprogramming CRLM pro-tumoral fibroblasts into anti-tumoral ones could be a feasible strategy.

In conclusion, a detailed understanding of TME from each HGP of CRLM, as well as an effective method to assess HGPs prior to surgery, could make a difference in the development of therapeutic strategies available for affected patients.

PREMISES AND HYPOTHESIS

PREMISES

- **Colorectal cancer liver metastases** (CRLM) diagnosed patient's treatment with curative aim is surgical removal. However, most studies reported a 10-year survival of 25% after resection. This fact, together with the high incidence of this disease, makes it a **health problem** in which many research efforts need to be employed.
- Many different factors, like node-positive primary colorectal cancer (CRC), right-sided CRC, multiple metastasis or CRLM large inside, have been studied to predict survival in the affected patients. Among those factors, a particular histopathological feature these resected lesions show has stand up in the last years as reliable prognostic factor: the **histological growth patterns** (HGP).
- These HGPs, which are largely explained in introduction sections, can be classified in two types depending on the features of the tumor-liver interface: the **desmoplastic (dHGP)** and the **non-desmoplastic subtype (non-dHGP)**. dHGP is characterized by showing a peripheral fibrotic rim in between tumoral glands and liver parenchyma, and by having a vascular strategy based on angiogenesis. Meanwhile, non-dHGP uses the already stablished sinusoids from liver parenchyma and does not show any rim between hepatocytes and tumoral cells.
- Since CRLM HGPs were firstly described, numerous studies have highlighted the utility of these HGP as **prognostic and predictive tool**, as they had observed that patients who presented a desmoplastic growth pattern had longer overall survival and disease-free survival after resection when compared with the non-desmoplastic ones.
- No molecular or histopathological characteristics of primary CRC tumor are associated with the appearance of desmoplastic or non-desmoplastic HGP. Moreover, the level of **desmoplasia** in these lesions is elevated, as it happens in CRC primary tumors. All this together highlights the importance of metastatic microenvironment in disease progression.

HYPOTHESIS

Considering all these premises, the hypothesis of this thesis is that **the tumor microenvironment of CRLM explain the differences observed in prognosis between desmoplastic (dHGP) and non-desmoplastic (non-dHGP) histological growth patterns.**

OBJECTIVES

To prove the previously exposed hypothesis, we defined the following **objectives**:

1. To quantify and characterize the spatial distribution of the different **T cell populations** present in dHGP and non-dHGP and their association with prognoses.
2. To quantify and characterize the spatial distribution the **tumor associated macrophages** (TAMs) present in each HGP and elucidate the role they are playing as well as to associate them with survival data from patients.
3. To describe and identify any **other immune infiltrates** populations that could be playing an important role in HGPs different biology.
4. To quantify and characterize the spatial distribution the different **CAFs subpopulations** that conform each HGP, and:
   - **a)** To characterize the contribution of **HSCs** and **PFs** to the global pool of CAFs in each HGP.
   - **b)** To assess their **functions**, pro-tumoral or anti-tumoral, including the relationship they could have with the studied immune infiltrates.
   - **c)** To assess their possible role in **predicting patient survival**.

MATERIALS AND METHODS

1. CELL CULTURE

1.1. Cell lines and culture conditions

In this project, we used three commercial hepatic stellate cells (HSCs) lines, primary portal (PF) fibroblasts from distal liver CRLM patients, primary CAFs lines, and four tumor cell lines of metastatic colorectal cancer.

1.1.1. Primary fibroblasts and CAFs isolation

PF and CAFs have a common process of isolation. These cells are isolated in our laboratory from biopsies of CRLM patients from *Hospital Universitari de Bellvitge*. Tumor samples were handled in sterile conditions under a laminar airflow cabinet.

The tumor sample was diced with a sterile scalpel in a petri dish with phosphate-buffered saline 1X (PBS, Gibco™ 14190-169). The small pieces of tissue were transferred to a gentleMACS™ C tube (Miltenyi Biotec) containing 2 mL of collagenase type IV (1 mg/mL) and 2 mL of dispase (1U/mL), both from STEMCELL™ Technologies. Then, the C tube was placed in the gentleMACS™ dissociator where three different predefined programs were run, followed by an incubation of 1 hour (h) at 37 °C in the rotator to dissociate the sample into very small pieces of tumor. In the middle of the incubation, the C tube was placed again in the dissociator and brought back to the incubator to continue at 37 °C for the remaining 30 minutes (min). This step was repeated at the end of the incubation. To stop the action of the enzymes contained in the C tube, we diluted them with PBS 5% fetal bovine serum (FBS, Gibco™ 10099-141). After that, the suspension was centrifuged at 350 rcf for 5 min. Then, we collected both the supernatant and the pellet separately, to keep the greatest number of cells present in the tube. After being strained through a 70 µm filter (Corning 352350), the pellet was seeded in a p60 plate, previously coated with Gibco Collagen I rat tail (Gibco™ A1048301). Meanwhile, the C tube supernatant was centrifuged at 1000 rpm and the pellet was also seeded in a coated plate. Plates were kept for 7-15 days at 37 °C in humidified air with 5% CO_2 content, to let cells attach and grow. Once the plates were at 70-90% of confluence, the following steps were performed to separate the fibroblasts from other cell types that could have grown in between them. The strategy used to separate the cell types was based on the expression of CD326. CD326, also known as an epithelial cell adhesion

molecule (EpCAM) is expressed on cells of epithelial origin, epithelium-derived tumor cells, circulating tumor cells, and cancer stem cells. First, we added 100 µL of CD326 (EpCAM) MicroBeads per 5×10^7 total cells, mixed well with the rotator and incubate for 30 min in the refrigerator (2–8 °C). Secondly, we washed the suspension with buffer B (PBS 1X, 0.1% BSA, 0.6% sodium citrate), placed the tubes into the magnet rack and waited for 2-5 min. After that time, EpCAM-positive cells were attracted by the magnet and EpCAM-negative cells remained on the supernatant. We collected the supernatant in a 15 mL tube and repeated this final step once more. Finally, the suspension on a 15 mL tube was centrifuged at 700 rcf for 5 min, aspirated the supernatant completely and resuspended in culture medium and seeded in a petri dish plate. Although EpCAM-negative cells include fibroblasts, endothelial cells and immune cells, the most favored growth population in cell culture is fibroblasts. However, a step of characterization through protein analysis was performed following the isolation, to dismiss the possibility of other cell types growing with fibroblasts.

1.1.2. Culture of mesenchymal cells

The culture medium used for PFs, HSCs and CAFs was Dulbecco's Modified Eagle Medium F-12 with GlutaMAX™ (DMEM/F-12-GlutaMAX™, Gibco™ 10565018) supplemented with 10% heat-induced activated FBS, 1% penicillin/streptomycin (P/S, Gibco™), and 1M HEPES (Sigma-Aldrich). Confluent cells (90-100%) were split 1:2 or 1:3 once a week until passage number. Cells were maintained at 37 °C and 5% CO_2 atmosphere.

1.1.3. Culture of tumoral cells

As tumor cell lines, we used LoVo, SW620 and T84 metastatic colorectal cancer cells from the ATCC (American Type Culture Collection); and SNU-503 from the Seoul National University cell line collection. Cells were maintained with DMEM/F-12-GlutaMAX™ + 10% heat-induced activated FBS, 1% P/S, and 1M HEPES. Confluent cells (90-100%) were split 1:2 or 1:3 once a week until passage number. Cells were kept at 37 °C and 5% CO_2 atmosphere. Sub-confluent cells (70-80%) were split 1:10 twice a week until passage number 30-40.

1.1.4. Co-culture of tumoral cells and mesenchymal cells

Direct co-culture

To evaluate the effect of paracrine communication as well as the effect of cell-to-cell contact between different cell types, the corresponding cell types were grown in the same culture dish. The proportion of mesenchymal cells and tumor cells was decided considering the doubling time of tumoral cells, to maintain the proportions as the assay took several days. Thus, the mesenchymal/tumoral cells seeding proportion was 1:1 for SNU-503 cells and 2:2 for LoVo cells. Co-cultured cells were maintained with DMEM/F-12-GlutaMAX™ supplemented with 2% FBS at 37 °C and 5% CO_2 atmosphere for 120 hours.

Indirect co-culture

The purpose of indirect co-culture was to assess the effect of soluble factors of the culture media in cell-to-cell communication between different cell types. For performing it, special inserts (Transwell®) are needed. Transwell® Permeable Supports (Corning®) are inserts with a polycarbonate permeable membrane that are placed in the well and allow for cell growth in both, the top part (membrane) and the bottom (well). Transwell® systems are available for different plate formats and with different membrane pore sizes, we used the 3 µm pore size which allows soluble factors to pass through the membrane.

1.2. Mycoplasma test

All cell lines were routinely tested for mycoplasma contamination by PCR using the following oligonucleotides:

Oligonucleotide	Sequence
MICO-1	5'- GGCGAATGGGTGAGTAACACG - 3'
MICO-2	5'- CGGATAACGCTTGCGACTATG - 3'

Table 4. Oligonucleotides used for the detection of mycoplasma contamination.

To perform the test, we seeded the cells in over-confluence in culture media without antibiotics. 48 h later the media were collected and diluted 1/100 to perform the analysis.

1.3. Cell counting

Cell counting was done manually using the trypan blue solution (Sigma-Aldrich) to distinguish viable cells, which do not absorb trypan blue, from non-viable cells. Firstly,

adherent cells were washed with PBS 1X and detached by incubating them for 5 min at 37 °C with pre-warmed 0.25% trypsin-EDTA (ethylenediaminetetraacetic acid), phenol red (Gibco™). Secondly, trypsin was inactivated adding fresh complete culture medium. The cell suspension was then centrifuged for 5 min at 1000 rpm and re-suspended again in fresh complete medium. Finally, to proceed with cell counting, 20 to 50 µL of cell suspension were diluted 1:1 with trypan blue solution and 10 µL of the mix was loaded on the loading groove in the Neubauer chamber. The number of cells from four squares/cell type were counted and cell concentration was calculated according to the following formula:

$$\text{Concentration}\left(\frac{\text{cells}}{\text{mL}}\right) = \frac{\text{viable cells per quadrant}}{\text{number of quadrants}} \times \frac{10^4}{\text{dilution factor}}$$

1.4. Cell cryopreservation and thawing

After trypsinization and centrifugation processes, cells were re-suspended in cold freezing medium (FBS with 10% DMSO (dimethyl sulfoxide, Sigma-Aldrich)) in a 1:3 dilution of a p100 plate of tumoral cells or a p100 plate of CAFs. The cell suspension was distributed in cryotubes (1 mL/tube) and cryotubes were placed in a Mr. Frosty™ freezing container (-1 °C/min ThermoScientific) filled with 100% isopropyl alcohol. For freezing, Mr. Frosty™ was stored at -80 °C for at least 24 h. Lastly, for long-term storage cryotubes were stored in a liquid nitrogen tank.

For cell thawing, cryotubes were warmed in the water bath at 37 °C and were diluted in a pre-warmed culture medium. Then, the cell suspension was centrifuged at 1000 rpm for 5 min and the cell pellet was re-suspended in fresh complete medium. Finally, they were grown into a p100 plate at 37 °C in humidified air with 5% CO_2 content.

1.5. Conditioned media harvesting

Conditioned medium (CM) is medium harvested from cultured cells under specific culture conditions. It contains metabolites, growth factors, and extracellular matrix proteins secreted into the medium by the cultured cells. To obtain the CMs used in this project, p100 plates containing cells at 80-90% of confluence were washed with PBS 1X and filled with 12

mL of media without FBS. After 48 h, the media was collected, filtered in a 22 µm filter (MillexR - GS), and stored at -80 °C until use.

2. MOLECULAR ANALYSIS

2.1. Cytometry assays

2.1.1. Fluorescence-activated cell sorting (FACS)

When performing direct co-cultures, FACS was the tool used to separate the different cell types to use them for further purposes, like culture after separation or RNA and protein extraction for posterior molecular analysis. To discriminate mesenchymal cells from tumor cells, we stained the mesenchymal population with Cell Trace™ CFSE (Carboxyfluorescein succinimidyl ester) from Invitrogen™ (Cat.no. C34554) before seeding the cells in the co-culture plate. Cell Trace™ staining was performed following the manufacturer's instructions at 2 µM concentration. On cell sorting day, seeded cells were trypsinized, centrifuged and resuspended with 500 µL of FACS buffer (PBS supplemented with 5% FBS and 1:1000 DNase 1 from BioLabs). Finally, 2 µL of 1 mg/mL propidium iodide (PI) was used to discard between live and dead cells. PI is a membrane impermeant dye, its staining method is based on a dye exclusion test which lies in the concept that viable cells do not absorb PI.

Beckman Coulter's MoFlo XDP was used to perform the cell sorting. First, we got PI negative viable cells and then, with CFSE staining we separated 2 populations of cells. On one hand mesenchymal cells as a CFSE positive population and the other the tumoral cells as a negative population. Obtained cell pellets were processed depending on the final purpose.

2.1.2. Fluorescence flow cytometry (FFC)

FCC is a technique used to detect and measure physical and chemical characteristics of a cell population. FFC was performed on a Gallios™ cytometer (Beckman Coulter), and data were processed with Kaluza Analysis version 2.1 software (Beckman Coulter). Propidium iodide was used to discard between live and dead. Staining and washes were performed using FFC buffer: PBS supplemented with 5% FBS. We used FFC to process different experiments. The

specific conditions and biological markers used are described in detail in each experiment, in following sections.

2.2. RNA analysis

2.2.1. RNA isolation and quantification

Cell pellets from cell sorting or from other cell culture assays were frozen at -80 °C until RNA extraction. RNA was isolated using the RNeasy Micro Kit (Qiagen) following the manufacturer's instructions. Obtained RNA was quantified in the spectrophotometer Nanodrop TM1000 (ThermoScientific). To avoid genomic DNA (gDNA) contamination, an additional DNase 1 treatment was performed by using the DNase I (RNase-free) from BioLabs, according to manufacturer's instructions.

When samples were for RNA sequencing, they were sent to CNAG (Centre Nacional d'Anàlisi Genòmica, Barcelona – Spain) to perform the process. If RNA samples were used to analyzed transcriptomic differences by qPCR, the RNA is retrotranscribed to cDNA as explained in the following section.

2.2.2. cDNA obtention from RNA

First-strand cDNA (complementary DNA) was obtained with SuperScript™ IV VILO™ Master Mix (Invitrogen™) reaction following the manufacturer's instructions. Briefly, a mix composed of 100-500 ng from each sample of RNA template, 4 µL of SuperScript™ IV VILO™ Master Mix and nuclease-free water until reach 20 µL was placed into a microcentrifuge tube. Then, this mix was placed in the thermocycler and the reverse transcription reaction took place with the following conditions: 10 min at 25 °C, 10 min at 50 °C, and 5 min at 85 °. Obtained cDNA was stored at -20 °C until use.

2.2.3. Real-Time quantitative PCR

RNA expression levels were detected by quantitative PCR (qPCR) using PowerUp™ SYBR Green Master Mix (Applied Biosystems). 1 µL of cDNA obtained from different cells were loaded onto 384-well plate mixed with 5 µL of PowerUp™ SYBR Green Master Mix, 0.2 µL of the probe of interest (Table 5) and ddH20 to a final volume of 10 µL. The plate was read at

the LightCyclerR 480 Instrument II (Roche). Results were visualized and analyzed using LightCyclerR 480 Software 1.5 (Roche).

Gene	**Forward (5'→3')**	**Reverse (5'→3')**
ACTG2	CCCCATTGAACACGGCATCA	ACATGATCTGGGTCATCTTTTCC
ACTA2	CATCACCAACTGGGACGACA	CAATGAGCTTCGTGTTGCCC
COL1A1	AGCCAGCAGATCGAGAACAT	TCTTGTCCTTGGGGTTCTTG
CYGB	TCAGCCAGTTCAAGCACATG	GTCACTGGCAAATTCCTCGG
DES	CAGTCCTACACCTGCGAGAT	CCATCTTCACGTTGAGCAGG
ELN	GGAGTTGGTGGCTTAGGAGT	TTAACTCCTGCTCCAGTGGG
F2R	CATTTGCTTCGGACCCACAA	TGCTGGGATCGGAACTTTCT
FBLN1	CAACACAGTGGGGTCTTTCC	ACGGGGCACTGATACTCAAA
GREM1	CATGTGACGGAGCGCAAATA	GTTCAGGGCAGTTGAGTGTG
HGF	TGGTAAAGGACGCAGCTACA	GCGTACCTCTGGATTGCTTG
IL18R1	CGCCGAGTTTGAAGATCAGG	TCAGCAAAGCAGAGCAGTTG
MFAP5	ATGTGACTCAAGCGACTCCA	CGGAAGTAATTGGAGCGACG
MME	AAGCTCCGAGAAAAGGTGGA	GCCATTGTGATCGAAGCCAT
NGFR	ACAAGACCTCATAGCCAGCA	TCCTTGCTTGTTCTGCTTGC
PDGFRA	ATGGATTAAGCCGGTCCCAA	TAAATGGGGCCTGACTTGGT
PDGFRB	AGACTGTTGGGCGAAGGTTA	CGGCAGTATAGAGGACGGAG
PDLIM3	TTCAGAGTGCTCCAGGGAAT	TCAGGGTGCCGGTACTTATC
PDPN	AACCAGCGAAGACCGCTATAA	CGAATGCCTGTTACACTGTTGA
PPARG	AGCCTGCGAAAGCCTTTTGGTG	GGCTTCACATTCAGCAAACCTGG
SERPINE1	AGAACCTCAAGAGTGCCTCC	GAGCTTCCCTTTCATCTGCG
SULF1	ACGGATACAGCAGGAACGAA	GCAGTTCTCGTTGTTGGTGT
THY1	ATCGCTCTCCTGCTAACAGTC	CTCGTACTGGATGGGTGAACT
ACTB	CCCCATTGAACACGGCATCA	ACATGATCTGGGTCATCTTTTCC

Table 5. List of genes and the sequences of the corresponding primers used in qPCR assays.

A standard curve was performed for each of the genes listed above. The differences between genes were assessed comparing the software extrapolated concentration in samples of interest, and normalized against the value of *ACTB*, used as housekeeping gene.

2.2.4. RNA sequencing of cultured mesenchymal cells and tumor cells

Stranded mRNA sequencing (RNA-seq; 50M PE reads, Ilumina® HiSeq 3000 system) was performed to detect differentially expressed genes (DEG) between experimental groups. Analyzed samples consisted of RNA coming from the pellet of co-cultured and mono-cultured cells of the experiment resumed in Figure 37, and from sorted $CD90^{hi}$ and $CD90^{lo}$ CAF subsets.

Poly-A pull-down was used to enrich for mRNAs from total RNA samples (0.2-1 µg per sample, RIN>8) and proceeded to library preparation using Illumina TruSeq RNA Prep Kit. Then, libraries were sequenced using Illumina® HiSeq3000 at the CNAG.

2.3. Protein analysis: Western Blot (WB)

Mesenchymal cells were seeded in different culture dishes in complete culture media. Once they reach a final confluence of 90%, plates were washed with PBS 1X and stored at -20 °C.

2.3.1. Protein lysate from cell culture

For western blotting of cellular lysates, mesenchymal cells were scrapped with RIPA protein lysis buffer (50 mM Tris-HCl pH 7.5, 150 mM NaCl, 1% NP-40, 0.10% SDS and 0.5% sodium deoxycholate) supplemented with complete EDTA-free Protease Inhibitor Cocktail Tablets (Roche), orthovanadate, PMSF, β-glycerol, aprotinin and leupeptin. Lysates were cleared by centrifugation at 12.000 rpm for 20 min. Protein lysates were stored at -80 °C until use.

2.3.2. Quantification of protein extract

Protein concentration was determined using colorimetric kit Pierce™ BCA Protein Assay (ThermoScientific, 23225) using a 96-round well plate. To perform a standard curve, decreased volumes of a standard of bovine serum albumin (BSA, 2 mg/µL) ranging from 0 to 2 mg/µL were loaded in duplicate. To quantify samples, 2 µL of samples of interest were loaded in triplicate. Then, BCA Working Reagent (50:1, Reagent A:B) was loaded onto wells to a final volume of 200 µL. The plate was incubated at 37 °C for 30 min and then the absorbance was measured at 560 nm wavelength by spectrophotometry (Victor™ X5,

PerkinElmer) using the PerkinElmer 2030 Workstation software. Finally, protein concentration was calculated by extrapolation in the BSA standard curve.

Once quantified, each lysate was boiled in sample buffer (2x Laemmli sample buffer from Bio-Rad Laboratories + 5% β-mercaptoethanol) at a final concentration of 1:1 for 5min at 95 °C to denature the proteins. Ready to use lysates were stored at -20 °C until use.

2.3.3. Electrophoresis, blotting, and detection

Ready to use protein lysates were loaded onto sodium dodecyl sulfatepolyacrylamide (SDS-PAGE) electrophoresis gels. These gels were composed of two fractions: the staking (up) and the resolving (down).

Gels were prepared with a mixture of dH_2O, 30% acrylamide-bis (Bio-Rad), Tris-HCl with 0.4% SDS, ammonium persulfate (APS) and TEMED (ApliChem). The volumes of each reagent depend on the acrylamide content of the gel. The staking fraction was always prepared with Tris-HCl 1.5 mM, pH 8.8 and at 4% acrylamide content. While the resolving fraction was made with Tris-HCl 0.5mM, pH 6.8 and the acrylamide concentration could range from 8 to 15% depending on the molecular weight of proteins of interest, this fraction separated the proteins by their molecular size. Usually, 30 µg of protein were loaded into the wells and a molecular weight marker (BenchMark™ pre-stained protein ladder, ThermoScientific) was used.

The gel was placed into the running buffer (25 mM Tris, 192 mM glycine, 0.1% SDS) and the separation of proteins was carried out at a constant voltage of 120V for 90 min at room temperature (RT).

For the blotting process, wet transfer was carried out. Proteins were transferred to 0.45 µm pore-size polyvinylidene fluoride (PVDF) membranes (Immobilon-P, Merck Millipore). The membranes were previously quickly activated in pure methanol and washed with dH_2O. The acrylamide gel together with the PVDF membrane, filter papers (Whatman® paper) and pads were assembled in a "transfer sandwich" as follows: pad – filter paper – acrylamide gel – PVDF membrane – filter paper – pad. Finally, this "transfer sandwich" was placed into the transfer tank full of transfer buffer (25 mM Tris, 192 mM glycine, 20% Methanol) and an 80V

constant voltage was applied for 120 min at 4 °C. In case of proteins smaller than 20kDa of molecular weight, transfer conditions were 40V of constant voltage for 30 min at 4 °C.

Once the transfer process finished and before primary antibody incubation, membranes must be blocked to prevent unspecific primary antibody unions. Membrane blocking was made in 5% nonfat milk in TBS-T (Tris-buffered saline + 0.1% Tween in TBS 1X) for 1 h at RT. After blocking, membranes were washed once with TBS-T, and incubated overnight (ON) at 4 °C with the corresponding dilution of primary antibodies in 1% nonfat milk in TBS-T listed on Table 6.

Primary antibody	Reference	Manufacturer	Clone	Host	Dilution
PDGFRβ	#3169	Cell Signaling	28E1	R	1:1000
CD31	ab28364	Abcam	polyclonal	R	1:500
FAPα	sc-100528	Santa Cruz	SS-13	M	1:100
CALD1	HPA008066	Atlas Antibodies	polyclonal	R	1:250
α-SMA	A2547	Sigma	1A4	M	1:1000
PDPN	HPA007534	Sigma	polyclonal	R	1:250
PDLIM3	HPA004749	Sigma	polyclonal	R	1:1000
β-ACT	A5441	Sigma	AC-15	M	1:1000

Table 6. List of secondary antibodies used in WB. *R, rabbit. M, mouse.*

The following day, after washing the membranes three times with TBS-T for 10 min, a secondary antibody incubation was performed using ECL horseradish peroxidase linked secondary mouse/rabbit antibody (Table 7) diluted in 1% nonfat milk in TBS-T for 1 h at RT.

Secondary antibody	Reference	Manufacturer	Dilution
Mouse	sc-516102	Santa Cruz Biotechnologies	1:2000
Rabbit	sc-2357	Santa Cruz Biotechnologies	1:2000

Table 7. List of secondary antibodies used in WB.

Finally, after washing the membranes three times with TBS-T for 10 min, blots of proteins were detected by ECL homemade chemiluminescent substrate (solution A: 1M Tris pH 8.5, 250 mM luminol, 90 mM coumaric acid; solution B: 1M Tris pH 8.5, hydrogen peroxidase) at 1:1 proportion with the ChemiDoc™ Touch imaging system (Bio-Rad Laboratories). All

measurements were performed without saturation and were normalized to β-actine (Sigma-Aldrich, A5441, mouse mAb) loading control. Band densiometric analyses were performed with Image Lab 6.0 software (Bio-Rad Laboratories).

3. *IN SILICO* ANALYSIS

3.1. Transcriptomic analysis: DEG

RNAseq was performed to detect mRNA expression differences between groups. In the case of co-culture experiment, those groups were monocultured HSCs, monocultured PFs, co-cultured HSCs with SNU-503 and with LoVo, co-cultured PFs with SNU-503 and with LoVo, monocultured SNU-503, monocultured LoVo, co-cultured SNU-503 with PFs and with HSCs, and co-cultured LoVo with PFs and with HSCs. We also performed RNAseq comparing $CD90^{hi}$ and $CD90^{lo}$ CAF groups. In all the analyses, both the differential expressed genes (DEG) list and principal component analysis (PCA) were provided by CNAG bioinformaticians, who followed the specifications above.

RNA-seq Illumina reads were mapped against the human reference genome (GRCh38) using aligner STAR version 2.7.8a (284) with ENCODE parameters. Annotated genes were quantified with RSEM version 1.3.0 (285), using the human GENCODE annotation v40 and default parameters.

Differential expression analysis was performed independently on mesenchymal and tumor samples with *limma v3.42.2 R package*. Data were normalized with TMM and the *voom function* (286) was used to estimate mean-variance relationship and to compute observation-level weights. The linear model was fitted adjusting for the replicate batch effect and contrasts were extracted. Genes were considered DEG with a p-value adjusted < 0.05 and the top50 DEG were represented in a heatmap with the heatmap R package.

Genes expressed in fewer than two libraries were filtered out before differential expression testing. The principal component analysis was calculated using the “prcomp” function available in R and plotted using a customized R script. Expression, normalization, and differential expression testing were performed using DESeq2, in case for comparison with two experimental groups. DESeq2 methodology estimate variance-mean dependence in

RNA-seq count data and test for differential expression based on a model using the negative binomial distribution.

3.2. Functional analysis of gene expression

3.2.1. Gene Set Enrichment Analysis (GSEA)

In order to explore the biological meaning of the gene expression of our experimental groups we used Gene Set Enrichment Analysis (GSEA). GSEA is a computational method that determines whether an *a priori* defined set of genes shows statistically significant, concordant differences between two biological states. Such *a priori* defined gene sets are compiled in the Molecular Signature Database (MSigDB). In addition, GSEA determines whether genes that constitute a predefined gene set tend to be represented at the top or bottom of our ordered list of genes, correlating with our experimental phenotypes. Also, one of the virtues of GSEA is that several small changes in expression of a set of genes, which in a coordinated way, have biological significance, are considered.

The expression profiles of our *in vitro* experimental conditions were subjected to a pre-ranked GSEA, using the T-statistics provided by Limma Package to assess and to rank the differentially expressed genes. We explored different collections of datasets: HALLMARKS, CANONICAL PATHWAYS and GO.BIOLOGICAL PROCESSESS.

3.2.2. HiPathia

The interpretation of the consequences of the combined changes of gene expression levels in the context of signaling pathways was performed using the HiPathia (High throughput pathway interpretation and analysis) web tool (287,288). HiPathia transforms uninformative gene expression data into signalling circuit activities, which carry information on the different cell functionalities. The information provided by HiPathia is complimentary of the information provided by GSEA.

Gene expression data after TMM normalization were used to analyze pathways activation status. HiPathia considers the expression of the genes in a pathway and the relation between them to obtain a value for the activation status of the pathway to each sample. The comparison of these data between groups showed up- or down-regulated pathways

regarding the control group. Results were also related to Gene Ontology (GO) functions. P-values were shown with FDR adjustment.

3.2.3. Metabolizer

Metabolizer is a web tool for analysis of modular architecture of metabolic pathways using transcriptomic data. This tool calculates the impact of modules on the production of metabolites (289). Metabolizer uses KEGG (Kyoto Encyclopedia of Genes and Genomes) Module activities and transcriptomic data. For the analyses, the t-test was applied for statistical assessment and p-values were adjusted by the Benjamini-Hochberg method. Log-fold changes were calculated as log (median).

4. CELL-BASED ASSAYS

4.1. Peripheral blood mononuclear cell migration assays

Peripheral blood mononuclear cells (PBMCs) were obtained from healthy donors. Fresh blood was collected in EDTA tube. The first step consists of isolating the PBMCs from total blood. For that, we used a Leucosep® tube (Greiner bio-one). First of all, Leucosep® tube was centrifuged 1 min at 300 rcf. Then, the whole blood sample was put into one 50 mL tube in which PBS was added until reaching a final volume of 25 mL. This blood mixed with PBS was carefully introduced into the Leucosep® tube and centrifuged during 15 min at 800 rcf, at RT and in a swinging bucket rotor. It is important to switch-off brakes of the centrifuge. After centrifugation, we obtained a sequence of layers which occurred as follows (Figure 8):

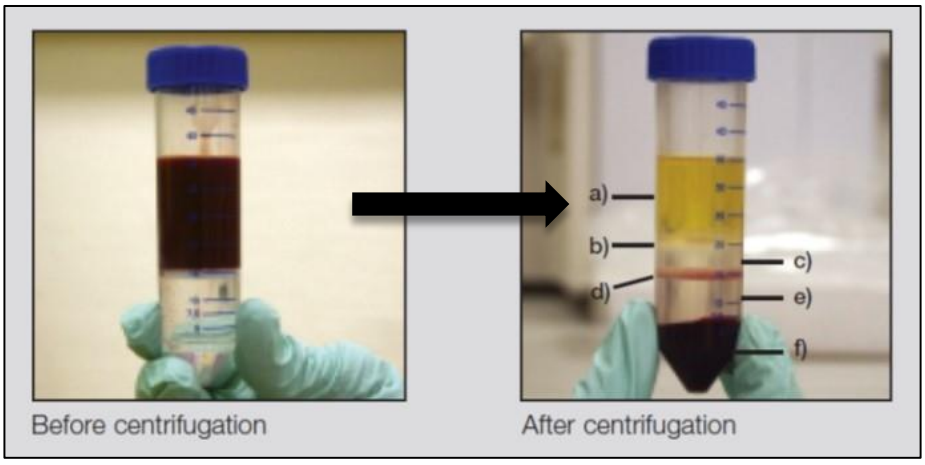

Figure 8. Blood sample before and after centrifugation*. From top to bottom: a) Plasma – b) enriched cell fraction (interphase consisting of lymphocytes / PBMC's) – c) separation medium – d) porous*

barrier – e) separation medium – f) pellet (erythrocytes and granulocytes). Adapted from www.gbo.com/bioscience.

We harvested the enriched cell fraction (interphase consisting of PBMCs - Peripheral Blood Mononuclear Cells) using a Pasteur pipette. Leucosep® tube's porous barrier effectively avoids recontamination with pelleted erythrocytes and granulocytes. We washed the collected cells with 10 mL of PBS, centrifuged them at 400 rcf for 5 min, and aspirate the supernatant. We washed again with 20 mL of PBS and centrifuged at 400 rcf for 5 min. The following wash was performed with 5 mL of PBS and at 250 rcf for 5 min. The last wash was done with 5 mL of PBS, at 200 rcf and for 5 min. The pellet obtained was re-suspended with 5 mL of PBS and counted using the Bio-rad TC10 automated cell counter. After that, we centrifuged the cells for 8 min at 400 rcf and resuspend the pellet with Roswell Park Memorial Institute medium (RPMI) GlutaMAX™ supplemented media (Gibco™, 61870044) at 2% FBS and 1% P/S, in a concentration of 200.000 cells per 100 µL.

For the migration assay, we used plates of 24 well and inserts of 8 µm (SARSTEDT, 83.3932.800), to evaluate PBMCs cell migration. First, we added the chemoattractant, in our case 600 µL of conditioned media or control media, at the lower chamber of the transwell, and let the plate in the incubator for 20 min. After that time, we seeded 100 µL of PBMCs cell solution, thus, 200.000 cells, at the upper chamber of the transwell (Figure 9). Moreover, we also kept a tube with 200.000 cells that served us as control, showing the proportions of each cell populations present at the beginning of the experiment.

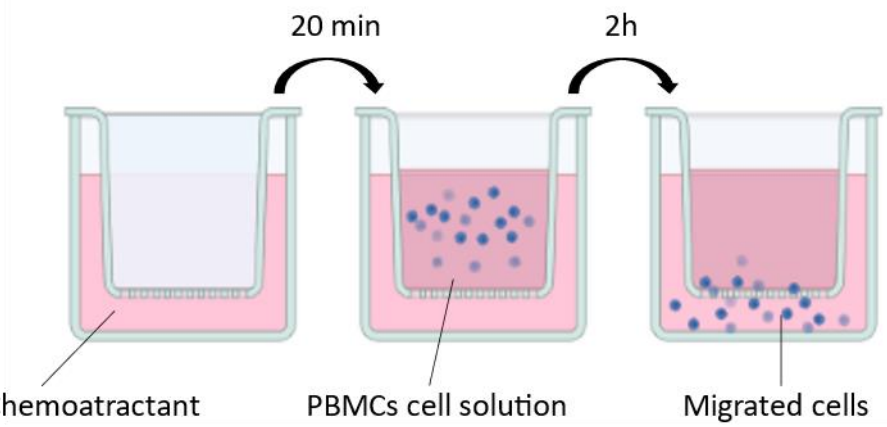

***Figure 9. Migration assay scheme**. Image created using Biorender (www.biorender.com).*

After 2 h of migration inside of the incubator (Figure 9), we collected the lower part of the transwell, which contained the migrated cells, to analyze them through flow cytometry. The collected cells were put in a 15 mL tube containing 2 mL of PBS and centrifuged during 8 min at 400 rcf. The pellet obtained was re-suspended with 20 µL of FACs Buffer and 5 µL of human FcR blocking reagent (Milteny Biotech, 130-059-901) and kept during 10 min in ice and darkness. FcR blocking reagent acts blocking Fc receptor of human cells to increase the specificity of the antibody and thereby improves the purity of target cells. Then, cells were stained with the combination of antibodies showed in Table 8, and incubated for 30 min in ice and darkness. After that, 3 washes with FACs buffer were done. Finally, each pellet was re-suspended in 500 µL of FACs buffer and 2 µL of 1 mg/mL propidium iodide were added.

Antibody	**Fluorochrome**	**Reference**
CD3	PE-Cy7 mouse anti-human CD3	5609190 (BD Pharmingen)
CD4	FITC mouse anti-human CD4	566320 (BD Pharmingen)
CD8	APC mouse anti-human CD8	561421 (BD Pharmingen)
CD25	BV421 mouse anti-human CD25	567486 (BD Horizon)
CD56	PE mouse anti-human NCAM-1	563238 (BD Pharmingen)
CD45	APC-H7 mouse anti-human CD45	560274 (BD Pharmingen)
CD193	BV510 mouse anti-human CD193	563071 (BD Horizon)

Table 8. List of antibodies used in flow cytometry.

4.2. Proliferation assays

Proliferation capacity of adherent cell cultures were evaluated with Real Time-Glo™ MT Cell Viability Assay (Promega- G9711). Cells were harvested onto white, clear bottom, 96-well plates (Corning® Costar plate, 3610). At a density of 2000-6000 cells/well, depending on the doubling time of the cell line assessed. After seeding, plates were revealed following manufacturer's instructions. The luminescence was measured in the PerkinElmer EnSpire Alpha 2390 Multilabel Reader. Cell proliferation was evaluated by comparing the luminescence values at different conditions.

4.3. Polarization assays

Macrophage polarization assays were performed thanks to the collaboration with Maria Rosa Sarrias' group, from *Institut Germans Trias i Pujol*. PBMCs isolated from healthy donors' buffy coats. Blood was put into one 50 mL tube, and sterile PBS 2% FBS was added up to a final volume of 50 mL/ tube. The volume was divided in two tubes containing 25 mL each. 300 µL of RossetteSep Human CD3 (STEMCELL Technologies, 15621) depletion cocktail to each tube. We mixed the solutions by inverting and incubated them 20 min at RT. Meanwhile, we prepared a 50 mL tube with 20 mL of Ficoll-Paque (Cytiva 17-1440-02) for each tube. We added 25 mL of cell suspension over 20 mL of Ficoll-Paque. It is important to preserve the interface between Ficoll solution and the cell suspension. Thus, the cell suspension has to be put slowly. Then, we centrifuged at 400 rcf for 20 min with fast acceleration "9" and slow deceleration "3" at room temperature. We prepared 50 mL tube with 10 mL of PBS 0.5% FBS for each sample. We recovered the PBMCs ring found in the interphase between the saline and Ficoll layers with a sterile plastic Pasteur pipette and put PBMCs in the 50 mL sterile tube with PBS 0.5% FBS. We added 10 mL extra of PBS 0.5% FBS to the PBMCs tubes. Then, we centrifuged at 400 rcf for 5 min (both acceleration and deceleration at maximum) and aspirated the supernatant. After that, we washed with 20 mL of PBS 0.5% FBS for three times, centrifuging at 400 rcf for 5 min the first time, 250 rcf the second and 200 rcf the third. We resuspended the pellet with 5 mL of PBS. With no light in the cabinet, we separated 25 µL of PBMCs in a FACs tube, mixed with 25 µL of Perfect-count microspheres (CYT-PCM-50) and added 5 µL of anti-CD14 antibody to count the number of PBMCs and CD14 cells. We added 150 µL of PBS 1% paraformaldehyde and counted cells on the cytometer. We took the corresponding volume containing the number of cells needed for the experiment and centrifuged at 400 rcf for 5 min.

Control Stimuli	Reference	Stock concentration	Final concentration
INF	300-02-A Peprotech	1 mg/mL	50 ng/mL
LPS	Invitrogen TLrLPS	5 mg/mL	200 ng/mL
IL-4	200-04 Peprotech	100 µg/mL	40 ng/mL
IL-10	200-10 Peprotech	100 µg/mL	50 ng/mL

Table 9. Control stimuli used in macrophage polarization assay.

We used 24 well plates and seeded 500.000 cells per well, in 250 µL RPMI 10% human AB serum + 1% P/S. We let PBMCs to attach inside the incubator for 1 hour. After confirming that cells were attached, we added the control stimuli (Table 9) and conditioned media in the proper wells.

4.4. TGFβ1 stimulation assay

In this assay, HSC were stimulated with 5 ng/mL recombinant TGFβ1 (Peprotech 100-21C) at different time points, and the subsequent expression of CD90 at protein level was assessed through flow cytometry (BD Horizon 559869). THY-1 gene as well as other TGFβ1 genes of response were assessed through qPCR.

4.5. $CD90^{hi}$ and $CD90^{lo}$ cell sorting

The primary CAF cell line that showed part of its cells negative for CD90 was stained by CD90-APC flow cytometry antibody, following the steps explained in 4.1 section. Negative cells for CD90 ($CD90^{lo}$) were separated from positive ones ($CD90^{hi}$) through MoFlo, for posterior RNA extraction, protein extraction or cell culture.

4.6. Repopulation assay

In this assay, $CD90^{hi}$ and $CD90^{lo}$ sorted cells were cultured for three passages and stained with CFSE Cell Trace™ ($CD90^{hi}$) and Violet Cell Trace™ (Invitrogen, C34557) following the same procedure described in section 2.1.1. Then, CFSE stained $CD90^{hi}$ cells were mixed with Violet stained $CD90^{lo}$ cells. This mixture was, in turn, incubated with CD90 flow cytometry antibody through the same steps explained in 4.1. section.

5. HISTOLOGICAL STUDIES

5.1. Hematoxylin & Eosin (H&E)

H&E stain is a tissue staining procedure to visualize the anatomy of tissues at microscopic level. Paraffin-embedded blocks were cut into 3 µm-thick sections using a microtome (ThermoScientific) and set down on poly-L-lysine pretreated slides (Deltalab, A100018). Tissue sections were deparaffinized by submitting them to submersions in a battery of xylene (4x10min), absolute ethanol (3x5min), 96% ethanol (3x5min), 70% ethanol (1x5min),

and 50% ethanol (1x5min). Lastly, sections were rehydrated by submerging them 5 min in dH_2O.

After deparaffination and rehydration processes slides were stained with H&E. For that, they were submerged for 10 min in Harris hematoxylin and rinsed in tap water to eliminate the excess. Next, they were submerged in 1% HCl until the tissue color turned to red and then in 2% ammonia water solution until the color shifted to blue. Sections were finally counterstained in 0.25% eosin for 1 min, dehydrated (2x96% ethanol, 2x absolute ethanol and 4x xylene; 3 min each one) and mounted using DPX (Merck).

Tissues were visualized using the Nikon Eclipse 80i microscope and images were taken with a Nikon DS-Ri1 digital camera using NIS-Elements BR 3.2 software.

5.2. Immunohistochemistry (IHC)

To evaluate protein expression in human tissues, paraffin-embedded tissue blocs were cut into 3-5 µm sections, which sections were deparaffinized and rehydrated.

The next step was antigen retrieval, it was done by submerging the tissue slides in the corresponding buffer (Table 10) depending on the antibody, for 15 min in a pressure cooker. Then, samples were cooled within the same buffer for 20-30 min and washed with dH_2O for 5 min. Endogenous peroxidase activity was blocked by incubation on dH_2O with 40% methanol and 6% H_2O_2 for 15 min. Slides were washed with dH_2O for 5 min and cell membranes were permeabilized by immersion in TBS-T for 10 min.

Afterward, to reduce non-specific antibody binding tissue sections were blocked with goat serum diluted 1:5 in TBS-T for 1 h at RT, followed by incubation overnight (ON) at 4 °C in a humid chamber with primary antibodies diluted in blocking solution.

The following day, slides were washed thrice with TBS-T for 10 min, then incubated with secondary anti-mouse or anti-rabbit EnVision+ System-HRP (Dako, K4001 o K4003) antibodies for 1 h at RT in a humid chamber. After that, samples were washed again and antigen-antibody unions were developed by adding 2 drops/tissue of DAB+ EnVision™ Kit (Dako, K3468), a chromogenic substrate. Samples were incubated from 1 to 5 min, depending on the antibody, until a brown precipitate appeared. DAB reaction was stopped

by rinsing the slides with tap water. Finally, sections were counterstained with hematoxylin, dehydrated, mounted, and analyzed as H&E stained slides.

Protein	Reference	Host	Retrieval Buffer	Dilution
CD90	Proteintech 66766	M	EDTA pH9	1:40000
CD90	Abcam ab92574	R	EDTA pH9	1:1000
Calprotectin	Dako M0747	M	EDTA pH9	1:1500
CCR4	Atlas Antibodies HPA0311613	R	Sodium Citrate pH6	1:40
CD163	Novocastra NCL-L-CD163	R	EDTA pH9	1:400
CD5L	Abnova MAB22048	R	EDTA pH9	1:200
CD8	Dako MA5-13473	M	EDTA pH9	1:400
F2R	Sc-13503 (ATAP2)	M	Sodium Citrate pH6	1:200
FAPα	Abcam ab227703	R	EDTA pH9	1:100
Fibronectin	Abcam ab207178	R	EDTA pH9	1:250
MARCO	Sigma HPA063793	R	EDTA pH9	1:500
Myeloperoxidase	CS14569	R	Sodium Citrate pH6	1:1000
MYH11	Sigma HPA015310	R	Sodium Citrate pH6	1:200
PDLIM3	Sigma HPA004749	R	Sodium Citrate pH6	1:200
Periostin	Abcam ab79946	R	Sodium Citrate pH6	1:50
Podoplanin	Sigma HPA007534	R	Sodium Citrate pH6	1:1000
pSMAD2	Cell Signalling CS3101	R	EDTA pH9	1:300
S100A4	Sigma HPA007973	R	Sodium Citrate pH6	1:1000
αSMA	M0851	M	Sodium Citrate pH6	1:400

Table 10. List of primary antibodies used for protein detection by IHC or Double immunofluorescent (D-IHF) *and their specific conditions. R, rabbit; M, mouse.*

5.3. Double immunofluorescence (D-IHF)

Double IHF allowed us to visualize the expression of two different proteins in the same tissue sample by a fluorescence method. The first steps were the same as for IHC. The main differences consist in the fact that slides were incubated with a mix of two primary antibodies (Table 10) diluted in a special IHF solution (1% BSA, 1% goat/horse serum, 0.3% Triton X-100, 0.01% sodium azide in PBS 1X). This solution was used to reduce the fluorescent background of paraffin. The slides were incubated with Alexa Fluor Secondary Antibodies diluted 1/200 and DAPI (Sigma) diluted 1/3000 for 1 h at RT. After washing the samples thrice with TBS-T, an extra step was added to prevent paraffin autofluorescence, it

consisted in an incubation with 0.1% Sudan black (Sigma) in 70% ethanol for 30 min at RT and darkness. Finally, after incubation, samples were washed again with TBS-T and mounted on slides using VECTASHIELD® Mounting Medium with DAPI so cell nuclei were counterstained with DAPI. Slides were stored at -20 °C until visualization with Zeiss Axio Observer Z1+ Apotome inverted fluorescent microscope and Nikon Eclipse 80i microscope. Images were analyzed using Image J software.

5.4. Patients

We obtained retrospective formalin-fixed paraffin-embedded (FFPE) CRCLM samples from surgical specimen from a consecutive CRCLM cohort (cohort 1) of 135 patients managed by the same surgical and pathological team from the Hospital de Bellvitge (L'Hospitalet de Llobregat, Barcelona, Spain). All patients did not receive neoadjuvant treatment before hepatic surgery. The baseline information for the cohort is summarised in Table 16.

The study samples were assembled after approval by the Ethics Committee of our institution. Signed, informed consent was obtained from each patient when possible. The study was conducted in accordance with the REMARK guidelines for the development of prognostic and predictive biomarkers.

A second cohort of 30 patients were used to validate some of the results obtained from cohort 1. The second cohort consisted in whole-slide sections from not pretreated CRCLM operated in the same center as cohort 1.

5.5. Whole-slide study and Tissue Microarray (TMA) cohorts

For the pilot whole-slide study, twenty-two consecutive cases of untreated CRLM were obtained with the approval of the Ethics Committee of the *Hospital Universitari de Bellvitge* after the informed consent of the patients. Thirteen cases were characterized as desmoplastic and nine as non-desmoplastic by a trained pathologist following the consensus guidelines (52,53). Five cases of twenty-two were synchronous metastases, three characterized as dHGP and two as non-dHGP.

For TMA preparation, one hundred cases of untreated CRLM were obtained also with the approval of the Ethics Committee of the *Hospital Universitari de Bellvitge* (IDIBELL) and after

the informed consent of the patients. The histological growth patterns of included patients were determined by trained pathologists following the mentioned consensus guidelines. For the selection of patients, we decided to include approximately 20% of pure desmoplastic HGP, reproducing the frequency in which this histologic pattern appears in large published cohorts. The invasive margin regions to include in tissue microarray (TMA) sections were manually selected by the pathologist of the team. TMA blocks were manufactured in an external platform. One hundred patients were included, using two TMA cores for each patient.

5.6. Multiplexed immunofluorescence (mIHC) staining and imaging

The mIHC could be performed thanks to the collaboration with Artur Mezheyeuski, PhD, from University of Uppsala. For performing the staining, 4 µm thick FFPE whole-slide or TMA sections were cut, de-paraffinized and rehydrated. After that, slides were subjected to 15 min heat-induced antigen retrieval (HIAR) performed using a pressure cooker or a microwave. The staining procedure included several iterative cycles, which included the incubations for primary antibody and the secondary polymerized reporter enzyme staining system, followed by tyramide signal amplification, and developing Opal fluorophore (1:100). After the final staining cycle, DAPI was applied to visualize nuclei. For whole-slide pilot study, which was performed in University of Uppsala laboratory, a previously stablished protocol was used for the panel of antibodies listed in Table 11.

Whole-slide Pilot Study	Marker 1	Marker 2	Marker 3	Marker 4	Marker 5	Marker 6	Marker 7	DAPI
Deparaffinization & Fixation								
Antigen Retrieval	AR9	AR6	AR6	AR6	AR6	AR6	AR6	
Wash (1X, 2 min)	TBST	TBST	TBST	TBST	TBST	TBST	TBST	TBST
Blocking (HS 2'5%)	10 min RT	10 min RT	10 min RT	10 min RT	10 min RT	10 min RT	10 min RT	
Antibody/CounterStain	Anti-CD4	Anti-CD8	Anti-CD20	Anti-FoxP3	Anti-CD45RO	Anti-PanCK	Anti-ASMA	DAPI
Dilution	1:100	1:200	1:1500	1:400	1:100	E-cad 1:2000 AE1/3 1:200	1:200	
Inc. Time	30 min RT	30 min RT	30 min RT	30 min RT	30 min RT	30 min RT	30 min RT	5 min RT
Wash (3X, 2 min)	TBST	TBST	TBST	TBST	TBST	TBST	TBST	
HRP Polymer, 10 min	ImPress M	ImPress M	Opal HRP Polymer	ImPress R	Opal HRP Polymer		Impress M	
Wash (3X, 2 min)	TBST	TBST	TBST	TBST	TBST	TBST	TBST	
Opal fluor, 10 min	Opal 520	Opal 570	Opal 540	Opal 620	Opal 650	Opal 480	Opal 780 *	
Wash (1X, 2 min)	TBST	TBST	TBST	TBST	TBST	TBST	TBST	

Table 11. Whole-Slide pilot study panel of antibodies and conditions. *AR9: antigen retrieval pH9; AR6: antigen retrieval pH6; TBST: Tris-Buffered Saline Tween20. RT: Room Temperature. All HIER were performed using microwave.*

For TMA samples three different panels were stablished: the lymphocyte panel (Table 12), the myeloid panel (Table 13), and the CAFs panel (Table 14). Antibodies and specific conditions are specified in each corresponding table. Antibody references of all mIHC panels are listed in Table 15. The pH9 antigen retrieval (AR) used was Dako S2367. The pH6 antigen retrieval, as well as Opal 520, Opal 540, Opal 570, Opal 620, Opal 650, and Opal 690, were from Opal 6-Plex Manual Detection Kit (NEL811001KT). Opal 780 (Akoya SKU FP1501001KT) was used following the manufacturer's instructions.

Lymphoid Panel	Marker 1	Marker 2	Marker 3	Marker 4	Marker 5	Marker 6	Marker 7	DAPI
Deparaffinization & Fixation								
Antigen Retrieval	AR9 **MW**	AR6 **MW**	AR6 MICRO **MW**	AR6 **MW**	AR6 **MW**	AR6 **MW**	AR6 **MW**	
Wash (1X, 2 min)	TBST	TBST	TBST	TBST	TBST	TBST	TBST	TBST
Blocking (HS 2'5%)	10 min RT	10 min RT	10 min RT	10 min RT	10 min RT	10 min RT	10 min RT	
Antibody/CounterStain	Anti-CD8	Anti-CD20	Anti-FoxP3	Anti-CD45RO	Anti-CD4	PanCK	Anti-HSA	DAPI
Dilution	1:400	1:3000	1:800	1:200	1:200	AE1/3 1:200	1:100	
Inc. Time	30 min RT	30 min RT	ON + 1h30min RT	30 min RT	30 min RT	30 min RT	30 min RT	5 min RT
Wash (3X, 2 min)	TBST	TBST	TBST	TBST	TBST	TBST	TBST	
HRP Polymer, 10 min	Envision M	Opal HRP Polymer	ImPressR (1h30min RT)	Opal HRP Polymer	Envision M	Opal HRP Polymer	Envision M	
Wash (3X, 2 min)	TBST	TBST	TBST	TBST	TBST	TBST	TBST	
Opal fluor, 10 min	Opal 570	Opal 540	Opal 650	Opal 620	Opal 520	Opal 690	Opal 780 *	
Wash (1X, 2 min)	TBST	TBST	TBST	TBST	TBST	TBST	TBST	

Table 12. Lymphoid panel of antibodies and conditions. *AR9: antigen retrieval pH9; AR6: antigen retrieval pH6; TBST: Tris-Buffered Saline Tween20. RT: Room Temperature. ON: overnight. MW: microwave HIAR.*

Myeloid Panel	Marker 1	Marker 2	Marker 3	Marker 4	Marker 5	Marker 6	Marker 7	DAPI
Deparaffinization & Fixation								
Antigen Retrieval	AR9 **PC**	AR6 **MW**	AR6 **MW**	AR6 **MW**	AR6 **MW**	AR6 **MW**	AR6 **MW**	
Wash (1X, 2 min)	TBST	TBST	TBST	TBST	TBST	TBST	TBST	TBST
Blocking (HS 2'5%)	10 min RT	10 min RT	10 min RT	10 min RT	10 min RT	10 min RT	10 min RT	
Antibody/CounterStain	Anti-CD8	Anti-CD68	Anti-163	Calprotectin	Anti-MARCO	PanCK	Anti-HSA	DAPI
Dilution	1:800	1:200	1:1000	1:500	1:750	AE1/3 1:200	1:100	
Inc. Time	30 min RT	30 min RT	30 min RT	30 min RT	30 min RT	30 min RT	30 min RT	5 min RT
Wash (3X, 2 min)	TBST	TBST	TBST	TBST	TBST	TBST	TBST	
HRP Polymer, 10 min	Envision M	Envision M	Envision M	Opal HRP Polymer	ImPressR	Opal HRP Polymer	Envision M	
Wash (3X, 2 min)	TBST	TBST	TBST	TBST	TBST	TBST	TBST	
Opal fluor, 10 min	Opal 540	Opal 570	Opal 520	Opal 650	Opal 620	Opal 690	Opal 780 *	
Wash (1X, 2 min)	TBST	TBST	TBST	TBST	TBST	TBST	TBST	

Table 13. Myeloid panel of antibodies and conditions. *AR9: antigen retrieval pH9; AR6: antigen retrieval pH6; TBST: Tris-Buffered Saline Tween20. RT: Room Temperature. MW: microwave HIAR. PC: pressure cooker HIAR.*

CAFs Panel	Marker 1	Marker 2	Marker 3	Marker 4	Marker 5	Marker 6	Marker 7	DAPI
Deparaffinization & Fixation								
Antigen Retrieval	AR9 **PC**	AR6 **MW**	AR6 **MW**	AR6 **MW**	AR6 **MW**	AR6 **MW**	AR6 **MW**	
Wash (1X, 2 min)	TBST	TBST	TBST	TBST	TBST	TBST	TBST	TBST
Blocking (HS 2'5%)	10 min RT	10 min RT	10 min RT	10 min RT	10 min RT	10 min RT	10 min RT	
Antibody/CounterStain	Anti-FAP	Anti-CD90	Anti-ASMA	Anti-NGFR	Anti-COL1A1	PanCK	Anti-HSA	DAPI
Dilution	1:1000	1:1500	1:2000	1:100	1:250	AE1/3 1:200	1:100	
Inc. Time	1 h RT	30 min RT	30 min RT	30 min RT	30 min RT	30 min RT	30 min RT	5 min RT
Wash (3X, 2 min)	TBST	TBST	TBST	TBST	TBST	TBST	TBST	
HRP Polymer, 10 min	ImPress R	ImPress R	Envision M	ImPress R	ImPress R	Envision M	Envision M	
Wash (3X, 2 min)	TBST	TBST	TBST	TBST	TBST	TBST	TBST	
Opal fluor, 10 min	Opal 520	Opal 570	Opal 540	Opal 650	Opal 620	Opal 690	Opal 780 *	
Wash (1X, 2 min)	TBST	TBST	TBST	TBST	TBST	TBST	TBST	

***Table 14. CAFs panel of antibodies and conditions**. AR9: antigen retrieval pH9; AR6: antigen retrieval pH6; TBST: Tris-Buffered Saline Tween20. RT: Room Temperature. MW: microwave HIAR. PC: pressure cooker HIAR.*

	mIHC Antibodies References
Primary Antibodies	
CD4	Dako M7319
CD8	Dako MA5-13473
CD20	Dako M0755
FoxP3	Cell Signalling D6O8R
CD45RO	ThermoFisher MA1-19452
E-cad	Bd Biosciences 610181
PanCK A1/3	Dako M3515
HSA	Merck 264M-9
CD68	Dako M0876
CD163	Novocastra NCL-L-CD163
Calprotectin	Dako M0747
MARCO	Sigma HPA063793
FAP	Abcam ab207178
CD90	Abcam ab92574
αSMA	Dako M0851
NGFR	Atlas Antibodies HPA004765
COL1A1	Boster PA214-2
Secondary Antibodies	
ImPress R	Vector MP-7401
ImPress M	Vector MP-7422-15
Envision M	Dako K4001
Opal HRP Polymer	From Opal 6-Plex Manual Detection Kit

Table 15. List of antibodies used for protein detection by mIHC.

Once the staining had been performed, scanning of the slides was done with Vectra Polaris system (Akoya Biosciences, Marlborough, MA, USA). For TMA samples, visualization was done using Phenoimager HT System (Akoya) in multispectral mode at 2 pixels/µm resolution. For whole-slide samples from the pilot study, first, each whole slide was scanned at 10x magnification. Then, representative regions (1'86 x 1'39 mm) for image acquisition were selected to capture areas from the central part and periphery of the metastases. The selected regions were imaged in a multispectral mote at 2 pixels/µm resolution. The multi-layer images obtained were subsequently processed through a spectral algorithm to generate a layer-composed image. This image was in grey-scale, and each of the layers

corresponded to either specific staining, DAPI and autofluorescence. However, one can change the color of each layer for visualization (Figure 10).

After that, inForm software was trained through a learning algorithm provided by the vendor. In case of whole-slides pilot study, the software was trained to split tissue into three categories: blank areas, epithelial and stromal compartments. In this study, epithelial compartment contained both tumor tissue and liver parenchyma. As we were interested in assessing invasive margin areas, we needed to stablish manually the line separating tumor from parenchyma. Thus, demarcations were defined as follows: tumor periphery, 100 µm of the proximal liver parenchyma until the first row of tumor cells, including the capsule in dHGP CRC-LM; invasive margin, 800 µm from the liver-tumor interface (non-dHGP) or capsule-tumor interface (dHGP) to the deeper tumor areas; central areas, deeper and distal tumor areas from the liver parenchyma. To simplify data visualization and analysis, the distances were split into four zones: 0 to 100 µm, 100 to 200 µm, 200 to 400 µm, 400 to 600 µm, taking as a reference two different measures (Figure 14). Thus, a certain number of the cells of interest was identified in each of the zones. Number of cells was normalized per mm^2.

In case of TMA samples, thanks to the inclusion of a specific marker for hepatocytes, HSA, we could segment the tissue in four categories: blank areas, liver, tumor, and stromal compartments. The software training was performed for each panel of markers separately (Figure 10).

The next step was cell segmentation, which was performed using DAPI nuclear staining as described in A. Mezheyeuski *et al.* (290,291). Area at 3 µm (6 pixels) around the nuclear border was considered the cytoplasm area. To stablish the thresholds for each marker positivity, inForm cell phenotyping function was used to choose a representative subset of positive cells as well as a representative negative subset (Figure 10).

Last step was to manually review all the images in order to exclude artefacts, necrotic regions, staining defects, damaged tissue or wrongly segmented areas (Figure 10).

The expression levels of the markers were used to classify cells into the four main subsets (immune cells in panel 1 or myeloid cells in panel 2 or CAFs in panel 3, tumor cells, hepatocytes, and marker-negative cells). Density plots of the protein expression of each

marker were used to set the thresholds for “marker-negative” and “marker-positive” cells. The number of cells of interest were normalized for mm^2 (cell density).

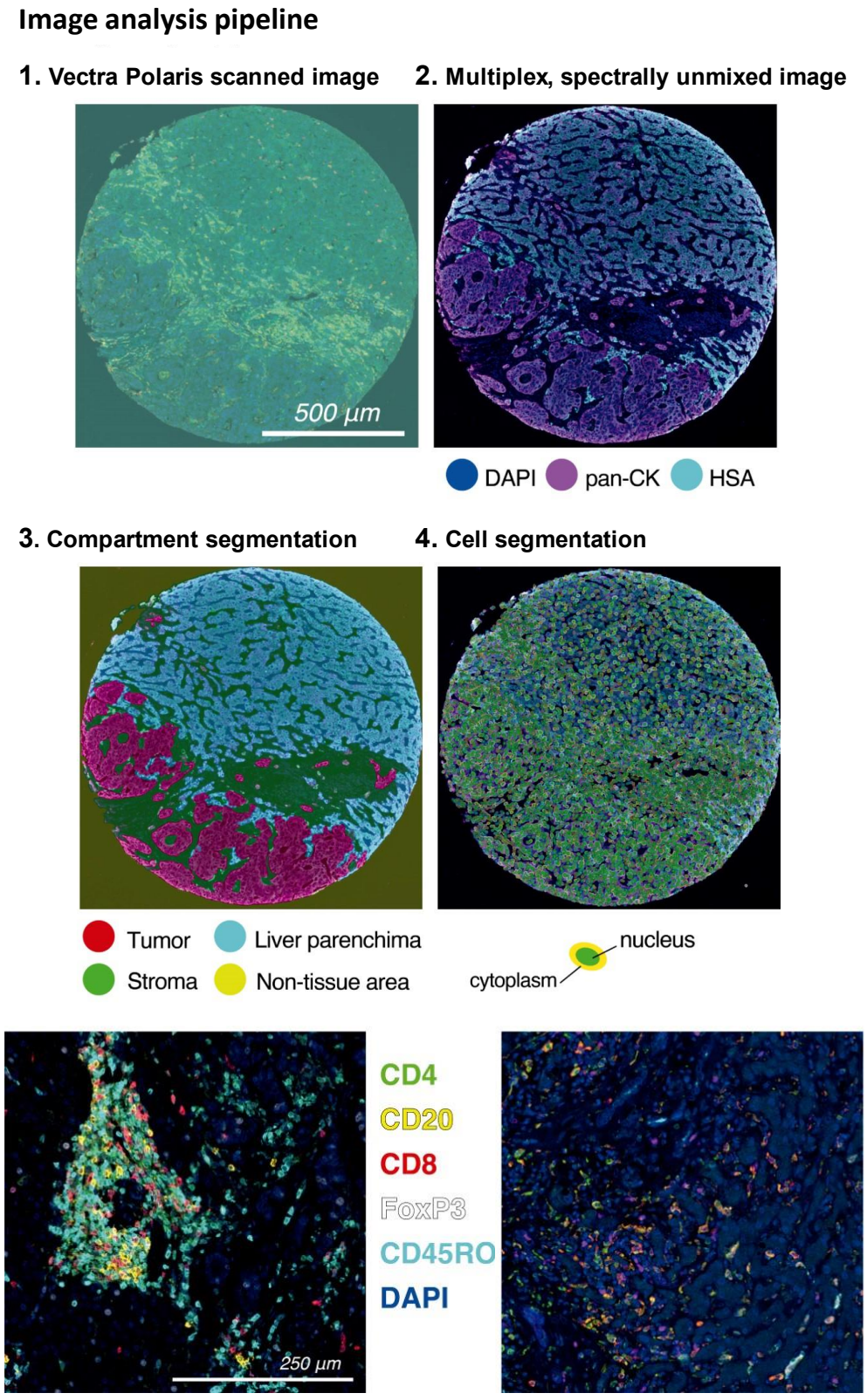

Figure 10. Steps of multiplex image processing and colors assigned to each lymphoid marker.

6. STATISTICAL ANALYSIS

Concerning clinical data of patient cohorts, overall survival curves were analyzed through Kaplan-Meier, and Chi-squared test was used to compare different characteristics between patients showing dHGP and non-dHGP.

About mIHC whole-slide pilot study, statistical analyses were performed using R Studio (Version 1.3.1073). The Ward algorithm was used for hierarchical clustering and the Mann Whitney U test was used to compare variables between central and peripheral of the same patient. The Mann Whitney U test with Pratt correction for tied data was used to compare variables between independent samples. $p < 0.05$ was considered statistically significant.

In mIHC TMA analysis, U Mann-Whitney test with Pratt correction for ties was applied. Moreover, to apply a correction for multiple testing, statistical significance reported was adjusted using Holm-Bonferroni correction and FDR adjustment. Adjusted $p < 0.05$ was considered statistically significant (Holm-Bonferroni adjustment).

In vitro experiments were carried out at least 3 independent times with at the minimum 3 technical replicates. Data were statistically analyzed with GraphPad Prism v8 software to determine if there were significant differences between samples. Results were presented as mean ± SD. Data were analyzed using the most appropriate statistical test for each experiment and specific analysis are described in the figure legends. In general terms, nonparametric statistics, U Mann Whitney for unpaired samples and Wilcoxon's test for paired samples were applied for *in vitro* experiments. For experiments involving more than two experimental groups, the Kruskal-Wallis test was used, subsequently applying the Dunns' test for multiple comparisons. More details are described in the figure legends.

RESULTS

1. Validation of the prognostic value of HGPs in the cohort of patients from Hospital de Bellvitge

Given the prognostic value of HGP observed in different series of patients (53), we aimed to validate this effect on survival in a consecutive series of patients operated at the Hospital de Bellvitge. The validation series consisted of 135 patients who have not received preoperative chemotherapy before liver surgery, as it has been described to have an impact on HGP appearance (82). The characteristics of the final included patients' series are described in Table 16 and Table 17.

The HGP was determined by our pathologist following the criteria described in the consensus guidelines (52,53). Briefly, patients showing a complete encapsulation (100% of the tumor-host interface surrounded by a fibrotic rim) were considered pure desmoplastic HGP (dHGP). This characteristic must be presented in all the slides available at the Pathology Service for a given patient. On the contrary, cases with any percentage of the tumor-host interface showing non-desmoplastic HGP, either replacement or pushing, were considered non-desmoplastic (non-HGP). Applying these parameters, 29 patients were categorized as dHGP (21’5%), and 106 patients were classified as non-dHGP (78’5%). These percentages of dHGP and non-dHGP match with the previously described in other cohorts (53). As observed in Figure 11 Kaplan-Meier plot, the overall survival was significantly longer in patients showing pure dHGP.

	N	Percentage
Sex		
male	103	76,30%
female	32	23,70%
Type of metastases		
synchronous	41	30,40%
metachronous	94	69,60%
Location of the primary tumor		
colon	87	64,40%
rectum	45	33,30%
lost	3	2,20%
Adjuvant treatment primary		
yes	83	61,50%
no	52	38,50%
Adjuvant treatment metastases		
yes	74	54,80%
no	42	31,10%
lost	19	14,10%
Mean age (years)	67,32	range 36-86
Mean size (cm)	3,08 cm	range 0,6-12,4

Table 16. Demographic data of 135 patients' cohort.

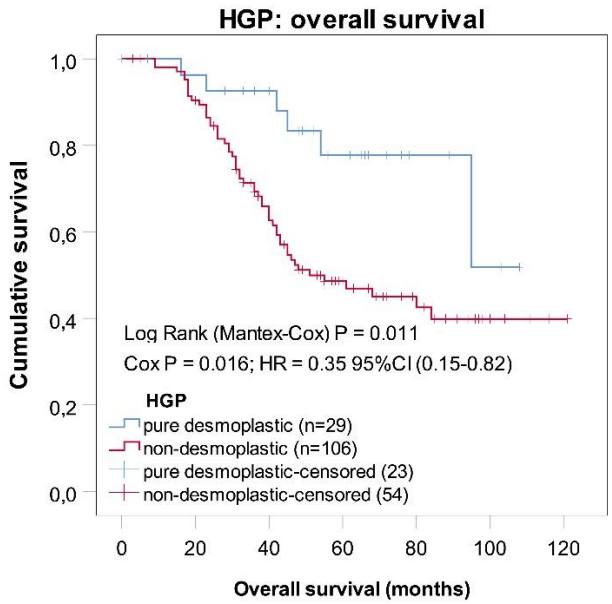

Figure 11. Kaplan-Meier plot for the overall survival (OS) of the 135-patient cohort from the Hospital de Bellvitge. *The blue line depicted patients with resected metastases with a pure desmoplastic HGP while the red line refers to patients with any percentage of non-desmoplastic HGP.*

	desmoplastic (dHGP)	non desmoplastic (non-HGP)	Chi Square p value
Sex			
male	23 (79,3%)	80 (75,5%)	0,667
female	6 (20,7%)	26 (24,5%)	
Status			
alive	19 (65,5%)	45 (42,5%)	**0,022**
dead with cancer	6 (20,7%)	53 (50%)	
dead no cancer	4 (13,8%)	6 (5,7%)	
lost	0	2 (1,9%)	
Adjuvant treatment metastases			
yes	12 (48%)	62 (68,1%)	0,064
no	13 (52%)	29 (31,9%)	
Type of metastases			
synchronous	15 (51,7%)	26 (24,5%)	**0,005**
metachronous	14 (48,3%)	80 (75,5%)	
Size (3 cm)			
< 3 cm	20 (69%)	55 (51,9%)	0,101
> 3 cm	9 (31%)	51 (48,1%)	
Location primary tumor			
colon	20 (74,1%)	67 (63,9%)	0,316
rectum	7 (25,9%)	38 (36,2%)	
Affected resection margin			
yes	4 (13,8%)	20 (19,2%)	0,501
no	25 (86,2%)	84 (80,8%)	
Adjuvant treatment primary			
yes	12 (41,4%)	71 (67%)	**0,012**
no	17 (58,6%)	35 (33%)	

Table 17. Chi-square test comparing 135 patients' cohort characteristics.

It is also important to highlight the clinical variables listed in Table 17. In the cohort of study, we observe that most of the patients diagnosed with non-dHGP metastases have received adjuvant treatment for the primary tumor. This could be explained by the fact that a higher percentage of non-dHGP lesions are metachronous (75.5%) (Table 17). Thus, it is more probable that these patients have previously been treated after the primary tumor diagnosis. Moreover, this is suggesting that primary tumor adjuvant chemotherapy could influence the HGP that will appear in future metastatic lesions, promoting non-dHGP. Meanwhile, it has been described that once the metastasis is diagnosed, neoadjuvant

treatment promotes an increase in the percentage of the desmoplastic tumor-liver interface (292). Hence, the chemotherapy's effect on HGP appearance would change depending on the stage of the metastatic lesion's development.

In conclusion, the data exposed validates the prognostic value of HGPs in the cohort of patients from Hospital de Bellvitge, as well as highlights the presence of biological differences between HGPs.

2. Spatial immunology in liver metastases from colorectal carcinoma according to the histologic growth pattern

Once validated the prognostic value of HGPs in Hospital de Bellvitge's cohort and observed evidence of biological differences between HGPs, we focused on characterizing dHGP and non-dHGP patterns. One of the most evident features characterizing dHGP is the presence of dense lympho-histiocytic infiltrates at the outer part of the fibrotic capsule, near the hepatocytes (Figure 12). Although recent advances have been done in immunoncology, with a special focus on the interaction of immune cells with tumor and other stromal cells, a detailed characterization of the immune infiltrates in the context of CRLM HGP as well as the biological role they are playing are still lacking. For these reasons, our first aim was to explore the spatial distribution of the mentioned lymphocytic infiltrates in CRLM in the context of HGPs.

For that, we decided to do a pilot study with whole-slide sections from 22 patients of our cohort, in which we planned to use a multiplex immunohistochemistry (mIHC) and perform a spatial image analysis.

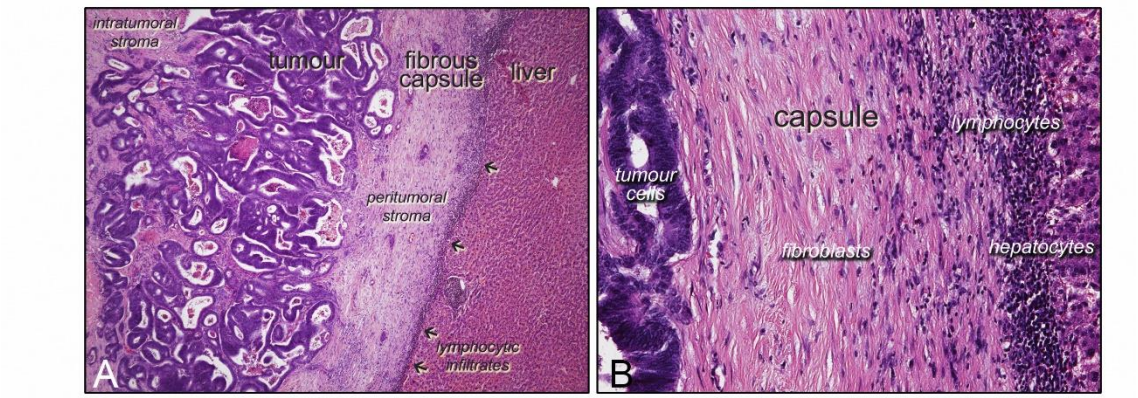

Figure 12. H&E staining of a dHGP liver metastasis showing most of the lymphocytes located in the outer part of the fibrotic capsule*. A) 10x magnification, displaying on the left side a well differentiated tumor glands, typical from this HGP and intratumoral stroma interspersed between glands. The malignant area is delimited by the peritumoral stroma (fibrous capsule) and then the normal liver parenchyma. B) Detailed magnification (20x) of the fibrotic capsule (peritumoral stroma) in which the arrangement of cells with elongated morphology typical of fibroblasts is clearly observed, as well as the arrangement of lymphocytes in the outermost part and close to the hepatocytes.*

2.1. The comparison of immune cell densities between dHGP and non-dHGP liver metastases

First, we compared tumor infiltrating lymphocyte (TIL) densities in dHGP vs. non-dHGP. The marker combination used to characterize TIL subclasses is displayed in Figure 13A. As we wanted to focus on the importance of the spatial context (293), we assessed separately areas from the central and peripheral regions of the lesions. When assessing the central areas, no differences were observed between HGPs (Figure 13B). Unexpectedly, we neither find differences when comparing the total immune infiltrates (epithelial + stroma compartments) in peripheral regions (Figure 13B). However, differences were observed when analyzing those infiltrates in different compartments separately, as non-dHGP samples showed higher infiltration of $CD4^+$, $CD4^+$ memory and $CD45RO^+$ retained in the stromal compartment (p=0.041, p=0.00005 and p=0.032, respectively). On the other hand, $CD4^+$ memory cells were the only cell type that showed higher infiltration in non-dHGP in the epithelial compartment (p=0.041) (Figure 13B).

In conclusion, we did not find statistically significant differences between immune infiltration in central regions of metastases with different HGP. In peripheral regions non-dHGP metastases showed higher infiltration of $CD4^+$ lymphocyte subsets and CD45R0+ cells.

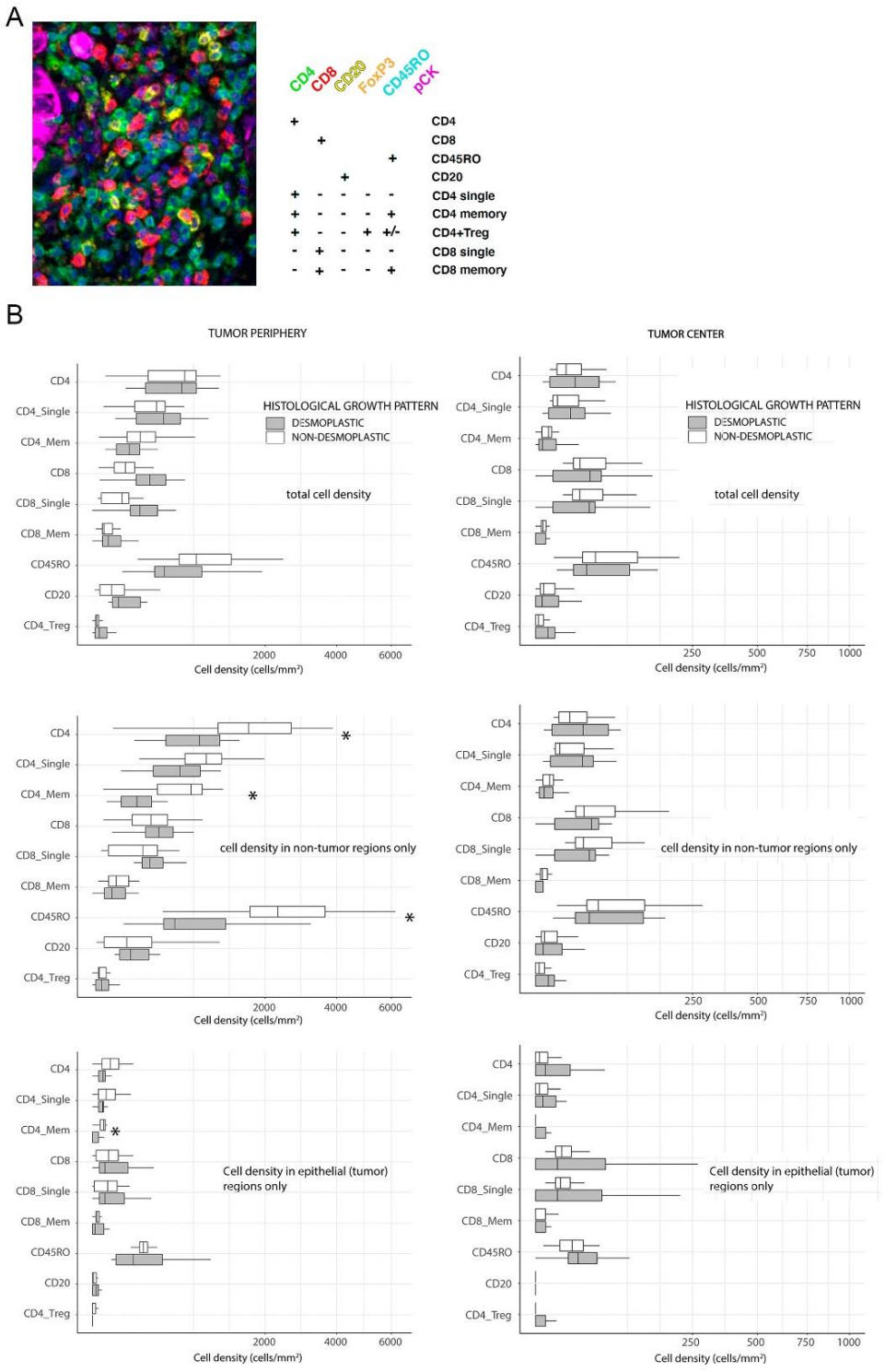

Figure 13. Immune cell densities dHGP vs. non-dHGP. *(A) Marker combination to identify each of the lymphocyte subsets assessed in the study. (B) Boxplots of cell densities (cells/mm^2) for each of the subsets assessed and stratified by HGP. We differentiated cell counts according to different topographic locations in the tumor, either in the tumor periphery or in central tumor areas as well as differentiating whether infiltrates were located in the stroma or in tumor glands. Tumor periphery was defined as the tissue fraction from 100 µm of the proximal liver parenchyma until the first row of tumor cells, thus, including the capsule in dHGP CRC-LM and any rare portion of peritumoral stroma in non-HGP CRC-LM. *p value < 0.05, U-Mann Whitney test comparing dHGP vs. non-HGP.*

2.2. Spatial Assessment of TILs in liver metastases

The initial analysis described above, however, did not take into account the differential histological characteristic represented by tumor encapsulation. Therefore, the analyzed peripheral regions in dHGP were mainly represented by the capsule, which retained most of the immune infiltrates, while the peripheral regions in non-dHGP, selected for analysis, mostly consisted of tumor tissue, liver parenchyma and small areas of reactive stroma. Such a difference in histological composition makes the direct comparison of peripheral regions suboptimal and suggests establishment of more reliable methods with comparable reference elements in both HGPs. Whith these results, we set out to evaluate lymphocyte infiltration, considering spatial location of immune infiltrates in relation to tumor and host tissue. However, the relation between these tissue elements is not equivalent in non-dHGP and dHGP.

Thus, the interface between healthy and tumoral tissue is easy to identify and could serve as reference for spatial analysis in non-dHGP metastases. However, in metastases with dHGP, the fibrotic capsule constitutes a barrier between host liver parenchyma and tumor tissue, and it is not clear whether to consider the capsule as an element of the host or of the tumor. Therefore, we decided to perform two measurement assessments: A and B, illustrated in Figure 14A. Measure A evaluates the 800 µm of cell distance from the interface between liver parenchyma and either capsule (in dHGP) or tumor (in non-dHGP) or small areas of reactive stroma (in non-dHGP).This area, that we termed as “tumor-liver interface”, includes the cells located in the capsule in dHGP metastases, in reactive stroma in non-dHGP lesions, and in tumor tissue in both HGPs. On the other hand, measure B evaluates the “invasive margin”, assessing the 800 µm of cell distance from the line delimited by tumor cells. Therefore, this measure excludes cells from stroma between liver parenchyma and tumor and includes only the cells from tumor tissue, strictly analyzing what corresponds to the invasive margin of the tumor.

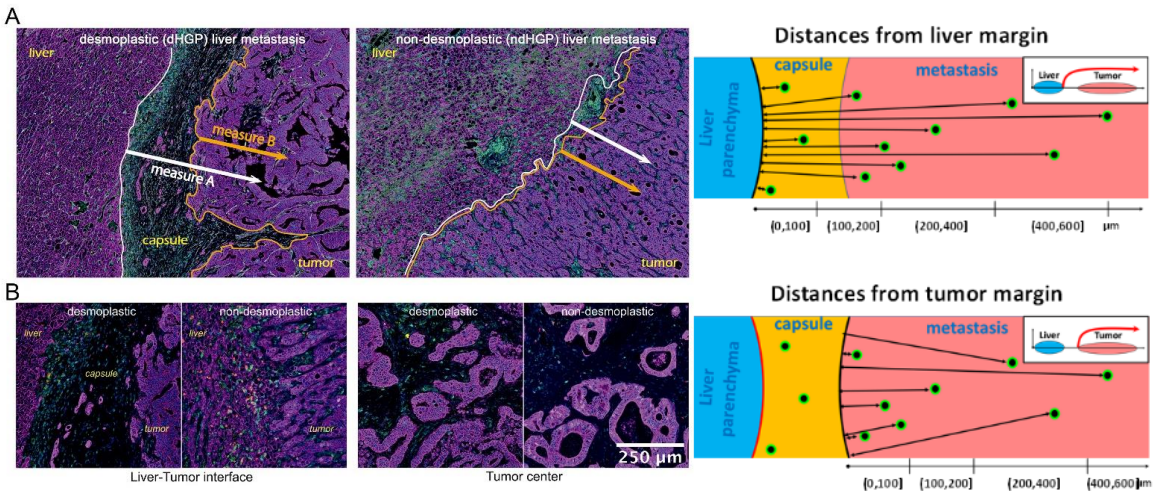

Figure 14. Spatial assessments of HGPs. *(A) Distances considered in relation to the tumor-host interface. Measure A, using as a reference the tumor-liver interface, including as part of the tumor, the fibrous capsule in case of dHGP or any small stromal area in the case of non-HGP; Measure B, using the tumor margin as a reference and then, not considering capsule or any peritumoral stromal. We use this measure throughout the manuscript to refer to the invasive margin. (B) Detailed magnification of the tumor/liver interface and central tumoral areas for both main histologic growth patterns.*

When analyzing measure A, dHGP displayed higher infiltration of $CD8^+$, $CD8^+$ single positive and $CD20^+$ lymphocytes, particularly in areas close to the liver parenchyma (Figure 15A, left panel). This distance, in encapsulated metastases, corresponds mainly to the outer capsule fragment closest to the liver, where a large quantity of TILs is retained, commonly arranged to form a crown of immune infiltrates. However, when moving away from parenchyma towards the tumor, the differences between HGP became less prominent and finally lost at 400 µm, where the comparison corresponds approximately to the invasive margin in dHGP and deeper tumoral regions in non-dHGP. Therefore, these results are in line with the previous observations from H&E stainings: TILs accumulate at the outer half part of the fibrotic rim of dHGP metastases. Moreover, most of these TILs populations conforming the crown are $CD8^+$ and $CD20^+$ cells.

On the other hand, when considering measure B the results were different: $CD4^+$, $CD4^+$ single positive, $CD4^+$ memory, CD4 Treg ($CD4^+$ and $FoxP3^+$), $CD20^+$ and $CD45RO^+$ cells showed significantly more infiltration in non-dHGP metastases (Figure 15A, right panel). Meanwhile, no difference was seen for $CD8^+$ cell subsets (Figure 15A, right panel).

Moreover, when assessing the overall cell density, for most of the immune subsets the total number was lower when using measure B, both for dHGP and non-dHGP. Thus, these results suggest that those populations of $CD8^+$ and $CD20^+$ observed in the fibrotic rim of dHGP keep retained on it, being not able to migrate properly through the capsule to reach the invasive margin. Furthermore, in the case of non-dHGP, it also shows that immune infiltrates keep on those small regions of reactive stroma (Figure 13B, right image). The immune cell subsets that showed higher infiltration capacity at non-dHGP invasive margin were $CD4^+$ populations, $CD20^+$ and $CD45RO^+$ cells.

Even larger prevalence of $CD4^+$, $CD4^+$ single positive, $CD4^+$ memory, CD4 Treg, and $CD45R0^+$ cells in terms of statistical significance and absolute cell counts was demonstrated in non-encapsulated metastases. Additionally, $CD20^+$ B cells showed higher levels in non-encapsulated samples, thus, demonstrating cellular composition in the regions of reactive stroma.

In conclusion, the fibrotic capsule in encapsulated metastases, especially the outer capsule part is characterized by increased quantity of $CD8^+$ positive lymphocyte subsets and B cells, in comparison to peripheral regions in non-dHGP metastases. However, the invasive margin of tumor tissue in encapsulated metastases did not demonstrate enrichment of these immune cell subsets, and conversely, showed a lower density of $CD4^+$ lymphocyte subsets and $CD45R0^+$ cells. The reactive stroma regions in non-encapsulated metastases are characterized by accumulation of $CD4^+$ lymphocyte subsets, $CD45R0^+$ cells, and $CD20^+$ cells.

2.3. The comparison of immune cell densities in the invasive margin of liver metastases

Spatial analysis revealed the importance of accurate assessment of the histological peculiarities of liver metastases with different HGP. Because we assumed that direct interaction between immune cells and malignant tissue is of major importance for immune surveillance in metastatic disease, we focused our next analyses on the metrics, derived using “Measure B” approach and performed manual selection of the invasive margin regions (e.g., tumor regions, excluding capsule, liver parenchyma, and reactive stroma) in both HGP.

Non-encapsulated metastases displayed higher quantity of total $CD4^+$, $CD4^+$ single positive, $CD4^+$ memory cells, as well as $CD20^+$ B cells in the invasive margin (Figure 15B, upper panel, p=0.011, p=0.038, p=0.008 and p=0.032, respectively). These differences corresponded mainly to inflammatory infiltrates circumscribed to the stromal compartment, which retained most of the identified infiltrates (Figure 15B, middle panel). The exception was $CD4^+$ memory cell subset, which also showed higher infiltration in epithelial compartment in non-dHGP (Figure 15B, lower panel).

In conclusion, the analysis of the invasive margin confirmed the spatial analysis and demonstrated that non-dHGP metastases have higher infiltration of several $CD4^+$ lymphocyte subsets.

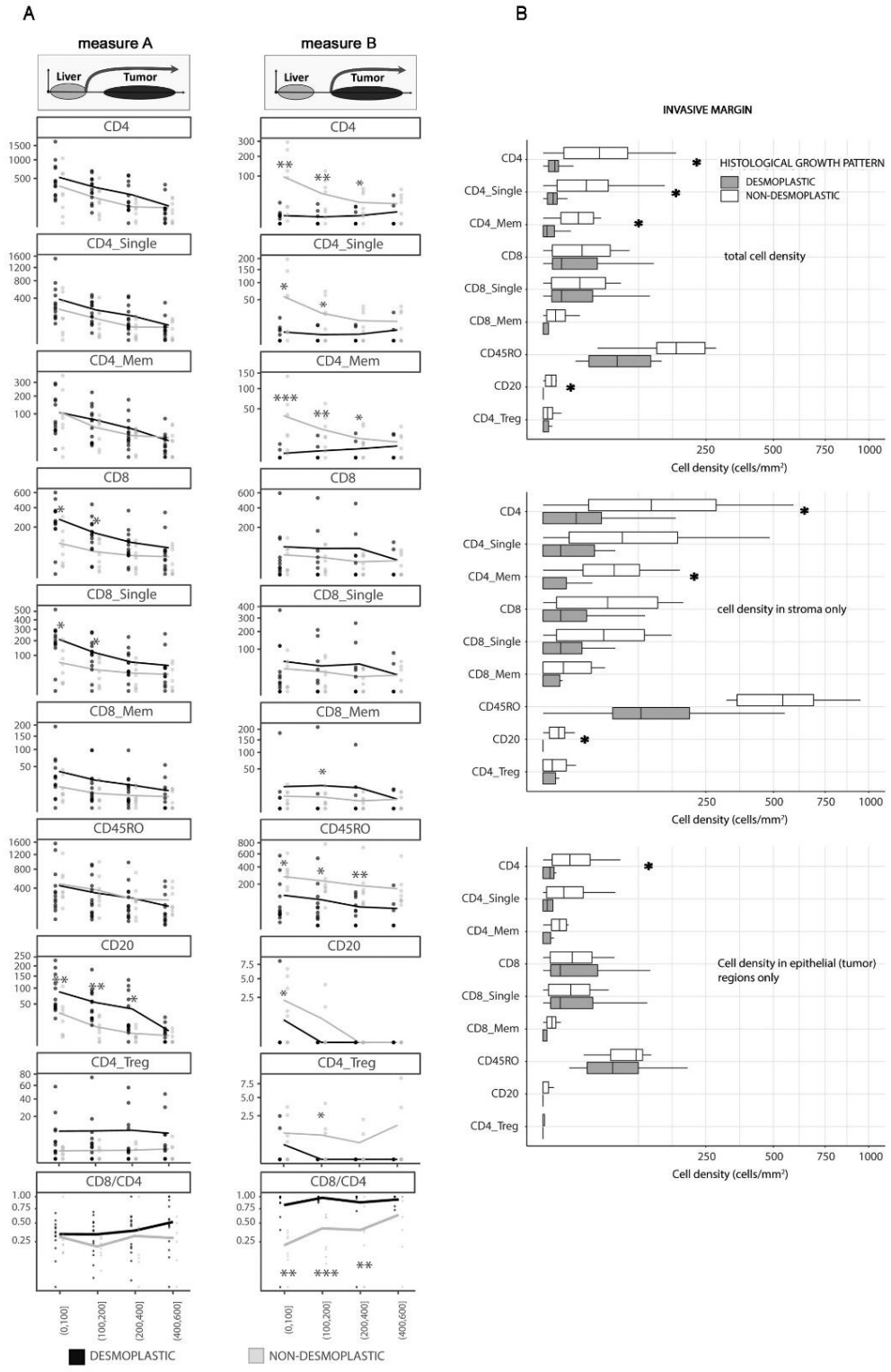

Figure 15. Invasive margin spatial assessment. *(A) Spatial assessment of lymphocyte subsets in dHGP and non-dHGP CRLM according to two different measures: measure A, from liver margin, and measure B, from the outer tumoral region (invasive margin). Lines show mean levels of cell densities. TMA cores show cell count/mm^2. X-axis is square root transformed (distant segments, µm). (B) Boxplots of cell densities (cells/mm^2) for each of the subsets were assessed and stratified by HGP according to the invasive margin (measure B). *p<0.05, **p<0.01, ***p<0.001. U Mann-Whitney test comparing dHGP vs. non-dHGP.*

2.4. The comparison of immune cell densities in the invasive margin and tumor center

Next, we compared in each sample, in a paired way, the inflammatory infiltrates between the invasive margin and central areas of each sample in a pairwise manner. In this analysis, dHGP showed higher infiltration of $CD4^+$ total, $CD4^+$ single and CD4 Treg cells in central areas. Meanwhile, the trend observed was the opposite in non-dHGP. Encapsulated metastases also showed more $CD20^+$ B cells in central areas when compared to invasive margin (Figure 16).

Therefore, in summary, we can state that the poorest immune infiltration is observed in the invasive margin of dHGP metastases, while their central parts as well as the invasive margin and central parts of non-dHGP metastases demonstrated comparable quantities of TILs.

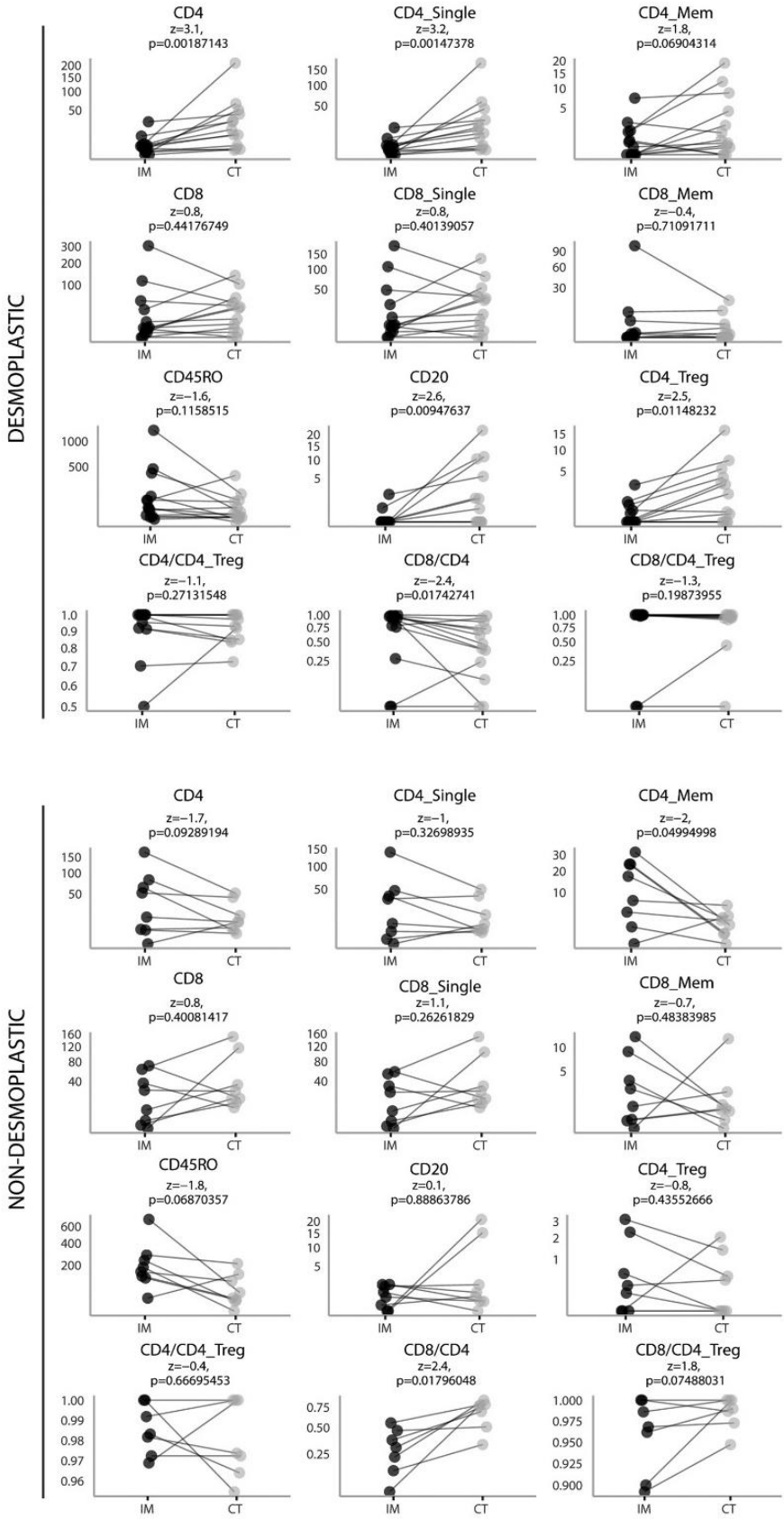

Figure 16. Pairwise comparison of immune cell densities in the invasive margin (IM) and central areas of the tumor (CT). *Wilcoxon signed-rank test with Pratt modification was used to look for statistically significant differences between the two areas.*

2.5. Anti-tumoral status of the immune infiltrates in the invasive margin and tumor center

The previous results showed the presence of higher TIL levels in the worse prognoses-associated non-dHGP metastases, which are the ones known to have substantially better prognosis. Thus, our results did not match with the stablished paradigm of TIL infiltration in tumors, which associates a greater number of immune infiltrates with better survival. For that reason, we hypothesized that such results may be explained by the presence of TILs with immune-suppressive functions in non-dHGP metastases. In line with this, CD8 lymphocytes are described to be the main tumor cell killers (113). Meanwhile, $CD4^+$ cell subsets include some populations that are described to be immuno-suppressive, like CD4 Tregs or $CD4^+$ Th2, which may be predominant in tumors (294). Among the Th2 cells described functions, they drive the polarization of macrophages towards M2-type and eventually create an immune-suppressive tumor microenvironment (295).

Thus, to prove our hypothesis, we sought to evaluate the overall anti-tumoral status of the TIL infiltrates. For that, we assumed that $CD8^+$ cells represent anti-tumor immunity, while $CD4^+$ cell subsets may contain a significant fraction of Th2 T cells and, therefore, reflect pro-tumor characteristics. To assess TIL antitumoral status, we generated a metric: CD8 / (CD8 + CD4), which further in the text is termed as “CD8/CD4 ratio”. According to this metric, high values of this ratio would mean high anti-tumoral activity while low values of it would mean a higher immune-suppressive and, thus, pro-tumoral activity.

The CD8/CD4 ratio was higher in the invasive margin than in central areas in dHGP cases, while opposite results were seen in non-dHGP cases (Figure 16), which suggests that the higher infiltration observed in non-dHGP central areas is explained by the presence of immune-suppressive cells. Moreover, when comparing invasive margin (considering measure B, thus, excluding any peritumoral stroma) between the two HGP, dHGP showed higher CD8/CD4 ratio (at tumor margin and up to 400 µm towards the tumor center; $p<0.05$) (Figure 15A, right panel). This results, which were confirmed in the specific analysis of this ratio for the invasive margin (Figure 17, upper panel), suggested that there is a higher anti-tumoral activity at this region in dHGP when compared with non-dHGP. On the other hand,

no differences were seen in CD8/CD4 ratio when assessing central areas of the two HGP (Figure 17, upper panel).

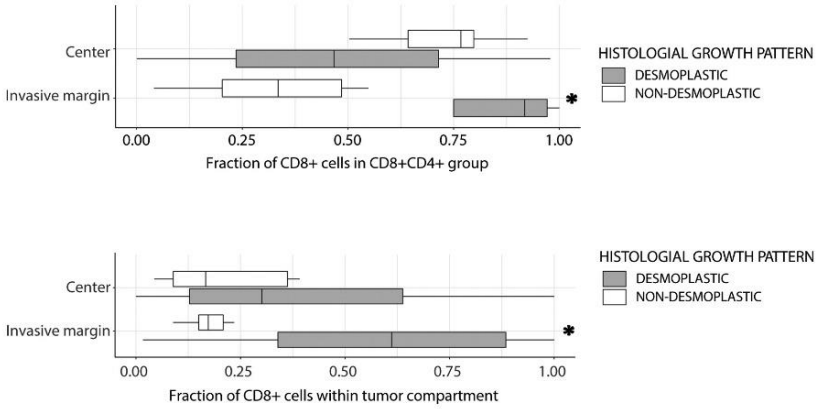

Figure 17. Anti-tumoral status of immune infiltrates*. Top panel, boxplot for CD8/CD4 ratio comparing dHGP and non-dHGP in central tumoral areas and at the invasive margin. Bottom panel, boxplot displaying the fraction of CD8⁺ cells within the epithelial compartment, both at the invasive margin and central tumor areas. *p<0.05, U-Mann-Whitney test comparing dHGP vs. non-dHGP.*

Finally, to corroborate the higher anti-cancer response in dHGP invasive margin that the previous results suggested, we performed a further analysis. The active anticancer response by cytotoxic cells requires their presence in the immediate vicinity of the malignant cells to enable their direct contact and cytotoxic function. Thus, if CD8/CD4 ratio reflects the antitumoral immune environment in dHGP, one would expect a higher number of CD8 (cytotoxic) cells in the epithelial compartment in dHGP samples. To assess that, we should analyze the number of CD8 at the epithelial compartment (the ones really acting as anti-tumoral cells) in relation to the CD8 cells that remain limited in the stromal compartment (retained, not performing an anti-tumoral activity). For that, we evaluated the following ratio: CD8 epithelial compartment/ (CD8 epithelial + CD8 stromal), in which higher values mean a more active anti-tumoral activity. This analysis also showed higher levels of this ratio at the invasive margin of dHGP (Figure 17, lower panel).

In conclusion, CD8/CD4, which we consider as a surrogate metric of the anti-tumoral status of the TIL infiltrates, was significantly elevated in the invasive margin in dHGP, in comparison to central areas and to the invasive margin in non-dHGP lesions, potentially reflecting an anti-tumoral immune microenvironment in dHGP metastases. Moreover, the invasive margin in encapsulated lesions was characterized by higher prevalence of CD8⁺ cells in the

epithelial compartment, suggesting the presence of an immune-suppressive, pro-tumoral microenvironment in non-dHGP lesions.

3. Tissue Microarray assessment of immune infiltrates

3.1. Lymphoid cells assessment in tissue microarray

The pilot study of whole slides from 22 patients showed interesting results. However, as the number of patients included was very low, we prepared a tissue microarray (TMA) with 100 patients available from our cohort of study. To analyse in more details the tumor interface, we specifically produced the TMA cores from this area. Our aim was to explore the same panel of markers to validate the results obtained previously in a bigger cohort of patients. The proportion of dHGP and non-dHGP patients was 20% and 80% respectively, reflecting patients' cohorts (52). The demographic characteristics of the patients are listed in Table 18.

	DESMOPLASTIC (dHGP)	NON DESMOPLASTIC (non-dHGP)	CHI SQUARE p value
Sex			
male	19 (86,4,3%)	59 (75,6%)	0,284
female	3 (13,6%)	19 (24,4%)	
Status			
alive	10 (45,5%)	35 (44,9%)	0,345
dead with cancer	9 (40,9%)	39 (50%)	
dead no cancer	3 (13,6%)	3 (3,8%)	
lost	0	1 (1,3%)	
Adjuvant treatment metastases			
yes	10 (50%)	44 (68.8%)	0,127
no	10 (50%)	20 (31,3%)	
Type of metastases			
synchronous	10 (45,5%)	17 (21,8%)	**0,027**
metachronous	12 (54,5%)	61 (78,2%)	
Size (3 cm)			
< 3 cm	14 (63,6%)	36 (46,2%)	0,148
> 3 cm	8 (36,4%)	42 (53,8%)	
Location primary tumor			
colon	16 (76,2%)	46 (59,7%)	0,166
rectum	5 (23,8%)	31 (40,3%)	
Affected resection margin			
yes	2 (9,1%)	17 (22,1%)	0,173
no	20 (90,9%)	60 (77,9%)	
Adjuvant treatment primary			
yes	12 (54,5%)	51 (67,1%)	0,279
no	10 (45,5%)	25 (32,9%)	
MSI/MSS status			
MSI	2 (9,1%)	8 (10,3%)	0,872
MSS	20 (90,9%)	70 (89,7%)	

Table 18. Clinicopathological characteristics of the patients included in the TMA.

3.1.1. Segmentation analysis results

The machine-learning algorithm in the InForm software was trained and applied to segment the tissues into liver, stroma, and tumor compartments. To avoid to manually stablish the

line delimiting the border of liver tumor compartments, as was done in a pilot study, for the current project we have added an extra marker, the Hepatocyte Specific Antigen (HSA). HSA allowed for software training for distinguishing between tumor compartment (Pan-Ck stained) and liver compartment (Pan-Ck and HAS stained).

3.1.2. Analyses of lymphocyte subsets

When looking at lymphocyte subsets in the TMA cohort, the striking differences were observed concerning $CD8^+$ cell population. This analysis showed higher infiltration in dHGP of $CD8^+$ cells when assessing the whole TMA core (total_tissue), thus, considering the cell densities encountered in the three compartments: stroma, tumor, and liver parenchyma (Figure 18, Figure 19, Table 19 and Table 20). Likewise, when excluding liver and considering only tumor compartment and its surrounding stroma (total_excluding_liver), the density of $CD8^+$ cells was also higher in dHGP (Figure 18, Figure 19, Table 19 and Table 20), suggesting that the changes observed in whole TMA core area were due to the differences present at the metastatic lesion rather than in the adjacent liver parenchyma.

In line with this, when assessing only the adjacent liver compartment, the number of $CD8^+$ cells was significantly higher in non-dHGP (Figure 18, Figure 19, Table 19 and Table 20). These results suggested that the capacity of cytotoxic cells recruitment is not necessarily higher in dHGP, but in this histological pattern, CD8 T lymphocytes would have higher infiltrative capacity, while in non-dHGP these cells were retained in liver parenchyma.

However, considering the total_excluding_liver compartment, the $CD8^+$ cells observed at higher levels in dHGP could be retained at the stromal compartment, as it happens in "immune-excluded" tumors. To discard this, we compared CD8 infiltration only in stromal compartment. With that, we observed no differences between dHGP and non-dHGP, suggesting that the differences observed in whole TMA core and tumor + stroma assessment were not a consequence of immune infiltrates restrained at the stromal compartment (Figure 18, Figure 19, Table 19 and Table 20). In fact, when assessing $CD8^+$ cells in tumor compartment, we observed greater numbers in dHGP, which further demonstrates that the infiltration of these cells was higher in desmoplastic cases and that these cytotoxic cells were located at the site where they carry out their function: over the tumor cells (Figure 18, Figure 19, Table 19 and Table 20).

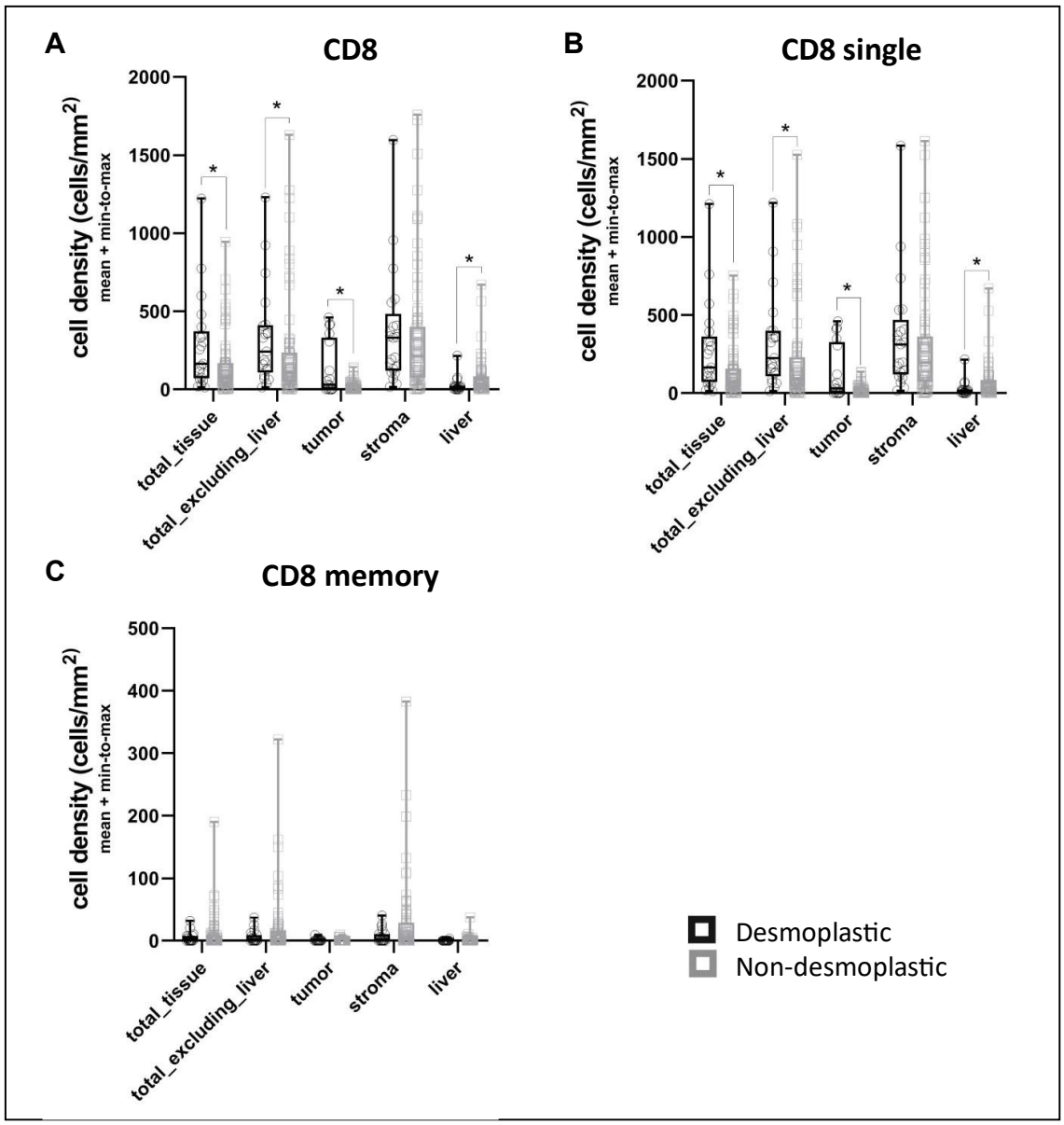

Figure 18. CD8⁺ cell densities in dHPG vs. non-dHPG*. Total CD8 positive cells (A), CD8_single positive cells (B), and CD8 memory (C) at the different compartments. U Mann-Whitney test (ties corrected) and Bonferroni correction for multitesting. *p<0.05*

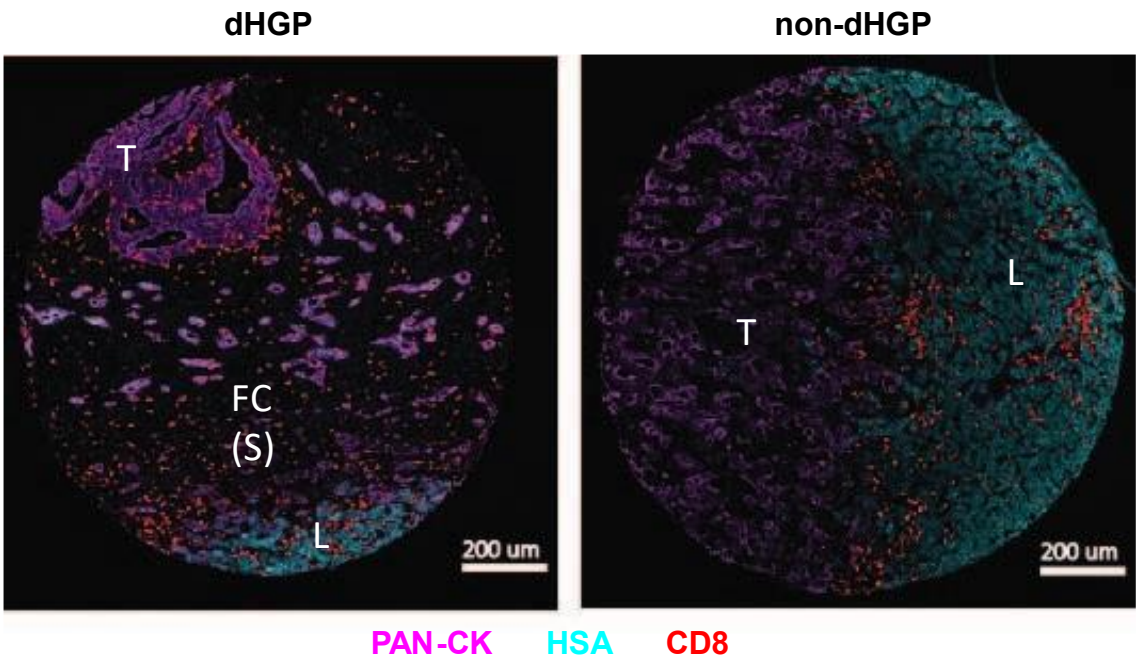

Figure 19. Images from multiplex IHC showing CD8 staining in TMA cores from dHGP and non-dHGP. *In dHGP image one can see that CD8⁺ cells are present in between tumoral cells at tumoral glands region. Meanwhile, in non-dHGP, although high infiltration of CD8⁺ cells can be observed at liver parenchyma, these cells do not infiltrate tumoral glands area and, thus, do not interact with cancerous cells. T: tumor; FC: fibrotic capsule, L: liver parenchyma, S: stroma. HSA stains hepatocytes and PAN-CK stains tumoral glands.*

In contrast with what we had observed in the pilot study, the number of $CD4^+$ cells did not demonstrate significant differences between patterns. Although, $CD4^+$ cells did show higher levels almost all the compartments and cell subsets of non-dHGP cases compared with dHGP, the difference did not reach statistical significance (Figure 20, Table 19 and Table 20).

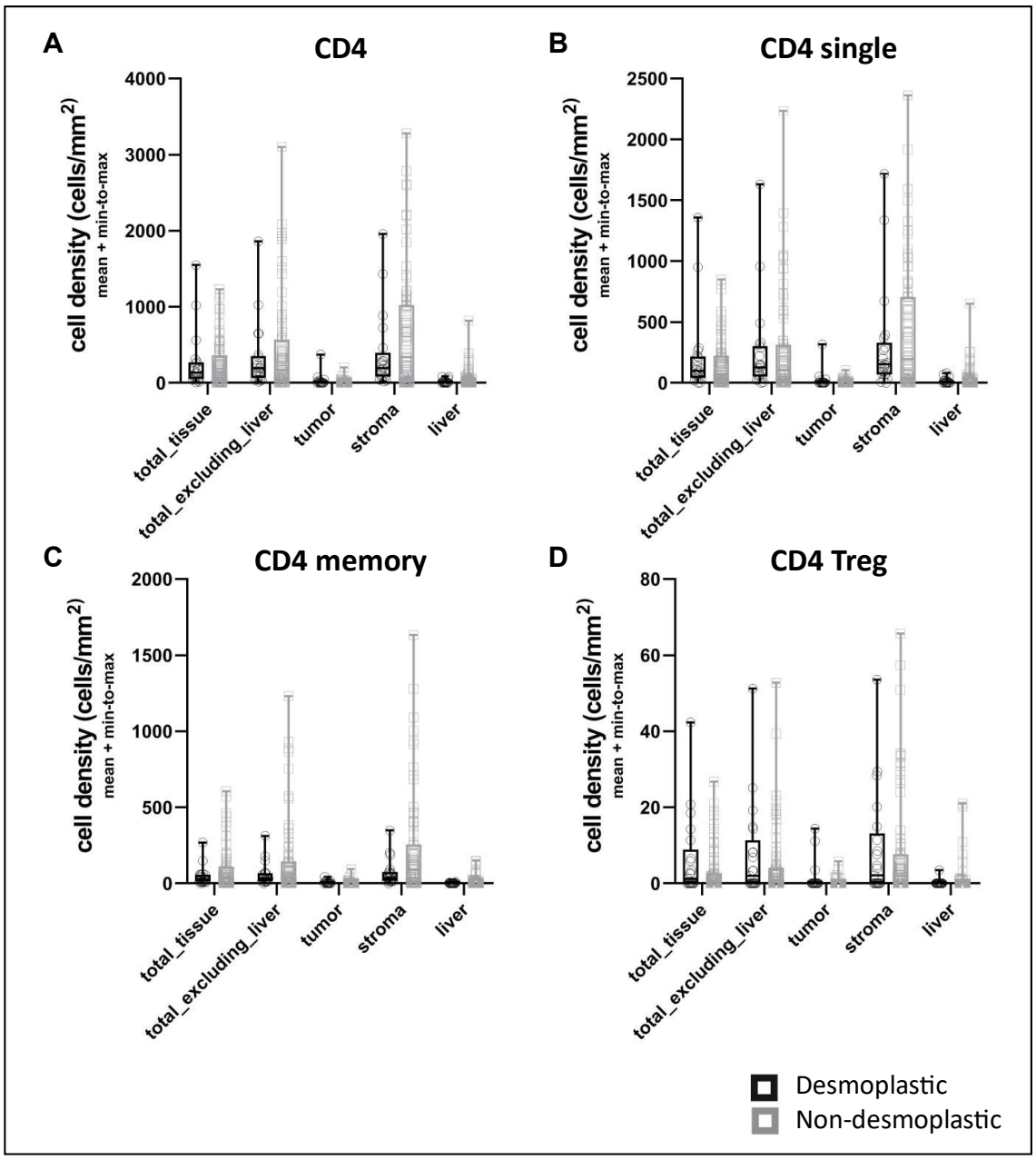

Figure 20. Densities of CD4⁺ cell subsets in dHGP vs. non-dHGP. *Total CD4⁺ cells (A), CD4_single positive cells (B), CD4 memory (C) and CD4 Tregs at the different compartments. U Mann-Whitney test (ties corrected) and Bonferroni correction for multitesting.*

Considering the rest of cell subsets, the density of cells marked for CD45RO, CD20 and FoxP3 are shown in Figure 21 and Table 19. CD45RO⁺ cells and CD20⁺ cells were present at higher numbers in the liver compartment of non-dHGP, which is in line with the previous observation of greater CD8⁺ levels at the same compartment. This supports the hypothesis that in this HGP most immune cell subsets keep retained at liver compartment, without infiltrating the tumor.

On the other hand, FoxP3$^+$ cells were increased in dHGP, both when assessing the total TMA core area and excluding liver region. According to the bibliography, the vast majority of FoxP3 positive cells are CD4$^+$ Tregs (296). However, this population showed no differences between patterns (Figure 21 and Table 19). Therefore, we hypothesized that there are other FoxP3$^+$ cells, which are CD4 negative. It is described that small but detectable numbers of peripheral CD8$^+$, CD4$^+$CD8$^+$, and CD4-CD8-TCRαβ$^+$ T cells express FoxP3, but their function remains unclear. Moreover, CD8$^+$ FoxP3$^+$ cells have been reported to lack the potent suppressive activity that CD4$^+$ FoxP3$^+$ cells have (296,297). This last-mentioned cell subset was also analysed in this assessment, but its presence was at extremely low levels (data not shown). Thus, further research is needed to elucidate the FoxP3$^+$ CD4$^-$ cell subset.

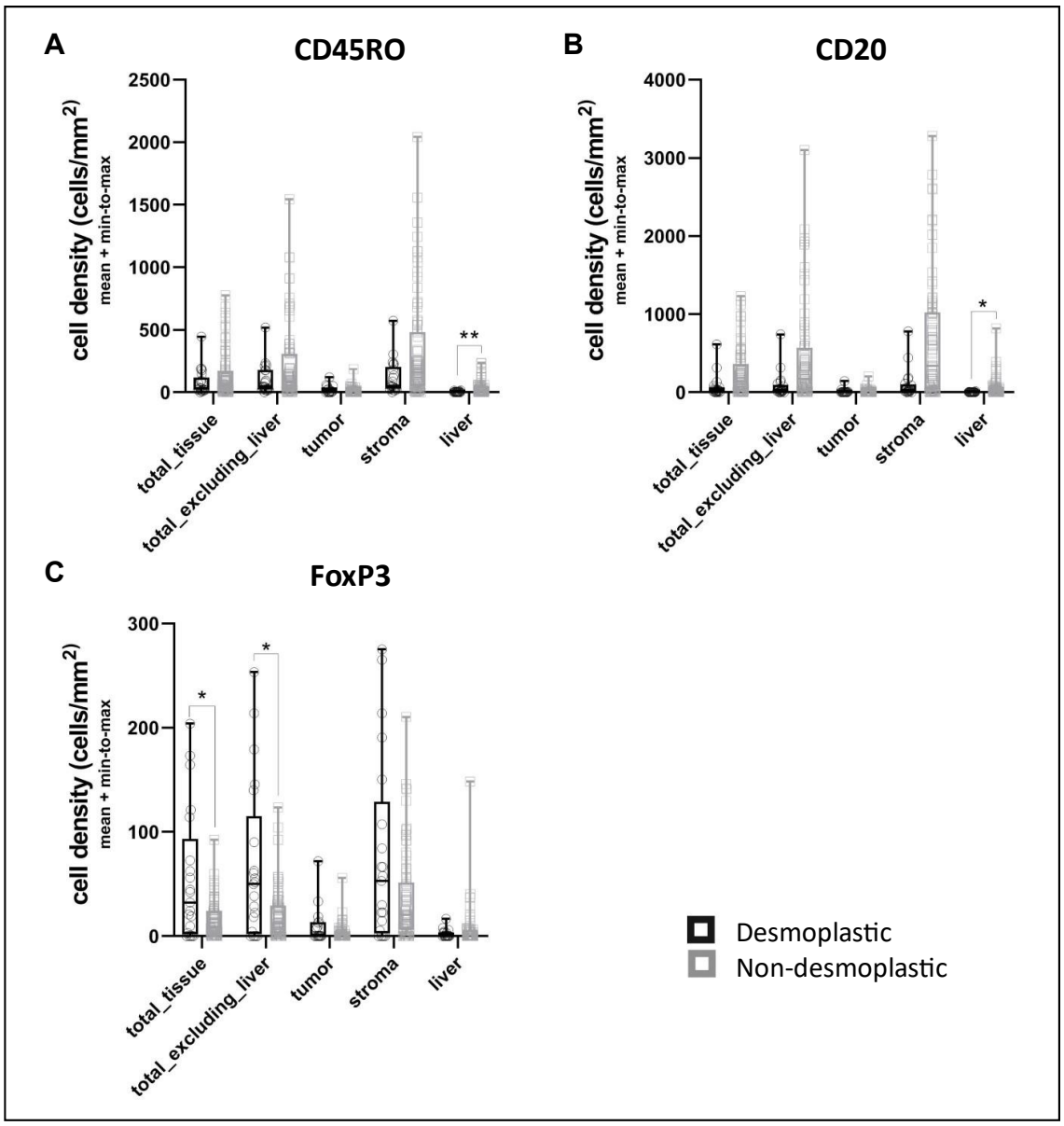

Figure 21. CD45RO⁺, CD20⁺ and FoxP3⁺ cell densities in dHGP vs. non-dHGP. *Total CD45RO positive cells (A), Total CD20 positive cells (B), and Total FOXP3 positive cells (C) at the different compartments. U Mann-Whitney test (ties corrected) and Bonferroni correction for multitesting. *p<0.05*

Cell type	Location	p value U Mann-Whitney	Adjustment multiple testing		Higher in
			p.adj (Bonferroni)	FDR	
CD4	Total tissue	0.475	1	0.662	nd
CD4	Total excluding liver	0.647	1	0.662	nd
CD4	Tumor	0.662	1	0.662	nd
CD4	Stroma	0.621	1	0.662	nd
CD4	Liver	0.146	0.73	0.662	nd
CD8	Total tissue	0.009	**0.045**	**0.021**	**dHGP**
CD8	Total excluding liver	0.010	**0.045**	**0.021**	**dHGP**
CD8	Tumor	0.018	**0.045**	**0.023**	**dHGP**
CD8	Stroma	0.231	0.23	0.231	nd
CD8	Liver	0.013	**0.045**	**0.021**	**non-dHGP**
CD20	Total tissue	0.761	1	0.761	nd
CD20	Total excluding liver	0.643	1	0.761	nd
CD20	Tumor	0.255	1	0.425	nd
CD20	Stroma	0.255	1	0.425	nd
CD20	Liver	0.002	**0.012**	**0.012**	**non-dHGP**
FoxP3	Total tissue	0.011	**0.043**	**0.027**	**dHGP**
FoxP3	Total excluding liver	0.008	**0.039**	**0.027**	**dHGP**
FoxP3	Tumor	0.121	0.24	0.151	nd
FoxP3	Stroma	0.080	0.24	0.133	nd
FoxP3	Liver	0.494	0.49	0.494	nd
CD45RO	Total tissue	0.397	0.84	0.397	nd
CD45RO	Total excluding liver	0.324	0.84	0.397	nd
CD45RO	Tumor	0.281	0.84	0.397	nd
CD45RO	Stroma	0.037	0.15	0.093	nd
CD45RO	Liver	0.000	**0.001**	**0.001**	**non-dHGP**

Table 19. P value, P adj and FDR for the total stained cells for each marker comparison between dHGP and non-dHGP in each compartment. *p.adj, p value adjusted; FDR, false discovery rate; nd, no differences.*

Cell type	Location	p value U Mann-Whitney	Adjustment multiple testing		Higher in
			p.adj (Bonferroni)	FDR	
CD4_Single	Total tissue	0.298	1	0.670	nd
CD4_Single	Total excluding liver	0.402	1	0.670	nd
CD4_Single	Tumor	0.674	1	0.843	nd
CD4_Single	Stroma	0.881	1	0.881	nd
CD4_Single	Liver	0.174	0.87	0.670	nd
CD4_Mem	Total tissue	0.825	1	0.825	nd
CD4_Mem	Total excluding liver	0.698	1	0.825	nd
CD4_Mem	Tumor	0.137	0.55	0.342	nd
CD4_Mem	Stroma	0.223	0.67	0.372	nd
CD4_Mem	Liver	0.012	0.059	0.059	nd
CD4_Treg	Total tissue	0.358	1	0.530	nd
CD4_Treg	Total excluding liver	0.424	1	0.530	nd
CD4_Treg	Tumor	0.290	1	0.530	nd
CD4_Treg	Stroma	0.634	1	0.634	nd
CD4_Treg	Liver	0.123	0.62	0.530	nd
CD8_Single	Total tissue	0.006	**0.032**	**0.017**	**dHGP**
CD8_Single	Total excluding liver	0.007	**0.032**	**0.017**	**dHGP**
CD8_Single	Tumor	0.018	**0.038**	**0.022**	**dHGP**
CD8_Single	Stroma	0.164	0.16	0.164	nd
CD8_Single	Liver	0.013	**0.038**	**0.021**	**non-dHGP**
CD8_Mem	Total tissue	0.495	1	0.495	nd
CD8_Mem	Total excluding liver	0.422	1	0.495	nd
CD8_Mem	Tumor	0.354	1	0.495	nd
CD8_Mem	Stroma	0.244	0.98	0.495	nd
CD8_Mem	Liver	0.044	0.22	0.220	nd

Table 20. P value, P adj and FDR for the single stained cells, and Treg (only in CD4⁺ cells) comparison between dHGP and non-dHGP in each compartment. *p.adj, p value adjusted; FDR, false discovery rate; nd, no differences.*

As we did in the whole-slides pilot study, we assessed the CD8 epithelial / CD8 stroma ratio, which represents the percentage of anti-tumoral associated CD8⁺ cells (epithelial compartment). As expected, and in line with the results obtained at the published pilot study, this ratio showed higher levels in desmoplastic pattern (Figure 22A). This reaffirmed

the fact that CD8⁺ T cells are not only present at greater numbers in dHGP, but also located in tumor nests where they presumably display their cytotoxic function.

Also following the analysis performed in whole-slides study, we analyzed the CD8/CD4 ratio, which was observed higher at dHGP when assessing the total tissue sample (p value=0.056) and the stromal compartment (p value=0.079), although it did not reach statistical significance (Figure 22B). In addition, the ratio between CD8 at tumor compartment / CD4 at stromal compartment was assessed, to evaluate the proportion of CD8 anti-tumoral functional cells (at the tumor compartment) vs. the potentially immunosuppressor activity of CD4⁺ cell subsets present in the stroma. This ratio showed significant differences between patterns, being higher in dHGP. Therefore, the results obtained from these analyses are in line not only with the results obtained when comparing lymphocyte cell subsets, but also with previous results observed in the pilot study.

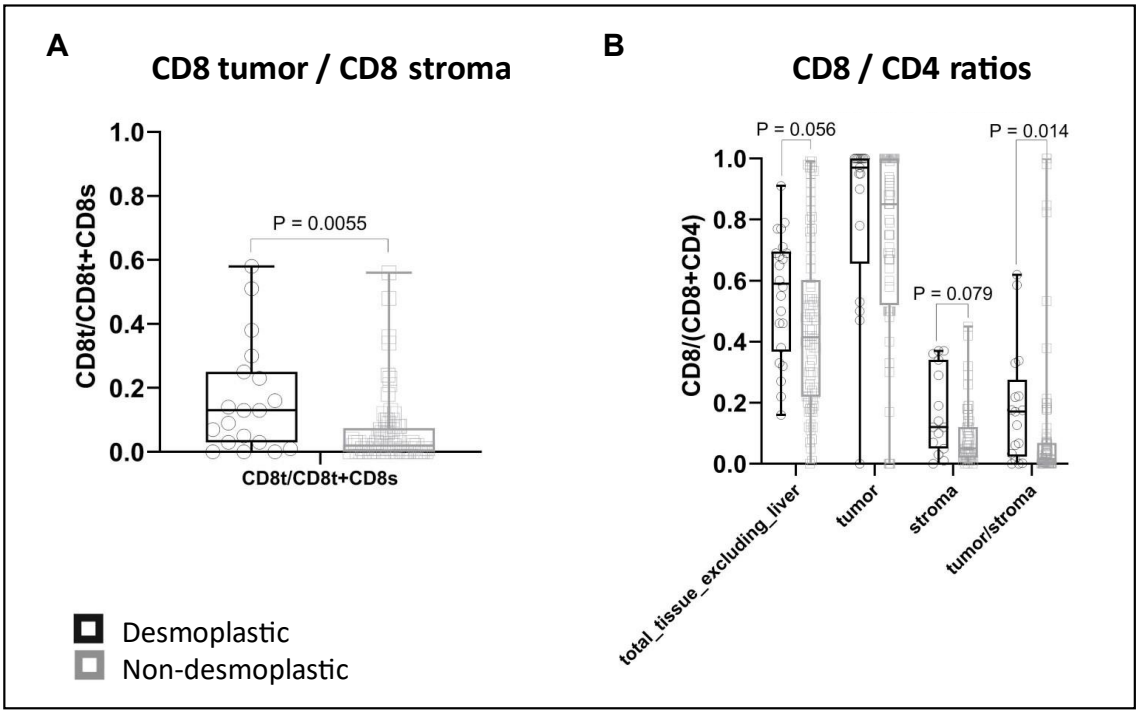

Figure 22. Anti-tumoral status of immune infiltrates in TMA assessment. *A) dHGP vs. non-dHGP comparison of the ratio CD8⁺ cells at tumor compartment / CD8⁺ cells at tumor compartment + CD8⁺ cells at stromal compartment. B) dHGP vs. non-dHGP comparison of the ratio CD8⁺ cells / CD8⁺ cells at total tissue excluding liver, tumor compartment, stromal compartment and CD8⁺ cells at tumor compartment / CD4⁺ cells at stromal compartment. U Mann-Whitney. Mean + min-to-max.*

In brief, the assessment of lymphoid immune infiltrates through mIHC in a cohort of 100 patients showed higher levels of cytotoxic lymphocytes in desmoplastic HPG. Moreover,

these $CD8^+$ cells were located in tumor nests instead of being restrained in stromal compartment, suggesting an activated state. On the other hand, CD8+, CD45RO+, and CD20+ cells were restrained in liver parenchyma and were not able to infiltrate cancer nests in the non-desmoplastic HGP metastatic lesions, suggesting an insufficient immune response or presence of strong local immunosuppressive factors in this HGP.

3.1.3. Additional lymphocyte cell population assessment

The results obtained through mIHC in the pilot study showed an anti-tumoral status of the immune infiltrates in the invasive margin of non-dHGP, as high level of $CD4^+$ and low level of $CD8^+$ cells were observed (Figure 17 upper panel). Moreover, with the spatial analysis, we had observed a modest increase in $CD4^+$ $FoxP3^+$ Tregs in non-dHGP (Figure 15A), although this was not observed when assessing the whole invasive margin area, neither in TMA results. Thus, we wondered if there could be other pro-tumoral T helper populations increased in non-dHGP. Among $CD4^+$ T helper subsets, the cells Th2 are present in many different tumors (294). These cells are described to drive the polarization of macrophages towards M2-type and, thus, contribute to create an immune-suppressive tumor microenvironment (295). For these reasons, we hypothesized that Th2 cells could be contributing to the worse prognoses observed in non-dHGP patients and decided to assess them through their typical CCR4 marker in TMA samples. This analysis revealed that $CCR4^+$ cells were significantly more abundant in non-dHGP (Figure 23), suggesting that these cells could be contributing to create an immune-suppressive environment in non-dHGP cases.

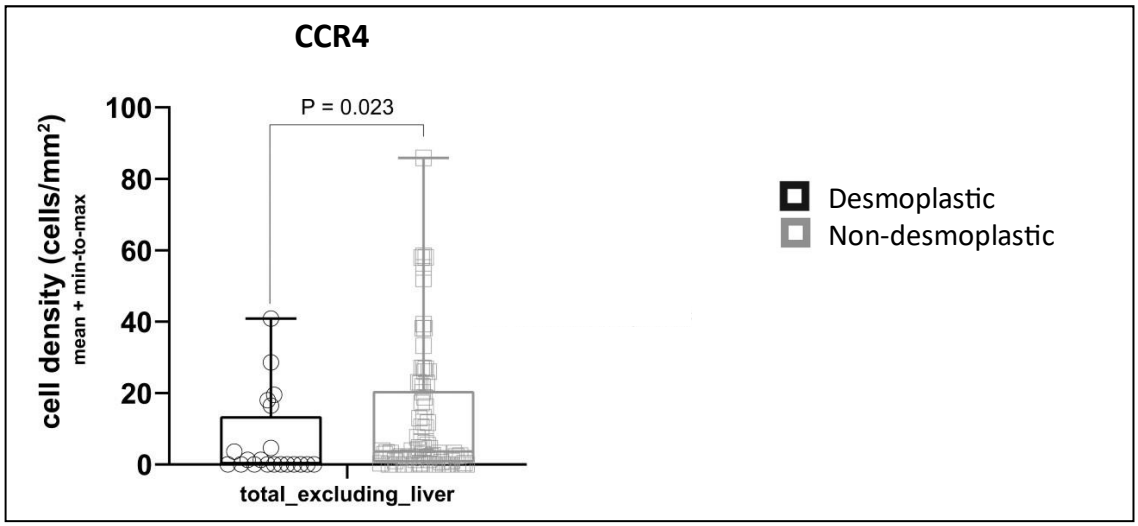

Figure 23. Comparison of CCR4 marker in TMA samples composed by 100 patients. *Cells were manually counted and normalized per tumor area. U Mann-Whitney.*

3.2. Myeloid cells assessment in tissue microarray

In the pilot study and lately in the TMA samples we assessed a panel of immune infiltrates markers focused on lymphoid cells. However, it has been extensively described that the presence of tumor-associated macrophages (TAMs) is associated with poor prognosis in solid tumors (298). TAMs can enhance tumor progression through different ways like promoting immune-suppression, angiogenesis, inflammation and chemoresistance (299). For this reason, we also decided to assess macrophage populations in the context of HGP of CRLM, and to do it through mIHC at TMA samples. For that, we selected CD68, as total macrophage marker; CD163, to determine M2 polarized macrophages (300); and MARCO, that is described to be expressed by tissue resident macrophages marker (116). In addition, we included Calprotectin, which is a heterodimer composed by S100A8 and S100A9 described to be expressed by neutrophils, monocytes, and myeloid-derived suppressor cells (301); as we had previously observed that there were high numbers of infiltrating immune cells positive for this marker in our samples. Concerning its function, Calprotectin, has previously been associated with worse prognoses in different contexts (302–304).

Except global identification of macrophages ($CD68^+$ cells) and M2 polarized macrophages ($CD68^+$ $CD163^+$ cells), the other assessed myeloid markers and the combinations of all of them are difficult to associate to one single subset of cells. There is controversy and promiscuity around these markers cell expression in many myeloid lineage cells, which, in

turn, are plastic cells capable to eventually change their phenotypes. Although the phenotype of these cells should be evaluated in connection to their function, we generated a simplified summary of marker-expression and related phenotypes (Table 21).

Cell population	Markers expressed
Macrophages (global number)	$CD68^+$
Kupffer cells (KC)	$CD68^+$ $MARCO^+$ ($CD163^+$)
Resident inflammatory macrophages	$CD68^+$ $Calprotectin^+$
M1 polarized macrophages	$CD68^+$ $CD163^-$
M2 polarized macrophages	$CD68^+$ $CD163^+$ ($MARCO^-$ if excluding KC)
Neutrophils and/or myeloid derived suppressor cells (MDSCs)	$Calprotectin^+$ (single)
Proinflammatory myeloid cells	$Calprotectin^+$ (total)
Myeloid non-macrophage cells	$CD68^-$ $CD163^+$

Table 21. Markers assessed in myeloid cells mIHC panel.

The obtained results showed higher levels of macrophages (total $CD68^+$ cells, M1-like and M2-like) in non-dHGP cases (Figure 24A-D; Figure 25). These data are in line with the already described association of macrophages with worse outcome, as non-dHGP is the poor survival related HGP (305–307). Moreover, M2 polarized macrophages are described to have a role as tumor tolerance inductors (308). Furthermore, the differences of these cell subsets were observed at total tissue, total excluding liver and stromal compartment, suggesting that the most important changes are located at the stroma, where these cells presumably display their immune-suppressive functions. Thus, macrophages may be inducing and maintaining the immune suppression environment in non-dHGP cases.

Moreover, we found an elevated number of $CD163^+$ cells, which were negative for CD68. Assuming that these cells were not macrophages, we named them “myeloid non-macrophage cells”, as CD163 is considered a marker of myeloid lineage (309). However, nor the cell subset neither its function is known for these cells. They were observed at higher numbers in the stromal compartment and liver of non-dHGP, which suggests that they might be related to the worse outcome of the patients showing this histologic pattern (Figure 24F, Figure 25).

Concerning MARCO staining, as a marker of resident Kupffer cells, no significant differences were observed. No MARCO positive cells were seen inside of the tumoral area (Figure 26), confirming our observations in whole-slides using conventional IHC (Figure 34a). This was validated through the IHC assessment of another Kuppffer cells marker: CD5L (Figure 34). This fact suggests two different situations: On the one hand, it could be that resident $MARCO^+$ cells are not capable to infiltrate the tumor. On the other hand, it could be that these cells infiltrate the tumor but loose MARCO expression. This last explanation would be in line with published single cell RNA sequencing works, in which MARCO expression is detected among tumor infiltrating macrophages (310).

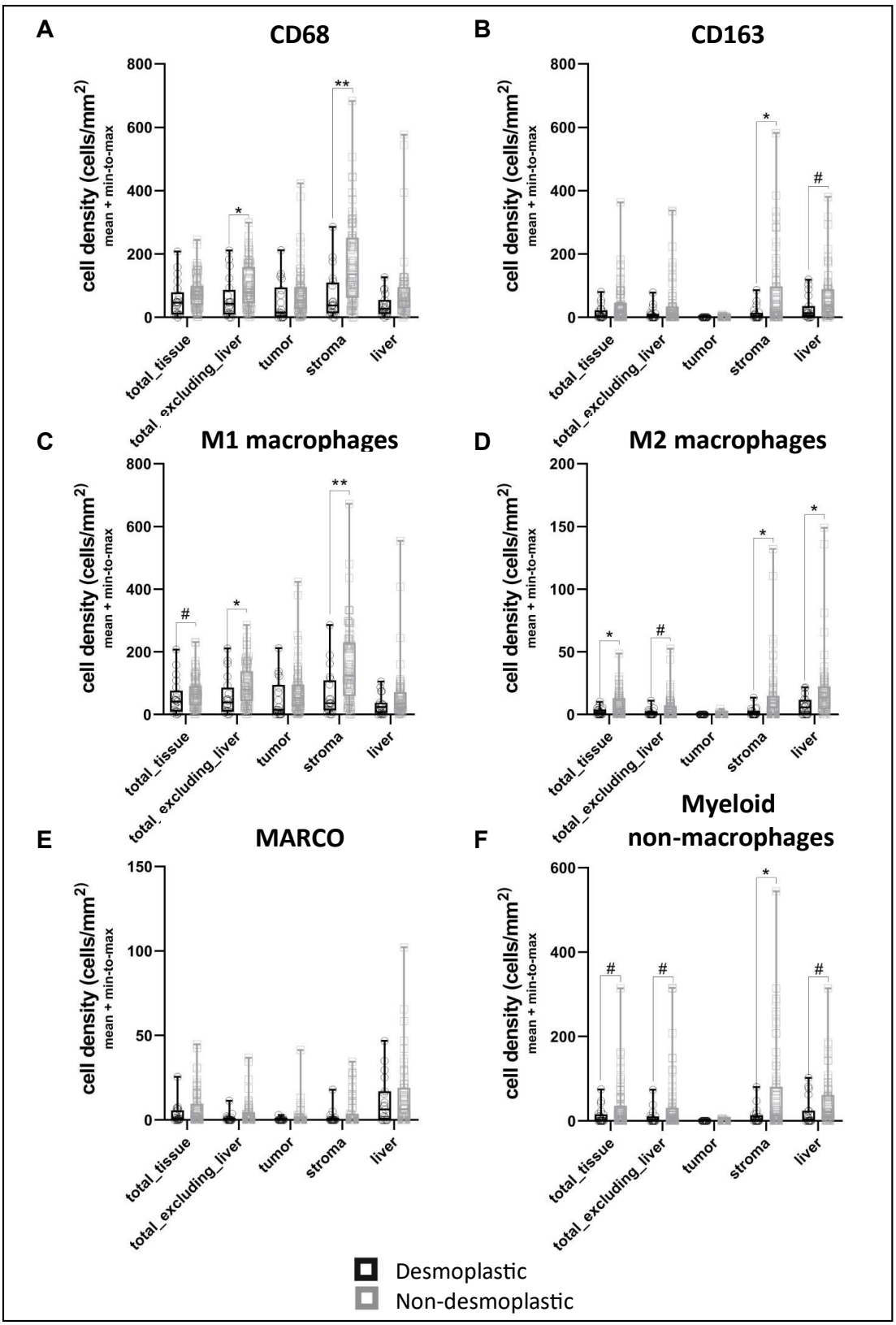

Figure 24. Myeloid cell subsets densities in dHGP vs. non-dHGP. *Total CD68 positive cells (A), Total CD163 positive cells (B), M1 macrophages (C), M2 macrophages (D), Total Marco positive cells (E), and non-macrophages myeloid cells positive for CD163 at the different compartments. U Mann-Whitney test (ties corrected) and Bonferroni correction for multitesting. *p value<0.05, **p value<0.01, *** p value<0.001; #FDR<0.05*

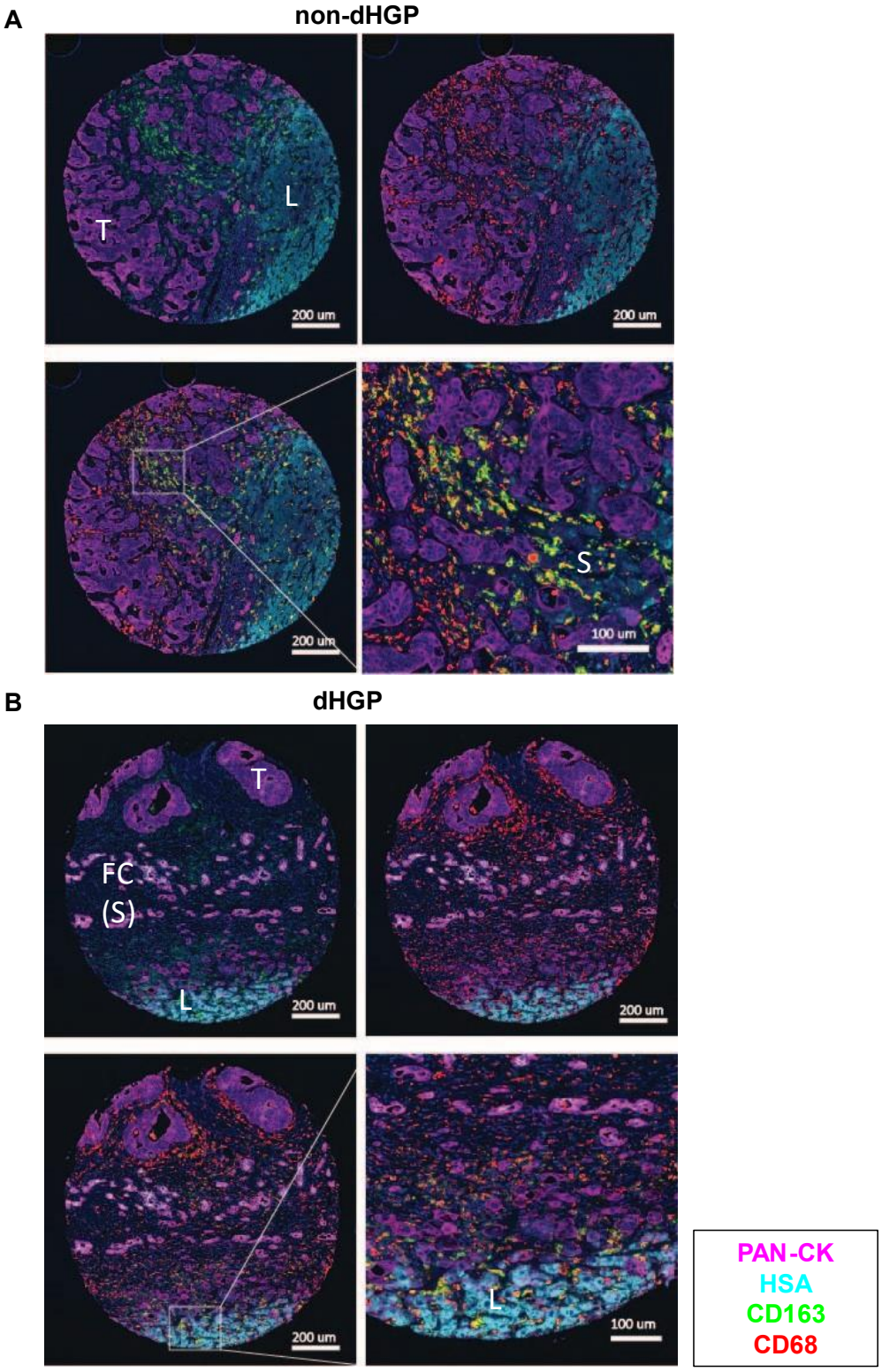

Figure 25. Images from multiplex IHC showing CD163 in green, and CD68 in red. *Yellow-stained cells are the ones in which both markers colocalize, thus, corresponding to M2 polarized macrophages. When comparing non-dHGP (A) with dHGP (B), we clearly observe that in the first ones there is higher amount of CD163 positive cells. This staining includes all CD163^{+} cells: M2 macrophages and "myeloid non-macrophage cells". Moreover, M2 polarized macrophages are present at the stromal compartment of non-dHGP (A), while in dHGP the number of M2 macrophages is slower and are retained at liver parenchyma (B).*

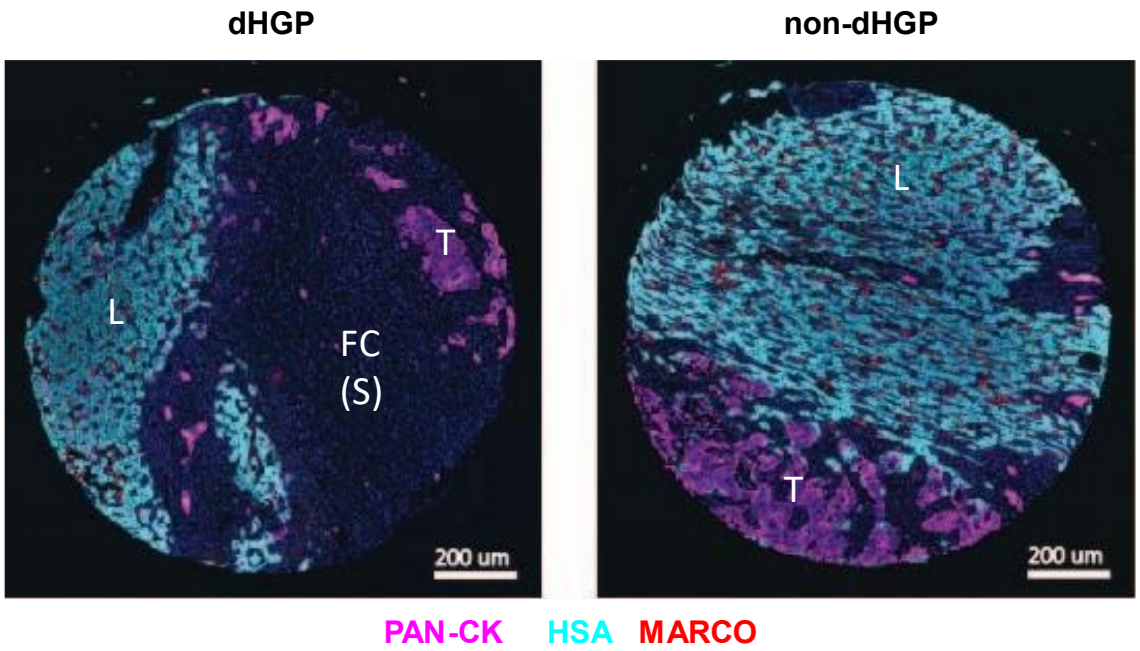

Figure 26. Images from multiplex IHC showing that MARCO staining is kept at liver parenchyma compartment, both in dHGP and non-dHGP.

When analysing Calprotectin marker data, we saw significantly higher levels of these cells in non-dHGP, both total and single Calprotectin^{+} cells, in almost all the compartments assessed (Figure 27). These results matched with the expected, as this marker is related to worse prognoses (311). We also observed that Calprotectin could be expressed in combination with other markers, mostly CD68 (data not shown), but the number of cells expressing a combination of Calprotectin with other markers was very low. Thus, most Calprotectin positive cells were only single-positive for this marker. Figure 28 exemplifies that CD68 do not colocalize with Calprotectin in most of the cases. Thus, this suggests that Calprotectin positive cells are not macrophages.

The statistical data of all the analysed markers is summarized in Table 22 and Table 23.

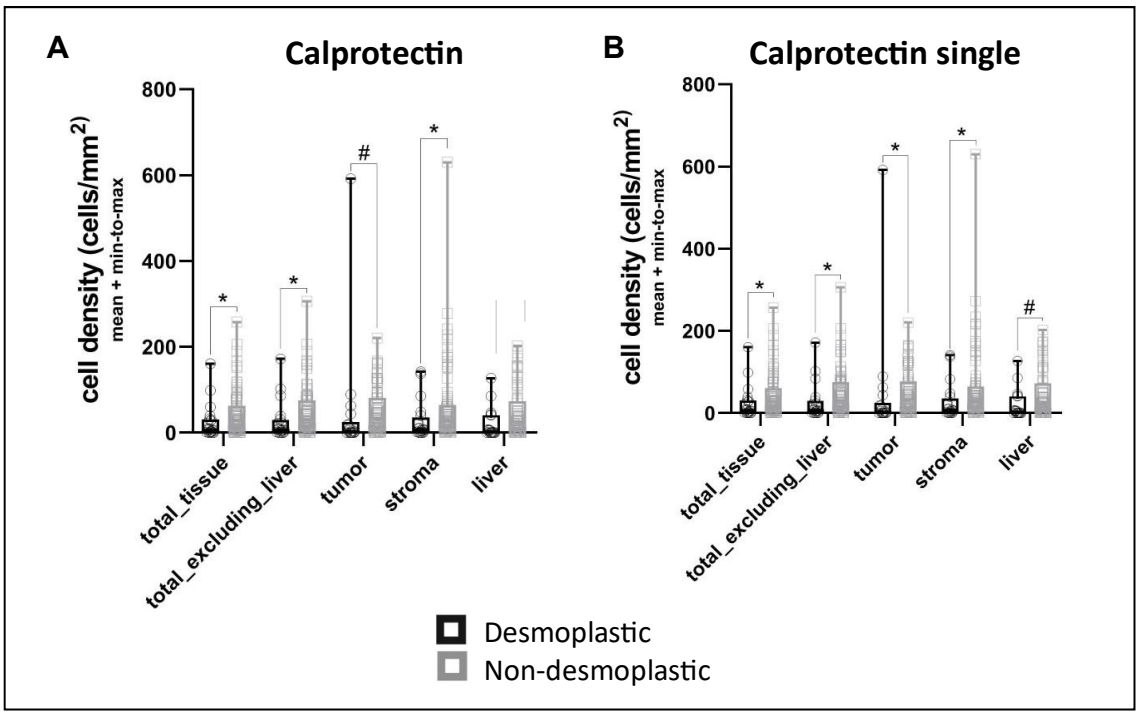

***Figure 27**. **Calprotectin⁺ cells densities in dHGP vs. non-dHGP.** Total Calprotectin positive cells (A), and single Calprotectin positive cells (B) at the different compartments. U Mann-Whitney test (ties corrected) and Bonferroni correction for multitesting. *p<0.05; #FDR<0.05.*

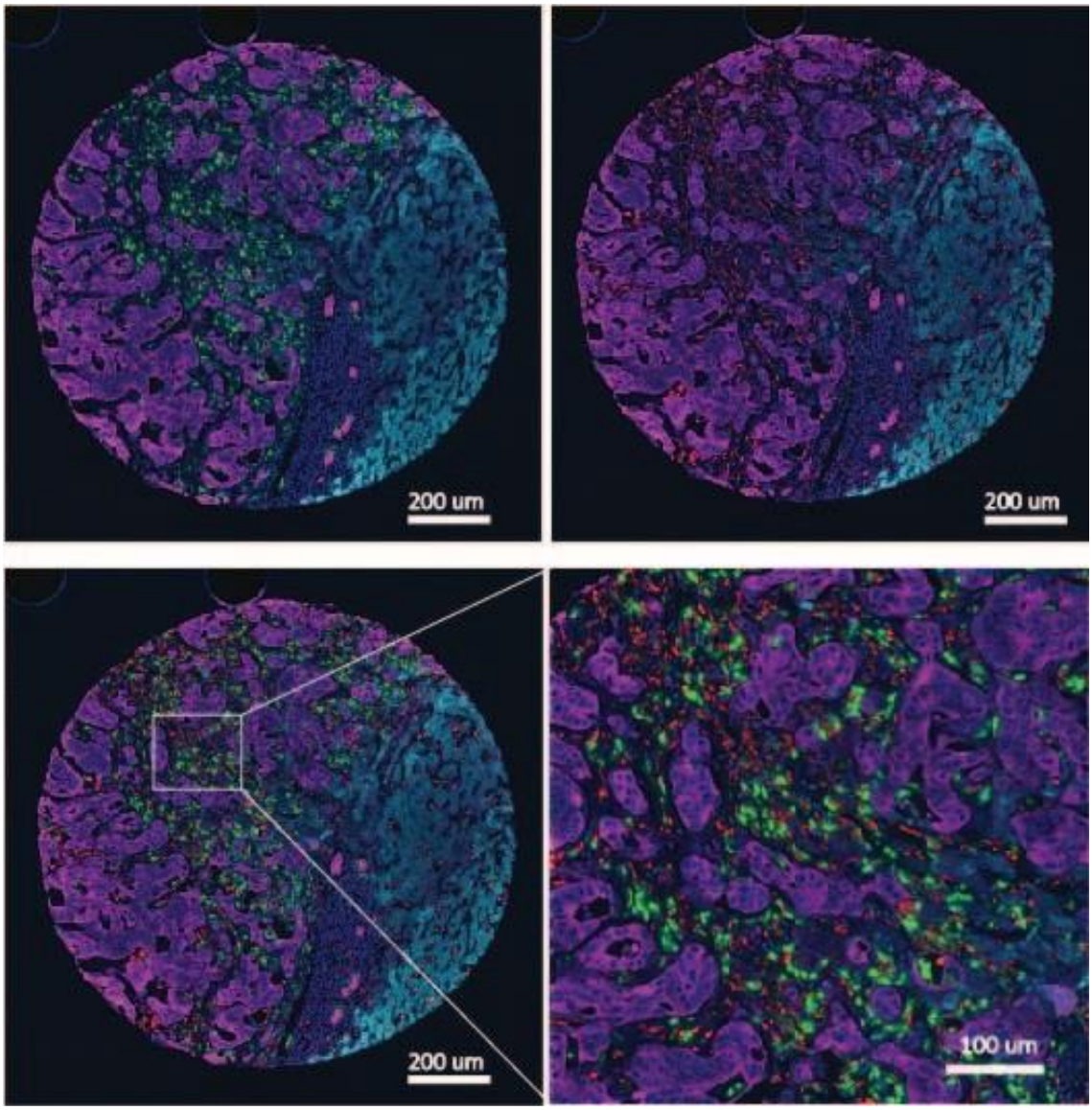

Figure 28. Images from multiplex IHC showing that CD68 and Calprotectin do not colocalize.

Cell Type	Location	p value U Mann-Whitney	Adjustment multiple testing		Higher in
			p.adj (Bonferroni)	FDR	
CD163	Liver	0.017	0.063	**0.031**	non-dHGP
CD163	Stroma	0.007	**0.020**	**0.009**	non-dHGP
CD163	Total excluding liver	0.043	0.086	0.057	nd
CD163	Total	0.043	0.098	0.058	nd
CD163	Tumor	0.089	0.270	0.124	nd
CD68	Liver	0.023	0.063	**0.031**	non-dHGP
CD68	Stroma	0.000	**0.002**	**0.002**	non-dHGP
CD68	Total excluding liver	0.010	**0.029**	**0.019**	non-dHGP
CD68	Total	0.033	0.098	0.058	nd
CD68	Tumor	0.093	0.270	0.124	nd
MARCO	Liver	0.916	0.920	0.916	nd
MARCO	Stroma	0.442	0.440	0.442	nd
MARCO	Total excluding liver	0.159	0.160	0.159	nd
MARCO	Total	0.498	0.500	0.498	nd
MARCO	Tumor	0.217	0.270	0.217	nd
Calprotectin	Liver	0.016	0.063	**0.031**	non-dHGP
Calprotectin	Stroma	0.007	**0.020**	**0.009**	non-dHGP
Calprotectin	Total excluding liver	0.004	**0.018**	**0.018**	non-dHGP
Calprotectin	Total	0.007	**0.029**	**0.029**	non-dHGP
Calprotectin	Tumor	0.002	**0.009**	**0.009**	non-dHGP

Table 22. P value, P adj and FDR for the total stained cells for each marker comparison between dHGP and non-dHGP in each compartment*. p.adj, p value adjusted; FDR, false discovery rate; nd, no differences.*

Cell Type	Location	p value U Mann-Whitney	Adjustment multiple testing		Higher in
			p.adj (Bonferroni)	FDR	
Calprotectin_single	Tumor	0.003	**0.011**	**0.011**	non-dHGP
Calprotectin_single	Total	0.009	**0.037**	**0.026**	non-dHGP
Calprotectin_single	Total excluding liver	0.005	**0.019**	**0.019**	non-dHGP
Calprotectin_single	Stroma	0.007	**0.022**	**0.010**	non-dHGP
Calprotectin_single	Liver	0.019	0.057	**0.028**	nd
M1-macrophages	Tumor	0.095	0.290	0.191	nd
M1-macrophages	Total	0.060	0.073	0.060	nd
M1-macrophages	Total excluding liver	0.010	**0.029**	**0.019**	non-dHGP
M1-macrophages	Stroma	0.000	**0.002**	**0.002**	non-dHGP
M1-macrophages	Liver	0.106	0.110	0.106	nd
M2-macrophages	Tumor	0.245	0.290	0.245	nd
M2-macrophages	Total	0.013	**0.039**	**0.026**	non-dHGP
M2-macrophages	Total excluding liver	0.029	0.059	**0.039**	nd
M2-macrophages	Stroma	0.007	**0.022**	**0.010**	non-dHGP
M2-macrophages	Liver	0.010	**0.038**	**0.028**	non-dHGP
Myeloid_non-macrophage	Tumor	0.147	0.290	0.196	nd
Myeloid_non-macrophage	Total	0.037	0.073	**0.049**	nd
Myeloid_non-macrophage	Total excluding liver	0.066	0.066	0.066	nd
Myeloid_non-macrophage	Stroma	0.019	**0.022**	**0.019**	non-dHGP
Myeloid_non-macrophage	Liver	0.021	0.057	**0.028**	nd

Table 23. P value, P adj and FDR for each cell subset comparing dHGP and non-dHGP in each compartment*. p.adj, p value adjusted; FDR, false discovery rate; nd, no differences.*

Moreover, we also evaluated the ratios between $CD8^+$ cells and M2 polarized macrophages, and the ratio between $CD8^+$ cells and myeloid non-macrophage cells. The first ratio corresponds to metric SIA (Signature of Immune Activation), is described elsewhere (312),

and is used as an approximation of the activity of the immune infiltration. Therefore, this parameter reflects the "balance" between anti-tumoral and pro-tumoral immunity. We observed higher levels of SIA metric in dHGP, both considering the total TMA core area and at stromal compartment (**Figure 29**A and Table 24). This suggests that immune activity is higher in desmoplastic cases. Furthermore, we assessed the second mentioned ratio as we had observed a lot of myeloid cells positive for CD163 and negative for CD68 in our samples, and we postulated that those cells may be playing a tumor-promoting role. The ratio CD8/Myeloid non-macrophage cells showed the same tendencies than SIA (Figure 29 and Table 24), suggesting that those cells display pro-tumoral functions. Moreover, M1 vs. M2 ratio was also assessed, but no differences between patterns were observed, suggesting that M1 macrophages are not playing as an anti-tumoral subset of cells in this context. Instead, M1 macrophages could be mediating inflammatory processes that may benefit tumor progression. In any case, further experiments may be needed to elucidate the role of M1 macrophages in CRLM lesions.

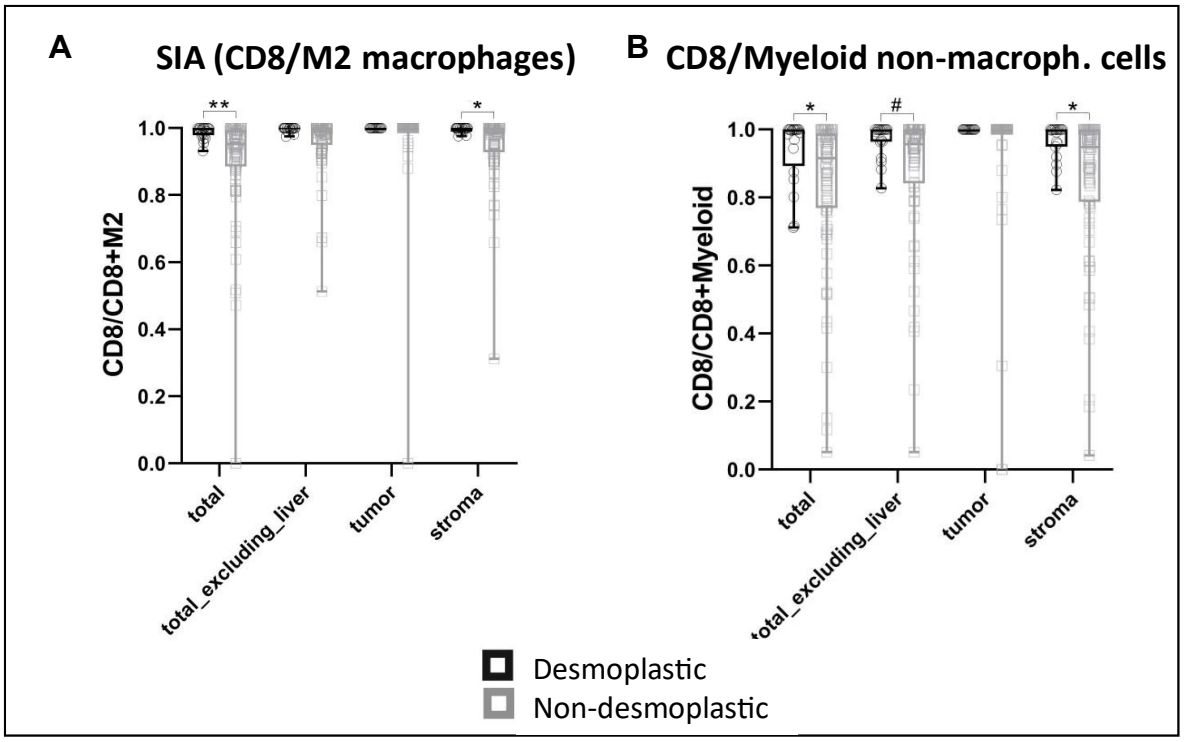

Figure 29. Signature of Immune activation (SIA) assessment in TMA samples. *A) SIA parameter ($CD8^+$ cells vs. M2 macrophages). B) $CD8^+$ cells vs. dHGP vs. myeloid non-macrophage cells. U Mann-Whitney. Mean + min-to-max. * p value<0.05, ** p value<0.01; #FDR<0.05.*

SIA and macrophage ratios	p value U Mann-Whitney	Adjustment multiple testing		Higher in
		p.adj (Bonferroni)	FDR	
CD8/M2_Total	0.001	**0.009**	**0.009**	dHGP
CD8/M2_Total_excluding_liver	0.010	0.077	**0.032**	dHGP
CD8/M2_Tumor	0.236	0.910	0.295	nd
CD8/M2_Stroma	0.005	**0.048**	**0.027**	dHGP
CD8/M2_Liver	0.634	0.910	0.634	nd
M1/M2_Total	0.167	0.910	0.244	nd
M1/M2_Total_excluding_liver	0.171	0.910	0.244	nd
M1/M2_Tumor	0.310	0.910	0.344	nd
M1/M2_Stroma	0.109	0.770	0.244	nd
M1/M2_Liver	0.151	0.910	0.244	nd
CD8/Myeloid_non-macrophage_Total	0.006	**0.025**	0.035	dHGP
CD8/Myeloid_non-macrophage_Total_excluding_liver	0.033	0.066	**0.044**	dHGP
CD8/Myeloid_non-macrophage_Tumor	0.125	0.125	0.125	nd
CD8/Myeloid_non-macrophage_Stroma	0.016	**0.048**	0.032	dHGP

Table 24. P value, P adj and FDR for SIA parameter and M1/M2 ratio comparing dHGP and non-dHGP in each compartment*. p.adj, p value adjusted; FDR, false discovery rate; nd, no differences.*

In conclusion, the assessment of a panel of myeloid cell markers through mIHC in the TMA cohort showed that non-dHGP samples, specially in the stromal compartment, are enriched in pro-tumoral myeloid cell subsets, including M1 and M2 macrophages, myeloid cells and Calprotectin$^+$ cells. Moreover, the SIA metric is higher in desmoplastic HGP, suggesting that the assessed myeloid immune cell subsets are mediating an immune-suppressive environment in non-dHGP cases.

3.2.1. Additional myeloid cell populations assessment

TMA mIHC showed that Calprotectin$^+$ cells were more abundant in non-dHGP. As mentioned before, high levels of cells positive for this marker have been associated with worse prognoses (304). Thus, we hypothesized that Calprotectin$^+$ cells conform a cell population with pro-tumoral functions. Moreover, as this marker can be expressed by different myeloid

cell subsets, we wondered to which cell type may these cells belong. Because of that, we decided to try other marker, Myeloperoxidase, by conventional IHC in our TMA samples. Myeloperoxidase is a peroxidase that is expressed mainly in neutrophils but can also be present at lower levels in monocytes and, in fact, in all myeloid cells (313). The results obtained showed significantly higher levels of Myeloperoxidase positive cells in non-dHGP (Figure 30). The shape of these cells was quite similar to the Calprotectin^{+} ones: more rounded than macrophages or myeloid non-macrophage cells. This, together with the fact that they are at higher levels in non-dHGP, lead us to postulate that they could be the same cell population.

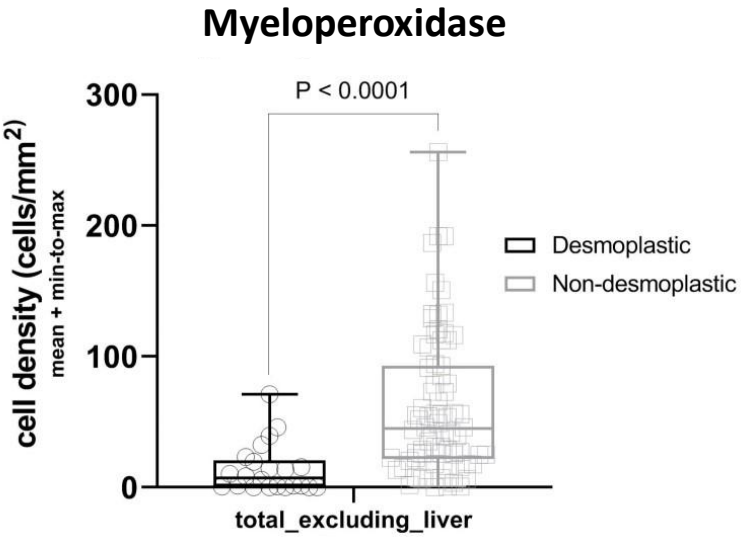

Figure 30. Comparison of Myeloperoxidase marker in TMA samples composed by 100 patients*. Cells were manually counted and normalized per tumor area analyzed. U Mann-Whitney test.*

3.3. TMA assessment of TGFβ1 pathway activation

Previous results exposed suggest a major grade of immunosuppression in non-dHGP cases. In CCR advanced stages, it is widely described the role of TGFβ1 as a promoter of the tolerogenic/immunesuppressor environment, which would be secreted by CAFs (314). Therefore, we assessed the activation of this pathway through IHC for pSMAD2, a protein that is activated downstream the binding between TGFβ1 and its receptor. pSMAD2 was observed to be more abundant in non-dHGP, considering both stroma and tumor compartment, which suggests that this already described mechanism is a particularity of non-dHGP CRLM (Figure 31).

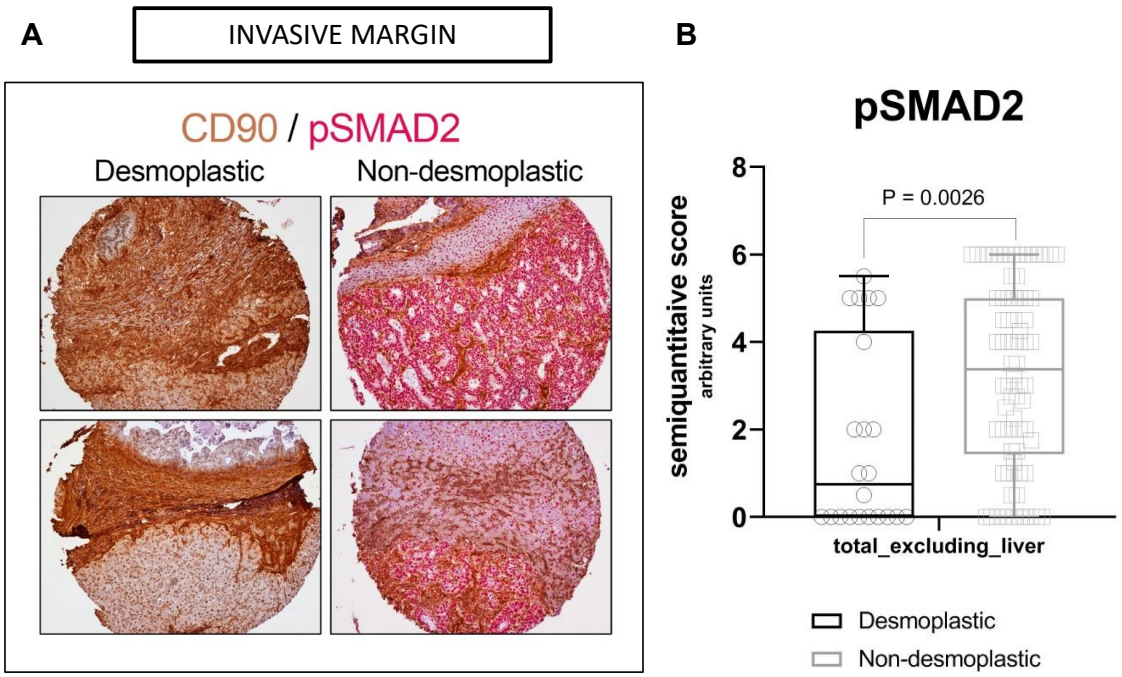

Figure 31. pSMAD2 conventional IHC assessment in TMA samples. *(A) 4x magnification representative TMA cores showing dHGP and non-dHGP samples staining for CD90 and pSMAD2. (B) Comparison of pSMAD2 marker in a TMA sample composed by 100 patients. Cells were manually counted and normalized per tumor area analyzed. U Mann-Whitney test.*

In summary, taking into account the results obtained from TMA samples, we can conclude that an immune-active environment, enriched in cytotoxic T cells, is characteristic of the desmoplastic HGP. Meanwhile, the non-desmoplastic HGP shows high densities of macrophages, myeloid non-macrophage cells and Calprotectin$^+$ cells. All of these cell subsets are associated to a tolerogenic/immunesuppressor environment, which could be mediated by TGFβ1 pathway, as its surrogate marker pSMAD2 is also present at higher levels in non-dHGP.

3.4. Whole slide IHC assessment of lymphoid cells

Moreover, to complete TMA information as it only includes TMA cores from invasive margin areas, we also assessed these markers that showed significant differences in whole-slide samples from a cohort of 30 CRLM patients. Concerning lymphoid cells, we performed a conventional IHC of CD8. This IHC showed higher levels of CD8 not only in the outer part of the fibrotic rim, but also infiltrating it and reaching central regions in dHGP liver metastases, in between tumoral cell niches, as shown in Figure 32A. This, added to the mIHC stainings observed in Figure 19, further confirms that the CD8$^+$ cells present in dHGP samples are

present between tumoral cells, which suggests that these cells are immunologically active. On the other hand, in non-dHGP CRLM, the number of $CD8^+$ positive cells was significantly lower, both in central regions and at the invasive margin. Moreover, the few cells observed were retained at stromal regions (Figure 32B), where they are most probably inactive.

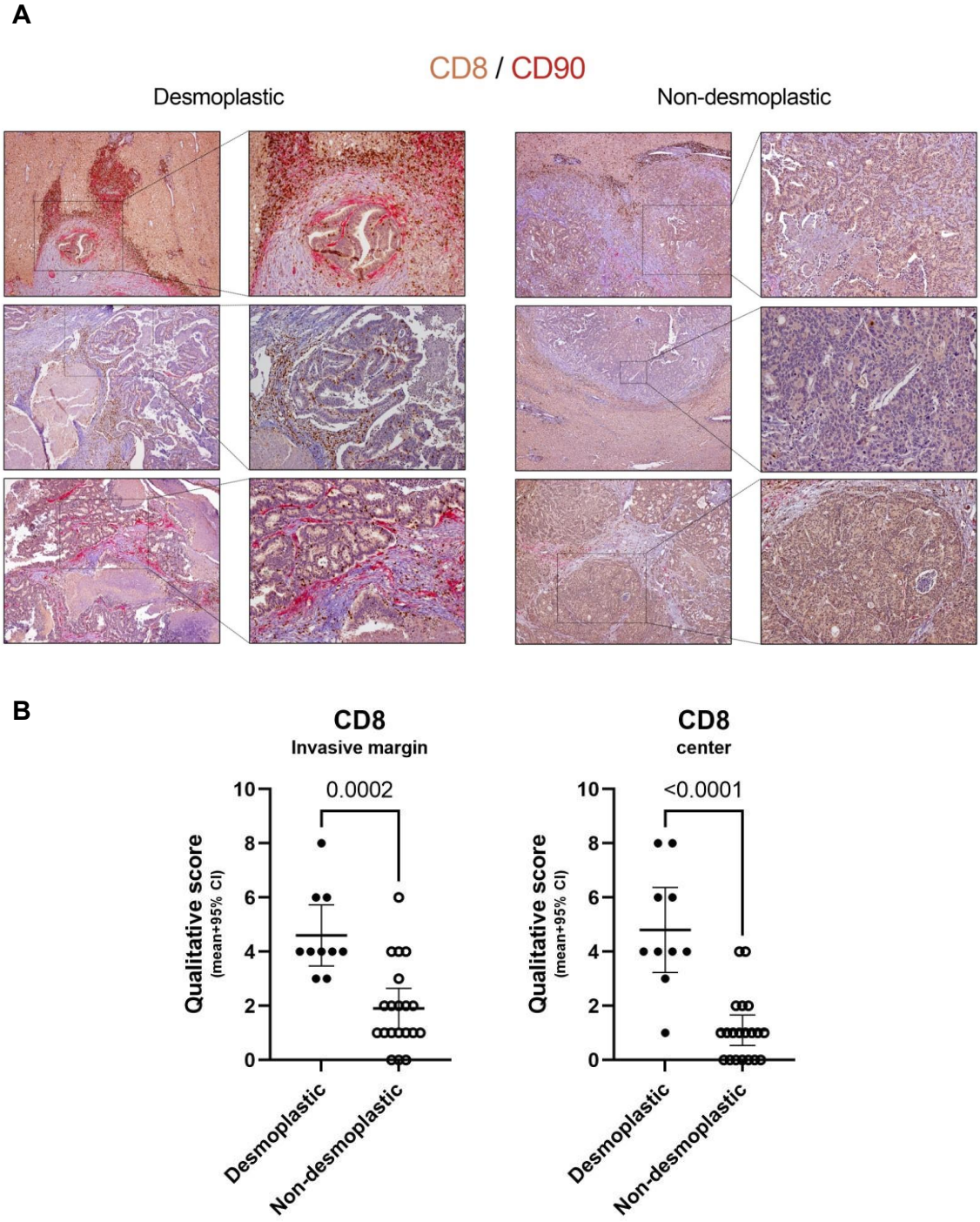

Figure 32. Whole slides $CD8^+$ conventional IHC. *(A) 4x (left column) and 10x (right column) magnification images from a CD8 and CD90 double IHC showing invasive margin and central regions of both dHGP and non-dHGP. (B) Qualitative score showing the presence of CD8 positive cells in dHGP*

and non-dHGP both in invasive margin and tumor centre. Cell density was evaluated in five categories (0-4, absent, slight, moderate, high, very high). The value of the score assigned was 2x when those infiltrates were inside of tumoral niches, while the value assigned was maintained if CD8$^+$ cells were in the stromal compartment. U Mann-Whitney test.

3.5. Whole slide IHC assessment of myeloid cells

We also assessed myeloid cell markers in the whole slides 30 patient cohort. Concerning Calprotectin, this marker was present at high levels in all the regions observed: at the invasive margin, as we had observed in TMA samples, but also in normal adjacent liver and tumor center regions. As expected, the levels of Calprotectin$^+$ cells were observed to be higher in non-dHGP samples (Figure 33A). The quantification of the IHC confirmed the previous observations, as significantly higher levels of Calprotectin$^+$ cells were shown both at the invasive margin and tumor center (Figure 33B). Thus, these results confirmed the ones obtained through mIHC in TMA samples, as well as added the higher presence of Calprotectin positive cells also in central areas of non-dHGP tumors.

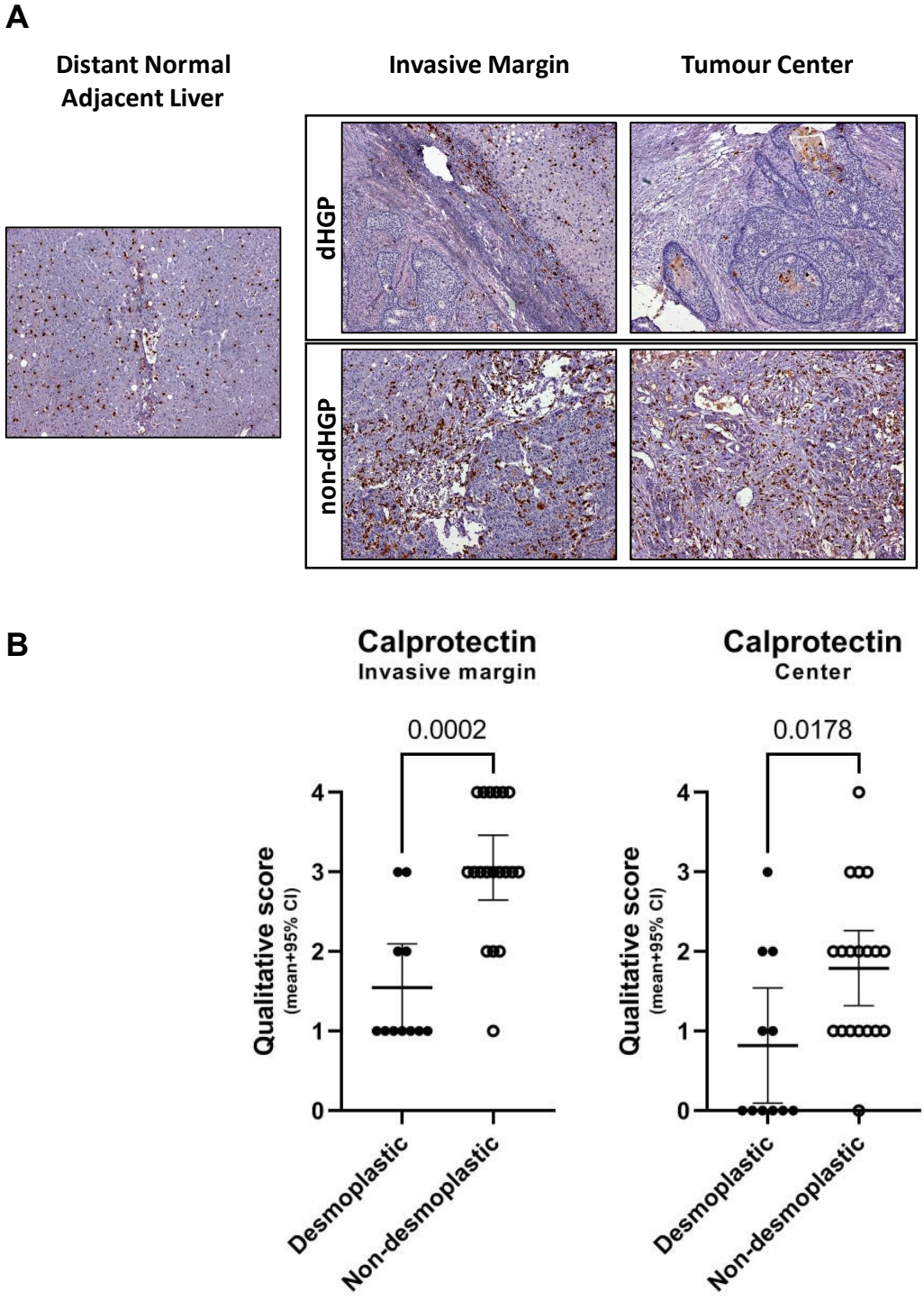

Figure 33. Whole slides Calprotectin⁺ conventional IHC. *(A) 20x magnification of S100A8/A9 (Calprotectin) IHC of both HGP. (B) Five categories qualitative score of the previous staining in 30 different patient samples through a qualitative score (0=absent, 1= less than 100 cells/field of view, 2= 100-200 cells/field of view, 3= 200-300 cells/field of view, 4=more than 300 cells/field of view). U Mann-Whitney test.*

The increased association of this marker with the histological condition with worse prognoses, as well as the already described relation of Calprotectin with worse prognoses,

makes us wonder which cell type could these cells be in CRLM context. As Calprotectin is described to be expressed in monocytes, macrophages, neutrophils, dendritic cells, and myeloid derived suppressor cells, we thought that the Calprotectin$^+$ cells of our samples may be part of one of these cell subsets.

Sonya A. *et al* work using single cell RNA sequencing described two populations of resident macrophages: one with tolerogenic functions, corresponding to Kupffer cells, expressing CD68, CD163 and MARCO; and one with proinflammatory functions, which would be expressing CD68 and Calprotectin (310). We postulated that the small population CD68$^+$ Calprotectin$^+$ observed in TMA results corresponds to the second population. However, TMA results show a very reduced number of CD68$^+$ Calprotectin$^+$ cells (data not shown), which suggest that the vast majority of Calprotectin$^+$ cells observed in CRLM samples are not macrophages.

In line with this, we also assessed CD5L marker, a protein enriched in Kupffer cells (315), which stained cells with the same shape and distribution that MARCO positive ones, confirming that both markers stain tissue resident macrophages. The distribution inside of the tumor was also different between Calprotectin and MARCO: while Calprotectin positive cells were found all around the tumor and liver near the tumor, MARCO positive cells were only observed in liver parenchyma, as we had already observed in TMA mIHC assessment of this marker (Figure 34A). The same happened with CD5L positive cells: they are observed in the liver, but the staining disappears inside of the tumor (Figure 34A). This suggested that MARCO and CD5L markers were staining the same cells, which were different from Calprotectin$^+$ cells.

In addition, we assessed CD163 in whole slide 30 patient's cohort, and compared this staining with consecutive sections stained by Calprotectin (Figure 34B). As it was also observed in TMA mIHC assessment, these conventional IHC demonstrated that Calprotectin positive cells use to be negative for CD163 (although few doble positive cells were observed in TMA mIHC assessment). In these images it could be observed that the shape and the distribution of CD163 and Calprotectin markers was different, suggesting also that they were different cells. Moreover, when observing Calprotectin expressing cells in distant adjacent

normal liver (Figure 33A), we see that these cells are round and show a different shape and location than Kupffer cells or other CD163 positive cells.

Furthermore, we did double IHC for MARCO and CD68 in the whole slide 30 patient's cohort. This IHC showed that MARCO and CD68 mostly colocalize in liver parenchyma, as observed through mIHC in TMA samples. However, in portal spaces there were CD68 positive cells negative for MARCO, suggesting that these cells are recruited macrophages (Figure 34A). Thus, CD68 cells present inside of the tumor, can be both resident macrophages losing MARCO and CD5L, recruited monocytes that become macrophages when reaching the liver, or a combination of both.

Finally, we also performed double MARCO and CD163 IHC, which showed that positive cells for these markers have a very similar shape and co-stain in a lot of cases, indicating that resident macrophages express this marker, but other macrophages, probably the recruited population, can do so. However, although some double positive cells are found at the closer regions of the tumor (Figure 34A, indicated by arrows), as already mentioned, MARCO staining is lost inside of the tumor. Thus, if MARCO cells are not able to infiltrate the tumor, CD163 positive cells found in there would be recruited macrophages.

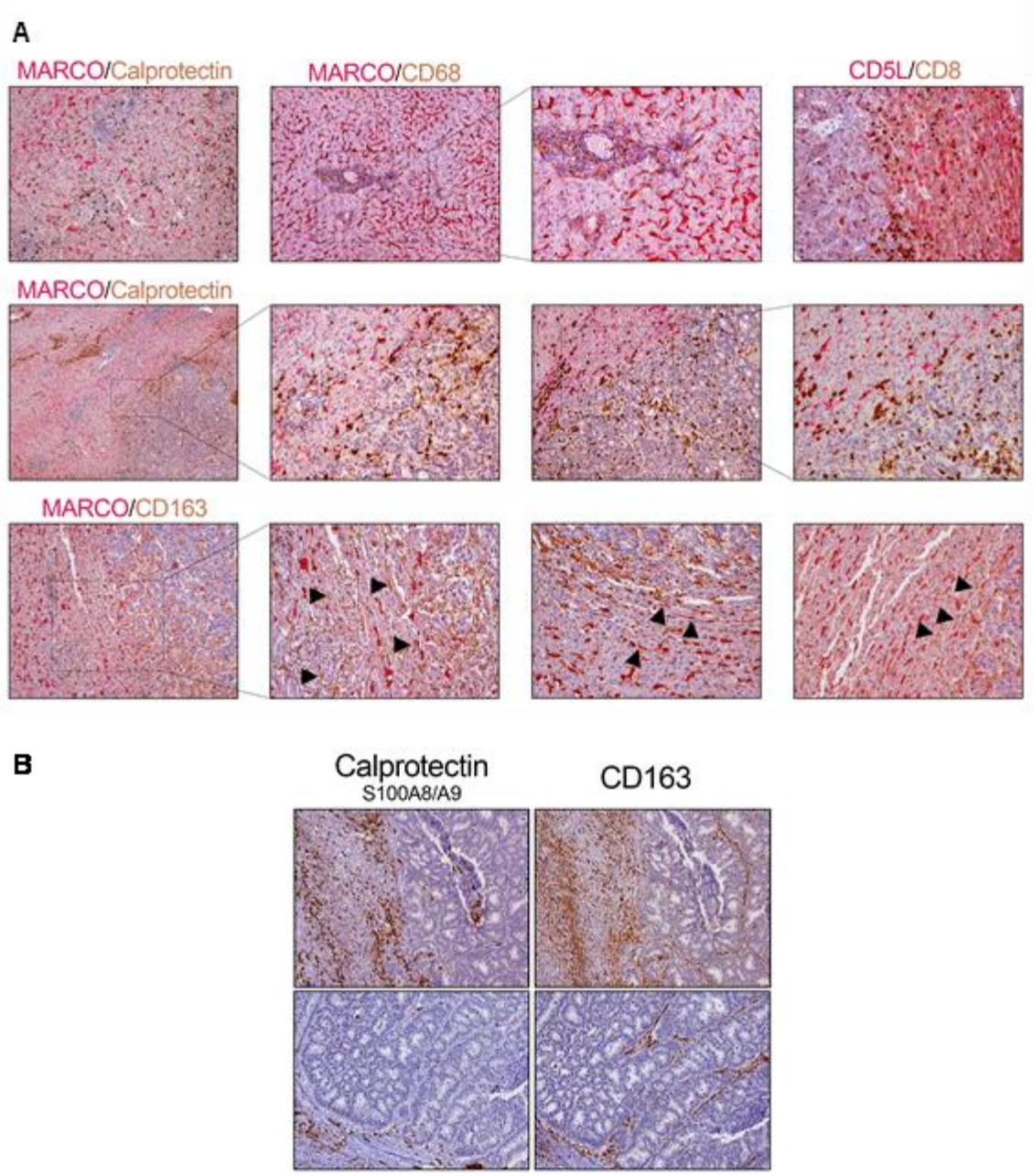

Figure 34. Whole slides MARCO, Calprotectin, CD5L, CD8 and CD163 conventional IHC. *(A) IHC images of CRLM samples. First row, from left to right: normal liver 4x magnification, normal liver 10x magnification, normal liver 20x magnification and non-dHGP invasive margin region. Second row: 4x, 20x, 10x and 20x magnification of non-dHGP invasive margin region. Third row: 10x and 20x magnification of non-dHGP invasive margin region. (B) 20x magnification serial section images showing S100A8/A9 and CD163 IHC staining.*

Considering these results, we assessed the expression of Myeloperoxidase in whole-slide samples, which showed higher levels of expression in non-dHGP, both at invasive margin, in line with TMA results, and tumor center (Figure 35B). Thus, the fact that both Calprotectin^{+} and Myeloperoxidase^{+} were present at higher densities in non-dHGP together with the

similarity they show in shape made us postulate that they could be the same cell subset, but further experiments need to be done to prove it. If these cells are part of the same population, it would suggest that they are neutrophils, which are described to polarize and perform pro-tumoral functions (247,249,250,313).

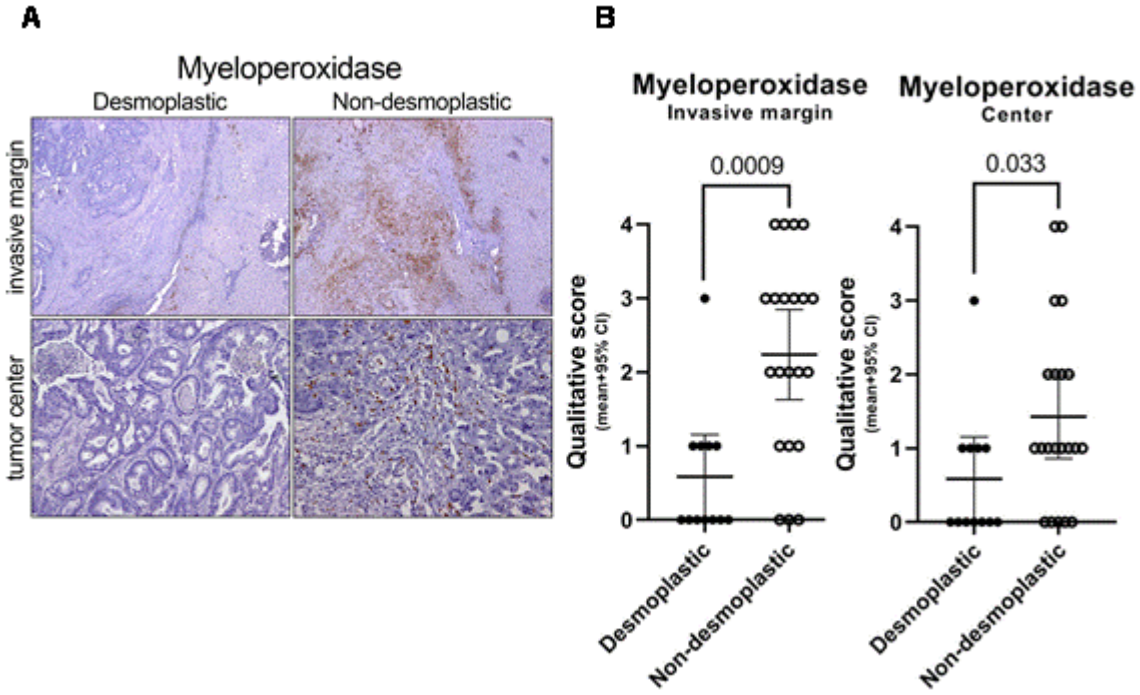

Figure 35. Whole slides Myeloperoxidase conventional IHC. *10x and 20x magnification of S100A8/A9 (Calprotectin) IHC of both HGP. (B) Quantification of the previous staining in 30 different patient samples through a qualitative score. U Mann-Whitney test.*

In conclusion, our results suggest that the Calprotectin positive cells present in CRLM lesions are not Kupffer cells, as they are negative for MARCO and CD5L. Moreover, the vast majority of Calprotectin cells are not macrophages, as TMA results showed that most of them are negative for CD68. Finally, they neither belong to the "myeloid non-macrophage" population observed in TMA ($CD68^-$ $CD163^+$) as their shape and distribution is very different to $CD163^+$ cells and these two markers are neither found together in TMA results. Thus, Calprotectin positive cells could be neutrophiles or dendritic cells. Although $Calprotectin^+$ cells are not $CD163^+$, with this data we cannot reject the possibility that they are myeloid derived suppressor cells, as MDSCs can express, or not, this marker. However, myeloperoxidase stainings suggest that $Myeloperoxidase^+$ cells and $Calprotectin^+$ cells could be the same population, indicating that they may be a pro-tumoral neutrophil subset.

4. Cancer Associated Fibroblasts subpopulations in liver metastases from colorectal carcinoma according to the histologic growth pattern

Cancer associated fibroblasts (CAFs) are the most abundant population of cells present in desmoplastic tumors such as liver metastases from CRC. The current knowledge about CAFs in different tumor types is extended and many different functions have been attributed to them. As CAFs are such a heterogenic cell type, due to the high number of markers they have been described to express as well as the different roles they could be playing, many CAF classifications have already been stablished. However, none of them has been proven to be valid for all contexts. CAFs can arise from different precursors and are very plastic cells, able to acquire different phenotypes depending on the specific signals they receive. Thus, it makes necessary to describe CAF populations in each tumoral context. In the case of liver metastases from colorectal cancer, the study of CAFs has a special interest, as they show the already mentioned histological growth patterns that differ, not only on the number of immune infiltrates present, but also on the type of desmoplasia they display, and the distribution of fibrotic areas present on them. Moreover, different resident cells, mainly HSCs and PFs, can give rise to CAFs. Thus, suggesting the presence of many CAF subpopulations, according to their origin. Moreover, there are three locations were CAFs can also be acting differently: peritumoral CAFs conforming the fibrotic capsule, intratumoral CAFs from the desmoplastic regions, and peritumoral CAFs present at the smaller stromal regions from non-dHGP. Therefore, we hypothesized that each HGP should have different CAFs subpopulations displaying different functions. Thus, we assessed the description of these subpopulations considering: i) markers from liver CAF precursors; ii) CD90 CAF markers; iii) classical CAFs markers.

4.1. CAFs subpopulations in CRLM can be defined according to markers from their precursors

Many origins of myofibroblasts have been described in the context of liver fibrosis: i) resident cells, which include quiescent hepatic stellate cells (HSCs) and portal-located liver fibroblasts (PF); ii) epithelial cells that had undergone epithelial to mesenchymal transition

(EMT), such as hepatocytes, cholangiocytes and endothelial cells; iii) bone-marrow-derived cells like fibrocytes or circulating mesenchymal cells (188). In the context of hepatocarcinoma and liver metastases, the ones that seem to be more implicated are resident cells, especially HSCs (316). Some studies have demonstrated using animal models that HSCs are the main source of CAFs in hepatocarcinoma, cholangiocarcinoma and liver metastases from PDAC and CRC (317–319). The authors of these works also describe two different HSCs-derived CAFs subpopulations, as well as a third present in a smaller proportion that would derive from portal fibroblasts (317–319). Another recently published study, which was performed in CAFs isolated from CRLM neoadjuvant-treated patients, described two main CAF populations. The most abundant of these populations showed an expression pattern similar to portal fibroblasts (320). This suggests that CAF populations may differ and be derived from different precursors and depending not only on the pathology but also on different factors like having received chemotherapy.

Specifically, the CAFs present in liver metastases in the context of the histologic growth patterns are not fully characterized either by the functions they display or the precursors they come from. We hypothesized that the different possible origins for myofibroblasts could give rise to different CAFs subpopulations with different functions. Thus, we aimed to characterize CAFs populations in the context of the histological growth patterns that arise in CRLM and to postulate what could be their origin.

The most reliable way to stablish the origin of any cell type is by performing cell trace experiments *in vivo*. However, animal models appropriate for studying HGP development are still lacking, thus, this kind of experiment cannot be done at the moment. However, as we hypothesised that the different precursor cells give rise to different subpopulations of CAFs, we postulated that we could find markers of HSCs and PFs present in myofibroblasts. Firstly, those markers would define different CAF subpopulations. Moreover, they would suggest the possible precursors to those populations could have arisen.

4.1.1. RNA characterization of HSCs and PFs

Typical markers from HSCs or PFs in conditions of normal liver were broadly described in the bibliography, particularly for the field of fibrosis research. Likewise, much of this research has been carried out in murine models, and this could have a significant bias due to

histological differences between the murine and human liver since it is well established that the amount of connective tissue in the portal tract is lower in rodents compared to humans (321). However, there was a lack of information when looking for specific HSCs and PFs markers that could be maintained when those cells get activated and become CAFs. For this reason, we performed an RNA sequencing (RNA seq) of HSCs and PFs in monoculture as well as HSCs and PF cocultured with two different cells CRC metastatic cell lines. That way, we could, not only know specific HSCs and PFs markers but also which of them were maintained when activated by the presence of tumoral cells, which simulated *in vitro* the activation to myofibroblasts they suffer *in vivo*, as well as specific changes of HSC and PF upon activation that might be suggesting unique roles or functions.

To do this experiment, we used PF previously isolated from normal liver parenchyma. Concerning HSCs, in our laboratory we work with three commercial HSCs: HSC-GFP, hTERT-HSCs, and LX2. To choose the best model for performing the RNAseq, we compared, through qPCR, our isolated PF with these different HSCs. We found that the three cell lines showed different RNA expression of the markers tested compared with PFs. Among these three cell lines, the ones that better fit with the marker expression of HSCs described in the bibliography are HSC-GFP, which are also the only ones that are not immortalized (LX-2 is described to suffer immortalization in low serum conditions) (Figure 36).

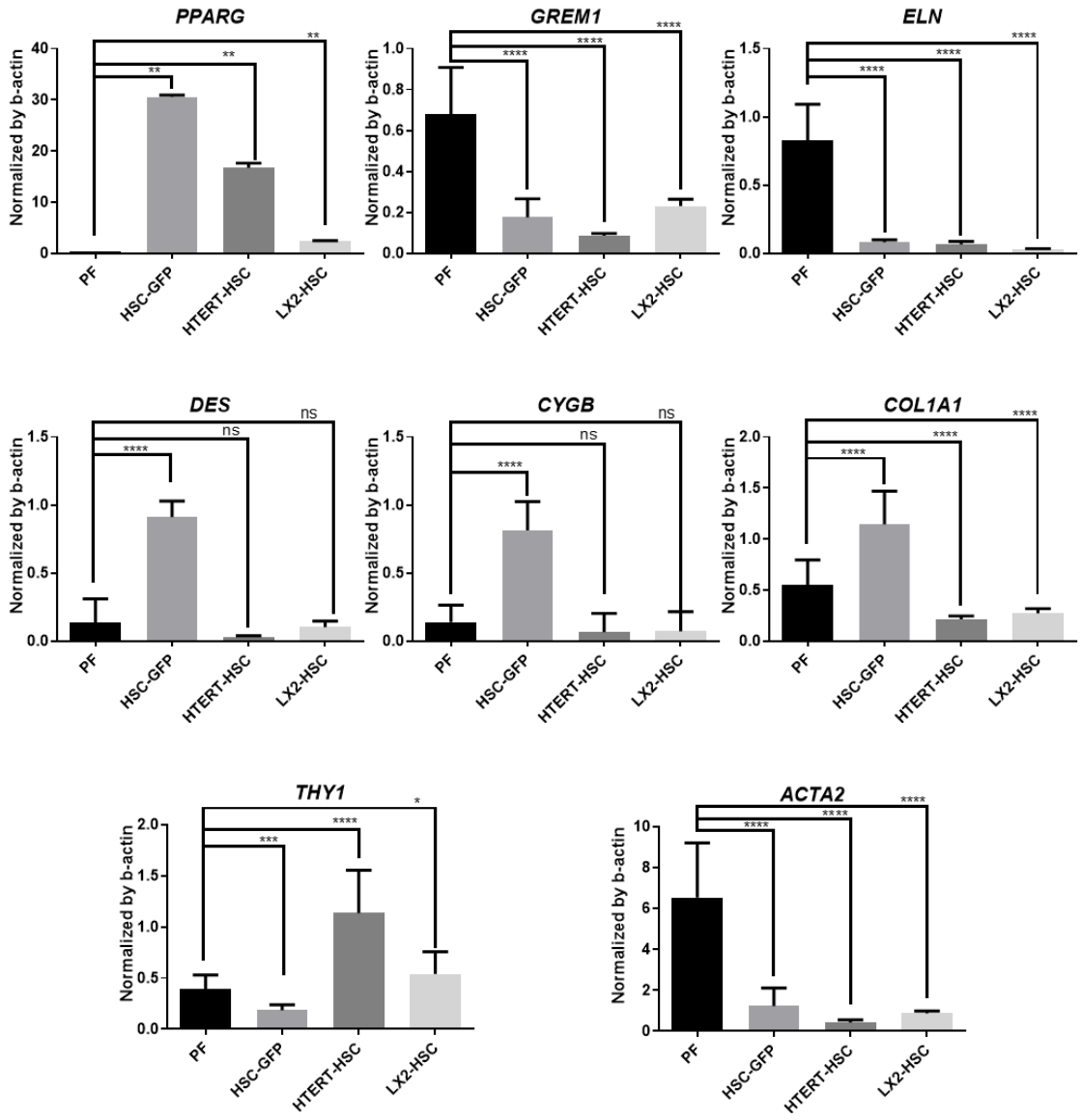

Figure 36. RNA characterization of HSCs and PFs. *Mann-Whitney test comparing the gene expression of PF with each of the HSC cell lines used at our laboratory. Mean with SD (n=4). Mann-Whitney test applied. * p value<0.05, ** p value<0.01, *** p value<0.001, **** p value<0.0001.*

A published article from 2021 (322) described that claudin-2 is characteristic of replacement HGP tumoral cells while claudin-8 is higher in dHGP. We took this information when choosing the two cell lines for the subsequent experiments: LoVo, which has a high expression of claudin 2; and SNU-503, which has a high expression of claudin 8. We also performed RNA seq with those cell lines in monoculture. Mesenchymal cells were stained with CFSE and separated through a cell sorter after 120h of cell culture. A scheme resuming the experiment is shown in Figure 37.

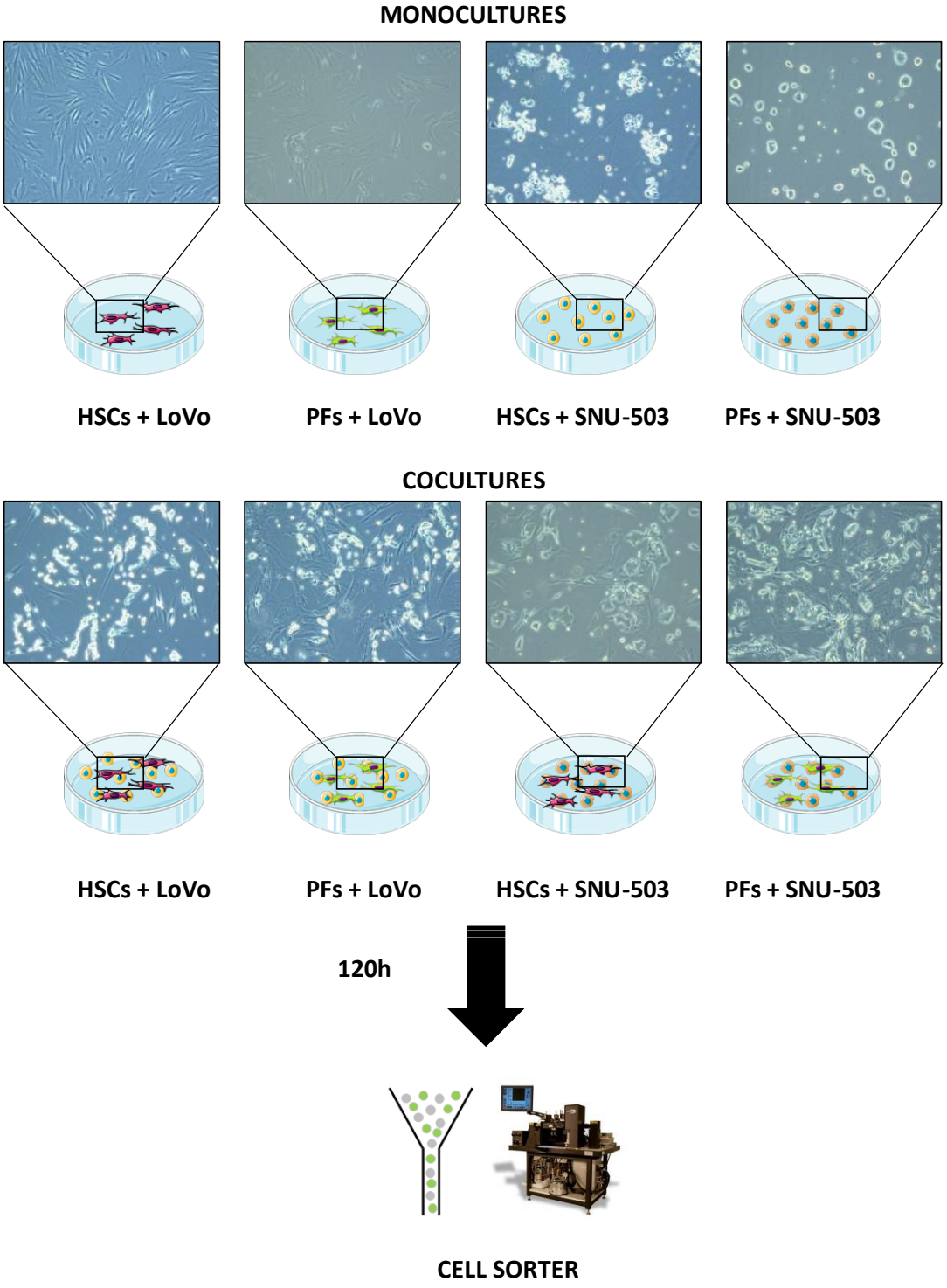

Figure 37. Schema that summarizes the different conditions of the experiment from which we obtained the RNAseq information*. Images shown are taken 120h after seeding the cells, just before the cell sorter.*

4.1.1.1. *RNA seq Principal Component (PC) analysis showed a proper clustering of the cell types analyzed*

The first analysis done with RNA seq information was a principal component (PC) analysis. In this analysis, the cell types cultured at different conditions grouped properly at PC1. Thus, proving that both cell types and the conditions in which they were maintained were different and well-replicated (Figure 38).

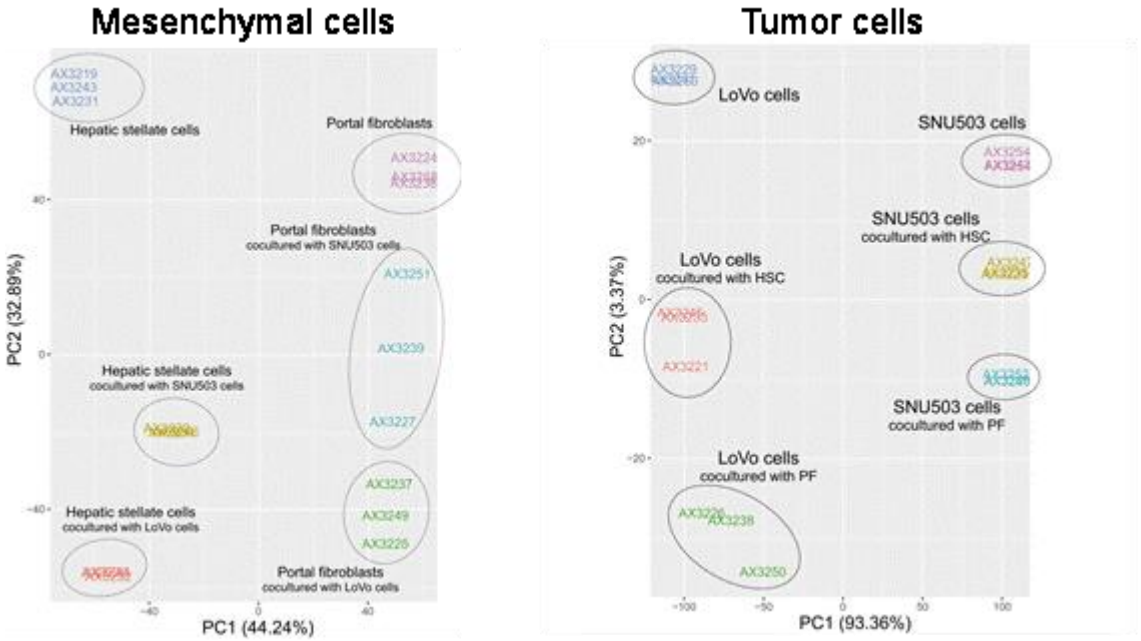

Figure 38. Principal Component representations *showing mesenchymal cells at the left panel and tumoral cells at the right panel groups.*

4.1.1.2. *Fibroblast and CAF genes were differently expressed in PFs compared with HSCs*

Differences in gene expression were observed when comparing HSCs and PFs, both in monoculture and co-culture. When assessing typical fibroblast and CAF markers, we saw that some of the changed between PFs and HSCs, meanwhile others showed no significant differences (Figure 39b).

Using a Log FC >2 or <-2 and p adj value <0.01, 1370 genes were observed to be differentially expressed in HSCs vs. PFs, 758 are upregulated in PFs (Log FC <-2, p.adj<0.01), and 612 are upregulated in HSCs (Log FC > 2, p.adj < 0.01). The 100 with better differences are shown in Figure 39A. Among all of them, we selected the ones that were differentially expressed in

monoculture and those differences were also observed in cocultured cells. That way, we could have a list of genes that were not only present in HSCs and PFs in normal conditions but also maintained when those cells become activated because of the presence of a tumoral cell. These selected genes are shown in the table that appears in Figure 39C.

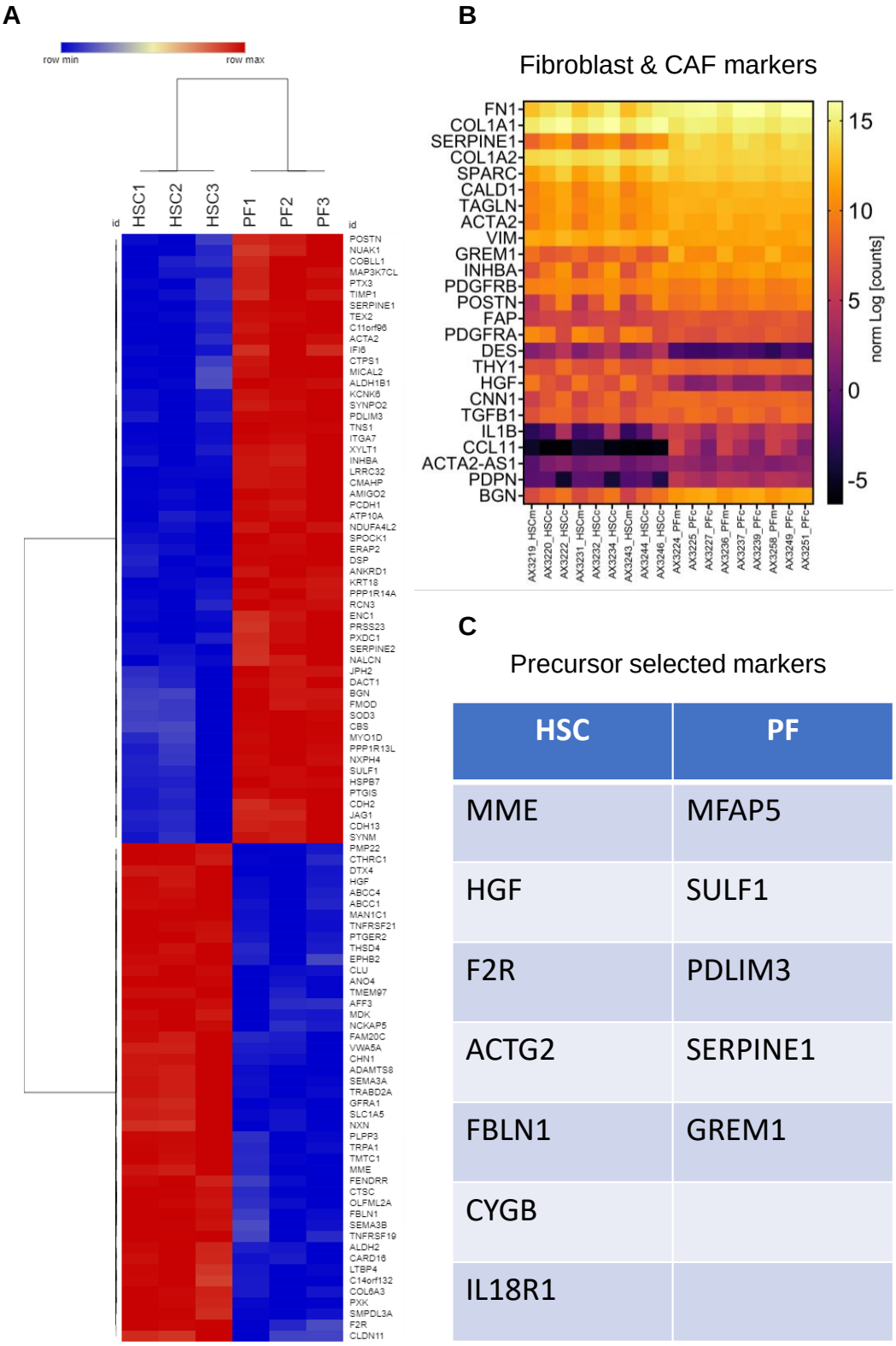

HSC	PF
MME	MFAP5
HGF	SULF1
F2R	PDLIM3
ACTG2	SERPINE1
FBLN1	GREM1
CYGB	
IL18R1	

Figure 39. Fibroblast and CAF genes differently expressed in PFs compared with HSCs. *(A) Heatmap showing the best 100 genes significantly differentiated when comparing HSCs vs. PFs. (B) Heatmap comparing the RNAseq analysis of fibroblast and CAF typical markers in HSCs vs. PFs, both in monoculture (HSCm, PFm) and in co-culture (HSCc, PFc). (C) Table showing a selection of markers that RNAseq analysis showed to be typical of HSCs and PFs that are conserved when activated to myofibroblasts.*

4.1.1.3. Gene set enrichment analysis (GSEA) and HiPathia analysis from RNAseq data showed differences between monocultured and cocultured PF

Gene set enrichment analysis (GSEA) analysis applied RNAseq obtained data revealed that the expression of many gene sets changed when coculturing the PFs (CC PFs). Among the pathways that had been observed to upregulate in co-culture, we find Wnt signaling, TGFβ1 response, PDGF signaling and some ECM formation pathways. Wnt signaling has been reported to be active in CAFs in breast, colon, and ovarian cancer stroma [87]. Although canonical Wnt signaling is not necessary for the function of CAFs in remodeling the ECM, it is needed to induce a tumor-promoting phenotype (323). Concerning TGFβ1, as mentioned before, it is described as a promoter of the tolerogenic/immunosuppressor environment, that is secreted by CAFs in many situations. However, it is involved in a huge number of functions including the promotion of tumor growth, invasive phenotype, and distant metastases dissemination (324). In breast cancer, a study demonstrated that the establishment of self-sustaining CXCL12 and TGFβ autocrine signaling pathways result in the formation of tumor-promoting CAFs (325). Thus, the upregulation of these pathway-related gene sets suggests activation of tumor-promoting CAFs of portal fibroblasts as a response to being co-cultured with tumoral cells. In line with this, as a consequence of this activation, the activated CAFs would increase the production of ECM components.

On the other hand, some oxidative metabolism-related pathways are downregulated, which may also be triggered by the coculture with tumoral cells, as the availability of oxygen in tumors is usually limited. All these results are shown in (Figure 40).

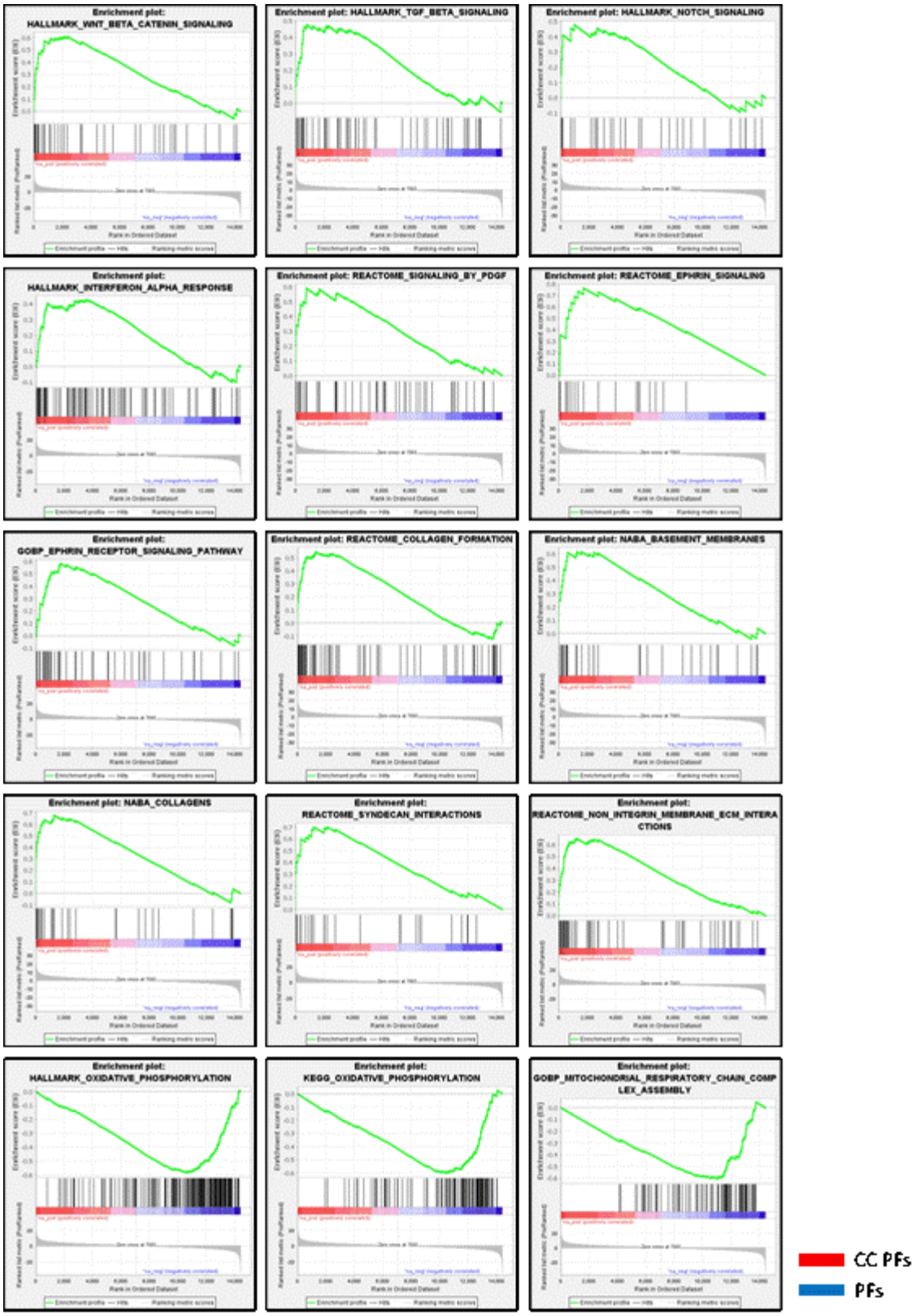

Figure 40. Upregulated and downregulated gene pathways comparing the RNAseq data from cocultured PFs (CC PFs) and monocultured PFs (PFs).

We also analyzed RNAseq data through HiPathia, which is a web tool that is also used for the interpretation of the changes in gene expression levels. HiPathia transforms gene expression data into signaling circuit activities, in the case of PFs shown in Figure 41. In turn, these signaling circuits carry information about the functions triggered by them, shown in Figure 42.

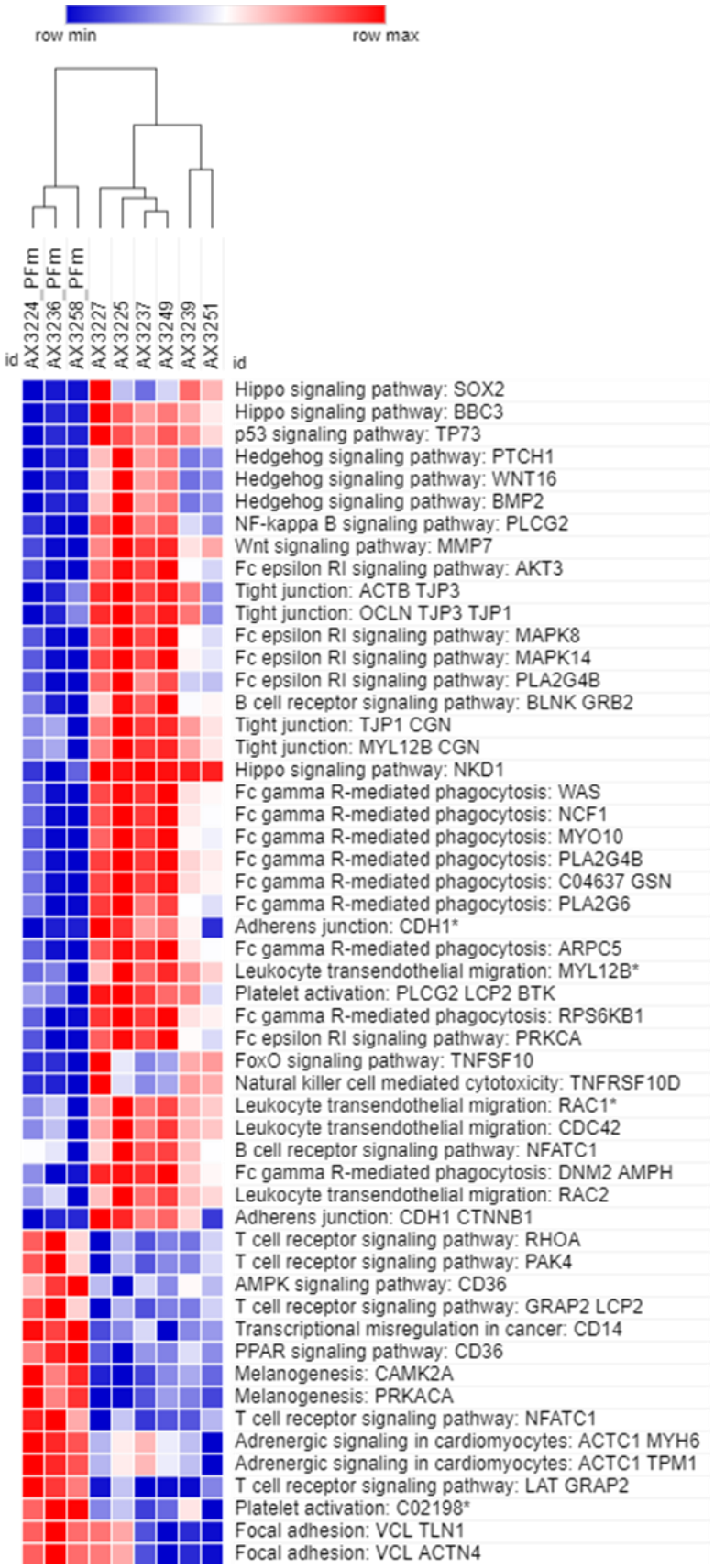

Figure 41. HiPathia transformation of monocultured and cocultured PFs gene expression to signaling circuit activities.

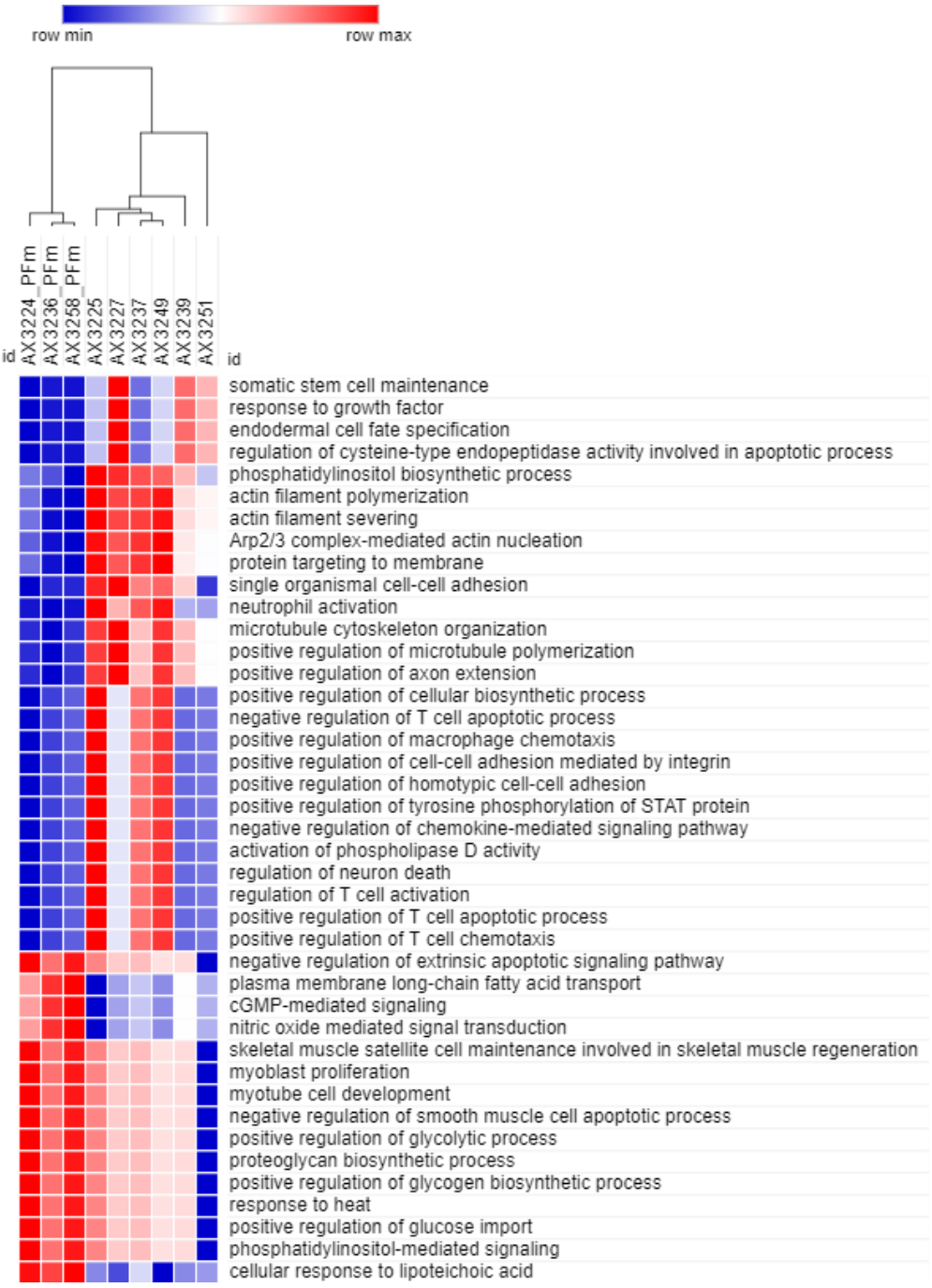

Figure 42. HiPathia transformation of monocultured and cocultured PFs signaling circuit activities to functions.

Considering this information, when cocultured, PFs gain stem cell maintenance, response to growth factors, actin organization related processes and chemotaxis of both macrophages and T cells. On the other hand, cocultured PFs show less glucose import and less negative regulation of apoptosis. These results suggest that, once activated by the presence of tumoral cells, PF acquire a less quiescent and more proliferative phenotype. Moreover, the

upregulation of some immune cell chemotaxis propose that they may play a role on promoting either an immune-active or immune-suppressive environment, depending on which cells are recruited to the tumor site.

In conclusion, when cocultured with tumoral cells, PF increase they expression of pathways related to inflammation and immune cell chemotaxis as well as their myofibroblastic features like actin or ECM organization. Concerning metabolic changes, they reduce oxygen required metabolic pathways as well as glucose import.

4.1.1.4. *Gene set enrichment analysis (GSEA) and HiPathia analysis from RNAseq data showed differences between monocultured and cocultured HSCs*

As we had previously did with PFs RNAseq data, we also analyzed through GSEA and HiPathia the RNAseq data from cocultured HSCs (CC HSCs) vs. monocultured HSCs (HSCs). When cocultured, HSCs gain EMT related pathways, proliferation related pathways, collagen synthesis, glycolysis and hypoxia induced genes. On the other hand, HSCs lose ROS triggered pathways, adipogenesis and complement related pathways (Figure 43). As it happened with PF, when cocultured, HSCs become less quiescent and more proliferative. As an indicator of their differentiation into CAFs, HSCs lose the expression of adipogenesis related genes, and they start producing ECM components, like collagens. However, ECM components produced by HSCs-derived CAFs may be different than the ones produced by PF-derived CAFs. Even different CAF subpopulations could arise from each CAF precursor, playing different roles (318,319) and producing different ECM components. The upregulation of glycolysis and hypoxia induced gens, as well as the loss of ROS triggered pathways, suggest a metabolic change towards Warburg effect, probably induced by tumor cells, due to the reduced oxygen availability in tumor conditions. About complement related pathways, in some tumors including CRC, complement genes have a potential immunosuppressive effect (326). Moreover, a recent report described the presence in CRLM of a CAF subpopulation termed “complement-secreting” (320). Thus, it suggests that HSCs, once activated, could give rise to one or some CAF subpopulations which displays these functions.

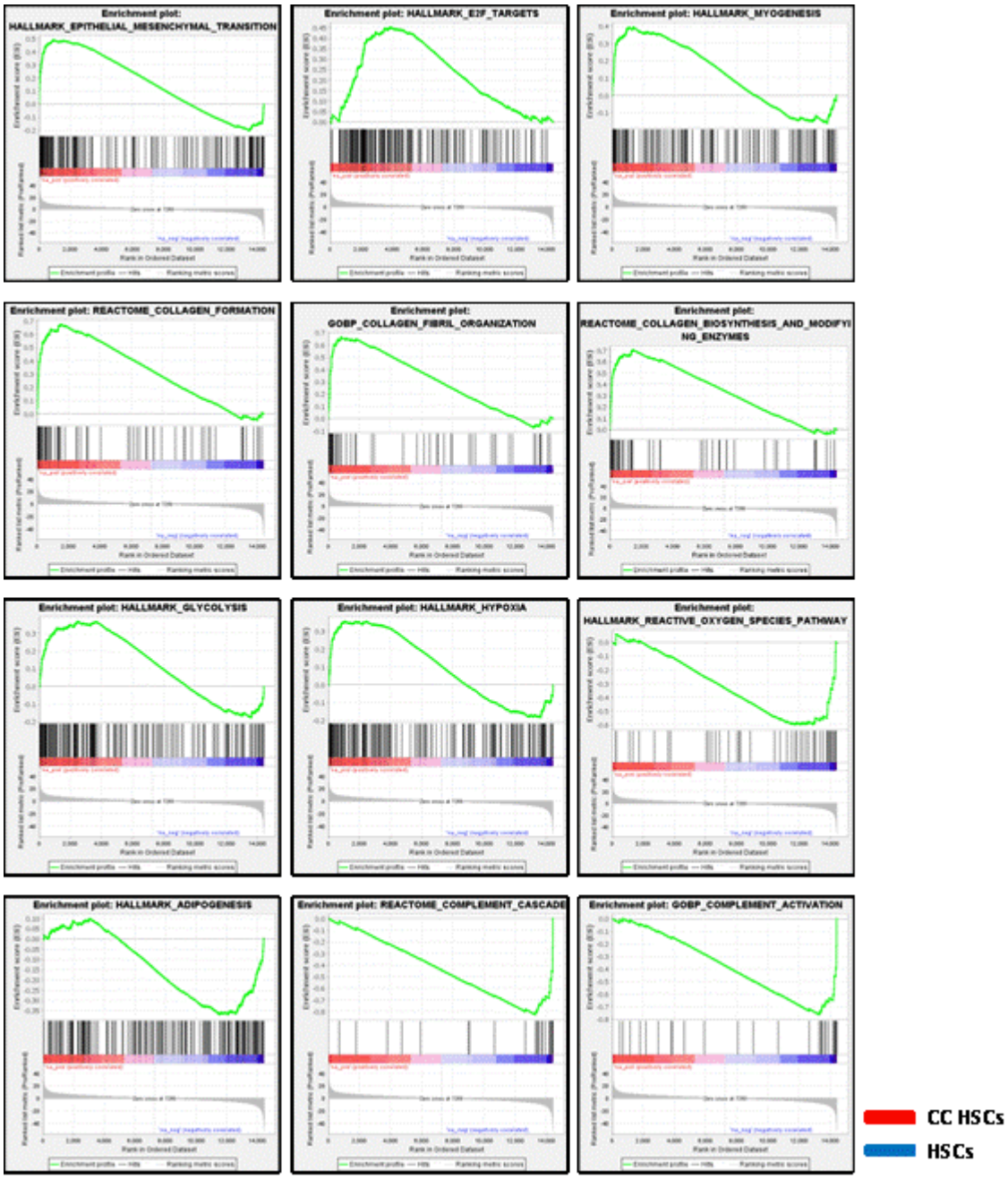

Figure 43. Upregulated and downregulated gene pathways comparing the RNAseq data from cocultured HSCs (CC HSCs) and monocultured HSCs (HSCs).

Like observed in GSEA analysis, HiPathia revealed that cocultured HSCs gain the activation of proliferation related processes, chemotaxis, inflammatory response and glycolysis. Moreover, HiPathia also showed an upregulation of functions like B cell activation, which suggest that co-cultured activated HSCs could be involved in creating an immune-activated environment. Meanwhile, among the functions that these cells lose, we manly find ion transport related functions (Figure 44).

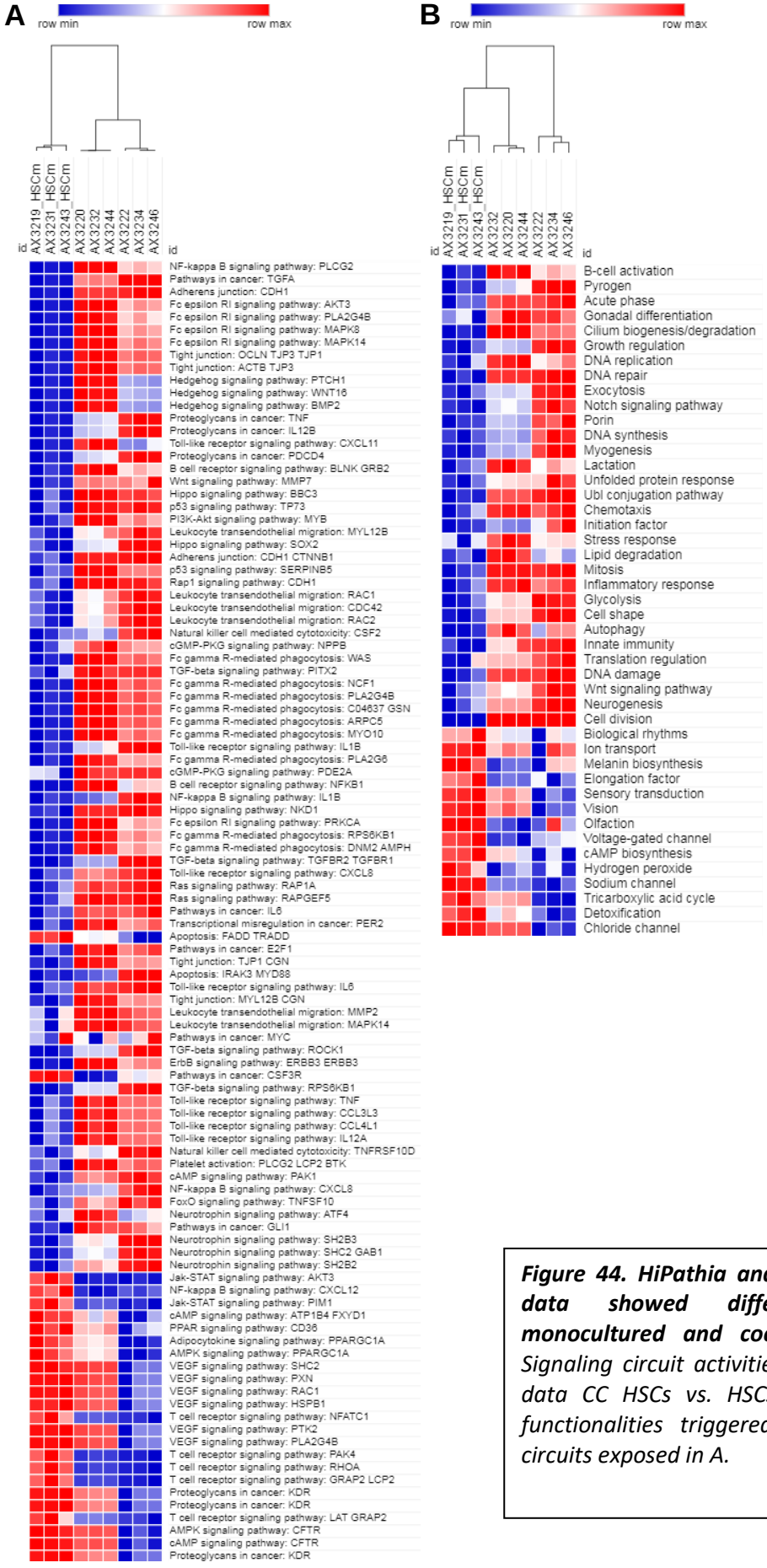

Figure 44. HiPathia analysis from RNAseq data showed differences between monocultured and cocultured HSCs. *(A) Signaling circuit activities obtained RNAseq data CC HSCs vs. HSCs analysis. (B) Cell functionalities triggered by the signaling circuits exposed in A.*

In conclusion, when cocultured with tumoral cells, HSCs increase they proliferation rate as well as acquire myofibroblastic features. Inflammatory response and immune cell chemotaxis also increase, as well as hypoxia related pathways and glycolysis. On the other hand, adipogenic pathways are diminished.

4.1.1.5. *Gene set enrichment analysis (GSEA) and HiPathia analysis RNAseq data showed differences between cocultured PFs and cocultured HSCs*

After analyzing the changes in PFs and HSCs produced by the tumoral exposition induced activation, we assessed the changes between the activated version of these two cell types. Through GSEA we find an upregulation in PFs of gene sets related to myogenesis, probably because their phenotype is closer to myofibroblasts, inflammation related pathways, immune recruitment and neurotrophin and other chemokines related pathways (Figure 45). On the other hand, HSCs showed an upregulation of proliferation and cholesterol metabolism (Figure 46), this last one probably because lipid storage is one of their functions in physiological conditions.

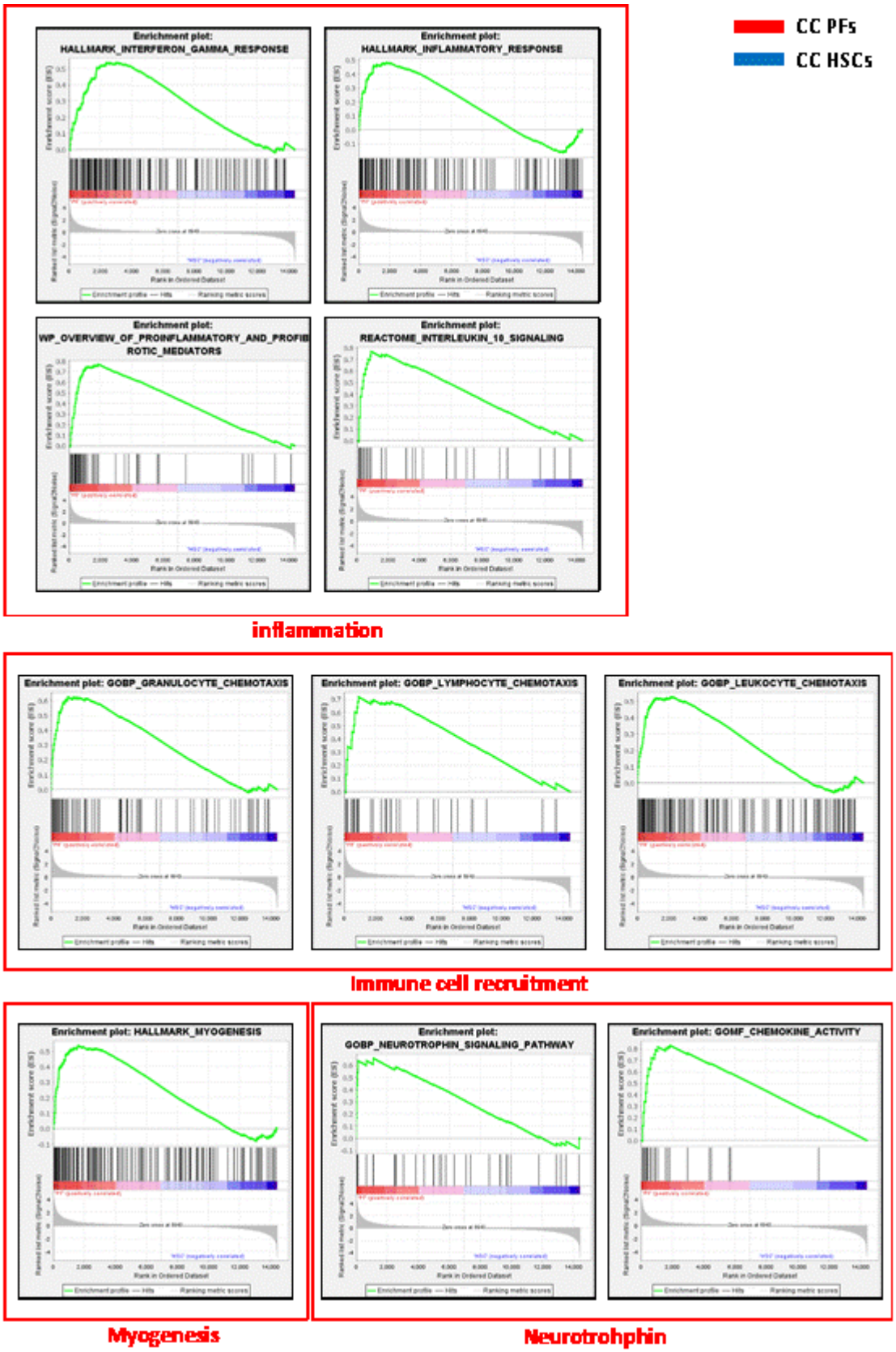

Figure 45. Upregulated gene pathways comparing the RNAseq data from cocultured PFs (CC PFs) and cocultured HSCs (CC HSCs).

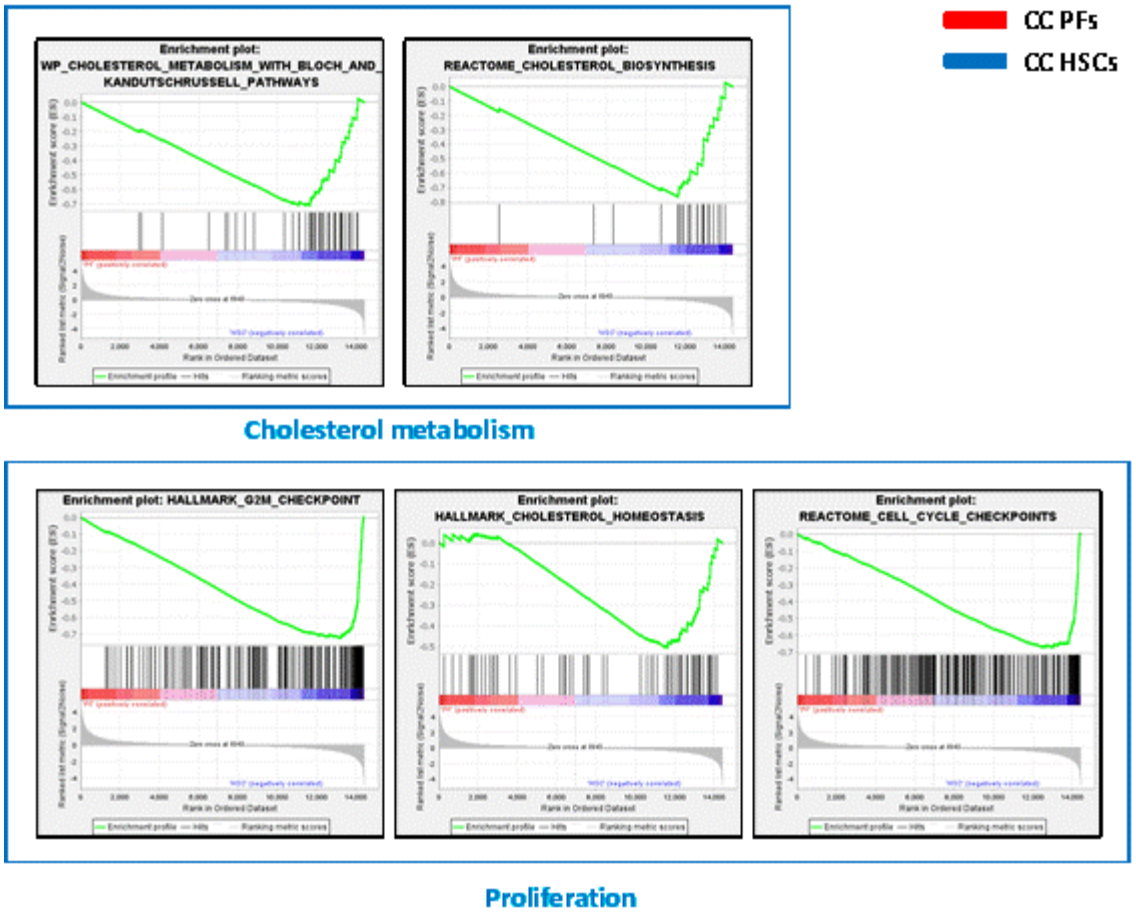

Figure 46. Downregulated gene pathways comparing the RNAseq data from cocultured PFs (CC PFs) and cocultured HSCs (CC HSCs).

Considering the HiPathia analysis, was performed including monoculture and co-culture conditions of both HSCs and PFs. When considering the differentially activated circuits, we observed more differences between HSCs and PFs than between monocultured and cocultured cells. Moreover, many of the differences observed depended on the tumoral cell with which the co-culture was done, although we focused on general HSCs vs. PFs differences. Some of the upregulated circuits observed in PFs were the natriuretic peptide B (NPPB) signaling pathway, proteoglycans in cancer, Toll-like receptor signaling, natural killer mediated cytotoxicity, NF-κB signaling, Strogen signaling and leucocyte trans endothelial migration. An NPPB signaling pathway is related to different anti-cancer mechanisms, like inhibiting VEGF, Wnt and AKT pathways (327). In this line, some of the proteoglycans upregulated in PF vs. HSCs are also related to anti-tumoral functions. It is the case of IL12B, which is described to promote anti-tumor immune response (328), and PDCD4, which shifts immune response towards a pro-inflammatory phenotype that suppresses tumor growth in

blood cancer (329). In the case of tumor necrosis factor (TNF) and HOXD10, they can be playing tumor-suppressive or tumor-restraining activities depending on the context (329–331). The toll-like receptor found at higher levels in PF, CD40 is correlated to type 1 anti-tumor response and better patient survival (332). On contrary, NF-κB signaling is described to have a major role in oncogenesis, specifically CXCL8, which is associated with tumour proliferation, invasion and migration as well as neovascularization (333). Thus, activated PF have shown both pro-tumoral and tumor-restraining upregulated functions, which suggests that these cells could give rise to different CAF subpopulations and/or that these subpopulations have different states between which they may switch.

On the other hand, some of the upregulated circuits in HSCs include neurotrophin signaling pathways, VEGF signaling pathways, proteoglycans in cancer (different than the upregulated in PFs) and adipocytokine signaling pathways (Figure 47). Specifically, the HSCs upregulated neurotrophin pathway is NFKB1, the role of which is not fully understood (334). However, VEGF signaling pathway activation suggests that HSCs may be contributing to new vessel formation (335). This added to the fact that the proteoglycan (KDR, also called VEGFR2) and the adipocytokine (NPY) upregulated are both associated with pro-tumoral functions like angiogenesis, proliferation, migration and tumor survival, suggest that HSCs give rise to tumor-promoting CAF populations (335,336).

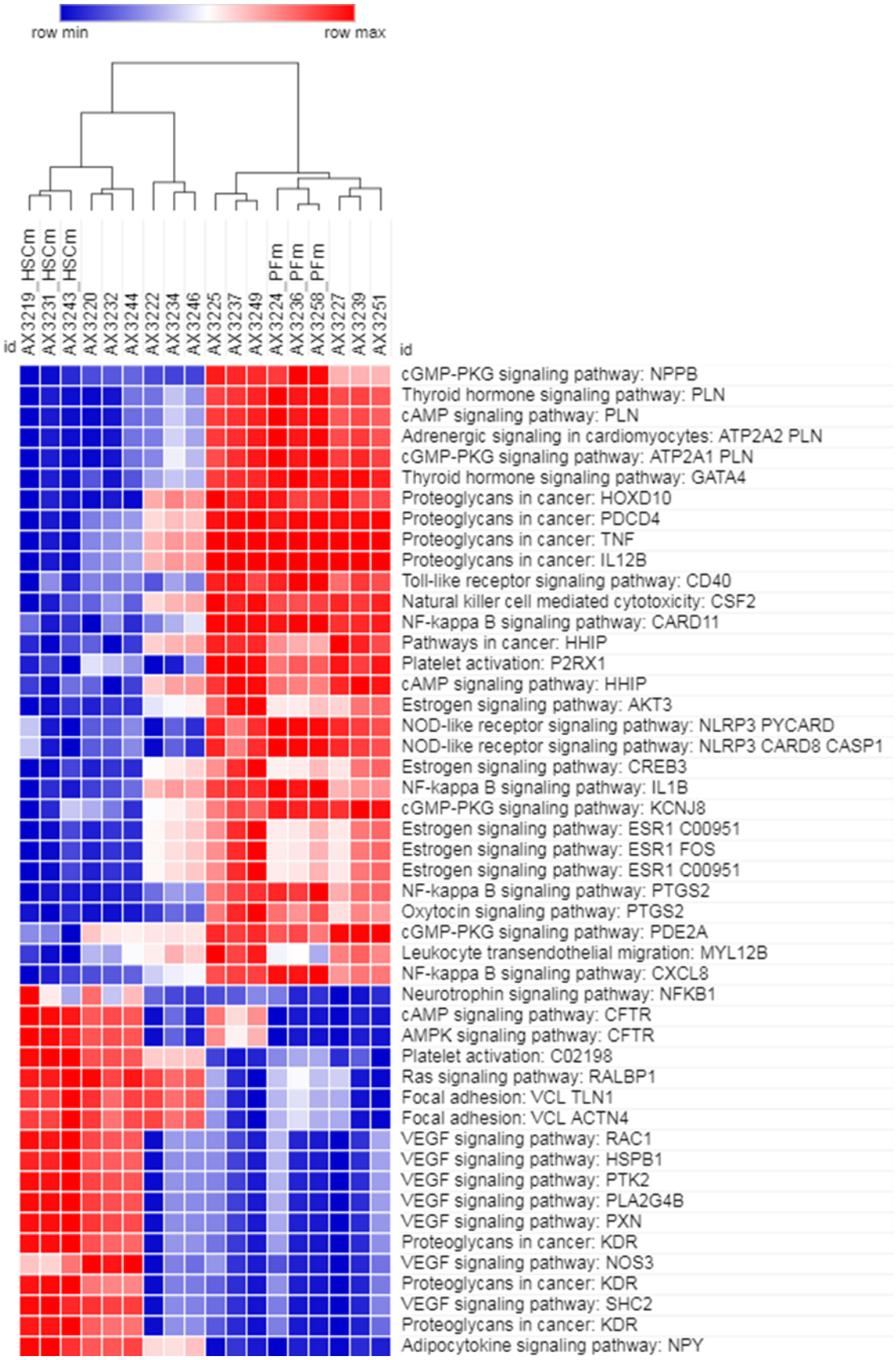

Figure 47. Signaling circuit activities obtained from RNAseq data HSCs vs. PFs.

When assessing the molecular functions derived from the circuits mentioned before, we observed again more differences between HSCs and PFs than between monoculture and co-culture. Moreover, PFs showed more functions upregulated when compared to HSCs. Once more, many differences were observed depending on the tumoral cell with which the CC is done. These differences are more notably in HSCs than in PFs, which could be explained by the fact that HSCs have become CAFs, while PFs are already fibroblasts before their activation. The upregulated functions in PFs are skeletal muscle fiber contraction and relaxation, intestinal epithelial cell differentiation, macrophage interactions, natural killer activation and cytokine production. Fiber contraction and relaxation suggests that these activated PF are more prompted to be myofibroblasts than HSCs. Macrophage interactions, natural killer activation and cytokine production suggest that PF may interact with immune system, whether promoting an immune-suppressive or an immune-active environment should be further assessed. The upregulated functions in HSCs are proliferation, proteoglycan biosynthesis, glucose import and glycolytic process, VEGF signaling pathway and nitric-oxide synthase (Figure 48). Considering these results, HSCs may display different pro-tumoral functions, mainly related to providing tumor cells energy and oxygen for survival, either being their selves the suppliers or promoting new-vessel formation.

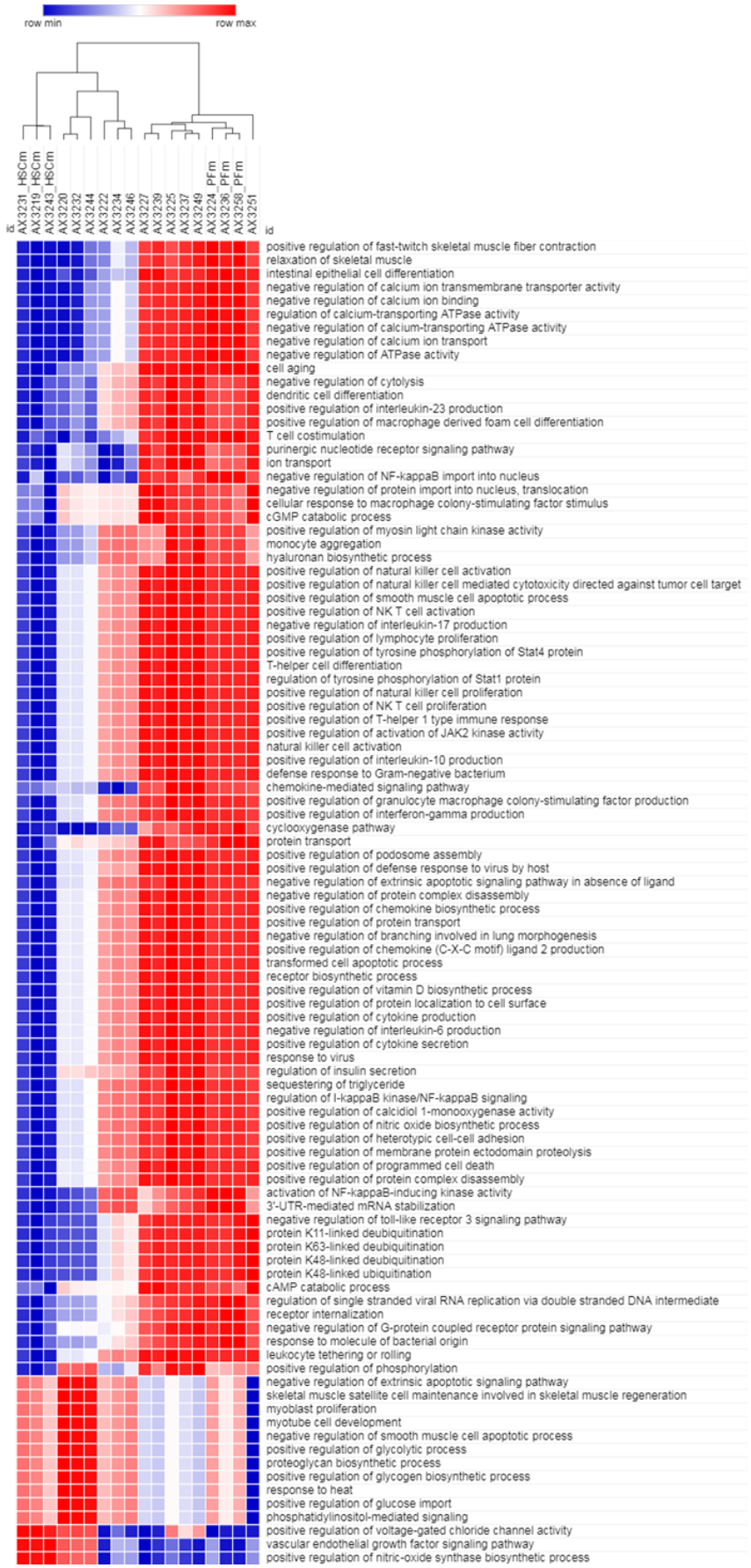

Figure 48. Cell functionalities triggered by the signaling circuits exposed in Figure 47.

In conclusion, once activated by the co-culture with tumoral cells, PFs and HSCs show different RNA expression. PFs show more myofibroblastic features as well as inflammation related pathways, chemokine production and immune cell recruitment. On the other hand, HSCs show increased pathways related to proliferation and angiogenesis. However, their main characteristic is the upregulation of many lipids' metabolism related pathways.

4.1.1.6. Metabolizer analysis revealed metabolic differences between HSCs vs. PFs

Metabolizer is a web tool for analyzing metabolic pathways from transcriptomic data. This tool calculates the impact of each gene module from Kegg database on production metabolites. The first analysis we did with this tool was to compare HSCs (monoculture + co-culture data) with PFs (monoculture + co-culture data). This comparison showed that PFs produce more amino acids (serine, cysteine), glycosphingolipids, nucleotide sugars for glycosylation reactions, glucose and o-glycans. Meanwhile, HSCs produce more phosphatidylcholine, fatty acids, N-glycans, PE (membrane component) and cholesterol (Figure 49).

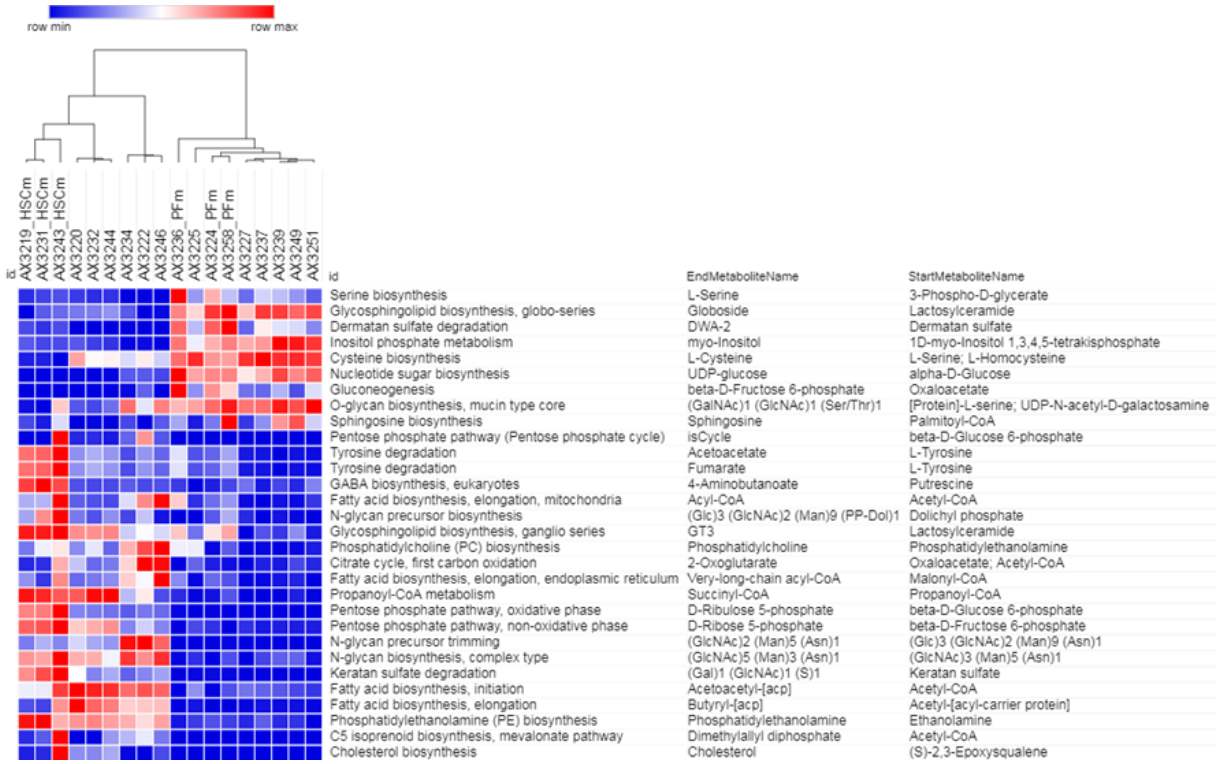

id	EndMetaboliteName	StartMetaboliteName
Serine biosynthesis	L-Serine	3-Phospho-D-glycerate
Glycosphingolipid biosynthesis, globo-series	Globoside	Lactosylceramide
Dermatan sulfate degradation	DWA-2	Dermatan sulfate
Inositol phosphate metabolism	myo-Inositol	1D-myo-Inositol 1,3,4,5-tetrakisphosphate
Cysteine biosynthesis	L-Cysteine	L-Serine; L-Homocysteine
Nucleotide sugar biosynthesis	UDP-glucose	alpha-D-Glucose
Gluconeogenesis	beta-D-Fructose 6-phosphate	Oxaloacetate
O-glycan biosynthesis, mucin type core	(GalNAc)1 (GlcNAc)1 (Ser/Thr)1	[Protein]-L-serine; UDP-N-acetyl-D-galactosamine
Sphingosine biosynthesis	Sphingosine	Palmitoyl-CoA
Pentose phosphate pathway (Pentose phosphate cycle)	isCycle	beta-D-Glucose 6-phosphate
Tyrosine degradation	Acetoacetate	L-Tyrosine
Tyrosine degradation	Fumarate	L-Tyrosine
GABA biosynthesis, eukaryotes	4-Aminobutanoate	Putrescine
Fatty acid biosynthesis, elongation, mitochondria	Acyl-CoA	Acetyl-CoA
N-glycan precursor biosynthesis	(Glc)3 (GlcNAc)2 (Man)9 (PP-Dol)1	Dolichyl phosphate
Glycosphingolipid biosynthesis, ganglio series	GT3	Lactosylceramide
Phosphatidylcholine (PC) biosynthesis	Phosphatidylcholine	Phosphatidylethanolamine
Citrate cycle, first carbon oxidation	2-Oxoglutarate	Oxaloacetate; Acetyl-CoA
Fatty acid biosynthesis, elongation, endoplasmic reticulum	Very-long-chain acyl-CoA	Malonyl-CoA
Propanoyl-CoA metabolism	Succinyl-CoA	Propanoyl-CoA
Pentose phosphate pathway, oxidative phase	D-Ribulose 5-phosphate	beta-D-Glucose 6-phosphate
Pentose phosphate pathway, non-oxidative phase	D-Ribose 5-phosphate	beta-D-Fructose 6-phosphate
N-glycan precursor trimming	(GlcNAc)2 (Man)5 (Asn)1	(Glc)3 (GlcNAc)2 (Man)9 (Asn)1
N-glycan biosynthesis, complex type	(GlcNAc)5 (Man)3 (Asn)1	(GlcNAc)3 (Man)5 (Asn)1
Keratan sulfate degradation	(Gal)1 (GlcNAc)1 (S)1	Keratan sulfate
Fatty acid biosynthesis, initiation	Acetoacetyl-[acp]	Acetyl-CoA
Fatty acid biosynthesis, elongation	Butyryl-[acp]	Acetyl-[acyl-carrier protein]
Phosphatidylethanolamine (PE) biosynthesis	Phosphatidylethanolamine	Ethanolamine
C5 isoprenoid biosynthesis, mevalonate pathway	Dimethylallyl diphosphate	Acetyl-CoA
Cholesterol biosynthesis	Cholesterol	(S)-2,3-Epoxysqualene

Figure 49. Upregulated and downregulated metabolic pathways HSCs vs. PFs.

When using the Metabolizer tool to compare cocultured HSCs with cocultured PFs, the results were so similar (Figure 50).

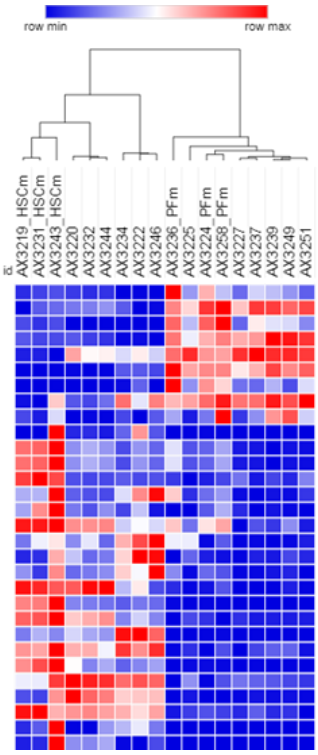

id	EndMetaboliteName	StartMetaboliteName
Serine biosynthesis	L-Serine	3-Phospho-D-glycerate
Glycosphingolipid biosynthesis, globo-series	Globoside	Lactosylceramide
Dermatan sulfate degradation	DWA-2	Dermatan sulfate
Inositol phosphate metabolism	myo-Inositol	1D-myo-Inositol 1,3,4,5-tetrakisphosphate
Cysteine biosynthesis	L-Cysteine	L-Serine; L-Homocysteine
Nucleotide sugar biosynthesis	UDP-glucose	alpha-D-Glucose
Gluconeogenesis	beta-D-Fructose 6-phosphate	Oxaloacetate
O-glycan biosynthesis, mucin type core	(GalNAc)1 (GlcNAc)1 (Ser/Thr)1	[Protein]-L-serine; UDP-N-acetyl-D-galactosamine
Sphingosine biosynthesis	Sphingosine	Palmitoyl-CoA
Pentose phosphate pathway (Pentose phosphate cycle)	isCycle	beta-D-Glucose 6-phosphate
Tyrosine degradation	Acetoacetate	L-Tyrosine
Tyrosine degradation	Fumarate	L-Tyrosine
GABA biosynthesis, eukaryotes	4-Aminobutanoate	Putrescine
Fatty acid biosynthesis, elongation, mitochondria	Acyl-CoA	Acetyl-CoA
N-glycan precursor biosynthesis	(Glc)3 (GlcNAc)2 (Man)9 (PP-Dol)1	Dolichyl phosphate
Glycosphingolipid biosynthesis, ganglio series	GT3	Lactosylceramide
Phosphatidylcholine (PC) biosynthesis	Phosphatidylcholine	Phosphatidylethanolamine
Citrate cycle, first carbon oxidation	2-Oxoglutarate	Oxaloacetate; Acetyl-CoA
Fatty acid biosynthesis, elongation, endoplasmic reticulum	Very-long-chain acyl-CoA	Malonyl-CoA
Propanoyl-CoA metabolism	Succinyl-CoA	Propanoyl-CoA
Pentose phosphate pathway, oxidative phase	D-Ribulose 5-phosphate	beta-D-Glucose 6-phosphate
Pentose phosphate pathway, non-oxidative phase	D-Ribose 5-phosphate	beta-D-Fructose 6-phosphate
N-glycan precursor trimming	(GlcNAc)2 (Man)5 (Asn)1	(Glc)3 (GlcNAc)2 (Man)9 (Asn)1
N-glycan biosynthesis, complex type	(GlcNAc)5 (Man)3 (Asn)1	(GlcNAc)3 (Man)5 (Asn)1
Keratan sulfate degradation	(Gal)1 (GlcNAc)1 (S)1	Keratan sulfate
Fatty acid biosynthesis, initiation	Acetoacetyl-[acp]	Acetyl-CoA
Fatty acid biosynthesis, elongation	Butyryl-[acp]	Acetyl-[acyl-carrier protein]
Phosphatidylethanolamine (PE) biosynthesis	Phosphatidylethanolamine	Ethanolamine
C5 isoprenoid biosynthesis, mevalonate pathway	Dimethylallyl diphosphate	Acetyl-CoA
Cholesterol biosynthesis	Cholesterol	(S)-2,3-Epoxysqualene

Figure 50. Upregulated and downregulated metabolic pathways CC HSCs vs. CC PFs.

Thus, considering only metabolic pathways, PFs produce more aminoacids, glycosphingolipids, nucleotide sugars, glucose and o-glycans; while HSCs would be producing membrane components, fatty acids, and cholesterol. This, added to previous results, suggest that these two CA precursors give rise to different CAF subpopulations that may be displaying different functions and/ or providing tumoral cells with different elements needed for their survival.

4.1.1.7. *Gene set enrichment analysis (GSEA), HiPathia and Metabolizer analysis from RNAseq data showed differences between tumoral cells cocultured with HSCs vs. cocultured with PFs*

After analyzing how the studied mesenchymal cells change between them and due to the influence of tumoral cells (TC), we wondered how tumoral cells change when they are cocultured with HSCs vs. when they are cocultured with PFs. For that, we did a GSEA that

revealed that in tumoral cells, when cocultured with HSCs, there was an upregulation of proliferation-related pathways (G2M checkpoint, DNA replication, MYC, cell cycle, pentose phosphate pathway), lipid and steroid biosynthesis, cholesterol homeostasis and propanoate metabolism. Thus, it all suggested that HSCs were inducing or promoting proliferation in the tumoral cells they were cocultured with. Meanwhile, tumoral cells cocultured with PFs showed an upregulation of inflammation-related pathways (interferon α, interferon γ and TNFα signaling), angiogenesis, apoptosis, chemotaxis and mediation of T cell responses and encapsulating structure organization (Figure 51). Therefore, PF was inducing tumoral cells the upregulation of several gene sets that suggested both pro-tumoral and tumor-restraining resulting functions. This is in line with the information obtained when comparing PF vs. HSCs, in which PF functions seem to be in both pro- and anti- tumoral directions, suggesting the presence of more than one CAF subpopulation. On the one hand, several gene sets upregulated in PF-cocultured tumoral cells were related to the recruitment and activation of the immune response. Moreover, apoptosis an encapsulating structure organization gene sets also may turn out to be growth-restraining. On the other hand, angiogenesis as well as some inflammation-related pathways may be associated with tumor progression. In conclusion, these data suggested that the coculture of PFs and HSCs were inducing different functions in tumoral cells.

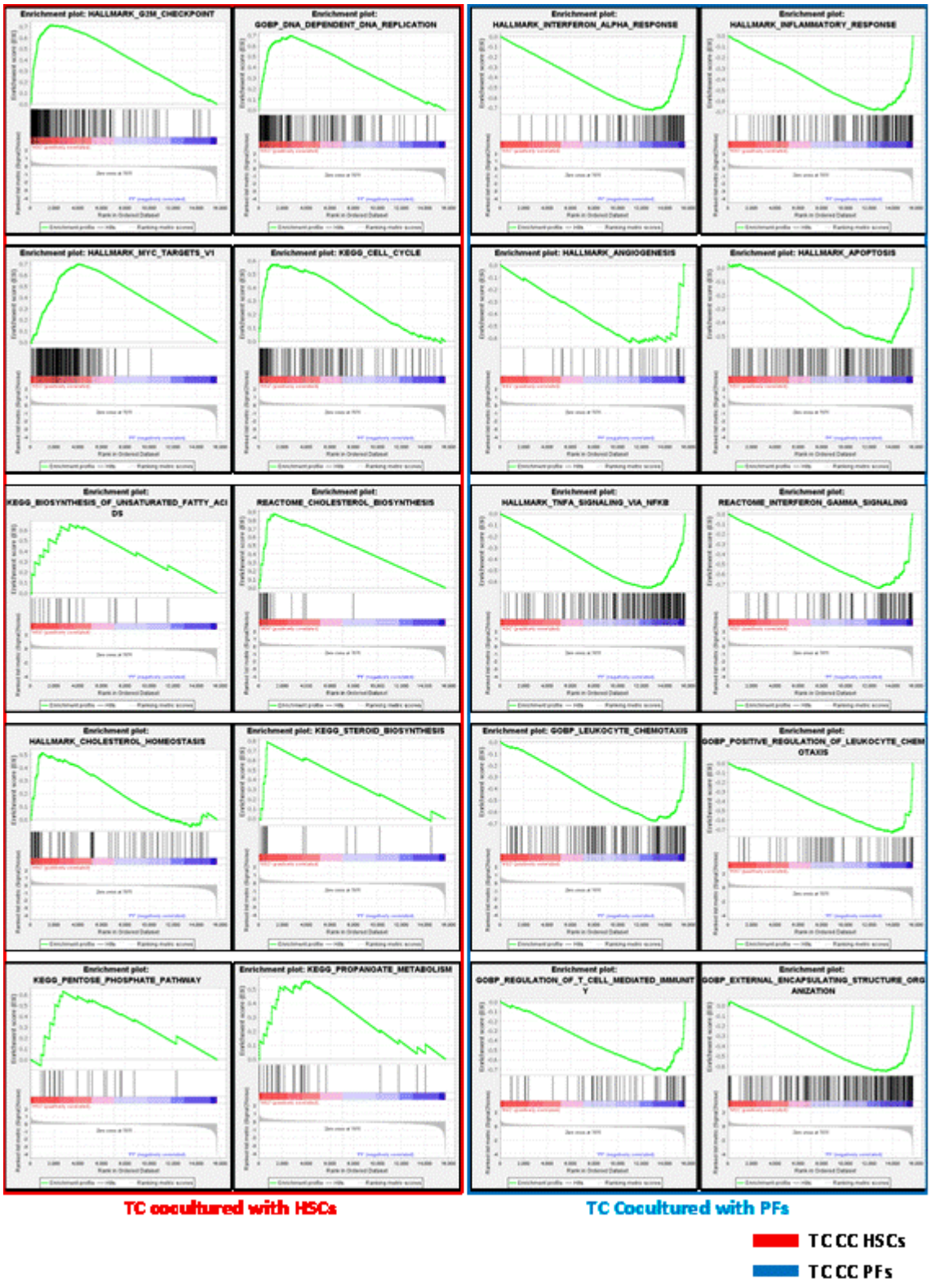

Figure 51. Upregulated and downregulated gene pathways comparing the RNAseq data from tumoral cells cocultured with PFs (TC CC PFs) and tumoral cells cocultured with HSCs (CC HSCs).

In the case of HiPathia, this analysis was done considering the two tumoral cell lines, LoVo and SNU-503, separately. Thus, we had four situations: each cell line cocultured with HSCs

and with PFs. The information obtained showed that the mesenchymal cells' induced changes were different depending on the tumoral cell line with which they were cocultured. In this line, many circuits upregulated in LoVo cells when cocultured with PF, among which we find natural killer cell-mediated cytotoxicity; NF-κB, TNF, sphingolipid, Wnt and MAPK signaling pathways. On the other hand, LoVo cells cocultured with HSCs showed an upregulation of the NFKB1 neurotrophin signaling pathway. Considering the few circuits that change in both LoVo and SNU-503 cell lines, we find apoptosis mediated by FADD and TRADD; CXCL10, IL6 and CCL5 toll-like receptor signaling pathways, transcriptional mis regulation in cancer (ITGAM) and pathways in cancer (IL6) (Figure 52).

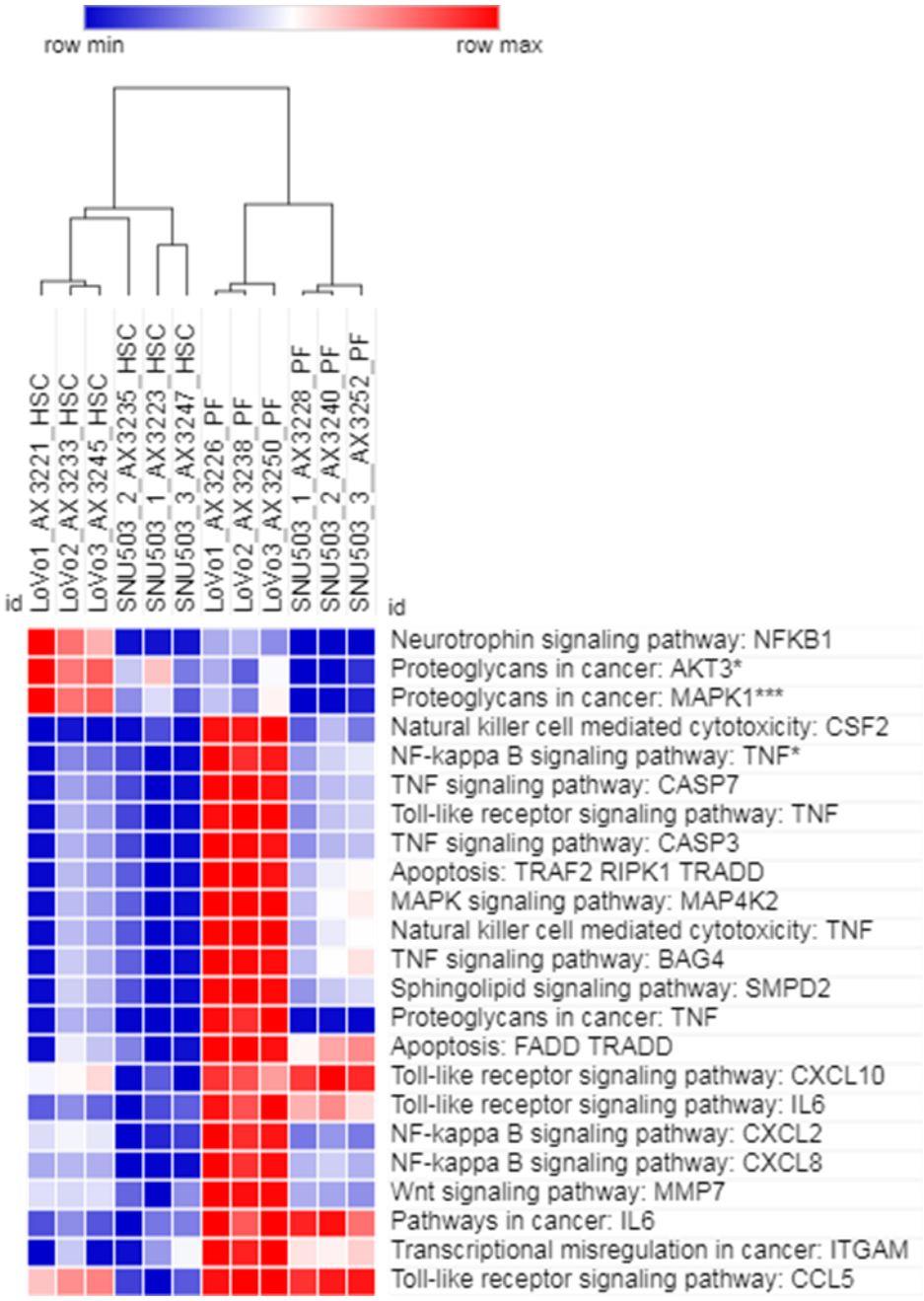

Figure 52. HiPathia transformation of LoVo and SNU-503 cocultured with PFs and HSCs gene expression to signaling circuit activities.

Metabolizer also showed differences depending on the mesenchymal cells the tumoral cells are cocultured with. In general terms, N-glycan precursor biosynthesis, fatty acid biosynthesis and phosphatidylethanolamine (PE) biosynthesis were increased when cocultured with HSCs. On the other hand, the metabolic pathway increased in PFs co-culture was galactose degradation (Figure 53). N-glycan is a fundamental and versatile protein modification that plays critical roles in various physiological and pathological events

including cancer progression (337), which further suggests a tumor-promoting role of HSCs. Considering the previously observed fact that HSCs induce tumor cell proliferation, cellular proliferation requires fatty acids for the synthesis of membranes and signaling molecules (338). Moreover, PE makes up greater than 50% of the total phospholipid species in eukaryotic membranes (339). Thus, these changes observed in HSCs-cocultured tumor cells could be explained by the need of generating cell membranes to keep proliferating. About the upregulation of galactose degradation observed in PF-cocultured tumor cells, some studies have shown that galactose, which is variably plentiful in fruit, might be playing a protective effect against tumor progression by binding and inhibiting a type of lectins that promote proliferation (340). Therefore, increased galactose degradation would suppose an advantage for tumor cell survival.

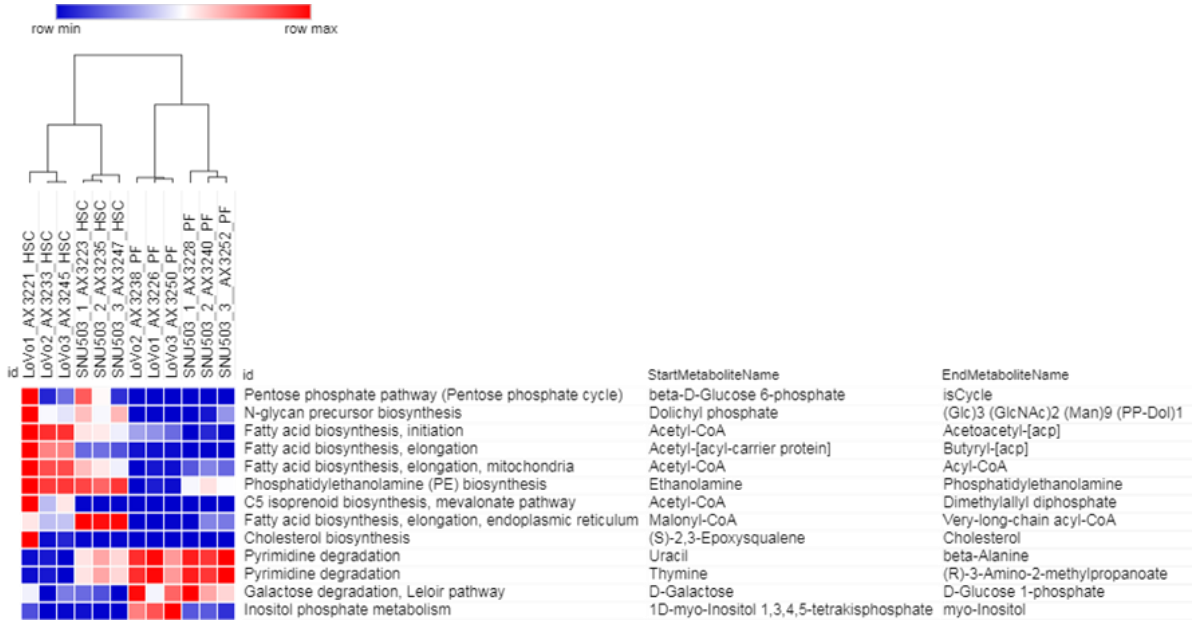

Figure 53. Upregulated and downregulated metabolic pathways in LoVo and SNU-503 cocultured with PFs and HSCs

In conclusion, although most of the changes in tumoral cells depend on the cell line, we can conclude that when assessing tumoral cells, they show an upregulation of proliferation-related processes, lipid, and cholesterol production when cocultured with HSCs. When cocultured with PFs, those cells increase inflammation-related pathways, immune cell chemotaxis and encapsulating structure.

4.1.1.8. qPCR validation of selected HSCs and PFs markers

The selection of genes for validation was done by manually curating the data obtained from RNAseq, considering the information published in the protein atlas. We validated the selected genes, which would serve as candidate markers for distinguishing HSCs from PFs, in newly generated *in vitro* samples, obtained following the same culture conditions as the ones used for the RNAseq. First, we validated them through qPCR. As expected, HSCs markers were highly expressed in HSCs (Figure 54) and PFs markers were highly expressed in PF (Figure 55). This made us conclude, not only that those genes were PF or HSC reliable markers, but also that our model was reproducible through.

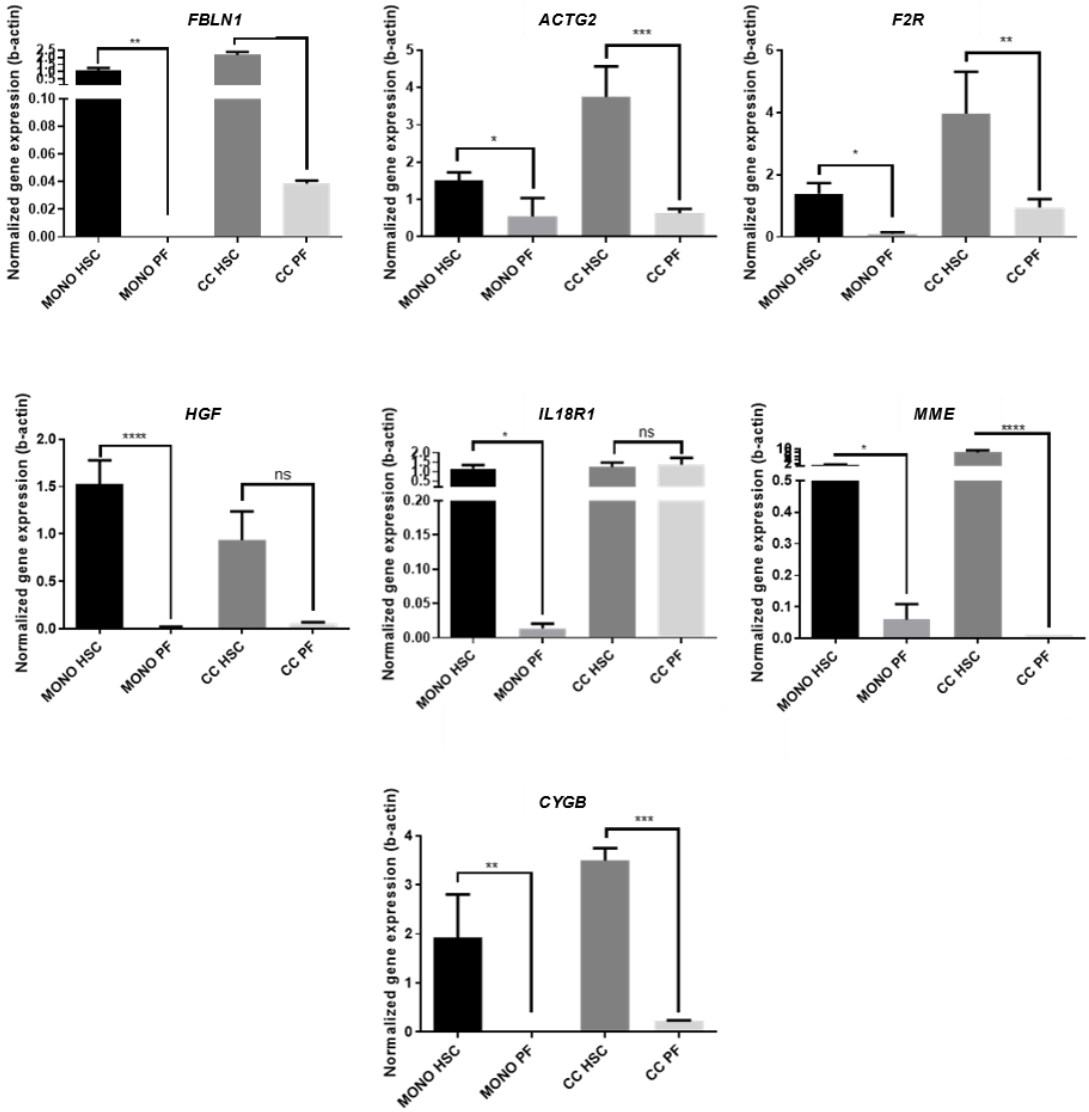

Figure 54. Validation of HSCs selected markers through qPCR. *Mean with SD (n=4). Dunn's multiple comparisons test applied. * p value<0.05, ** p value<0.01, *** p value<0.001, **** p value<0.0001.*

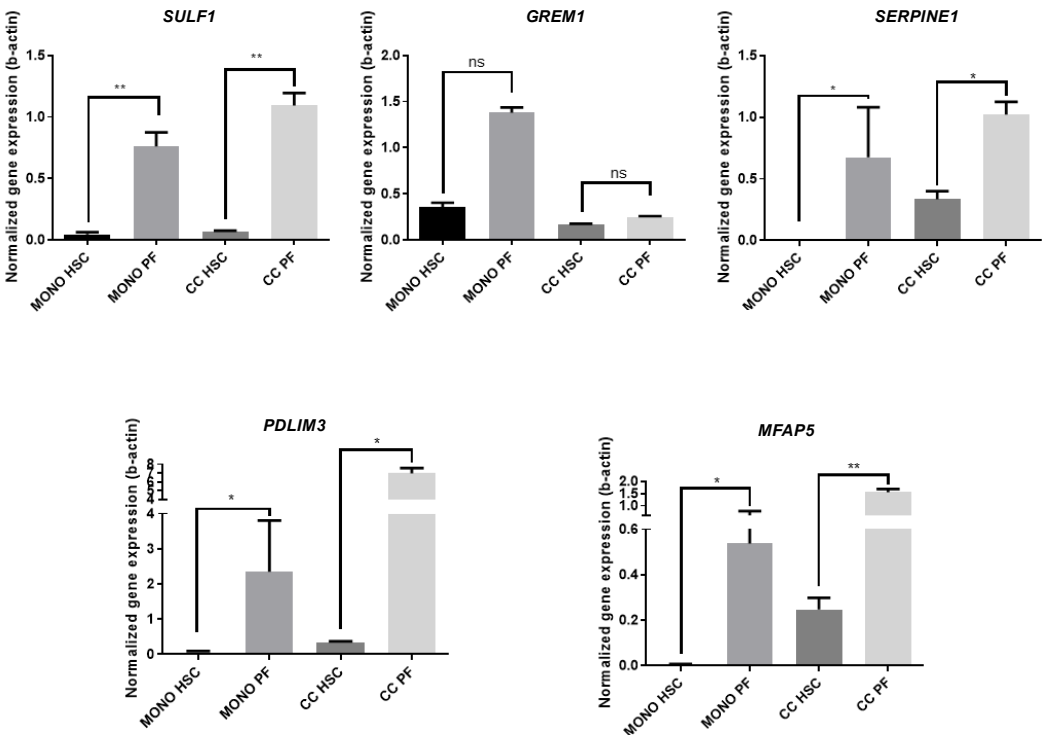

Figure 55. Validation of PFs selected markers through qPCR. *Mean with SD (n=4). * p value<0.05, ** p value<0.01, *** p value<0.001, **** p value<0.0001.*

4.1.1.9. Immunohistochemistry validation of selected HSCs and PFs markers

After validating RNA seq obtained HSCs and PFs markers through qPCR, we aimed to validate some of them through immunohistochemistry (IHC), in samples coming from a cohort of 32 CRLM patients. To choose the best markers to validate, we considered all the possible comparisons of the different conditions from the RNAseq (monocultured HSCs, HSCs cocultured with each cell line, monocultured PF, PFs cocultured with each cell line; plus, the comparison of the whole HSCs conditions with the ones of PFs.) Then, we performed a double IHC staining with two antibody combinations: as an HSCs marker we selected F2R, while as a PF marker, we used MFAP5 and PDLIM3.

Regarding about F2R and MFAP5 combination, we observed clear staining of MFAP5 in portal spaces of the normal liver parenchyma, while sinusoids showed not staining for this marker. Meanwhile, F2R stained in normal liver inside of the sinusoids, where HSCs are expected to be (Figure 56A), while this protein was not present in portal space's fibrosis. Thus, this observation let us conclude that MFAP5 and F2R are suitable markers to define

PFs and HSCs, respectively. Moreover, the fact that RNAseq-obtained candidate genes mark properly the expected cell populations suggest that our *in vitro* model reproduces what happens in the patient's tissue.

Concerning metastatic lesion tissue, we observed that inside the tumor, the predominant staining was F2R while MFAP5 was kept around the lesion on most of the occasions (Figure 56B and C), although MFAP5^{+} areas were also observed at central tumor regions (Figure 56E). Moreover, these two markers do not use to colocalize, although it can happen in a few cells (Figure 56D). This suggests that MFAP5^{+} PFs-derived CAFs and F2R^{+} HSCs-derived CAFs conform to two different subpopulations inside the tumor.

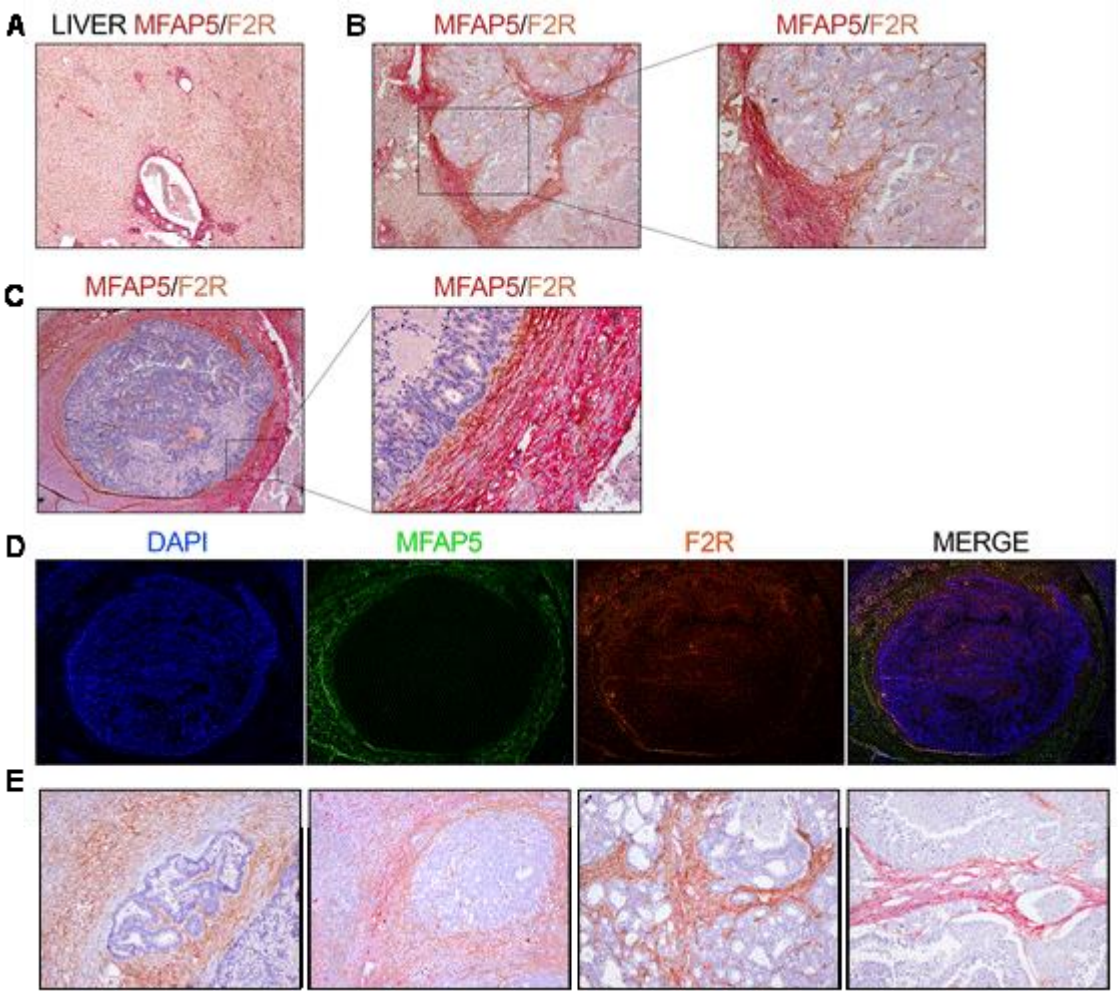

Figure 56. MFAP5 and F2R double IHC and IHF. *(A) 4x magnification of a normal liver region showing MFAP5 staining (red) in portal spaces and F2R staining (brown) in sinusoids. (B) 4x and 10x magnification of a non-dHGP tumor periphery in which F2R^{+} myofibroblasts are observed inside of the tumor and MFAP5^{+} cells are surrounding it. (C) 4x and 20x magnification of a complete dHGP lesion in which F2R^{+} cells are shown inside of the tumor as well as at the firs tumor line at the fibrotic rim, while MFAP5^{+} cells are at the outer part of the rim. (D) Immunofluorescence shows the previous lesion in which one can see the same MFAP5 and F2R distribution. Moreover, colocalization is*

observed in some cells. (E) The first and second images correspond to 10x magnification dHGP tumor interphase regions. The third and fourth images correspond to 10x magnification central regions.

We also wondered if PFs-derived and HSCs-derived CAFs follow a specific distribution inside the metastatic lesions. For example, one possible situation could have been that one of these populations would be mainly present at the fibrotic rim, meanwhile the other would be responsible for fibrotic regions placed at tumor centre. However, contrary to our postulations, in our stained samples we could observe $MFAP5^+$ and $F2R^+$ areas both at the tumor interphase and in central regions (Figure 56E), without following any perceptible tumor-induced distribution rule. This fact suggested that PF-derived $MFAP5^+$ and HSCs-derived $F2R^+$ myofibroblasts may not migrate to different locations inside of the tumor to conform intratumorally fibrotic rumbles or surrounding capsules. Instead of it, at the tumor interface, we observed $MFAP5^+$ regions near fibrotic regions of the surrounding normal liver, such as portal spaces. For example, in the case of dHGP samples, it could be observed $MFAP5^+$ fibrotic rim areas close to portal tracts, suggesting that PFs from portal spaces have migrated and contributed to the encapsulating fibrosis in these regions. In this line, relatively large $MFAP5^+$ areas were seen at central regions, suggesting that pre-existing normal liver fibrotic areas or portal spaces could have been located there. Thus, one possible explanation for this observed distribution could be that the tumor invades the host tissue and, that way encompasses all the pre-existing structures present in its path. That way, there would be MFAP5-positive cells in those regions were there had been portal spaces, while F2R-positive myofibroblasts would be in those tumoral regions that were previously occupied by sinusoids, which would also explain why they are more abundant.

Thus, we concluded that the distribution of MFAP5 and F2R both in tumor periphery and tumor central regions is heterogeneous an seems to depend on the previous structure that was in each zone.

Furthermore, we performed a semi-quantitative visual evaluation of MFAP5 and F2R staining to assess the presence of these two markers in dHGP and non-dHGP. We evaluated three regions of a cohort of 30 patient samples: tumor proximal liver, invasive margin and tumor central regions. Thus, the fibrotic rim is not evaluated as it only appears in one of the HGP. Through this evaluation, we observed that MFAP5 was more expressed in dHGP when assessing the proximal liver, while no differences were seen concerning center and invasive

margin regions (Figure 57A). Therefore, this suggests that the contribution of PFs-derived MFAP5$^+$ CAFs to tumor fibrotic areas does not change depending on the histologic pattern. In other words, PF would not be recruited at different levels in dHGP vs. non-dHGP.

On the other hand, F2R-positive cells showed no differences between HGP in proximal liver or tumor central regions, but they did in the invasive margin (Figure 57B). At this last region, higher staining of HSCs-derived F2R$^+$ cells was shown in dHGP, suggesting a higher capacity of this type of tumor lesions to recruit HSCs and/or induce their activation.

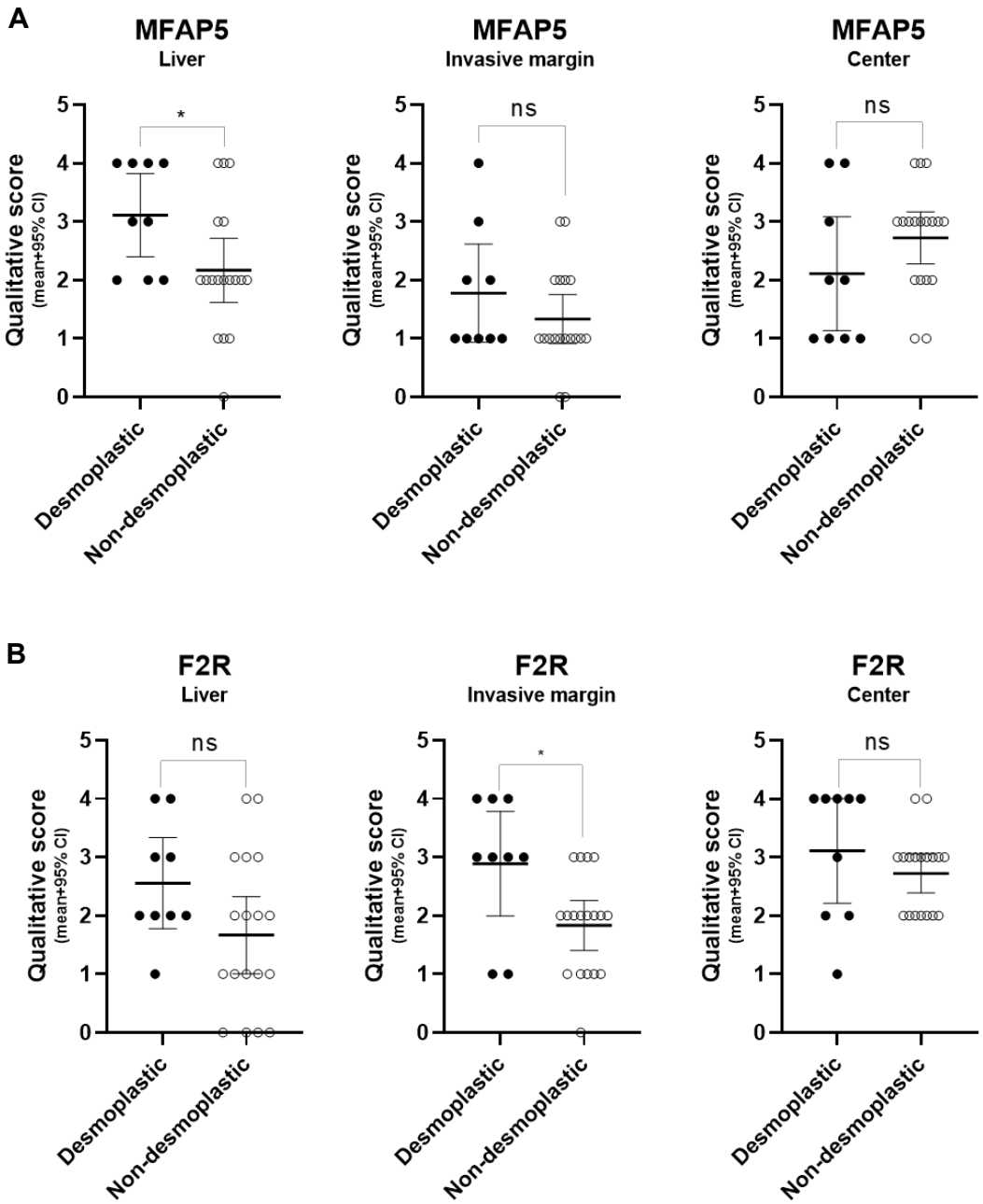

Figure 57. Visual evaluation of MFAP5 and F2R staining. *Three regions (liver, invasive margin and tumor center) from 30 CRLM patient samples were evaluated. The evaluation was performed by the assignment of one category, which was from 0 to 5, with being 0 the lower and 5 being the higher levels of staining. (A) MFAP5 evaluation. (B) F2R evaluation. U Mann-Whitney test. * p value<0.05. ns, non-significant.*

Concerning F2R and PDLIM3 double IHC, when assessing liver regions near the tumor we observed that PDLIM3 was not staining portal space fibrosis (Figure 58A), as MFAP5 did (Figure 56A). In portal spaces, PDLIM3 was only staining epithelial cells from the structures present in this area. However, at tumoral regions, both central and invasive margins, PDLIM3-stained cells were observed (Figure 58). This suggests that PDLIM3 may be expressed at RNA level by all PF, but only expressed at protein level by highly activated PFs-derived CAFs. That PDLIM3 would be a marker of only a subset of PFs-derived CAFs, which we postulate may be associated with high activation. However, it could also be that PDLIM3 is staining a CAF subpopulation derived from PFs that would be performing specific functions. Third, another option, less probable, would be that PDLIM3$^+$ CAFs are derived from these stained portal space's epithelial cells that may have undergone an EMT process.

Moreover, when assessing PDLIM3 and F2R combination through IF, we observed that these two markers do not colocalize, thus, being two different subpopulations inside of the tumor. F2R is stained CAFs, which are nearer to tumoral cells, are more abundant than PDLIM3$^+$ CAFs (Figure 58B). This is in line with the postulation that these CAFs do not derive form HSCs, as they do not express F2R marker and are present at lower levels than F2R$^+$ HSCs-derived CAFs.

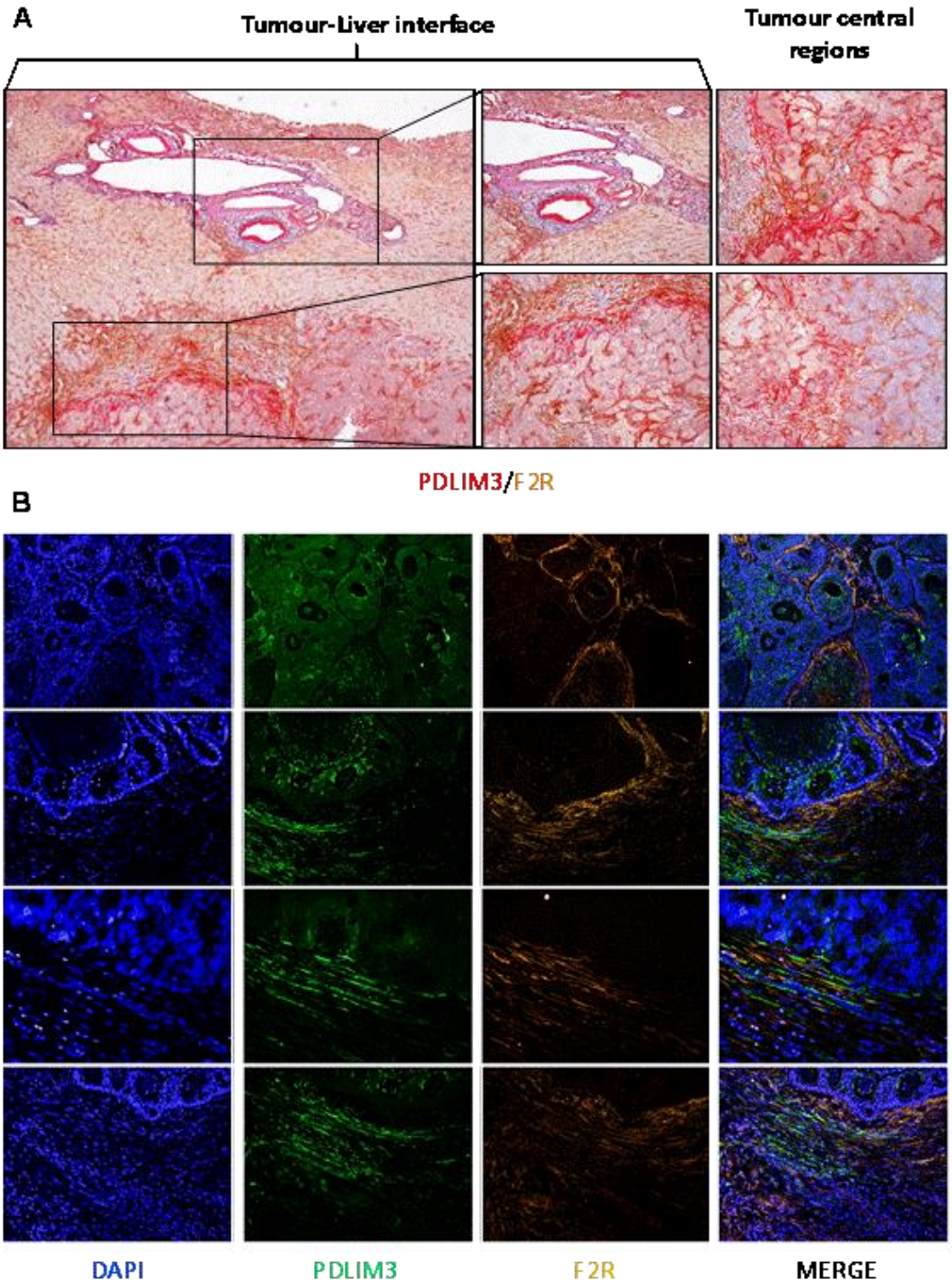

Figure 58. PDLIM3 and F2R double IHC and IHF. *(A) IHC showing PDLIM3 and F2R staining. 4x image is shown on the right, 10x images are shown on left. (B) 10x magnification images showing PDLIM3 and F2R staining. The first row shows a central tumor region while the rest of the rows are taken from a fibrotic capsule.*

In conclusion, MFAP5 and F2R are good markers for identifying PF and HSCs, respectively in paraffin embedded CRLM tissues. On the other hand, our results suggest that PDLIM3 only stains a subset of PF-derived CAFs.

4.1.2. Activated HSCs and PFs can recruit different immune cell populations

As RNAseq analysis suggested that PFs, when activated by the presence of tumoral cells, were producing more chemokines and recruiting immune cells, we decided to perform an *in vitro* transwell migration assay to test this capacity. For doing that, conditioned media from monocultured and cocultured HSCs and PFs was collected and stored at -80ºC. On the day of the experiment, this conditioned media served as the migration stimuli placed at the plate well in which the transwell would be located. At the upper part of the transwell, PBMCs isolated from healthy donors were seeded. After two hours of migration, we assessed which immune cells had migrated through flow cytometry. When performing this experiment with conditioned media coming from monocultured HSCs and PFs, not significantly differences were observed (Figure 59), suggesting that these cells do have not different recruitment capacities when they are not activated by any stimuli. When doing the experiment with media from cocultures, we observed that PFs have a significantly higher capacity to recruit Tregs and Th2 cells. Thus, these *in vitro* experiments show that PFs recruit immune cell populations that are described to create an immune-suppressive environment.

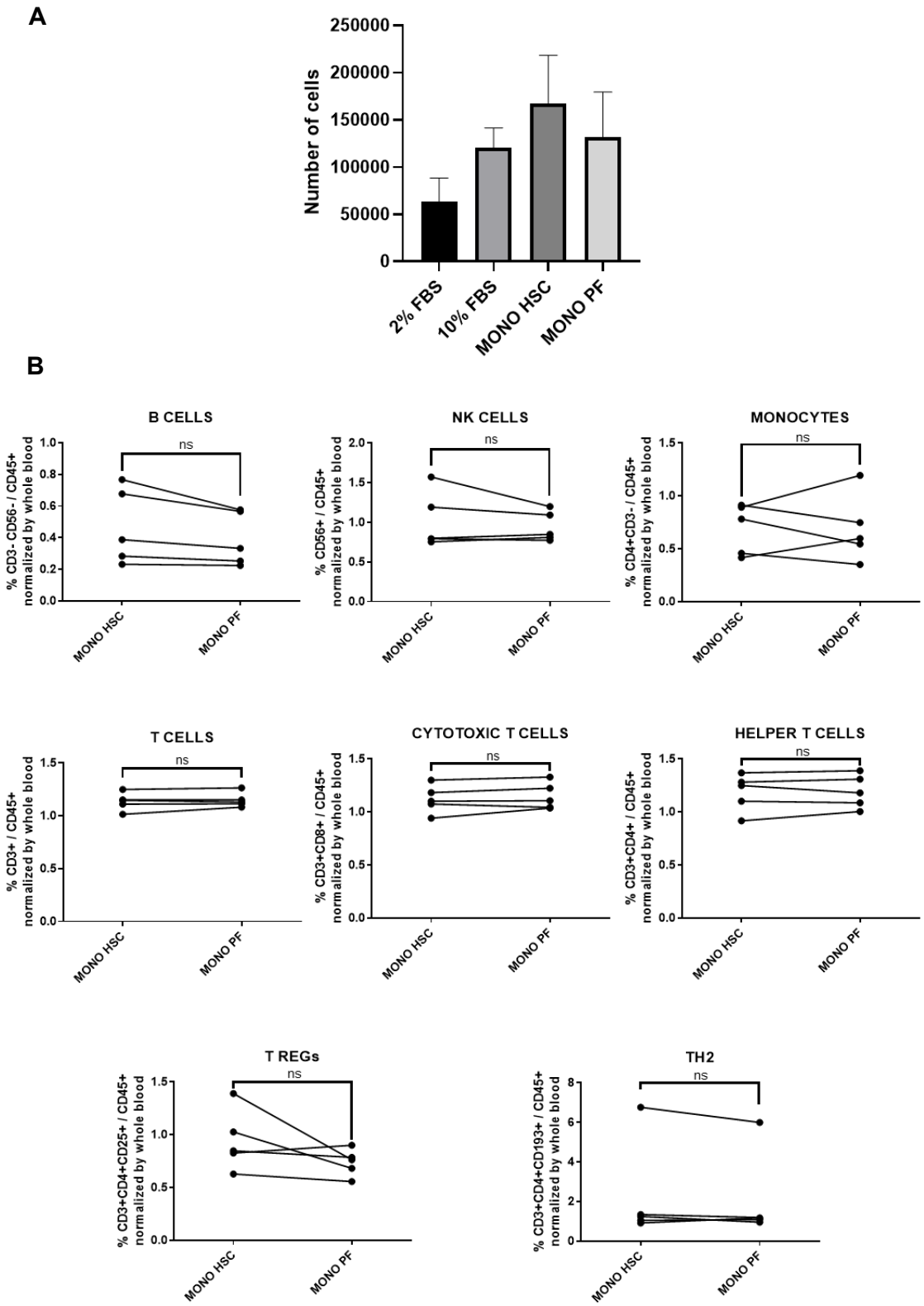

Figure 59. Migration assay using monocultured HSCs and PFs conditioned media. *(A) Number of cells at the lower part of the transwell of each condition. (B) Graphical representation of PBMC's migration assay performed with conditioned media from HSCs (MONO HSC) and PFs (MONO PF) in monoculture conditions. The percentage of CD45 for each cell type was calculated and subsequently normalized by the corresponding percentage of the whole blood sample. Wilcoxon test was applied. Mean with SD (n=5). ns, non-significant.*

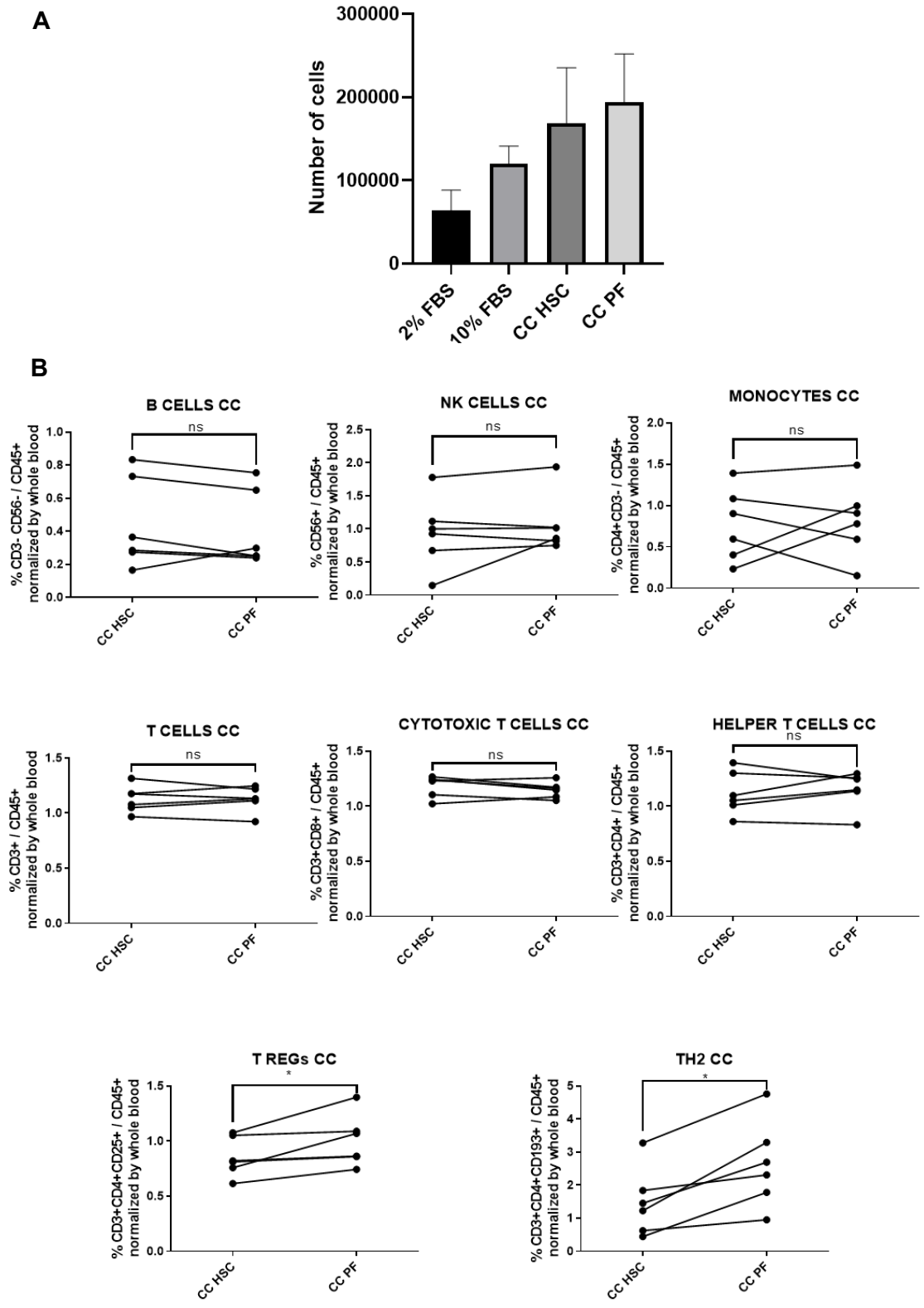

Figure 60. Migration assay using co-cultured HSCs and PFs conditioned media. *(A) Number of cells at the lower part of the transwell of each condition. (B) Graphical representation of PBMC's migration assay performed with conditioned media from HSCs (CC HSC) and PFs (CC PF) in co-culture conditions. The percentage of CD45 for each cell type was calculated and subsequently normalized by the corresponding percentage of the whole blood sample. Wilcoxon test was applied. Mean with SD (n=5). * p value<0.05. ns, non-significant.*

In conclusion, conditioned media coming from monocultures did not show differences in recruiting the assessed immune cell populations. However, conditioned media from cocultured portal fibroblasts showed higher recruitment of Tregs and Th2 T helper subpopulations.

4.1.3. Activated HSCs and PFs conditioned media affects tumoral cells proliferation

RNAseq data suggested that HSCs not only proliferate more than PFs but also are able to induce an increase of proliferation-related pathways to the tumoral cells they are cocultured with. To test that, we performed a proliferation assay using conditioned media from monocultured and cocultured HSCs and PFs and exposed four different CRC metastatic cell lines to it: SNU-503, T84, LoVo and SW620. We observed that conditioned media coming from monocultures did not induce a higher proliferation rate in tumoral cells. However, contrary to what we expected, conditioned media coming from cocultured portal fibroblasts increased proliferation in tumoral cells (Figure 61). This could be explained by the fact that RNAseq information was obtained from direct co-cultured mesenchymal and tumoral cells. Thus, these cells were able to communicate between themselves both through paracrine signals and through cell-to-cell signaling across gap junctions. On contrary, in this experiment, we used conditioned media from mesenchymal cells, in which only paracrine signals were present. Thus, this suggests that the signaling induced by the direct culture of tumoral cells with mesenchymal cells differs from the induced only by the conditioned media. Thus, the induction of proliferation may be mediated by cell-to-cell signaling.

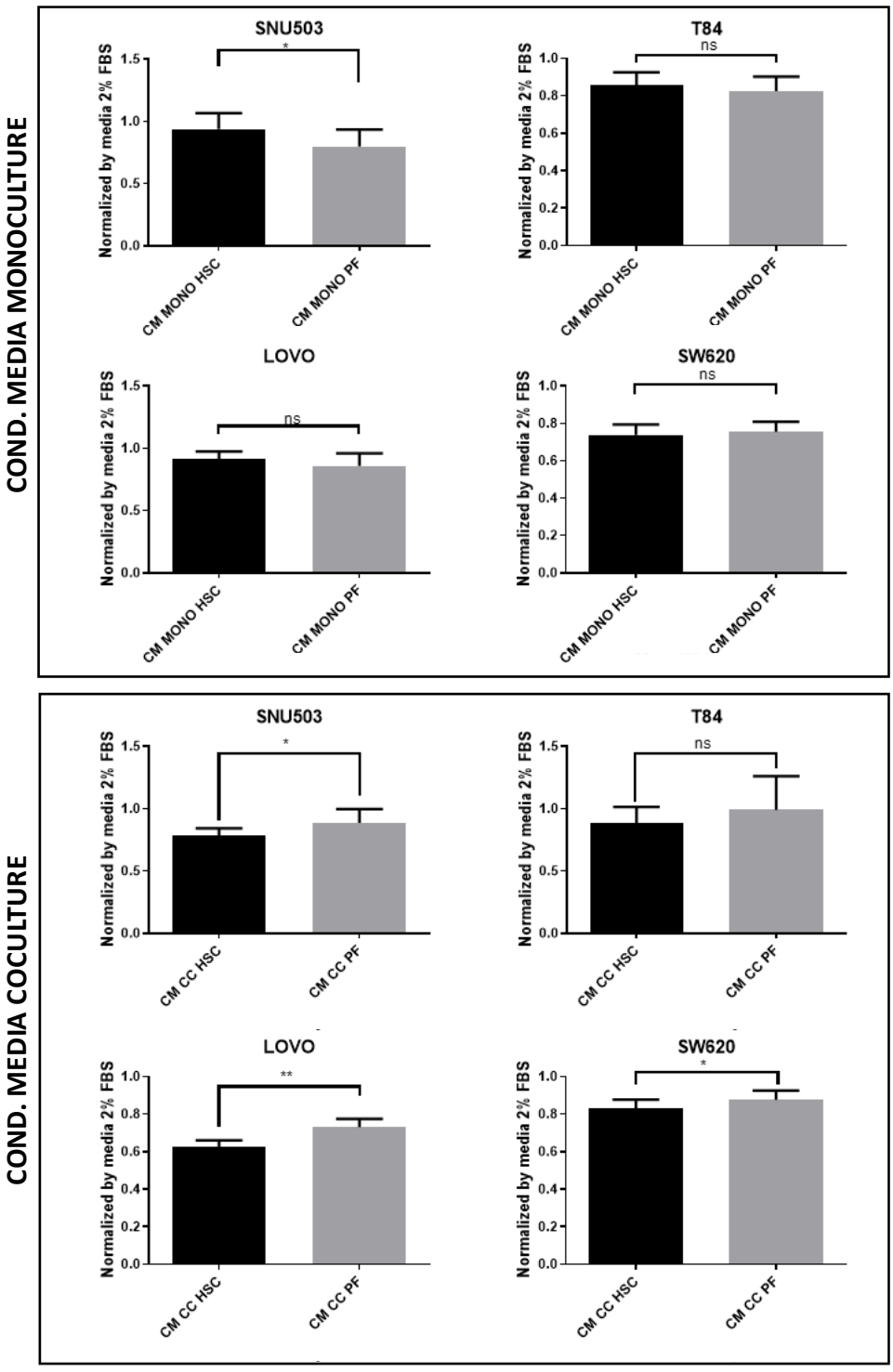

Figure 61. Proliferation assay of SNU-503, T84, LoVo and SW620 cell lines *(upper panel) with media from monocultured HSCs (CM MONO HSC) and PFs (CM MONO PF), (lower panel) and with media from cocultured HSCs (CM CC HSC) and PFs (CM CC PF). Mann-Whitney test. Mean with SD (n=4). * p value<0.05, ** p value<0.01. ns, non-significant.*

4.2. The fibroblast marker CD90 defines two CAF subpopulations according to the level of its expression

CD90 fibroblast marker is regularly used in our laboratory as a CAF marker. When using it by flow cytometry, we had already observed that, although at different staining intensities, most of the CAFs isolated from patients were positive for CD90. However, on one occasion the CAFs isolated showed as low expression of CD90 that part of the population was negative when analyzed through flow cytometry (Figure 62, first panel). It was uncommon to see a part of an isolated CAFs population negative for CD90. For this reason, we hypothesized that CD90 may be a marker useful to distinguish different CAF subpopulations. Thus, we decided to further study the CAFs isolated from this patient. To do that, we started isolating through cell sorter CD90 positive and CD90 negative CAFs and assessing the RNA levels of CD90 gene, *THY1*, through qPCR. With that, we saw that, although CD90 was significantly lower in sorted CD90 negative cells at RNA level, these CAFs had a low expression of *THY1* gene. For this reason, we started referring to them as CD90 high (CD90^{hi}) and CD90 low (CD90^{lo}) CAFs.

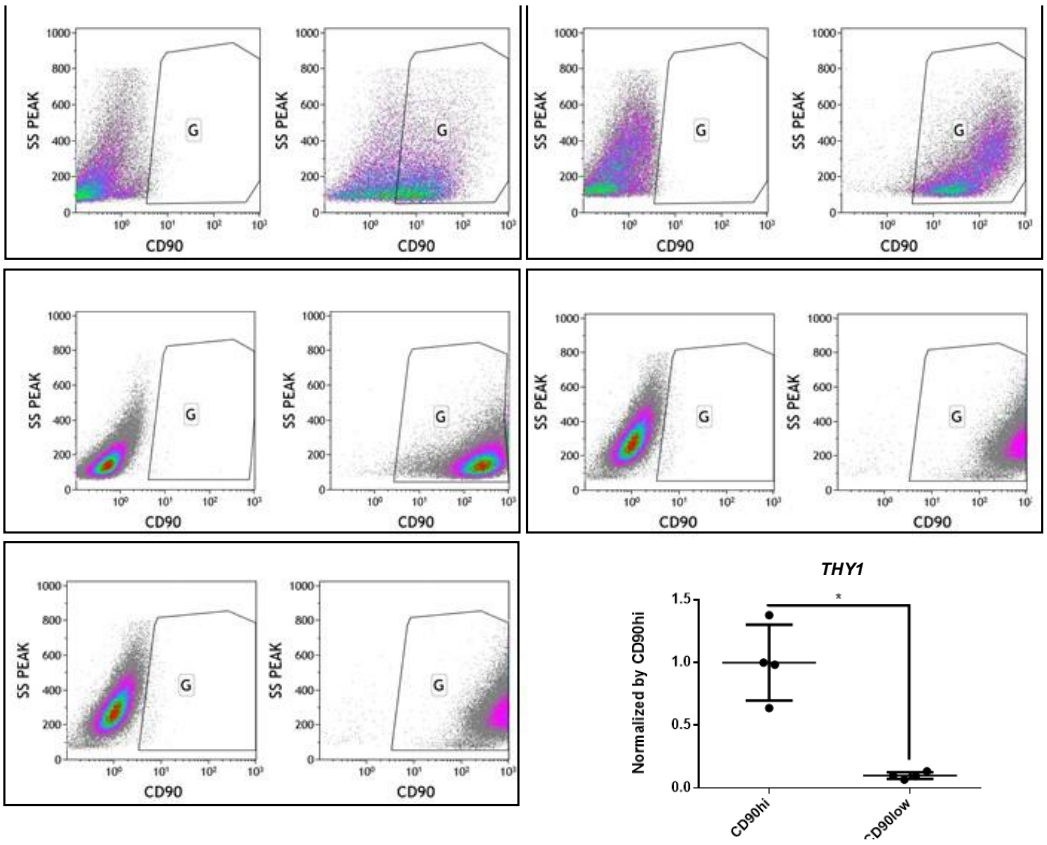

Figure 62. Flow cytometry analysis of five CRLM CAFs isolated from patient samples. *Unstained control at the left panel of the five populations. Different CD90 expression level is shown in the five cases.*

4.2.1. CD90 can be expressed both by PFs and HSCs

In the bibliography, CD90 is defined as a CAF marker in different tumor types. Concerning normal liver, CD90 is considered specific to fibroblasts present in portal spaces (PFs). Thus, when we observed the different expression levels of CD90 in the isolated CAFs, our first postulation was that, possibly, $CD90^{hi}$ CAFs could be coming from PFs, while $CD90^{lo}$ or negative cells could come from HSCs. However, we observed that the HSCs we worked with *in vitro* expressed THY-1 (CD90 gene), although at lower levels when compared with PFs (Figure 36). It is also described that plastic from cell culture plates can activate HSCs and fibroblasts. Thus, we hypothesized that, although CD90 marker is not typical of HSCs, its expression can increase in these cells when they are activated by a stimulus. To prove this, we stimulated HSC-GFP with TGFβ1, a factor that is described to transform fibroblasts to myofibroblasts and expected to observe higher expression of CD90.

First, we treated HSC-GFP cells with TGFβ1 for 5 days and assessed their CD90 expression at the protein level through flow cytometry. After this time, we observed that the media acidification was different as well as that the morphology of the cells had slightly changed (Figure 63A). Concerning CD90 expression at the protein level, the intensity of the staining increased a little with the treatment, but no significant differences were observed (Figure 63B and C).

Moreover, we also assessed the RNA levels of *THY-1* as well as *ACTA2*, *SERPINF1*, *CYGB* and *NGFR* genes when HSC-GFP cells were treated with TGFβ1 (Figure 63D). Again, we observed not significant differences concerning *THY1* gene while other myofibroblast markers increased their expression (*ACTA2* and *SERPINF1*). We also assessed two HSCs markers, *CYGB* and *NGFR*, and observed that they diminished due to the treatment (Figure 63D). Thus, it suggests that CD90 protein is not regulated by TGFβ1 or, at least, in HSC-GFP cells. However, in both treated and non-treated HSC-GFP cells we observed CD90 expression at RNA and protein level, confirming that these cells can express this marker in some conditions, for example when they are cultured *in vitro*. Furthermore, when HSCs express CD90, they do it at lower levels compared with control CAFs, isolated from different patients depending on the day of the experiment.

In conclusion, as we had observed CD90 expression in HSCs under some conditions, but at lower levels than PFs or the CAFs used as control, we could not discard the possibility that CD90lo CAFs were HSCs-derived CAFs.

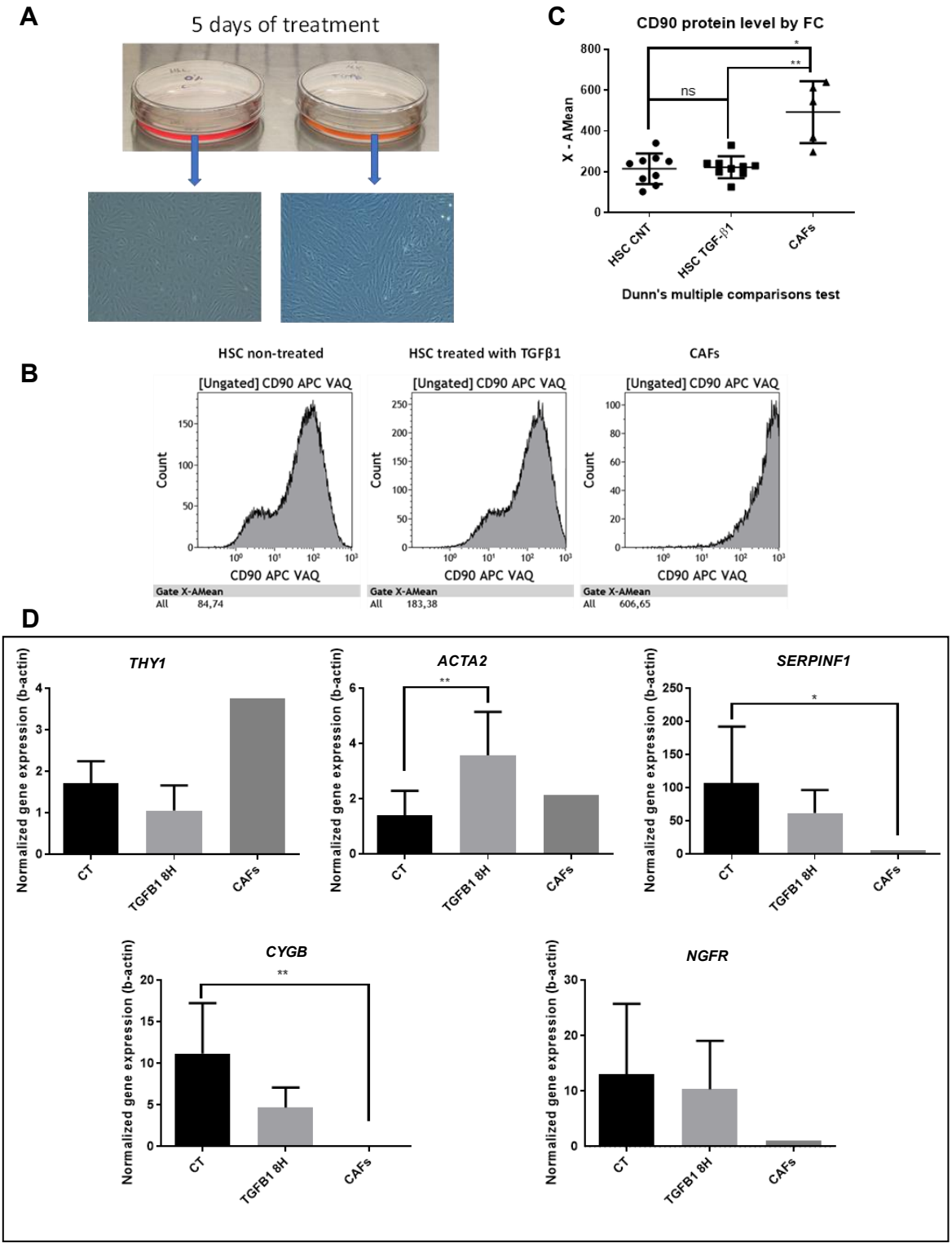

Figure 63. HSCs response to TGFβ1 stimulus. *(A) HSC-GFP plates untreated and treated with TGFβ1 after 5 days. (B) Flow cytometry obtained histogram showing CD90 staining intensities in untreated*

*HSCs, treated HSCs and CAFs. (C) Analysis of CD90 staining intensity assessed by flow cytometry. (D) qPCR assessment of a pool of genes in response to TGFβ1 treatment. Dunn's multiple comparisons test applied. Mean with SD. * p value<0.05, ** p value<0.01.*

4.2.2. Sorted CD90 low expression CAFs increase they expression level of this marker after three cell culture passages

To study if CD90 expression level was determining different CAF populations with different functions, we isolated through cell sorter $CD90^{hi}$ and $CD90^{lo}$ expression CAFs from the population of patient isolated CAFs that showed the lower level of CD90 at flow cytometer. As most of CAFs isolated from patients had flow cytometry detectable levels of CD90, we thought that maybe this protein needed to be expressed at least in some fibroblasts to keep growing in cell culture. Thus, after observing that both $CD90^{hi}$ and $CD90^{lo}$ sorted CAFs could be seeded and keep growing separately, we wondered if CD90 levels would maintain during passages or if, on contrary, the expression of this protein would be restored in $CD90^{lo}$ sorted CAFs.

For this reason, we maintained both populations in cell culture during three passages before performing a "repopulation" assay. This assay consisted of staining with two different cell traces $CD90^{hi}$ and $CD90^{lo}$ populations and, after that, mixing them and staining the solution with CD90 flow cytometry antibody.

With this experiment, we observed that the population $CD90^{lo}$ cells, shown in violet, had cells stained in the whole range of intensities, although they had been sorted only for the flow cytometer negative intensity of CD90 (Figure 64A). However, the mean intensity is still higher in $CD90^{hi}$ sorted cells (Figure 64A), as well as the RNA levels of its transcript (Figure 64B). These results suggest that CD90 is a dynamic marker the levels of which can vary under different conditions. Specifically, in our case study, it could be that CD90 expression is required for better survival *in vitro*, and/or induced by plastic cell culture plates or some substances from the media. However, these results are neither enough to discard the hypothesis that $CD90^{lo}$ CAFs derive from HSCs, as the global value of CD90 expression keeps being lower than $CD90^{hi}$ CAFs. Another plausible hypothesis would be that CD90 expression is linked to the level of fibroblast activation. That way, CAFs would express high levels of

CD90 when they are receiving activation stimuli like the contact with cancer cells or growing in plastic cell culture plates.

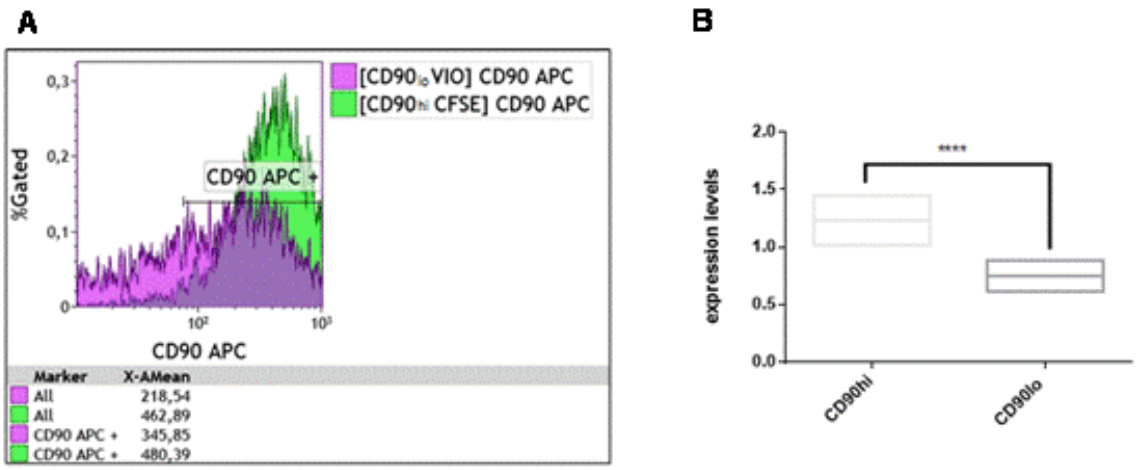

Figure 64. CD90 repopulation assay. *(A) Flow cytometry plot showing the CD90 expression of CD90^{hi} (green) and CD90^{lo} (violet) sorted CAFs after three passages of cell culture. (B) qPCR showing RNA levels of CD90 gene transcript, Thy-1. **** p value< 0.0001.*

4.2.3. CD90^{hi} and CD90^{lo} qPCR characterization

Further to the "repopulation" assay we also wondered if CD90^{hi} and CD90^{lo} cells had different RNA expression levels for other CAF genes. For that, we extracted RNA from recently sorted CD90^{hi} and CD90^{lo} CAFs and assessed a set of gens through qPCR. Among them, the only ones that showed significant differences were *THY1*, as expected, *PDPN* and *NGFR* (Figure 65). *PDPN* expression in CD90^{hi} CAFs is especially interesting as it has been described to be upregulated in different CAF subpopulations and associated with the promotion of M2-like pro-tumoral macrophages as well as with monocyte recruitment (341). Moreover, some of the markers selected are typical of HSCs (*CYGB*) and PFs (*GREM1*). Thus, as there are no differences between CD90^{hi} and CD90^{lo} concerning these markers, it suggests that both populations would have arisen from the same precursor cell, although further assessment of precursor associated genes would be needed to conclude this.

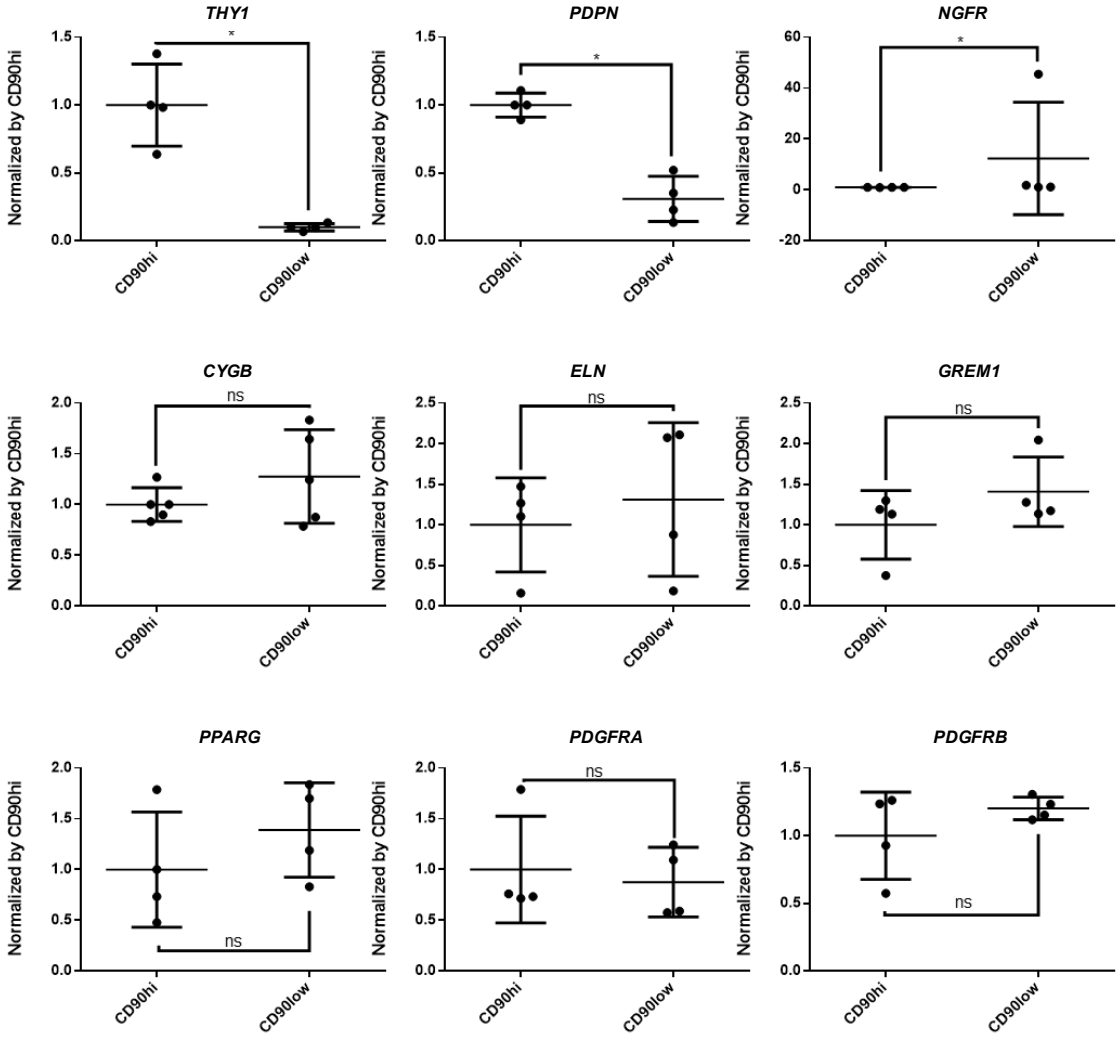

Figure 65. qPCR characterization of CD90^{hi} and CD90^{lo} sorted CAFs. *Mann-Whitney test applied. Mean ± SD (n=4). * p value<0.05. ns, non-significant.*

4.2.4. CD90^{hi} and CD90^{lo} Western Blot characterization

We also assessed some CAFs markers at protein level to ensure that our cells of study, which were isolated from patients, were fibroblasts. Positivity in PDGFRβ, FAPα, CALD1 and α-SMA, as well as negativity in CD31 (endothelial cell marker), showed that CD90^{hi} and CD90^{lo} isolated cells are CAFs. The high expression CD90^{hi} and CD90^{lo} show in PDLIM3 suggest that those CAFs have both arose from the same mesenchymal precursor, which is in line with the previous qPCR characterization results. As PDLIM3 is a PF marker, CD90^{hi} and CD90^{lo} CAFs seem to come from this mesenchymal population. Moreover, as observed in previous qPCR, the expression of PDPN at protein level is also higher in CD90^{hi} than in CD90^{lo} (Figure 66).

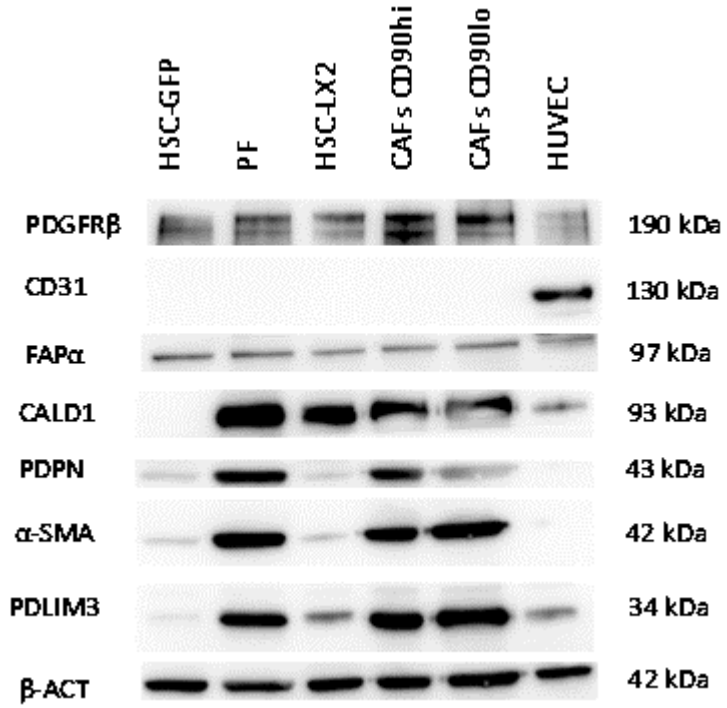

Figure 66. Western Blot characterization of two HSC cell lines (HSC-GFP and HSC-LX2), PF, CAFs CD90^{hi} and CAF CD90^{lo}. *HUVEC cells were also included as CD31 positive marker.*

4.2.5. CD90^{hi} and CD90^{lo} showed a different secretome profile

As we had observed that CD90^{hi} and CD90^{lo} cells had not only differences in CD90 expression level, but also the expression of other genes and proteins, we wondered if their secretome profile would be also different. For that, we performed a Raybiotech cytokine array that showed that these CAFs secrete a different pool of molecules. This analysis showed that CD90^{hi} CAFs secreted higher amounts of CCL11 and angiogenin; while MIF, bFGF, ANGPT2, IGFBP-3, adiponectin and CCL25, among others, were highly secreted by CD90^{lo} CAFs (Figure 67).

CCL11 is associated with TAMs recruitment and angiogenesis promotion (342). Concerning angiogenin, it not only activates endothelial cells to induce tumor angiogenesis, but also targets tumor cells to promote cell survival, proliferation and/or migration, and is associated with metastasis in CRC patients (343). Thus, CD90^{hi} CAF's secretome suggests that this CAF population is involved in tumor-promoting processes.

On contrary, among the molecules highly secreted by CD90^{lo} cells we find CCL25, which has controversial functions in cancer contexts. On one side, it is described to participate in the

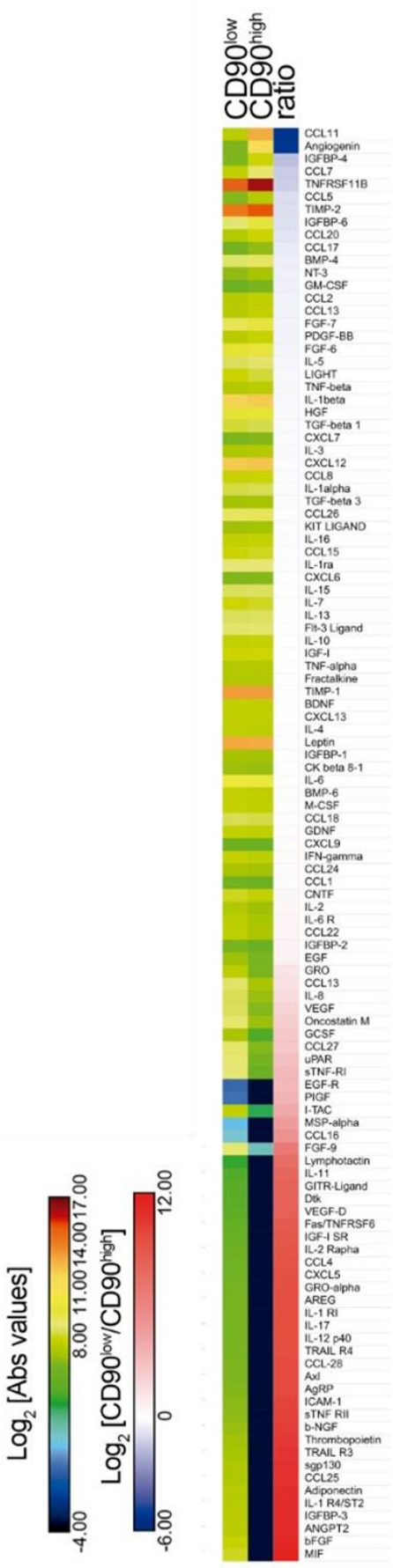

migration and invasion of cancer cells, stimulate tumor cell proliferation, and being associated with apoptosis and drug resistance. On the other side, colon cancer inhibits cancer cell migration. Moreover, CCL25 have been associated with cytotoxic lymphocytes infiltration, which have an anticancer effect, as these cells express its receptor: CCR9 (344).

Similarly, IGFBP-3, also oversecreted in CD90^{lo} CAFs, is described to play pro-apoptotic and growth-inhibitory actions or to have cytoprotective and growth-potentiating properties depending on the context and/or the cancer type (345). In colorectal cancer, low levels of this protein are associated with better survival, while in cholangiocarcinoma it is the other way around (346).

Concerning the CD90^{lo} highly secreted adiponectin, multiple evidence suggests low adiponectin levels are associated with the threat of developing several types of cancers. Moreover, this molecule has been described to orchestrate multiple biological functions to inhibit cancer progression, like angiogenesis, growth and proliferation, invasion, migration, and metastasis (347).

Considering the CD90^{lo} secreted molecules mentioned before, we could postulate that this CAF subpopulation may be displaying tumor-restraining functions including cytotoxic lymphocytes recruitment, pro-apoptotic and growth-inhibitory actions and inhibition of angiogenic process.

Figure 67. Raybiotech cytokine array showing the secretome comparison between CD90^{hi} and CD90^{lo} CAFs.

However, these CD90^{lo} CAFs also secrete molecules that are extensively associated with cancer progression. It is the case of MIF, bFGF, ANGPT2. The first one was discovered as macrophage migration inhibitory factor. Taking into account that the presence of macrophages is usually an indicator of poor prognosis, the secretion of this factor would be inhibiting cancer progression. However, the pro-tumoral functions of MIF are widely described (348,349). In the same line, bFGF and ANGPT2 are also described to be tumor-promoting, their functions are mainly associated with the angiogenic process (350,351).

In conclusion, whether CD90^{hi} and CD90^{lo} are tumor-promoting or tumor restraining CAF subpopulations needs to be further assessed through functional experiments. However, Raybiotech cytokine array obtained information suggests that CD90^{lo} has a greater secretory phenotype when compared with CD90^{hi}.

4.2.6. CD90^{hi} and CD90^{lo} qPCR characterization for "origin" selected markers

We had observed that CD90^{hi} and CD90^{lo} CAFs differ in their expression of some proteins as well as on the factors they secrete, which suggested that this marker defined two CAF subpopulations that probably were performing different functions. Thus, as we also had observed that both PF and HSCs could express CD90 marker and had postulated that different CAF subpopulations could arise from different liver mesenchymal precursors, we wondered if these CD90 subpopulations arose from HSCs or from PFs. For this, we assessed the previously selected "origin" markers through qPCR. This analysis showed no differences between CD90^{hi} and CD90^{lo} concerning the selected HSC and PF markers. In fact, when comparing the expression of them with HSC and PF, the levels of expression suggest that CD90^{hi} and CD90^{lo} are CAFs derived from PF (Figure 68).

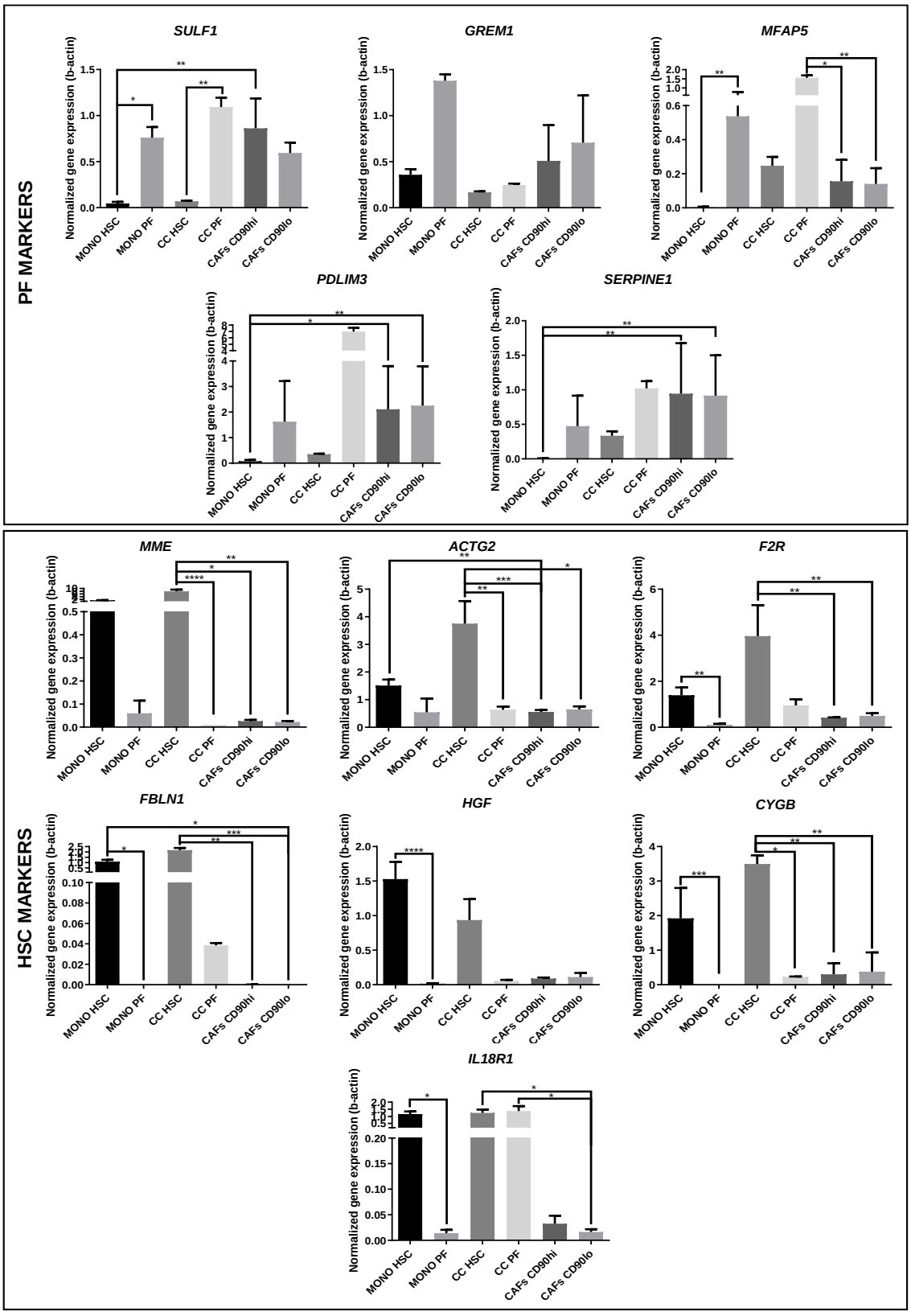

Figure 68. "Origin" markers RNA levels of monocultured HSCs (MONO HSC), monocultured PFs (MONO PFs), cocultured HSCs (CC HSC), cocultured PF (CC PF), CD90^{hi} sorted CAFs and CD90^{lo} sorted CAFs*. Dunn's multiple comparisons test applied. Mean with SD (n=4). *p value<0.05, **p value<0.01, ***p value<0.001, ****p value<0.0001.*

4.2.7. CD90^{hi} and CD90^{lo} RNAseq Gene set enrichment analysis (GSEA)

We observed that there were differences in protein and RNA expression, and that the secretome changed between CD90^{hi} and CD90^{lo} cells. Because of that, we decided to perform RNAseq to better characterize these CAFs at RNA level. This RNAseq showed an increase of proliferation, complement, extracellular matrix production and monocytes migration related pathways in CD90^{hi} when compared with CD90^{lo} (Figure 69).

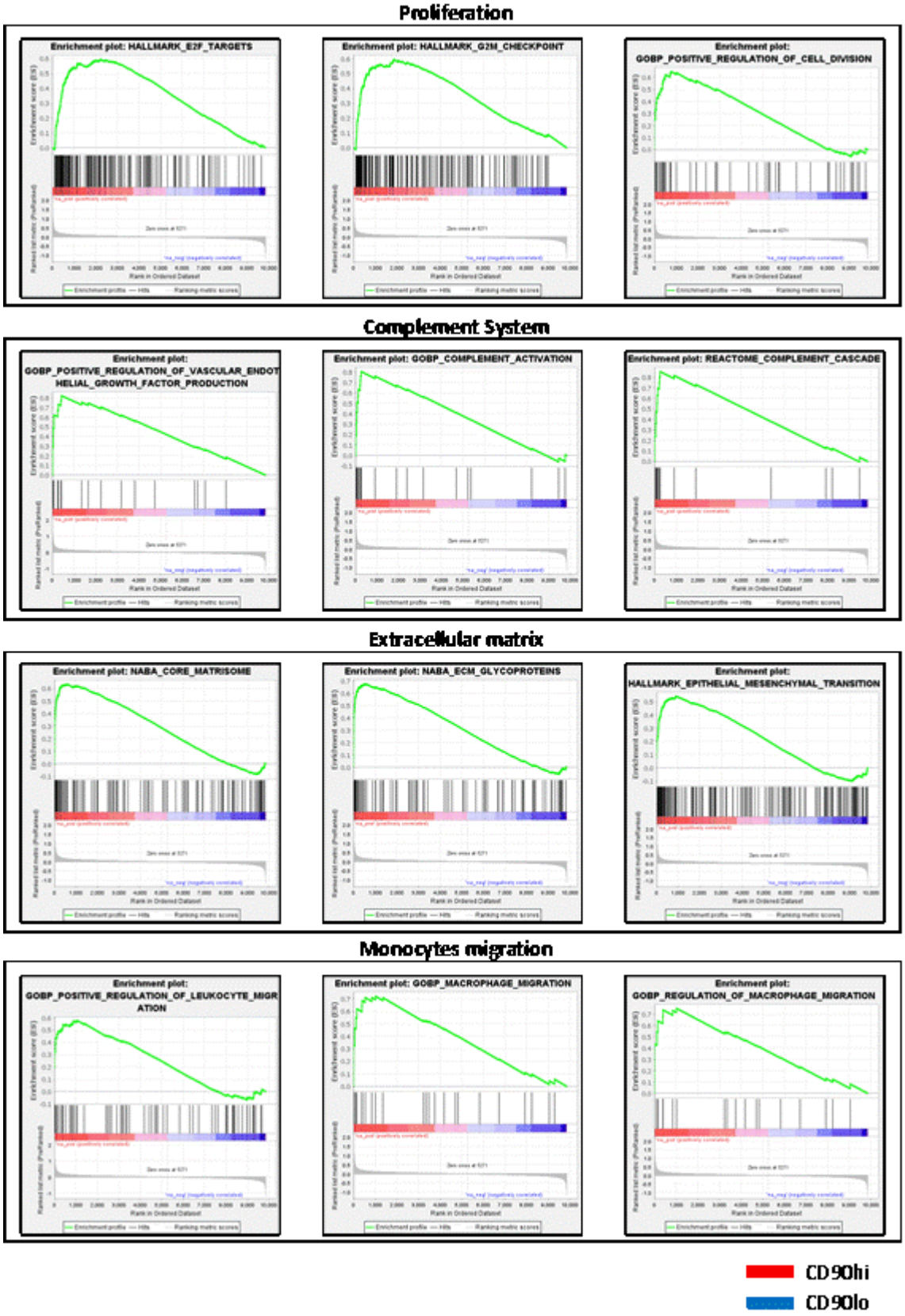

Figure 69. Gene set enrichment analysis of RNAseq data from CD90^{hi} and CD90^{lo} CAFs.

4.2.8. CD90^{hi} and CD90^{lo} CAFs recruit different immune cell populations

The previous GSEA RNAseq analysis showed that CD90^{hi} cells highly expressed pathways related to monocyte recruitment. Moreover, CCL11, which was secreted at higher amounts by CD90^{hi} CAFs, is associated with TAMs recruitment. On the other hand, one of de functions of CCL25, that was highly secreted by CD90lo CAFs, is cytotoxic T cell recruitment. For all these reasons, we decided to test which PBMC populations were CD90^{hi} and CD90^{lo} able to recruit through an in vitro transwell migration assay. For that, conditioned media from CD90^{hi} and CD90^{lo} previously sorted cells was placed at the well were transwell inserts would be placed, acting as the migration stimuli. At the upper part of the insert, PBMCs isolated from healthy donors were seeded. After two hours in cell culture, we assessed which immune cells had migrated through flow cytometry. Doing that, we observed that conditioned media coming from CD90^{hi} and CD90^{lo} CAFs showed the recruitment of different immune cell populations. In line with our previous observations, CD90^{hi} CAFs recruit more monocytes while CD90^{lo} CAFs recruit more T cells, both T cytotoxic and T helper. Among the last group, T helper cells recruited are not Treg, neither Th2, thus it suggests that they would be mediating a functional immune response. (Figure 70). Moreover, higher monocyte recruitment by CD90^{hi} CAFs is in line with the high expression of *PDPN* in these CAFs, as the expression of this marker has been associated to it (341).

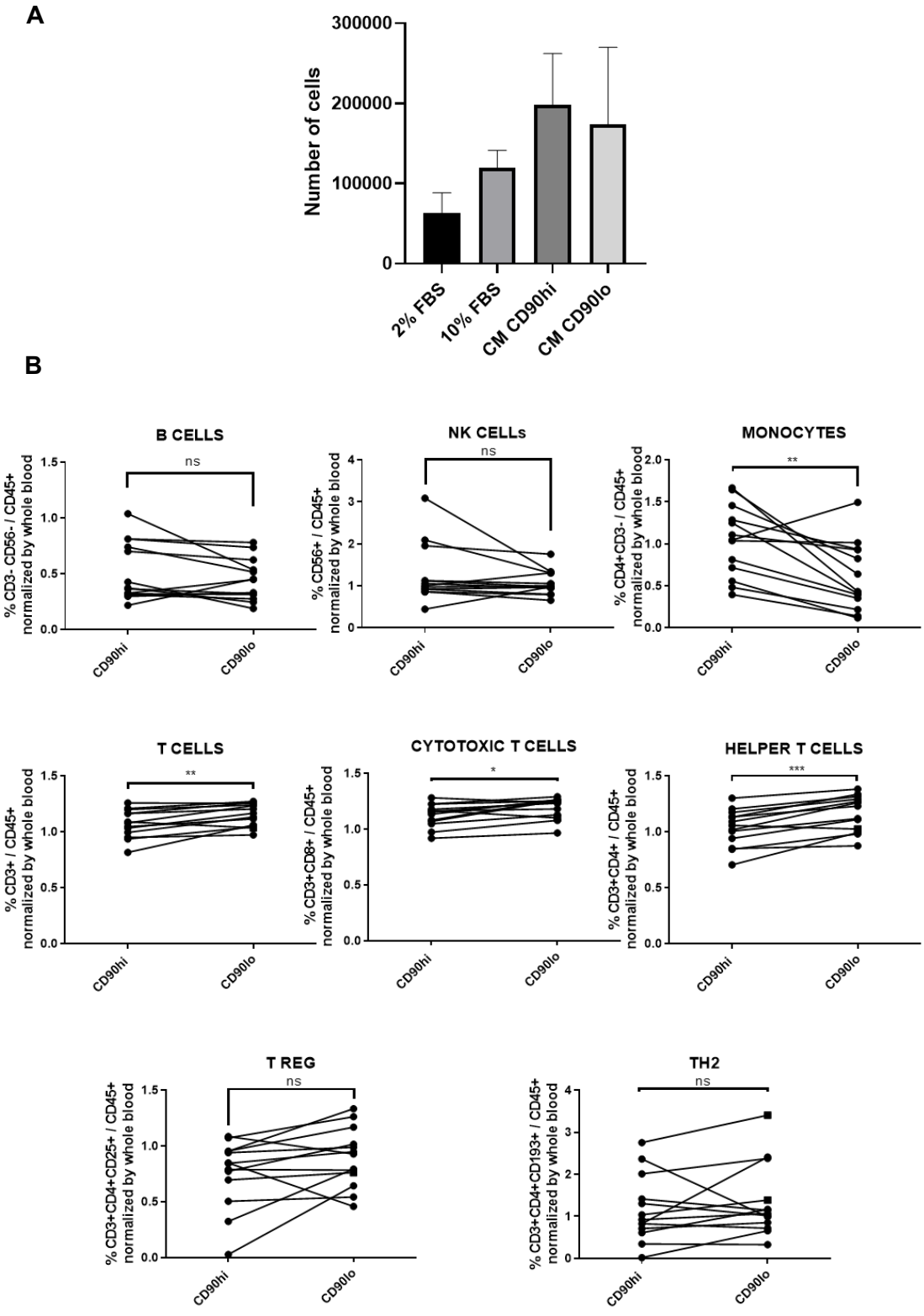

Figure 70. Migration assay using CD90^{hi} and CD90^{lo} conditioned media. *(A) Number of cells at the lower part of the transwell of each condition. (B) Graphical representation of PBMC's migration assay performed with conditioned media from CD90^{hi} and CD90^{lo}. Percentage on CD45 for each cell type was calculated and subsequently normalized by the corresponding percentage of whole blood sample. Wilcoxon test was applied. Mean with SD (n=15). *p value<0.05, **p value<0.01, ***p value<0.001, ****p value<0.0001. ns, non-significant.*

4.2.9. CD90^{hi} conditioned media can induce monocyte M2 polarization

As we had observed that CD90^{hi} conditioned media factors recruited a higher percentage of monocytes, we wondered if this media also was also capable to polarize these monocytes to M1 or M2 phenotype. For that, we did a M1/M2 polarization assay with blood monocytes isolated from six healthy donors. These monocytes were exposed to CD90^{hi} and CD90^{lo} conditioned media, as well as with media with different factors that serve as controls of polarization. Control factors induced the M1 or M2 polarization as expected (Figure 71a), confirming that the experiment was well performed. This experiment showed that isolated monocytes cultured with CD90^{hi} conditioned media expressed higher levels of CD163, suggesting that CD90^{hi} population of CAFs can polarize monocytes to M2 macrophages (Figure 71b). This M2 polarization mediated by CD90^{hi} CAFs is in line with the already described association of high expression of *PDPN* with tolerogenic polarization (341).

In conclusion, these two subpopulations of CAFs have a different impact on the immune response. On the one hand, CD90^{hi} CAFs are able to recruit higher numbers of macrophages and to polarize them to M2 phenotype. These results would be in line with the already described association between PDPN expression in CAFs and the recruitment and polarization of macrophages. On the other hand, CD90^{lo} CAFs would recruit higher levels of T cells, both cytotoxic and helper, which would not include Tregs or Th2.

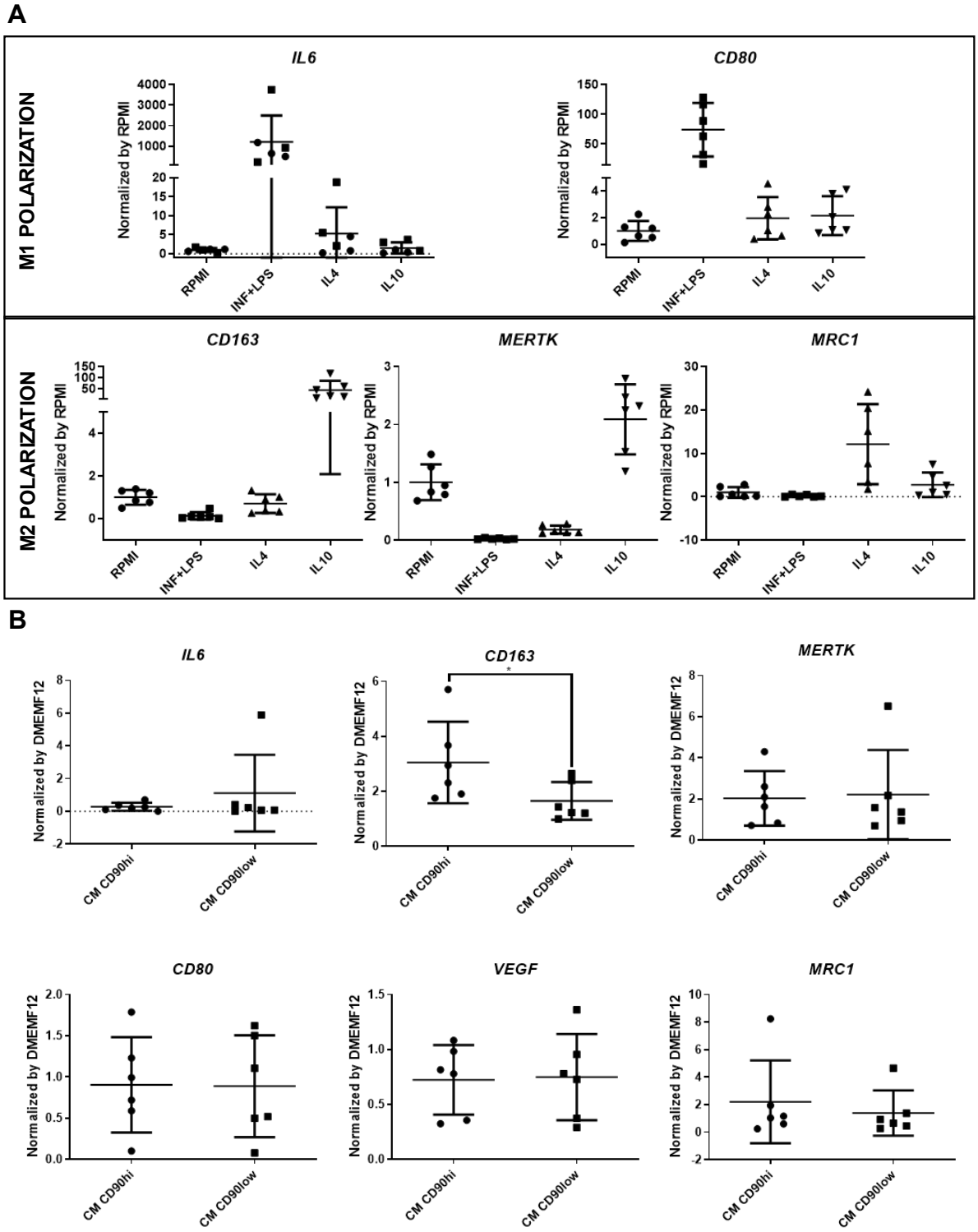

Figure 71. Macrophage polarization assay. *(A) M1 and M2 polarization marker genes expression in response to the control factors. (B) M1 and M2 polarization marker genes expression in response to the conditioned medias they were exposed. Mean with SD (n=6). Wilcoxon test applied. *p value<0.05.*

4.2.10. CD90^{hi} conditioned media affects tumoral cells proliferation

In addition, although we had no information concerning the effect of CD90^{hi} and CD90^{lo} CAFs on tumoral cells, we wondered if they could affect on their proliferation. Thus, we performed a proliferation assay using conditioned media from these two CAF subpopulations. We observed that conditioned media from CD90^{hi} induced an increase on the proliferation of three of the four CRC metastatic cell lines tested (Figure 72).

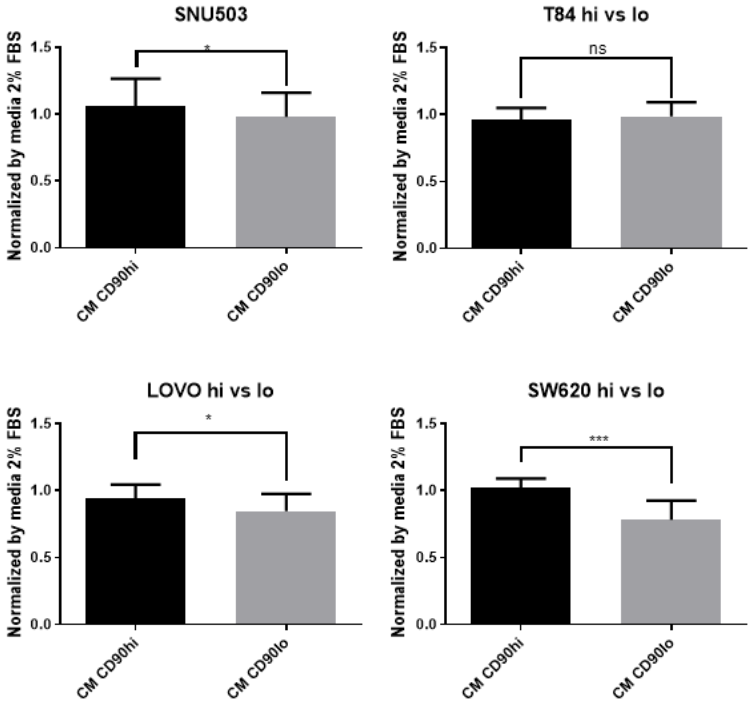

Figure 72. Proliferation assay SNU-503, T84, LoVo and SW620 cell lines cultured with CD90^{hi} and CD90^{lo} conditioned media. *Mann-Whitney test applied. Mean with SD (n=4). Wilco *p value<0.05, ***p value<0.001, ns. not significant.*

4.2.11. CD90 marker distribution in tissues from dHGP and non-dHGP CRLM patients

We had observed in *in vitro* that CD90 expression level was linked to different CAF subpopulations with different functions. Therefore, we wondered how this marker was expressed in CRLM patients. For that, we performed IHC for CD90 in whole-slides of paraffin embedded tissue samples from both dHGP and non-dHGP. This experiment showed that CD90 was staining most of the CAFs in central regions of both HGP. CD90 was also expressed at the invasive margin of both HGP. Concerning the fibrotic rim of dHGP, it contained both

positive and negative cells for CD90 (Figure 73), suggesting that the fibrotic capsule is composed by different CAF subpopulations.

Moreover, it is important to highlight that, when stablishing this IHC conditions, we observed that diluting or concentrating CD90 antibody the number of cells stained decreased or increased. Thus, it indicated that CD90 is expressed in most of the CAFs but at different levels. We postulate that this high or low expression would be the one linked to the functions described. However, in this whole-slide IHCs we did not observed differences between HGP concerning CD90 stained cells.

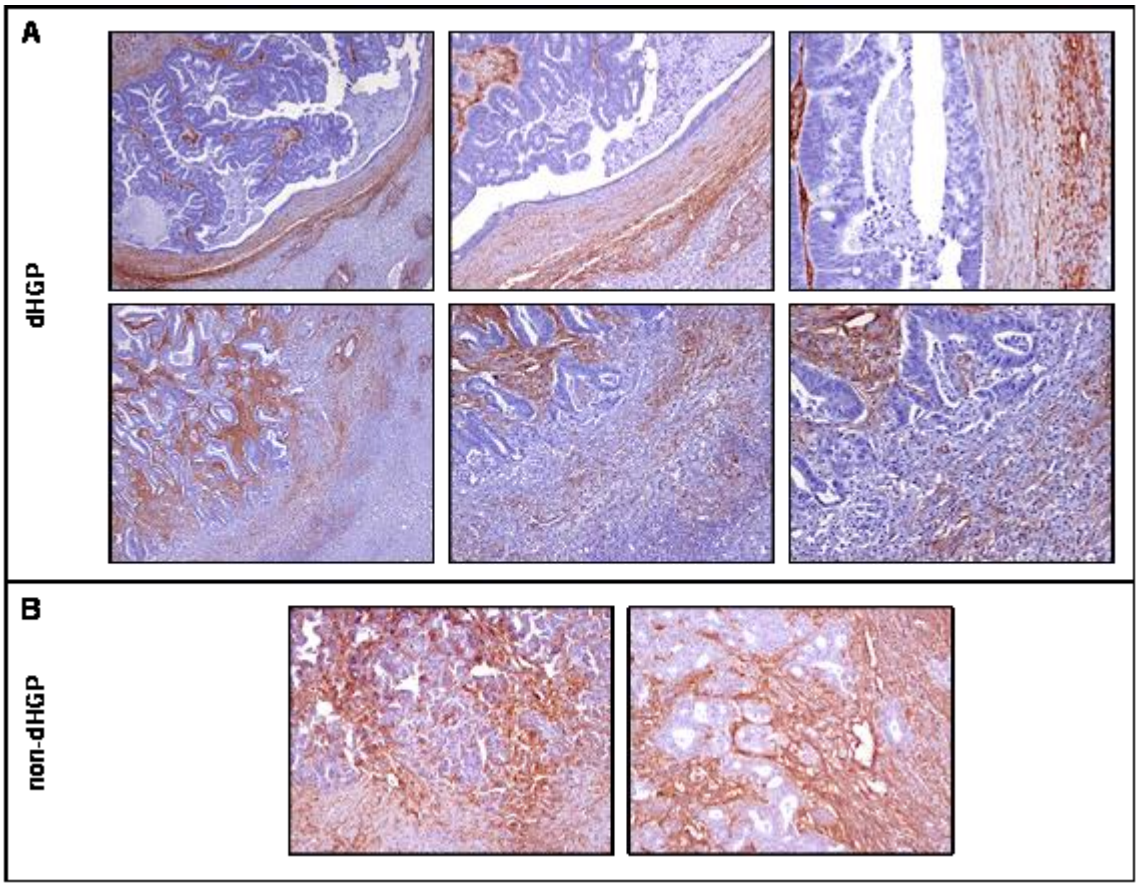

Figure 73. CD90 marker distribution in tissues from dHGP and non-dHGP. *(A) dHGP images from two different patients (each row corresponds to a patient) showing CD90 staining. Images from the first, second and third column are taken at 4x, 10x and 20x magnification, respectively. (B) 20x magnification non-dHGP images from invasive margin (left image) and central region (right image).*

4.2.12. Immunofluorescence in tissue samples from CRLM patients showed that CD90 staining does not colocalize with F2R

We had observed no differences between $CD90^{hi}$ and $CD90^{lo}$ concerning the RNA expression of our previously selected markers of origin (Figure 68). Thus, both CAF populations may come from the same origin. Their RNA expression for the origin markers suggested that they both would come from PF. In addition, papers focused on liver fibrosis define CD90 as a good marker for portal fibroblasts. We performed double IF for CD90 and F2R in to see if they are completely different populations or if they colocalize. With that we observed that generally they are different populations. However, we could see colocalization in very few cells (Figure 74). These results suggest that HSCs (F2R positive cells) usually do not express CD90 (or express it at low levels, not detectable through IF), although they can do it under some conditions, which is in line with our previously exposed experiments done *in vitro* (Figure 63).

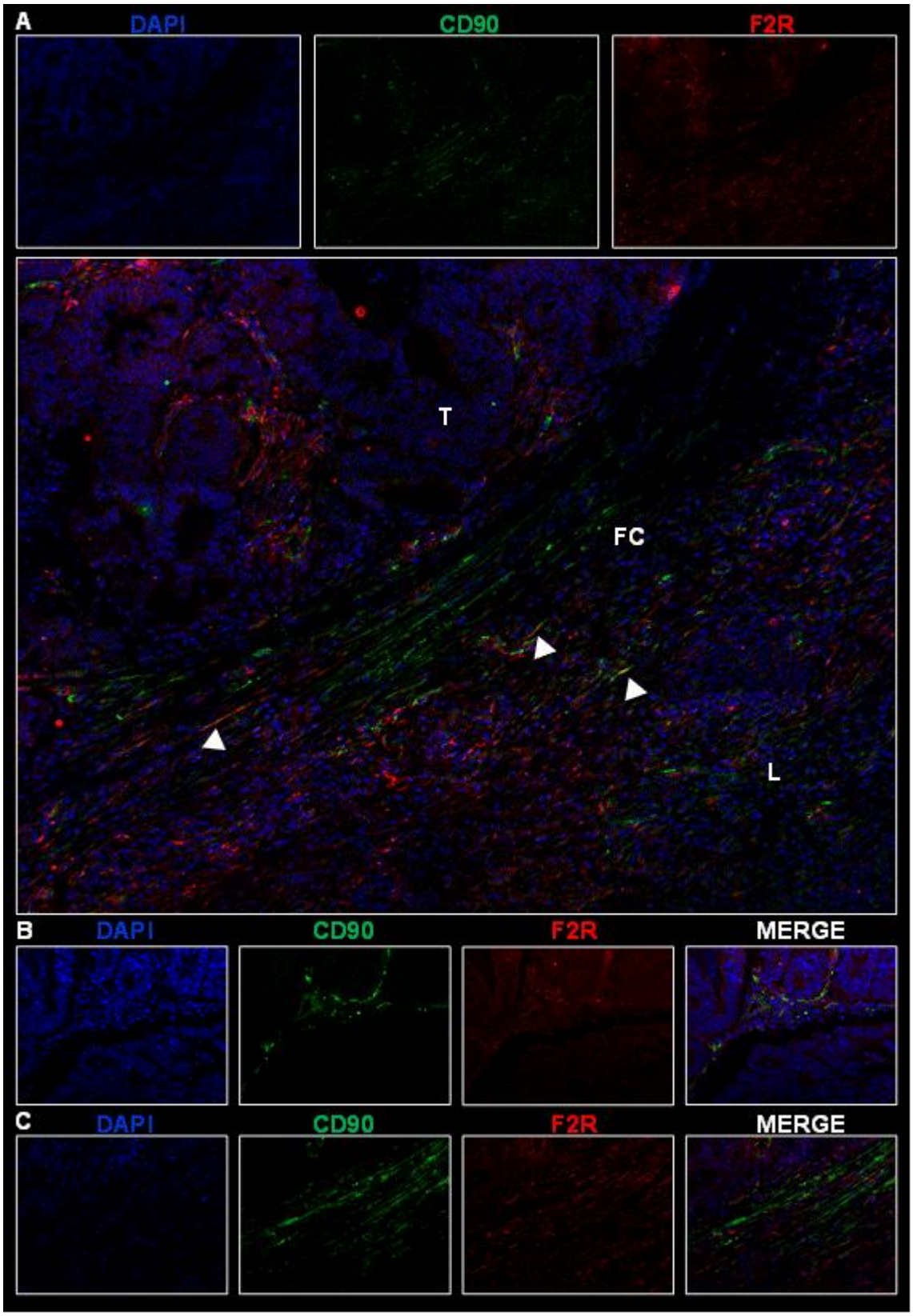

Figure 74. Double immunofluorescence showing CD90 in green and F2R in red. *(A) Mosaic image that shows a dHGP tumor interphase (T: tumor, FC: fibrotic capsule, L: liver). Arrows indicate colocalization. (B) 20x magnification images corresponding to a tumor central region. (C) 20x magnification image corresponding to a dHGP tumor interphase.*

4.3. CRLM CAF subpopulations assessment according to CAF classical markers in HGP context

Since they have been described, CAFs have been identified through a set of commonly used fibroblast markers in between we can find αSMA, FAP and IL1β, among others. However, CAFs are such a heterogeneous population that varies depending on the tissue or the factors at which they are exposed. Because of that, none of the commonly used markers is useful to identify all of them, but they are staining different CAFs subpopulations. Moreover, in pancreatic cancer, it has been described two subpopulations of CAFs: myofibroblasts (myCAF), expressing high levels of αSMA; and inflammatory CAFs (iCAFs), expressing low levels of αSMA and secreting cytokines like IL1β or IL6 (162). Thus, we aimed to assess how the most used CAF classical markers and myCAF/iCAF subpopulations are distributed in the context of CRLM HGP, both in our cell models *in vitro* and in paraffin embedded patient samples.

4.3.1. qPCR classical markers assessment of HSCs, PF and CD90^{hi} and CD90^{lo} populations

We assessed if the HSCs, PFs and CD90^{hi} and CD90^{lo} we work with are more like myCAFs or like iCAFs. For that, we performed qPCR for *ACTA2* (αSMA coding gene), *IL1β* and *FAP*. This last one, FAP, is also a classical CAF marker used to identify these cells, but it is not clear if the subpopulation it stains is closer to myCAF or to iCAF.

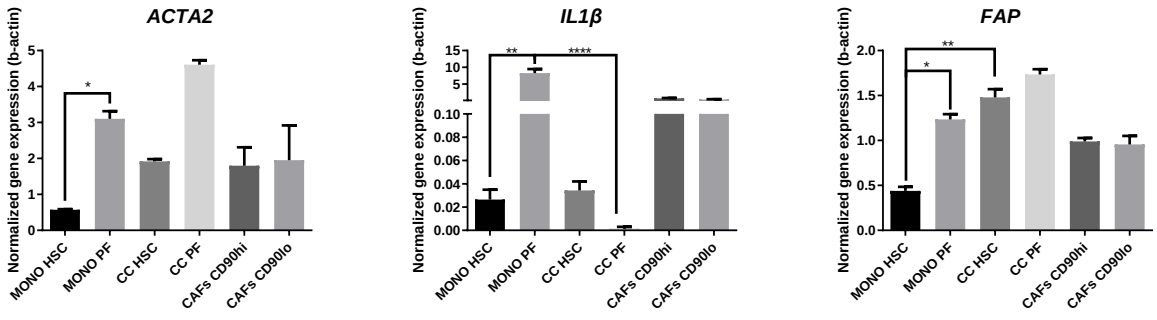

Figure 75. CAF classical markers qPCR assessment. *Dunn's multiple comparisons test applied. Mean with SD (n=4). *p value<0.05, **p value<0.01, ***p value<0.001, ****p value<0.0001.*

Thus, considering these three classical markers, it seems that, in monoculture, PF have more expression of all of them, which one could expect as PF are already fibroblasts while HSCs

are not. However, once activated by the presence of tumoral cells, in co-culture, these expression levels change: Cocultured HSCs show higher levels of *IL1β* when compared with PF, which express high levels of *ACTA2*. This suggests that CC HSCs would be acting iCAFs while CC PF would be myofibroblasts. In the case of $CD90^{hi}$ and $CD90^{lo}$, they do not show differences concerning these markers (Figure 75).

4.3.2. RNAseq data demonstrates a decrease of iCAF genes in both HSCs and PF when they are co-cultured

To further study myCAF and iCAF classification in HSCs and PFs, we created a gene set of 25 myCAF specific genes and one of 25 iCAF genes and assessed them in RNAseq data. With this analysis, we observed that iCAF genes decrease in co-culture both in HSCs and PFs, while myCAF genes increase (Figure 76A and B). On the other hand, when comparing HSC with PF, HSCs showed lower levels of both myCAF and iCAF signatures (Figure 76A and C).

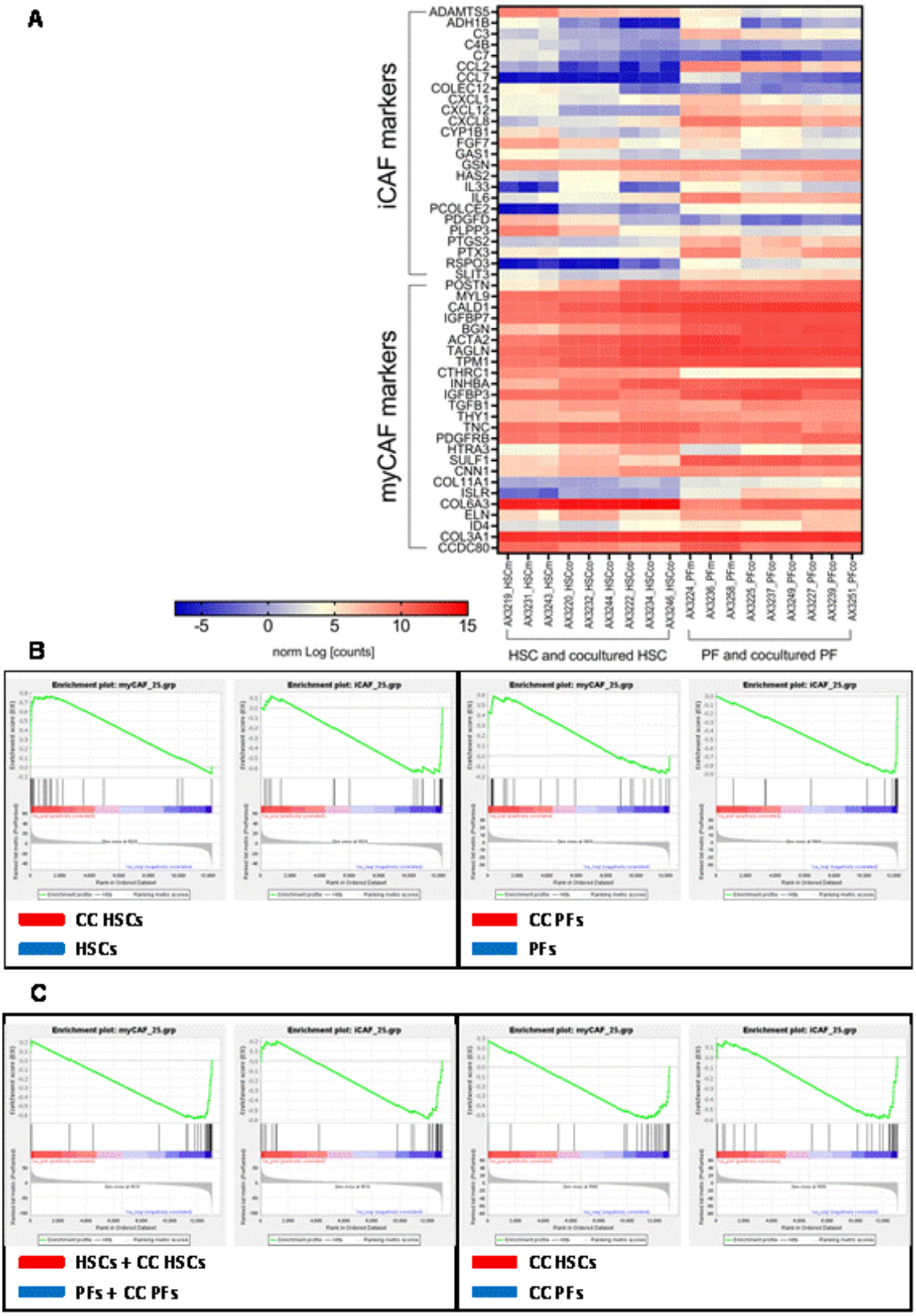

Figure 76. myCAF and iCAF gene sets assessment in CD90^{hi} and CD90^{lo} RNAseq data. *(A) Heatmap showing HSCs and PFs RNAseq data for 25 myCAF and 25 iCAF genes. (B) GSEA analysis comparing myCAF and iCAF gene sets between monocultured and cocultured of both HSCs and PFs. (C) GSEA analysis comparing myCAF and iCAF gene sets between HSCs and PFs.*

4.3.3. qPCR showed that direct co-culture promotes an increase of myCAF genes while indirect co-culture promotes an increase of iCAF genes

We had observed from RNAseq data that both HSCs and PFs increased myCAF gene set and diminished iCAF gene set when co-cultured with tumoral cells. To obtain the samples for RNAseq, we had carried out a direct co-culture, in which both paracrine and cell-to-cell communications are taking place. Thus, we wondered if an indirect co-culture, that allows only paracrine signaling to take place, would induce a different gene expression pattern on mesenchymal cells.

To test that, we performed an experiment in which we co-cultured HSCs both in a direct and an indirect way in parallel. We also add the monoculture condition, and an extra condition in which a monolayer of HSCs was indirectly co-cultured with a mix of HSCs and tumoral cells (INDIRECT CC/CC) (Figure 77).

As genes representative for the myCAF phenotype we chose ACTA2 and POSTN. As expected, both genes were increased in the direct co-culture condition. As genes representative for the iCAF phenotype we chose CCL2 and IL6 and observed that both genes were increased in the indirect co-culture condition. Meanwhile, these genes diminished (CCL2) or showed no significand differences (IL6) when looking at direct co-culture (Figure 77).

In conclusion, our results suggest that cell-to-cell communications that occur between tumoral and mesenchymal cells in direct co-culture induce a myCAF phenotype. On the other hand, paracrine signals present in indirect co-culture promote the differentiation of mesenchymal cells towards an iCAF phenotype. Thus, it would be interesting to explore the changes on the expression pattern of HSCs and PFs in indirect co-culture conditions, as these mesenchymal cells may give rise to different CAF subpopulations depending on the kind of signals they receive.

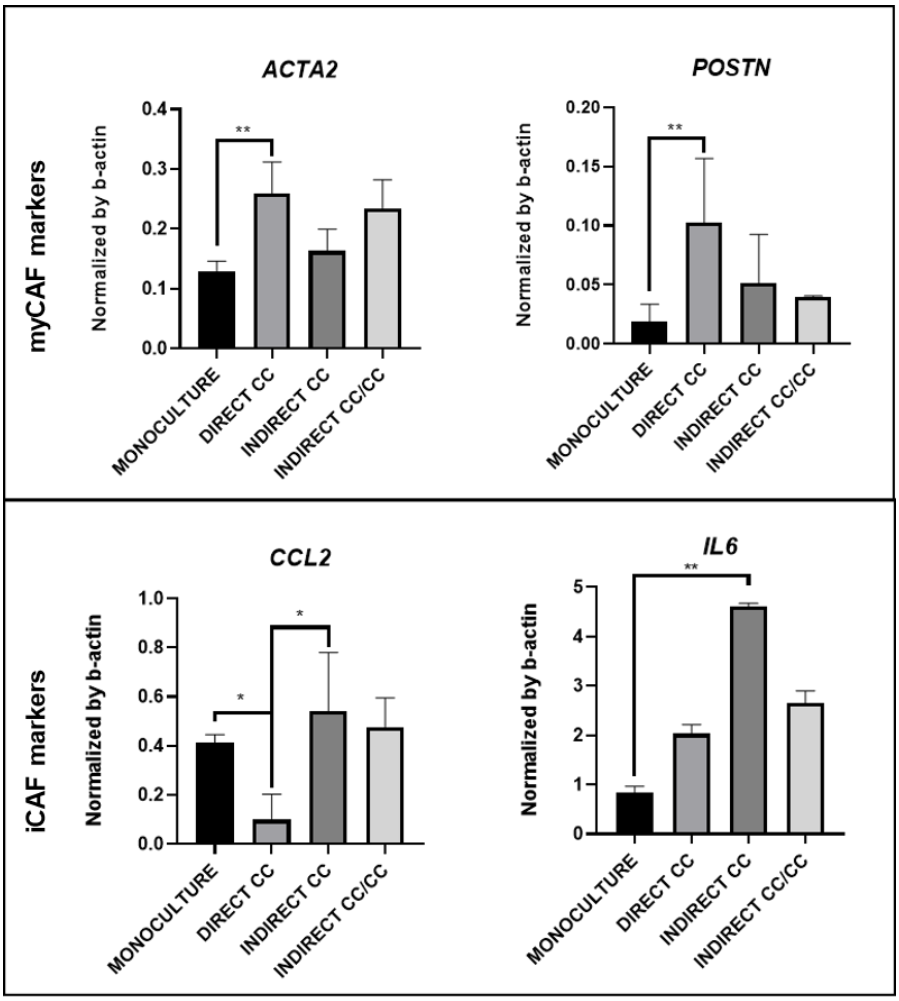

Figure 77. myCAF and iCAF markers qPCR assessment. *Kruskal-Wallis test applied. Mean with SD (n=4). *p value<0.05, **p value<0.01.*

4.3.4. Classical CAF markers distribution in tissues from dHGP and non-dHGP CRLM patients

αSMA and FAP are the most common CAF markers used in the literature, being αSMA the most established marker associated to myCAF phenotype. Thus, we investigated the distribution of these markers in paraffin embedded samples from CRLM patients. IHC for αSMA and FAP showed an intense staining of both at invasive margin areas (Figure 78A-D). These areas are those where there is a constant tissue remodeling and where tumor cells show more aggressive phenotypes, higher proliferation, and migration capabilities. On contrary, there is a progressive decrease in FAP staining from the liver-tumor interface to central areas (Figure 78E-H). On the other hand, αSMA staining is quite homogeneous in the whole tumor. These markers distribution could be explained by the fact that central areas

usually correspond to areas of secondary fibrosis, which are enriched in myCAFs. Thus, the activation pattern of CAFs from central regions would be different from those areas closer to the invasive margin.

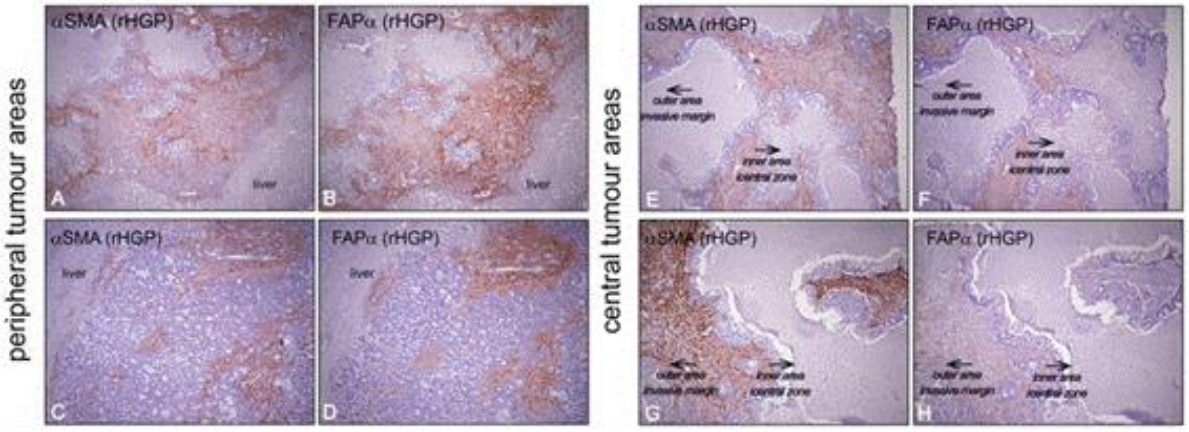

Figure 78. αSMA and FAPα distribution in replacement HGP. *10x magnification images of αSMA and FAP IHC from peripherial and central tumor areas of replacement HGP (rHGP).*

Moreover, concerning fibrotic capsules of liver metastases, these two classical markers also follow an specific distribution: αSMA positive CAFs are observed in the outer area of the capsule, the one closest to the liver parenchyma, this positivity progressively disappears when being closer to the tumor cells; meanwhile FAP-expressing fibroblasts are the ones touching tumor cells (Figure 79A-B).

We also assessed the distribution in the fibrotic rim of other classical CAF markers like Podoplanin, Periostin, Fibronectin, s100A4 and MYH11. The outer half of the capsule stained for αSMA; while the iner half stained for FAPα, podoplanin, periostin and fibronectin. On contrary, capsule did not show s100A4 or MYH11 positive cells (Figure 79B).

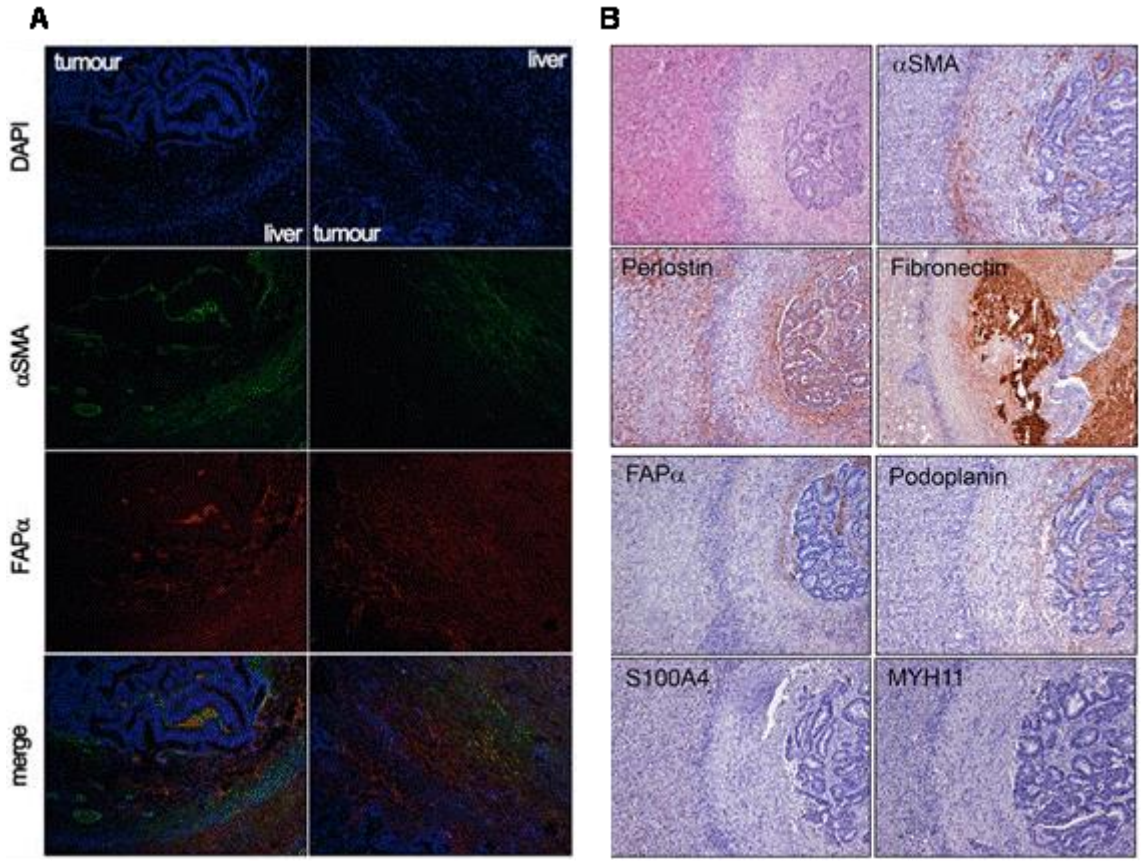

Figure 79. Classical CAF markers distribution in dHGP fibrotic rim. *(A) 10x magnification αSMA and FAPα double IF images showing fibrotic rim areas from two different dHGP CRLM patients. (B) 10x magnification images of H&E staining and different classical CAF markers IHC from a fibrotic rim area.*

In conclusion, the IHC assessment of classical CAFs markers showed that the fibrosis present at the invasive margin or CRLMs differs from the one encountered at tumor central areas. Moreover, when assessing the fibrotic rim in dHGP samples we observed that the studied markers followed a specific distribution inside of it, suggesting that the capsule is conformed by different CAF subpopulations displaying different functions.

5. Tissue Microarray assessment of Cancer Associated Fibroblasts subpopulations

One of the most characteristic features of the histologic growth patterns that appear in CRLM lesions is the presence or the absence of a fibrotic rim separating tumor cells from parenchyma, which is composed of CAFs and elements of the extracellular matrix. However, CAFs are not only present in the capsule of desmoplastic lesions: the invasive margin of both dHGP and non-dHGP cases also contain high amounts of activated fibroblasts surrounding tumoral glands. For this reason, we wondered if CAFs subpopulations vary depending on the HGP. To answer this question, in parallel to the experiments explained above focused on the study of CAFs, we assessed a panel of CAF markers through mIHC in the same TMA cohort in which we had evaluated lymphoid and myeloid immune infiltrates (Table 18). Like in previous mIHCs, TMA samples contained tissue cores of the invasive margin. In those areas, we assessed liver, tumor, and stromal compartments. Figure 80 shows an example of CAFs present in the region segmented as "tumor" as well as CAFs present in the liver and stromal compartment. It also shows how stromal regions look at the invasive margin of non-dHGP.

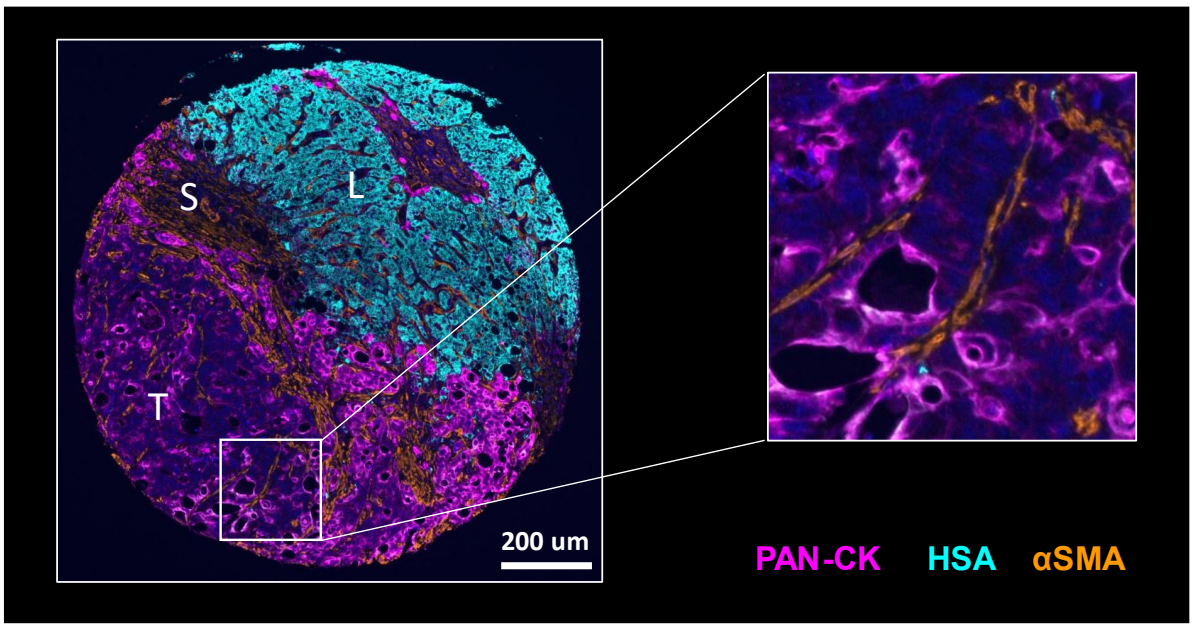

Figure 80. Multiplex IHC image showing CAFs in the region segmented as "tumor compartment". *Images from multiplex IHC showing αSMA staining in orange. Magnified image shows small rims of αSMA⁺ CAFs located between tumor glands. T: tumor; L: Liver; PS: Portal Space.*

As it has been extensively explained in previous sections, several definitions of CAF subpopulations could be found, which differ depending on the circumstances and the type of cancer. In the context of histologic growth patterns of CRLM lesions, CAF subpopulations are not determined. Thus, to select the most relevant markers to include in the multiplex panel we looked up the bibliography. Similar to lymphoid and myeloid cell panels, to distinguish tumoral cells and hepatocytes we included Pan-CK and HSA markers.

Among the markers of election, first, we choose αSMA and FAP, as we wanted to know the distribution along HGP of these classical CAF markers. We also decided to include CD90, not only because we were observing in our *in vitro* experiments that this marker was linked to some functions, but also because in the bibliography it had already been used to define CAF subpopulations (352–354). Moreover, studies focused on liver fibrosis and cancer associated with this marker with PF (355,356). Thus, we believed that it could also be useful as a marker for PFs-derived CAFs, although later our experiments would suggest that other markers like MFAP5 would probably be better elections for this purpose.

In line with the inclusion of a potentially suitable PFs-derived CAFs marker, we added NGFR, as it was described to be a HSCs marker (356–359). However, not all HSCs express the same level of this protein. Specifically, HSCs closer or into portal spaces express higher levels of NGFR (357,360). Thus, for this objective, F2R would probably have been a better candidate, according to the results we obtained from our *in vitro* assays. These assays were performed temporarily at different times, we may have chosen different markers for the mIHC panel if possible. However, Figure 81 shows that these two precursor-associated markers were distributed in normal liver as expected: NGFR mainly stains the inner part of sinusoids while CD90 is basically expressed on portal spaces (PSs).

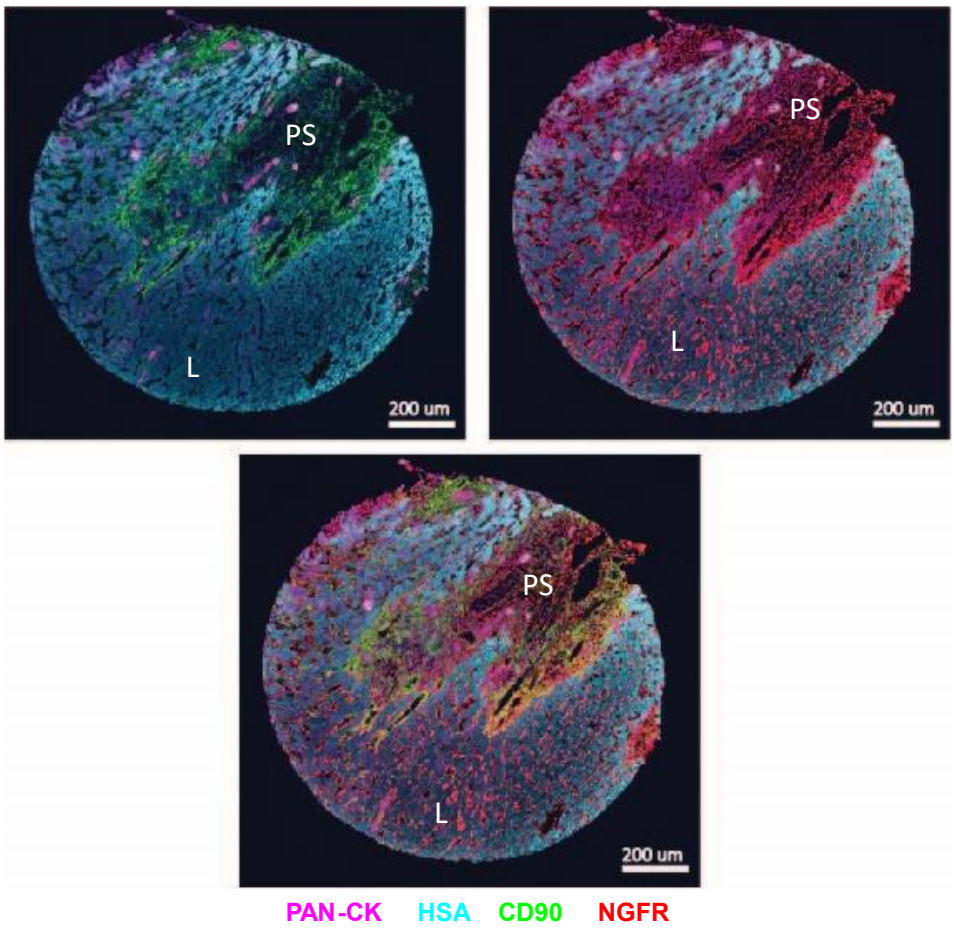

***Figure 81**. **CD90 and NGFR expression in normal liver.** Images from multiplex IHC showing CD90 in green, and NGFR in red. L: Liver; PS: Portal Space.*

Finally, we also included an element of the extracellular matrix and choose the major component of it: collagen. Specifically, we selected Collagen type I, a myCAF marker the role of which had been already studied in pancreatic cancer (361), cholangiocarcinoma (318), glioma (362), hepatocarcinoma (363) and liver metastases (364). Collagen type I protein consists of two collagen type I alpha 1 (COL1A1) and one collagen type I alpha 2 (COL1A2) chains (362). We identified the presence of this protein in our samples through the IHC staining of COL1A1.

Depending on the context, Collagen type I has been involved in a variety of biological behaviors, including both promoting or restraining tumor growth functions. On the one hand, COL1A1 is described to promote tumors via increased stiffness and mechanosensitive signaling (365). Moreover, the change in ECM stiffness can reduce the immune cell influx, reducing the immune anti-tumor response (363). On the other hand, ECM can also act as a mechanical barrier restricting tumor spread (318). In line with this, a study focused on PDAC

and CRC liver metastases proposed that COL1A1, despite activating mechanosensitive signals in tumor cells, could establish mechanical barriers that restrict tumor growth, overriding its tumor-promoting stiffness signals (364). Furthermore, in pancreatic cancer, Collagen type I has been associated with high levels of desmoplasia and associated with tumor-restraining functions. Specifically, its deletion in murine models showed an altered profile of immune cells: MDSCs and M2 macrophages increased, while T and B cells diminished (361).

Considering the information obtained from this panel of markers, we performed a first analysis assessing the total cell numbers for each marker, the results of which are shown in Figure 82 and Table 25. With this initial analysis we saw that there were few differences between HGP concerning the classical CAF markers αSMA and FAP. Taking into account Bonferroni-adjusted analysis, αSMA only shows significant differences in liver compartment, in which non-dHGP has higher levels of αSMA^+ cells (Figure 82A). However, when considering a less stringent statistic (FDR adjustment) we observed that these cells were significantly higher in non-dHGP in tumor and stromal compartment (Table 25). This suggested that non-desmoplastic pattern contained higher levels of αSMA^+ CAFs, although among the population of αSMA^+ cells we also find a small proportion of pericytes.

On the contrary, through Bonferroni analysis, FAP did not show any differences between HGPs in the CRLM lesions (Figure 82B and Table 25).

In contrast, in this initial analysis, we could observe huge differences between HGPs concerning CD90 marker, which was present at higher levels in total tissue (adjusted p value<0.01), total excluding liver (adjusted p value<0.01), tumor compartment (adjusted p value<0.05) and stromal compartment (FDR<0.05) in desmoplastic HGP (Figure 82C and Table 25). As CD90 is a marker of myofibroblasts, it suggests that dHGP contain higher amounts of myCAF. CD90 is also described as a PFs marker. Thus, it is possible that most of the myofibroblasts present at dHGP are derived from these cells. This could be associated to the fact that dHGP tumors show higher level of differentiation, being closer to the colon glands, which are lined with bundles of fibroblasts that provide structural support. Moreover, dHGP metastases could grow close to or inside portal tracts, which would further explain the higher density of myofibroblasts in this HGP.

About NGFR, this marker was present at higher levels in tumor compartment (adjusted p value<0.05), total tissue (FDR<0.05), total excluding liver (FDR<0.05) and stromal compartment (FDR<0.05) of desmoplastic HGP. Thus, this suggests that $NGFR^+$ HSCs were more abundant in dHGP. As this marker is higher in desmoplastic pattern, which is associated with better prognoses, these HSCs-derived CAF subpopulation may be displaying tumor-restraining functions, which would be interesting to study in depth.

Interestingly, COL1A1 marker, which is considered a myCAF marker like CD90, also showed great differences between HGPs. Its density was higher in desmoplastic cases, specifically in total tissue, total excluding liver and stromal compartment, suggesting higher amounts of myCAFs in dHGP. The fact that we observe higher amounts of COL1A1 in the HGP associated with better prognoses, dHGP, is in line with the previously mentioned results of Bhattcharfee *et al*. work (364). This study describes $COL1A1^+$ CAFs as a tumor-restraining myCAF population, while other myCAF populations display pro-tumoral functions.

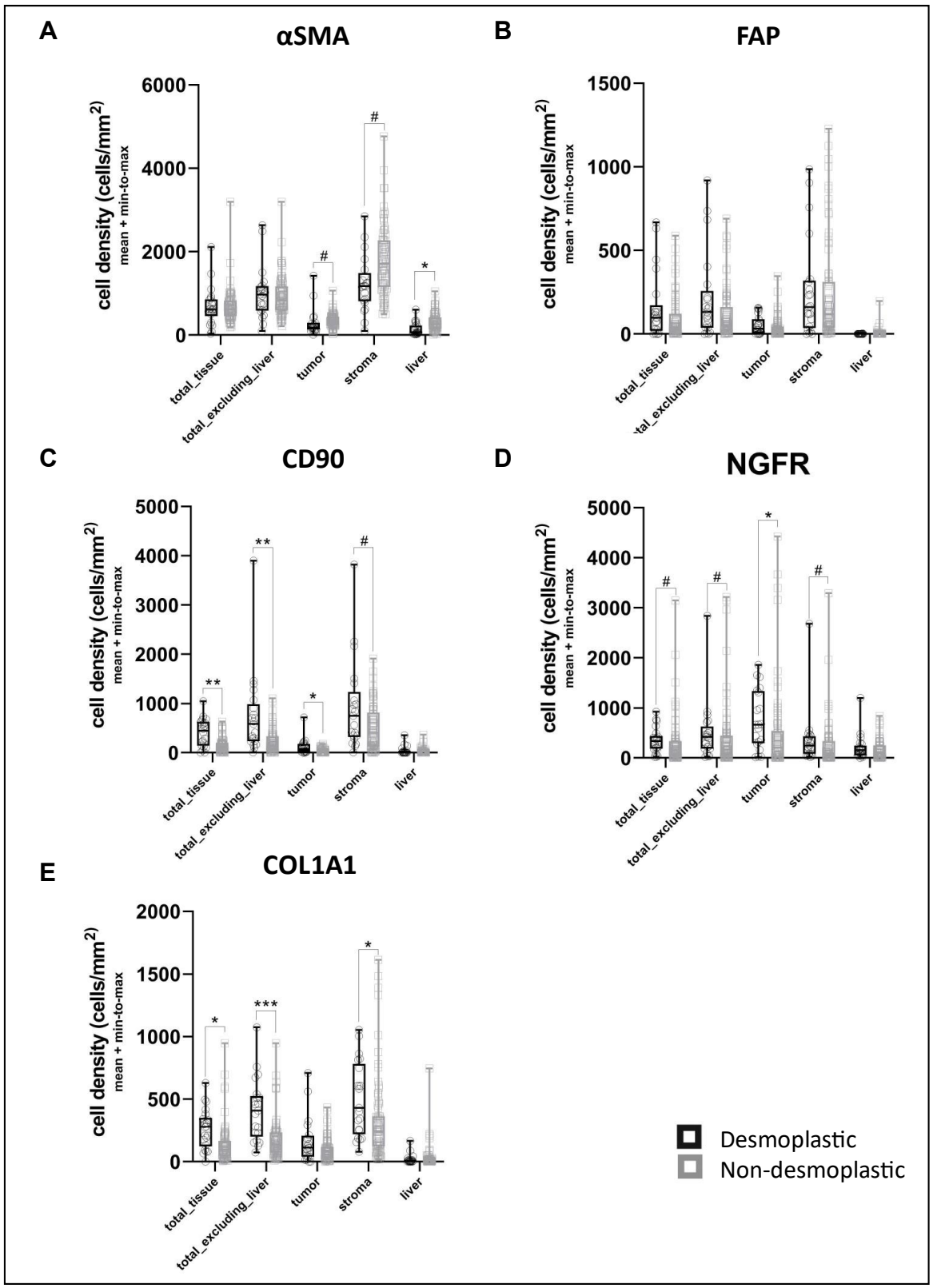

Figure 82. Analysis of total cells positive for each CAF marker. *Total αSMA positive cells (A), Total FAP positive cells (B), Total CD90 positive cells (C), Total NGFR positive cells (D), Total COL1A1 positive cells. U Mann-Whitney test (ties corrected) and Bonferroni correction for multitesting. * p value<0.05, ** p value<0.01, *** p value<0.001; #FDR<0.05.*

Cell Type	Location	p value U Mann-Whitney	Adjustment multiple testing		Higher in
			p.adj (Bonferroni)	FDR	
FAP	Total	0.195	1.000	0.270	nd
αSMA	Total	0.884	1.000	0.921	nd
CD90	Total	0.000	**< 0.001**	< 0.0005	dHGP
COL1A1	Total	0.000	**0.002**	< 0.001	dHGP
NGFR	Total	0.010	0.140	**0.021**	dHGP
FAP	Total_excluding_liver	0.139	1.000	0.217	nd
αSMA	Total_excluding_liver	0.555	1.000	0.630	nd
CD90	Total_excluding_liver	0.000	**< 0.001**	< 0.0005	dHGP
COL1A1	Total_excluding_liver	0.000	**< 0.0005**	< 0.0005	dHGP
NGFR	Total_excluding_liver	0.015	0.190	**0.027**	dHGP
FAP	Tumor	0.265	1.000	0.315	nd
αSMA	Tumor	0.004	0.073	**0.012**	non-dHGP
CD90	Tumor	0.001	**0.018**	0.004	dHGP
COL1A1	Tumor	0.227	1.000	0.298	nd
NGFR	Tumor	0.002	**0.040**	0.007	dHGP
FAP	Stroma	0.724	1.000	0.787	nd
αSMA	Stroma	0.009	0.140	**0.021**	non-dHGP
CD90	Stroma	0.017	0.190	**0.028**	dHGP
COL1A1	Stroma	0.003	**0.050**	0.009	dHGP
NGFR	Stroma	0.014	0.190	**0.027**	dHGP
FAP	Liver	0.005	0.074	**0.012**	non-dHGP
αSMA	Liver	0.000	**0.010**	0.002	non-dHGP
CD90	Liver	0.933	1.000	0.933	nd
COL1A1	Liver	0.247	1.000	0.309	nd
NGFR	Liver	0.171	1.000	0.252	nd

Table 25. P value, P adj and FDR for total cells positive for each CAF marker. *p.adj, p value adjusted; FDR, false discovery rate; nd, no differences.*

After the first analysis explained above, we decided to perform a second one focused on αSMA and CD90 markers, as they can be staining different CAF subpopulations depending on their level of expression. Concerning αSMA, CAFs that express high levels of this protein are considered myCAFs, whereas iCAFs express αSMA but at lower levels (364,366). About CD90, we observed in our previous experiments that it can be expressed both by portal fibroblasts (188,195,197,205,206,355) and by HSCs, this second ones at lower levels. Furthermore, as mentioned previously, CAFs isolated with high and low expression of this marker were associated with different functions (352–354,367–373). Through multiplex IHC it is possible to stablish a threshold of intensities to differentiate between high and low

expressing cells. In our case, we stablished the threshold at the value of the arithmetic media considering all positive cells for both αSMA and CD90. That way, we hypothesized that αSMA^{hi} cells would correspond to myCAFs while αSMA^{lo} would be iCAFs. The results of this analysis showed that both αSMA^{hi} and αSMA^{lo} cells were present at higher levels in non-dHGP (Figure 83 and Table 26). However, significant results for αSMA^{hi} at stromal compartment were lost. It is important to have in mind that some of the αSMA^{hi} cells that only express this marker (single) could be pericytes. For this reason, we have not evaluated the population of αSMA^{hi} single cells in any of the analysis performed. Alternatively, we have assessed αSMA^{hi} total cells, in which the population of pericytes is diluted among all the αSMA^{hi} cells, and in combination with other CAF markers in the latest and conclusive analysis.

On the other hand, when assessing αSMA^{lo} cells, these showed highly significant differences between HGPs. Thus, suggesting that iCAFs (αSMA^{lo} cells), which are described as tumor-promoting CAFS (366), were more abundant in non-dHGP. Meanwhile, the differences in myCAFs, considered αSMA^{hi} cells, would be less prominent. Moreover, considering Bhattacharjee *et al.* work (364), myCAF population would include both tumor-promoting and tumor-restraining CAFs.

Concerning CD90, related to precursor cells, we hypothesized that CD90^{hi} are portal fibroblasts or portal fibroblasts-derived CAFs; while CD90^{lo} would correspond to HSCs-derived myofibroblasts. Results showed that both CD90^{hi} and CD90^{lo} CAF populations were higher in dHGP (Figure 83 and Table 26), which further demonstrates that there is a greater amount of myofibroblasts in this pattern that, according to our postulation, would be derived from both PFs and HSCs.

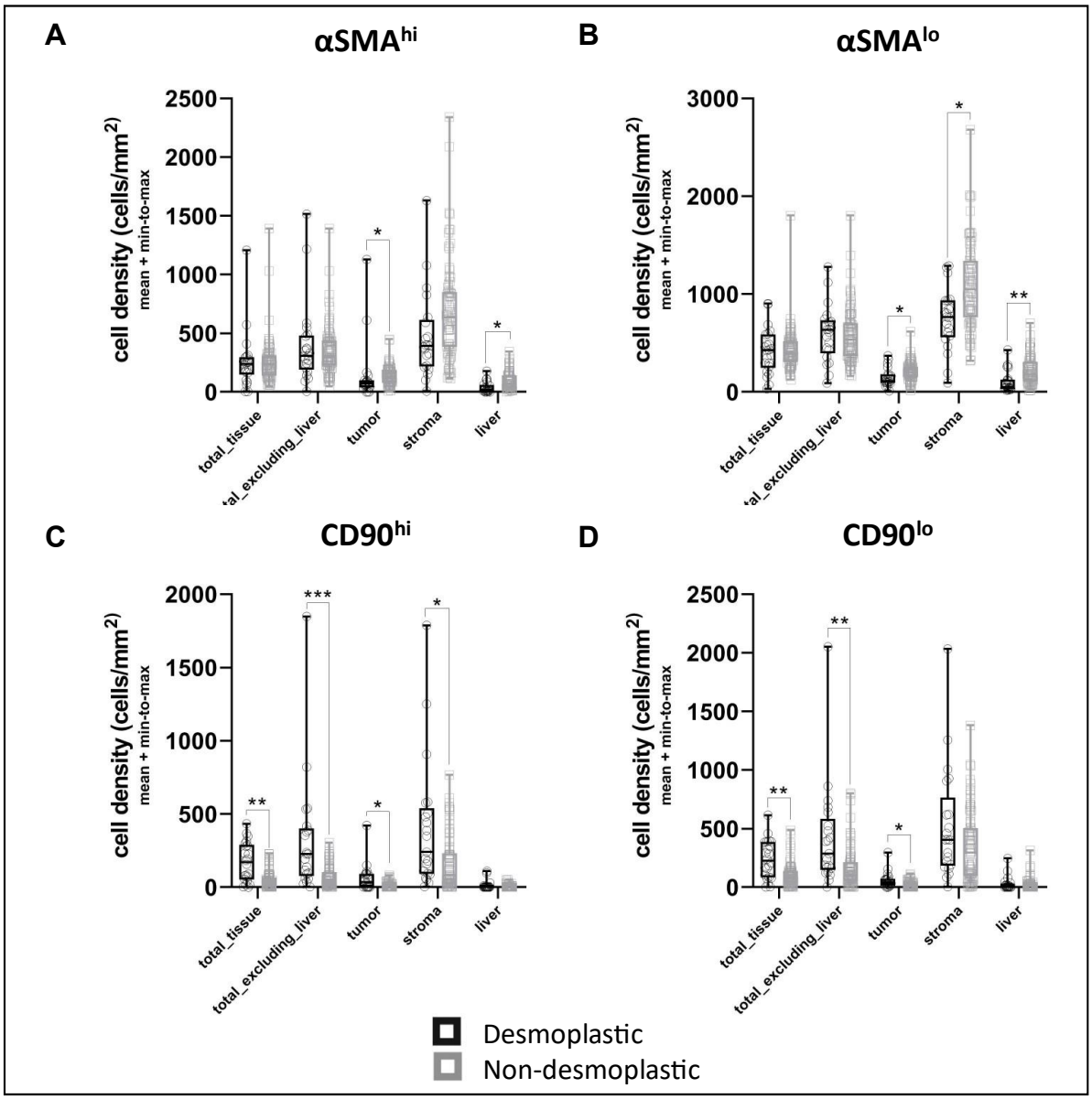

Figure 83. Analysis of αSMA^{hi} and αSMA^{lo}, CD90^{hi} and CD90^{lo} cell subsets. *Total αSMA^{hi} cells (A), Total αSMA^{lo} cells (B), Total CD90^{hi} cells (C), Total CD90^{lo} cells (D). U Mann-Whitney test (ties corrected) and Bonferroni correction for multitesting. * p value<0.05, ** p value<0.01, *** p value<0.001*

Cell Type	Location	p value U Mann-Whitney	Adjustment multiple testing		Higher in
			p.adj (Bonferroni)	FDR	
CD90^{low}	Total	1.45E-04	**0.0025**	0.0007	dHGP
CD90^{high}	Total	1.45E-05	**0.0003**	0.0001	dHGP
αSMA^{low}	Total	9.18E-01	1.0000	0.9623	nd
αSMA^{high}	Total	8.57E-01	1.0000	0.9526	nd
CD90^{low}	Total_excluding_liver	1.01E-04	**0.0018**	0.0007	dHGP
CD90^{high}	Total_excluding_liver	5.87E-06	**0.0001**	0.0001	dHGP
αSMA^{low}	Total_excluding_liver	4.43E-01	1.0000	0.5909	nd
αSMA^{high}	Total_excluding_liver	7.11E-01	1.0000	0.8890	nd
CD90^{low}	Tumor	2.35E-03	**0.0330**	0.0055	dHGP
CD90^{high}	Tumor	3.52E-03	**0.0390**	0.0070	dHGP
αSMA^{low}	Tumor	5.11E-03	**0.0460**	0.0085	non-dHGP
αSMA^{high}	Tumor	4.30E-03	**0.0430**	0.0078	non-dHGP
CD90^{low}	Stroma	5.69E-02	0.4000	0.0813	dHGP
CD90^{high}	Stroma	2.50E-03	**0.0330**	0.0055	dHGP
αSMA^{low}	Stroma	2.43E-03	**0.0330**	0.0055	non-dHGP
αSMA^{high}	Stroma	3.51E-02	0.2800	0.0541	nd
CD90^{low}	Liver	9.62E-01	1.0000	0.9623	nd
CD90^{high}	Liver	8.19E-01	1.0000	0.9526	nd
αSMA^{low}	Liver	6.05E-04	**0.0091**	0.0020	non-dHGP
αSMA^{high}	Liver	2.00E-04	**0.0032**	0.0008	non-dHGP

Table 26. P value, P adj and FDR for αSMA^{hi} and αSMA^{lo}, CD90^{hi} and CD90^{lo} cell subsets. *p.adj, p value adjusted; FDR, false discovery rate; nd, no differences.*

Finally, we aimed to establish combinations of markers that could define populations of CAFs associated with their functionality. To select the proper combinations of markers, we considered a first analysis which included all the combinatory possibilities (data not shown). Among them, we selected those combinations that established a population with a certain number of cells and dismissed all those with too few cells. Then, we took into consideration the previously exposed bibliography to associate each CAF population defined by a combination of markers with its function.

According to the bibliography, αSMA is a marker of myCAFs, which can be pro-tumoral or tumor-restraining. Moreover, COL1A1 is an indicator of ECM-producing tumor-restraining CAFs. Thus, we define the αSMA^{+} COL1A1^{+} CAF population as one of the tumor-restraining CRLM CAF subsets. In addition, as CD90 is also described as a myofibroblastic marker, CD90^{+} COL1A1^{+} CAFs may also constitute a tumor-restrictive CAF population. Finally, among ECM-

producing COL1A1$^+$ CAFs we find NGFR$^+$ COL1A1$^+$ cells, which may constitute a third CAF subset with tumor-restraining functions. Furthermore, according to our postulations, COL1A1$^+$ CAFs that also expressed CD90 would most likely be derived from PFs. In line with this, COL1A1$^+$ CAFs that also express NGFR may be derived from HSCs.

On the other hand, FAP has been described on many occasions as a myofibroblast marker associated to pro-tumoral functions like immune-suppression (366,374). Thus, we postulate that CAFs positive for αSMA and FAP, but negative for COL1A1, are pro-tumoral fibroblasts, representing the tumor-promoting myCAF population. In addition, Figure 84A and B show that COL1A1 and FAP markers do never colocalize. In fact, they are distributed at different regions as it is clearly shown in desmoplastic cases from Figure 84A. Figure 84B further confirms that this two markers are mutually exclusive, as it shows two graphs from the first preliminary analysis in which we can see that the number of cells positive for FAP and αSMA is high, while the population positive for FAP, αSMA and COL1A1 has numbers so low that it is negligible. Finally, CAFs expressing only αSMA at low levels, αSMA^{lo}, would represent the pro-tumoral iCAF subset, although the assessment of specific markers for iCAFs are needed to reinforce this idea. All these CAF populations are resumed in Table 27.

Functionality	CAF population	myCAF / iCAF Classification
Tumor-restraining CAFs	αSMA^{hi} COL1A1$^+$	myCAFs
	CD90$^+$ COL1A1$^+$	
	NGFR$^+$ COL1A1$^+$	
Tumor-promoting CAFs	FAP$^+$ αSMA$^+$ COL1A1^{neg}	
	αSMA^{lo} single	iCAFs

Table 27. CAF populations assessed through mIHC in TMA samples.

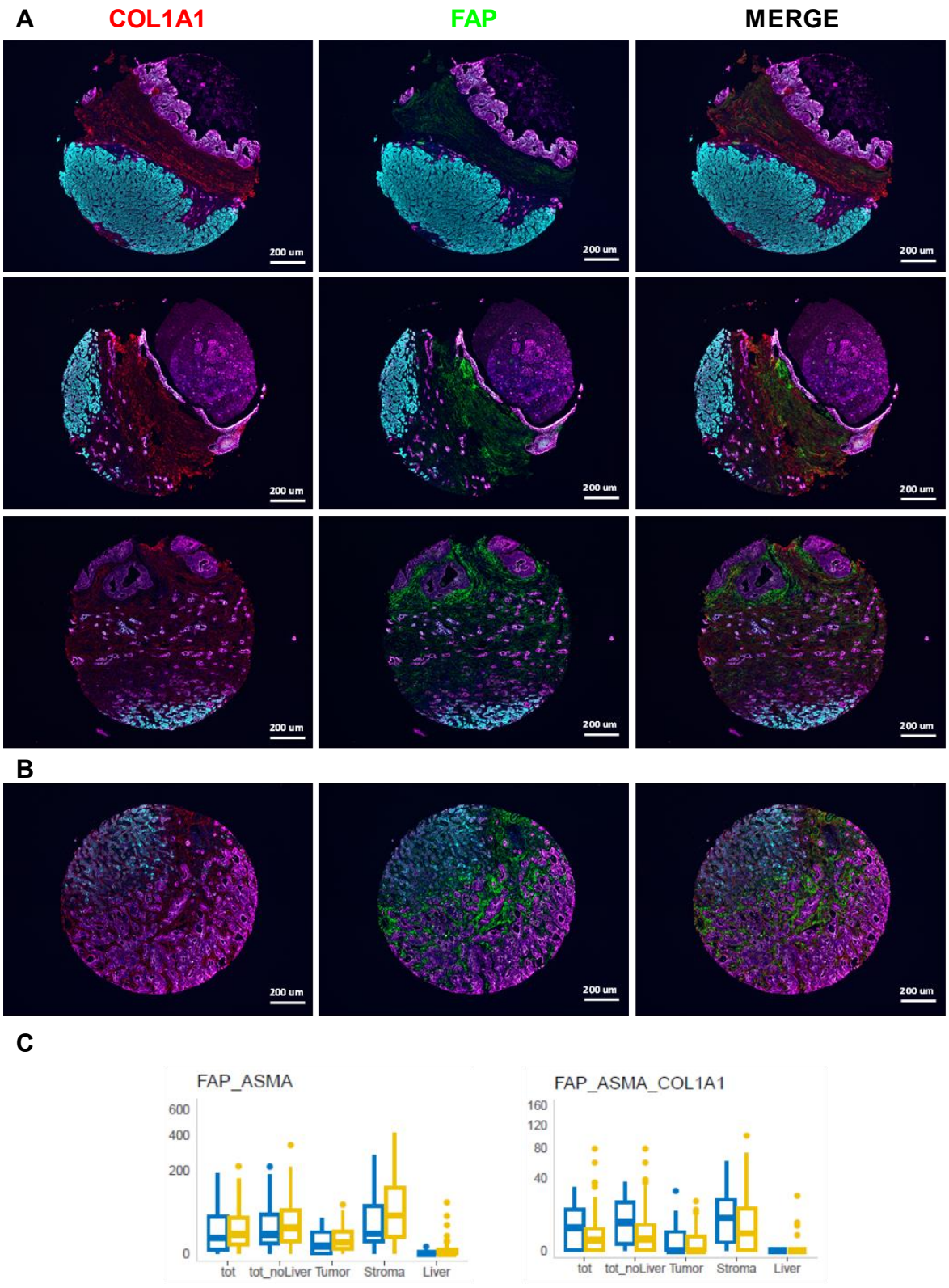

Figure 84. COL1A1 and FAP distribution in desmoplastic and non-desmoplastic HGPs. *(A) Three dHGP examples showing that COL1A1 is mainly expressed at the fibrotic rim and never colocalizes with FAP. (B) Representative example of a non-dHGP case showing that COL1A1 and FAP neither colocalize in this HGP. (C) Graphs from a preliminary analysis used to select the CAF populations of study. These graphs show that the number of FAP⁺ αSMA⁺ COL1A1⁺ cells is very low.*

When assessing the described above CAF subpopulations, we observed that αSMA^{lo} single CAF population, considered iCAF, was enriched in tumor, liver, and stromal compartments of non-desmoplastic cases (Figure 85A and Table 28), according with the previous analysis (Figure 83 and Table 26). Thus, iCAF pro-tumoral population would be present at higher levels in non-dHGP.

About myCAF populations, all the tumor-restraining subsets were found at higher densities in dHGP. αSMA^{hi} COL1A1^{+} showed greater levels in total tissue, total excluding liver, and stromal compartment of dHGP, the same happened in NGFR^{+} COL1A1^{+} population (Figure 85C and E, and Table 28). The fact that COL1A1 was found at higher levels in dHGP stromal compartment added to the observation of COL1A1 at the fibrotic rim (Figure 84A) suggests that this protein could be acting as a barrier with a physical tumor-restraining role.

Meanwhile, CD90^{+} COL1A1^{+} was found increased in all the compartments assessed excepting the liver (Figure 85D, and Table 28). Thus, probably this population is not only contributing to the fibrotic rim physical barrier, but also playing tumor-suppressive roles at tumor compartment, like immune cell recruitment.

Considering the tumor-promoting myCAF subpopulation, defined by FAP^{+} αSMA^{+} COL1A1^{neg}, no differences were observed between HGPs, suggesting that this pro-tumoral subpopulation of myCAFs is present at equal levels in both histologic patterns. However, the fact that the tumor-restraining myCAFs show lower levels in non-dHGP, added to the high content of pro-tumoral iCAF subpopulation in this pattern, suggests that the balance of tumor-promoting vs. tumor-restraining CAFs shifts to pro-tumoral CAF populations in non-dHGP. To evaluate this, we decided to perform a ratio between tumor-restraining (rCAFs) and tumor-promoting (ptCAFs, including pro-tumoral myCAFs and iCAFs), which showed that this balance is significantly inclined to restraining CAFs in desmoplastic HGP (Figure 85F).

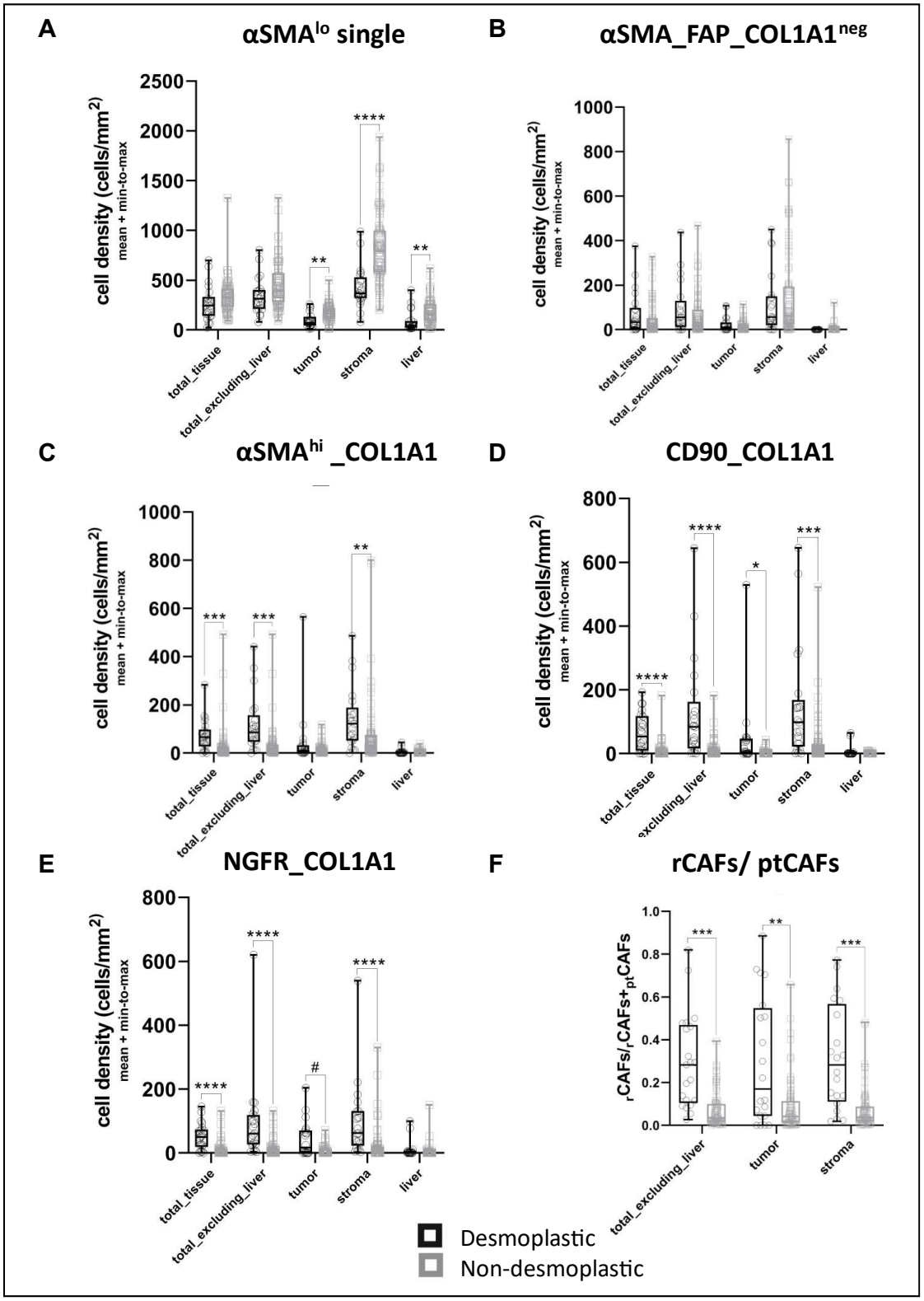

Figure 85. Analysis of function associated CAF subpopulations. *Single αSMA^{lo} cells (A), Total FAP^{+} αSMA^{+} COL1A1^{neg} cells (B), Total αSMA^{hi} COL1A1^{+} cells (C), Total CD90^{+} COL1A1^{+} cells (D), Total NGFR^{+} COL1A1^{+} (E), ratio of tumor-restraining CAFs (rCAFs) and tumor-promoting CAFs (ptCAFs). U Mann-Whitney test (ties corrected) and Bonferroni correction for multitesting. * p value<0.05, ** p value<0.01, *** p value<0.001, ****p value<0.0001; #FDR<0.05*

Cell Type	Location	p value U Mann-Whitney	Adjustment multiple testing		Higher in
			p.adj (Bonferroni)	FDR	
αSMA^{low}_single	Total	4.802E-02	0.48	0.075034	nd
αSMA^{high}_ COL1A1	Total	3.185E-05	**0.00054**	8.85E-05	dHGP
NGFR_ COL1A1	Total	6.828E-07	**0.000016**	5.69E-06	dHGP
CD90_ COL1A1	Total	2.285E-06	**0.000046**	9.52E-06	dHGP
FAP_αSMA_COL1A1^{neg}	Total	5.634E-01	1	0.612384	nd
αSMA^{low}_ single	Total_excluding_liver	7.498E-02	0.67	0.110266	nd
αSMA^{high}_ COL1A1	Total_excluding_liver	4.110E-06	**0.000078**	1.47E-05	dHGP
NGFR_ COL1A1	Total_excluding_liver	4.999E-08	**1.2E-06**	1.25E-06	dHGP
CD90_ COL1A1	Total_excluding_liver	2.616E-07	**6.3E-06**	3.27E-06	dHGP
FAP_αSMA_COL1A1^{neg}	Total_excluding_liver	4.698E-01	1	0.559247	nd
αSMA^{low}_ single	Tumor	2.069E-04	**0.0033**	0.000517	non-dHGP
αSMA^{high}_ COL1A1	Tumor	4.585E-01	1	0.559247	nd
NGFR_ COL1A1	Tumor	8.658E-03	0.1	**0.015461**	nd
CD90_ COL1A1	Tumor	3.792E-03	**0.049**	0.007293	dHGP
FAP_αSMA_COL1A1^{neg}	Tumor	8.274E-01	1	0.842715	nd
αSMA^{low}_ single	Stroma	1.936E-06	**0.000041**	9.52E-06	non-dHGP
αSMA^{high}_ COL1A1	Stroma	3.118E-04	**0.0047**	0.00065	dHGP
NGFR_ COL1A1	Stroma	1.397E-06	**0.000031**	8.73E-06	dHGP
CD90_ COL1A1	Stroma	1.074E-05	**0.00019**	3.36E-05	dHGP
FAP_αSMA_ COL1A1^{neg}	Stroma	5.029E-01	1	0.571455	nd
αSMA^{low}_ single	Liver	3.117E-04	**0.0047**	0.00065	non-dHGP
αSMA^{high}_COL1A1	Liver	1.836E-01	1	0.254993	nd
NGFR_COL1A1	Liver	2.915E-01	1	0.383512	nd
CD90_COL1A1	Liver	8.427E-01	1	0.842715	nd
FAP_αSMA_ COL1A1^{neg}	Liver	1.433E-02	0.16	**0.023888**	nd

Table 28. P value, P adj and FDR for function associated CAF subpopulations. *p.adj, p value adjusted; FDR, false discovery rate; nd, no differences.*

In conclusion, desmoplastic HGP is enriched in tumor-restraining CAF subpopulations, which are characterized by expressing COL1A1. This protein has been described to act as a mechanical barrier, restraining tumor growth. Thus, COL1A1 would be displaying this function at the fibrotic rim of dHGP cases. Moreover, it has also been associated with inflammatory response, specifically to induce B and T cell recruitment and avoid the presence of MDSCs and M2 macrophages. This suggests that COL1A1 could also be mediating the higher levels of $CD8^+$ cells observed in dHGP, as well as the high levels of MDSCs and macrophages in non-dHGP. On the other hand, non-desmoplastic HGP is enriched in the tumor-promoting iCAF population. Thus, although the myCAF pro-tumoral subpopulation did not show differences between HGPs, the tumor-restraining vs. pro-tumoral CAFs balance shifts to pro-tumoral populations in non-dHGP, as it is indicated by rCAFs/ptCAFs ratio.

DISCUSSION

1. PROGNOSTIC EFFECT OF HGPs IN CRLM PATIENTS

The histological growth patterns observed in liver metastases have caught the attention of pathologists for many years. In fact, the first reported work focused on them was published in 1996 (57) and, since then, interest and research in this histopathological feature of liver metastases have increased. In the 2000s and 2010s, several studies have been published around how the different ways of tumor growth in the liver could be related to patient prognoses. These studies also assessed the biological features of each growth pattern. However, poor reproducibility and concordance were observed between them, probably due to the lack of an established way of assessing HGPs. It was not until 2017 that the scientific community proposed a consensual method to determine the HGPs (52). The guidelines proposed in 2017 are in constant revision and updating. In fact, the last revision was published in 2022 (53). The establishment of these consensual guidelines has permitted a reliable evaluation of HGPs value as a prognostic and predictive tool, in which desmoplastic HGP has been clearly associated with better outcomes when compared with patients showing non-desmoplastic patterns (53). Many reasons explaining the differences observed in survival have been proposed. First, the implications that HGPs have in terms of surgical resection, as it is the standard gold therapy for CRLM patients. Non-dHGP cases have been described to have a higher risk of positive resection margins. However, positive and negative margins have been observed in both HGPs, suggesting that the resection margin is not the only player in predicting patient outcomes. Biology must also be playing an important role (69,275). For this reason, many efforts are employed in deciphering the molecular mechanisms underlying each HGP, including our project.

Thus, as we aimed to focus on the biological aspects of each HGP, we first validated the already described effect of HGPs on survival in a consecutive series of patients operated at *Hospital de Bellvitge*, a highly experienced CRLM surgery center with which we collaborate. With that, we could conclude that, as expected, HGPs also predict prognoses in the cohort of patients with which we planned to work.

After primary tumor resection, adjuvant chemotherapy is administered in those patients that show a high risk of recurrence factors, such as histological high grade, R1 resection margin or cancer growth in blood/lymphatic vessels (375). In our cohort of patients, those

that have received adjuvant treatment showed a higher percentage of non-dHGP. This could be explained by the fact that patient selection factors for adjuvant treatment are usually related to a more aggressive disease, which could be linked to undifferentiated tumoral cells, able to develop a worse prognosis growth pattern. On the other hand, it could also be attributed to the effect of adjuvant chemotherapy, which could be performing a "selection" of the most aggressive cells, which would be the ones growing in the metastatic site.

Moreover, in our cohort of patients, we observed a higher percentage of non-dHGP lesions in those patients with metachronous metastases, while synchronous metastases tend to be desmoplastic. An explanation for that could be the presence of adjuvant-treated patients in the metachronous diagnosed subset of liver metastasis, in line with the previous postulation. On the contrary, neoadjuvant chemotherapy before metastases surgical resection has been associated with a higher proportion of desmoplastic pattern (54). A possible explanation for this apparent contradiction could be that the timing in which the chemotherapy is administered determines the effect that it would cause. That way, adjuvant treatment after primary tumor surgery would be affecting the possible remaining tumoral cells, at a stage where these cells have not yet settled in the metastatic organ or are undetectable clinically. In this situation, chemotherapy would promote non-dHGP metastatic development. On the other hand, neoadjuvant chemotherapy administered before metastatic resection would be affecting already established metastases and, hence, would be promoting a possible change to dHGP.

Much research is still needed to prove the postulations exposed above, as poor studies have been published concerning the effect of chemotherapy on HGP, or on assessing if the desmoplastic rim observed in neoadjuvant-treated patients is the same type of fibrotic capsule present in the chemo-naive dHGP cases, as chemotherapy agents probably affect the biology of each pattern. Moreover, published studies associating metachronic or synchronic metastases with HGPs are still lacking.

Another aspect to be mentioned considering the predictive value of HGPs is the high interest in studying pushing histologic pattern. This pattern is observed on few occasions and usually appears in a mix with desmoplastic or replacement. When simplifying in dHGP and non-dHGP, the pushing HGP is considered non-dHGP, although it shows some characteristics that

are closer to dHGP, like no contact between tumoral cells and hepatic parenchyma, or angiogenesis as a vascularization strategy. Thus, assessing the percentage of pushing could be useful to predict treatment response or to take therapeutic decisions.

2. SPATIAL IMMUNOLOGY IN HGP FROM CRLMs

2.1. Spatial immunology whole-slide assessment

In the published pilot study (376), we aimed to characterize the spatial distribution of lymphocytic infiltrates in the context of HGP from CRLM. For that, we analyzed 22 samples from chemo-naive patients considering their characteristic HGP. We assessed the spatial distribution in three tissue levels: a) distinguishing tumor center, parenchymal peripheral regions and tumor invasive margin, b) doing a distance assessment in which we accurately measured the immune cell distribution with different histological hallmarks, and c) analyzing both stromal and epithelial compartments. This study was, to our knowledge, the first study providing an approach for the topographic distribution of lymphocytic infiltrates in HGPs from CRLM.

Many studies have related HGP characteristics to their prognosis value, including the already mentioned surgical (377), histopathological (378), molecular (94) or immunological parameters (379). In this line, the immunological parameters, like Immunoscore® (380), have gained interest as their importance has become evident.

It has already been published that lymphocytic infiltrates are not uniformly distributed in CRLM, instead, immune cells tend to be located in the peripheral areas of the tumor (381–384). However, most of published studies do not take into consideration the HGPs, and neither do any spatial distribution assessments. Bretel A *et al.* (385) reported distinct patterns of immune cell infiltration in CRLM, in which the distribution of the immune cell populations depended on their distance from the invasive margin. However, this study neither considered HGPs. On the other hand, Hoppener D *et al.* (386) reported that encapsulated metastases have higher cell density of different cytotoxic populations, to which the authors attributed the better survival of patients. In line with this observation, some authors have suggested that non-dHGP should be considered as “immune desert” tumors. In contrast, the fact that most of the immune cells keep retained in the fibrotic rim in dHGP has made some authors consider them as “immune excluded” (387). This

affirmation can be suggesting that, although dHGP show higher levels of cytotoxic cells, they never reach tumoral cells. Thus, the differences observed between HGPs could not be explained by the presence of higher immune infiltration. However, both in the pilot study and in the posterior TMA assessment, we evaluated the immune cells that reach the tumor in dHGP and non-dHGP and saw differences that could be explaining the better outcome of the desmoplastic one.

Concerning the 22 patients pilot study, we observed higher immune cell densities in the invasive margin of non-dHGP lesions, but most of the cells that were present at high levels were subsets of $CD4^+$ cells. Although we could not dissect the functional characteristics of $CD4^+$ cells, with the information obtained in the pilot study we analyzed CD8/CD4 ratio, which was significantly lower in non-desmoplastic tumors (Figure 17). Moreover, we also assessed the distribution of $CD8^+$ cells, which showed to be enriched in the epithelial compartment from the invasive margin of desmoplastic tumors. Altogether this suggests that the high number of $CD4^+$ cells observed in non-dHGP was mediating an immune suppressive environment, while the higher presence of cytotoxic cells in the tumor compartment of dHGP suggests higher cytotoxic activity in this pattern.

Taken together, from the pilot study we could conclude that, although the densities of cytotoxic T cells are low in both dHGP and non-dHGP, in non-dHGP CD8 infiltrates are mainly retained at the stromal compartment (tumor-excluded). Meanwhile, in dHGP, $CD8^+$ cells are present at high levels at tumoral niches, suggesting that these cells are immunologically active. However, this study was done including a few clinical cases. Thus, it is needed to replicate its results in a bigger cohort or patients.

2.2. Lymphoid immune infiltrates assessment in TMA samples

To validate the results obtained from the pilot study and to increase the number of patients, we constructed a tissue microarray (TMA) allowing evaluation of 100 patients. Tumors from different HGP have different histology in the whole lesion, although it is evident in tumor invasive margins. Moreover, the pilot study had shown the most interesting and valuable information from this region of the tumor, as no differences were observed between HGPs concerning tumor center. For this reason, the TMA cores were taken from the invasive margin of the lesion. In the TMA samples we assessed each of the compartments, tumor,

liver, and stroma, and analyze the lymphoid cell subsets present in them to extract valuable information. On the other hand, the small size of TMA cores limited the possibilities of performing the distance analysis, which is a limitation of this part of the project.

To analyze the data obtained from TMA samples through mIHC, we assessed different locations: total tissue, total excluding liver, tumor, stroma, and liver. “Total tissue” refers to the density of each cell population considering the whole core. “Total excluding liver” assesses the densities eliminating the part of liver present in the TMA core. “Tumor”, “stroma” and “liver” compartments were defined thanks to PanCK and HSA markers.

The analysis of the lymphoid cells revealed higher infiltration of $CD8^+$ cells in dHGP. Next, we evaluated the stromal and tumor compartment separately, and showed that infiltration was significantly higher in dHGP at tumor compartment while no difference was seen between HGPs at the stromal compartment, suggesting that $CD8^+$ cells in dHGP are functional cytotoxic cells, which demonstrate tendency for interaction with cancer cells.

On the contrary, $CD8^+$ cells were significantly higher in the liver compartment from non-dHGP lesions, which suggests that these cells keep retained in host parenchyma, unable to infiltrate the tumor, in non-desmoplastic pattern (Figure 18). Thus, the results obtained in TMA samples are more robust and reliable. Moreover, the study of Bretel A et al. (385) determines a pattern of infiltration depending on the distance from the invasive margin, which in our pilot study showed differences in the CD4 Tregs population but could not be assessed in TMA study.

As mentioned, through TMA multiplex IHC assessment, we did not observe significant differences concerning $CD4^+$ cell subsets. However, the pilot study indicated, not only an increase of Tregs in non-dHGP through the distance assessment but also a lower ratio of CD8/CD4 in this histologic pattern, indicating less antitumoral activity in it. The differences in this ratio were subsequently validated in TMA samples. Thus, we strongly believed that in non-dHGP an immune suppressive environment was present, limiting the immune anti-tumoral activity. Because of this, we added to the lymphoid immune infiltrates assessment, the study of Th2, a subset of T helper lymphocytes that is described to facilitate tumor growth, both by promoting angiogenesis and by inhibiting cell-mediated immunity and subsequent tumor cell killing (221). For that we assessed CCR4, a chemokine receptor

expressed predominantly by Th2 cells, through regular IHC in TMA samples (388). As expected, we found a higher number of CCR4-positive cells in non-dHGP, suggesting that these cells are contributing to the immuno-suppressive microenvironment that we postulate non-desmoplastic lesions to have.

Following on TMA lymphoid subsets assessment, higher levels of CD45RO and CD20 positive cells were observed in the liver compartment of non-desmoplastic cases (Figure 21). As it happens with $CD8^+$ cells, it seems that most of the immune infiltrates that reach non-dHGP are not able to infiltrate tumoral tissue.

We observed higher number of FoxP3 positive cells in dHGP when considering the total area of the TMA sample or excluding the liver compartment (Figure 21C). As $CD4^+$ $FoxP3^+$ cells, thus, Treg subset, and $CD8^+$ $FoxP3^+$ (data not shown) showed no statistically significant differences between HGP, we concluded this difference was not due to Treg or $CD8^+$ $FoxP3^+$ cell subsets. The same happened with $CD8^+$ $FoxP3^+$ cells (data not shown). Thus, these $FoxP3^+$ cells present at higher levels in desmoplastic HGP should belong to another cell type (297,389–391). Following T cells, but at considerably lower RNA levels, Kupffer cells and hepatocytes can also express FoxP3. At even lower levels, fibroblasts, adipocytes, plasma cells and macrophages can do so (392). In hepatocytes, FoxP3 is described to locate in the mitochondrial compartment and to play a non-canonical role, which is not yet elucidated (389). Moreover, it has also been associated with hepatocarcinoma. Moreover, FoxP3 have also been found in tumor cells of some cancer types (393). Specifically, in gastric cancer, which has been described to impair proliferation and induce apoptosis (394). In addition, $FoxP3^+$ cells negative for CD4 or CD8 have also been observed in the stromal compartment, being CD45ROhigh or CD45ROlow, which suggests that they could be part of γδ T cells or NKT cells (393). However, the role and functional properties of FoxP3 expression in CD4-negative cells have not been fully understood. In our samples, FoxP3 expression was found in tumor cells, $CD45RO^+$ cells and liver parenchyma (Figure 86). Thus, it would be interesting to further investigate which is the predominant dHGP $FoxP3^+$ cell type, and the function these cells are playing in the CRLM context.

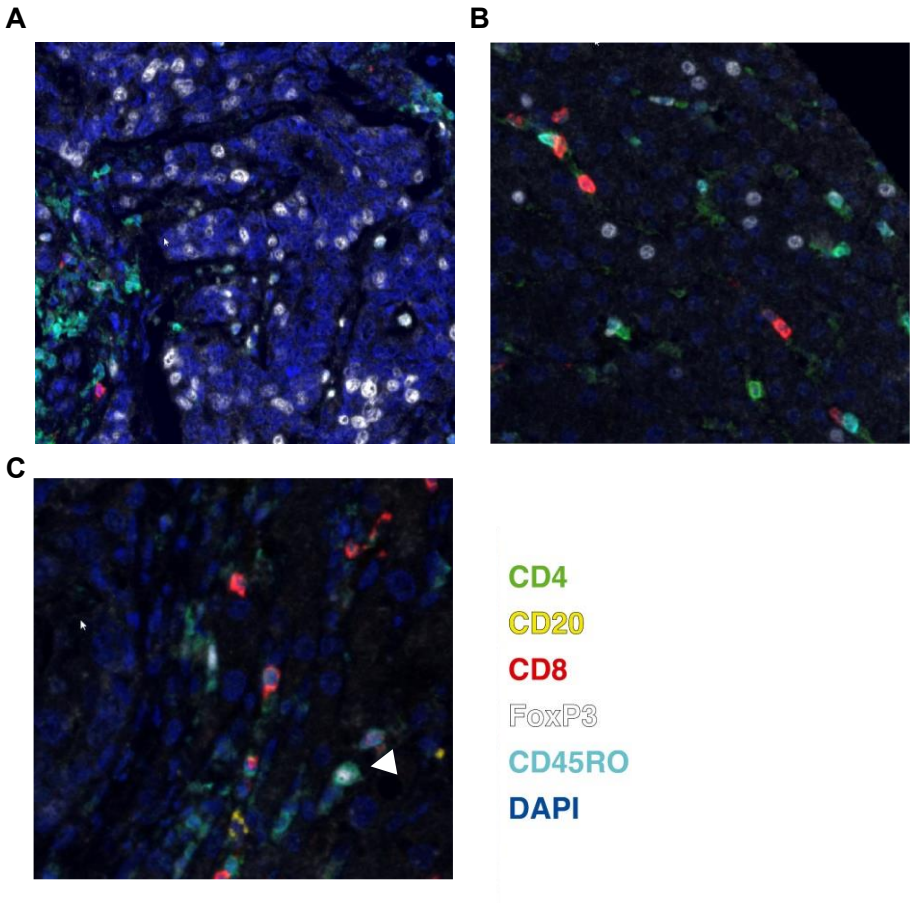

Figure 86. FoxP3 expression *in tumoral cells (A), hepatocytes (B) and CD45RO⁺ cells (C).*

Taken together with the lymphoid lineage immune infiltrates data, the quantity of cytotoxic $CD8^+$ cells is comparable in invasive margins in both HGP, but the immune microenvironment in dHGP seems to be more competent due to the cytotoxic activity of $CD8^+$ cells.

2.3. Myeloid immune infiltrates assessment in TMA samples

Lymphocyte cell subsets are not the only immune cells capable of reaching the tumor. Macrophages, myeloid lineage cells, are numerous and important players in disease development. For this reason, we decided to assess a pool of selected myeloid cell markers through mIHC in TMA samples.

With the selected markers we aimed to answer different questions. On the one hand, we wanted to know the contribution of tumor-associated macrophages (TAMs) to the tumor microenvironment of CRC metastatic lesions. Specifically, we wanted to assess if different TAM populations had an impact on HGPs. However, the total number of macrophages is

already associated with worse patient outcomes in the context of cancer (233). To assess the total number of macrophages, we used the CD68 marker, which, in line with the expected, showed to be at higher levels in non-dHGP, specifically located in the stroma.

Macrophages are plastic cells able to change their phenotype in response to a variety of factors, thus, giving rise to different TAMs subsets. Following total macrophages, we wanted to assess if different TAMs subsets were present in our samples. We focused on the classical M1-M2 paradigm, which establishes that macrophages can be polarized into two categories: M1 and M2. According to this paradigm, M1 would be promoting inflammatory responses, or anti-tumoral ones in the context of cancer, meanwhile M2 would be mediating anti-inflammatory functions, or pro-tumoral ones in cancer conditions (232). However, hybrid or intermediate phenotypes have been described, as well as different grades of activation. It has also been proved that M2 macrophages can express M1-associated markers and the other way around.

Moreover, different subtypes of M2 are defined, depending on the pool of factors that promote this differentiation, which will also determine the specific function that those cells will carry out (395,396). Thus, the M1-M2 paradigm is a simplified classification. To assess M2 polarization in our samples, we included CD163, an M2-associated marker. That way, M2 macrophages ($CD68^+$ $CD163^+$) showed to be present at higher levels in non-dHGP. This was in line with our previously postulated immunosuppressive environment in non-desmoplastic metastases. Moreover, M1 and M2 polarization concepts emerged in association with two subsets of helper T cells, mentioned above: Th1 and Th2. Th1 cells were described to secrete factors, like IFN-γ, which can drive macrophage polarization towards M1 phenotype. Meanwhile, Th2 would be secreting factors that promote M2-polarization, like IL-4 and IL-13 (395). This M2 polarization is classified by some authors like the “product of Th2 activation one”, or M2a, which is one related to type II inflammation and allergy. On the other hand, M2-polarized macrophages can also promote Th2 activation. Then they are termed “product of Th2 activation two” or “M2b” and are associated with immunoregulatory functions (395,397). As we had observed higher levels of Th2 cells in non-dHGP, it could be that these cells are secreting the mentioned factors and promoting M2 polarization in this histologic pattern. On the contrary, it could also be happening in the opposite situation: M2 macrophages are the ones promoting Th2 activation. Specifically, in

the central nervous system, it has been described that tissue-resident macrophages, termed microglia, express the macrophage-derived chemokine CCL22 that induces chemotaxis of Th2 through its receptor CCR4 (398), the one used to assess this cell subset in our TMA samples. Thus, it would be interesting to assess the interaction between Th2 and M2 macrophages in the non-desmoplastic pattern, in order not only to understand the biological process underlying its immunosuppressor environment but also to find possible therapeutic targets.

Other cells that can be inducing the recruitment and polarization of M2 macrophages are tumoral cells and Tregs, through the secretion of factors such as IL-10 or TGFβ (396), and CAFs (180,307,399–401).

Concerning M1 macrophages, we have not used any specific marker to assess this population, but the absence of CD163. Thus, considering that macrophages are plastic and that it has been described that M1 polarized ones can express M2 markers and vice versa, the assessment based only on CD163 markers could be considered a limitation of the study. However, the results obtained are in line with the expected, as both the total number of macrophages ($CD68^+$) and M2 polarized ones ($CD68^+$ $CD163^+$) were higher in worse prognoses histologic condition. However, when considering M1 macrophages ($CD68^+$ $CD163^-$), this cell subset that is classically been associated with anti-tumoral activities is also at higher levels in non-dHGP. This result could be explained by a lack of specific markers to determine M1 macrophages displaying pro-inflammatory functions. However, it could also be that M1 in this context are acting as a pro-tumoral cell subset, as it has been described to happen in other cancer contexts like melanoma (402).

It is important to highlight that, while $CD8^+$ cells in dHGP were specifically present at higher levels in tumor compartment, macrophage differences were observed in the stromal and liver compartment. It is important to note that $CD8^+$ cells are functional in tumor compartment, while if they are found in the stroma probably, they are retained there, or are not able to infiltrate the tumor if found in the liver. On the contrary, macrophages do not need to be in the tumor compartment to display their pro-tumoral functions. Among these functions, it has been reported that M2 macrophages can interact with CD8 lymphocytes when they are in proximity and inactivate them in a process called cell siphoning (281). This

interaction between macrophages and cytotoxic T cells is a particularity that would also be interesting to study in the context of HGP.

In a non-dHGP context, it would also be interesting further investigate the role that M2 macrophages are playing in this histologic pattern lesions. M2 macrophages are involved in multiple pro-tumoral functions. Among them, we find the already mentioned mediation of immune suppression, through PDL-1 and CTLA4 expression (403–405). Moreover, these polarized macrophages can also affect cancer cell proliferation through the expression of members of the fibroblast growth factor (FGF) family, like TGFβ and EGF (406,407). In addition, M2 macrophages secrete pro-angiogenic cytokines that promote the formation of leaky blood vessels (408). However, this angiogenic involvement is associated with the previously mentioned subcategorized M2a, also called alternatively activated macrophages; and a third subtype termed Mc or regulatory macrophages. M2b, the one that promotes Th2 recruitment and mediates immune suppression, would not be mediating new vessel formation (409). This is in line with what happens in non-dHGP, where the tumor vascularization strategy is based on vessel co-option.

Moreover, M1 or M2 polarization is also associated with the origin of the macrophages. Macrophages can arise from bone marrow-derived circulating monocytes or can be embryonic-derived populations present in many organs, known as resident macrophages, that can self-renew and maintain throughout adulthood (410,411). It would be the case of Kupffer cells, that are tolerogenic by nature because the liver is responsible for filtering the blood coming from the portal vein, which is full of food antigens. Thus, Kupffer cells usually express CD163. Tumor-associated macrophages have historically been observed as being exclusively derived from a circulating monocyte origin that undergoes differentiation once infiltrate the tumoral tissue. However, a high fraction of resident macrophages has also been described in solid tumors (412). In addition, the developmental origin of macrophages has been associated with some changes in polarization state. On the one hand, it has been described that that bone marrow-derived macrophages are more capable to respond to local signals than embryonic macrophages. On the other hand, embryonic macrophages would be less susceptible to these signals, thus, they would be less plastic than those derived from the bone-marrow (413). Furthermore, polarization signals from the tissue appear to overcome the embryonic developmental signals, which makes polarization states reflect the

signals from the environment rather than the ones typical from their ontogeny (414). Considering this information, with the mIHC applied to the TMA samples, we also wanted to assess the origin of the metastatic-associated macrophages present in our samples. For that, we included the marker MARCO, which is described to be typical of Kupffer cells, the liver resident population of macrophages. This marker showed no differences between HGP. In addition, when observing both conventional and multiplex IHC, MARCO-positive cells were present in the liver parenchyma but not inside of the tumor (Figure 26 and Figure 34). Through conventional IHC we also assessed CD5L, another marker typical of liver resident macrophages (415), and observed the same distribution (Figure 34). This would be in line with the studies that affirm the main contribution of bone marrow-derived macrophages conforming the TAME population. However, there are studies based on single-cell RNA sequencing that show tumor-infiltrating macrophages expressing these markers at RNA levels (104,125,310). Thus, we cannot reject the possibility that resident cells do infiltrate the tumor to contribute to the TAMs population but lose the expression of MARCO and CD5L at the protein level.

In addition, in line with our observations concerning MARCO, a study published in 2017 (416) established a relationship between this scavenger receptor expression and the progression and prognosis of hepatocellular carcinoma. In this work, the authors corroborated the expression of MARCO by Kupffer cells, as well as demonstrated an inverse correlation of this marker with the severity of the tumor. This published article it is shown a higher level of MARCO RNA expression in normal liver tissues when compared with hepatocellular ones, which is also corroborated at the protein level. The differences observed increased in metastatic hepatocellular carcinoma, indicating that the expression of MARCO decreases as well as the stage of the disease advances. This MARCO-negative association with tumor progression and poor prognoses had previously been described in prostate cancer context (417). Tumor encapsulation can occur in hepatocarcinoma and is associated with less severity of cancer. Interestingly, the authors of this work observed that MARCO expression in patients without tumor capsules was reduced compared with that of those with tumor capsules. In our case, there are no MARCO-positive macrophages infiltrating tumor tissue. Thus, according to this paper, it suggests that the metastatic CRC stage that we study may be in a so advanced stage that the expression of this marker is non-existent inside the tumor.

However, tumor periphery is rich in $MARCO^+$ cells. Whether MARCO expression loss is a causative element, or a consequence of poor prognosis remains unknown. In fact, in our samples of study we had observed a transition at the tumor liver interface considering MARCO and CD5L scavenger markers: the closer we get to the tumor, the less expression there is of these markers (data not shown). Therefore, it cannot be excluded that macrophages may be altered when MARCO expression changes, becoming tumor-promoter cells. Thus, the detailed mechanisms underlying the role of MARCO in the CRLM context need further research.

To further assess the role of M2 macrophages in HGPs, we performed the CD8/M2 ratio at the different tissue compartments. This ratio, termed Signature of Immune Activation (SIA) (418), was described to define prognosis in immunogenic cancers. Specifically, colon cancer has been shown to predict survival better than immune score and to contribute to survival prediction when compared to the established clinical parameter (418). In our samples, CD8/M2 showed statistically significantly higher levels in dHGP vs. non-dHGP when assessing the total area of the TMA core, the total area excluding the liver compartment, and the stromal compartment (Figure 29 and Table 24). Thus, this ratio is indicating that the cytotoxic T cells are present at higher numbers than those cells that inactivate them, M2 macrophages.

Another fraction that we analyzed in all the mentioned compartments is M1/M2, which gave no differences in any of them (Table 22). According to the bibliography, this ratio is elevated at the early stages of tumor development, as at the very beginning there is a process of high inflammation. However, cancer cells can promote M2 polarization to the recruited macrophages. Thus, with tumor development, this ratio is progressively inverted (419). Some authors have postulated that the replacement (non-dHGP) pattern is the “default” one. Thus, it would be the first to appear, which could develop as dHGP or maintain non-dHGP histology (53). As no differences in M1/M2 ratio are observed when comparing dHGP vs. non-dHGP, this feature is not corroborating this hypothesis. However, many other characteristics, like the presence of remanent portal triads inside of both HGP lesions, are in line with the postulation of these authors. Thus, it cannot be rejected.

Additionally, when analyzing CD163 to assess M2 polarized macrophages ($CD68^+$, $CD163^+$), we observed a big population of $CD163^+$ that were negative for CD68. These cells were statistically higher in non-dHGP, both at stromal and liver compartments. Thus, as these cells are mostly present in the worst prognoses histologic pattern, we postulate that they have pro-tumoral functions, probably contributing to create the immune suppressive environment that characterizes this HGP. CD163 expression is linked to the down-regulatory phase of the inflammatory process. It is described to be specific to monocyte/macrophage cells, particularly those subsets with strong anti-inflammatory potential. Moreover, its expression is also associated with the level of monocyte maturation. That way, monocytes increase their CD163 expression when they differentiate to macrophages and downregulate their levels if this differentiation is towards dendritic cells. Taking this into account, $CD68^-$ $CD163^+$ cells that we observe in our samples of study could be recruited monocytes that have recently arrived at the CRLM. Dendritic cells and granulocytes can eventually express CD163, but they do it at very lower levels (420). In any case, CD163 is a myeloid lineage-expressed protein. Thus, as we cannot precisely define which cell subtype are $CD68^-$ $CD163^+$ cells, we termed them "non-macrophage myeloid cells". In addition, CD163 expression is regulated by anti-inflammatory mediators, such as IL-10 and glucocorticoids. Considering that, in this project, we describe an immunosuppressive environment in non-dHGP lesions, the microenvironment in these metastases should be enriched in factors promoting CD163 expression.

In addition to the myeloid markers mentioned above, we had previously observed that S100A8/A9, also called "Calprotectin", was present at high numbers in CRLM samples. Calprotectin is an heterodimer described to be expressed by neutrophils, monocytes, and myeloid-derived suppressor cells (301). This caught our attention and decided to include this marker among the ones assessed through mIHC. The amount of Calprotectin was observed higher in the tumor, stromal and liver compartments of non-dHGP, as well as when assessing the whole tissue core. Moreover, IHC performed in whole-slide samples also showed higher levels of this marker at central parts of non-dHGP metastases. Thus, the Calprotectin-positive cell population may be contributing to the tumor-favoring environment that these lesions show. Multiplex IHC analysis demonstrated that the vast majority of $S100A8/9^+$ cells were not macrophages, as they were negative for CD68. However, a small proportion of the

stained cells was also positive for CD68. We postulate that this $CD68^+$ S100A8/A9 population corresponds to the resident inflammatory macrophage subset described by Sonya *et al.* (117). Pro-inflammatory cell subsets are usually linked with tumor suppressive functions. However, inflammation is a double-edged sword, as it can act as a protective response against the tumor, but at later stages, it can become cancer-associated inflammation and contribute to disease development and progression (421). Thus, pro-inflammatory cell subsets can also do pro-tumoral functions. In any case, the levels of $CD68^+$ $Calprotectin^+$ cells are very low in both HGP, which suggests that they may not be playing a decisive role in the CRLM context. The same happens with $CD163^+$ $Calprotectin^+$ cells, these cells are detected by mIHC (data not shown) but at very low levels. Thus, we decided to not focus on them.

On the other hand, the fact that single S100A8/A9 cells were present at high levels in non-dHGP lesions makes us wonder which cell type would these cells be. S100A8/A9 are calcium-binding proteins belonging to the S100 family. They often exist in the form of a heterodimer, termed Calprotectin, as a homodimer has little stability (301). Thus, published articles sometimes refer to one of the members of the heterodimer and sometimes to both, but in most cases, we can consider that they refer to the same. S100 proteins are involved in a variety of biological processes and are expressed in various cell types. In the case of Calprotectin, it is described to play an indispensable role as a mediator in inflammatory processes (420). Moreover, it is associated with poor outcomes in melanoma (422), colorectal, gastric, liver, pancreatic and prostate cancer (423–430). On the other hand, it has been observed to act as a negative regulator of lymph node metastasis in gastric adenocarcinoma (425,426). Thus, although in most contexts it has tumorigenic activity, on some occasions it can act as antitumoral. Concerning its expression, it is mainly expressed by cells of the myeloid lineage, specifically neutrophils, monocytes, macrophages, myeloid-derived suppressor cells and dendritic cells (301,302,311). All these cells are associated with poor prognoses in melanoma (422). At lower levels, $CD34^+$ endothelial cells and $CD3^+$ T cells can express Calprotectin (430). In some cancer types, like lung, prostate, nasopharyngeal and breast, S100A9 can be expressed by neoplastic tumor cells (431–434), which is related to poorly differentiated carcinomas (435). In the hepatocarcinoma context, S100A9 is expressed mainly by neutrophils, although a considerable number of monocytes also expressed it (430). Calprotectin is described to play an important role in malignant

development and cancer progression by triggering protumor immune responses. Among them, it acts as a chemotactic molecule for inflammatory cells such as MDSCs and neutrophils. This leads to a proinflammatory microenvironment that, in this case, is promoting tumor progression. Additionally, Calprotectin can also be in a soluble form, which is released to promote inflammation (436,437) and can be present in serum, which is also associated with bad prognoses (422). In melanoma, it has also been shown to predict response to immunotherapy with pembrolizumab, an anti-PDL-1 antibody (438,439). Another function linked to S100A8/A9 is myeloid-derived suppressor cells recruitment and stimulation of their immunosuppressive functions (438,439), which may be explaining its influence on pembrolizumab treatment response. Furthermore, S100A8/A9 expression can also play a role in establishing the metastatic niche, as some tumoral cells express surface receptors that bind to Calprotectin, thereby migrating into tissues with high expression of this protein, where they can initiate metastases (438–440).

In our samples, S100A8/A9 did not show co-expression with pan-CK. Thus, it is not expressed by tumoral cells in the CRLM context. It is neither expressed by endothelial cells, as the morphology observed is rounded and distributed around the whole tissue, very different from endothelial cells' morphology and location. As mentioned before, co-expression with $CD68^+$ cells occur in a few numbers of cells. Thus, we postulated that the main Calprotectin cells present in our samples could be neutrophils and MDSCs. For this reason, we assessed the Myeloperoxidase marker, which is mainly expressed by these neutrophils, although it can be expressed by monocytes at lower levels. Myeloperoxidase staining was applied through current IHC in TMA samples and showed the same tendencies as Calprotectin staining (Figure 30). When assessing this marker in whole-slide samples, the morphology and distribution were quite similar between Calprotectin and Myeloperoxidase (Figure 33). Thus, it is highly probable that positive cells for both markers conform to the same cell population. However, a double IF to confirm this is needed, and ongoing at the moment of this thesis writing. The confirmation of the $Myeloperoxidase^+$ $Calprotectin^+$ population would highly suggest that these cells are neutrophils.

About the foregoing, it has been described in the breast cancer context, that S100A8 and S100A9 expressing neutrophils suppress $CD8^+$ T cell activation (441). Tumor-associated neutrophils (TANs), as happens with macrophages, may differentiate into N1 or N2

phenotypes under the stimulation of different cytokines or chemokines. In the context of cancer, they play a dual role, antitumor or tumor-promoting, through direct or indirect ways. As mentioned in previous sections, in CRLM, the involvement of neutrophils is reported to have mainly pro-tumoral effects and to be associated with worse prognoses (249–251). Thus, if Calprotectin^{+} cells are neutrophils, they may be polarized towards the N2 phenotype.

Although the staining with Myeloperoxidase suggests that Calprotectin cells are neutrophils, we cannot reject myeloid-derived suppressor cells. These cells are described to be recruited by S100A8/A9 and to express this protein in an autocrine way. Moreover, S100A8/A9 is expressed by hematopoietic progenitor cells, which downregulate its expression during their process of differentiation. Thus, Calprotectin cells observed in CRLM samples could be immature recruited cells that still have high levels of this marker. In this line, circulant immature myeloid cells are described to differentiate when reaching their target tissue. There, depending on the tumor-host signals that they receive, they can differentiate into different phenotypes, which include “monocyte-like” (M-MDSCs) and “granulocyte-like” (G-MDSCs) cells. In the context of cancer, G-MDSCs suppress T cell proliferation, while M-MDSCs inhibit T cell function and prevent its accumulation (442). It is not known which phenotype is induced by the S100A8/A9 soluble factor, but it is described that MDSCs acquire an immunosuppressive role in response to it (443). MDSCs have been shown to be reliable biomarkers for non-response to immune-checkpoint inhibition (444,445). Thus, it would be of great interest to know in detail the role of Calprotectin-positive cells and their relationship with myeloid-derived suppressor cells.

Despite the postulations exposed above, we cannot affirm to which cell subset belongs the single Calprotectin-positive cell population observed at higher levels in non-dHGP. However, concerning that the presence of all the possible cell types is associated with poor prognoses, that S100A8/A9 expression predicts worse outcomes in many cancer types, and that Calprotectin cells appear at a higher level in non-dHGP, it suggests that this population plays a pro-tumoral role. Therefore, it would be interesting to further assess this population, to elucidate not only its cell type but also, more important, its function in the CRLM context.

2.4. TGFβ in the context of CRLM HGPs

We observed numerous clues indicating an immune-suppressive environment in non-dHGP. Further to specific cell subsets playing immune-suppressive roles, in CCR advanced stages, it is widely described the role of TGFβ as a promoter of the tolerogenic/immunosuppressor environment. TGFβ has three main isoforms, TGFβ1, TGFβ2, TGFβ3. However, TGFβ1 is one related to fibrogenesis, carcinogenesis, immune modulation, cell proliferation, and differentiation, as it has a pleiotropic nature, able to adopt different trans-activations depending on the context (446,447). Moreover, this TGFβ group of cytokines can trigger the activation of a canonical pathway, or some non-canonical ones (442). In the cancer context, this protein can have a dual role, being both a tumor suppressor in pre-malignant cells and a tumor promoter in cancer cells (448). In turn, cancer cells are able to inactivate the tumor suppressive components of the TGFβ canonical pathway, which implies Smad signaling and create an immune suppressive tumor microenvironment (449,450). Specifically, in colorectal cancer, it has been described an increased TGFβ in the tumor microenvironment, which represented a primary mechanism of immune evasion that promotes T cell exclusion and blocks the differentiation towards the Th1 phenotype (314). We had observed this effect in the metastatic context, in a non-desmoplastic pattern: an exclusion of $CD8^+$ cells infiltration, and high levels of Th2 cells. Thus, we wondered if TGFβ signaling was active in our samples, thus promoting the immune suppressive environment observed in them. For this reason, we assessed the activation of this pathway through IHC for pSMAD2, a protein that is activated downstream of the binding between TGFβ1 and its receptor. pSMAD2 was observed to be more abundant in non-dHGP, considering both stroma and tumor compartment, which reveals that this mechanism is active in non-dHGP CRLM (Figure 31).

The next questions to be assessed in the future, thus, are which cells are responsible for the high TGFβ expression and which ones are affected by its presence. TGFβ can be secreted by CAFs, macrophages and tumoral cells, among others, and is a mediator of multiple functions in many cell types. In neutrophils, TGFβ promotes polarization towards protumor N2 phenotype (247,451). Moreover, neutrophils can also contribute to TGFβ signaling pathway activation through the secretion of MMP-9, which is capable to convert TGFβ precursor into an active form. In line with this, public CRC gene expression datasets verified that the T cell

activity is lower in those tumors that show neutrophil infiltration combined with TGFβ activation (452).

Considering macrophages, TGFβ can also act as a polarizing factor for these cells towards pro-tumoral M2 phenotypes via activating the Smad2/3 and PI3K/AKT pathways, which enhance the transcription of pro-tumoral factors like IL-10 (453–455). Thus, in non-dHGP CRLM lesions, TGFβ would also be contributing to creating the immunosuppressor environment by guiding the M2 polarization observed in these metastases.

In addition, the canonical TGFβ pathway mediates endothelial-mesenchymal transformation in tumor endothelial cells and promotes the accumulation of myofibroblasts and CAFs in TME (456). In this line, TGFβ is also crucial for activating CAFs to modulate migration and invasion of cancer cells (457,458). TGFβ induces fibroblasts to become myofibroblasts and increases their contractility, as well as enhances the expression of extracellular matrix remodeling genes, including Thy1/CD90 (459). Moreover, it is also described in the context of pancreatic cancer that tumor cell derived TGFβ1 is implicated in the promotion of CAFs heterogeneity (460).

Among the multiple pro-tumoral functions of CAFs, these cells mediate migration and invasion of the cancer cells through the extracellular matrix components that they secret. In line with this, TGFβ promotes the production of some of these ECM factors, among which we find Fibronectin and different types of collagens (442).

Regarding TGFβ role in immunosuppression, it has been mentioned that TGFβ mediates cytotoxic cell exclusion and promotes Th2 phenotype in T helper cells. In addition to this, TGFβ can induce programmed cell death of B and T lymphocytes and block the development of cytotoxic T cells (442,446,447). Tregs secrete this factor to suppress $CD8^+$ cell activity (461). In turn, TGFβ promotes the survival of immature $CD4^+$ T cells to later promote its differentiation from uncommitted to Tregs (462,463). In cancer cells, TGFβ reduces the expression of class II major histocompatibility complex antigens to diminish their surface immunogenicity (464). Concerning CAFs secreted TGFβ, it hinders the maturation of dendritic cells and educates them to secrete large amounts of immunosuppressive cytokines (465). Moreover, CAFs can help circulating monocytes to differentiate into immunosuppressive M2-like phenotype (466), program immature myeloid cells to myeloid-

derived suppressor cells and mediate the recruitment of both monocytic and granulocytic MDSCs (467,468). Tumor-associated macrophages can also secrete TGFβ, in this case, it has been implicated in EMT induction (469).

Thereby, all the mentioned TGFβ functions may occur in the worse prognosis associated with HGP, influencing almost all cell subsets of the tumor microenvironment, and resulting in an immune-suppressive microenvironment.

2.5. Immune infiltrates assessment conclusions

Considering the results exposed, it is suggested that in dHGP there is an anti-tumoral environment in which, when compared with non-dHGP, a higher number of $CD8^+$ cells is functional and able to interact with tumoral cells, as these cells are located at tumor niches. On the other hand, non-dHGP shows the presence of a variety of cell subsets that are described to play pro-tumoral functions, mainly through the inactivation of cytotoxic T cells. The value of this postulation relies on the fact that, in recent years, immune checkpoint inhibitors, which can activate T cells to achieve antitumor effects, have demonstrated promising results but only in a very exclusive subset of patients. CRC patients that have a good response to ICIs belong to the microsatellite-instability-high (MSI-H) or deficient-DNA-mismatch repair (dMMR) group, which are the ones with higher immune infiltration but represent only 15% of patients affected by this disease. Concerning this, it is important to highlight that as it can be observed in Table 18, in our samples of study there was the same percentage of MSI patients in both groups, dHGP and non-dHGP, which was very low.. Thus, this does not explain the immune infiltrate differences observed in this project. Considering liver metastases of CRC, the currently performed trials show a failure of immunotherapy in most of the cases. However, these studies do not consider HGP. Thus, we postulate a need for patient segregation according to the HGP, as most of the patients have a non-dHGP, which shows an immunosuppressive environment, but dHGP patients should respond properly to this type of therapy (247).

In this line, most of the studies focused on CRLM characteristics and/or their relationship with primary tumor features do not consider the histologic pattern of the metastatic lesions. We believe that many aspects are masked by the lack of HGP segregation. Therefore, it is

important to consider histologic growth patterns in any study assessing liver metastases from CRC.

3. CAFs POPULATIONS IN HGP FROM CRLMs

CAFs are the most abundant cell type present in desmoplastic tumors like CRC liver metastases. Moreover, these lesions are classified according to how fibrosis, whose main components are ECM, is distributed in them, describing the different histologic growth patterns. Thus, we believed that CAFs should be playing a determining role in the outcome of these patients. In addition, stromal cells are good therapeutic targets as they are relatively genetically stable in comparison with tumoral cells, which have unstable genomes. For this reason, we decided to study the different populations that could be present in each HGP, as well as their function. For doing that, we considered different approaches, that could be grouped into the following categories: i) study of markers from liver resident mesenchymal cells, ii) evaluation the functional and phenotypic implications of the regulation of a known CAFs marker iii) assessment of a set of classical CAF markers, including FAP and αSMA.

3.1. CAF populations according to precursor markers

Different CAF classifications have been proposed, according to the heterogeneous characteristics of these cells. However, it is still not known whether these different CAFs are indicators of distinct CAF lineages, or if the same CAFs can adopt different states depending on the changes in TME, two ideas that are not mutually exclusive. However, the recently described antigen-presenting CAFs, which are able to induce regulatory T cells and suppress anti-tumor immunity, are shown to be derived from mesothelial cells (470). In addition, all the referred heterogeneity has an extra layer of complexity. CAF precursors, whether resident fibroblasts or other resident mesenchymal cells, the most plausible CAFs precursors, hav a global topographic differentiation (471). It means that depending on the anatomical location, fibroblasts will display particular transcriptional programs that might be retained, partially or totally when they become CAFs. Thus, the observations described for a given tumor type in relation to the different subpopulations of CAFs must be considered with caution when trying to extrapolate to another kind of tumor. However, broadly speaking, we can refer to two main CAF subsets from the transcriptional point of view,

myofibroblastic CAF or myCAF, and inflammatory CAF or iCAF, which also seems plausible that functionally they are acting differently. Probably, and in light of the myriad of articles that use single cell technology, different subpopulations can be differentiated from each main type, each of which can perform different of overlapping functions (104,164,167,357,360,374,472,473).

In line with this complexity, heterogeneity, and topographic differentiation, we aimed to assess the origin of CAFs present in CRLM. The two main sources of CAFs in the liver are described to be portal fibroblasts and hepatic stellate cells. We postulated that in CRC liver metastases there may be CAFs from both origins and that their markers and their relative abundance might also differ according to the HGP. What we do not know yet is whether their fate as myCAF or iCAF is determined by their origin as portal fibroblasts or hepatic stellate cells. Murine models reproducing desmoplastic and non-desmoplastic histologic growth patterns are still lacking, thus tracing experiments cannot be done to elucidate how PFs, and HSCs derived CAFs are distributed in each HGP, which is a limitation of this project. Because of that, we sought which were the most appropriate markers to assess PF-derived and HSCs-derived CAFs in patient samples, once the metastasis is already developed. For this purpose, we consulted the bibliography in search of PF and HSC markers, mostly linked to malignancies other than cancer, as fibrosis (474–476). After performing IHC in human tissue samples with various candidate markers, we found that CD90 was the most suitable to stain PFs, while NGFR was the most appropriate to identify HSCs. However, the results of this thesis show that HSCs can express CD90 when cultured *in vitro*, although at lower levels than CAFs or PFs. Moreover, despite CD90 is expressed by almost all CAF subpopulations, the level of expression of this marker is not equal for all of them, suggesting that the levels of this protein could be linked to different functionalities or cell subsets. About NGFR, this marker is also described to be dynamic, as some studies based on single-cell analysis of human samples described that it is differently expressed in HSCs depending on the zonation of the liver (357). Thus, although the markers proposed were useful, maybe they were not the most suitable for our purpose to distinguish CAFs' precursors. A possible explanation for this could be that the papers that we took into account, which assessed PFs and HSCs as precursors of activated fibroblasts, were performed in mice models. Therefore, although the chosen markers are valid, it could be that in human context there are other markers with a

more relevant role. For this reason, we decided to perform RNA sequencing from an *in vitro* approximation to get candidate markers to distinct PF-derived and HSCs-derived CAFs.

RNAseq of hepatic stellate cells and portal fibroblasts revealed different gene expressions of these cells both in monoculture and in co-culture. Among the most differentially expressed genes observed *MME*, *HGF*, *F2R*, *ACTG2*, *FBLN1*, *CD82, CYGB* and *IL18R1* were characteristic of HSCs, while *MFAP5*, *SULF1*, *PDLIM3*, *SERPINE1* and *GREM1* were expressed on PFs. Immunohistochemistry assays showed that F2R and MFAP5 were good HSCs and PFs markers at the protein level, respectively. In normal liver IHC, F2R was shown in between the sinusoids, where HSCs are located, and portal tracts were negative for this marker. On the other hand, MFAP5 clearly stained portal tracts, while sinusoids did not show their expression. Inside the lesion, we could observe high staining of F2R, which was spread all around the lesion. In the case of MFAP5, the staining was located at some regions near the capsule, where the fibrosis came from a portal tract, but also at central regions of the tumor, suggesting a pre-existing portal tract that had been encompassed by the tumor. These observations are in line with the "replacement is the default" hypothesis of HGPs formation (53,272).

In line with the aforementioned, the criteria of HGPs classification establishes that fibrotic rim closer to a portal tract should not be considered, as the fibrosis observed could be due to the proximity to this parenchymal structure (53). We have observed MFAP5 staining in portal tracts in normal liver and in regions of the fibrotic rim in proximity with these structures, which should be excluded according to the consensus guidelines. However, MFAP5 also stained regions in the fibrotic capsules in which the presence of a portal tract was not evident, as well as in central regions inside of the tumor. This staining makes us think that MFAP5-positive areas have previously been portal tracts encompassed by the tumor and that fibrosis becomes part of it consequently. Because of that, we wonder if portal tracts fibrosis should be also considered as part of tumor-mediated fibrosis and, thus, may not be excluded from HGP classification. Alternatively, if portal tracts-derived fibrosis should be excluded, then the MFAP5 marker could help distinguish when the fibrosis observed is an extension of these structures.

In addition, the functional analysis of differential expressed genes showed that, when co-cultured with tumoral cells, PF increase the expression of pathways related to inflammation and immune cell chemotaxis as well as their myofibroblastic features like actin or ECM organization. Considering this information, PF seemed to form the "good" stroma present at higher levels in the better prognostic HGP, dHGP, as these CAFs would be recruiting higher levels of immune cells and creating the fibrotic rim. However, migration assays showed that conditioned media from PFs was more capable to recruit Th2 cells, a pro-tumoral T helper subset that we have observed at higher levels in non-dHGP. Thus, we could conclude that PFs are more prompted to recruit immune infiltrates, probably pro-tumoral cell subsets, when they are activated by tumoral cells when compared with their basal monoculture state. Even so, we cannot rule out the possibility that the co-culture results show only the conversion of FP to pro-tumoral CAFs. Thus, in vitro coculture would not be a good system for modeling tumor-restraining phenotypes.

On the other hand, when co-cultured with tumoral cells, HSCs increase their proliferation rate as well as acquire myofibroblastic features. These pathways were not upregulated when comparing monoculture and co-cultured PFs, probably because PFs are already playing fibroblastic functions, in contrast to HSCs. Inflammatory response and immune cell chemotaxis also increase, as well as hypoxia-related pathways and glycolysis. Meanwhile, adipogenic pathways are diminished. Both hypoxia and immune cell chemotaxis-related pathways were also upregulated in PFs, suggesting that both cell types react to the co-culture similarly. Nevertheless, the immune cell subsets recruited by HSCs and PFs may be different, according to the migration assay's results. Concerning the diminution of adipogenic pathways, in physiological conditions, HSCs are rich in lipid droplets containing a variety of triglycerides, cholesterol, phospholipids and free fatty acids. It has already been described that, during activation and myofibroblast transformation, these cells loss their lipid droplets (477). Thus, this fact further proves that our *in vitro* model is reliable, as it reproduces previously described data.

In addition, once activated by the co-culture with tumoral cells, PFs and HSCs show different RNA expressions. This is in line with our postulation that PF-derived and HSC-derived CAFs may differ in their functions. Hereby, it highlights the relevance of studying CAFs regarding their precursor cells. PFs show more myofibroblastic features as well as inflammation-

related pathways, chemokine production and immune cell recruitment. On the other hand, HSCs show increased pathways related to proliferation and angiogenesis. However, their main characteristic is the upregulation of many lipids' metabolism-related pathways. As mentioned before, portal fibroblasts are already fibroblastic cells, which become highly activated when in contact with tumoral cells; meanwhile, HSCs are characterized by storing lipids. Thereby, it suggests that these two functional differences between PF-derived and HSC-derived CAFs are marked by the physiological function of their precursor cells. On contrary, differences like immune cell recruitment, proliferation and angiogenesis would be related to the CAF functions that each CAF subset would be carrying out.

It is important to mention that PFs and HSCs are the main sources of activated fibroblasts both in cancer and fibrosis. However, other origins are described, like fibrocytes, mesenchymal stem cells, or even hepatocytes that have undergone EMT. Thus, although most of the fibrotic area of CRLMs is stained by either F2R or MFAP5, negative cells for both markers do exist, suggesting the presence of CAFs derived from other origins (95).

Moreover, Vidal-Vanaclocha proposes in chapter 3 of "Liver Metastasis: Biology and Clinical Management" (478) that PFs contribute to fibrosis in CRLMs when, during the first phases of the metastatic process, the metastatic niche is located at the portal tract. According to what is exposed in this chapter, when this happens, the metastases grow following a pushing histologic pattern. However, we have observed MFAP5 staining, which marks accurately portal tracts, in both dHGP and non-dHGP. Thus, although during the establishment of the metastasis's precursor cells closer to the metastatic niche may have the greatest contribution, in fully developed metastases, all the precursor cells have contributed to the metastatic fibrosis.

In line with this, Vidal-Vanaclocha also proposes that there are two models of blood supply: the sinusoidal-like, corresponding to co-option, which appears in replacement HGP; and the portal-like, that would be the one that appears in pushing and desmoplastic HGPs. Linked to this, in sinusoidal-like tumor vascularization, there is a high contribution of CAFs expressing desmin and glial fibrillary acidic protein, two HSCs typical markers. Therefore, this is suggesting a predominant presence of HSCs in replacement HGP. However, we observe similar levels of HSCs, assessed through F2R staining, in dHGP and non-dHGP.

Taking all this together, our results suggest no differences between HGPs concerning PF or HSC contribution. Nevertheless, to strongly confirm these observations the assessment of the described PF and HSCs markers in a larger cohort of patients through multiplex IHC would be needed.

Considering tumoral cells, the vast majority of the results obtained vary depending on the cell line. These differences may be explained by the expression of claudin 2 or claudin 8 (322), but they can also be a consequence of other specific features of each cell line. In any case, we decided to focus on the changes they have in common, as a way to include the variety of inter cellular lines. Thus, it would be interesting to assess the differences associated to the tumor cell lines in future experiments. If we look at the differences in common in both cell lines, they show an upregulation of proliferation-related processes, and lipid and cholesterol production when co-cultured with HSCs. When co-cultured with PFs, those cells increase inflammation-related pathways, immune cell chemotaxis and the formation of encapsulated structures. Thus, these results suggest an induction of proliferation rate increase in tumoral cells mediated by HSCs, in which lipid and cholesterol production would be linked with the need for the creation of new membranes. However, conditioned media from PF promoted an increase in tumor cell proliferation when compared to HSCs. The *in vitro* approximation analyzed through RNAseq consisted of co-cultured cells, in which there was direct contact between cells. On the contrary, the proliferation assay was performed using mesenchymal cell's conditioned media, in which only paracrine signals were preserved. Therefore, our results suggest a different effect of cell-cell and paracrine signals on tumoral cell proliferation.

About myCAF and iCAF classification, gene sets for myCAF and iCAF specific genes assessment in RNAseq data revealed that iCAF genes decrease in co-culture in both HSCs and PFs, while myCAF genes increase. Moreover, when comparing HSC with PF, HSCs showed lower levels of both myCAF and iCAF signatures. These results suggest that both HSCs and PFs can give rise to iCAF or myCAF, although they are more predisposed to become myCAFs at least in our *in vitro* model of cocultures growing in the same culture plate. Taking this into account and concerning CAF classifications, we postulate that CAFs derived from both origins can become iCAF or myCAF, but each origin-derived CAF subset would be more inclined to perform different iCAF or myCAF associated functions. In this line, both PF and

HSC-derived CAFs could be displaying pro-tumoral or anti-tumoral functions depending on the context.

3.2. CAF populations according to CD90 expression

Regarding cancer-associated fibroblast assessment considering the CD90 marker, the characterization of $CD90^{hi}$ and $CD90^{lo}$ sorted cells showed no differences between them when assessing PF and HSCs markers through qPCR. However, both $CD90^{hi}$ and $CD90^{lo}$ populations showed expression levels closer to PFs than to HSCs. This suggested that both could have arisen from the PF precursor cell subset. A possible explanation for this fact could be that the process of CAFs isolation and maintenance *in vitro* favors the growth of PF-derived CAFs rather than HSC-derived CAFs. The procedures needed to isolate HSCs are complex and require several specific reactives and steps (479). In line with this, in the context of pancreatic cancer, it has been observed that NGFR expression, which stains pancreatic stellate cells derived CAFs, decreases after cell isolation (480). In our isolated CAFs, we also observe low levels of NGFR, suggesting that it could also be occurring in the context of CRLM. This may be a limitation of working with isolated CAFs, as we could be selecting specific CAF populations that may survive better under *in vitro* conditions.

Moreover, when looking at CD90 staining in patient samples through IHC, we observed that CD90 could be expressed in a huge amount of CAFs but at different expression levels. Thus, we hypothesized that CD90 expression is variable and seems to be regulated. Its expression may be associated with different CAF functions and/or with the myofibroblastic potential. In conclusion, CD90 may be a good marker for PF and PFs-derived CAFs, although MFAP5 would be a more stable PF marker.

In addition, $CD90^{hi}$ and $CD90^{lo}$ cell populations showed different secretomes, which confirmed that they are part of different CAF subsets or phenotypes and suggested that they could be mediating different functions.

$CD90^{hi}$ showed higher levels of Podoplanin than $CD90^{lo}$, both at RNA and protein levels (Figure 65 and Figure 66). It is described that this protein is upregulated in CAFs that mediate the recruitment of macrophages and their polarization of the M2 phenotype (399). Moreover, both $CD90^{hi}$ and $CD90^{lo}$ CAF populations expressed high levels of IL1β, a marker

of iCAFs (Figure 75). Migration assays showed higher recruitment of monocytes in $CD90^{hi}$-conditioned media conditions (Figure 70). Furthermore, the macrophage polarization assay showed an increased polarization of macrophages (CD163 RNA expression) in those monocytes cultured with $CD90^{hi}$ conditioned media (Figure 71). On the other hand, $CD90^{lo}$ conditioned media recruited higher numbers of T cells, both cytotoxic and T helper (Figure 70). In addition, $CD90^{hi}$-conditioned media increased the proliferation rates of tumoral cells cultured with it (Figure 72). Thus, these results suggest that $CD90^{hi}$ and $CD90^{lo}$ CAFs might be different subpopulations of iCAFs. However, more research is needed to validate this postulation.

Nevertheless, the results obtained from mIHC CAF subpopulations assessment in TMA, which will be commented in later sections, go in the opposite direction. First, total CD90 staining was seen at higher levels in dHGP, suggesting that $CD90^{+}$ CAFs are associated with better prognosis. Moreover, when we stablished a threshold to segregate between $CD90^{hi}$ and $CD90^{lo}$, both populations were present at greater densities in dHGP. It is important to highlight that the levels of CD90 expression of mIHC assessed $CD90^{hi}$ and $CD90^{lo}$ are not comparable with $CD90^{hi}$ and $CD90^{lo}$ populations stablished through flow cytometry, not only because the sensitivity of detection is different according to the technique used, but also because the *in vitro* maintained CAFs may have changed their original CD90 expression. Moreover, these two populations we worked with *in vitro* came from CAFs isolated from one patient, which means that the differences observed between them could be patient-specific. Other reason why these results do not match could be that functional experiments are done *in vitro*, while the information of mIHC comes from patient samples.

3.3. CAF populations according to classical CAF markers

αSMA and FAP are classical CAF markers hugely described in the literature. Other widely used markers to identify these elements of the tumor microenvironment are Periostin, Fibronectin, Podoplanin, s100A4 and MYH11. These markers have been extensively studied and their functions have already been assessed. Thus, we found it interesting to assess how these markers are distributed in the particular histology of dHGP. Doing that, we observed a CAF expression pattern inside of the capsule, suggesting CAF heterogeneity in the fibrotic structure, which could be linked to different CAF functions, and could be determined by the

distance of each CAF subset from tumoral cells or parenchyma. In this line, the markers observed at the closest proximity of cancer cells were FAP, Periostin, Fibronectin and Podoplanin. Meanwhile, αSMA, was present at the nearest part of parenchyma, suggesting that this marker appears highly expressed when being in touch with hepatocytes. On contrary, s100A4 and MYH11 showed no expression in the fibrotic rim.

In addition, we assessed the expression of αSMA and FAP in replacement histologic patterns. In this pattern, FAP was highly expressed in invasive margin areas in contrast to central regions, suggesting that this marker is playing a role in those regions in which tissue remodeling and invasion are taking place. On the other hand, αSMA was highly expressed both in peripheral and central tumor areas.

In conclusion, classical CAF markers, which are usually associated to functions, are showing a specific distribution pattern inside each HGP. On the other hand, this distribution was not observed when assessing MFAP5 and F2R origin-associated markers. Therefore, this suggests that both PFs and HSCs can give rise to different CAF subpopulations with diverse functions. It would have a special interest to look for associations between PF-derived and HSC-derived CAFs and the mentioned classical markers, in order to better define the CAF subpopulations, present in CRLMs and their function. Hence, from a histologic point of view, invasive margin and central tumor areas may be showing two scenarios that occur at different time points: In central areas there is a scarring fibrosis, characterized by matrix deposition, being less cellular and suggesting an already cured wound. Meanwhile, at the invasive margin there may be a tissue remodeling process, typical of a tumor in its phase of growth and expansion, with a more cellular, reactive, and unstructured fibrosis.

3.4. CAF subpopulations assessment in TMA samples

In order to assess the role of CAFs in CRLM, we studied these cells though different perspectives. On the one hand, we performed *in vitro* experiments to elucidate how PF and HSCs change when they are activated by the presence of tumoral cells, as well as to find proper markers to distinguish these precursor cells in patient samples. On the other hand, we also studied the association of CD90, a classical CAF marker to different functions through *in vitro* experiments. Moreover, we assessed the distribution inside the lesions of a set of markers of interest in dHGP and non-dHGP patient samples.

However, we thought that CAF subpopulations will, not only distribute in a specific way inside CRLM lesion, but also differ in densities depending on the HGP. Thus, a comparison of CAF subpopulations between dHGP and non-dHGP in a big cohort of patients was needed. For this reason, in parallel to all the mentioned experiments, we applied mIHC at the same TMA samples in which we studied lymphoid and myeloid immune cells. This allowed us to study five selected CAF markers that served us to define various CAF subpopulations. These CAF subsets showed significantly different densities when comparing dHGP with non-dHGP.

With the selected CAF markers for mIHC, some of the questions we aimed to answer were (a) which were the most abundant CAF precursors in each histologic pattern, (b) how did the classical markers αSMA and FAP distribute through HGPs and (c) how COL1A1, an abundant ECM protein, was disseminated in dHGP and non-dHGP. The reasons for selecting each of the mentioned markers are explained in the corresponding results section. However, the selection of these markers was done prior to knowing the results from the other experiments. Thus, considering all the information obtained, other markers, like F2R and MFAP5 may be more suitable, especially for the purpose of assessing CAF precursor cells.

When looking at the densities of the total cells expressing each studied marker (Figure 82 and Table 25), we observed few differences between dHGP and non-dHGP for the classical makers αSMA and FAP. In the case of FAP, it did not show differences between HGPs of CRLM lesions. Considering αSMA, it was observed statistically significant higher in tumor and stromal compartments of non-dHGP, but only through the less stringent statistical test. Concerning αSMA, CAFs that express high levels of this protein are considered myCAFs, whereas iCAFs express αSMA but at lower levels (364,366). Interestingly, when we stablished a threshold to distinguish between αSMA^{hi} and αSMA^{lo} cells, we could see significant differences using the most restrictive statistical test in both αSMA subpopulations (Figure 83 and Table 26). αSMA^{hi} was higher in tumor and liver compartments of non-dHGP and αSMA^{lo} was higher in the tumor, stromal and liver compartments of the same HGP. Thus, it suggested that αSMA^{+} CAFs contained different subpopulations which may have different functions and distribute in a distinct way between HGPs.

We postulated that αSMA^{lo} constitute the population of iCAFs, which may display pro-tumoral functions and be present at higher levels in non-dHGP. As expected, non-dHGP was

enriched in this CAF population. However, it would be useful to assess a specific iCAF marker through the same TMA samples and study its distribution to further confirm these results. This work is ongoing in the lab at the moment of delivering this manuscript.

Considering αSMA^{hi} CAFs, the differences of this population between HGPs were less pronounced than the observed in αSMA^{lo}. In fact, we postulated that αSMA^{hi} subset of CAFs correspond to myCAFs, which may include different CAF subpopulations. In between the CAF subsets αSMA^{hi}, we may encounter both tumor-promoting a tumor-restraining myCAFs. Thus, as αSMA^{hi} CAF subset include pro-tumoral and anti-tumoral subsets, it would include populations present at higher levels in dHGP and populations typical of non-dHGP, which would explain the less strongly marked differences between HGPs.

In some studies, αSMA has been described as a TGFβ response gene (481,482). Although TGFβ is associated to poor prognoses, it is unclear whether αSMA is associated to tumor-promoting or tumor-restraining CAFs (481). In our context, TGFβ is higher in non-dHGP (assessment through the surrogated protein p-SMAD2) in the same way that αSMA is, which suggests that both proteins may be associated to worse survival. Nevertheless, among αSMA^{+} cells we find both pro-tumoral and anti-tumoral subsets. Therefore, total levels of αSMA may be associated to worse prognoses, but the existence of different subpopulations of αSMA^{+} could explain the controversy around this marker. In conclusion, αSMA by itself is only a good myCAF marker when expressed at high levels. Thus, the combination of αSMA with other markers to define CAF subsets is the key to reveal the value of αSMA in each situation.

Regarding total CD90^{+} cells, we observed substantial differences between HGPs. Contrary to what we may expected considering the *in vitro* functional assays done with two populations isolated from one patient, this marker was present at higher levels in the good prognoses condition: desmoplastic HGP. Mainly, CD90 is a myofibroblast marker. Thus, these results suggest that dHGP is enriched in myCAFs, at least in the invasive margin. his fact is also related to the well-differentiated histology of dHGP metastases and could be associated with the fact that well-structured glands require supporting myofibroblasts, which structure and contribute to giving shape to the mentioned glands. The non-desmoplastic HGP display a non-differentiated histology, mainly at the invasive margin, displaying also an unstructured

stroma. Moreover, we also selected this marker because of its association with portal fibroblasts, suggesting a higher contribution of PFs in desmoplastic HGP. However, as we have observed in previous experiments, CD90 is a dynamic marker that could be changing depending on the context. Thus, the assessment of other markers like MFAP5 would be needed to state this more reliably.

About NGFR, which was selected because of being an HSCs marker, it was also observed at higher levels in dHGP. Thus, desmoplastic HGP would also have a higher contribution of HSCs-derived CAFs. Interestingly, the average number of total $NGFR^+$ cells was so elevated, suggesting a high contribution of HSCs in CAFs present at CRLM lesions. In murine models of cholangiocarcinoma, HSCs have been described to be the main source of CAFs and the dominant population interacting with tumor cells (318). In the same line, Bhattacharjee *et al*. also observed that these precursor cells constitute the main source of CAFs in liver metastases from CRC and PDAC (364). However, whole-slide staining of MFAP5 and F2R showed that both PFs-derived and HSCs-derived CAFs were present in CRLM lesions. Moreover, although high levels of $NGFR^+$ cells were seen through mIHC, the levels of $CD90^+$ CAFs were also high. Thus, our results suggest that both CAF precursor cells, HSCs and PFs, contribute at approximately the same level to CRLM fibrosis. These data are in line with Giguelay A *et al*. work, in which CAFs derived from hepatic stellate cells, portal fibroblasts (termed "cells strongly associated with fibrosis"), and vascular smooth muscle cells were described (320).

However, the expression of NGFR have been described to vary following a zonation inside the liver parenchyma and the hepatic lobule structure (357). Therefore, the expression of this marker in the context of tumoral lesions may also be changing depending on the context. Thus, as it happened with CD90, the assessment of other markers, like F2R, would be needed to better determine HSCs-derived CAFs.

Furthermore, a study performed by Fujiwara K *et al.* in PDAC associated NGFR to better prognoses (480), which would match with our results. Interestingly, the same work proposed that pancreatic stellate cells, the pancreatic homologous cell type of hepatic stellate cells, once activated, can give rise to different populations of myofibroblasts, which may perform restraining or promoting tumoral functions (480). This supports the hypothesis that CAFs

coming from HSCs can derive into different CAF subpopulations, including pro-tumoral and anti-tumoral subsets, which may depend on TME context. We postulate that the same would happen in the case of PF-derived CAFs. This would be in line with the theory that CAF subpopulations are an "state" that depends on TME features, rather than a lineage predetermination. On contrary, the data of Giguelay A *et al*. study show that CAF heterogeneity is mainly based on the distinct origins (320). However, we propose that both postulations are not mutually exclusive. Otherwise, we postulate that signals from the TME modulate CAF states, but the functional possibilities of each population would depend on its lineage. The work of Street K *et al*. in PDAC is in agreement with this hypothesis as it concludes that, although TME changes during tumor progression affect fibroblast evolution, pre-existing fibroblast heterogeneity of normal pancreas dictates the development trajectories of activated murine CAFs (483,484).

Considering CD90 and NGFR, both markers are associated with tissue-resident mesenchymal cells: PFs and HSCs, respectively. There are studies that suggest that tissue-resident fibroblasts, at physiological conditions, prevent tumor growth and invasiveness. Then, once they become reprogrammed by unknown mechanisms induced by tumor cells, they provide a tumor-promoting environment (485–487). In line with this, Fujiwara K. *et al*. work describes that NGFR is a temporary marker of the first activation stages of pancreatic stellate cells, as a result of the interaction of these cells with tumoral cells. However, a long-term exposition to cancer cells may induce an NGFR loss on them (480). Thus, considering that both CD90 and NGFR markers are present at higher levels in dHGP, it could be that are PFs and HSCs at their first activation stages, thus, displaying tumor-restraining defensive roles (480,481).

Nevertheless, with the information provided by CD90 and NGFR markers, we cannot infer which CAF precursor has the greatest contribution in each HGP. Thus, only with this information we cannot associate the PFs and HSCs functions observed *in vitro* with desmoplastic or non-desmoplastic patterns.

When considering the total positive cells for each marker, the most pronounced differences were seen in COL1A1. This marker was present at higher levels in total tissue, total-excluding liver, and stromal compartment of desmoplastic HGP. This protein is also considered a

myCAF marker. Thus, these results further confirmed that myofibroblasts were present at higher density in dHGP. As COL1A1 is associated with both pro-tumoral and anti-tumoral functions, observing larger amounts of this marker in desmoplastic HGP suggested that, in the context of CRLM HGPs, it is playing a tumor-restrictive role. In fact, this ECM protein has been associated before with high levels of desmoplasia by Chen Y *et al.* (361). However, the same study concludes that COL1A1 has no impact in the blood vessel density, as the vascular basement membranes associated with capillaries is predominantly composed of type IV collagen (361). Thus, according to this paper, in our context, COL1A1 would not be contributing to the angiogenic process observed in dHGP. In PDAC, Chen Y *et al.* (361) conclude that, although COL1A1 increases the ECM biophysical stiffness facilitating abnormal cellular interactions and migration, in balance it has a tumor-restraining function that reduces the proliferation of tumoral cells and increases the inflammatory response. In fact, they observe that COL1A1 deletion in αSMA$^+$ CAFs significantly alters the profile of immune cells, increasing the presence of MDSCs and M2 macrophages, while diminishing T and B cells (361). Thereby, in PDAC, αSMA$^+$ COL1A1$^+$ CAFs may constitute a tumor-restricting myofibroblast population. This CAF subset could also be present in CRLM.

Furthermore, an anti-tumor function of COL1A1 in the context of CRLMs was already described by Bhattacharjee *et al.* (364), in a study on mice models focused on PDAC and CRC liver metastases. This work also defined two populations of myCAFs: myCAF expressing hyaluronic acid, which would be tumor-promoting, and myCAF expressing Collagen type I, being tumor-restraining CAFs. Moreover, it also describes a protumoral population of iCAF expressing hepatocyte growth factor (HGF). Therefore, in our context, dHGP lesions would be enriched in the second described myCAF subpopulation. Among the described anti-tumoral functions of COL1A1 we find the mechanical restriction of tumor growth, and the recruitment of T and B cells to promote an immune active environment.

On the contrary, Junyu Ren *et al.* study correlates COL1A1 with poor prognoses in different cancer types. Moreover, in lower grade glioma (LLG), it has been associated with M1 and M2 macrophage recruitment and T cell exhaustion markers, as well as with markers of different T helper cell populations. In fact, COL1A1 has been correlated to high Immunoscore® and associated with the recruitment of many immune cell types, including T cells. However, it seems that in LLG it could be promoting an immune suppressive

environment (362). It is worth mentioning that tumors in which COL1A1 is correlated to worse prognoses do not show fibrotic encapsulation, suggesting that the context of the HGPs is different. Thus, COL1A1-provided stiffness may be involved in pro-tumoral or tumor-restraining functions, depending on the context.

Finally, we stablished five combinations of the markers assessed in mIHC, which defined 5 different CAF subpopulations according to the bibliography and the numbers of cells that constituted each combination. Similarly, Pellinen T *et al.* used multiplex IHC to study CAF subpopulations in the context of non-small cell lung cancer (NSCL). In this study, the authors also defined multimarker CAF subsets through high-content spatial profiling (488). Among the defined CAF subpopulations we included four myCAF subpopulations and one iCAF, defined by being αSMA^{lo} single. Among the myCAF populations, the subset defined by FAP^{+} αSMA^{+} $COL1A1^{neg}$ may be displaying pro-tumoral functions according to the bibliography, as FAP is associated with tumor-promoting functions like immunosuppression (366,374). The other three myCAF populations would be αSMA^{hi} $COL1A1^{+}$, $CD90^{+}$ $COL1A1^{+}$, $NGFR^{+}$ $COL1A1^{+}$. These three last CAF subsets may be ECM-producing tumor-restraining CAFs due to the expression of COL1A1, that in our context is associated to good prognoses. It is worth to mention that, as we are assessing the total of the cells expressing each combination of markers, there may be overlapping between the mentioned $COL1A1^{+}$ myCAF subsets. In this manner, αSMA^{hi} $COL1A1^{+}$ cell subset may include some $CD90^{+}$ $COL1A1^{+}$ cells and some $NGFR^{+}$ $COL1A1^{+}$ cells.

In a similar way, Giuguelay A *et al*. performed single cell at CAFs isolated from CRLM patients and found 2 main CAF populations expressing αSMA: ECM-remodeling CAFs and contractile-CAFs (320). ECM-remodeling CAFs are described to produce high amounts of collagen, which makes the ECM stiffer hampering cell growth, and to accumulate at areas of strong desmoplastic reaction (320).

It is also important to have in mind that αSMA^{+} cells include pericytes. However, as pericytes express high levels of αSMA, αSMA^{lo} population may contain a negligible number of these cells. Meanwhile, αSMA^{hi} subpopulations are assessed in combination with other CAF markers, which allows us to avoid αSMA stained pericytes.

Moreover, the low number of cells positive for both FAP and COL1A1 (Figure 84C) and the lack of colocalization of these two markers in mIHC obtained images suggest that these two markers are mutually exclusive (Figure 84A and B). That way, FAP would be labeling tumor-promoting subpopulations, while COL1A1 may be staining tumor-restraining CAF subsets. In a similar way, in NSCL, Pellinen T *et al.* defined the poor prognoses associated CAF subsets as FAP^+, while the good prognoses correlated CAF subsets were negative for this marker and positive for PDGFRα (488).

With this analysis we saw that the three CAF subpopulations associated with tumor-restraining functions were present at higher levels in dHGP. Meanwhile, the pro-tumoral myCAF population, defined by FAP^+ αSMA^+ $COL1A1^{neg}$ showed no differences between HGPs. However, in dHGP the balance of tumor-promoting vs. tumor-restraining CAFs is bend to tumor-restraining, as these cases have higher amounts of anti-tumoral myCAF subpopulations. On contrary, this balance is inclined to pro-tumoral CAFs in non-dHGP, as this HGP is enriched in tumor-promoting iCAFs.

About future perspectives, we plan to further describe the markers of each of the defined CAF subpopulations. Moreover, considering that Bhattacharjee *et al*. observed pro-tumoral hyaluronan-expressing myCAFs and hepatocyte growth factor-expressing iCAFs in murine models of CRLM (364), it would be interesting to study the role of these molecules associated to each HGP.

In conclusion, we postulate that the pro-tumoral subpopulation of myCAFs, defined as FAP^+ αSMA^+ $COL1A1^{neg}$, is equally present in both desmoplastic and non-desmoplastic HGP invasive margins. Meanwhile, non-dHGP may be rich in iCAFs and present low levels of all tumor-restraining $COL1A1^+$ CAF subsets. According to the already bibliography mentioned, the high levels of COL1A1 present in dHGP would be mechanically restraining tumor growth, especially when expressed at the fibrotic rim. Moreover, COL1A1 could also act recruiting T cells to create an immune active environment against the tumor. On the other hand, the lower levels of this collagen in non-dHGP may contribute to the immune-suppressive environment associated to this HGP through the recruitment of M2 macrophages and MDSCs.

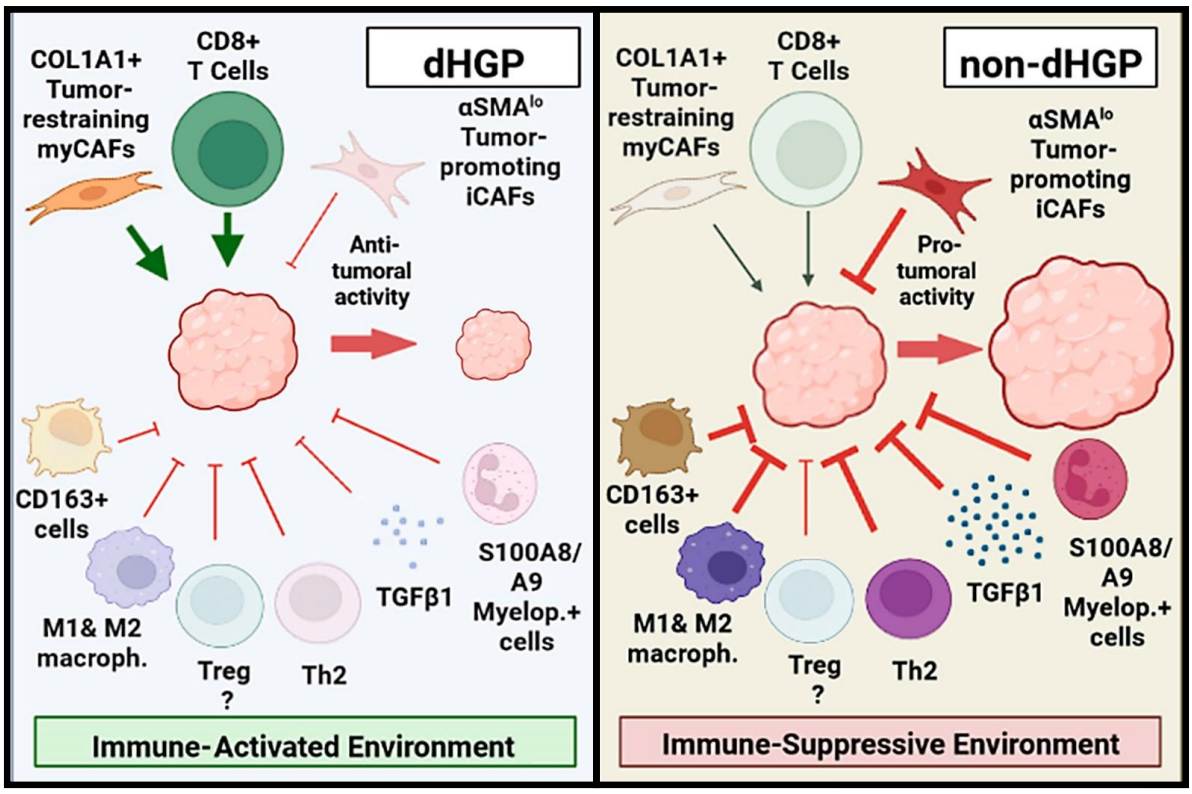

Figure 87. Schematic summary of the proposed dHGP and non-dHGP environment considering immune infiltrates and CAF populations. *Image created in Biorender.com.*

4. THERAPEUTIC CONSEQUENCES OF THE RESULTS OBTAINED

The results obtained from this project suggest that the histologic growth patterns found in CRLM may be playing an important role in the response to some treatments. The higher presence of cytotoxic T cells in tumoral niches of the encapsulated lesions show that these cells are able to infiltrate dHGP metastases. In contrast, non-desmoplastic lesions show, not only a lower density of $CD8^+$ cells, but also greater levels of different subsets of myeloid cells that are described to be immunosuppressive (249,250,298,300,305–307,313,402,406,409,451,452,489–492). As mentioned before, taking into account that non-dHGP accounts for 80% of the cases, our results may be explaining the failure of immunotherapy in most patients with hepatic metastases of CRC (279–281,298,493). But this is not the only context in which HGPs influence treatment response. It has been already described that desmoplastic HGPs are characterized by using angiogenesis as a blood supply, instead of vessel co-option for replacement metastases. Thus, anti-angiogenics are particularly effective in patients with this HGP (54,85,292). Taking this into account, it would be especially useful to consider the histologic pattern for clinical decision-making. However,

at present is useless since it is determined at the pathology process after surgery. For this reason, there are studies that are assessing how to evaluate the HGP through advanced medical imaging techniques like computed tomography or magnetic resonance, in order to build a predictive radiomic signature, which are showing encouraging results (278,494–497). Knowing the histologic pattern before surgery would be of special interest, not only to be able to choose the most appropriate treatment for those patients optimal for surgery, but also to provide more effective treatment options in those cases that cannot be operated. Thus, patients with an encapsulated pattern could benefit from the antiangiogenic treatments already described and, taking into account our results, they would also be good candidates for adoptive T-cell therapies, since in dHGP $CD8^+$ cells can reach tumor niches, displaying a diminished pressure for tumor exclusion or siphoning by myeloid cells. On the other hand, patients with non-dHGP pattern could positively respond to treatments against immunosuppressive myeloid cells. Targeting M2 macrophages and other suppressive myeloid cells would relief the tumor exclusion, restoring the function of the infiltrative T cells. There are already different compounds on clinical trials, which include MERKT (498) or CSF1R (499,500) inhibitors, compounds against the immunosuppression that target molecules like arginase (501), inhibitors or antibodies suppressing recruitment targeting cytokines like CCL2 (502) or CSF1 (503), or even drugs that induce repolarization of M2 macrophages towards M1 phenotype (504). However, the segregation of patients according to the HGP will be still needed.

CONCLUSIONS

1. The lymphoid infiltration of CRLM differed according to the HGP. Encapsulated metastasis displayed higher density of cytotoxic CD8 cells, particularly over the tumor cells nests. This fact, combined with i) higher ratio tumor CD8/stroma CD8, ii) higher ratio tumor CD8/stroma CD4 in encapsulated metastases and iii) higher density of Th2 lymphocytes on non-desmoplastic metastases, suggested a higher immune anti-tumor activity in dHGP compared to non-dHGP.

2. The assessment of myeloid cell subsets showed higher levels of macrophages both M1 and M2 polarized in non-dHGP stromal compartment. Myeloid non-macrophage cells Calprotectin, and Myeloperoxidase positive cells were also observed at higher levels in non-dHGP. These facts, combined with the presence of moderate infiltration of CD8 retained in the stromal compartment, suggested a pro-tumoral immune environment in non-dHGP liver metastases.

3. The ratio CD8 /M2 polarized macrophages and CD8/Myeloid non macrophage cells, which illustrate the activation status of the immune system, revealed significant differences between HGPs, being at significantly lower levels in the stromal compartment of non-dHGP, suggesting a mechanism of CD8 retention and inactivation mediated by myeloid immune-suppressive cells.

4. Considering all the mentioned above, non-dHGP liver metastases display a powerful immune suppressive environment, which has been further confirmed by a higher activity of TGFβ1 pathway in this pattern, assessed through the surrogated marker pSMAD2.

5. The assessment of five defined CAF subpopulations showed that three Collagen 1-producing myCAF populations were present at higher levels in dHGP, suggesting a tumor-restraining role of COL1A1 in CRLM context. The tumor-promoting myCAF subset showed no differences between HGPs. However, the pro-tumoral inflammatory CAF subpopulation was present at higher density in non-dHGP. Thus, the higher ratio restraining-CAFs vs. pro-tumoral-CAFs in dHGP might contribute to the better outcome of patients harboring encapsulated metastases.

6. Thus, the evaluation of HGPs could have a benefit for clinical decision-making, particularly regarding adoptive T cell therapies for encapsulated metastases, as well as therapies based on myeloid cell inhibition for non-desmoplastic cases.

7. The transcriptional analysis of HSC and PF co-cultured with tumor cells provided us specific markers of the two mesenchymal lineages that are maintained in the conversion to CAFs. Two of them, MFAP5 and F2R, characteristic of PF and HSC respectively, were successfully validated in human tumor samples, making it possible to determine the contribution of these two cell types in the stroma of liver metastases.

8. The transcriptional analysis of HSC and PF co-cultured with tumor cells provided us specific markers of the two mesenchymal lineages that are maintained in the conversion to CAFs. Two of them, MFAP5 and F2R, characteristic of PF and HSC respectively, were successfully validated in human tumor samples, making it possible to determine the contribution of these two cell types in the stroma of liver metastases.

9. On the other hand, the cocultured HSCs showed an increase in proliferation, as well as in pathways that involve the synthesis of fatty acids and phospholipids, essential requirements for the demanding growth of plasma membranes.

10. Considering tumoral cells, they show an upregulation of proliferation related processes, lipid, and cholesterol production when co-cultured with HSCs.

11. Instead, when co-cultured with PFs, tumor cells display a proinflammatory phenotype, as well as the induction of processes involving the encapsulation of structures, a biological process that requires the participation of collagens, collagenases, MMPs and other extracellular matrix components, which could be related to the formation of the fibrotic rim in dHGP.

12. In primary cell culture, we isolated from one patient two populations of CAFs with different expression of CD90: $CD90^{hi}$ and $CD90^{lo}$. These CAF subsets had a different secretory profile as well as different functions: $CD90^{hi}$ showed a higher capacity to recruit monocytes, to drive M2 polarization, and to increase tumor cells proliferation; while $CD90^{lo}$ recruited higher numbers of T cells.

REFERENCES

1. AECC [Internet]. Available from: www.aecc.es

2. National Institutes of Health [Internet]. Available from: www.nih.gov

3. National Cancer Institute [Internet]. Available from: www.cancer.gov

4. World Health Organization [Internet]. Available from: www.who.int

5. (GLOBOSCAN). IA for R on CancerWHO. Cancer Today [Internet]. Available from: http://gco.iarc.fr/today/data/pdf/fact-sheets/cancers/cancer-fact-sheets-6.pdfReferences

6. Weinberg RA. The Biology of Cancer. 2nd ed. New York: Garland Science, Taylor & Francis Group; 2014.

7. Hanahan D, Weinberg RA. The hallmarks of Cancer. Cell. 2000;100:57–70.

8. Hanahan D, Weinberg RA. Hallmarks of cancer: The next generation. Cell. 2011;144(5):646–74.

9. Hanahan D. Hallmarks of Cancer: New Dimensions. Cancer Discov. 2022;12(1):31–46.

10. Sung H, Ferlay J, Siegel RL, Laversanne M, Soerjomataram I, Jemal A, et al. Global Cancer Statistics 2020: GLOBOCAN Estimates of Incidence and Mortality Worldwide for 36 Cancers in 185 Countries. CA Cancer J Clin. 2021;71(3):209–49.

11. Dienstmann R, Vermeulen L, Guinney J, Kopetz S, Tejpar S, Tabernero J. Consensus molecular subtypes and the evolution of precision medicine in colorectal cancer. Nat Rev Cancer. 2017;17(2):79–92.

12. André T, Boni C, Navarro M, Tabernero J, Hickish T, Topham C, et al. Improved overall survival with oxaliplatin, fluorouracil, and leucovorin as adjuvant treatment in stage II or III colon cancer in the MOSAIC trial. Journal of Clinical Oncology. 2009;27(19):3109–16.

13. Siegel RL, Miller KD, Jemal A. Cancer statistics, 2019. CA Cancer J Clin. 2019;69(1):7–34.

14. Siegel RL, Miller KD, Goding Sauer A, Fedewa SA, Butterly LF, Anderson JC, et al. Colorectal cancer statistics, 2020. CA Cancer J Clin. 2020;70(3):145–64.

15. Henrikson NB, Webber EM, Goddard KA, Scrol A, Piper M, Williams MS, et al. Family history and the natural history of colorectal cancer: Systematic review. Genetics in Medicine. 2015;17(9):702–12.

16. Kastrinos F, Samadder NJ, Burt RW. Use of Family History and Genetic Testing to Determine Risk of Colorectal Cancer. Gastroenterology. 2020;158(2):389–403.

17. Straussman R, Morikawa T, Shee K. Tumor microenvironment induces innate RAF-inhibitor resistance through HGF secretion. Nature. 2012;487(7408):500–4.

18. Mármol I, Sánchez-de-Diego C, Dieste AP, Cerrada E, Yoldi MJR. Colorectal carcinoma: A general overview and future perspectives in colorectal cancer. Int J Mol Sci. 2017;18(1).

19. Müller MF, Ibrahim AEK, Arends MJ. Molecular pathological classification of colorectal cancer. Virchows Archiv. 2016;469(2):125–34.

20. George Poulogiannis, Koichi Ichimura, Rifat A Hamoudi, Feijun Luo, Suet Y Leung STY, David J Harrison AHW, Arends and MJ. Prognostic relevance of DNA copy number changes in colorectal cancer. Journal of Pathology. 2010;220(October 2009):338–47.

21. MJ A. Pathways of Colorectal Carcinogenesis. Mol Morphol. 2013;21(2):97–102.

22. Ibrahim AE, Arends MJ, Silva A-L, Wyllie AH, Greger L IY, Vowler SL, Huang TH, Tavaré S MA. Sequential DNA methylation changes are associated with DNMT3B overexpression in colorectal neoplastic progression. Gut. 2011;60(4):499–598.

23. Colussi D, Brandi G, Bazzoli F RL. Molecular pathways involved in colorectal cancer: implications for disease behavior and prevention. Int J Mol Sci. 2013;14:16365–85.

24. Grady WM CJM. Genomic and epigenetic instability in colorectal cancer pathogenesis. Gastroenterology. Gastroenterology. 2008;135:1079–99.

25. E. R. Fearon and B. Vogelstein. A genetic model for colorectal tumorigenesis. Cell. 1990;

26. Domenica F, Palma E De, Argenio VD, Pol J, Kroemer G, Maiuri MC, et al. The Molecular Hallmarks of the Serrated Pathway in Colorectal Cancer. Cancers (Basel). 2019;11(7):1–25.

27. B. Vogelstein and K. W. Kinzler. The multistep nature of cancer. Trends in Genetics. 1993;9 (4):138–41.

28. Z. Herceg and P. Hainaut. Genetic and epigenetic alterations as biomarkers for cancer detection, diagnosis and prognosis. Mol Oncol. 2007;1 (1):26–41.

29. J. Guinney. The consensus molecular subtypes of colorectal cancer. Nat Med. 2015;

30. W. K. Kim et al. Identification and selective degradation of neopeptide-containing truncated mutant proteins in the tumors with high microsatellite instability. Clinical Cancer Research. 19(13):3369–82.

31. Ros J, Baraibar I, Martini G, Salvà F, Saoudi N, Cuadra-Urteaga JL, et al. The Evolving Role of Consensus Molecular Subtypes: a Step Beyond Inpatient Selection for Treatment of Colorectal Cancer. Curr Treat Options Oncol. 2021;22(12):1–18.

32. E. Fessler and J. P. Medema. Colorectal Cancer Subtypes: Developmental Origin and Microenvironmental Regulation. Trends Cancer. 2016;2(9).

33. Jordan P. Targeted Therapy of Colorectal Cancer Subtypes. 2018. 1–6 p.

34. Treanor D, Quirke P. Pathology of Colorectal Cancer. Vol. 19, Clinical Oncology. 2007. p. 769–76.

35. Fleming M, Ravula S, Tatishchev SF, Wang HL. Colorectal carcinoma: Pathologic aspects. J Gastrointest Oncol. 2021;3(3):153–73.

36. Luo C, Cen S, Ding G WW. Mucinous colorectal adenocarcinoma: clinical pathology and treatment options. Cancer Commun (Lond). 2019;39(1):13.

37. E. J. Kuipers et al. Colorectal Cancer. Nat Rev Dis Primers. 2015;1.

38. Marques I, Araújo A, de Mello RA. Anti-angiogenic therapies for metastatic colorectal cancer: current and future perspectives. World J Gastroenterol [Internet]. 2013 Nov 28 [cited 2022 Nov 28];19(44):7955–71. Available from: https://pubmed.ncbi.nlm.nih.gov/24307789/

39. Tabernero J, van Cutsem E, Díaz-Rubio E, Cervantes A, Humblet Y, André T, et al. Phase II trial of cetuximab in combination with fluorouracil, leucovorin, and oxaliplatin in the first-line treatment of metastatic colorectal cancer. J Clin Oncol [Internet]. 2007 Nov

20 [cited 2022 Nov 28];25(33):5225–32. Available from: https://pubmed.ncbi.nlm.nih.gov/18024868/

40. van Cutsem E, Köhne CH, Hitre E, Zaluski J, Chang Chien CR, Makhson A, et al. Cetuximab and chemotherapy as initial treatment for metastatic colorectal cancer. N Engl J Med [Internet]. 2009 Apr 2 [cited 2022 Nov 28];360(14):1408–17. Available from: https://pubmed.ncbi.nlm.nih.gov/19339720/

41. Biller LH, Schrag D. Diagnosis and treatment of metastatic colorectal cancer: A review. JAMA - Journal of the American Medical Association. 2021;325(7):669–85.

42. Kahi CJ, Boland CR, Dominitz JA et al. Colonoscopy surveillance after colorectal cancer resection: recommendations of the US Multi-Society Task Force on Colorectal Cancer. Am J Gastroenterol. 2016;111(3):31–44.

43. Tauriello DVF, Calon A, Lonardo E, Batlle E. Determinants of metastatic competency in colorectal cancer. Mol Oncol. 2017;11(1):97–119.

44. Riihimäki M, Hemminki A SJ, K. H. Patterns of metastasis in colon and rectal cancer. Sci Rep. 2016;6(1):29765.

45. Jang KU, Kim CW, Kim KH, Lim SB, Yu CS, Kim TW, et al. Prognostic factors in terms of the number of metastatic nodules in patients with colorectal cancer liver metastases. Ann Coloproctol. 2016;32(3):92–100.

46. Garcia-vicién G, Mezheyeuski A, Bañuls M, Ruiz-roig N, Molleví DG. The tumor microenvironment in liver metastases from colorectal carcinoma in the context of the histologic growth patterns. Int J Mol Sci. 2021;22(4):1–21.

47. Liu J, Cho YB, Hong HK, Wu S, Ebert PJ, Bray SM, et al. Molecular dissection of CRC primary tumors and their matched liver metastases reveals critical role of immune microenvironment, EMT and angiogenesis in cancer metastasis. Sci Rep. 2020;10(1):1–15.

48. Rinn JL, Bondre C, Gladstone HB, Brown PO, Chang HY. Anatomic demarcation by positional variation in fibroblast gene expression programs. PLoS Genet. 2006;2(7):1084–96.

49. Berdiel-Acer M, Cuadras D, Díaz-Maroto NG, Sanjuan X, Serrano T, Berenguer A, et al. A monotonic and prognostic genomic signature from fibroblasts for colorectal cancer initiation, progression, and metastasis. Molecular Cancer Research. 2014;12(9):1254–66.

50. Berdiel-Acer M, Berenguer A, Sanz-Pamplona R, Cuadras D, Sanjuan X, Paules MJ, et al. A 5-gene classifier from the carcinoma-associated fibroblast transcriptomic profile and clinical outcome in colorectal cancer. Oncotarget. 2014;5(15):6437–52.

51. Cheng ML, Nakib D, Perciani CT, MacParland SA. The immune niche of the liver. Clin Sci. 2021;135(20):2445–66.

52. van Dam PJ, van der Stok EP, Teuwen LA, van den Eynden GG, Illemann M, Frentzas S, et al. International consensus guidelines for scoring the histopathological growth patterns of liver metastasis. Br J Cancer. 2017;117(10):1427–41.

53. Latacz E, Höppener D, Bohlok A, Leduc S, Tabariès S, Fernández Moro C, et al. Histopathological growth patterns of liver metastasis: updated consensus guidelines for pattern scoring, perspectives and recent mechanistic insights. Br J Cancer. 2022;(May).

54. Galjart B, Nierop PMH, van der Stok EP, van den Braak RRJC, Höppener DJ, Daelemans S, et al. Angiogenic desmoplastic histopathological growth pattern as a prognostic marker of good outcome in patients with colorectal liver metastases. Angiogenesis [Internet]. 2019;22(2):355–68. Available from: http://dx.doi.org/10.1007/s10456-019-09661-5

55. Buisman FE, van der Stok EP, Galjart B, Vermeulen PB, Balachandran VP, Coebergh van den Braak RRJ, et al. Histopathological growth patterns as biomarker for adjuvant systemic chemotherapy in patients with resected colorectal liver metastases. Clin Exp Metastasis. 2020;37(5):593–605.

56. Frentzas S, Simoneau E, Bridgeman VL, Vermeulen PB, Eynden G Van Den, Daley F, et al. Europe PMC Funders Group Vessel co-option mediates resistance to anti-angiogenic therapy in liver metastases. 2017;22(11):1294–302.

57. Terayama N, Terada T, Nakanuma Y. Histologic growth patterns of metastatic carcinomas of the liver. Jpn J Clin Oncol. 1996;26(1):24–9.

58. Vermeulen PB, Colpaert C, Salgado R, Royers R, Hellemans H, van den Heuvel E, et al. Liver metastases from colorectal adenocarcinomas grow in three patterns with different angiogenesis and desmoplasia. Journal of Pathology. 2001;195(3):336–42.

59. Van Den Eynden GG, Majeed AW, Illemann M, Vermeulen PB, Bird NC, Høyer-Hansen G, et al. The multifaceted role of the microenvironment in liver metastasis: Biology and clinical implications. Cancer Res. 2013;73(7):2031–43.

60. Latacz E, Caspani E, Barnhill R, Lugassy C, Verhoef C, Grünhagen D, et al. Pathological features of vessel co-option versus sprouting angiogenesis. Angiogenesis. 2020;23(1):43–54.

61. Brodt P. Role of the microenvironment in liver metastasis: From pre- to prometastatic niches. Clinical Cancer Research. 2016;22(24):5971–82.

62. van Dam PJ, Daelemans S, Ross E, Waumans Y, van Laere S, Latacz E, et al. Histopathological growth patterns as a candidate biomarker for immunomodulatory therapy. Semin Cancer Biol. 2018;52(January):86–93.

63. Allison KH; Fligner CL; Parks WT. Radiographically occult, diffuse intrasinusoidal hepatic metastases from primary breast carcinomas: a clinicopathologic study of 3 autopsy cases. Arch Pathol Lab Med. 2004;128:1418–23.

64. AJ W. Diffuse intra-sinusoidal metastatic carcinoma of the liver. J Pathol Bacteriol. 195(69):207–17.

65. Vaideeswar P et al. Hepatic diffuse intra-sinusoidal metastases of pulmonary small-cell carcinoma. J Postgrad Med. 2012;58:230–1.

66. Höppener DJ, Galjart B, Nierop PMH, Buisman FE, van der Stok EP, Coebergh van den Braak RRJ, et al. Histopathological Growth Patterns and Survival After Resection of Colorectal Liver Metastasis: An External Validation Study. JNCI Cancer Spectr. 2021;5(3):1–9.

67. Okano K, Yamamoto J, Kosuge T, Yamamoto S, Sakamoto M, Nakanishi Y, et al. Fibrous pseudocapsule of metastatic liver tumors from colorectal carcinoma: Clinicopathologic study of 152 first resection cases. Cancer. 2000;89(2):267–75.

68. Nielsen K, Rolff HC, Eefsen RL, Vainer B. The morphological growth patterns of colorectal liver metastases are prognostic for overall survival. Modern Pathology. 2014;27(12):1641–8.

69. Nierop PMH, Ho¨ppener DJ, van der Stok EP et al. Histopathological growth patterns and positive margins after resection of colorectal liver metastases. HPB (Oxford). 2020;22(6):911–9.

70. Oliveira RC, Alexandrino H, Cipriano MA, Alves FC, Tralhão JG. Predicting liver metastases growth patterns: Current status and future possibilities. Semin Cancer Biol. 2020;(July):0–1.

71. Temido MJ, Oliveira RC, Martins R, Serôdio M, Costa B, Carvalho C, et al. Prognostic factors after hepatectomy for gastric adenocarcinoma liver metastases: Desmoplastic growth pattern as the key to improved overall survival. Cancer Manag Res. 2020;12:11689–99.

72. Stessels F, van den Eynden G, van der Auwera I, Salgado R, van den Heuvel E, Harris AL, et al. Breast adenocarcinoma liver metastases, in contrast to colorectal cancer liver metastases, display a non-angiogenic growth pattern that preserves the stroma and lacks hypoxia. Br J Cancer. 2004;90(7):1429–36.

73. Liao A, Mittal P, Lawson DH, Yang JJ, Szalai E, Grossniklaus HE. Radiologic and Histopathologic Correlation of Different Growth Patterns of Metastatic Uveal Melanoma to the Liver. Ophthalmology. 2018;125(4):597–605.

74. Barnhill R, Vermeulen P, Daelemans S, van Dam PJ, Roman-Roman S, Servois V, et al. Replacement and desmoplastic histopathological growth patterns: A pilot study of prediction of outcome in patients with uveal melanoma liver metastases. J Pathol Clin Res. 2018;4(4):227–40.

75. Barnhill R, van Dam PJ, Vermeulen P, Champenois G, Nicolas A, Rawson RV et al. Replacement and desmoplastic histopathological growth patterns in cutaneous

melanoma liver metastases: frequency, characteristics, and robust prognostic value. Replacement and desmoplastic histopathological growth patterns in cutaneous melanoma liver metastases: frequency, characteristics, and robust prognostic value. 2020;6:195–206.

76. Bohlok A, Vermeulen P, Leduc S, Latacz E, Botzenhart L, Richard F et al. Association between the histopathological growth patterns of liver metastases and survival after hepatic surgery in breast cancer patients. NPJ Breast Cancer. 2020;6:64.

77. Teng S, Li YE, Yang M, Qi R, Huang Y, Wang Q, et al. Tissue-specific transcription reprogramming promotes liver metastasis of colorectal cancer. Cell Res. 2020;30(1):34–49.

78. Welter S, Arfanis E, Christoph D, Hager T, Roesel C, Aigner C, et al. Growth patterns of pulmonary metastases: Should we adjust resection techniques to primary histology and size? European Journal of Cardio-thoracic Surgery. 2017;52(1):39–46.

79. Fink K, Fink J. Imaging of brain metastases. Surg Neurol Int. 2013;4(SUPPL4):209–19.

80. Nierop PM, Hoppener DJ, Buisman FE, van der Stok EP, Galjart B B, VP et al. Preoperative systemic chemotherapy alters the histopathological growth patterns of colorectal liver metastases. J Pathol Clin Res. 2022;(8):48–64.

81. Matsuda Y, Inoue Y, Hiratsuka M, Kawakatsu S, Arai T, Matsueda K, et al. Encapsulating fibrosis following neoadjuvant chemotherapy is correlated with outcomes in patients with pancreatic cancer. PLoS One. 2019;14(9):1–18.

82. Mentha G, Terraz S, Morel P, Andres A, Giostra E, Roth A et al. Dangerous halo after neoadjuvant chemotherapy and two-step hepatectomy for colorectal liver metastases. Br J Surg. 2009;96:95–103.

83. Rubbia-Brandt L, Giostra E, Brezault C, Roth AD, Andres A, Audard V et al. Importance of histological tumor response assessment in predicting the outcome in patients with colorectal liver metastases treated with neo-adjuvant chemotherapy followed by liver surgery. Ann Oncol. 2007;18:299–304.

84. Kuczynski EA, Yin M, Bar-Zion A, Lee CR, Butz H, Man S et al. Co-option of liver vessels and not sprouting angiogenesis drives acquired sorafenib resistance in hepatocellular carcinoma. J Natl Cancer Inst. 2016;108.

85. Bridgeman VL, Vermeulen PB, Foo S, Bilecz A, Daley F, Kostaras E et al. Vessel co-option is common in human lung metastases and mediates resistance to anti-angiogenic therapy in preclinical lung metastasis models. J Pathol. 2017;241:362–74.

86. Leenders WP, Kusters B, Verrijp K, Maass C, Wesseling P, Heerschap A et al. Antiangiogenic therapy of cerebral melanoma metastases results in sustained tumor progression via vessel co-option. Clinical Cancer Research. 2004;10:6222–30.

87. Martens T, Laabs Y, Gunther HS, Kemming D, Zhu Z, Witte L et al. Inhibition of glioblastoma growth in a highly invasive nude mouse model can be achieved by targeting epidermal growth factor receptor but not vascular endothelial growth factor receptor-2. Clinical Cancer Research. 2008;14:5447–58.

88. Eefsen RL, Engelholm L, Alpizar-Alpizar W, Van den Eynden GGE, Vermeulen PB, Christensen IJ, et al. Inflammation and uPAR-Expression in Colorectal Liver Metastases in Relation to Growth Pattern and Neo-adjuvant Therapy. Cancer Microenvironment. 2015;8(2):93–100.

89. Höppener DJ, Stook JLPL, Galjart B, Nierop PMH, Nagtegaal ID, Vermeulen PB, et al. The relationship between primary colorectal cancer histology and the histopathological growth patterns of corresponding liver metastases. BMC Cancer [Internet]. 2022;22(1):911. Available from: https://doi.org/10.1186/s12885-022-09994-3

90. Wu JB, Sarmiento AL, Fiset PO, Lazaris A, Metrakos P, Petrillo S, et al. Histologic features and genomic alterations of primary colorectal adenocarcinoma predict growth patterns of liver metastasis. World J Gastroenterol. 2019;25(26):3408–25.

91. Rajaganeshan R, Prasad R, Guillou PJ, Chalmers CR, Scott N, Sarkar R, et al. The influence of invasive growth pattern and microvessel density on prognosis in colorectal cancer and colorectal liver metastases. Br J Cancer. 2007;96(7):1112–7.

92. Buisman FE, Giardiello D, Kemeny NE, Steyerberg EW, Höppener DJ, Galjart B, et al. Predicting 10-year survival after resection of colorectal liver metastases; an international study including biomarkers and perioperative treatment. Eur J Cancer. 2022;168:25–33.

93. Liu J, Cho YB, Hong HK, Wu S, Ebert PJ, Bray SM, et al. Molecular dissection of CRC primary tumors and their matched liver metastases reveals critical role of immune microenvironment, EMT and angiogenesis in cancer metastasis. Sci Rep. 2020;10(1):1–15.

94. Schlicker A, Ellappalayam A, Beumer IJ, Snel MHJ, Mittempergher L, Diosdado B, et al. Investigating the concordance in molecular subtypes of primary colorectal tumors and their matched synchronous liver metastasis. Int J Cancer. 2020;147(8):2303–15.

95. Vidal-Vanaclocha F. The Tumor microenvironment at different stages of hepatic metastasis. In: Brodt P, editor. Liver metastasis: biology and clinical management. 1st ed. Dordecht (Netherlands): Springer Netherlands; 2011. p. 43–87.

96. Schwitalla S, Fingerle AA, Cammareri P NT, G€oktuna SI, Ziegler PK, Canli O, Heijmans J H, DJ MG et al. Intestinal tumorigenesis initiated by dedifferentiation and acquisition of stemcell- like properties. Cell. 2013;152:25–38.

97. Drost J, van Jaarsveld RH, Ponsioen B, Zimberlin C V, Boxtel R, Buijs A, Sachs N, Overmeer RM O, GJ BH et al. Sequential cancer mutations in cultured human intestinal stem cells. Nature. 2015;521:43–7.

98. Fujii M, Shimokawa M, Date S, Takano A MM, Nanki K, Ohta Y, Toshimitsu K NY, Al. KK et. A colorectal tumor organoid library demonstrates progressive loss of niche factor requirements during tumorigenesis. Cell Stem Cell. 2016;18:827–38.

99. Urosevic J, Garcia-Alb eniz X, Planet E, Real S C espedes, MV, Guiu M, Fernandez E, Bellmunt A GS, Al. PM et. Colon cancer cells colonize the lung from established liver metastases through p38 MAPK signalling and PTHLH. Nat Cell Biol. 2014;16:685–94.

100. Massague J and Obenauf AC. Metastatic colonization by circulating tumour cells. Nature. 2016;529:298–306.

101. JM SD and T. Transmission of donor melanoma by organ transplantation. Lancet Oncol. 2010;(11):790–6.

102. Sosa MS BP and AGJ. Mechanisms of disseminated cancer cell dormancy: an awakening field. Nat Rev Cancer. 2014;14:611–22.

103. Dalerba P, Dylla SJ, Park I-K, Liu R, Wang X CR, Hoey T, Gurney A, Huang EH SD et al. Phenotypic characterization of human colorectal cancer stem cells. Proc Natl Acad Sci USA. 2007;104:10158– 10163.

104. Dalerba P, Kalisky T, Sahoo D RP, Rothenberg ME, Leyrat AA, Sim S OJ, Johnston DM QD et al. Single-cell dissection of transcriptional heterogeneity in human colon tumors. Nat Biotechnol. 2011;29:1120–1127.

105. Sonoshita M, Itatani Y, Kakizaki F SK, Terashima T, Katsuyama Y SY and TM. Promotion of colorectal cancer invasion and metastasis through activation of NOTCH–DAB1–ABL–RHOGEF protein TRIO. Cancer Discov. 2015;5:198–211.

106. Page C this, Kalra A, Yetiskul E, Wehrle CJ et al. Physiology, Liver [Internet]. Treasure Island (FL): StatPearls. 2022. Available from: https://www.ncbi.nlm.nih.gov/books/NBK535438/

107. Trefts E, Gannon M, Wasserman DH. The liver. 2018;27(21).

108. Zheng M, Tian Z. Liver-Mediated Adaptive Immune Tolerance. 2019;10(November).

109. Crispe IN. Hepatic T cells and liver tolerance. Nat Rev Immunol. 2003;3:51–62.

110. Crispe IN. Immune tolerance in liver disease. Hepatology. 2014;60:2109–17.

111. Breous, E., Somanathan, S., Vandenberghe, L.H. and Wilson JM. Hepatic regulatory T cells and Kupffer cells are crucial mediators of systemic T cell tolerance to antigens targeting murine liver. Hepatology. 2009;50:612–21.

112. Xiaoliang Zhu and Jinfang Zhu. CD4 T Helper Cell Subsets and Related Human Immunological Disorders. Int J Mol Sci. 2020;21(21):8011.

113. Raskov H, Orhan A, Christensen JP, Gögenur I. Cytotoxic CD8+ T cells in cancer and cancer immunotherapy. Br J Cancer. 2021;124(2):359–67.

114. Engelhard V, Conejo-Garcia JR, Ahmed R, Nelson BH, Willard-Gallo K, Bruno TC FWH. B cells and cancer. Cancer Cell. 2021;39(10):12193–1296.

115. Peter D. Pioli. Plasma Cells, the Next Generation: Beyond Antibody Secretion. Front Immunol. 2019;10:2768.

116. Wen Y, Lambrecht J, Ju C, Tacke F. Hepatic macrophages in liver homeostasis and diseases-diversity, plasticity and therapeutic opportunities. Cell Mol Immunol. 2021;18(1):45–56.

117. MacParland SA, Liu JC, Ma XZ, Innes BT, Bartczak AM, Gage BK, et al. Single cell RNA sequencing of human liver reveals distinct intrahepatic macrophage populations. Nat Commun. 2018;9(1):1–21.

118. Heymann F TF. Immunology in the liver--from homeostasis to disease. Nat Rev Gastroenterol Hepatol. 2016;13(2):88–110.

119. Bandyopadhyay K, Marrero I K V. NKT cell subsets as key participants in liver physiology and pathology. Cell Mol Immunol. 2016;13(3):337–46.

120. Kurioka A, Walker LJ, Klenerman P WCB. MAIT cells: new guardians of the liver. Immunology. 2016;5(8):98.

121. Rahman AH AC. Dendritic cells and liver fibrosis. Biochim Biophys Acta. 2013;1832(7):998–1004.

122. Hammerich L TF. Role of gamma-delta T cells in liver inflammation and fibrosis. Gastrointest Pathophysiol. 2014;5(2):107–13.

123. Clottu AS, Humbel M, Fluder N, Karampetsou MP CD. Innate Lymphoid Cells in Autoimmune Diseases. Front Immunol. 2022;12:789788.

124. Krenkel, O. and Tacke F. Liver macrophages in tissue homeostasis and disease. Nat Rev Immunol. 2017;17:306–21.

125. Stamataki, Z. and Swadling L. The liver as an immunological barrier redefined by single-cell analysis. Immunology. 2020;160:157–70.

126. Aizarani, N., Saviano, A., Sagar, Mailly, L., Durand, S., Herman JS et al. A human liver cell atlas reveals heterogeneity and epithelial progenitors. Nature. 2019;572:199–204.

127. David, B.A., Rezende, R.M., Antunes, M.M., Santos, M.M., Freitas Lopes, M.A., Diniz AB et al. Combination of mass cytometry and imaging analysis reveals origin, location, and functional repopulation of liver myeloid cells in mice. Gastroenterology. 2016;151:1176–91.

128. Soysa, D.R. and Crispe IN. Subcapsular hepatic dendritic cells: hiding in plain sight. Gastroenterology. 2016;151:311–23.

129. Crispe IN. The liver as a lymphoid organ. Annu Rev Immunol. 2009;27:147–63.

130. Robinson, M.W., Harmon, C. and O'Farrelly C. Liver immunology and its role in inflammation and homeostasis. Cell Mol Immunol. 2016;13:267–76.

131. Hernández-Gea, V., Ghiassi-Nejad, Z., Rozenfeld, R., Gordon, R., Fiel, M.I., Yue Z et al. Autophagy releases lipid that promotes fibrogenesis by activated hepatic stellate cells in mice and in human tissues. Gastroenterology. 2012;142:938–46.

132. Ilyas, G., Zhao, E., Liu, K., Lin, Y., Tesfa, L., Tanaka KE et al. Macrophage autophagy limits acute toxic liver injury in mice through down regulation of interleukin-1β. J Hepatol. 2016;64:118–27.

133. Jeffery, H.C., Braitch, M.K., Brown, S. and Oo YH. Clinical potential of regulatory T cell therapy in liver diseases: an overview and Perspectives. Front Immunol. 2016;7:334.

134. Perciani, C.T. and MacParland SA. Lifting the veil on macrophage diversity in tissue regeneration and fibrosis. Sci Immunol. 2019;4.

135. Sommerfeld, S.D., Cherry, C., Schwab, R.M., Chung, L., Maestas, D.R., Laffont P et al. Interleukin-36γ-producing macrophages drive IL-17-mediated fibrosis. Sci Immunol. 2019;4.

136. Sadtler, K., Estrellas, K., Allen, B.W., Wolf, M.T., Fan, H., Tam AJ et al. Developing a pro-regenerative biomaterial scaffold microenvironment requires T helper 2 cells. Science (1979). 2016;352:366–70.

137. van den Eynden GG, Majeed AW, Illemann M, Vermeulen PB, Bird NC, Høyer-Hansen G, et al. The multifaceted role of the microenvironment in liver metastasis: Biology and clinical implications. Cancer Res. 2013;73(7):2031–43.

138. Braet F, Nagatsuma K, Saito M, Soon L, Wisse E, Matsuura T. The hepatic sinusoidal endothelial lining and colorectal liver metastases. World J Gastroenterol. 2007;13(6):821–5.

139. Ou J, Peng Y, Deng J, Miao H, Zhou J, Zha L, et al. Endothelial cell-derived-fibronectin extra domain A promotes colorectal cancer metastasis via inducing epithelialmesenchymal transition. Carcinogenesis. 2014;35(7):1661–70.

140. Hu CT, Guo LL, Feng N, Zhang L, Zhou N, Ma LL, et al. MIF, secreted by human hepatic sinusoidal endothelial cells, promotes chemotaxis and outgrowth of colorectal cancer in liver prometastasis. Oncotarget. 2015;6(26):22410–23.

141. Banerjee, D.; Hernandez, S.L.; Garcia, A.; Kangsamaksin, T.; Sbiroli, E.; Andrews, J.; Forrester, L.A.; Wei N; KC, A.; Shawber CJ; Notch suppresses angiogenesis and progression of hepatic metastases. Cancer Res. 2015;75:1592–602.

142. Im JH, Tapmeier T, Balathasan L, Gal A, Yameen S, Hill S, et al. G-CSF rescues tumor growth and neo-angiogenesis during liver metastasis under host angiopoietin-2 deficiency. Int J Cancer. 2013;132(2):315–26.

143. Solaun MS, Mendoza L, De Luca M, Gutierrez V, López MP, Olaso E, et al. Endostatin inhibits murine colon carcinoma sinusoidal-type metastases by preferential targeting of hepatic sinusoidal endothelium. Hepatology. 2002;35(5):1104–16.

144. van Dam PJ, Daelemans S, Ross E, Waumans Y, Van Laere S, Latacz E, et al. Histopathological growth patterns as a candidate biomarker for immunomodulatory therapy. Semin Cancer Biol. 2018;52(August 2017):86–93.

145. Arteta B, Lasuen N, Lopategi A, Sveinbjörnsson B, Smedsrød B, Vidal-Vanaclocha F. Colon carcinoma cell interaction with liver sinusoidal endothelium inhibits organ-specific antitumor immunity through interleukin-1-induced mannose receptor in mice. Hepatology. 2010;51(6):2172–82.

146. Yamamoto Y, Kasashima H, Fukui Y, Tsujio G, Yashiro M, Maeda K. The heterogeneity of cancer- associated fibroblast subpopulations : Their origins , biomarkers , and roles in the tumor microenvironment. 2022;(May):1–9.

147. Ünlü M, Çetinayak HO, Önder D, Ecevit C, Akman F, Ikiz AÖ, et al. The prognostic value of tumor-stroma proportion in laryngeal squamous cell carcinoma. Turk Patoloji Dergisi/Turkish Journal of Pathology. 2013;29(1):27–35.

148. Hynes SO, Coleman HG, Kelly PJ, Irwin S, O'Neill RF, Gray RT, et al. Back to the future: routine morphological assessment of the tumour microenvironment is prognostic in stage II/III colon cancer in a large population-based study. Histopathology. 2017;71(1):12–26.

149. Huijbers A, Tollenaar RAEM, Pelt GWV, Zeestraten ECM, Dutton S, McConkey CC, et al. The proportion of tumor-stroma as a strong prognosticator for stage II and III colon cancer patients: Validation in the victor trial. Annals of Oncology [Internet]. 2013;24(1):179–85. Available from: https://doi.org/10.1093/annonc/mds246

150. Gonçalves-Ribeiro S, Díaz-Maroto NG, Berdiel-Acer M, Soriano A, Guardiola J, Martínez-Villacampa M, et al. Carcinoma-associated fibroblasts affect sensitivity to oxaliplatin and 5FU in colorectal cancer cells. Oncotarget. 2016;7(37):59766–80.

151. Sabath DE. Minimal Residual Disease ☆. Reference Module in Biomedical Sciences. 2018;9(SEpTEMbER):665–74.

152. Paraiso KHT, Smalley KSM. Fibroblast-mediated drug resistance in cancer. Biochem Pharmacol [Internet]. 2013;85(8):1033–41. Available from: http://dx.doi.org/10.1016/j.bcp.2013.01.018

153. Mark B Meads 1, Robert A Gatenby WSD. Environment-mediated drug resistance: a major contributor to minimal residual disease. Nat Rev Cancer. 2009;(9):665-74.

154. Berdiel-Acer M, Sanz-Pamplona R, Calon A, Cuadras D, Berenguer A, Sanjuan X, et al. Differences between CAFs and their paired NCF from adjacent colonic mucosa reveal functional heterogeneity of CAFs, providing prognostic information. Mol Oncol. 2014;8(7):1290–305.

155. Herrera M, Islam ABMMK, Herrera A, Martín P, García V, Silva J, et al. Functional heterogeneity of cancer-associated fibroblasts from human colon tumors shows specific prognostic gene expression signature. Clinical Cancer Research. 2013;19(21):5914–26.

156. Ueno H, Konishi T, Ishikawa Y, Shimazaki H, Ueno M, Aosasa S, et al. Histologic categorization of fibrotic cancer stroma in the primary tumor is an independent prognostic index in resectable colorectal liver metastasis. American Journal of Surgical Pathology. 2014;38(10):1380–6.

157. Díaz-Maroto NG, Sanz-Pamplona R, Berdiel-Acer M, Cimas FJ, García E, Gonçalves-Ribeiro S, et al. Noncanonical TGFb pathway relieves the blockade of IL1B/TGFb-mediated crosstalk between tumor and stroma: TGFBR1 and TAK1 inhibition in colorectal cancer. Clinical Cancer Research. 2019;25(14):4466–79.

158. Berna C Özdemir 1 , Tsvetelina Pentcheva-Hoang 2 , Julienne L Carstens 3 , Xiaofeng Zheng 3 , Chia-Chin Wu 4 , Tyler R Simpson 2 , Hanane Laklai 5 , Hikaru Sugimoto 1 , Christoph Kahlert 1 , Sergey V Novitskiy 6 , Ana De Jesus-Acosta 7 , Padmanee Sharma 2 RK 10. Depletion of carcinoma-associated fibroblasts and fibrosis induces immunosuppression and accelerates pancreas cancer with reduced survival. Cancer Cell. 2014;25(6):719–34.

159. Erkan M, Michalski CW, Rieder S, Reiser-Erkan C, Abiatari I, Kolb A, et al. The Activated Stroma Index Is a Novel and Independent Prognostic Marker in Pancreatic Ductal Adenocarcinoma. Clinical Gastroenterology and Hepatology. 2008;6(10):1155–61.

160. Calon A, Lonardo E, Berenguer-Llergo A, Espinet E, Hernando-Momblona X, Iglesias M, et al. Stromal gene expression defines poor-prognosis subtypes in colorectal cancer. Nat Genet [Internet]. 2015;47(4):320–9. Available from: http://dx.doi.org/10.1038/ng.3225

161. Peng H, Zhu E, Zhang Y. Advances of cancer-associated fibroblasts in liver cancer. Biomark Res. 2022;10(1):1–18.

162. Zeltz C, Primac I, Erusappan P, Alam J, Noel A, Gullberg D. Cancer-associated fibroblasts in desmoplastic tumors: emerging role of integrins. Semin Cancer Biol

[Internet]. 2020;62(5009):166–81. Available from: https://doi.org/10.1016/j.semcancer.2019.08.004

163. Costa A, Kieffer Y, Scholer-Dahirel A, Pelon F, Bourachot B, Cardon M, et al. Fibroblast Heterogeneity and Immunosuppressive Environment in Human Breast Cancer. Cancer Cell [Internet]. 2018;33(3):463-479.e10. Available from: http://dx.doi.org/10.1016/j.ccell.2018.01.011

164. Bartoschek M, Oskolkov N, Bocci M, Lövrot J, Larsson C, Sommarin M, et al. Spatially and functionally distinct subclasses of breast cancer-associated fibroblasts revealed by single cell RNA sequencing. Nat Commun [Internet]. 2018;9(1). Available from: http://dx.doi.org/10.1038/s41467-018-07582-3

165. Berdiel-Acer M, Cuadras D, Díaz-Maroto NG, Sanjuan X, Serrano T, Berenguer A, et al. A monotonic and prognostic genomic signature from fibroblasts for colorectal cancer initiation, progression, and metastasis. Molecular Cancer Research. 2014;12(9):1254–66.

166. Kilvaer TK, Rakaee M, Hellevik T, Vik J, Petris L de, Donnem T, et al. Differential prognostic impact of platelet-derived growth factor receptor expression in NSCLC. Sci Rep. 2019;9(1):1–11.

167. Xie T, Wang Y, Deng N, Huang G, Taghavifar F, Geng Y, et al. Single-Cell Deconvolution of Fibroblast Heterogeneity in Mouse Pulmonary Fibrosis. Cell Rep [Internet]. 2018 Mar 27 [cited 2022 Nov 29];22(13):3625–40. Available from: https://pubmed.ncbi.nlm.nih.gov/29590628/

168. Li R, Bernau K, Sandbo N, Gu J, Preissl S, Sun X. Pdgfra marks a cellular lineage with distinct contributions to myofibroblasts in lung maturation and injury response. Elife [Internet]. 2018 Sep 1 [cited 2022 Nov 29];7. Available from: https://pubmed.ncbi.nlm.nih.gov/30178747/

169. Su S, Chen J, Yao H, Liu J, Yu S, Lao L, et al. CD10+GPR77+ Cancer-Associated Fibroblasts Promote Cancer Formation and Chemoresistance by Sustaining Cancer Stemness. Cell [Internet]. 2018;172(4):841-856.e16. Available from: https://doi.org/10.1016/j.cell.2018.01.009

170. Bonneau C, Eliès A, Kieffer Y, Bourachot B, Ladoire S, Pelon F, et al. A subset of activated fibroblasts is associated with distant relapse in early luminal breast cancer. Breast Cancer Research. 2020;22(1):1–22.

171. Nielsen MFB, Mortensen MB, Detlefsen S. Typing of pancreatic cancer-associated fibroblasts identifies different subpopulations. World J Gastroenterol. 2018;24(41):4663–78.

172. Dekker TJA, van de Velde CJH, van Pelt GW, Kroep JR, Julien JP, Smit VTHBM, et al. Prognostic significance of the tumor-stroma ratio: Validation study in node-negative premenopausal breast cancer patients from the EORTC perioperative chemotherapy (POP) trial (10854). Breast Cancer Res Treat. 2013;139(2):371–9.

173. Miyai Y, Esaki N, Takahashi M, Enomoto A. Cancer-associated fibroblasts that restrain cancer progression: Hypotheses and perspectives. Cancer Sci [Internet]. 2020 Apr 1 [cited 2022 Nov 29];111(4):1047–57. Available from: https://pubmed.ncbi.nlm.nih.gov/32060987/

174. Mizutani Y, Kobayashi H, Iida T, Asai N, Masamune A, Hara A, et al. Meflin-Positive Cancer-Associated Fibroblasts Inhibit Pancreatic Carcinogenesis. Cancer Res [Internet]. 2019 Oct 15 [cited 2022 Nov 29];79(20):5367–81. Available from: https://pubmed.ncbi.nlm.nih.gov/31439548/

175. Gerling M, Büller NVJA, Kirn LM, Joost S, Frings O, Englert B, et al. Stromal Hedgehog signalling is downregulated in colon cancer and its restoration restrains tumour growth. Nat Commun [Internet]. 2016 Aug 5 [cited 2022 Nov 29];7. Available from: https://pubmed.ncbi.nlm.nih.gov/27492255/

176. Neesse A, Algül H, Tuveson DA, Gress TM. Stromal biology and therapy in pancreatic cancer: a changing paradigm. Gut [Internet]. 2015 Sep 1 [cited 2022 Nov 29];64(9):1476–84. Available from: https://pubmed.ncbi.nlm.nih.gov/25994217/

177. Rhim AD, Oberstein PE, Thomas DH, Mirek ET, Palermo CF, Sastra SA, et al. Stromal elements act to restrain, rather than support, pancreatic ductal adenocarcinoma. Cancer Cell [Internet]. 2014 Jun 16 [cited 2022 Nov 29];25(6):735–47. Available from: https://pubmed.ncbi.nlm.nih.gov/24856585/

178. Chen Y, McAndrews KM, Kalluri R. Clinical and therapeutic relevance of cancer-associated fibroblasts. Nat Rev Clin Oncol [Internet]. 2021 Dec 1 [cited 2022 Nov 29];18(12):792–804. Available from: https://pubmed.ncbi.nlm.nih.gov/34489603/

179. Tauriello DVF, Palomo-Ponce S, Stork D, Berenguer-Llergo A, Badia-Ramentol J, Iglesias M, et al. TGFβ drives immune evasion in genetically reconstituted colon cancer metastasis. Nature [Internet]. 2018 Feb 22 [cited 2022 Nov 29];554(7693):538–43. Available from: https://pubmed.ncbi.nlm.nih.gov/29443964/

180. Mao X, Xu J, Wang W, Liang C, Hua J, Liu J, et al. Crosstalk between cancer-associated fibroblasts and immune cells in the tumor microenvironment: new findings and future perspectives. Mol Cancer [Internet]. 2021 Dec 1 [cited 2022 Nov 29];20(1). Available from: https://pubmed.ncbi.nlm.nih.gov/34635121/

181. Kim R, Emi M, Tanabe K. Cancer immunosuppression and autoimmune disease: beyond immunosuppressive networks for tumour immunity. Immunology [Internet]. 2006 Oct [cited 2022 Nov 29];119(2):254–64. Available from: https://pubmed.ncbi.nlm.nih.gov/17005005/

182. Sun Q, Zhang B, Hu Q, Qin Y, Xu W, Liu W, et al. The impact of cancer-associated fibroblasts on major hallmarks of pancreatic cancer. Theranostics [Internet]. 2018 [cited 2022 Nov 29];8(18):5072–87. Available from: https://pubmed.ncbi.nlm.nih.gov/30429887/

183. Shiga K, Hara M, Nagasaki T, Sato T, Takahashi H, Takeyama H. Cancer-Associated Fibroblasts: Their Characteristics and Their Roles in Tumor Growth. Cancers (Basel) [Internet]. 2015 Dec 11 [cited 2022 Nov 29];7(4):2443–58. Available from: https://pubmed.ncbi.nlm.nih.gov/26690480/

184. Johnson SJ, Hines JE, Burt AD. Phenotypic modulation of perisinusoidal cells following acute liver injury: A quantitative analysis. Int J Exp Pathol. 1992;73(6):765–76572.

185. Driskell RR, Lichtenberger BM, Hoste E, Kretzschmar K, Simons BD, Charalambous M, et al. Distinct fibroblast lineages determine dermal architecture in skin development and repair. Nature. 2013;504(7479):277–81.

186. Guyot C, Lepreux S, Combe C, Doudnikoff E, Bioulac-Sage P, Balabaud C, et al. Hepatic fibrosis and cirrhosis: The (myo)fibroblastic cell subpopulations involved. International Journal of Biochemistry and Cell Biology. 2006;38(2):135–51.

187. Cassiman D, Roskams T. Beauty is in the eye of the beholder: Emerging concepts and pitfalls in hepatic stellate cell research. J Hepatol. 2002;37(4):527–35.

188. Brenner DA, Kisseleva T, Scholten D, Paik YH, Iwaisako K, Inokuchi S, et al. Origin of myofibroblasts in liver fibrosis. Fibrogenesis Tissue Repair [Internet]. 2012;5(SUPPL.1):S17. Available from: http://www.fibrogenesis.com/content/5/S1/S17

189. Mederacke I, Hsu CC, Troeger JS, Huebener P, Mu X, Dapito DH et al. Fate tracing reveals hepatic stellate cells as dominant contributors to liver fbrosis independent of its aetiology. Nat Commun. 2013;4:2823.

190. Pellicoro A, Raschperger E, Betsholtz C, Ruminski PG, Griggs DW P, MJ et al. Targeting of αv integrin identifes a core molecular pathway that regulates fbrosis in several organs. Nat Med. 2013;19(12):1617–24.

191. wang SS, Tang XT, Lin M, Yuan J, Peng YJ, Yin X et al. Perivenous stellate cells are the main source of myofbroblasts and cancerassociated fbroblasts formed after chronic liver injuries. Hepatology. 2021;74(3):1578–94.

192. Bhattacharjee S, Hamberger F, Ravichandra A, Miller M NA, Afo S et al. tumor restriction by type 1 collagen opposes tumor-promoting effects of cancer-associated fibroblasts. Journal of Clinical Investigation. 2021;131(11):e146987.

193. Kruepunga N, Hakvoort TBM, Hikspoors JPJM, Köhler SE LWH. Anatomy of rodent and human livers: What are the differences? Biochim Biophys Acta Mol Basis Dis. 2019;1865(5):869–78.

194. Jang HK, Lee CE, Choi GS, Lee YJ, Noh SJ. Temperature dependent I-V characteristics of plasma hydrogenated Poly-Si TFTs in the low voltage region. Journal of the Korean Physical Society. 1997;30(SUPPL. PART 1):125–72.

195. Mueller L, Goumas FA, Affeldt M, Sandtner S, Gehling UM, Brilloff S, et al. Stromal fibroblasts in colorectal liver metastases originate from resident fibroblasts and

generate an inflammatory microenvironment. American Journal of Pathology. 2007;171(5):1608–18.

196. Olaso E, Salado C, Egilegor E, Gutierrez V, Santisteban A, Sancho-Bru P, et al. Proangiogenic role of tumor-activated hepatic stellate cells in experimental melanoma metastasis. Hepatology. 2003;37(3):674–85.

197. Iwaisako K, Jiang C, Zhang M, Cong M, Moore-Morris TJ, Park TJ, et al. Origin of myofibroblasts in the fibrotic liver in mice. Proc Natl Acad Sci U S A. 2014;111(32).

198. Dudas J, Mansuroglu T, Batusic D, Ramadori G. Thy-1 is expressed in myofibroblasts but not found in hepatic stellate cells following liver injury. Histochem Cell Biol. 2009;131(1):115–27.

199. Motoyama H, Komiya T, Thuy LTT, Tamori A, Enomoto M, Morikawa H, et al. Cytoglobin is expressed in hepatic stellate cells, but not in myofibroblasts, in normal and fibrotic human liver. Laboratory Investigation. 2014;94(2):192–207.

200. Karin D, Koyama Y, Brenner D, Kisseleva T. The characteristics of activated portal fibroblasts/myofibroblasts in liver fibrosis. Differentiation. 2016;92(3):84–92.

201. Ingrid Lua, Yuchang Li, Jessica A. Zagori, Kasper S. Wang, Samuel W. French, Jean Sévigny and KA. Characterization of hepatic stellate cells, portal fibroblasts, and mesothelial cells in normal and fibrotic livers. J Hepatol. 2016;64(5):1137–46.

202. Kisseleva T. The origin of fibrogenic myofibroblasts in fibrotic liver. Hepatology. 2017;65(3):1039–43.

203. Frentzas S, Simoneau E, Bridgeman VL, Vermeulen PB, Foo S, Kostaras E, et al. Vessel co-option mediates resistance to anti-angiogenic therapy in liver metastases. Nat Med [Internet]. 2016 Nov 1 [cited 2022 Nov 29];22(11):1294–302. Available from: https://pubmed.ncbi.nlm.nih.gov/27748747/

204. van den Eynden GG, Bird NC, Majeed AW, van Laere S, Dirix LY, Vermeulen PB. The histological growth pattern of colorectal cancer liver metastases has prognostic value. Clin Exp Metastasis. 2012;29(6):541–9.

205. Paku S, Lapis K. Morphological aspects of angiogenesis in experimental liver metastases. American Journal of Pathology. 1993;143(3):926–36.

206. Paku S, Kopper L, Nagy P. Development of the vasculature in “pushing-type” liver metastases of an experimental colorectal cancer. Int J Cancer. 2005;115(6):893–902.

207. Vidal-Vanaclocha F. The prometastatic microenvironment of the liver. Cancer Microenvironment. 2008;1(1):113–29.

208. van den Eynden GG, Majeed AW, Illemann M, Vermeulen PB, Bird NC, Høyer-Hansen G, et al. The multifaceted role of the microenvironment in liver metastasis: Biology and clinical implications. Cancer Res. 2013;73(7):2031–43.

209. Bogdanos DP, Gao B, Gershwin ME. Liver immunology. Compr Physiol [Internet]. 2013 [cited 2022 Nov 29];3(2):567–98. Available from: https://pubmed.ncbi.nlm.nih.gov/23720323/

210. Tay SS, Wong YC, McDonald DM, Wood NAW, Roediger B, Sierro F, et al. Antigen expression level threshold tunes the fate of CD8 T cells during primary hepatic immune responses. Proc Natl Acad Sci U S A [Internet]. 2014 Jun 24 [cited 2022 Nov 29];111(25). Available from: https://pubmed.ncbi.nlm.nih.gov/24927525/

211. Crispe IN, Giannandrea M, Klein I, John B, Sampson B, Wuensch S. Cellular and molecular mechanisms of liver tolerance. Immunol Rev [Internet]. 2006 Oct [cited 2022 Nov 29];213(1):101–18. Available from: https://pubmed.ncbi.nlm.nih.gov/16972899/

212. Kee JY, Ito A, Hojo S, Hashimoto I, Igarashi Y, Tsukada K, et al. Chemokine CXCL16 suppresses liver metastasis of colorectal cancer via augmentation of tumor-infiltrating natural killer T cells in a murine model. Oncol Rep [Internet]. 2013 Mar [cited 2022 Nov 29];29(3):975–82. Available from: https://pubmed.ncbi.nlm.nih.gov/23242131/

213. López-Soto A, Gonzalez S, Smyth MJ, Galluzzi L. Control of Metastasis by NK Cells. Cancer Cell [Internet]. 2017 Aug 14 [cited 2022 Nov 29];32(2):135–54. Available from: https://pubmed.ncbi.nlm.nih.gov/28810142/

214. Vivier E, Tomasello E, Baratin M, Walzer T, Ugolini S. Functions of natural killer cells. Nat Immunol [Internet]. 2008 May [cited 2022 Nov 29];9(5):503–10. Available from: https://pubmed.ncbi.nlm.nih.gov/18425107/

215. Wang F, Lau JKC, Yu J. The role of natural killer cell in gastrointestinal cancer: killer or helper. Oncogene 2020 40:4 [Internet]. 2020 Dec 1 [cited 2022 Nov 29];40(4):717–30. Available from: https://www.nature.com/articles/s41388-020-01561-z

216. Donadon M, Hudspeth K, Cimino M, di Tommaso L, Preti M, Tentorio P, et al. Increased Infiltration of Natural Killer and T Cells in Colorectal Liver Metastases Improves Patient Overall Survival. J Gastrointest Surg [Internet]. 2017 Aug 1 [cited 2022 Nov 29];21(8):1226–36. Available from: https://pubmed.ncbi.nlm.nih.gov/28536806/

217. Krijgsman D, Hokland M, Kuppen PJK. The Role of Natural Killer T Cells in Cancer-A Phenotypical and Functional Approach. Front Immunol [Internet]. 2018 Feb 27 [cited 2022 Nov 29];9(FEB). Available from: https://pubmed.ncbi.nlm.nih.gov/29535734/

218. Zeng X, Zhou J, Xiong Z, Sun H, Yang W, Mok MTS, et al. Cell cycle-related kinase reprograms the liver immune microenvironment to promote cancer metastasis. Cell Mol Immunol [Internet]. 2021 Apr 1 [cited 2022 Nov 29];18(4):1005–15. Available from: https://pubmed.ncbi.nlm.nih.gov/32879468/

219. Yang W, Li H, Mayhew E, Mellon J, Chen PW, Niederkorn JY. NKT cell exacerbation of liver metastases arising from melanomas transplanted into either the eyes or spleens of mice. Invest Ophthalmol Vis Sci [Internet]. 2011 May [cited 2022 Nov 29];52(6):3094–102. Available from: https://pubmed.ncbi.nlm.nih.gov/21330669/

220. Seki S, Nakashima H, Nakashima M, Kinoshita M. Antitumor immunity produced by the liver Kupffer cells, NK cells, NKT cells, and CD8 CD122 T cells. Clin Dev Immunol [Internet]. 2011 [cited 2022 Nov 29];2011. Available from: https://pubmed.ncbi.nlm.nih.gov/22190974/

221. Ellyard JI, Simson L, Parish CR. Th2-mediated anti-tumour immunity: friend or foe? Tissue Antigens [Internet]. 2007 Jul [cited 2022 Nov 23];70(1):1–11. Available from: https://pubmed.ncbi.nlm.nih.gov/17559575/

222. Nishimura T, Iwakabe K, Sekimoto M, Ohmi Y, Yahata T, Nakui M, et al. Distinct Role of Antigen-Specific T Helper Type 1 (Th1) and Th2 Cells in Tumor Eradication in Vivo. J Exp Med [Internet]. 1999 Sep 9 [cited 2022 Nov 23];190(5):617. Available from: /pmc/articles/PMC2195611/

223. Ruterbusch M, Pruner KB, Shehata L, Pepper M. In Vivo CD4+ T Cell Differentiation and Function: Revisiting the Th1/Th2 Paradigm. Annu Rev Immunol [Internet]. 2020 Apr 26 [cited 2022 Nov 23];38:705–25. Available from: https://pubmed.ncbi.nlm.nih.gov/32340571/

224. Vinay DS, Ryan EP, Pawelec G, Talib WH, Stagg J, Elkord E, et al. Immune evasion in cancer: Mechanistic basis and therapeutic strategies. Semin Cancer Biol [Internet]. 2015 Dec 1 [cited 2022 Nov 23];35 Suppl:S185–98. Available from: https://pubmed.ncbi.nlm.nih.gov/25818339/

225. Kidd P. Th1/Th2 balance: the hypothesis, its limitations, and implications for health and disease. Altern Med Rev [Internet]. 2003 Aug [cited 2022 Nov 23];8(3):223–46. Available from: https://pubmed.ncbi.nlm.nih.gov/12946237/

226. Knochelmann HM, Dwyer CJ, Bailey SR, Amaya SM, Elston DM, Mazza-McCrann JM, et al. When worlds collide: Th17 and Treg cells in cancer and autoimmunity. Cell Mol Immunol [Internet]. 2018 May 1 [cited 2022 Nov 23];15(5):458–69. Available from: https://pubmed.ncbi.nlm.nih.gov/29563615/

227. Katz SC, Bamboat ZM, Maker A v., Shia J, Pillarisetty VG, Yopp AC, et al. Regulatory T cell infiltration predicts outcome following resection of colorectal cancer liver metastases. Ann Surg Oncol [Internet]. 2013 Mar [cited 2022 Nov 29];20(3):946–55. Available from: https://pubmed.ncbi.nlm.nih.gov/23010736/

228. Saura-Esteller J, de Jong M, King LA, Ensing E, Winograd B, de Gruijl TD, et al. Gamma Delta T-Cell Based Cancer Immunotherapy: Past-Present-Future. Front Immunol [Internet]. 2022 Jun 16 [cited 2022 Nov 23];13. Available from: https://pubmed.ncbi.nlm.nih.gov/35784326/

229. Hof J, Visser L, Höppener DJ, Nierop PMH, Terpstra MM, Gouw ASH, et al. B Cells as Prognostic Biomarker After Surgery for Colorectal Liver Metastases. Front Oncol

[Internet]. 2020 Mar 5 [cited 2022 Nov 23];10:249. Available from: /pmc/articles/PMC7066250/

230. Engelhard V, Conejo-Garcia JR, Ahmed R, Nelson BH, Willard-Gallo K, Bruno TC, et al. B cells and cancer. Cancer Cell [Internet]. 2021 Oct 11 [cited 2022 Nov 23];39(10):1293–6. Available from: http://www.cell.com/article/S1535610821004967/fulltext

231. Zhao L, Lim SY, Gordon-Weeks AN, Tapmeier TT, Im JH, Cao Y, et al. Recruitment of a myeloid cell subset (CD11b/Gr1 mid) via CCL2/CCR2 promotes the development of colorectal cancer liver metastasis. Hepatology [Internet]. 2013 Feb [cited 2022 Nov 29];57(2):829–39. Available from: https://pubmed.ncbi.nlm.nih.gov/23081697/

232. Yunna C, Mengru H, Lei W, Weidong C. Macrophage M1/M2 polarization. Eur J Pharmacol. 2020 Jun 15;877:173090.

233. Takemura N, Saiura A. Role of surgical resection for non-colorectal non-neuroendocrine liver metastases. World J Hepatol [Internet]. 2017 [cited 2022 Nov 29];9(5):242–51. Available from: https://pubmed.ncbi.nlm.nih.gov/28261381/

234. Khatib AM, Auguste P, Fallavollita L, Wang N, Samani A, Kontogiannea M, et al. Characterization of the host proinflammatory response to tumor cells during the initial stages of liver metastasis. Am J Pathol [Internet]. 2005 [cited 2022 Nov 29];167(3):749–59. Available from: https://pubmed.ncbi.nlm.nih.gov/16127154/

235. Gardner CR, Wasserman AJ, Laskin DL. Liver macrophage-mediated cytotoxicity toward mastocytoma cells involves phagocytosis of tumor targets. Hepatology [Internet]. 1991 Aug 1 [cited 2022 Nov 29];14(2):318–24. Available from: https://onlinelibrary.wiley.com/doi/full/10.1002/hep.1840140219

236. Seki S, Nakashima H, Nakashima M, Kinoshita M. Antitumor immunity produced by the liver Kupffer cells, NK cells, NKT cells, and CD8 CD122 T cells. Clin Dev Immunol [Internet]. 2011 [cited 2022 Nov 29];2011. Available from: https://pubmed.ncbi.nlm.nih.gov/22190974/

237. Heymann F, Peusquens J, Ludwig-Portugall I, Kohlhepp M, Ergen C, Niemietz P, et al. Liver inflammation abrogates immunological tolerance induced by Kupffer cells.

Hepatology [Internet]. 2015 Jul 1 [cited 2022 Nov 29];62(1):279–91. Available from: https://pubmed.ncbi.nlm.nih.gov/25810240/

238. Qian BZ, Li J, Zhang H, Kitamura T, Zhang J, Campion LR, et al. CCL2 recruits inflammatory monocytes to facilitate breast-tumour metastasis. Nature [Internet]. 2011 Jul 14 [cited 2022 Nov 29];475(7355):222–5. Available from: https://pubmed.ncbi.nlm.nih.gov/21654748/

239. Valls AF, Knipper K, Giannakouri E, Sarachaga V, Hinterkopf S, Wuehrl M, et al. VEGFR1+ Metastasis-Associated Macrophages Contribute to Metastatic Angiogenesis and Influence Colorectal Cancer Patient Outcome. Clin Cancer Res [Internet]. 2019 Sep 15 [cited 2022 Nov 29];25(18):5674–85. Available from: https://pubmed.ncbi.nlm.nih.gov/31239322/

240. Nielsen SR, Quaranta V, Linford A, Emeagi P, Rainer C, Santos A, et al. Macrophage-secreted granulin supports pancreatic cancer metastasis by inducing liver fibrosis. Nat Cell Biol [Internet]. 2016 May 1 [cited 2022 Nov 29];18(5):549–60. Available from: https://pubmed.ncbi.nlm.nih.gov/27088855/

241. Lim SY, Gordon-Weeks A, Allen D, Kersemans V, Beech J, Smart S, et al. Cd11b(+) myeloid cells support hepatic metastasis through down-regulation of angiopoietin-like 7 in cancer cells. Hepatology [Internet]. 2015 Aug 1 [cited 2022 Nov 29];62(2):521–33. Available from: https://pubmed.ncbi.nlm.nih.gov/25854806/

242. Lim SY, Yuzhalin AE, Gordon-Weeks AN, Muschel RJ. Targeting the CCL2-CCR2 signaling axis in cancer metastasis. Oncotarget [Internet]. 2016 May 10 [cited 2022 Nov 29];7(19):28697–710. Available from: https://pubmed.ncbi.nlm.nih.gov/26885690/

243. Quaranta V, Rainer C, Nielsen SR, Raymant ML, Ahmed MS, Engle DD, et al. Macrophage-Derived Granulin Drives Resistance to Immune Checkpoint Inhibition in Metastatic Pancreatic Cancer. Cancer Res [Internet]. 2018 Aug 1 [cited 2022 Nov 29];78(15):4253–69. Available from: https://pubmed.ncbi.nlm.nih.gov/29789416/

244. Ciner AT, Jones K, Muschel RJ, Brodt P. The unique immune microenvironment of liver metastases: Challenges and opportunities. Semin Cancer Biol [Internet]. 2020;(April):0–1. Available from: https://doi.org/10.1016/j.semcancer.2020.06.003

245. Harmon C, Robinson MW, Hand F, Almuaili D, Mentor K, Houlihan DD, et al. Lactate-Mediated Acidification of Tumor Microenvironment Induces Apoptosis of Liver-Resident NK Cells in Colorectal Liver Metastasis. Cancer Immunol Res [Internet]. 2019 Feb 1 [cited 2022 Nov 29];7(2):335–46. Available from: https://pubmed.ncbi.nlm.nih.gov/30563827/

246. Ducimetière L, Lucchiari G, Litscher G, Nater M, Heeb L, Nuñez NG, et al. Conventional NK cells and tissue-resident ILC1s join forces to control liver metastasis. Proc Natl Acad Sci U S A [Internet]. 2021 Jul 6 [cited 2022 Nov 29];118(27). Available from: https://pubmed.ncbi.nlm.nih.gov/34183415/

247. Zheng W, Wu J, Peng Y, Sun J, Cheng P, Huang Q. Tumor-Associated Neutrophils in Colorectal Cancer Development, Progression and Immunotherapy. Cancers (Basel) [Internet]. 2022 Oct 1 [cited 2022 Nov 24];14(19). Available from: https://pubmed.ncbi.nlm.nih.gov/36230676/

248. Donadon M, Hudspeth K, Cimino M, di Tommaso L, Preti M, Tentorio P, et al. Increased Infiltration of Natural Killer and T Cells in Colorectal Liver Metastases Improves Patient Overall Survival. J Gastrointest Surg [Internet]. 2017 Aug 1 [cited 2022 Nov 29];21(8):1226–36. Available from: https://pubmed.ncbi.nlm.nih.gov/28536806/

249. Mizuno R, Kawada K, Itatani Y, Ogawa R, Kiyasu Y, Sakai Y. The Role of Tumor-Associated Neutrophils in Colorectal Cancer. Int J Mol Sci [Internet]. 2019 Feb 1 [cited 2022 Nov 29];20(3). Available from: https://pubmed.ncbi.nlm.nih.gov/30691207/

250. Walsh SR, Cook EJ, Goulder F, Justin TA, Keeling NJ. Neutrophil-lymphocyte ratio as a prognostic factor in colorectal cancer. J Surg Oncol [Internet]. 2005 Sep 1 [cited 2022 Nov 29];91(3):181–4. Available from: https://pubmed.ncbi.nlm.nih.gov/16118772/

251. Jackstadt R, van Hooff SR, Leach JD, Cortes-Lavaud X, Lohuis JO, Ridgway RA, et al. Epithelial NOTCH Signaling Rewires the Tumor Microenvironment of Colorectal

Cancer to Drive Poor-Prognosis Subtypes and Metastasis. Cancer Cell [Internet]. 2019 Sep 16 [cited 2022 Nov 29];36(3):319-336.e7. Available from: https://pubmed.ncbi.nlm.nih.gov/31526760/

252. Cools-Lartigue J, Spicer J, McDonald B, Gowing S, Chow S, Giannias B, et al. Neutrophil extracellular traps sequester circulating tumor cells and promote metastasis. J Clin Invest [Internet]. 2013 Aug 1 [cited 2022 Nov 29];123(8):3446–58. Available from: https://pubmed.ncbi.nlm.nih.gov/23863628/

253. Gabrilovich DI. Myeloid-Derived Suppressor Cells. Cancer Immunol Res [Internet]. 2017 Jan 1 [cited 2022 Nov 29];5(1):3–8. Available from: https://pubmed.ncbi.nlm.nih.gov/28052991/

254. Sade-Feldman M, Kanterman J, Ish-Shalom E, Elnekave M, Horwitz E, Baniyash M. Tumor necrosis factor-α blocks differentiation and enhances suppressive activity of immature myeloid cells during chronic inflammation. Immunity [Internet]. 2013 Mar 21 [cited 2022 Nov 29];38(3):541–54. Available from: https://pubmed.ncbi.nlm.nih.gov/23477736/

255. Gabrilovich DI, Nagaraj S. Myeloid-derived suppressor cells as regulators of the immune system. Nat Rev Immunol [Internet]. 2009 Mar [cited 2022 Nov 29];9(3):162–74. Available from: https://pubmed.ncbi.nlm.nih.gov/19197294/

256. Gabrilovich DI, Ostrand-Rosenberg S, Bronte V. Coordinated regulation of myeloid cells by tumours. Nat Rev Immunol [Internet]. 2012 Apr [cited 2022 Nov 29];12(4):253–68. Available from: https://pubmed.ncbi.nlm.nih.gov/22437938/

257. Gulubova M v., Ananiev JR, Vlaykova TI, Yovchev Y, Tsoneva V, Manolova IM. Role of dendritic cells in progression and clinical outcome of colon cancer. Int J Colorectal Dis [Internet]. 2012 Feb [cited 2022 Nov 24];27(2):159–69. Available from: https://pubmed.ncbi.nlm.nih.gov/22065108/

258. Chandra R, Karalis JD, Liu C, Murimwa GZ, Park JV, Heid CA, et al. The Colorectal Cancer Tumor Microenvironment and Its Impact on Liver and Lung Metastasis. Cancers (Basel) [Internet]. 2021 Dec 1 [cited 2022 Nov 24];13(24). Available from: /pmc/articles/PMC8699466/

259. Legitimo A, Consolini R, Failli A, Orsini G, Spisni R. Dendritic cell defects in the colorectal cancer. Hum Vaccin Immunother [Internet]. 2014 Nov 1 [cited 2022 Nov 24];10(11):3224–35. Available from: https://pubmed.ncbi.nlm.nih.gov/25483675/

260. Orsini G, Legitimo A, Failli A, Ferrari P, Nicolini A, Spisni R, et al. Defective generation and maturation of dendritic cells from monocytes in colorectal cancer patients during the course of disease. Int J Mol Sci [Internet]. 2013 Nov 7 [cited 2022 Nov 24];14(11):22022–41. Available from: https://pubmed.ncbi.nlm.nih.gov/24213603/

261. Berthel A, Zoernig I, Valous NA, Kahlert C, Klupp F, Ulrich A, et al. Detailed resolution analysis reveals spatial T cell heterogeneity in the invasive margin of colorectal cancer liver metastases associated with improved survival. Oncoimmunology [Internet]. 2017;6(3):1–10. Available from: http://dx.doi.org/10.1080/2162402X.2017.1286436

262. Brunner SM, Kesselring R, Rubner C, Martin M, Jeiter T, Boerner T, et al. Prognosis according to histochemical analysis of liver metastases removed at liver resection. British Journal of Surgery. 2014;101(13):1681–91.

263. Chen DS, Mellman I. Elements of cancer immunity and the cancer-immune set point. Nature. 2017;541(7637):321–30.

264. Latacz E, van Dam PJ, Vanhove C, Llado L, Descamps B, Ruiz N, et al. Can medical imaging identify the histopathological growth patterns of liver metastases? Semin Cancer Biol [Internet]. 2020;(July):1–9. Available from: https://doi.org/10.1016/j.semcancer.2020.07.002

265. Stremitzer S, Vermeulen P, Graver S, Kockx M, Dirix L, Yang D, et al. Immune phenotype and histopathological growth pattern in patients with colorectal liver metastases. Br J Cancer [Internet]. 2020;122(10):1518–24. Available from: http://dx.doi.org/10.1038/s41416-020-0812-z

266. 'Revertant' DCIS in human axillary breast carcinoma metastases - Barsky - 1997 - The Journal of Pathology - Wiley Online Library [Internet]. [cited 2022 Nov 29]. Available from: https://onlinelibrary.wiley.com/doi/10.1002/(SICI)1096-9896(199710)183:2%3C188::AID-PATH898%3E3.0.CO;2-7

267. Dezso K, Papp V, Bugyik E, Hegyesi H, Sáfrány G, Bödör C, et al. Structural analysis of oval-cell-mediated liver regeneration in rats. Hepatology [Internet]. 2012 Oct [cited 2022 Nov 29];56(4):1457–67. Available from: https://pubmed.ncbi.nlm.nih.gov/22419534/

268. Schuppan D, Kim YO. Evolving therapies for liver fibrosis. J Clin Invest [Internet]. 2013 May 1 [cited 2022 Nov 29];123(5):1887–901. Available from: https://pubmed.ncbi.nlm.nih.gov/23635787/

269. Ding B sen, Cao Z, Lis R, Nolan DJ, Guo P, Simons M, et al. Divergent angiocrine signals from vascular niche balance liver regeneration and fibrosis. Nature [Internet]. 2014 [cited 2022 Nov 29];505(7481):97–102. Available from: https://pubmed.ncbi.nlm.nih.gov/24256728/

270. Rada M, Kapelanski-Lamoureux A, Petrillo S, Tabariès S, Siegel P, Reynolds AR, et al. Runt related transcription factor-1 plays a central role in vessel co-option of colorectal cancer liver metastases. Commun Biol [Internet]. 2021 Dec 1 [cited 2022 Nov 29];4(1). Available from: https://pubmed.ncbi.nlm.nih.gov/34376784/

271. Lugassy C, Kleinman HK, Vermeulen PB, Barnhill RL. Angiotropism, pericytic mimicry and extravascular migratory metastasis: an embryogenesis-derived program of tumor spread. Angiogenesis [Internet]. 2020 Feb 1 [cited 2022 Nov 29];23(1):27–41. Available from: https://pubmed.ncbi.nlm.nih.gov/31720876/

272. Fernández Moro C, Bozóky B, Gerling M. Growth patterns of colorectal cancer liver metastases and their impact on prognosis: a systematic review. BMJ Open Gastroenterol [Internet]. 2018 [cited 2022 Nov 29];5(1). Available from: https://pubmed.ncbi.nlm.nih.gov/30073092/

273. Fernández Moro C, Harrizi S, Hamidi Y, Geyer N, Kuznyecov D, Tidholm-Qvist E, et al. An idiosyncratic, zonated stroma encapsulates desmoplastic liver metastases and originates from injured liver. [cited 2022 Nov 24]; Available from: https://doi.org/10.1101/2022.08.24.22279162

274. Ciner AT, Jones K, Muschel RJ, Brodt P. The unique immune microenvironment of liver metastases: Challenges and opportunities. Semin Cancer Biol [Internet]. 2021 Jun 1

[cited 2022 Nov 29];71:143–56. Available from: https://pubmed.ncbi.nlm.nih.gov/32526354/

275. Oliveira RC, Alexandrino H, Cipriano MA, Alves FC, Tralhão JG. Predicting liver metastases growth patterns: Current status and future possibilities. Semin Cancer Biol [Internet]. 2021 Jun 1 [cited 2022 Nov 29];71:42–51. Available from: https://pubmed.ncbi.nlm.nih.gov/32679190/

276. Latacz E, van Dam PJ, Vanhove C, Llado L, Descamps B, Ruiz N, et al. Can medical imaging identify the histopathological growth patterns of liver metastases? Semin Cancer Biol [Internet]. 2021 Jun 1 [cited 2022 Nov 29];71:33–41. Available from: https://pubmed.ncbi.nlm.nih.gov/32735852/

277. Liu Z, Zhang XY, Shi YJ, Wang L, Zhu HT, Tang Z, et al. Radiomics Analysis for Evaluation of Pathological Complete Response to Neoadjuvant Chemoradiotherapy in Locally Advanced Rectal Cancer. Clin Cancer Res [Internet]. 2017 Dec 1 [cited 2022 Nov 29];23(23):7253–62. Available from: https://pubmed.ncbi.nlm.nih.gov/28939744/

278. Cheng J, Wei J, Tong T, Sheng W, Zhang Y, Han Y, et al. Prediction of Histopathologic Growth Patterns of Colorectal Liver Metastases with a Noninvasive Imaging Method. Ann Surg Oncol [Internet]. 2019 Dec 1 [cited 2022 Nov 29];26(13):4587–98. Available from: https://pubmed.ncbi.nlm.nih.gov/31605342/

279. Lee JC, Mehdizadeh S, Smith J, Young A, Mufazalov IA, Mowery CT, et al. Regulatory T cell control of systemic immunity and immunotherapy response in liver metastasis. Sci Immunol [Internet]. 2020 Oct 16 [cited 2022 Nov 25];5(52). Available from: https://pubmed.ncbi.nlm.nih.gov/33008914/

280. Wang C, Park J, Ouyang C, Longmate JA, Tajon M, Chao J, et al. A Pilot Feasibility Study of Yttrium-90 Liver Radioembolization Followed by Durvalumab and Tremelimumab in Patients with Microsatellite Stable Colorectal Cancer Liver Metastases. Oncologist [Internet]. 2020 May 1 [cited 2022 Nov 25];25(5):382-e776. Available from: https://pubmed.ncbi.nlm.nih.gov/31857446/

281. Yu J, Green MD, Li S, Sun Y, Journey SN, Choi JE, et al. Liver metastasis restrains immunotherapy efficacy via macrophage-mediated T cell elimination. Nat Med

[Internet]. 2021 Jan 1 [cited 2022 Nov 25];27(1):152–64. Available from: https://pubmed.ncbi.nlm.nih.gov/33398162/

282. Le DT, Uram JN, Wang H, Bartlett BR, Kemberling H, Eyring AD, et al. PD-1 Blockade in Tumors with Mismatch-Repair Deficiency. N Engl J Med [Internet]. 2015 Jun 25 [cited 2022 Nov 29];372(26):2509–20. Available from: https://pubmed.ncbi.nlm.nih.gov/26028255/

283. Overman MJ, McDermott R, Leach JL, Lonardi S, Lenz HJ, Morse MA, et al. Nivolumab in patients with metastatic DNA mismatch repair-deficient or microsatellite instability-high colorectal cancer (CheckMate 142): an open-label, multicentre, phase 2 study. Lancet Oncol [Internet]. 2017 Sep 1 [cited 2022 Nov 29];18(9):1182–91. Available from: https://pubmed.ncbi.nlm.nih.gov/28734759/

284. Dobin A, Davis CA, Schlesinger F, Drenkow J, Zaleski C, Jha S, et al. STAR: ultrafast universal RNA-seq aligner. Bioinformatics [Internet]. 2013 Jan [cited 2023 Feb 6];29(1):15–21. Available from: https://pubmed.ncbi.nlm.nih.gov/23104886/

285. Li B, Dewey CN. RSEM: accurate transcript quantification from RNA-Seq data with or without a reference genome. BMC Bioinformatics [Internet]. 2011 Aug 4 [cited 2023 Feb 6];12. Available from: https://pubmed.ncbi.nlm.nih.gov/21816040/

286. Law CW, Chen Y, Shi W, Smyth GK. voom: Precision weights unlock linear model analysis tools for RNA-seq read counts. Genome Biol [Internet]. 2014 Feb 3 [cited 2023 Feb 6];15(2). Available from: https://pubmed.ncbi.nlm.nih.gov/24485249/

287. Hidalgo MR, Cubuk C, Amadoz A, Salavert F, Carbonell-Caballero J, Dopazo J. High throughput estimation of functional cell activities reveals disease mechanisms and predicts relevant clinical outcomes. Oncotarget [Internet]. 2017 [cited 2022 Dec 18];8(3):5160–78. Available from: https://pubmed.ncbi.nlm.nih.gov/28042959/

288. Hipathia [Internet]. [cited 2022 Dec 18]. Available from: http://hipathia.babelomics.org/

289. Metabolizer [Internet]. [cited 2022 Dec 18]. Available from: http://metabolizer.babelomics.org/

290. Lundgren S, Elebro J, Heby M, Nodin B, Leandersson K, Micke P, et al. Quantitative, qualitative and spatial analysis of lymphocyte infiltration in periampullary and pancreatic adenocarcinoma. Int J Cancer [Internet]. 2020 Jun 15 [cited 2022 Dec 18];146(12):3461–73. Available from: https://pubmed.ncbi.nlm.nih.gov/32129882/

291. Mezheyeuski A, Bergsland CH, Backman M, Djureinovic D, Sjöblom T, Bruun J, et al. Multispectral imaging for quantitative and compartment-specific immune infiltrates reveals distinct immune profiles that classify lung cancer patients. J Pathol [Internet]. 2018 Apr 1 [cited 2022 Dec 18];244(4):421–31. Available from: https://pubmed.ncbi.nlm.nih.gov/29282718/

292. Lugassy C, Vermeulen PB, Ribatti D, Pezzella F, Barnhill RL. Vessel co-option and angiotropic extravascular migratory metastasis: a continuum of tumour growth and spread? Br J Cancer. 2022;126(7):973–80.

293. Fu T, Dai LJ, Wu SY, Xiao Y, Ma D, Jiang YZ, et al. Spatial architecture of the immune microenvironment orchestrates tumor immunity and therapeutic response. J Hematol Oncol. 2021;14(1):1–25.

294. Lisa M. Coussens LZ and AKP. Neutralizing Tumor-Promoting Chronic Inflammation: A Magic Bullet? Science (1979). 2013;339(6117):286–91.

295. Pollard JW. Trophic macrophages in development and disease. Nat Rev Immunol. 2009;9(4):259–70.

296. Rudensky AY. Regulatory T Cells and Foxp3. Immunol Rev [Internet]. 2011 May [cited 2022 Dec 2];241(1):260. Available from: /pmc/articles/PMC3077798/

297. Mayer CT, Floess S, Baru AM, Lahl K, Huehn J, Sparwasser T. CD8+ Foxp3+ T cells share developmental and phenotypic features with classical CD4+ Foxp3+ regulatory T cells but lack potent suppressive activity. Eur J Immunol [Internet]. 2011 Mar [cited 2022 Dec 2];41(3):716–25. Available from: https://pubmed.ncbi.nlm.nih.gov/21312192/

298. David G. DeNardo BR. Macrophages as regulators of tumor immunity and immunotherapy. Vol. 19, Nat Rev Immunol. 2019. 369–382 p.

299. Kielbassa K, Vegna S, Ramirez C, Akkari L. Understanding the origin and diversity of macrophages to tailor their targeting in solid cancers. Front Immunol. 2019;10(SEP):1–15.

300. Larionova I, Tuguzbaeva G, Ponomaryova A, Stakheyeva M, Cherdyntseva N, Pavlov V, et al. Tumor-Associated Macrophages in Human Breast, Colorectal, Lung, Ovarian and Prostate Cancers. Front Oncol. 2020;10(October):1–34.

301. Wang S, Song R, Wang Z, Jing Z, Wang S, Ma J. S100A8/A9 in inflammation. Front Immunol. 2018;9(JUN).

302. Huang M, Wu R, Chen L, Peng Q, Li S, Zhang Y, et al. S100A9 Regulates MDSCs-Mediated Immune Suppression via the RAGE and TLR4 Signaling Pathways in Colorectal Carcinoma. Front Immunol. 2019;10(September):1–13.

303. Cheng P, Corzo CA, Luetteke N, Yu B, Nagaraj S, Bui MM, et al. Inhibition of dendritic cell differentiation and accumulation of myeloid-derived suppressor cells in cancer is regulated by S100A9 protein. Journal of Experimental Medicine. 2008;205(10):2235–49.

304. Wagner NB, Weide B, Gries M, Reith M, Tarnanidis K, Schuermans V, et al. Tumor microenvironment-derived S100A8/A9 is a novel prognostic biomarker for advanced melanoma patients and during immunotherapy with anti-PD-1 antibodies. J Immunother Cancer. 2019;7(1):1–10.

305. Cassetta L, Pollard JW. Tumor-associated macrophages. Current Biology [Internet]. 2020;30(6):R246–8. Available from: http://dx.doi.org/10.1016/j.cub.2020.01.031

306. Cortese N, Soldani C, Franceschini B, Barbagallo M, Marchesi F, Torzilli G, et al. Macrophages in colorectal cancer liver metastases. Cancers (Basel). 2019;11(5):1–12.

307. Ireland L v., Mielgo A. Macrophages and fibroblasts, key players in cancer chemoresistance. Front Cell Dev Biol. 2018;6(OCT):1–14.

308. Tripathi C, Tewari BN, Kanchan RK, Baghel KS, Nautiyal N, Shrivastava R, et al. Macrophages are recruited to hypoxic tumor areas and acquire a Pro-Angiogenic M2-Polarized phenotype via hypoxic cancer cell derived cytokines Oncostatin M and Eotaxin. Oncotarget. 2014;5(14):5350–68.

309. Behzatoglu K. Osteoclasts in Tumor Biology: Metastasis and Epithelial-Mesenchymal-Myeloid Transition. Pathol Oncol Res [Internet]. 2021 Apr 30 [cited 2022 Dec 5];27. Available from: https://pubmed.ncbi.nlm.nih.gov/34257573/

310. MacParland, S.A., Liu, J.C., Ma, X.-Z., Innes, B.T., Bartczak, A.M., Gage BK et al. Single cell RNA sequencing of human liver reveals distinct intrahepatic macrophage populations. Nat Commun. 2018;9:43–83.

311. Zhao F, Hoechst B, Duffy A, Gamrekelashvili J, Fioravanti S, Manns MP, et al. S100A9 a new marker for monocytic human myeloid-derived suppressor cells. Immunology. 2012;136(2):176–83.

312. Mezheyeuski A, Backman M, Mattsson J, Martín-Bernabé A, Larsson C, Hrynchyk I, et al. An immune score reflecting pro- and anti-tumoural balance of tumour microenvironment has major prognostic impact and predicts immunotherapy response in solid cancers. EBioMedicine [Internet]. 2023 Feb 1 [cited 2023 Feb 15];88. Available from: http://www.thelancet.com/article/S2352396423000178/fulltext

313. Aratani Y. Myeloperoxidase: Its role for host defense, inflammation, and neutrophil function. Arch Biochem Biophys. 2018;640(January):47–52.

314. Tauriello DVF, Palomo-Ponce S, Stork D, Berenguer-Llergo A, Badia-Ramentol J, Iglesias M, et al. TGFβ drives immune evasion in genetically reconstituted colon cancer metastasis. Nature. 2018;554(7693):538–43.

315. Uhlén M, Fagerberg L, Hallström BM, Lindskog C, Oksvold P, Mardinoglu A, et al. Tissue-based map of the human proteome. Science (1979). 2015 Jan 23;347(6220).

316. Mueller L, Goumas FA, Affeldt M, Sandtner S, Gehling UM, Brilloff S, et al. Stromal fibroblasts in colorectal liver metastases originate from resident fibroblasts and generate an inflammatory microenvironment. American Journal of Pathology. 2007;171(5):1608–18.

317. Filliol A, Saito Y, Nair A, Dapito DH, Yu LX, Ravichandra A, et al. Opposing roles of hepatic stellate cell subpopulations in hepatocarcinogenesis. Nature [Internet]. 2022 Oct 13 [cited 2023 Jan 19];610(7931):356–65. Available from: https://pubmed.ncbi.nlm.nih.gov/36198802/

318. Affo S, Nair A, Brundu F, Ravichandra A, Bhattacharjee S, Matsuda M, et al. Promotion of cholangiocarcinoma growth by diverse cancer-associated fibroblast subpopulations. Cancer Cell. 2021 Jun 14;39(6):866-882.e11.

319. Bhattacharjee S, Hamberger F, Ravichandra A, Miller M, Nair A, Affo S, et al. Tumor restriction by type I collagen opposes tumor-promoting effects of cancer-associated fibroblasts. J Clin Invest [Internet]. 2021 Jun 6 [cited 2023 Jan 19];131(11). Available from: /pmc/articles/PMC8159701/

320. Giguelay A, Turtoi E, Khelaf L, Tosato G, Dadi I, Chastel T, et al. The landscape of cancer-associated fibroblasts in colorectal cancer liver metastases. Theranostics [Internet]. 2022 [cited 2023 Jan 19];12(17):7624–39. Available from: https://pubmed.ncbi.nlm.nih.gov/36438498/

321. Kruepunga N, Hakvoort TBM, Hikspoors JPJM, Köhler SE, Lamers WH. Anatomy of rodent and human livers: What are the differences? Biochimica et Biophysica Acta (BBA) - Molecular Basis of Disease. 2019 May 1;1865(5):869–78.

322. Tabariès S, Annis MG, Lazaris A, Petrillo SK, Huxham J, Abdellatif A, et al. Claudin-2 promotes colorectal cancer liver metastasis and is a biomarker of the replacement type growth pattern. Commun Biol [Internet]. 2021;4(1):1–14. Available from: http://dx.doi.org/10.1038/s42003-021-02189-9

323. Ferrari N, Ranftl R, Chicherova I, Slaven ND, Moeendarbary E, Farrugia AJ, et al. Dickkopf-3 links HSF1 and YAP/TAZ signalling to control aggressive behaviours in cancer-associated fibroblasts. Nat Commun [Internet]. 2019 Dec 1 [cited 2023 Jan 19];10(1). Available from: https://pubmed.ncbi.nlm.nih.gov/30631061/

324. Massagué J. TGFbeta in Cancer. Cell [Internet]. 2008 Jul 25 [cited 2023 Jan 19];134(2):215–30. Available from: https://pubmed.ncbi.nlm.nih.gov/18662538/

325. Kojima Y, Acar A, Eaton EN, Mellody KT, Scheel C, Ben-Porath I, et al. Autocrine TGF-beta and stromal cell-derived factor-1 (SDF-1) signaling drives the evolution of tumor-promoting mammary stromal myofibroblasts. Proc Natl Acad Sci U S A [Internet]. 2010 Nov 16 [cited 2023 Jan 19];107(46):20009–14. Available from: https://pubmed.ncbi.nlm.nih.gov/21041659/

326. Roumenina LT, Daugan M v., Petitprez F, Sautès-Fridman C, Fridman WH. Context-dependent roles of complement in cancer. Nat Rev Cancer [Internet]. 2019 Dec 1 [cited 2023 Jan 19];19(12):698–715. Available from: https://pubmed.ncbi.nlm.nih.gov/31666715/

327. Vesely DL. Natriuretic peptides' metabolic targets for treatment of cancer. J Investig Med [Internet]. 2013 [cited 2023 Jan 20];61(5):816–22. Available from: https://pubmed.ncbi.nlm.nih.gov/23612148/

328. Yuzhalin AE, Kutikhin AG. Interleukin-12: clinical usage and molecular markers of cancer susceptibility. Growth Factors [Internet]. 2012 Jun [cited 2023 Jan 20];30(3):176–91. Available from: https://pubmed.ncbi.nlm.nih.gov/22515181/

329. Joo MK, Park JJ, Chun HJ. Impact of homeobox genes in gastrointestinal cancer. World J Gastroenterol [Internet]. 2016 Oct 10 [cited 2023 Jan 20];22(37):8247. Available from: /pmc/articles/PMC5055856/

330. Wei J, Hu M, Huang K, Lin S, Du H. Roles of Proteoglycans and Glycosaminoglycans in Cancer Development and Progression. Int J Mol Sci [Internet]. 2020 Sep 1 [cited 2023 Jan 20];21(17):1–28. Available from: /pmc/articles/PMC7504257/

331. Freeman AJ, Kearney CJ, Silke J, Oliaro J. Unleashing TNF cytotoxicity to enhance cancer immunotherapy. Trends Immunol [Internet]. 2021 Dec 1 [cited 2023 Jan 20];42(12):1128–42. Available from: https://pubmed.ncbi.nlm.nih.gov/34750058/

332. Yan C, Richmond A. Hiding in the dark: pan-cancer characterization of expression and clinical relevance of CD40 to immune checkpoint blockade therapy. Mol Cancer [Internet]. 2021 Dec 1 [cited 2023 Jan 20];20(1). Available from: https://pubmed.ncbi.nlm.nih.gov/34758832/

333. Liu Q, Li A, Tian Y, Wu JD, Liu Y, Li T, et al. The CXCL8-CXCR1/2 pathways in cancer. Cytokine Growth Factor Rev [Internet]. 2016 Oct 1 [cited 2023 Jan 23];31:61–71. Available from: https://pubmed.ncbi.nlm.nih.gov/27578214/

334. Concetti J, Wilson CL. NFKB1 and Cancer: Friend or Foe? Cells [Internet]. 2018 Sep 7 [cited 2023 Jan 20];7(9). Available from: https://pubmed.ncbi.nlm.nih.gov/30205516/

335. Melincovici CS, Boşca AB, Şuşman S, Mărginean M, Mihu C, Istrate M, et al. Vascular endothelial growth factor (VEGF) - key factor in normal and pathological angiogenesis. Rom J Morphol Embryol [Internet]. 2018 [cited 2023 Jan 20];59(2):455–67. Available from: https://pubmed.ncbi.nlm.nih.gov/30173249/

336. Kasprzak A, Adamek A. The Neuropeptide System and Colorectal Cancer Liver Metastases: Mechanisms and Management. Int J Mol Sci [Internet]. 2020 May 2 [cited 2023 Jan 23];21(10). Available from: /pmc/articles/PMC7279011/

337. Kizuka Y, Taniguchi N. Enzymes for N-Glycan Branching and Their Genetic and Nongenetic Regulation in Cancer. Biomolecules [Internet]. 2016 Jun 1 [cited 2023 Jan 24];6(2). Available from: /pmc/articles/PMC4919920/

338. Currie E, Schulze A, Zechner R, Walther TC, Farese R v. Cellular fatty acid metabolism and cancer. Cell Metab [Internet]. 2013 Aug 6 [cited 2023 Jan 24];18(2):153–61. Available from: https://pubmed.ncbi.nlm.nih.gov/23791484/

339. Gibellini F, Smith TK. The Kennedy pathway--De novo synthesis of phosphatidylethanolamine and phosphatidylcholine. IUBMB Life [Internet]. 2010 Jun [cited 2023 Jan 24];62(6):414–28. Available from: https://pubmed.ncbi.nlm.nih.gov/20503434/

340. Evans RC, Fear S, Ashby D, Williams E, van der Vliet M, Rhodes JM, et al. Diet and colorectal cancer: An investigation of the lectin/galactose hypothesis. Gastroenterology [Internet]. 2002 [cited 2023 Jan 24];122(7):1784–92. Available from: https://pubmed.ncbi.nlm.nih.gov/12055585/

341. Gunaydin G. CAFs Interacting With TAMs in Tumor Microenvironment to Enhance Tumorigenesis and Immune Evasion. Front Oncol. 2021;11(July):1–29.

342. Korbecki J, Kojder K, Simińska D, Bohatyrewicz R, Gutowska I, Chlubek D, et al. CC Chemokines in a Tumor: A Review of Pro-Cancer and Anti-Cancer Properties of the Ligands of Receptors CCR1, CCR2, CCR3, and CCR4. Int J Mol Sci [Internet]. 2020 Nov 1 [cited 2023 Jan 25];21(21):1–29. Available from: /pmc/articles/PMC7665155/

343. Li S, Shi X, Chen M, Xu N, Sun D, Bai R, et al. Angiogenin promotes colorectal cancer metastasis via tiRNA production. Int J Cancer [Internet]. 2019 Sep 1 [cited 2023 Jan 25];145(5):1395–407. Available from: https://pubmed.ncbi.nlm.nih.gov/30828790/

344. Korbecki J, Grochans S, Gutowska I, Barczak K, Baranowska-Bosiacka I. CC Chemokines in a Tumor: A Review of Pro-Cancer and Anti-Cancer Properties of Receptors CCR5, CCR6, CCR7, CCR8, CCR9, and CCR10 Ligands. Int J Mol Sci [Internet]. 2020 Oct 2 [cited 2023 Jan 25];21(20):1–34. Available from: /pmc/articles/PMC7590012/

345. Johnson MA, Firth SM. IGFBP-3: A cell fate pivot in cancer and disease. Growth Hormone & IGF Research. 2014 Oct 1;24(5):164–73.

346. Cai Q, Dozmorov M, Oh Y. IGFBP-3/IGFBP-3 Receptor System as an Anti-Tumor and Anti-Metastatic Signaling in Cancer. Cells [Internet]. 2020 May 20 [cited 2023 Jan 26];9(5). Available from: /pmc/articles/PMC7290346/

347. Parida S, Siddharth S, Sharma D. Adiponectin, Obesity, and Cancer: Clash of the Bigwigs in Health and Disease. Int J Mol Sci [Internet]. 2019 May 2 [cited 2023 Jan 26];20(10). Available from: /pmc/articles/PMC6566909/

348. Mora Barthelmess R, Stijlemans B, van Ginderachter JA. Hallmarks of Cancer Affected by the MIF Cytokine Family. Cancers (Basel) [Internet]. 2023 Jan 6 [cited 2023 Jan 26];15(2):395. Available from: https://pubmed.ncbi.nlm.nih.gov/36672343/

349. Zhang Z, Zhou X, Guo J, Zhang F, Qian Y, Wang G, et al. TA-MSCs, TA-MSCs-EVs, MIF: their crosstalk in immunosuppressive tumor microenvironment. J Transl Med [Internet]. 2022 Dec 1 [cited 2023 Jan 26];20(1):320. Available from: /pmc/articles/PMC9287873/

350. Li CY, Kuang KL, Du JR, Eymin B, Jia T. Far beyond anti-angiogenesis: Benefits for anti-basicFGF therapy in cancer. Biochimica et Biophysica Acta (BBA) - Molecular Cell Research. 2022 Jul 1;1869(7):119253.

351. Leong A, Kim M. The Angiopoietin-2 and TIE Pathway as a Therapeutic Target for Enhancing Antiangiogenic Therapy and Immunotherapy in Patients with Advanced Cancer. Int J Mol Sci [Internet]. 2020 Nov 2 [cited 2023 Jan 26];21(22):1–20. Available from: https://pubmed.ncbi.nlm.nih.gov/33217955/

352. Zhao H, Peehl DM. Tumor-promoting phenotype of CD90hi prostate cancer-associated fibroblasts. Prostate [Internet]. 2009 Jun 15 [cited 2023 Jan 27];69(9):991–1000. Available from: https://pubmed.ncbi.nlm.nih.gov/19267366/

353. Karpus ON, Westendorp BF, Vermeulen JLM, Meisner S, Koster J, Muncan V, et al. Colonic CD90+ Crypt Fibroblasts Secrete Semaphorins to Support Epithelial Growth. Cell Rep [Internet]. 2019 Mar 26 [cited 2023 Jan 27];26(13):3698-3708.e5. Available from: https://pubmed.ncbi.nlm.nih.gov/30917322/

354. Zhang Q, Yi DY, Xue BZ, Wen WW, Lu YP, Abdelmaksou A, et al. CD90 determined two subpopulations of glioma-associated mesenchymal stem cells with different roles in tumour progression. Cell Death Dis [Internet]. 2018 Nov 1 [cited 2023 Jan 27];9(11). Available from: https://pubmed.ncbi.nlm.nih.gov/30368520/

355. Dudas J, Mansuroglu T, Batusic D, Ramadori G. Thy-1 is expressed in myofibroblasts but not found in hepatic stellate cells following liver injury. Histochem Cell Biol [Internet]. 2009 [cited 2023 Jan 27];131(1):115–27. Available from: https://pubmed.ncbi.nlm.nih.gov/18797914/

356. Xu J, Liu X, Koyama Y, Wang P, Lan T, Kim IG, et al. The types of hepatic myofibroblasts contributing to liver fibrosis of different etiologies. Front Pharmacol [Internet]. 2014 [cited 2023 Jan 27];5. Available from: https://pubmed.ncbi.nlm.nih.gov/25100997/

357. Dobie R, Wilson-Kanamori JR, Henderson BEP, Smith JR, Matchett KP, Portman JR, et al. Single-Cell Transcriptomics Uncovers Zonation of Function in the Mesenchyme during Liver Fibrosis. Cell Rep [Internet]. 2019 Nov 12 [cited 2023 Jan 27];29(7):1832-1847.e8. Available from: https://pubmed.ncbi.nlm.nih.gov/31722201/

358. Suzuki K, Tanaka M, Watanabe N, Saito S, Nonaka H, Miyajima A. p75 Neurotrophin receptor is a marker for precursors of stellate cells and portal fibroblasts in mouse fetal liver. Gastroenterology [Internet]. 2008 [cited 2023 Jan 27];135(1). Available from: https://pubmed.ncbi.nlm.nih.gov/18515089/

359. Yamamoto Y, Kasashima H, Fukui Y, Tsujio G, Yashiro M, Maeda K. The heterogeneity of cancer-associated fibroblast subpopulations: Their origins, biomarkers, and roles in

the tumor microenvironment. Cancer Sci [Internet]. 2023 Jan 1 [cited 2023 Jan 27];114(1). Available from: https://pubmed.ncbi.nlm.nih.gov/36197901/

360. Ramachandran P, Matchett KP, Dobie R, Wilson-Kanamori JR, Henderson NC. Single-cell technologies in hepatology: new insights into liver biology and disease pathogenesis. Nat Rev Gastroenterol Hepatol [Internet]. 2020 Aug 1 [cited 2023 Jan 27];17(8):457–72. Available from: https://pubmed.ncbi.nlm.nih.gov/32483353/

361. Chen Y, Kim J, Yang S, Wang H, Wu CJ, Sugimoto H, et al. Type I collagen deletion in αSMA+ myofibroblasts augments immune suppression and accelerates progression of pancreatic cancer. Cancer Cell [Internet]. 2021 Apr 12 [cited 2023 Jan 27];39(4):548-565.e6. Available from: https://pubmed.ncbi.nlm.nih.gov/33667385/

362. Ren J, Da J, Hu N. Identification of COL1A1 associated with immune infiltration in brain lower grade glioma. PLoS One [Internet]. 2022 Jul 1 [cited 2023 Jan 30];17(7). Available from: https://pubmed.ncbi.nlm.nih.gov/35789341/

363. Filliol A, Saito Y, Nair A, Dapito DH, Yu LX, Ravichandra A, et al. Opposing roles of hepatic stellate cell subpopulations in hepatocarcinogenesis. Nature [Internet]. 2022 Oct 13 [cited 2023 Jan 30];610(7931):356–65. Available from: https://pubmed.ncbi.nlm.nih.gov/36198802/

364. Bhattacharjee S, Hamberger F, Ravichandra A, Miller M, Nair A, Affo S, et al. Tumor restriction by type I collagen opposes tumor-promoting effects of cancer-associated fibroblasts. J Clin Invest [Internet]. 2021 Jun 1 [cited 2023 Jan 30];131(11). Available from: https://pubmed.ncbi.nlm.nih.gov/33905375/

365. Barbazán J, Matic Vignjevic D. Cancer associated fibroblasts: is the force the path to the dark side? Curr Opin Cell Biol [Internet]. 2019 Feb 1 [cited 2023 Jan 30];56:71–9. Available from: https://pubmed.ncbi.nlm.nih.gov/30308331/

366. Biffi G, Tuveson DA. Diversity and Biology of Cancer-Associated Fibroblasts. Physiol Rev [Internet]. 2021 Jan 1 [cited 2023 Feb 1];101(1):147. Available from: /pmc/articles/PMC7864232/

367. Kawka E, Witowski J, Bartosova M, Catar R, Rudolf A, Philippe A, et al. Thy-1+/- fibroblast subsets in the human peritoneum. Am J Physiol Renal Physiol. 2017;313(5):F1116–23.

368. Schliekelman MJ, Creighton CJ, Baird BN, Chen Y, Banerjee P, Bota-Rabassedas N, et al. Thy-1+ Cancer-associated Fibroblasts Adversely Impact Lung Cancer Prognosis. Sci Rep [Internet]. 2017;7(1):1–12. Available from: http://dx.doi.org/10.1038/s41598-017-06922-5

369. Burgos-Bravo F, Figueroa NL, Casanova-Morales N, Quest AFG, Wilson CAM, Leyton L. Single-molecule measurements of the effect of force on Thy-1/αvβ3-integrin interaction using nonpurified proteins. Mol Biol Cell. 2018;29(3):326–38.

370. Shentu TP, Huang TS, Cernelc-Kohan M, Chan J, Wong SS, Espinoza CR, et al. Thy-1 dependent uptake of mesenchymal stem cell-derived extracellular vesicles blocks myofibroblastic differentiation. Sci Rep [Internet]. 2017;7(1):1–11. Available from: http://dx.doi.org/10.1038/s41598-017-18288-9

371. Cohen PY, Breuer R, Wallach-Dayan SB. A profibrotic phenotype in naïve and in fibrotic lung myofibroblasts is governed by modulations in thy-1 expression and activation. Mediators Inflamm. 2018;2018:36–9.

372. Kumar A, Bhanja A, Bhattacharyya J, Jaganathan BG. Multiple roles of CD90 in cancer. Tumor Biology [Internet]. 2016;37(9):11611–22. Available from: http://dx.doi.org/10.1007/s13277-016-5112-0

373. Pascal LE, Ai J, Vêncio RZN, Vêncio EF, Zhou Y, Page LS, et al. Differential inductive signaling of CD90+ prostate cancer-associated fibroblasts compared to normal tissue stromal mesenchyme cells. Cancer Microenvironment. 2011;4(1):51–9.

374. Kieffer Y, Hocine HR, Gentric G, Pelon F, Bernard C, Bourachot B, et al. Single-Cell Analysis Reveals Fibroblast Clusters Linked to Immunotherapy Resistance in Cancer. Cancer Discov [Internet]. 2020 Sep 1 [cited 2023 Feb 1];10(9):1330–51. Available from: https://pubmed.ncbi.nlm.nih.gov/32434947/

375. Tratamiento del cáncer de colon según la etapa [Internet]. [cited 2022 Dec 1]. Available from: https://www.cancer.org/es/cancer/cancer-de-colon-o-recto/tratamiento/por-etapas-colon.html

376. Garcia-Vicién G, Mezheyeuski A, Micke P, Ruiz N, Ruffinelli JC, Mils K, et al. Spatial Immunology in Liver Metastases from Colorectal Carcinoma according to the Histologic Growth Pattern. Cancers (Basel). 2022;14(3).

377. Adam R, de Gramont A, Figueras J, Guthrie A, Kokudo N, Kunstlinger F, et al. The oncosurgery approach to managing liver metastases from colorectal cancer: a multidisciplinary international consensus. Oncologist [Internet]. 2012 Oct 1 [cited 2022 Dec 1];17(10):1225–39. Available from: https://pubmed.ncbi.nlm.nih.gov/22962059/

378. Höppener DJ, Galjart B, Nierop PMH, Buisman FE, van der Stok EP, Coebergh van den Braak RRJ, et al. Histopathological Growth Patterns and Survival After Resection of Colorectal Liver Metastasis: An External Validation Study. JNCI Cancer Spectr [Internet]. 2021 May 6 [cited 2022 Dec 1];5(3). Available from: https://pubmed.ncbi.nlm.nih.gov/34056541/

379. Tanis E, Julié C, Emile JF, Mauer M, Nordlinger B, Aust D, et al. Prognostic impact of immune response in resectable colorectal liver metastases treated by surgery alone or surgery with perioperative FOLFOX in the randomised EORTC study 40983. Eur J Cancer [Internet]. 2015 [cited 2022 Dec 1];51(17):2708–17. Available from: https://pubmed.ncbi.nlm.nih.gov/26342674/

380. Pagès F, Mlecnik B, Marliot F, Bindea G, Ou FS, Bifulco C, et al. International validation of the consensus Immunoscore for the classification of colon cancer: a prognostic and accuracy study. The Lancet. 2018;391(10135):2128–39.

381. Brunner SM, Kesselring R, Rubner C, Martin M, Jeiter T, Boerner T, et al. Prognosis according to histochemical analysis of liver metastases removed at liver resection. Br J Surg [Internet]. 2014 Dec 1 [cited 2022 Dec 20];101(13):1681–91. Available from: https://pubmed.ncbi.nlm.nih.gov/25331841/

382. Mlecnik B, van den Eynde M, Bindea G, Church SE, Vasaturo A, Fredriksen T, et al. Comprehensive intrametastatic immune quantification and major impact of immunoscore on survival. J Natl Cancer Inst. 2018 Jan 1;110(1):97–108.

383. van den Eynde M, Mlecnik B, Bindea G, Fredriksen T, Church SE, Lafontaine L, et al. The Link between the Multiverse of Immune Microenvironments in Metastases and the Survival of Colorectal Cancer Patients. Cancer Cell [Internet]. 2018 Dec 10 [cited 2022 Dec 20];34(6):1012-1026.e3. Available from: https://pubmed.ncbi.nlm.nih.gov/30537506/

384. Baldin P, van den Eynde M, Mlecnik B, Bindea G, Beniuga G, Carrasco J, et al. Prognostic assessment of resected colorectal liver metastases integrating pathological features, RAS mutation and Immunoscore. J Pathol Clin Res [Internet]. 2021 Jan 1 [cited 2022 Dec 20];7(1):27–41. Available from: https://pubmed.ncbi.nlm.nih.gov/32902189/

385. Berthel A, Zoernig I, Valous NA, Kahlert C, Klupp F, Ulrich A, et al. Detailed resolution analysis reveals spatial T cell heterogeneity in the invasive margin of colorectal cancer liver metastases associated with improved survival. Oncoimmunology [Internet]. 2017 Mar 4 [cited 2022 Dec 20];6(3). Available from: https://pubmed.ncbi.nlm.nih.gov/28405518/

386. Höppener DJ, Nierop PMH, Hof J, Sideras K, Zhou G, Visser L, et al. Enrichment of the tumour immune microenvironment in patients with desmoplastic colorectal liver metastasis. Br J Cancer [Internet]. 2020 Jul 21 [cited 2022 Dec 20];123(2):196–206. Available from: https://pubmed.ncbi.nlm.nih.gov/32418992/

387. van Dam PJ, Daelemans S, Ross E, Waumans Y, van Laere S, Latacz E, et al. Histopathological growth patterns as a candidate biomarker for immunomodulatory therapy. Semin Cancer Biol [Internet]. 2018 Oct 1 [cited 2022 Dec 20];52(Pt 2):86–93. Available from: https://pubmed.ncbi.nlm.nih.gov/29355613/

388. Yoshie O, Matsushima K. CCR4 and its ligands: from bench to bedside. Int Immunol [Internet]. 2015 Jan 1 [cited 2022 Dec 7];27(1):11–20. Available from: https://pubmed.ncbi.nlm.nih.gov/25087232/

389. Rojas J, Teran-Angel G, Barbosa L, Peterson DL, Berrueta L, Salmen S. Activation-dependent mitochondrial translocation of Foxp3 in human hepatocytes. Exp Cell Res [Internet]. 2016 May 1 [cited 2022 Dec 7];343(2):159–67. Available from: https://pubmed.ncbi.nlm.nih.gov/27068374/

390. Jia H, Qi H, Gong Z, Yang S, Ren J, Liu Y, et al. The expression of FOXP3 and its role in human cancers. Biochim Biophys Acta Rev Cancer [Internet]. 2019;1871(1):170–8. Available from: https://doi.org/10.1016/j.bbcan.2018.12.004

391. Vadasz Z, Toubi E. FoxP3 Expression in Macrophages, Cancer, and B Cells—Is It Real? Clin Rev Allergy Immunol. 2017;52(3):364–72.

392. Karlsson M, Zhang C, Méar L, Zhong W, Digre A, Katona B, et al. A single–cell type transcriptomics map of human tissues. Sci Adv. 2021 Jul 1;7(31).

393. Lundgren S, Elebro J, Heby M, Nodin B, Leandersson K, Micke P, et al. Quantitative, qualitative and spatial analysis of lymphocyte infiltration in periampullary and pancreatic adenocarcinoma. Int J Cancer [Internet]. 2020 Jun 15 [cited 2022 Dec 8];146(12):3461–73. Available from: https://pubmed.ncbi.nlm.nih.gov/32129882/

394. Ma GF, Chen SY, Sun ZR, Miao Q, Liu YM, Zeng XQ, et al. FoxP3 inhibits proliferation and induces apoptosis of gastric cancer cells by activating the apoptotic signaling pathway. Biochem Biophys Res Commun [Internet]. 2013 Jan 11 [cited 2022 Dec 7];430(2):804–9. Available from: https://pubmed.ncbi.nlm.nih.gov/23201402/

395. Martinez FO, Gordon S. The M1 and M2 paradigm of macrophage activation: time for reassessment. F1000Prime Rep [Internet]. 2014 Mar 3 [cited 2022 Dec 7];6. Available from: https://pubmed.ncbi.nlm.nih.gov/24669294/

396. Boutilier AJ, Elsawa SF. Macrophage Polarization States in the Tumor Microenvironment. Int J Mol Sci [Internet]. 2021 Jul 1 [cited 2022 Dec 7];22(13). Available from: /pmc/articles/PMC8268869/

397. Verreck FAW, de Boer T, Langenberg DML, Hoeve MA, Kramer M, Vaisberg E, et al. Human IL-23-producing type 1 macrophages promote but IL-10-producing type 2 macrophages subvert immunity to (myco)bacteria. Proc Natl Acad Sci U S A [Internet].

2004 Mar 30 [cited 2022 Dec 8];101(13):4560–5. Available from: https://pubmed.ncbi.nlm.nih.gov/15070757/

398. Columba-Cabezas S, Serafini B, Ambrosini E, Sanchez M, Penna G, Adorini L, et al. Induction of macrophage-derived chemokine/CCL22 expression in experimental autoimmune encephalomyelitis and cultured microglia: Implications for disease regulation. J Neuroimmunol [Internet]. 2002 Sep 1 [cited 2022 Dec 8];130(1–2):10–21. Available from: http://www.jni-journal.com/article/S0165572802001704/fulltext

399. Friedman G, Levi-Galibov O, David E, Bornstein C, Giladi A, Dadiani M, et al. Cancer-associated fibroblast compositions change with breast cancer progression linking the ratio of S100A4+ and PDPN+ CAFs to clinical outcome. Nat Cancer [Internet]. 2020;1(7):692–708. Available from: http://dx.doi.org/10.1038/s43018-020-0082-y

400. Alkasalias T, Moyano-Galceran L, Arsenian-Henriksson M, Lehti K. Fibroblasts in the tumor microenvironment: Shield or spear? Int J Mol Sci. 2018;19(5):1–21.

401. Lee K, Hwang H, Nam KT. Immune response and the tumor microenvironment: How they communicate to regulate gastric cancer. Gut Liver. 2014;8(2):131–9.

402. Falleni M, Savi F, Tosi D, Agape E, Cerri A, Moneghini L, et al. M1 and M2 macrophages' clinicopathological significance in cutaneous melanoma. Melanoma Res [Internet]. 2017 [cited 2022 Dec 8];27(3):200–10. Available from: https://pubmed.ncbi.nlm.nih.gov/28272106/

403. Anderson KM, Czinn SJ, Redline RW, Blanchard TG. Induction of CTLA-4-mediated anergy contributes to persistent colonization in the murine model of gastric Helicobacter pylori infection. J Immunol [Internet]. 2006 May 1 [cited 2022 Dec 20];176(9):5306–13. Available from: https://pubmed.ncbi.nlm.nih.gov/16621997/

404. Geng Y, Wang H, Lu C, Li Q, Xu B, Jiang J, et al. Expression of costimulatory molecules B7-H1, B7-H4 and Foxp3+ Tregs in gastric cancer and its clinical significance. Int J Clin Oncol. 2015 Apr 1;20(2):273–81.

405. Bloch O, Crane CA, Kaur R, Safaee M, Rutkowski MJ, Parsa AT. Gliomas promote immunosuppression through induction of B7-H1 expression in tumor-associated

macrophages. Clin Cancer Res [Internet]. 2013 Jun 15 [cited 2022 Dec 20];19(12):3165–75. Available from: https://pubmed.ncbi.nlm.nih.gov/23613317/

406. Allavena P, Mantovani A. Immunology in the clinic review series; focus on cancer: tumour-associated macrophages: undisputed stars of the inflammatory tumour microenvironment. Clin Exp Immunol [Internet]. 2012 Feb [cited 2022 Dec 20];167(2):195–205. Available from: https://pubmed.ncbi.nlm.nih.gov/22235995/

407. Obermajer N, Muthuswamy R, Odunsi K, Edwards RP, Kalinski P. PGE(2)-induced CXCL12 production and CXCR4 expression controls the accumulation of human MDSCs in ovarian cancer environment. Cancer Res [Internet]. 2011 Dec 15 [cited 2022 Dec 20];71(24):7463–70. Available from: https://pubmed.ncbi.nlm.nih.gov/22025564/

408. Jeong H, Kim S, Hong BJ, Lee CJ, Kim YE, Bok S, et al. Tumor-Associated Macrophages Enhance Tumor Hypoxia and Aerobic Glycolysis. Cancer Res [Internet]. 2019 Feb 15 [cited 2022 Dec 20];79(4):795–806. Available from: https://pubmed.ncbi.nlm.nih.gov/30610087/

409. Jetten N, Verbruggen S, Gijbels MJ, Post MJ, de Winther MPJ, Donners MMPC. Anti-inflammatory M2, but not pro-inflammatory M1 macrophages promote angiogenesis in vivo. Angiogenesis [Internet]. 2014 Jan [cited 2022 Dec 20];17(1):109–18. Available from: https://pubmed.ncbi.nlm.nih.gov/24013945/

410. Murray PJ. Macrophage Polarization. Annu Rev Physiol [Internet]. 2017 Feb 10 [cited 2022 Dec 8];79:541–66. Available from: https://pubmed.ncbi.nlm.nih.gov/27813830/

411. Wynn TA, Chawla A, Pollard JW. Macrophage biology in development, homeostasis and disease. Nature [Internet]. 2013 Apr 25 [cited 2022 Dec 8];496(7446):445–55. Available from: https://pubmed.ncbi.nlm.nih.gov/23619691/

412. Laviron M, Boissonnas A. Ontogeny of Tumor-Associated Macrophages. Front Immunol [Internet]. 2019 [cited 2022 Dec 8];10:1799. Available from: https://pubmed.ncbi.nlm.nih.gov/31417566/

413. van de Laar L, Saelens W, de Prijck S, Martens L, Scott CL, van Isterdael G, et al. Yolk Sac Macrophages, Fetal Liver, and Adult Monocytes Can Colonize an Empty Niche and

Develop into Functional Tissue-Resident Macrophages. Immunity [Internet]. 2016 Apr 19 [cited 2022 Dec 8];44(4):755–68. Available from: https://pubmed.ncbi.nlm.nih.gov/26992565/

414. Lavin Y, Winter D, Blecher-Gonen R, David E, Keren-Shaul H, Merad M, et al. Tissue-resident macrophage enhancer landscapes are shaped by the local microenvironment. Cell [Internet]. 2014 Dec 4 [cited 2022 Dec 8];159(6):1312–26. Available from: https://pubmed.ncbi.nlm.nih.gov/25480296/

415. CD5L protein expression summary - The Human Protein Atlas [Internet]. [cited 2022 Dec 8]. Available from: https://www.proteinatlas.org/ENSG00000073754-CD5L

416. Sun H, Song J, Weng C, Xu J, Huang M, Huang Q, et al. Association of decreased expression of the macrophage scavenger receptor MARCO with tumor progression and poor prognosis in human hepatocellular carcinoma. J Gastroenterol Hepatol [Internet]. 2017 May 1 [cited 2022 Dec 9];32(5):1107–14. Available from: https://pubmed.ncbi.nlm.nih.gov/27806438/

417. Takayama H, Nonomura N, Nishimura K, Oka D, Shiba M, Nakai Y, et al. Decreased immunostaining for macrophage scavenger receptor is associated with poor prognosis of prostate cancer. BJU Int [Internet]. 2009 Feb [cited 2022 Dec 9];103(4):470–4. Available from: https://pubmed.ncbi.nlm.nih.gov/18778349/

418. Mezheyeuski A, Backman M, Mattsson J, Martín-Bernabé A, Larsson C, Hrynchyk I, et al. The ratio of cytotoxic lymphocytes to M2-like macrophages is prognostic in immunogenic tumors. bioRxiv [Internet]. 2021 Mar 24 [cited 2022 Dec 9];2021.03.24.436814. Available from: https://www.biorxiv.org/content/10.1101/2021.03.24.436814v1

419. Fan Z, Yu P, Wang Y, Wang Y, Fu ML, Liu W, et al. NK-cell activation by LIGHT triggers tumor-specific CD8+ T-cell immunity to reject established tumors. Blood [Internet]. 2006 Feb 15 [cited 2022 Dec 20];107(4):1342–51. Available from: https://pubmed.ncbi.nlm.nih.gov/16223768/

420. Kowal K, Silver R, Sławińska E, Bielecki M, Chyczewski L, Kowal-Bielecka O. CD163 and its role in inflammation. Folia Histochem Cytobiol [Internet]. 2011 [cited 2022 Dec 9];49(3):365–74. Available from: https://pubmed.ncbi.nlm.nih.gov/22038213/

421. Öhlund D, Handly-Santana A, Biffi G, Elyada E, Almeida AS, Ponz-Sarvise M, et al. Distinct populations of inflammatory fibroblasts and myofibroblasts in pancreatic cancer. J Exp Med. 2017;214(3):579–96.

422. Wagner NB, Weide B, Gries M, Reith M, Tarnanidis K, Schuermans V, et al. Tumor microenvironment-derived S100A8/A9 is a novel prognostic biomarker for advanced melanoma patients and during immunotherapy with anti-PD-1 antibodies. J Immunother Cancer [Internet]. 2019 Dec 5 [cited 2022 Dec 10];7(1). Available from: https://pubmed.ncbi.nlm.nih.gov/31806053/

423. Huang CH, Kuo CJ, Liang SS, Chi SW, Hsi E, Chen CC, et al. Onco-proteogenomics identifies urinary S100A9 and GRN as potential combinatorial biomarkers for early diagnosis of hepatocellular carcinoma. BBA Clin [Internet]. 2015 Jun 1 [cited 2022 Dec 10];3:205–13. Available from: https://pubmed.ncbi.nlm.nih.gov/26675302/

424. Meng J, Gu F, Fang H, Qu B. Elevated Serum S100A9 Indicated Poor Prognosis in Hepatocellular Carcinoma after Curative Resection. J Cancer [Internet]. 2019 [cited 2022 Dec 10];10(2):408. Available from: /pmc/articles/PMC6360318/

425. Zhao Z, Zhang C, Zhao Q. S100A9 as a novel diagnostic and prognostic biomarker in human gastric cancer. Scand J Gastroenterol [Internet]. 2020 Mar 3 [cited 2022 Dec 10];55(3):338–46. Available from: https://pubmed.ncbi.nlm.nih.gov/32172630/

426. Nedjadi T, Evans A, Sheikh A, Barerra L, Al-Ghamdi S, Oldfield L, et al. S100A8 and S100A9 proteins form part of a paracrine feedback loop between pancreatic cancer cells and monocytes. BMC Cancer [Internet]. 2018 Dec 17 [cited 2022 Dec 10];18(1). Available from: https://pubmed.ncbi.nlm.nih.gov/30558665/

427. Zhou M, Li M, Liang X, Zhang Y, Huang H, Feng Y, et al. The Significance of Serum S100A9 and TNC Levels as Biomarkers in Colorectal Cancer. J Cancer [Internet]. 2019 [cited 2022 Dec 10];10(22):5315–23. Available from: https://pubmed.ncbi.nlm.nih.gov/31632476/

428. Tidehag V, Hammarsten P, Egevad L, Granfors T, Stattin P, Leanderson T, et al. High density of S100A9 positive inflammatory cells in prostate cancer stroma is associated with poor outcome. Eur J Cancer [Internet]. 2014 [cited 2022 Dec 10];50(10):1829–35. Available from: https://pubmed.ncbi.nlm.nih.gov/24726733/

429. Salama I, Malone PS, Mihaimeed F, Jones JL. A review of the S100 proteins in cancer. Eur J Surg Oncol [Internet]. 2008 Apr [cited 2022 Dec 10];34(4):357–64. Available from: https://pubmed.ncbi.nlm.nih.gov/17566693/

430. Liao J, Li JZ, Xu J, Xu Y, Wen WP, Zheng L, et al. High S100A9+ cell density predicts a poor prognosis in hepatocellular carcinoma patients after curative resection. Aging [Internet]. 2021 Jun 30 [cited 2022 Dec 10];13(12):16367–80. Available from: https://pubmed.ncbi.nlm.nih.gov/34157683/

431. Arai K, Takano S, Teratani T, Ito Y, Yamada T, Nozawa R. S100A8 and S100A9 overexpression is associated with poor pathological parameters in invasive ductal carcinoma of the breast. Curr Cancer Drug Targets [Internet]. 2008 Jun 3 [cited 2022 Dec 10];8(4):243–52. Available from: https://pubmed.ncbi.nlm.nih.gov/18537548/

432. Yan LL, Huang YJ, Yi X, Yan XM, Cai Y, He Q, et al. Effects of silencing S100A8 and S100A9 with small interfering RNA on the migration of CNE1 nasopharyngeal carcinoma cells. Oncol Lett [Internet]. 2015 [cited 2022 Dec 10];9(6):2534–40. Available from: https://pubmed.ncbi.nlm.nih.gov/26137102/

433. Hermani A, Hess J, de Servi B, Medunjanin S, Grobholz R, Trojan L, et al. Calcium-binding proteins S100A8 and S100A9 as novel diagnostic markers in human prostate cancer. Clin Cancer Res [Internet]. 2005 Jul 15 [cited 2022 Dec 10];11(14):5146–52. Available from: https://pubmed.ncbi.nlm.nih.gov/16033829/

434. Kawai H, Minamiya Y, Takahashi N. Prognostic impact of S100A9 overexpression in non-small cell lung cancer. Tumour Biol [Internet]. 2011 [cited 2022 Dec 10];32(4):641–6. Available from: https://pubmed.ncbi.nlm.nih.gov/21369941/

435. Arai K, Yamada T, Nozawa R. Immunohistochemical investigation of migration inhibitory factor-related protein (MRP)-14 expression in hepatocellular carcinoma.

Med Oncol [Internet]. 2000 [cited 2022 Dec 10];17(3):183–8. Available from: https://pubmed.ncbi.nlm.nih.gov/10962528/

436. Hermani A, Hess J, de Servi B, Medunjanin S, Grobholz R, Trojan L, et al. Calcium-binding proteins S100A8 and S100A9 as novel diagnostic markers in human prostate cancer. Clin Cancer Res [Internet]. 2005 Jul 15 [cited 2022 Dec 10];11(14):5146–52. Available from: https://pubmed.ncbi.nlm.nih.gov/16033829/

437. Wagner NB, Weide B, Reith M, Tarnanidis K, Kehrel C, Lichtenberger R, et al. Diminished levels of the soluble form of RAGE are related to poor survival in malignant melanoma. Int J Cancer [Internet]. 2015 Dec 1 [cited 2022 Dec 10];137(11):2607–17. Available from: https://pubmed.ncbi.nlm.nih.gov/26018980/

438. Sinha P, Okoro C, Foell D, Freeze HH, Ostrand-Rosenberg S, Srikrishna G. Proinflammatory S100 proteins regulate the accumulation of myeloid-derived suppressor cells. J Immunol [Internet]. 2008 Oct 1 [cited 2022 Dec 10];181(7):4666–75. Available from: https://pubmed.ncbi.nlm.nih.gov/18802069/

439. Cheng P, Corzo CA, Luetteke N, Yu B, Nagaraj S, Bui MM, et al. Inhibition of dendritic cell differentiation and accumulation of myeloid-derived suppressor cells in cancer is regulated by S100A9 protein. J Exp Med [Internet]. 2008 Sep 29 [cited 2022 Dec 10];205(10):2235–49. Available from: https://pubmed.ncbi.nlm.nih.gov/18809714/

440. Hibino T, Sakaguchi M, Miyamoto S, Yamamoto M, Motoyama A, Hosoi J, et al. S100A9 is a novel ligand of EMMPRIN that promotes melanoma metastasis. Cancer Res [Internet]. 2013 Jan 1 [cited 2022 Dec 10];73(1):172–83. Available from: https://pubmed.ncbi.nlm.nih.gov/23135911/

441. Coffelt SB, Kersten K, Doornebal CW, Weiden J, Vrijland K, Hau CS, et al. IL-17-producing γδ T cells and neutrophils conspire to promote breast cancer metastasis. Nature [Internet]. 2015 Jun 18 [cited 2022 Dec 10];522(7556):345–8. Available from: https://pubmed.ncbi.nlm.nih.gov/25822788/

442. Chung JYF, Chan MKK, Li JSF, Chan ASW, Tang PCT, Leung KT, et al. TGF-β Signaling: From Tissue Fibrosis to Tumor Microenvironment. International Journal of Molecular Sciences 2021, Vol 22, Page 7575 [Internet]. 2021 Jul 15 [cited 2022 Dec

11];22(14):7575. Available from: https://www.mdpi.com/1422-0067/22/14/7575/htm

443. Huang M, Wu R, Chen L, Peng Q, Li S, Zhang Y, et al. S100A9 Regulates MDSCs-Mediated Immune Suppression via the RAGE and TLR4 Signaling Pathways in Colorectal Carcinoma. Front Immunol [Internet]. 2019 Sep 18 [cited 2022 Dec 10];10. Available from: https://pubmed.ncbi.nlm.nih.gov/31620141/

444. Weide B, Martens A, Zelba H, Stutz C, Derhovanessian E, di Giacomo AM, et al. Myeloid-derived suppressor cells predict survival of patients with advanced melanoma: comparison with regulatory T cells and NY-ESO-1- or melan-A-specific T cells. Clin Cancer Res [Internet]. 2014 [cited 2022 Dec 10];20(6):1601–9. Available from: https://pubmed.ncbi.nlm.nih.gov/24323899/

445. Gebhardt C, Sevko A, Jiang H, Lichtenberger R, Reith M, Tarnanidis K, et al. Myeloid Cells and Related Chronic Inflammatory Factors as Novel Predictive Markers in Melanoma Treatment with Ipilimumab. Clin Cancer Res [Internet]. 2015 Dec 15 [cited 2022 Dec 10];21(24):5453–9. Available from: https://pubmed.ncbi.nlm.nih.gov/26289067/

446. Prud'homme GJ. Pathobiology of transforming growth factor beta in cancer, fibrosis and immunologic disease, and therapeutic considerations. Lab Invest [Internet]. 2007 Nov [cited 2022 Dec 11];87(11):1077–91. Available from: https://pubmed.ncbi.nlm.nih.gov/17724448/

447. Meng XM, Tang PMK, Li J, Lan HY. TGF-β/Smad signaling in renal fibrosis. Front Physiol [Internet]. 2015 [cited 2022 Dec 11];6(MAR). Available from: https://pubmed.ncbi.nlm.nih.gov/25852569/

448. Zhao H, Wei J, Sun J. Roles of TGF-β signaling pathway in tumor microenvirionment and cancer therapy. Int Immunopharmacol [Internet]. 2020 Dec 1 [cited 2022 Dec 11];89(Pt B). Available from: https://pubmed.ncbi.nlm.nih.gov/33099067/

449. Tang PMK, Zhou S, Meng XM, Wang QM, Li CJ, Lian GY, et al. Smad3 promotes cancer progression by inhibiting E4BP4-mediated NK cell development. Nat Commun

[Internet]. 2017 Mar 6 [cited 2022 Dec 11];8. Available from: https://pubmed.ncbi.nlm.nih.gov/28262747/

450. David CJ, Massagué J. Contextual determinants of TGFβ action in development, immunity and cancer. Nat Rev Mol Cell Biol [Internet]. 2018 Jul 1 [cited 2022 Dec 11];19(7):419–35. Available from: https://pubmed.ncbi.nlm.nih.gov/29643418/

451. Fridlender ZG, Sun J, Kim S, Kapoor V, Cheng G, Ling L, et al. Polarization of tumor-associated neutrophil phenotype by TGF-beta: "N1" versus "N2" TAN. Cancer Cell [Internet]. 2009 Sep 8 [cited 2022 Dec 11];16(3):183–94. Available from: https://pubmed.ncbi.nlm.nih.gov/19732719/

452. Germann M, Zangger N, Sauvain M, Sempoux C, Bowler AD, Wirapati P, et al. Neutrophils suppress tumor-infiltrating T cells in colon cancer via matrix metalloproteinase-mediated activation of TGFβ. EMBO Mol Med [Internet]. 2020 Jan 9 [cited 2022 Dec 11];12(1). Available from: https://pubmed.ncbi.nlm.nih.gov/31793740/

453. Regis S, Dondero A, Caliendo F, Bottino C, Castriconi R. NK Cell Function Regulation by TGF-β-Induced Epigenetic Mechanisms. Front Immunol [Internet]. 2020 Feb 25 [cited 2022 Dec 11];11. Available from: https://pubmed.ncbi.nlm.nih.gov/32161594/

454. Zhang F, Wang H, Wang X, Jiang G, Liu H, Zhang G, et al. TGF-β induces M2-like macrophage polarization via SNAIL-mediated suppression of a pro-inflammatory phenotype. Oncotarget [Internet]. 2016 Aug 1 [cited 2022 Dec 11];7(32):52294–306. Available from: https://pubmed.ncbi.nlm.nih.gov/27418133/

455. Rodell CB, Arlauckas SP, Cuccarese MF, Garris CS, Li R, Ahmed MS, et al. TLR7/8-agonist-loaded nanoparticles promote the polarization of tumour-associated macrophages to enhance cancer immunotherapy. Nat Biomed Eng [Internet]. 2018 Aug 1 [cited 2022 Dec 11];2(8):578–88. Available from: https://pubmed.ncbi.nlm.nih.gov/31015631/

456. Welch-Reardon KM, Ehsan SM, Wang K, Wu N, Newman AC, Romero-Lopez M, et al. Angiogenic sprouting is regulated by endothelial cell expression of Slug. J Cell Sci

[Internet]. 2014 [cited 2022 Dec 11];127(Pt 9):2017–28. Available from: https://pubmed.ncbi.nlm.nih.gov/24554431/

457. Flier JS, Underhill LH, Dvorak HF. Tumors: wounds that do not heal. Similarities between tumor stroma generation and wound healing. N Engl J Med [Internet]. 1986 Dec 25 [cited 2022 Dec 11];315(26):1650–9. Available from: https://pubmed.ncbi.nlm.nih.gov/3537791/

458. Rybinski B, Franco-Barraza J, Cukierman E. The wound healing, chronic fibrosis, and cancer progression triad. Physiol Genomics [Internet]. 2014 Apr 1 [cited 2022 Dec 11];46(7):223–44. Available from: https://pubmed.ncbi.nlm.nih.gov/24520152/

459. Lamprecht S, Sigal-Batikoff I, Shany S, Abu-Freha N, Ling E, Delinasios GJ, et al. Teaming Up for Trouble: Cancer Cells, Transforming Growth Factor-β1 Signaling and the Epigenetic Corruption of Stromal Naïve Fibroblasts. Cancers (Basel) [Internet]. 2018 Mar 1 [cited 2022 Dec 11];10(3). Available from: https://pubmed.ncbi.nlm.nih.gov/29495500/

460. Biffi G, Oni TE, Spielman B, Hao Y, Elyada E, Park Y, et al. IL1-Induced JAK/STAT Signaling Is Antagonized by TGFβ to Shape CAF Heterogeneity in Pancreatic Ductal Adenocarcinoma. Cancer Discov [Internet]. 2019 [cited 2022 Dec 11];9(2):282–301. Available from: https://pubmed.ncbi.nlm.nih.gov/30366930/

461. Chen ML, Pittet MJ, Gorelik L, Flavell RA, Weissleder R, von Boehmer H, et al. Regulatory T cells suppress tumor-specific CD8 T cell cytotoxicity through TGF-beta signals in vivo. Proc Natl Acad Sci U S A [Internet]. 2005 Jan 11 [cited 2022 Dec 11];102(2):419–24. Available from: https://pubmed.ncbi.nlm.nih.gov/15623559/

462. Zhu J, Davidson TS, Wei G, Jankovic D, Cui K, Schones DE, et al. Down-regulation of Gfi-1 expression by TGF-beta is important for differentiation of Th17 and CD103+ inducible regulatory T cells. J Exp Med [Internet]. 2009 Feb 16 [cited 2022 Dec 11];206(2):329–41. Available from: https://pubmed.ncbi.nlm.nih.gov/19188499/

463. Das J, Ren G, Zhang L, Roberts AI, Zhao X, Bothwell ALM, et al. Transforming growth factor beta is dispensable for the molecular orchestration of Th17 cell differentiation.

J Exp Med [Internet]. 2009 Oct 26 [cited 2022 Dec 11];206(11):2407–16. Available from: https://pubmed.ncbi.nlm.nih.gov/19808254/

464. Valderrama-Carvajal H, Cocolakis E, Lacerte A, Lee EH, Krystal G, Ali S, et al. Activin/TGF-beta induce apoptosis through Smad-dependent expression of the lipid phosphatase SHIP. Nat Cell Biol [Internet]. 2002 Dec 1 [cited 2022 Dec 11];4(12):963–9. Available from: https://pubmed.ncbi.nlm.nih.gov/12447389/

465. Ruffell B, Chang-Strachan D, Chan V, Rosenbusch A, Ho CMT, Pryer N, et al. Macrophage IL-10 blocks CD8+ T cell-dependent responses to chemotherapy by suppressing IL-12 expression in intratumoral dendritic cells. Cancer Cell [Internet]. 2014 Nov 10 [cited 2022 Dec 11];26(5):623–37. Available from: https://pubmed.ncbi.nlm.nih.gov/25446896/

466. Li X, Bu W, Meng L, Liu X, Wang S, Jiang L, et al. CXCL12/CXCR4 pathway orchestrates CSC-like properties by CAF recruited tumor associated macrophage in OSCC. Exp Cell Res [Internet]. 2019 May 15 [cited 2022 Dec 11];378(2):131–8. Available from: https://pubmed.ncbi.nlm.nih.gov/30857971/

467. Zhang Y, Ertl HCJ. Depletion of FAP+ cells reduces immunosuppressive cells and improves metabolism and functions CD8+T cells within tumors. Oncotarget [Internet]. 2016 Apr 26 [cited 2022 Dec 11];7(17):23282–99. Available from: https://pubmed.ncbi.nlm.nih.gov/26943036/

468. Yang X, Lin Y, Shi Y, Li B, Liu W, Yin W, et al. FAP Promotes Immunosuppression by Cancer-Associated Fibroblasts in the Tumor Microenvironment via STAT3-CCL2 Signaling. Cancer Res [Internet]. 2016 Jul 15 [cited 2022 Dec 11];76(14):4124–35. Available from: https://pubmed.ncbi.nlm.nih.gov/27216177/

469. Zhang S, Che D, Yang F, Chi C, Meng H, Shen J, et al. Tumor-associated macrophages promote tumor metastasis via the TGF-β/SOX9 axis in non-small cell lung cancer. Oncotarget [Internet]. 2017 [cited 2022 Dec 11];8(59):99801–15. Available from: https://pubmed.ncbi.nlm.nih.gov/29245941/

470. Huang H, Wang Z, Zhang Y, Pradhan RN, Ganguly D, Chandra R, et al. Mesothelial cell-derived antigen-presenting cancer-associated fibroblasts induce expansion of

regulatory T cells in pancreatic cancer. Cancer Cell [Internet]. 2022 Jun 13 [cited 2022 Dec 19];40(6):656-673.e7. Available from: https://pubmed.ncbi.nlm.nih.gov/35523176/

471. Foote AG, Wang Z, Kendziorski C, Thibeault SL. Tissue specific human fibroblast differential expression based on RNAsequencing analysis. BMC Genomics [Internet]. 2019 Apr 23 [cited 2023 Feb 17];20(1). Available from: https://pubmed.ncbi.nlm.nih.gov/31014251/

472. Elyada E, Bolisetty M, Laise P, Flynn WF, Courtois ET, Burkhart RA, et al. Cross-species single-cell analysis of pancreatic ductal adenocarcinoma reveals antigen-presenting cancer-associated fibroblasts. Cancer Discov. 2019;9(8):1102–23.

473. Dominguez CX, Müller S, Keerthivasan S, Koeppen H, Hung J, Gierke S, et al. Single-cell RNA sequencing reveals stromal evolution into LRRC15+ myofibroblasts as a determinant of patient response to cancer immunotherapy. Cancer Discov. 2020;10(2):232–53.

474. Karin D, Koyama Y, Brenner D, Kisseleva T. The characteristics of activated portal fibroblasts/myofibroblasts in liver fibrosis. Differentiation [Internet]. 2016 Sep 1 [cited 2023 Feb 17];92(3):84–92. Available from: https://pubmed.ncbi.nlm.nih.gov/27591095/

475. Wells RG. The portal fibroblast: not just a poor man's stellate cell. Gastroenterology [Internet]. 2014 [cited 2023 Feb 17];147(1):41–7. Available from: https://pubmed.ncbi.nlm.nih.gov/24814904/

476. Katsumata LW, Miyajima A, Itoh T. Portal fibroblasts marked by the surface antigen Thy1 contribute to fibrosis in mouse models of cholestatic liver injury. Hepatol Commun [Internet]. 2017 [cited 2023 Feb 17];1(3):198–214. Available from: https://pubmed.ncbi.nlm.nih.gov/29404454/

477. Jing XY, Yang XF, Qing K, Ou-Yang Y. Roles of the lipid metabolism in hepatic stellate cells activation △. Chin Med Sci J [Internet]. 2013 Dec [cited 2022 Dec 19];28(4):233–6. Available from: https://pubmed.ncbi.nlm.nih.gov/24382226/

478. Brodt P, editor. Liver Metastasis: Biology and Clinical Management. 2011 [cited 2022 Dec 20];16. Available from: http://link.springer.com/10.1007/978-94-007-0292-9

479. Shang L, Hosseini M, Liu X, Kisseleva T, Brenner DA. Human hepatic stellate cell isolation and characterization. J Gastroenterol [Internet]. 2018 Jan 1 [cited 2023 Feb 5];53(1):6–17. Available from: https://pubmed.ncbi.nlm.nih.gov/29094206/

480. Fujiwara K, Ohuchida K, Mizumoto K, Shindo K, Eguchi D, Kozono S, et al. CD271^{+} subpopulation of pancreatic stellate cells correlates with prognosis of pancreatic cancer and is regulated by interaction with cancer cells. PLoS One [Internet]. 2012 Dec 27 [cited 2023 Feb 5];7(12). Available from: https://pubmed.ncbi.nlm.nih.gov/23300742/

481. Ando R, Sakai A, Iida T, Kataoka K, Mizutani Y, Enomoto A. Good and Bad Stroma in Pancreatic Cancer: Relevance of Functional States of Cancer-Associated Fibroblasts. Cancers (Basel) [Internet]. 2022 Jul 1 [cited 2023 Feb 6];14(14). Available from: https://pubmed.ncbi.nlm.nih.gov/35884375/

482. Principe DR, DeCant B, Mascariñas E, Wayne EA, Diaz AM, Akagi N, et al. TGFβ signaling in the pancreatic tumor microenvironment promotes fibrosis and immune evasion to facilitate tumorigenesis. Cancer Res [Internet]. 2016 May 5 [cited 2023 Feb 20];76(9):2525. Available from: /pmc/articles/PMC4873388/

483. Street K, Risso D, Fletcher RB, Das D, Ngai J, Yosef N, et al. Slingshot: cell lineage and pseudotime inference for single-cell transcriptomics. BMC Genomics [Internet]. 2018 Jun 19 [cited 2023 Feb 6];19(1). Available from: https://pubmed.ncbi.nlm.nih.gov/29914354/

484. Bryce AS, Dreyer SB, Froeling FEM, Chang DK. Exploring the Biology of Cancer-Associated Fibroblasts in Pancreatic Cancer. Cancers (Basel) [Internet]. 2022 Oct 28 [cited 2023 Feb 6];14(21):5302. Available from: https://pubmed.ncbi.nlm.nih.gov/36358721/

485. Bronisz A, Godlewski J, Wallace JA, Merchant AS, Nowicki MO, Mathsyaraja H, et al. Reprogramming of the tumour microenvironment by stromal PTEN-regulated miR-

320. Nat Cell Biol [Internet]. 2011 Feb [cited 2023 Feb 5];14(2):159–67. Available from: https://pubmed.ncbi.nlm.nih.gov/22179046/

486. Bhowmick NA, Neilson EG, Moses HL. Stromal fibroblasts in cancer initiation and progression. Nature [Internet]. 2004 Nov 18 [cited 2023 Feb 5];432(7015):332–7. Available from: https://pubmed.ncbi.nlm.nih.gov/15549095/

487. Mueller MM, Fusenig NE. Friends or foes - bipolar effects of the tumour stroma in cancer. Nat Rev Cancer [Internet]. 2004 Nov [cited 2023 Feb 5];4(11):839–49. Available from: https://pubmed.ncbi.nlm.nih.gov/15516957/

488. Pellinen T, Paavolainen L, Martín-Bernabé A, Papatella Araujo R, Strell C, Mezheyeuski A, et al. Fibroblast subsets in non-small cell lung cancer: Associations with survival, mutations, and immune features. J Natl Cancer Inst [Internet]. 2023 Jan 10 [cited 2023 Feb 6];115(1). Available from: https://pubmed.ncbi.nlm.nih.gov/36083003/

489. Pan Y, Yu Y, Wang X, Zhang T. Tumor-Associated Macrophages in Tumor Immunity. Front Immunol [Internet]. 2020 Dec 3 [cited 2022 Dec 7];11. Available from: https://pubmed.ncbi.nlm.nih.gov/33365025/

490. Jackaman C, Tomay F, Duong L, Abdol Razak NB, Pixley FJ, Metharom P, et al. Aging and cancer: The role of macrophages and neutrophils. Ageing Res Rev [Internet]. 2017 Jul 1 [cited 2022 Dec 7];36:105–16. Available from: https://pubmed.ncbi.nlm.nih.gov/28390891/

491. Cheng Y, Li H, Deng Y, Tai Y, Zeng K, Zhang Y, et al. Cancer-associated fibroblasts induce PDL1+ neutrophils through the IL6-STAT3 pathway that foster immune suppression in hepatocellular carcinoma. Cell Death Dis. 2018;9(4).

492. Stadler M, Pudelko K, Biermeier A, Walterskirchen N, Gaigneaux A, Weindorfer C, et al. Stromal fibroblasts shape the myeloid phenotype in normal colon and colorectal cancer and induce CD163 and CCL2 expression in macrophages. Cancer Lett. 2021;520(July):184–200.

493. Mowery CT, Daud A, Bluestone JA. Immunotherapy Response in Liver Metastasis. 2021;5(52).

494. Han Y, Chai F, Wei J, Yue Y, Cheng J, Gu D, et al. Identification of Predominant Histopathological Growth Patterns of Colorectal Liver Metastasis by Multi-Habitat and Multi-Sequence Based Radiomics Analysis. Front Oncol [Internet]. 2020 Aug 14 [cited 2023 Feb 14];10. Available from: https://pubmed.ncbi.nlm.nih.gov/32923388/

495. Starmans MPA, Buisman FE, Renckens M, Willemssen FEJA, van der Voort SR, Groot Koerkamp B, et al. Distinguishing pure histopathological growth patterns of colorectal liver metastases on CT using deep learning and radiomics: a pilot study. Clin Exp Metastasis [Internet]. 2021;38(5):483–94. Available from: https://doi.org/10.1007/s10585-021-10119-6

496. Wei S, Han Y, Zeng H, Ye S, Cheng J, Chai F, et al. Radiomics diagnosed histopathological growth pattern in prediction of response and 1-year progression free survival for colorectal liver metastases patients treated with bevacizumab containing chemotherapy. Eur J Radiol [Internet]. 2021 Sep 1 [cited 2023 Feb 14];142. Available from: https://pubmed.ncbi.nlm.nih.gov/34343846/

497. Li WH, Wang S, Liu Y, Wang XF, Wang YF, Chai RM. Differentiation of histopathological growth patterns of colorectal liver metastases by MRI features. Quant Imaging Med Surg [Internet]. 2022 Jan 1 [cited 2023 Feb 14];12(1):608–17. Available from: https://pubmed.ncbi.nlm.nih.gov/34993105/

498. Rios-Doria J, Favata M, Lasky K, Feldman P, Lo Y, Yang G, et al. A Potent and Selective Dual Inhibitor of AXL and MERTK Possesses Both Immunomodulatory and Tumor-Targeted Activity. Front Oncol. 2020 Dec 7;10:2759.

499. Cannarile MA, Weisser M, Jacob W, Jegg AM, Ries CH, Rüttinger D. Colony-stimulating factor 1 receptor (CSF1R) inhibitors in cancer therapy. J Immunother Cancer [Internet]. 2017 Jul 18 [cited 2023 Feb 14];5(1). Available from: https://pubmed.ncbi.nlm.nih.gov/28716061/

500. Evaluation of Safety and Activity of an Anti-PDL1 Antibody (DURVALUMAB) Combined With CSF-1R TKI (PEXIDARTINIB) in Patients With Metastatic/Advanced Pancreatic or Colorectal Cancers - Full Text View - ClinicalTrials.gov [Internet]. [cited 2023 Feb 14]. Available from:

https://clinicaltrials.gov/ct2/show/NCT02777710?term=csf1r&cond=cancer&draw=2&rank=1

501. A Study of INCMGA00012, INCB001158, and the Combination in Japanese Participants With Advanced Solid Tumors - Full Text View - ClinicalTrials.gov [Internet]. [cited 2023 Feb 15]. Available from: https://clinicaltrials.gov/ct2/show/NCT03910530?term=NCT03910530&draw=2&rank=1

502. Brana I, Calles A, LoRusso PM, Yee LK, Puchalski TA, Seetharam S, et al. Carlumab, an anti-C-C chemokine ligand 2 monoclonal antibody, in combination with four chemotherapy regimens for the treatment of patients with solid tumors: an open-label, multicenter phase 1b study. Target Oncol [Internet]. 2015 Mar 1 [cited 2023 Feb 15];10(1):111–23. Available from: https://clinicaltrials.gov/ct2/show/NCT01204996

503. Efficacy Study of MCS110 Given With Carboplatin and Gemcitabine in Advanced Triple Negative Breast Cancer (TNBC) - Full Text View - ClinicalTrials.gov [Internet]. [cited 2023 Feb 15]. Available from: https://clinicaltrials.gov/ct2/show/NCT02435680?term=NCT02435680&draw=2&rank=1

504. Duan Z, Luo Y. Targeting macrophages in cancer immunotherapy. Signal Transduct Target Ther [Internet]. 2021 Dec 1 [cited 2023 Feb 15];6(1). Available from: https://pubmed.ncbi.nlm.nih.gov/33767177/

PUBLICATIONS

International Journal of
Molecular Sciences

MDPI

Review

The Tumor Microenvironment in Liver Metastases from Colorectal Carcinoma in the Context of the Histologic Growth Patterns

Gemma Garcia-Vicién [1,2], Artur Mezheyeuski [3], María Bañuls [1,2], Núria Ruiz-Roig [1,4] and David G. Molleví [1,2,*]

1 Tumoral and Stromal Chemoresistance Group, Molecular Mechanisms and Experimental Therapy in Oncology Program (ONCOBELL), Institut d'Investigació Biomèdica de Bellvitge—IDIBELL, 08908 L'Hospitalet de Llobregat, Spain; ggarciav@idibell.cat (G.G.-V.); maria.banuls@iconcologia.net (M.B.); nuria.ruiz@bellvitgehospital.cat (N.R.-R.)
2 Program Against Cancer Therapeutic Resistance (ProCURE), Catalan Institute of Oncology, 08908 L'Hospitalet de Llobregat, Spain
3 Department of Immunology, Genetics and Pathology, Uppsala University, 752 37 Uppsala, Sweden; artur.mezheyeuski@igp.uu.se
4 Department of Pathology, Hospital Universitari de Bellvitge, 08908 L'Hospitalet de Llobregat, Spain
* Correspondence: dgmollevi@iconcologia.net

Abstract: Colorectal carcinoma (CRC) is the third most common cancer. Likewise, it is a disease that has a long survival if it is prematurely detected. However, more than 50% of patients will develop metastases, mainly in the liver (LM-CRC), throughout the evolution of their disease, which accounts for most CRC-related deaths. Treatment it is certainly a controversial issue, since it has not been shown to increase overall survival in the adjuvant setting, although it does improve disease free survival (DFS). Moreover, current chemotherapy combinations are administered based on data extrapolated from primary tumors (PT), not considering that LM-CRC present a very particular tumor microenvironment that can radically condition the effectiveness of treatments designed for a PT. The liver has a particular histology and microenvironment that can determine tumor growth and response to treatments: double blood supply, vascularization through fenestrated sinusoids and the presence of different mesenchymal cell types, among other particularities. Likewise, the liver presents a peculiar immune response against tumor cells, a fact that correlates with the poor response to immunotherapy. All these aspects will be addressed in this review, putting them in the context of the histological growth patterns of LM-CRC, a particular pathologic feature with both prognostic and predictive repercussions.

Keywords: histologic growth patterns; desmoplasia; carcinoma-associated fibroblasts; microenvironment; liver; hepatic stellate cells; capsule

Citation: Garcia-Vicién, G.; Mezheyeuski, A.; Bañuls, M.; Ruiz-Roig, N.; Molleví, D.G. The Tumor Microenvironment in Liver Metastases from Colorectal Carcinoma in the Context of the Histologic Growth Patterns. *Int. J. Mol. Sci.* **2021**, *22*, 1544. https://doi.org/10.3390/ijms22041544

Academic Editor: Alfred King-Yin Lam
Received: 2 January 2021
Accepted: 29 January 2021
Published: 3 February 2021

1. Introduction

Colorectal carcinoma (CRC) is the third most frequent tumor in the world and the second in Europe. Taking both sexes into account, there are 1,850,000 new cases annually worldwide [1]. The incidence of this tumor increases by 2% each year and it is the primary cause of death due to cancer. The annual number of deaths is approximately half that of the incidence (880,000 deaths worldwide in 2020). Therefore, tackling this disease is one of the highest priority challenges in healthcare. Despite the best survival results with adjuvant chemotherapy since the publication of the MOSAIC study [2], approximately 20% of patients will develop metachronous metastases in the liver in less than three years following resection of the primary tumor and 25% displayed liver metastases at diagnosis (synchronous) [3]. In liver metastases from CRC (LM-CRC), curative surgery is the treatment of choice if it is performed in specialized centers. However, in these

advanced stages of the disease, the 5-year survival rates are less than 10%. Although only about 15% of metastases are initially resectable, this percentage can reach 30% if conversion chemotherapy is administered to selected patients. In the past few years, many treatment advances, such as more effective chemotherapy or staged hepatectomies, have emerged. However, despite the curative intent, there is a high rate of intrahepatic recurrence. Moreover, despite the fact that many retrospective studies have identified poor prognostic factors such as tumor size or number of lesions [4], none of them provide enough information to take surgical decisions. This fact highlights the need for new prognostic factors to select the best therapeutic approach for each patient.

In addition, a few advances in preclinical research have been translated into significant benefits, either in clinical terms or with respect to the quality of life of patients with LM-CRC. Despite important preclinical discoveries about aberrant biological pathways associated with the development and progression of the primary tumor, certain pathological aspects of the formation of liver metastases remain unknown.

A very common approach to study the biology of the metastatic process has been to compare the primary tumor and the metastatic lesions. Although great similarities between both tumors have been described at the genomic level [5], at the transcriptional level, relevant differences that reflect the particular microenvironment of each different location have been determined. The liver, to name a few examples, has exclusive stromal cells at this location, e.g., Kupffer cells, hepatic stellate cells (HSC) and portal fibroblasts (PF). Due to the great influence of the microenvironment on both the tumor biology and the response mechanisms to chemotherapy and targeted therapies, this fact should have a determining impact on the clinical management of patients with LM-CRC compared to patients without distant lesions.

Moreover, LM-CRC present different histological characteristics that accentuate their morphological differences from primary colorectal tumors. Thus, a remarkable presence of cancer-associated fibroblasts (CAFs), constituting the main stromal cell type and reaching 75–80% of the entire tumor mass, high interstitial pressure that hampers the delivery of drugs and a defective immunologic response from the host are essential to understand the therapeutic resistances of LM-CRC. Even considering possible therapeutic strategies focused on stromal cells, we must bear in mind that fibroblasts demonstrate certain topographic differentiation [6]. This means that the CAFs of a primary tumor may present different characteristics to the CAFs of a liver lesion [7,8] in the same patient, and therefore therapies designed against colonic CAFs may not be efficient enough over hepatic CAFs. On the other hand, liver metastases have displayed a unique histologic feature, a histologic growth pattern (HGP) [9], that will be described in more detail in the next section (Figure 1). Interestingly, these HGPs displayed prognostic [10,11] and predictive [12] value, suggesting that possibly intratumoral CAFs and peritumoral CAFs are exerting different functions that could be a consequence of either different origins or different cellular precursors, or particular responses of the host against the tumor type.

Thus, the tumor microenvironment in liver lesions presents unique and differential characteristics that are going to be highly relevant in the management of the patients. In the following sections, we will elucidate the relevance of the different cell types that shape up the liver microenvironment, the way in which they are structured, the altered immune response and the clinical and therapeutic consequences that can be derived from them.

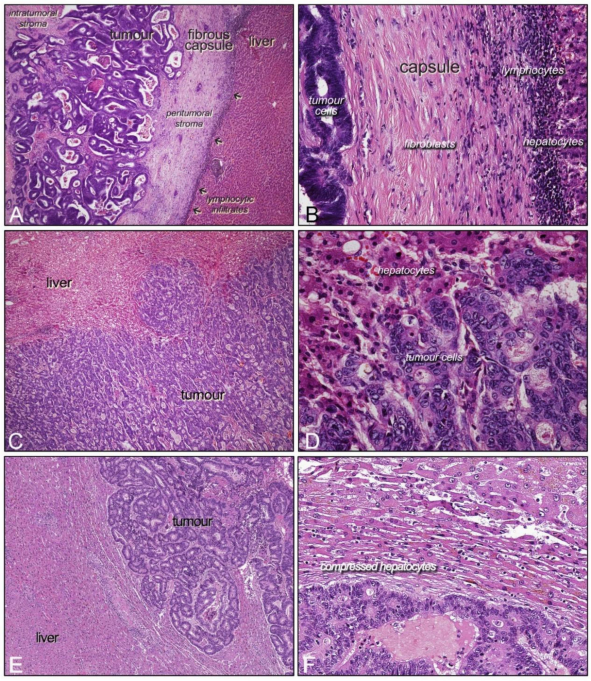

Figure 1. Hematoxylin and eosin staining of histologic growth patterns (HGPs) of liver metastases from colorectal cancer (LM-CRC). (**A**,**B**) encapsulating/desmoplastic, (**C**,**D**) invasive/replacement, and (**E**,**F**) expansive/pushing, the different HGPs at low magnification. In the right column, same patterns at detailed magnification.

2. Histology of LM-CRC

As mentioned before, LM-CRC are characterized at the histological level by their way of growing and infiltrating liver parenchyma. It is widely accepted by the scientific community that there are three main HGPs named "pushing", "replacement" and "desmoplastic", which were described for the first time in 1996 (including a fourth subtype, sinusoidal) [13], although the terminology was finally coined in 2001 [14] (Figure 1). The "desmoplastic" HGP is also named "encapsulated" and its most important feature is that tumoral cells are separated from liver parenchyma by a fibrotic stromal capsule; thus, tumoral cells and hepatocytes never touch. Conversely, in the "replacement" subtype, there is a direct contact between hepatocytes and tumoral cells. In "replacement" HGP, also called "invasive", tumor cells infiltrate liver parenchyma, replacing the hepatocytes and following the hepatic sinusoidal structure, which makes it difficult to clearly distinguish the tumor border [15]. Finally, in the "pushing" or "expansive" HGP, tumoral cells literally "push" the hepatocytes, which become flattened in consequence, and the tumor border is clearly demarcated, but no fibrotic tissue intervenes. However, there is no direct contact between hepatocytes and tumor cells.

The relevance of these distinct HGPs falls in their possible utility as a prognostic and predictive tool, due to its numerously described association with tumor recurrence and overall survival [10,16–18] as well as prediction of response to anti-angiogenic therapies [12]. On this matter, patients who present a predominantly desmoplastic growth pattern have superior survival after resection with curative intent when compared with patients presenting the replacement type [9–11,16,18,19]. Although a significant percentage of patients present a mixed pattern, with dHGP and non-dHGP areas, the most favorable prognosis is in those patients who present a pure dHGP pattern, complete throughout the entire liver–tumor interface [10]. Interesting, prognosis has also been related to the thickness of the capsule: the thicker the capsule, the better the prognosis [20].

These differences in survival could partially rely on the fact that, in the desmoplastic growth pattern, there is a band of stroma enriched in collagen and with dense lymphocytic infiltration that may act as a physical obstacle for the tumor expansion. This is particularity

emphasized by an increase in collagen type IV and integrin blockade, which reduces the infiltration capacity of tumoral cells through liver parenchyma [14,18].

In this line, the differences in recurrence rates could be explained by the HGP surgical implications. For mCRC, liver resection is the gold standard therapy, with a curative aim. The success of this therapy is closely related to the percentage of R0 resections achieved. It has been described that desmoplastic patterns are associated with an increased rate of R0 (tumor-cell-clean resection margins), probably because the stromal tissue surrounding the metastases protects against a margin-positive resection. Therefore, a resection with a more extended margin could benefit replacement and pushing cases [21].

Interestingly, HGPs have also been described in liver metastases from other types of cancer such as uveal melanoma [22,23], gastric cancer [24] and breast cancer [25], which adds interest to the predictive value of HGPs. However, because hepatectomy is less common in these cases, the prognostic role of HGPs is much less explored [21].

The lung is the second most common place where CRC metastasizes [26]. In fact, three different HGPs have also been described in CRC lung metastases. First, a pushing pattern, where tumoral cells compress pulmonary parenchyma. Second, a desmoplastic pattern, which also shows a desmoplastic rim containing immune infiltrates. Finally, third, an aerogenous pattern that can be considered as the analogue to the replacement pattern in liver as the tumor cells spread in the pulmonary air spaces without disrupting the lung architecture [27]. These HGPs observed in lung metastases also have clinical meaning, and the aerogenous pattern displays a poor prognosis, which concurs with liver replacement HGP as well. The brain is another organ where three metastatic patterns have been reported: a well-demarcated one, vascular co-option and diffuse infiltration; however, their impact on overall survival could not be assessed in autopsy studies [28]. Therefore, HGPs could have a role in guiding therapeutic decisions in many different contexts apart from LM-CRC. This also implies the need for predicting the HGP on different imaging modalities.

Another aspect to consider is how preoperative neoadjuvant treatment received by a proportion of patients with LM-CRC could affect the HGP and the ratios of cells that constitute the metastatic tumor microenvironment (TME). Concerning this, it has been described that in neoadjuvantly treated patients, the percentage of dHGP is higher. However, further investigation is needed, as most of the studies that attend this issue englobe different chemotherapeutic regimens [10]. Moreover, it has been reported that some features, such as the expression of a plasminogen receptor or the presence of CD68+ macrophages, differ between desmoplastic and non-desmoplastic HGPs but not in neoadjuvantly treated patients [29]. Thus, neoadjuvant chemotherapy is altering tumor growth in many different aspects, the study of which could be crucial for the development of better treatment strategies.

Taken together, HGPs are not only a distinct morphological feature of LM-CRC, but also a valuable prognostic marker. HGPs also reflect the biological processes underlying tumor growth. Moreover, therapy-induced conversion of non-dHGP into dHGP would improve the survival for the patients with metastatic disease dramatically. The development of such treatment, however, requires better understanding of the biological processes underlying metastatic growth.

3. Biology of LM-CRC

From a biology perspective, the mode through which metastases grow in the liver has awaked high interest as it should conceal the mechanisms underlying the previously described differences in prognosis. First, it is important to take into account that the progression of liver metastases consists of four phases, proposed for the first time by Vidal-Vanaclocha in 2011 [30], in which the hepatic microenvironment can play opposing roles [31]. The first one, called the microvascular phase, occurs in sinusoidal vessels when circulating tumor cells arrive [31,32]. At this timepoint, cancer cells need to be able to attach and adhere to the endothelial cell layer and, eventually, transmigrate through the vascular endothelium. This complex process is called extravasation and leads to the following second phase: pre-angiogenic or intra-lobular micrometastatic phase. In this

phase, stromal cells from liver and immune cells are recruited, but the micrometastases still do not show vascularization. In the third angiogenic or pan-lobular phase, the hypoxic microenvironment induces the recruitment of endothelial cells and formation of blood vessels. Finally, in the fourth lobar growth phase, the new tumor can be clinically detectable. The progression of these phases and the following growth of the metastasis depend on the interactions that occur between malignant cells and the liver microenvironment [31,32].

Thus, this process can be assessed in two ways. The local microenvironment can be considered as the major determinant of the host reaction on the tumor progression. In this case, the host tissue defines the development of a certain HGP and thus contains the key for explaining worse or better outcome. On the other hand, metastasized cancer cells interact with the different host cell types and, through the paracrine signaling, transform host stroma and determine HGP development. However, up to now, the formation of a particular HGP is still an unknown process, and there are no clues for a tumor-driven or a host-driven mechanism. A concept proposed by Fernando Vidal-Vanaclocha [33] distinguishes at least three different "entry points" for the cancer cells and thus three different metastatic niches which shape up the tumor–host interaction and drive the evolution of the tumor: periportal, perisinusoidal and intrasinusoidal. According to this concept, cancer cells which enter periportal and perisinusoidal spaces develop according to the "classical" process, following four phases, as described above. During the intra-lobular and pan-lobular phases, malignant cells invade parenchymal cell plates (perisinusoidal location) or the portal space (periportal location) and develop a pushing–desmoplastic phenotype, while intrasinusoidal metastases start proliferation already in the intravascular space, avoiding the extravasation phase. These metastases develop in a very distinct microenvironment, surrounded by liver sinusoidal endothelial cells (LSEC) and elements of the blood, which require different surviving mechanisms. During further growth, intrasinusoidal micrometastasis disrupts the sinusoid and develops a replacement HGP. However, these processes have not been experimentally demonstrated so far.

Concerning the host microenvironment, the liver harbors different stromal cells, which include host macrophages (Kupffer cells), host fibroblasts (HSC and PF), LSEC, liver-associated lymphocytes and dendritic cells [31,32]. Moreover, there are also circulating and bone marrow-derived immune cells that are recruited in response to the malignant growth. These host cells, as well as the recruited cells of the immune system, interact in a complex interplay of cytokines and chemokines that conform to the microenvironment in which the metastatic tumor growth takes place.

3.1. Liver Sinusoidal Endothelial Cells (LSEC)

LSEC play a crucial role, as they are the first host cells to be in direct contact with tumoral cells. LSEC are part of the first line of defense, also accompanied by Kupffer cells and hepatic natural killers, which may destroy tumor cells through the release of pro-apoptotic signals prior to extravasation [31,34]. However, LSEC can also promote attachment and adherence of the cancer cells by expressing cell surface adhesion molecules (CAM), thus facilitating metastasis formation [31]. Moreover, LSEC secrete fibronectin, which can induce an epithelial–mesenchymal transition in cancer cells, and macrophage migration inhibitory factor [35,36]. In addition, LSEC can also be a key player for HGP development as they are closely related to the metastasis vascularization pattern [31,37–39].

Finally, LSEC are endocytic cells that scavenge molecules from the bloodstream and present them to hepatic lymphocytes, which leads to a physiological immune regulation towards tolerance preventing liver parenchymal damage. However, during hepatic metastasis development, tumor-activated LSEC become highly inflamed which fosters their immune suppressive effect, especially in the replacement HGP [27]. As shown in an experimental model of hepatic CRC metastasis, the mechanism is contributed by IL-1-induced LSEC mannose receptors [40].

3.2. Cancer-Associated Fibroblasts

As it happens in primary tumors [8], LM-CRC are characterized by desmoplasia, which is defined as the presence of a high amount of stroma among the malignant cells. This reactive stroma creates the proper environment for tumor development and CAFs are the main component of it. In a desmoplastic TME, CAFs interact with the extracellular matrix and with the other cells and mediate processes that favor tumor cells: promoting tumor cell proliferation and migration, supporting stem cell niche generation, regulating immune suppression and influencing chemoresistance.

In general terms, fibroblasts in physiological conditions remain in a quiescent state and become activated in case of tissue damage. Similarly, CAFs are fibroblasts that have been activated by the interaction with tumor cells. This activation implies morphological changes and the expression of a plethora of CAFs markers, such as α-smooth muscle actin, periostin and fibroblast activating protein (FAP). This marker expression pattern changes markedly depending on the CAFs' location both inside the tumor and in their anatomic demarcation [7]. Once they are activated, CAFs generate the collagens and fibronectin that conform to the extracellular matrix, as well as crosstalking with tumor cells through cytokines and growth factors [41].

Moreover, in different types of cancer, the quantity of CAFs is associated with bad prognosis [42–44]. However, the existence of different CAF subpopulations associated with different functions has been demonstrated [45,46]. Thus, they have to be considered as heterogeneous cells and the biomarkers to characterize these different subpopulations need to be defined [8,47,48].

In addition, CAFs also play an important role in the process of chemoresistance [49]. They can create a physical barrier that hinders the drugs to reach the tumor cells or alter drugs' function through factors production [50–52].

For all these reasons, CAFs are considered to be a potential therapeutic target for desmoplastic tumors. Therefore, many research groups have focused on developing therapeutic strategies for the elimination of CAFs, which have shown opposite effects. Thus, the inhibition of CAFs' functions had a positive effect on sensitizing tumoral cells to treatments [48,53–55]. On the contrary, other studies have shown that CAF depletion can also result in a protumoral effect [53]. Therefore, this further suggests the coexistence of different CAF subpopulations associated with different functions [53].

In the context of LM-CRC, the function of CAFs remains unclear. However, as these metastases have been shown to grow in different HGPs associated with prognosis, CAFs located in particular topographic areas of the tumor, e.g., peritumoral/encapsulating CAFs, CAFs in invasive margins or CAFs in central tumoral areas, might be playing different roles and probably reflect different temporal processes (Figure 2).

In other types of cancer, such as pancreas [56], breast [57] and lung cancer [58,59], different subpopulations of CAFs have already been described. These publications highlight the fact that CAFs may change from one state to another depending on the context [60]. Other authors have classified CAFs according to their spatial location in pancreatic tumors, having observed a particular transcriptional signature at each location [61]. Despite these results, clearly more research is needed to elucidate the most accurate classification and association of particular subsets with functionality and spatial location.

Taking together, these data provide evidence that there may coexist subpopulations of CAFs performing both tumor-supportive and tumor-suppressive functions. These subpopulations can be shaped up by multiple factors such as the location inside the tumor, the origin of the CAF and the effect of chemotherapy and may vary between different tissues and anatomic demarcations. In this line, characterizing the degree of fibroblast heterogeneity as well as the dynamics of the different biomarkers would provide highly valuable tools to design new therapeutic strategies.

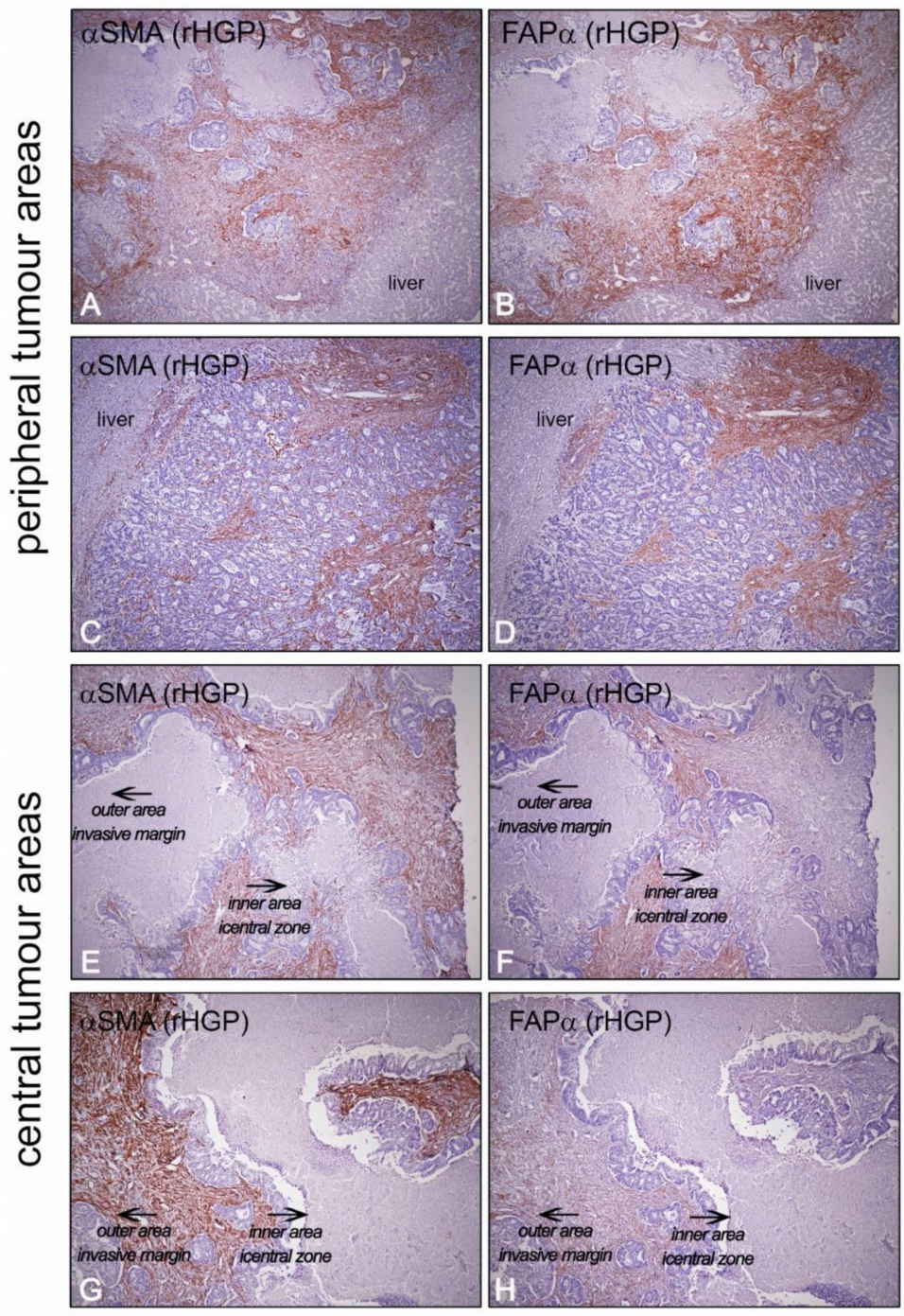

Figure 2. Different cancer-associated fibroblast (CAF) subsets might be topographically located in particular areas inside the LM-CRC. Although it is a fact that should be explored in detail with dedicated technologies such as spatial transcriptomics, invasive margins (**A**–**D**) displayed an intense staining of both αSMA and FAP. The outer regions of the liver metastases are those areas where there is a constant tissue remodeling and where tumor cells show more aggressive phenotypes, higher proliferation and migration capabilities. On the contrary, in central areas of the tumor (**E**–**H**), having the liver–tumor interface as a reference, a progressive decrease in FAP staining is observed, becoming negative in the most central and internal areas of the tumor. The staining of αSMA is quite homogeneous. These areas usually correspond to areas of secondary fibrosis enriched in myofibroblasts, probably corresponding to myCAFs. These areas are progressively repaired as the tumor grows. In these areas, the activation pattern of CAFs is different from those closest to the invasive margin (rHGP stands for the replacement histologic growth pattern).

Concerning the stromal reaction of the three HGPs, they can be simplified in two groups, the ones which show a fibrotic rim, the desmoplastic HGP (dHGP), and the ones that do not (non-dHGP). In this context, three different topographic locations of CAFs can be distinguished. First, CAFs present in the fibrotic rim of the dHGP, i.e., in peritumoral stromal areas. Second, CAFs located at the invasive margin, i.e., intratumoral CAFs located in outer tumoral areas. As the prognoses differ drastically in metastases that show 100% of dHGP, it may be plausible that peritumoral and intratumoral fibroblasts near to the host–tumor interface are different subsets with different functions, or particular juxtacrine and paracrine crosstalk with tumor cells might induce phenotypic differences with functional consequences (Figure 2). Third, intratumoral CAFs located in central tumoral regions, common for the different HGPs. These areas usually present large extensions formed mainly by myofibroblastic CAFs and extracellular matrix components and are often related to secondary fibrosis processes. These are areas where CAFs do not usually express FAP or other inflammatory CAF markers. In colloquial terms, we could say that these are areas where the battle between the tumor and the host has already ended—areas of injury that must be repaired.

The fibrotic rim of the dHGP is considered by many authors as a response to the inflammation and damage in the host tissue to the growing tumor. Moreover, the link between the presence of the desmoplastic capsule and a considerable better prognosis makes it possible to hypothesize that these CAFs play a tumor suppressor role, limiting physically and chemically the tumor growth and attracting immune infiltrates to act against malignant cells.

A few results seem to indicate that the fibrotic rim could be acting as a defensive barrier. First, the capsule could be mechanically acting as a protective shield avoiding local spreading. Second, it might be acting as a chemical barrier. Lunevicius et al. [62] described that the inner side of the capsule was enriched in collagen fibers and fibroblastic cells negative for metalloproteases. In contrast, the outer portion of the capsule was formed by cells expressing matrix metalloproteins (MMPs). In a similar vein, Illemann et al. [63] also described a difference in the cellular composition of the capsules, with the outer portion being enriched in αSMA-positive CAFs. What we observed in our laboratory is a certain gradient of positivity for some characteristic CAF markers. As summarized in Figure 3, we observed that the outer part of the capsule, the half side in contact with hepatocytes, is enriched in αSMA-expressing cells, while the inner part, in contact with tumor cells, is enriched in FAP-positive CAFs.

This gradient was also observed for periostin, fibronectin and podoplanin, which indicates that a certain differential degree of activation or a differential cellular composition could be occurring (Figure 4).

The differences observed in terms of the differential expression of certain proteins in the fibrotic rim raises the controversy whether this fact is due to the presence of different types of CAFs depending on their location in the capsule. In turn, the coexistence of different CAFs could imply that each of them came from a different precursor, a fact that has yet to be demonstrated. Another possibility is that it is a single cell type with high plasticity, as a consequence of the influence of tumor cells on the inner half of the capsule. However, defining the origin of activated myofibroblasts is one of the major challenges of the research on fibrosis, as those cells might be potential therapeutic targets against this remodeling process. In addition, several fibroblastic cells have been defined in the human liver [64]. In animal models, many different fibroblast origins have been also identified. Fibrocyte invasion, endogenous resident fibroblasts, pericytes and gli1-positive mesenchymal stem cells would be some examples. In the context of cancer, it is also a recurrent aspect to focus on, especially in the desmoplastic kind of tumor. This is the case of pancreatic cancer, where the two major stromal sources are resident pancreatic fibroblasts and stellate cells. In breast cancer, CAFs are thought to derive from pericytes, resident fibroblasts and even from the transformed epithelial cells via EMT. Thereby, the

origin of CAFs, as well as the origin of myofibroblasts in fibrosis, varies depending on the tissue [57,65].

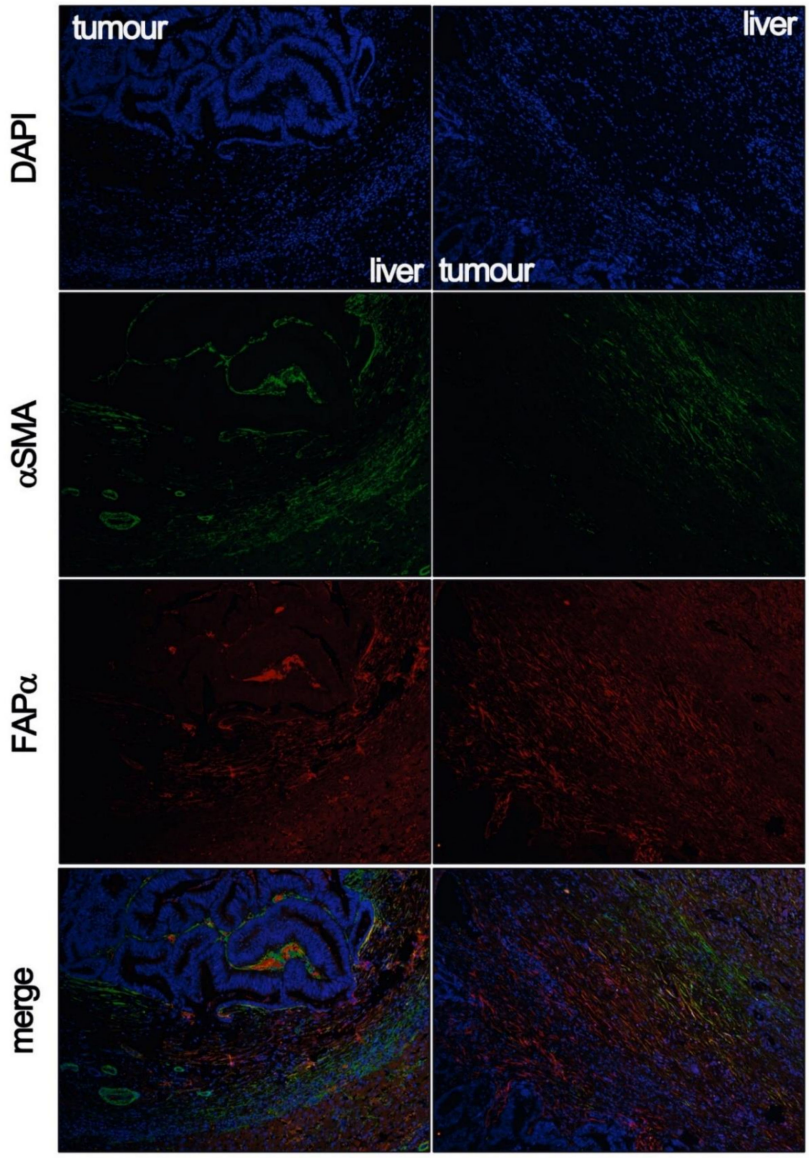

Figure 3. The fibrous capsules of liver metastases present CAFs that express different biomarkers classically associated with the activation of these cells. This fact enables two hypotheses, pending to be proved. On the one hand, it could be that different subpopulations coexisted in the same peritumoral area. On the other hand, it could be the same cells, which, depending on their proximity to the tumor cells, could establish a paracrine crosstalk with them, which would modulate the phenotype of the CAFs. The two columns of images correspond to two different encapsulating tumors, where positive αSMA CAFs (green immunofluorescence) are observed in the outer area of the capsule, the one closest to the liver parenchyma. On the contrary, in the inner area, αSMA positivity progressively disappears, while FAP-expressing cells (red immunofluorescence) appear as fibroblasts approach tumor cells. The FAP protein has two main locations, as a protein anchored to the plasma membrane, or as a component of the extracellular matrix (ECM). In some publications, it has been mentioned that fibrous capsules are formed by fibroblasts on their outermost layer and by acellular components on their innermost layer, mainly ECM components. However, DAPI staining indicates the presence of elongated nuclei that are compatible with the existence of CAFs in the deeper areas of the fibrous capsule.

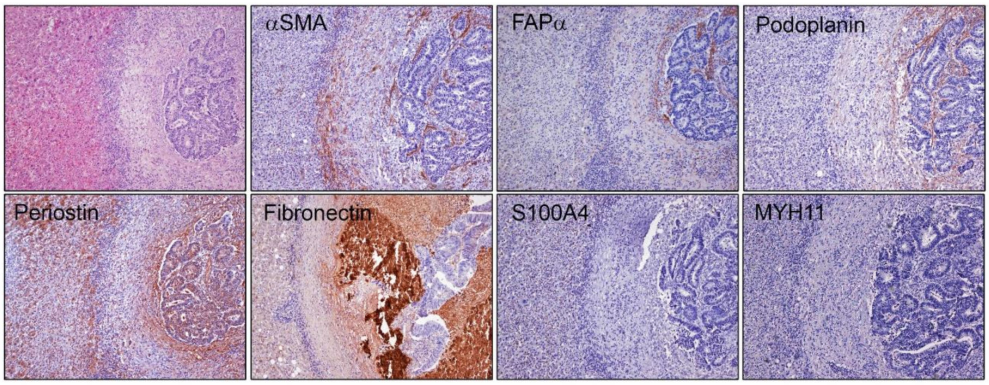

Figure 4. Immunohistochemical staining of a desmoplastic liver metastasis from CRC. We used classical markers for carcinoma-associated fibroblasts (αSMA, FAPα and S100A4). As shown in the microphotographs, the outer half of the capsule stains for αSMA-positive fibroblastic cells, while the inner half does it for FAPα, as also shown in Figure 3. We did not observe staining for S100A4 (also known as FSP1, Fibroblast Specific Protein 1) on cells of the capsule. Podoplanin, which is a type 1 integral membrane glycoprotein and is characteristic of particular CAF subsets, also stains in cells of the inner half of the membrane, as is the case for various proteins of the extracellular matrix, such as fibronectin and periostin (among others, not shown).

In the context of LM-CRC and fibrotic diseases of the liver, the three main sources described are resident mesenchymal cells, which include quiescent HSC and resident PF, but we cannot exclude other cells that have undergone EMT (hepatocytes, cholangiocytes and endothelial cells), and bone-marrow derived cells, consisting of fibrocytes and circulating mesenchymal cells. However, the origin of myofibroblasts may be different depending on the liver disease that causes the fibrosis [66].

In LM-CRC, many cell types have been discussed to contribute to the stromal reaction, such as smooth muscle cells or circulating mesenchymal cells. However, as currently considered, the main CAF sources in the liver are HSC, PF [67] and fibroblasts surrounding the centrolobular vein, the so-called second-layer cells [68].

HSC are in the space of Disse, around the sinusoidal LSEC, and represent 5% to 8% of the liver cellular population. In normal conditions, they are characterized for being in a quiescent state and containing lipid droplets with vitamin A [68]. Once activated, HSC acquire myofibroblast features such as αSMA expression and extracellular matrix deposition and become the orchestrating cells of the liver injury response [69]. In vitro, these cells have been reported to be able to undergo myofibroblastic transdifferentiation [70]. In hepatic metastases, HSC release growth factors and metalloproteinases and deposit type I and IV collagens and laminin [31]. They are also involved in endothelial cell recruitment and neoangiogenesis [71], as well as in tumor cell invasion and proliferation [31]. On the other hand, PF can also be the origin of CAFs when cancer cells are located in portal tracts, but they probably initiate the stromal response through a different process.

Finally, another origin that has been explored are hepatocytes located at the periphery of the metastases, which can undergo EMT and contribute to fibrosis and angiogenesis [70].

In the context of HGP and spatial localization, the different types of CAFs lead us to question which cell type is the precursor of fibrotic capsules or if is it a mixture of the cell types described above. In this sense, we can learn a lot from the research carried out on fibrotic liver diseases, which will probably follow processes similar to liver tumoral malignancies. Therefore, it is crucial to know in detail the differences between HSC and PF, especially in the context of the activation of both cell types. This can also be affected by the route of entrance of the tumor cell into the liver, that is, whether it extravasates in a centrolobular vein, in a portal tract or directly into a sinusoid. It has been observed in experimental models of fibrosis that depending on the etiology, there is a differential activation of both HSC and PF. For example, HSC are the main source of myofibroblasts in

lesions induced by Tetrachloromethane (CCl_4), whereas PF are the main source in lesions induced by bile duct occlusion [72]. Likewise, the differences between activated HSC and activated PF have been characterized, and some characteristic biomarkers of each cell type have been reported once they have undergone an activation process. It has been described that PF are characterized by the expression of CD90, while activated HSC would be negative for this marker [73]. On the contrary, cytoglobin has been described as a good characteristic marker of activated HSC and that it is not expressed in activated PF [74]. What seems very plausible is that CAFs from different origins coexist in LM-CRC. Data from our laboratory reinforce this fact, since we isolated CD90-positive CAFs and CD90-negative CAFs that could correspond to a differential origin or precursor (data not shown).

However, we cannot rule out that the generation of the capsule is due to intrinsic properties of the tumor cell. In any case, they are important aspects that must be taken into account because they could provide future therapeutic strategies.

Therefore, all this knowledge leads us to speculate that each HGP contains CAFs coming from a distinct origin among those earlier described. This would be in line with the hypothesis on the HGP predetermination by the different access routes of circulating tumor cells into hepatic tissue [30]. On the one hand, if tumoral cells enter through a portal tract, they would first interact with PF and those would mediate the stromal reaction. On the other hand, if they reach hepatic sinusoids, they will be able to activate HSC and the process of fibrosis would be orchestrated by them [75,76].

3.3. Tumor Vascularization

Different HGPs have also been associated with different types of tumor vascularization. In fact, another common classification for HGPs considers only two patterns: the angiogenic, which includes desmoplastic and pushing HGPs, and the non-angiogenic one that refers to the replacement HGP [27].

In the replacement HGP, the tumoral cells benefit from the hepatic architecture: they progressively "replace" the hepatocyte plates and use the already existing connective tissue and blood vessels. Hence, tumor vascularization is carried out by a non-angiogenic process called vessel "co-option" [12,14,25]. On the other hand, in desmoplastic and pushing HGPs, the tumor completely disturbs the hepatic architecture, creating its own supporting stroma, new blood vessels through an angiogenic process and, in the dHGP, forming the desmoplastic rim that separates the tumor from parenchyma. As an effect of vascular endothelial growth factor (VEGF), these new angiogenic blood vessels are composed by proliferating endothelial cells and form what is called "vascular hot spots". Moreover, as they are not covered by pericytes, VEGF also induces the deposition of fibrin in a perivascular space [16,25].

Some studies have suggested that these different tumor vascularization types can be related to the route that tumoral cells take during the extravasation phase. In this line, a study performed with a murine model found that, if the cancer cells had invaded between LSEC in the space of Disse [75], the metastases with a co-option sinusoidal system developed. On contrary, as showed in the other study, if tumoral cells were injected via the portal route, near the portal tracts, they demonstrated the development of an angiogenic pattern [76]. However, at the moment, further investigation is needed to prove this fact. This might explain why the patients with a replacement (presumably non-angiogenic) HGP obtain less clinical benefit from bevacizumab-chemo treatment, which is a VEGF inhibitor, when compared with the patients with desmoplastic (angiogenic) metastases [27]. This concept may explain the failure of anti-angiogenic therapy in breast cancer liver metastases, which predominantly show the replacement HGP [12].

Thus, the tumor vascularization strategy used by each HGP is another feature to consider in order to understand their biological processes and finally select the best treatment option in each case.

3.4. Immune Infiltrates

The immune system plays crucial role in controlling tumor growth and dissemination. With the introduction of immune checkpoint inhibitors (ICI) into clinical practice, the interest of the research community in the tumor immune microenvironment has been raised and a growing body of preclinical and clinical studies has been accumulated. With this background, the immune microenvironment of LM-CRC has not been fully investigated.

In 2018, Pagès et al. [77] reported a study based on 603 resected synchronous and metachronous metastases from mCRC patients. When compared to primary tumors, metastases were characterized by higher levels of CD3, CD8 and CD45RO lymphocytes and lower levels of CD20 cells, while the FoxP3-positive cell count did not demonstrate a difference. This observation, however, was based on either hot spot analysis or the whole slide average immune cell count and did not consider the spatial context. A certain pattern was observed in relation to the size of the metastasis and lymphocyte infiltration: the average infiltration was higher in small metastases; however, larger-size lesions often had "hot spots" with very high lymphocyte density, not observed in small tumors. This pattern was also seen when analyzing small and large metastases in patients with multiple metastases. Importantly, although the average lymphocyte density did not differ between cases with different metastatic burdens, the individual lesions in patients with multiple metastases demonstrated significant heterogeneity with regard to immune density. This observation is in consistence with earlier work of Halama et al. [78] performed with a focus on partially different immune cell subsets (CD3+, CD8+ and granzyme B+ cells) and overall may suggest that the tumor-related factors are more important for the local immune response than individual variations in the immune background of the host organ. However, Brunner et al. [79], although based on very few samples (n = 5), reported a conflicting observation, i.e., the homogeneity of immune infiltration patterns (CD4, CD8, CD45RO) between different lesions in patients with multiple metastases.

Immune infiltration is not evenly distributed in liver metastases. Thus, peripheral regions of the metastases have higher infiltration of CD3, CD8, C45RO and CD20 lymphocytes [79–82] and probably of NKp46+ cells [82] in comparison to the central regions of the lesion. Further, peripheral regions have higher infiltration of CD4, CD45RO and CD8 cells in comparison to distant peritumoral liver parenchyma [79]. However, the definition and extent of the peripheral region (or invasive margin) of the metastases are not set up and vary between the studies. For example, sometimes, such peripheral region contained marginal tumor tissue, and other times, it was defined as a peritumoral, non-malignant zone of a certain depth. Attempts for more detailed spatial analysis are rare and until now are limited to very few samples [78].

What is even more important in the contexts of the current review is that the above-mentioned studies did not adjust the scoring technique according to different HGPs and almost never considered the HGP in reports. However, the evaluation of inflammatory infiltrates in the context of HGPs is of crucial importance, since they topographically delimit structures that end up being physical and chemical barriers to infiltration by these cells. Concerning intratumoral regions, FoxP3, CD79A and Kappa/Lambda were more frequent in dHGP according to Höppener et al. [79]. Importantly, only intraepithelial, but not stromal, CD8 cells demonstrated such difference.

A few studies investigated peritumoral tissue. Thus, Brunner et al. reported that high levels of CD4, CD45RO and CD8 in the near peritumoral region (when normalized to immune infiltration in distant peritumoral regions) were associated with the dHGP [79]. This was further developed by Höppener et al. [83], who showed higher counts for CD8, CD45, CD79A, Kappa/Lambda and SLAMF7 cells in peritumoural areas of dHGP CRLMs in comparison to the rHGP. At the same time, FoxP3 cells did not demonstrate such difference. Digital image analysis on an independent tissue set confirmed the results for CD8 cells but also revealed the same association for FoxP3 cells (higher in the peritumoral dHGP). These in situ analyses did not reveal a difference in CD4 infiltration, but flow cytometry demonstrated a relative increase in CD4+ cells within the band of CD3+ T lymphocytes in the

non-dHGP. Authors speculated that such effect must be due to an increase in CD4+FoxP3- helper cells because no difference was found for Tregs (CD4+FoxP3+). Interestingly, even in individual metastases with a combination of HGPs, a high density of CD8 cells is seen in the area of the dHGP while being very low in the regions of the rHGP [27].

The concept based on the different spatial patterns of the immune response was developed in recent years. Thus, tumors demonstrating high lymphocyte infiltration were designated "inflamed" or "hot", while tumors with a low immune cell content were classified as "desert" or "cold" tumors [84]. The third category of tumors was characterized by high abundance of immune cells, which, however, do not penetrate cancer cell nests but are instead retained in the stroma. This phenotype was termed "immune-excluded". Interestingly, immune infiltration in "immune-excluded" tumors may be limited to the peritumoral stroma or capsule (if present) but may also infiltrate the tumor itself and stay retained in intratumoral stromal bulks [84]. We believe that these two types of "immune-excluded" phenotype may be characterized by qualitative differences in the existing antitumor response and by different mechanisms of the blockage of immune cells. The important observation regarding lymphocyte infiltration in the dHGP of LM-CRC is that the majority of lymphocytes accumulate at the interface between the outer part of the desmoplastic rim and the adjacent liver parenchyma [27]. Most immune cells, thus, although present in a high number, are kept at a distance from the malignant tissue. Due to such an immune phenotype, Jan van Dam [27,85] suggested considering metastases with the dHGP as "immune-excluded" tumors. However, some other reports considered an association of the dHGP with an inflamed phenotype [86]. In the rHGP, lymphocytes are present in the interface between liver parenchyma and the tumor and thus directly approach malignant cells, although being in relatively low numbers. We believe that a certain level of the confusion and discordance in results is caused by several reasons. First, different immune cells and different visualization methods may capture distinct lymphocyte subclasses with potentially different biology. Second, the absence of proper definitions for the immune phenotypes. Third, a lack of standardized criteria for the assessment and reporting of the spatial immune cell distribution in different HGPs.

It remains a question as to why there is such a lack of an immune-competent response from the liver tumor microenvironment [86]. However, different cells can contribute to such unresponsiveness. Thus, cancer-associated fibroblasts can express PD-L1 [87–90] or may induce its expression in other cells [82–84], contributing to immunologic silencing. Particular CAF subtypes can also induce the expression of PD-1 and CTLA4 in surrounding lymphocytes [88–91], contributing to immunosuppression and resistance to immunotherapy. Liver endothelial sinusoidal cells can also induce T cell exhaustion and suppress innate responses [92]. Kupffer cells [93] and HSC [93] contribute to such hypo-reactivity. However, the balance between responsiveness or unresponsiveness seems to be predetermined according to the HGP.

The overall impact of the prognostic role of immune infiltration was recently summarized elsewhere [94]. Despite heterogeneous study designs, cells of interest and scoring criteria, a clear overall trend with high intratumoral infiltration of CD4, CD8 or CD45RO and improved survival could be stated. Interestingly, out of nine studies, six considered peritumoral regions as of separate interest; however, none of them distinguished HGPs. The prognostic impact of immune cell infiltration in peritumoral regions is not clear. To the best of our knowledge, only one study evaluated both HGPs and immune phenotypes of LM-CRC with regard to survival. In this study, Stremitzer et al. classified 118 metastases into an inflamed immune phenotype and a non-inflamed immune phenotype, based on CD8-positive cell infiltration [86]. The inflamed immune phenotype was associated with the dHGP and both of them were linked to improved survival. Unfortunately, the survival differences between all three groups and their distribution across HGPs remained unreported.

Studies have demonstrated that patients with MSI-H cancer, which develop distant metastases, may benefit from immunotherapy [95,96]. These results led to FDA approval for ICI pembrolizumab and nivolumab for the treatment of chemoresistant MSI-H

(microsatellite-instability high) metastatic CRC. Despite pioneering studies of the Galon group [80,97,98], the dynamics of the immune microenvironment under immunotherapy in metastatic lesions remains unclear.

Thus, LM-CRC can have different immune infiltration patterns. The crude rate of lymphocyte immune infiltration in the resected metastatic lesions seems to be expectedly associated with improved survival. However, the role and impact of peritumoral immune infiltration and inflammation status in liver parenchyma and their impact on prognosis are yet to be discovered. There is evidence that certain immune patterns are associated with certain HGPs. The HGP may be one of the key factors sculpting the development of certain immune phenotypes of LM-CRC. Further studies using standardized evaluation and reporting systems are needed to confirm and clarify such association.

4. Clinical Opportunities of TME in the Context of the HGP

LM-CRC are a defiance for cancer treatment, since they are entities that have the particularity of recruiting a large number of cells with an immunosuppressive capacity and, even more challenging, that have characteristic resistance to a multitude of antitumor drugs, aspects very well summarized in Ciner AT et al. [99].

However, the particular pathological and histological characteristics of the TME in hepatic metastases, as well as the particular biology of the different phenotypes, are the aspects that could be exploited clinically. We have already commented that HGPs have a prognostic and predictive value, although prospective studies are warranted to validate this. Thus, knowing the HGP prior to surgery, i.e., being able to determine metastases with an established capsule, could contribute to the better selection of patients for a curative surgical resection. Knowing the HGP at the pre-operative stage could improve patient selection for neoadjuvant treatment, minimizing the toxicity effects and surgery-related risks. This fact could be approached by using modern medical imaging techniques and is extensively reviewed by Oliveira RC et al. and Latacz E et al. [21,85]. Radiomics is another powerful non-invasive tool capable of classifying tumors at the morphological [100] and molecular levels [101]. Thus, in a retrospective study, Cheng et al. used pre- and post-contrast (arterial and portal venous) phase MDCT images to build a radiomic classifier which predicted the HGP with remarkable accuracy [102]. According to the authors, they could distinguish a clear tumor–liver interface in the tumors with a dHGP and fibrotic capsule, while a poorly defined tumor–liver interface would be associated with a replacement growth pattern.

Another important feature of liver metastases, linked to the HGP, is the type of vascularization which the tumor develops. As we described above, two vascularization strategies, i.e., vessel co-option (in tumors with a replacement HGP) or neoangiogenesis (in tumors with a dHGP), can be clearly distinguished. In this regard, patients whose metastases have a desmoplastic HGP would be candidates for receiving anti-angiogenics drugs in neoadjuvant settings. Non-invasive imaging for the classification of the HGP is the pre-requisite for such therapeutic approach.

Another opportunity relies on the observation that regardless of the HGP, LM-CRC are characterized by some degree of immune suppression, at least in central areas of the tumor lesion, as above reviewed. However, anti-angiogenic [103] and anti-fibrotic [104–107] therapies could be interesting strategies to re-establish the anti-tumoral immunity and are thus direct targets of immunotherapeutic approaches. Current clinical trials are assessing this hypothesis (NCT03698461), although no criteria for selection of patients according to the HGP have been applied. However, some caution must be exercised since some approaches have turned out to be counterproductive and report the opposite observation [108], especially if they are not accompanied by ICI.

The counterproductive results obtained so far using the deletion or silencing of particular mesenchymal cells raise the question for different CAF subsets, as stated throughout the text. This fact is especially relevant in the context of HGPs and taking into account different potential precursors of CAFs in the liver. It could be hypothesized that the fibroblasts that form the capsule are different from those that are located in the central regions of the tumor.

Thus, the fibroblasts that form the fibrotic rim may exert a protective role by enveloping the tumor and hindering the invasion into the liver tissue. The capsule in the dHGP may have certain similarities to the peritumoral host reaction against benign tumors or abscesses.

Thus, these observations open the door for researchers in the field to try to reprogram intratumoral fibroblasts. We usually find these cells in large numbers in rHGP metastases but also in dHGP metastases. However, intratumoral CAFs in invasive versus central deeper areas could probably be performing different functions. The conceptual idea is to differentiate those CAFs into fibroblasts that would have the ability to envelop, as a shield or shell, the tumor itself, preventing the spreading of the tumor inside the liver plates. Reprogramming fibroblasts has been a successful strategy at the preclinical level so far. As in all organs, resident mesenchymal cells are transformed into CAFs due to the selective pressures exerted by the tumor–stroma crosstalk. In pancreatic cancer, as well as in pancreatitis, pancreatic stellate cells (PSC) are differentiated to CAFs. In this process of loss of quiescence, they lose the expression of the vitamin D receptor, a fact that has been reversed by administering synthetic derivatives of vitamin D such as calcipotriol, inducing quiescence in the CAFs, and, in turn, the reestablishment of the transcriptional programs of the PSC [109]. In the same vein, all-trans retinoic acid (ATRA), the active metabolite of vitamin A, is able to restore quiescence of PSC by means of a reduction in the myofibroblastic properties of activated PSC, a process involving RARβ [110]. However, it is still a matter of major concert determining which is the trigger that induces the encapsulating response. Is it a host response or tumor-driven?

Thus, the particular histology of colorectal carcinoma liver metastases, conditioned by the characteristics of the TME, should be taken into account when designing therapeutic clinical trials and could be known in advance using conventional medical imaging techniques.

5. Conclusions

Thus, as final thoughts and comments, LM-CRC are tumors that have particular characteristics in terms of their content in TME cells, both qualitatively and quantitatively. This fact makes them distinct entities with respect to their corresponding primary tumors. Furthermore, this fact should have an impact on the way we treat metastases. However, treatments have not been designed according to these particularities so far. Be that as it may, we need to better understand the particularities of the cells that form the TME in each particular location, since we already know that, e.g., fibroblasts display anatomic demarcation that affects their transcriptional repertoire.

All these facts acquire even greater relevance since LM-CRC present different HGPs, having a great impact on the way the stroma is organized. In this sense, the new spatial transcriptomic technologies can contribute to improving such knowledge. However, much more affordable and feasible technologies could also contribute with relevant clinical answers. The prospective assessment of the HGP is needed in terms of reinforcing the prognostic and predictive value described so far. Further, it would be highly recommended to include such feasible assessment in the pathological anatomy reports on a routine basis. Furthermore, having this information available prior to surgery could, on the one hand, help design more efficient neoadjuvant treatments for those resectable patients and, on the other hand, be able to offer potentially curative strategies to those initially non-surgical patients. This clinical information can only be obtained through medical imaging techniques, and there are different initiatives underway to demonstrate the feasibility of this option. However, in order to obtain a clinical benefit with an impact on affected patients, it is necessary to deepen the knowledge of the biology of HGPs. We still do not know with certainty which is the cause that motivates the formation of the capsules. However, it would be of great interest to be able to pharmacologically induce the formation of such fibrotic capsules. In any case, the combination of both better knowledge and routine assessment by means of medical imaging would have an impact on the selection of patients for personalized treatments, particularly relevant for the majority of patients that could not benefit from a potentially curative resection.

Funding: This work has been supported by grant PI18/1140 from the Fondo de Investigaciones Sanitarias of the Spanish Government, Fondo Europeo de Desarrollo Regional (FEDER) "Una manera de hacer Europa"/"A way of shaping Europe" and AGAUR grant number SGR771. In addition, GGV is recipient of the 2019 FI_B 00673 grant, funded by AGAUR the Department of Health of the Generalitat de Catalunya by the call "Ajuts per a la contractació de personal investigador novell FI 2019". We also thank CERCA Programme/Generalitat de Catalunya for institutional support to IDIBELL.

Conflicts of Interest: The authors declare no conflict of interest.

References

1. (GLOBOSCAN). IA for R on CWHO. Cancer Today. Available online: http://gco.iarc.fr/today/data/pdf/fact-sheets/cancers/cancer-fact-sheets-6.pdf (accessed on 20 November 2020).
2. André, T.; Boni, C.; Navarro, M.; Tabernero, J.; Hickish, T.; Topham, C.; Bonetti, A.; Clingan, P.; Bridgewater, J.; Rivera, F. Improved overall survival with oxaliplatin.; fluorouracil.; and leucovorin as adjuvant treatment in stage II or III colon cancer in the MOSAIC trial. *J. Clin. Oncol.* **2009**, *27*, 3109–3116. [CrossRef]
3. Adam, R.; De Gramont, A.; Figueras, J.; Guthrie, A.; Kokudo, N.; Kunstlinger, F.; Loyer, E.; Poston, G.; Rougier, P.; Rubbia-Brandt, L.; et al. The oncosurgery approach to managing liver metastases from colorectal cancer: A multidisciplinary international consensus. *Oncologist* **2012**, *17*, 1225–1239.
4. Jang, K.U.; Kim, C.W.; Kim, K.H.; Lim, S.B.; Yu, C.S.; Kim, T.W.; Kim, P.N.; Kim, J.H.; Kim, J.C. Prognostic factors in terms of the number of metastatic nodules in patients with colorectal cancer liver metastases. *Ann. Coloproctol.* **2016**, *32*, 92–100. [CrossRef]
5. Liu, J.; Cho, Y.B.; Hong, H.K.; Wu, S.; Ebert, P.J.; Bray, S.M.; Wong, S.S.; Ting, J.C.; Calley, J.N.; Whittington, C.F.; et al. Molecular dissection of CRC primary tumors and their matched liver metastases reveals critical role of immune microenvironment, EMT and angiogenesis in cancer metastasis. *Sci. Rep.* **2020**, *10*, 1–15. [CrossRef]
6. Rinn, J.L.; Bondre, C.; Gladstone, H.B.; Brown, P.O.; Chang, H.Y. Anatomic demarcation by positional variation in fibroblast gene expression programs. *PLoS Genet.* **2006**, *2*, 1084–1096. [CrossRef] [PubMed]
7. Berdiel-Acer, M.; Cuadras, D.; Díaz-Maroto, N.G.; Sanjuan, X.; Serrano, T.; Berenguer, A.; Moreno, V.; Gonçalves-Ribeiro, S.; Salazar, R.; Villanueva, A.; et al. A monotonic and prognostic genomic signature from fibroblasts for colorectal cancer initiation, progression, and metastasis. *Mol. Cancer Res.* **2014**, *12*, 1254–1266. [CrossRef] [PubMed]
8. Berdiel-Acer, M.; Berenguer, A.; Sanz-Pamplona, R.; Cuadras, D.; Sanjuan, X.; Paules, M.J.; Santos, C.; Salazar, R.; Moreno, V.; Capella, G.; et al. A 5-gene classifier from the carcinoma-associated fibroblast transcriptomic profile and clinical outcome in colorectal cancer. *Oncotarget* **2014**, *5*, 6437–6452. [CrossRef] [PubMed]
9. Van Dam, P.J.; van der Stok, E.P.; Teuwen, L.A.; Van den Eynden, G.G.; Illemann, M.; Frentzas, S.; Majeed, A.W.; Eefsen, R.L.; Coebergh van den Braak, R.R.J.; Lazaris, A.; et al. International consensus guidelines for scoring the histopathological growth patterns of liver metastasis. *Br. J. Cancer* **2017**, *117*, 1427–1441. [CrossRef]
10. Galjart, B.; Nierop, P.M.H.; van der Stok, E.P.; van den Braak, R.; Höppener, D.J.; Daelemans, S.; Dirix, L.Y.; Verhoef, C.; Vermeulen, P.B.; Grünhagen, D.J. Angiogenic desmoplastic histopathological growth pattern as a prognostic marker of good outcome in patients with colorectal liver metastases. *Angiogenesis* **2019**, *22*, 355–368. [CrossRef]
11. Buisman, F.E.; van der Stok, E.P.; Galjart, B.; Vermeulen, P.B.; Balachandran, V.P.; Coebergh van den Braak, R.R.J.; Creasy, J.M.; Höppener, D.J.; Jarnagin, W.R.; Kingham, T.P.; et al. Histopathological growth patterns as biomarker for adjuvant systemic chemotherapy in patients with resected colorectal liver metastases. *Clin. Exp. Metastasis* **2020**, *37*, 593–605. [CrossRef]
12. Frentzas, S.; Simoneau, E.; Bridgeman, V.L.; Vermeulen, P.B.; Foo, S.; Kostaras, E.; Nathan, M.; Wotherspoon, A.; Gao, Z.H.; Shi, Y.; et al. Vessel co-option mediates resistance to anti-angiogenic therapy in liver metastases. *Nat. Med.* **2017**, *22*, 1294–1302. [CrossRef] [PubMed]
13. Terayama, N.; Terada, T.; Nakanuma, Y. Histologic growth patterns of metastatic carcinomas of the liver. *Jpn. J. Clin. Oncol.* **1996**, *26*, 24–29. [CrossRef] [PubMed]
14. Vermeulen, P.B.; Colpaert, C.; Salgado, R.; Royers, R.; Hellemans, H.; Van Den Heuvel, E.; Goovaerts, G.; Dirix, L.Y.; Van Marck, E. Liver metastases from colorectal adenocarcinomas grow in three patterns with different angiogenesis and desmoplasia. *J. Pathol.* **2001**, *195*, 336–342. [CrossRef] [PubMed]
15. Kurebayashi, Y.; Kubota, N.; Sakamoto, M. Immune microenvironment of hepatocellular carcinoma, intrahepatic cholangiocarcinoma and liver metastasis of colorectal adenocarcinoma: Relationship with histopathological and molecular classifications. *Hepatol. Res.* **2020**. [CrossRef] [PubMed]
16. Van Den Eynden, G.G.; Bird, N.C.; Majeed, A.W.; Van Laere, S.; Dirix, L.Y.; Vermeulen, P.B. The histological growth pattern of colorectal cancer liver metastases has prognostic value. *Clin. Exp. Metastasis* **2012**, *29*, 541–549. [CrossRef] [PubMed]
17. Eefsen, R.L.; Vermeulen, P.B.; Christensen, I.J.; Laerum, O.D.; Mogensen, M.B.; Rolff, H.C.; Van den Eynden, G.G.; Høyer-Hansen, G.; Osterlind, K.; Vainer, B.; et al. Growth pattern of colorectal liver metastasis as a marker of recurrence risk. *Clin. Exp. Metastasis* **2015**, *32*, 369–381. [CrossRef] [PubMed]
18. Nielsen, K.; Rolff, H.C.; Eefsen, R.L.; Vainer, B. The morphological growth patterns of colorectal liver metastases are prognostic for overall survival. *Mod. Pathol.* **2014**, *27*, 1641–1648. [CrossRef] [PubMed]

19. Höppener, D.J.; Nierop, P.M.H.; Herpel, E.; Rahbari, N.N.; Doukas, M.; Vermeulen, P.B.; Grünhagen, D.J.; Verhoef, C. Histopathological growth patterns of colorectal liver metastasis exhibit little heterogeneity and can be determined with a high diagnostic accuracy. *Clin. Exp. Metastasis* **2019**, *36*, 311–319. [CrossRef] [PubMed]
20. Okano, K.; Yamamoto, J.; Kosuge, T.; Yamamoto, S.; Sakamoto, M.; Nakanishi, Y.; Hirohashi, S. Fibrous pseudocapsule of metastatic liver tumors from colorectal carcinoma: Clinicopathologic study of 152 first resection cases. *Cancer* **2000**, *89*, 267–275. [CrossRef]
21. Oliveira, R.C.; Alexandrino, H.; Cipriano, M.A.; Alves, F.C.; Tralhão, J.G. Predicting liver metastases growth patterns: Current status and future possibilities. *Semin. Cancer Biol.* **2020**. [CrossRef]
22. Liao, A.; Mittal, P.; Lawson, D.H.; Yang, J.J.; Szalai, E.; Grossniklaus, H.E. Radiologic and Histopathologic Correlation of Different Growth Patterns of Metastatic Uveal Melanoma to the Liver. *Ophthalmology* **2018**, *125*, 597–605. [CrossRef] [PubMed]
23. Barnhill, R.; Vermeulen, P.; Daelemans, S.; van Dam, P.J.; Roman-Roman, S.; Servois, V.; Hurbain, I.; Gardrat, S.; Raposa, G.; Nicolas, A.; et al. Replacement and desmoplastic histopathological growth patterns: A pilot study of prediction of outcome in patients with uveal melanoma liver metastases. *J. Pathol. Clin. Res.* **2018**, *4*, 227–240. [CrossRef] [PubMed]
24. Temido, M.J.; Caetano Oliveira, R.; Martins, R.; Serôdio, M.; Costa, B.; Carvalho, C.; Santos, E.; Ferreira, L.; Teixeira, P.; Cipriano, M.A.; et al. Prognostic factors after hepatectomy for gastric adenocarcinoma liver metastases: Desmoplastic growth pattern as the key to improved overall survival. *Cancer Manag. Res.* **2020**, *12*, 11689–11699. [CrossRef] [PubMed]
25. Stessels, F.; Van den Eynden, G.; Van der Auwera, I.; Salgado, R.; Van den Heuvel, E.; Harris, A.L.; Jackson, D.G.; Colpaert, C.G.; van Marck, E.A.; Dirix, L.Y.; et al. Breast adenocarcinoma liver metastases.; in contrast to colorectal cancer liver metastases.; display a non-angiogenic growth pattern that preserves the stroma and lacks hypoxia. *Br. J. Cancer* **2004**, *90*, 1429–1436. [CrossRef]
26. Welter, S.; Arfanis, E.; Christoph, D.; Hager, T.; Roesel, C.; Aigner, C.; Weinreich, G.; Theegarten, D. Growth patterns of pulmonary metastases: Should we adjust resection techniques to primary histology and size? *Eur. J. Cardio Thorac. Surg.* **2017**, *52*, 39–46. [CrossRef]
27. Van Dam, P.J.; Daelemans, S.; Ross, E.; Waumans, Y.; Van Laere, S.; Latacz, E.; Van Steen, R.; De Pooter, C.; Kockx, M.; Dirix, L.; et al. Histopathological growth patterns as a candidate biomarker for immunomodulatory therapy. *Semin. Cancer Biol.* **2018**, *52*, 86–93. [CrossRef]
28. Fink, K.; Fink, J. Imaging of brain metastases. *Surg. Neurol. Int.* **2013**, *4*, 209–219. [CrossRef]
29. Eefsen, R.L.; Engelholm, L.; Alpizar-Alpizar, W.; Van den Eynden, G.G.; Vermeulen, P.B.; Christensen, I.J.; Laerum, O.D.; Rolff, H.C.; Høyer-Hansen, G.; Vainer, B.; et al. Inflammation and uPAR-Expression in Colorectal Liver Metastases in Relation to Growth Pattern and Neo-adjuvant Therapy. *Cancer Microenviron* **2015**, *8*, 93–100. [CrossRef]
30. Vidal-Vanaclocha, F. The Tumor microenvironment at different stages of hepatic metastasis. In *Liver Metastasis: Biology and Clinical Managemen*, 1st ed.; Brodt, P., Ed.; Springer: Dordecht, The Netherlands, 2011; pp. 43–87.
31. Van den Eynden, G.G.; Majeed, A.W.; Illemann, M.; Vermeulen, P.B.; Bird, N.C.; Høyer-Hansen, G.; Eefsen, R.L.; Reynolds, A.R.; Brodt, P. The multifaceted role of the microenvironment in liver metastasis: Biology and clinical implications. *Cancer Res.* **2013**, *73*, 2031–2043. [CrossRef]
32. Brodt, P. Role of the microenvironment in liver metastasis: From pre- to prometastatic niches. *Clin. Cancer Res.* **2016**, *22*, 5971–5982. [CrossRef]
33. Vidal-Vanaclocha, F. The prometastatic microenvironment of the liver. *Cancer Microenviron.* **2008**, *1*, 113–129. [CrossRef] [PubMed]
34. Braet, F.; Nagatsuma, K.; Saito, M.; Soon, L.; Wisse, E.; Matsuura, T. The hepatic sinusoidal endothelial lining and colorectal liver metastases. *World J. Gastroenterol.* **2007**, *13*, 821–825. [CrossRef] [PubMed]
35. Ou, J.; Peng, Y.; Deng, J.; Miao, H.; Zhou, J.; Zha, L.; Zhou, R.; Yu, L.; Shi, H.; Liang, H. Endothelial cell-derived-fibronectin extra domain A promotes colorectal cancer metastasis via inducing epithelialmesenchymal transition. *Carcinogenesis* **2014**, *35*, 1661–1670. [CrossRef] [PubMed]
36. Hu, C.T.; Guo, L.L.; Feng, N.; Zhang, L.; Zhou, N.; Ma, L.L.; Shen, L.; Tong, G.H.; Yan, Q.W.; Zhu, S.J.; et al. MIF, secreted by human hepatic sinusoidal endothelial cells.; promotes chemotaxis and outgrowth of colorectal cancer in liver prometastasis. *Oncotarget* **2015**, *6*, 22410–22423. [CrossRef]
37. Banerjee, D.; Hernandez, S.L.; Garcia, A.; Kangsamaksin, T.; Sbiroli, E.; Andrews, J.; Forrester, L.A.; Wei, N.; Kadenhe-Chiweshe, A.; Shawber, C.J.; et al. Notch suppresses angiogenesis and progression of hepatic metastases. *Cancer Res.* **2015**, *75*, 1592–1602. [CrossRef]
38. Im, J.H.; Tapmeier, T.; Balathasan, L.; Gal, A.; Yameen, S.; Hill, S.; Smart, S.; Noterdaeme, O.; Kelly, M.; Brady, M.; et al. G-CSF rescues tumor growth and neo-angiogenesis during liver metastasis under host angiopoietin-2 deficiency. *Int. J. Cancer* **2013**, *132*, 315–326. [CrossRef]
39. Solaun, M.S.; Mendoza, L.; De Luca, M.; Gutierrez, V.; López, M.P.; Olaso, E.; Lee Sim, B.K.; Vidal-Vanaclocha, F. Endostatin inhibits murine colon carcinoma sinusoidal-type metastases by preferential targeting of hepatic sinusoidal endothelium. *Hepatology* **2002**, *35*, 1104–1116. [CrossRef]
40. Arteta, B.; Lasuen, N.; Lopategi, A.; Sveinbjörnsson, B.; Smedsrød, B.; Vidal-Vanaclocha, F. Colon carcinoma cell interaction with liver sinusoidal endothelium inhibits organ-specific antitumor immunity through interleukin-1-induced mannose receptor in mice. *Hepatology* **2010**, *51*, 2172–2182. [CrossRef]
41. Paulsson, J.; Micke, P. Prognostic relevance of cancer-associated fibroblasts in human cance. *Semin. Cancer Biol.* **2014**, *25*, 61–68. [CrossRef]

42. Ünlü, M.; Çetinayak, H.O.; Önder, D.; Ecevit, C.; Akman, F.; Ikiz, A.Ö.; Ada, E.; Karaçali, B.; Sarioğlu, S. The prognostic value of tumor-stroma proportion in laryngeal squamous cell carcinoma. *Turk. Patoloji Derg./Turk. J. Pathol.* **2013**, *29*, 27–35. [CrossRef]
43. Van Pelt, G.W.; Huijbers, A.; Tollenaar, R.A.E.M.; Mesker, W.E. In reply to Hynes et al.: Back to the future: Routine morphological assessment of the tumour microenvironment is prognostic in stages II/III colon cancer in a large population-based study. *Histopathology* **2018**, *72*, 531–532. [CrossRef] [PubMed]
44. Huijbers, A.; Tollenaar, R.A.E.M.; Pelt, G.W.V.; Zeestraten, E.C.M.; Dutton, S.; McConkey, C.C.; Domingo, E.; Smit, V.T.; Midgley, R.; Warren, B.F.; et al. The proportion of tumor-stroma as a strong prognosticator for stage II and III colon cancer patients: Validation in the victor trial. *Ann. Oncol.* **2013**, *24*, 179–185. [CrossRef] [PubMed]
45. Erkan, M.; Michalski, C.W.; Rieder, S.; Reiser-Erkan, C.; Abiatari, I.; Kolb, A.; Giese, N.A.; Esposito, I.; Friess, H.; Kleeff, J. The Activated Stroma Index Is a Novel and Independent Prognostic Marker in Pancreatic Ductal Adenocarcinoma. *Clin. Gastroenterol. Hepatol.* **2008**, *6*, 1155–1161. [CrossRef] [PubMed]
46. Calon, A.; Lonardo, E.; Berenguer-Llergo, A.; Espinet, E.; Hernando-Momblona, X.; Iglesias, M.; Sevillano, M.; Palomo-Ponce, S.; Tauriello, D.V.; Byrom, D.; et al. Stromal gene expression defines poor-prognosis subtypes in colorectal cancer. *Nat. Genet.* **2015**, *47*, 320–329. [CrossRef] [PubMed]
47. Dekker, T.J.A.; Van De Velde, C.J.H.; Van Pelt, G.W.; Kroep, J.R.; Julien, J.P.; Smit, V.T.H.B.M.; Tollenaar, R.A.; Mesker, W.E. Prognostic significance of the tumor-stroma ratio: Validation study in node-negative premenopausal breast cancer patients from the EORTC perioperative chemotherapy (POP) trial (10854). *Breast Cancer Res. Treat* **2013**, *139*, 371–379. [CrossRef] [PubMed]
48. Berdiel-Acer, M.; Sanz-Pamplona, R.; Calon, A.; Cuadras, D.; Berenguer, A.; Sanjuan, X.; Paules, M.J.; Salazar, R.; Moreno, V.; Batlle, E.; et al. Differences between CAFs and their paired NCF from adjacent colonic mucosa reveal functional heterogeneity of CAFs, providing prognostic information. *Mol. Oncol.* **2014**, *8*, 1290–1305. [CrossRef]
49. Gonçalves-Ribeiro, S.; Díaz-Maroto, N.G.; Berdiel-Acer, M.; Soriano, A.; Guardiola, J.; Martínez-Villacampa, M.; Salazar, R.; Capellà, G.; Villanueva, A.; Martínez-Balibrea, E.; et al. Carcinoma-associated fibroblasts affect sensitivity to oxaliplatin and 5FU in colorectal cancer cells. *Oncotarget* **2016**, *7*, 59766–59780. [CrossRef]
50. Sabath, D.E. Minimal Residual Disease ☆. *Ref. Modul. Biomed. Sci.* **2018**, *9*, 665–674.
51. Paraiso, K.H.T.; Smalley, K.S.M. Fibroblast-mediated drug resistance in cancer. *Biochem. Pharmacol.* **2013**, *85*, 1033–1041. [CrossRef]
52. Mark, M.B.; Robert, A.; Gatenby, W.S.D. Environment-mediated drug resistance: A major contributor to minimal residual disease. *Nat. Rev. Cancer* **2009**, *9*, 665–674.
53. Herrera, M.; Islam, A.B.M.M.K.; Herrera, A.; Martín, P.; García, V.; Silva, J.; Garcia, J.M.; Salas, C.; Casal, I.; de Herreros, A.G.; et al. Functional heterogeneity of cancer-associated fibroblasts from human colon tumors shows specific prognostic gene expression signature. *Clin. Cancer Res.* **2013**, *19*, 5914–5926. [CrossRef] [PubMed]
54. Ueno, H.; Konishi, T.; Ishikawa, Y.; Shimazaki, H.; Ueno, M.; Aosasa, S.; Saiura, A.; Hase, K.; Yamamoto, J. Histologic categorization of fibrotic cancer stroma in the primary tumor is an independent prognostic index in resectable colorectal liver metastasis. *Am. J. Surg. Pathol.* **2014**, *38*, 1380–1386. [CrossRef] [PubMed]
55. Díaz-Maroto, N.G.; Sanz-Pamplona, R.; Berdiel-Acer, M.; Cimas, F.J.; García, E.; Gonçalves-Ribeiro, S.; Albert, N.; Garcia-Vicién, G.; Capella, G.; Moreno, V.; et al. Noncanonical TGFb pathway relieves the blockade of IL1B/TGFb-mediated crosstalk between tumor and stroma: TGFBR1 and TAK1 inhibition in colorectal cancer. *Clin. Cancer Res.* **2019**, *25*, 4466–4479. [CrossRef] [PubMed]
56. Neuzillet, C.; Tijeras-Raballand, A.; Ragulan, C.; Cros, J.; Patil, Y.; Martinet, M.; Erkan, M.; Kleeff, J.; Wilson, J.; Apte, M.; et al. Inter- and intra-tumoural heterogeneity in cancer-associated fibroblasts of human pancreatic ductal adenocarcinoma. *J. Pathol.* **2019**, *248*, 51–65. [CrossRef] [PubMed]
57. Costa, A.; Kieffer, Y.; Scholer-Dahirel, A.; Pelon, F.; Bourachot, B.; Cardon, M.; Sirven, P.; Magagna, I.; Fuhrmann, L.; Bernard, C.; et al. Fibroblast Heterogeneity and Immunosuppressive Environment in Human Breast Cancer. *Cancer Cell* **2018**, *33*, 463–479.e10. [CrossRef] [PubMed]
58. Su, S.; Chen, J.; Yao, H.; Liu, J.; Yu, S.; Lao, L.; Wang, M.; Luo, M.; Xing, Y.; Chen, F.; et al. CD10+GPR77+ Cancer-Associated Fibroblasts Promote Cancer Formation and Chemoresistance by Sustaining Cancer Stemness. *Cell* **2018**, *172*, 841–856.e16. [CrossRef] [PubMed]
59. Bonneau, C.; Eliès, A.; Kieffer, Y.; Bourachot, B.; Ladoire, S.; Pelon, F.; Hequet, D.; Guinebretière, J.M.; Blanchet, C.; Vincent-Salomon, A.; et al. A subset of activated fibroblasts is associated with distant relapse in early luminal breast cancer. *Breast Cancer Res.* **2020**, *22*, 1–22. [CrossRef]
60. Öhlund, D.; Handly-Santana, A.; Biffi, G.; Elyada, E.; Almeida, A.S.; Ponz-Sarvise, M.; Corbo, V.; Oni, T.E.; Hearn, S.A.; Lee, E.J.; et al. Distinct populations of inflammatory fibroblasts and myofibroblasts in pancreatic cance. *J. Exp. Med.* **2017**, *214*, 579–596. [CrossRef]
61. Nielsen, M.F.B.; Mortensen, M.B.; Detlefsen, S. Typing of pancreatic cancer-associated fibroblasts identifies different subpopulations. *World J. Gastroenterol.* **2018**, *24*, 4663–4678. [CrossRef]
62. Lunevicius, R.; Nakanishi, H.; Ito, S.; Kozaki, K.I.; Kato, T.; Tatematsu, M.; Yasui, K. Clinicopathological significance of fibrotic capsule formation around liver metastasis from colorectal cancer. *J. Cancer Res. Clin. Oncol.* **2001**, *127*, 193–199. [CrossRef]
63. Illemann, M.; Bird, N.; Majeed, A.; Lærum, O.D.; Lund, L.R.; Danø, K.; Nielsen, B.S. Two distinct expression patterns of urokinase.; urokinase receptor and plasminogen activator inhibitor-1 in colon cancer liver metastases. *Int. J. Cance* **2009**, *124*, 1860–1870. [CrossRef] [PubMed]

64. Johnson, S.J.; Hines, J.E.; Burt, A.D. Phenotypic modulation of perisinusoidal cells following acute liver injury: A quantitative analysis. *Int. J. Exp. Pathol.* **1992**, *73*, 765–76572. [PubMed]
65. Driskell, R.R.; Lichtenberger, B.M.; Hoste, E.; Kretzschmar, K.; Simons, B.D.; Charalambous, M.; Ferron, S.R.; Herault, Y.; Pavlovic, G.; Ferguson-Smith, A.C.; et al. Distinct fibroblast lineages determine dermal architecture in skin development and repair. *Nature* **2013**, *504*, 277–281. [CrossRef] [PubMed]
66. Brenner, D.A.; Kisseleva, T.; Scholten, D.; Paik, Y.H.; Iwaisako, K.; Inokuchi, S.; Schnabl, B.; Seki, E.; De Minicis, S.; Oesterreicher, C.; et al. Origin of myofibroblasts in liver fibrosis. *Fibrogenes Tissue Repair* **2012**, *5*, S17. [CrossRef] [PubMed]
67. Guyot, C.; Lepreux, S.; Combe, C.; Doudnikoff, E.; Bioulac-Sage, P.; Balabaud, C.; Desmoulière, A. Hepatic fibrosis and cirrhosis: The (myo)fibroblastic cell subpopulations involved. *Int. J. Biochem. Cell Biol.* **2006**, *38*, 135–151. [CrossRef] [PubMed]
68. Cassiman, D.; Roskams, T. Beauty is in the eye of the beholder: Emerging concepts and pitfalls in hepatic stellate cell research. *J. Hepatol.* **2002**, *37*, 527–535. [CrossRef]
69. Jang, H.K.; Lee, C.E.; Choi, G.S.; Lee, Y.J.; Noh, S.J. Temperature dependent I-V characteristics of plasma hydrogenated Poly-Si TFTs in the low voltage region. *J. Korean Phys. Soc.* **1997**, *30*, 125–172.
70. Mueller, L.; Goumas, F.A.; Affeldt, M.; Sandtner, S.; Gehling, U.M.; Brilloff, S.; Walter, J.; Karnatz, N.; Lamszus, K.; Rogiers, X.; et al. Stromal fibroblasts in colorectal liver metastases originate from resident fibroblasts and generate an inflammatory microenvironment. *Am. J. Pathol.* **2007**, *171*, 1608–1618. [CrossRef]
71. Olaso, E.; Salado, C.; Egilegor, E.; Gutierrez, V.; Santisteban, A.; Sancho-Bru, P.; Friedman, S.L.; Vidal-Vanaclocha, F. Proangiogenic role of tumor-activated hepatic stellate cells in experimental melanoma metastasis. *Hepatology* **2003**, *37*, 674–685. [CrossRef]
72. Iwaisako, K.; Jiang, C.; Zhang, M.; Cong, M.; Moore-Morris, T.J.; Park, T.J.; Liu, X.; Xu, J.; Wang, P.; Paik, Y.H.; et al. Origin of myofibroblasts in the fibrotic liver in mice. *Proc. Natl. Acad. Sci. USA* **2014**, *111*, E3297–E3305. [CrossRef]
73. Dudas, J.; Mansuroglu, T.; Batusic, D.; Ramadori, G. Thy-1 is expressed in myofibroblasts but not found in hepatic stellate cells following liver injury. *Histochem. Cell Biol.* **2009**, *131*, 115–127. [CrossRef] [PubMed]
74. Motoyama, H.; Komiya, T.; Thuy, L.T.T.; Tamori, A.; Enomoto, M.; Morikawa, H.; Iwai, S.; Uchida-Kobayashi, S.; Fujii, H.; Hagihara, A.; et al. Cytoglobin is expressed in hepatic stellate cells.; but not in myofibroblasts.; in normal and fibrotic human liver. *Lab. Investig.* **2014**, *94*, 192–207. [CrossRef] [PubMed]
75. Paku, S.; Lapis, K. Morphological aspects of angiogenesis in experimental liver metastases. *Am. J. Pathol.* **1993**, *143*, 926–936. [PubMed]
76. Paku, S.; Kopper, L.; Nagy, P. Development of the vasculature in "pushing-type" liver metastases of an experimental colorectal cancer. *Int. J. Cancer* **2005**, *115*, 893–902. [CrossRef]
77. Pagès, F.; Mlecnik, B.; Marliot, F.; Bindea, G.; Ou, F.S.; Bifulco, C.; Lugli, A.; Zlobec, I.; Rau, T.T.; Berger, M.D.; et al. International validation of the consensus Immunoscore for the classification of colon cancer: A prognostic and accuracy study. *Lancet* **2018**, *391*, 2128–2139. [CrossRef]
78. Berthel, A.; Zoernig, I.; Valous, N.A.; Kahlert, C.; Klupp, F.; Ulrich, A.; Weitz, J.; Jaeger, D.; Halama, N. Detailed resolution analysis reveals spatial T cell heterogeneity in the invasive margin of colorectal cancer liver metastases associated with improved survival. *Oncoimmunology* **2017**, *6*, 1–10. [CrossRef]
79. Brunner, S.M.; Kesselring, R.; Rubner, C.; Martin, M.; Jeiter, T.; Boerner, T.; Ruemmele, P.; Schlitt, H.J.; Fichtner-Feigl, S. Prognosis according to histochemical analysis of liver metastases removed at liver resection. *Br. J. Surg.* **2014**, *101*, 1681–1691. [CrossRef]
80. Mlecnik, B.; Van Den Eynde, M.; Bindea, G.; Church, S.E.; Vasaturo, A.; Fredriksen, T.; Lafontaine, L.; Haicheur, N.; Marliot, F.; Debetancourt, D.; et al. Comprehensive intrametastatic immune quantification and major impact of immunoscore on survival. *J. Natl. Cancer Inst.* **2018**, *110*, 97–108. [CrossRef]
81. Van den Eynde, M.; Mlecnik, B.; Bindea, G.; Fredriksen, T.; Church, S.E.; Lafontaine, L.; Haicheur, N.; Marliot, F.; Angelova, M.; Vasaturo, A.; et al. The Link between the Multiverse of Immune Microenvironments in Metastases and the Survival of Colorectal Cancer Patients. *Cancer Cell* **2018**, *34*, 1012–1026.e3. [CrossRef]
82. Donadon, M.; Hudspeth, K.; Cimino, M.; Di Tommaso, L.; Preti, M.; Tentorio, P.; Roncalli, M.; Mavilio, D.; Torzilli, G. Increased Infiltration of Natural Killer and T Cells in Colorectal Liver Metastases Improves Patient Overall Survival. *J. Gastrointest Surg.* **2017**, *21*, 1226–1236. [CrossRef]
83. Höppener, D.J.; Nierop, P.M.H.; Hof, J.; Sideras, K.; Zhou, G.; Visser, L.; Gouw, A.S.H.; de Jong, K.P.; Sprengers, D.; Kwekkeboom, J.; et al. Enrichment of the tumour immune microenvironment in patients with desmoplastic colorectal liver metastasis. *Br. J. Cancer* **2020**, *123*, 196–206. [CrossRef] [PubMed]
84. Chen, D.S. Mellman Elements of cancer immunity and the cancer-immune set point. *Nature* **2017**, *541*, 321–330. [CrossRef] [PubMed]
85. Latacz, E.; van Dam, P.J.; Vanhove, C.; Llado, L.; Descamps, B.; Ruiz, N.; Joye, I.; Grünhagen, D.; Van Laere, S.; Dirix, P.; et al. Can medical imaging identify the histopathological growth patterns of liver metastases? *Semin. Cancer Biol.* **2020**. [CrossRef] [PubMed]
86. Stremitzer, S.; Vermeulen, P.; Graver, S.; Kockx, M.; Dirix, L.; Yang, D.; Zhang, W.; Stift, J.; Wrba, F.; Gruenberger, T.; et al. Immune phenotype and histopathological growth pattern in patients with colorectal liver metastases. *Br. J. Cancer* **2020**. [CrossRef]
87. Koji, T.; Tomoyuki, I.; Yoko, K.; Mitsuaki, I.; Jun, H.; Hidetoshi, S.; Yataro, D. Clinical significance of PD-L1-positive cancer-associated fibroblasts in pN0M0 non-small cell lung cancer. *Lung Cancer* **2019**, *137*, 56–63.

88. Inoue, C.; Miki, Y.; Saito, R.; Hata, S.; Abe, J.; Sato, I.; Okada, Y.; Sasano, H. PD-L1 induction by cancer-associated fibroblast-derived factors in lung adenocarcinoma cells. *Cancers* **2019**, *11*, 1257. [CrossRef]
89. Li, Z.; Zhou, J.; Zhang, J.; Li, S.; Wang, H.; Du, J. Cancer-associated fibroblasts promote PD-L1 expression in mice cancer cells via secreting CXCL5. *Int. J. Cancer* **2019**, *145*, 1946–1957. [CrossRef]
90. Cheng, Y.; Li, H.; Deng, Y.; Tai, Y.; Zeng, K.; Zhang, Y.; Liu, W.; Zhang, Q.; Yang, Y. Cancer-associated fibroblasts induce PDL1+ neutrophils through the IL6-STAT3 pathway that foster immune suppression in hepatocellular carcinoma. *Cell Death Dis.* **2018**, *9*, 422. [CrossRef]
91. Kieffer, Y.; Hocine, H.R.; Gentric, G.; Pelon, F.; Bernard, C.; Bourachot, B.; Lameiras, S.; Albergante, L.; Bonneau, C.; Guyard, A.; et al. Single-Cell Analysis Reveals Fibroblast Clusters Linked to Immunotherapy Resistance in Cancer. *Cancer Discov.* **2020**, *10*, 1330–1351. [CrossRef]
92. Klugewitz, K.; Blumenthal-Barby, F.; Schrage, A.; Knolle, P.A.; Hamann, A.; Crispe, I.N. Immunomodulatory Effects of the Liver: Deletion of Activated CD4 + Effector Cells and Suppression of IFN-γ-Producing Cells After Intravenous Protein Immunization. *J. Immunol.* **2002**, *169*, 2407–2413. [CrossRef]
93. Doherty, D.G. Immunity, tolerance and autoimmunity in the liver: A comprehensive review. *J. Autoimmun.* **2016**, *66*, 60–75. [CrossRef] [PubMed]
94. Hof, J.; Kok, K.; Sijmons, R.H.; De Jong, K.P. Systematic review of the prognostic role of the immune system after surgery of colorectal liver metastases. *Front. Oncol.* **2019**, *9*, 1–12. [CrossRef] [PubMed]
95. Diaz, L.A., Jr.; Le, D.T. PD-1 Blockade in Tumors with Mismatch-Repair Deficiency. *N. Engl. J. Med.* **2015**, *373*, 1979.
96. Overman, M.J.; McDermott, R.; Leach, J.L.; Lonardi, S.; Lenz, H.J.; Morse, M.A.; Desai, J.; Hill, A.; Axelson, M.; Moss, R.A.; et al. Nivolumab in patients with metastatic DNA mismatch repair-deficient or microsatellite instability-high colorectal cancer (CheckMate 142): An open-label, multicentre, phase 2 study. *Lancet Oncol.* **2017**, *18*, 1182–1191. [CrossRef]
97. Mlecnik, B.; Bindea, G.; Kirilovsky, A.; Angell, H.K.; Obenauf, A.C.; Tosolini, M.; Church, S.E.; Maby, P.; Vasaturo, A.; Angelova, M.; et al. The tumor microenvironment and Immunoscore are critical determinants of dissemination to distant metastasis. *Sci. Transl. Med.* **2016**, *8*, 327ra26. [CrossRef] [PubMed]
98. Angelova, M.; Mlecnik, B.; Vasaturo, A.; Bindea, G.; Fredriksen, T.; Lafontaine, L.; Buttard, B.; Morgand, E.; Bruni, D.; Jouret-Mourin, A.; et al. Evolution of Metastases in Space and Time under Immune Selection. *Cell* **2018**, *175*, 751–765.e16. [CrossRef]
99. Ciner, A.T.; Jones, K.; Muschel, R.J.; Brodt, P. The unique immune microenvironment of liver metastases: Challenges and opportunities. *Semin. Cancer Biol.* **2020**. [CrossRef]
100. Liu, Z.; Zhang, X.Y.; Shi, Y.J.; Wang, L.; Zhu, H.T.; Tang, Z.; Wang, S.; Li, X.T.; Tian, J.; Sun, Y.S. Radiomics analysis for evaluation of pathological complete response to neoadjuvant chemoradiotherapy in locally advanced rectal cancer. *Clin. Cancer Res.* **2017**, *23*, 7253–7262. [CrossRef]
101. Yang, L.; Dong, D.; Fang, M.; Zhu, Y.; Zang, Y.; Liu, Z.; Zhang, H.; Ying, J.; Zhao, X.; Tian, J. Can CT-based radiomics signature predict KRAS/NRAS/BRAF mutations in colorectal cancer? *Eur. Radiol.* **2018**, *28*, 2058–2067. [CrossRef]
102. Cheng, J.; Wei, J.; Tong, T.; Sheng, W.; Zhang, Y.; Han, Y.; Gu, D.; Hong, N.; Ye, Y.; Tian, J.; et al. Prediction of Histopathologic Growth Patterns of Colorectal Liver Metastases with a Noninvasive Imaging Method. *Ann. Surg. Oncol.* **2019**, *26*, 4587–4598. [CrossRef]
103. Wallin, J.J.; Bendell, J.C.; Funke, R.; Sznol, M.; Korski, K.; Jones, S.; Hernandez, G.; Mier, J.; He, X.; Hodi, F.S.; et al. Atezolizumab in combination with bevacizumab enhances antigen-specific T-cell migration in metastatic renal cell carcinoma. *Nat. Commun.* **2016**, *7*, 12624. [CrossRef] [PubMed]
104. Schliekelman, M.J.; Creighton, C.J.; Baird, B.N.; Chen, Y.; Banerjee, P.; Bota-Rabassedas, N.; Ahn, Y.H.; Roybal, J.D.; Chen, F.; Zhang, Y.; et al. Thy-1+ Cancer-associated Fibroblasts Adversely Impact Lung Cancer Prognosis. *Sci. Rep.* **2017**, *7*, 1–12. [CrossRef]
105. Pretzsch, E.; Bösch, F.; Neumann, J.; Ganschow, P.; Bazhin, A.; Guba, M.; Werner, J.; Angele, M. Mechanisms of Metastasiss in Colorectal Cancer and Metastatic Organotropism: Hematogenous versus Peritoneal Spread. *J. Oncol.* **2019**, *2019*. [CrossRef] [PubMed]
106. Feig, C.; Jones, J.O.; Kraman, M.; Wells, R.J.B.; Deonarine, A.; Chan, D.S.; Connell, C.M.; Roberts, E.W.; Zhao, Q.; Caballero, O.L.; et al. Targeting CXCL12 from FAP-expressing carcinoma-associated fibroblasts synergizes with anti-PD-L1 immunotherapy in pancreatic cance. *Proc. Natl. Acad. Sci. USA* **2013**, *110*, 20212–20217. [CrossRef] [PubMed]
107. Kraman, M.; Bambrough, P.J.; Arnold, J.N.; Roberts, E.W.; Magiera, L.; Jones, J.O.; Gopinathan, A.; Tuveson, D.A.; Fearon, D.T. Suppression of antitumor immunity by stromal cells expressing fibroblast activation protein-α. *Science* **2010**, *330*, 827–830. [CrossRef] [PubMed]
108. Özdemir, B.C.; Pentcheva-Hoang, T.; Carstens, J.L.; Zheng, X.; Wu, C.-C.; Simpson, T.R.; Laklai, H.; Sugimoto, H.; Kahlert, C.; Novitskiy, S.V.; et al. Depletion of carcinoma-associated fibroblasts and fibrosis induces immunosuppression and accelerates pancreas cancer with reduced survival. *Cancer Cell* **2014**, *25*, 719–734. [CrossRef]
109. Sherman, M.H.; Yu, R.T.; Engle, D.D.; Ding, N.; Atkins, A.R.; Tiriac, H.; Collisson, E.A.; Connor, F.; Van Dyke, T.; Kozlov, S. Vitamin D receptor-mediated stromal reprogramming suppresses pancreatitis and enhances pancreatic cancer therapy. *Cell* **2014**, *159*, 80–93. [CrossRef]
110. Chronopoulos, A.; Robinson, B.; Sarper, M.; Cortes, E.; Auernheimer, V.; Lachowski, D.; Attwood, S.; García, R.; Ghassemi, S.; Fabry, B.; et al. ATRA mechanically reprograms pancreatic stellate cells to suppress matrix remodelling and inhibit cancer cell invasion. *Nat. Commun.* **2016**, *7*, 12630. [CrossRef]

cancers

MDPI

Article

Spatial Immunology in Liver Metastases from Colorectal Carcinoma according to the Histologic Growth Pattern

Gemma Garcia-Vicién [1], Artur Mezheyeuski [2,*], Patrick Micke [2], Núria Ruiz [1,3], José Carlos Ruffinelli [1,4], Kristel Mils [1,5], María Bañuls [1], Natàlia Molina [1], Ferran Losa [1,4], Laura Lladó [1,5] and David G. Molleví [1,6,*]

1 Tumoral and Stromal Chemoresistance Group, Oncobell Program, Institut d'Investigacions Biomèdiques de Bellvitge (IDIBELL), Gran Via 197-203, L'Hospitalet de Llobregat, 08908 Barcelona, Catalonia, Spain; ggarciav@idibell.cat (G.G.-V.); nuria.ruiz@bellvitgehospital.cat (N.R.); jruffinelli@iconcologia.net (J.C.R.); kristel.mils@bellvitgehospital.cat (K.M.); maria.banuls@iconcologia.net (M.B.); nmolina@idibell.cat (N.M.); flosa@iconcologia.net (F.L.); laurallado@bellvitgehospital.cat (L.L.)

2 Department of Immunology, Genetics and Pathology, Uppsala University, S-75105 Uppsala, Sweden; patrick.micke@igp.uu.se

3 Department of Pathology, Hospital Universitari de Bellvitge, L'Hospitalet de Llobregat, 08908 Barcelona, Catalonia, Spain

4 Department of Medical Oncology, Institut Català d'Oncologia, L'Hospitalet de Llobregat, 08908 Barcelona, Catalonia, Spain

5 Department of Surgery, Hospital Universitari de Bellvitge, L'Hospitalet de Llobregat, 08908 Barcelona, Catalonia, Spain

6 Program Against Cancer Therapeutic Resistance (ProCURE), Institut Català d'Oncologia, L'Hospitalet de Llobregat, 08908 Barcelona, Catalonia, Spain

* Correspondence: artur.mezheyeuski@igp.uu.se (A.M.); dgmollevi@iconcologia.net (D.G.M.); Tel.: +34-93-260-7370 (D.G.M.); Fax: +34-93-260-7466 (D.G.M.)

Simple Summary: In the era of immunotherapy, the tumor microenvironment (TME) has attracted special interest. However, colorectal liver metastases (CRC-LM) present histological peculiarities that could affect the interaction of immune and tumor cells such as fibrotic encapsulation and dense intratumoral stroma. We explored the spatial distribution of lymphocytic infiltrates in CRC-LM in the context of the histologic growth patterns using multispectral digital pathology providing data on three different scenarios, tumor periphery, invasive margin, and central tumoral areas. Our results illustrate a similar poor cell density of $CD8^+$ cells between different metastases subtypes in intratumoral regions. However, in encapsulated metastases, cytotoxic cells reach the tumor cells while remaining retained in stromal areas in non-encapsulating metastases. Some aspects are still unresolved, such as understanding the reason why most lymphocytes are largely retained in the capsule.

Abstract: Colorectal cancer liver metastases (CRC-LM) present differential histologic growth patterns (HGP) that determine the interaction between immune and tumor cells. We explored the spatial distribution of lymphocytic infiltrates in CRC-LM in the context of the HGP using multispectral digital pathology. We did not find statistically significant differences of immune cell densities in the central regions of desmoplastic ($_{d}$HGP) and non-desmoplastic ($_{nd}$HGP) metastases. The spatial evaluation reported that $_{d}$HGP-metastases displayed higher infiltration by $CD8^+$ and $CD20^+$ cells in peripheral regions as well as $CD4^+$ and $CD45RO^+$ cells in $_{nd}$HGP-metastases. However, the reactive stroma regions at the invasive margin (IM) of $_{nd}$HGP-metastases displayed higher density of $CD4^+$, $CD20^+$, and $CD45RO^+$ cells. The antitumor status of the TIL infiltrates measured as CD8/CD4 reported higher values in the IM of encapsulated metastases up to 400 µm towards the tumor center ($p < 0.05$). Remarkably, the IM of $_{d}$HGP-metastases was characterized by higher infiltration of $CD8^+$ cells in the epithelial compartment parameter assessed with the ratio $CD8^{epithelial}/CD8^{stromal}$, suggesting anti-tumoral activity in the encapsulating lesions. Taking together, the amount of $CD8^+$ cells is comparable in the IM of both HGP metastases types. However, in $_{d}$HGP-metastases some cytotoxic cells reach the tumor nests while remaining retained in the stromal areas in $_{nd}$HGP-metastases.

check for updates

Citation: Garcia-Vicién, G.; Mezheyeuski, A.; Micke, P.; Ruiz, N.; Ruffinelli, J.C.; Mils, K.; Bañuls, M.; Molina, N.; Losa, F.; Lladó, L.; et al. Spatial Immunology in Liver Metastases from Colorectal Carcinoma according to the Histologic Growth Pattern. *Cancers* **2022**, *14*, 689. https://doi.org/10.3390/cancers14030689

Academic Editors: Alessandro Ottaiano, Michele Caraglia and Luisa Circelli

Received: 23 December 2021
Accepted: 27 January 2022
Published: 29 January 2022

Publisher's Note: MDPI stays neutral with regard to jurisdictional claims in published maps and institutional affiliations.

Keywords: liver metastases; lymphocyte; immunology; desmoplasia; growth pattern; multiplex

1. Introduction

Colorectal carcinoma (CRC) is the third most frequent tumor in the world, with 1,932,000 new cases annually worldwide (GLOBOCAN 2020). The incidence of this tumor increases by 2% each year and is the primary cause of death due to cancer. The number of deaths annually is approximately half that of its incidence. Therefore, tackling this disease is one of the highest priority health challenges. In addition, approximately 50% of patients will develop either synchronous or metachronous colorectal liver metastases (CRC-LM) [1], with less than 10% of 5-year survival rates in these cases [2]. Moreover, the great majority of patients with metastasis (around 70%) are treated solely with chemotherapy, biologics in a selected group of patients [3] and immunotherapy in cases of mismatch repair deficiency [4]. Therefore, it is important to improve our knowledge of these tumors particularly for the metastatic setting.

Recent advances in immunoncology have sparked interest in the interaction of immune cells with tumor cells and other stromal cells. However, CRC-LM present histological peculiarities that could affect such interaction. CRC-LM grow according to three histological growth patterns (HGP) [5], desmoplastic ($_{d}$HGP), pushing ($_{p}$HGP) and replacement ($_{r}$HGP). Pushing and replacement subtypes are normally grouped in a single class, as non-desmoplastic ($_{nd}$HGP). The desmoplastic subtype is characterized by a dense fibrotic capsule surrounding the tumors. No contact takes place between tumor cells and hepatocytes. Around 40% of CRC-LM displayed such encapsulation in at least more than 50% of its interface with the normal parenchyma and 20% displayed a complete fibrotic rim, this group of patients being those with a very good outcome [6]. This fibrotic rim is formed by cancer-associated fibroblasts (CAFs) and a dense lympho-histiocytic infiltrate and massive matrix deposition. Using conventional histology staining, the lymphocytic infiltration in $_{d}$HGP is easily identifiable as a well-defined belt in the most distal half of the fibrotic rim. However, its detailed characterization, as well as the biologic reason for the lack of infiltration in more central areas of the fibrotic rim and closer to the tumor has still not been fully elucidated.

The aim of this study was to explore the spatial distribution of lymphocytic infiltrates in CRC-LM in the context of the HGPs using a multiplex immunohistochemistry (mIHC) and spatial image analysis.

2. Materials and Methods

2.1. Study Cohort/Material

Twenty-two consecutive cases of untreated CRC-LM were obtained with the approval of the Ethics Committee of the Hospital Universitari de Bellvitge (IDIBELL) after the informed consent of the patients. Thirteen cases were characterized as desmoplastic/encapsulated ($_{d}$HGP) and nine cases as non-desmoplastic ($_{nd}$HGP), characterized by the absence of the fibrotic rim between the liver parenchyma and the tumor. Five cases out of twenty-two were synchronous metastases, three characterized as $_{d}$HGP and two as $_{nd}$HGP. HGP was scored following previously reported consensus guidelines [7]. No MSI samples were included.

2.2. Multiplex Immunofluorescence Staining

Quantitative multiplex staining was performed in whole surgical FFPE sections.

Briefly, four µm thick sections were de-paraffinized, rehydrated and subjected to HIAR (microwave, pH9, 15 min). To enable multiplexing, the staining procedure included several iterative cycles. In each of them the primary antibody (incubation time 30 min, RT) and the secondary polymerized reporter enzyme staining system (undiluted, incubation time 10 min, RT) were applied, and followed by tyramide signal amplification and developing

with Opal™ fluorophore (1:100, incubation time 10 min, RT) (Akoya Biosciences). After a target was completed, HIAR (microwave, pH6, 15 min) was applied to quench endogenous peroxidase activity, to allow both antigen retrieval and removal of antibodies and polymer system from the previous cycle. After the final staining cycle, 4′,6-diamidino-2-phenylindole (DAPI) was applied to visualize nuclei.

A detailed procedure of retrieval buffers, primary antibodies, and amplification systems are described in supplementary material and methods.

2.3. Imaging

Imaging was performed with the Vectra Polaris system (Akoya Biosciences, Marlborough, MA, USA). First, each whole slide was scanned at 10× magnification. Then, the regions (1.86 × 1.39 mm) for image acquisition were selected to capture areas from the central part of the metastases and from the periphery. The selected regions were imaged in a multispectral mode at a resolution of 2 pixels per 1 µm.

2.4. Image Analysis, Thresholding and Immune Cell Subclasses

Image spectral deconvolution and analysis were performed by inForm (2.4.8) software (Akoya), described in detail previously [8,9] In short, images were classified into three categories: two tissue compartments (the epithelial compartment and stroma compartment), and blank areas. DAPI nuclear staining was used to perform cell segmentation. The images were reviewed for artifacts, staining defects, and the accumulation of immune cells in necrotic areas and intraglandular structures, which were manually excluded.

Marker intensity thresholds were defined as described before [9].

Because tissue-classifier did not allow liver parenchyma to be distinguished from tumor tissue, as Pan-cytokeratin stained both tumor cells and hepatocytes, manual selection on each of the regions was performed. Thus, three tissue categories were segmented: Tumor tissue (can contain both epithelial and small regions of stroma between adjacent tumor glands), liver parenchyma (can contain both epithelial and stroma compartments), and stroma, including the fibrotic capsule in $_{d}$HGP metastases and some eventual stromal areas between liver and tumor cells in $_{nd}$HGP metastases.

2.5. Spatial Analysis

We evaluated cell distribution at the tumor periphery, the invasive margin, and central areas of metastatic tissue. These demarcations were defined as follows: tumor periphery, 100 µm of the proximal liver parenchyma until the first row of tumor cells, including the capsule in $_{d}$HGP CRC-LM; invasive margin, 800 µm from the liver-tumor interface ($_{nd}$HGP) or capsule-tumor interface ($_{d}$HGP) to the deeper tumor areas; central areas, deeper and distal tumor areas from the liver parenchyma. Certain tissue category(ies) (for example, liver parenchyma and stroma) were used as 'reference tissue', while the cells of interest were identified in other tissue categories (for example, tumor tissue). Each cell of interest was defined by marker combination as described above. For each cell of interest in the tumor tissue, the nearest neighboring cell (of any subclass) in liver parenchyma or stroma was identified and the distance was measured. To simplify data visualization and analysis, the distances were split into four zones: 0 to 100 µm, 100 to 200 µm, 200 to 400 µm, 400 to 600 µm, taking as a reference two different measures (described in Figure 1B). Thus, a certain number of the cells of interest was identified in each of the zones. To normalize the cell counts, the zone area had to be assessed. For this purpose, spatial coordinates of all cells in the zone were retrieved. Further, a convex-hull algorithm was used to generate a polygon, covering the retrieved coordinates and to calculate the polygon area. Cell count was normalized per mm [2].

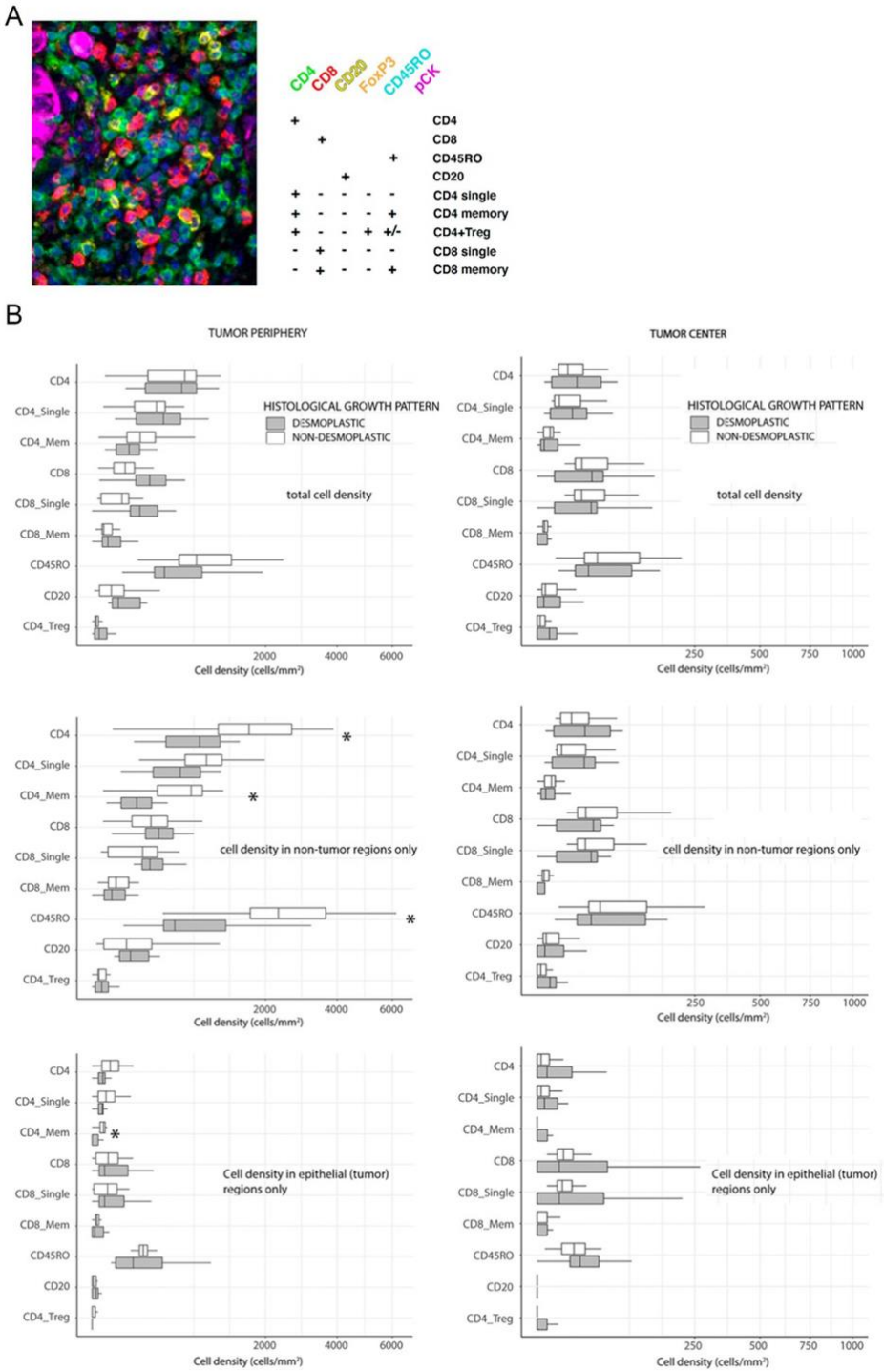

Figure 1. (**A**) Marker combination to identify each of the lymphocyte subsets assessed in the study. (**B**) Boxplots of cell densities (cells/mm^2) for each of the subsets assessed and stratified by HGP. We differentiated cell counts according to different topographic locations in the tumor, either in the tumor periphery or in central tumor areas as well as differentiating whether infiltrates were located in the stroma or in tumor glands. Tumor periphery was defined as the tissue fraction from 100 µm of the proximal liver parenchyma until the first row of tumor cells, thus, including the capsule in dHGP CRC-LM and any rare portion of peritumoral stroma in ndHGP CRC-LM. Asterisks illustrate p value < 0.05, U-Mann Whitney test comparing dHGP vs. ndHGP.

2.6. Statistics

Statistical analyses were performed using R Studio (Version 1.3.1073). The Ward algorithm was used for hierarchical clustering and the Wilcoxon signed rank test was used to compare variables between central and peripheral of the same patient. The Mann–Whitney U test with Pratt correction for tied data was used to compare variables between independent samples. $p < 0.05$ was considered statistically significant.

3. Results

3.1. The Comparison of Immune Cell Densities between Encapsulated and Non-Encapsulated Liver Metastases

First, we aimed to compare immune infiltrating lymphocyte (TIL) densities in $_{d}$HGP and $_{nd}$HGP metastases. The marker combination used to characterize TIL subclasses is displayed in Figure 1A. Because of the importance of the spatial context [10], we assessed separately the central and peripheral regions of the malignant lesions (Figure 1B). No differences were observed in central areas between metastases with different HGP (Figure 1B). Surprisingly, we also did not observe substantial differences between $_{d}$HGP and $_{nd}$HGP metastases when analyzing total immune infiltrates (epithelial + stroma compartments) in peripheral regions (Figure 1B). When analyzing immune infiltrates in different compartments separately, we observed in $_{nd}$HGP metastases higher infiltration of $CD4^+$, $CD4^+$ memory, $CD45RO^+$ cells in stroma compartment ($p = 0.041$, $p = 0.0005$ and $p = 0.032$ respectively), and $CD4^+$ memory cells in the epithelial compartment ($p = 0.041$).

In conclusion, we did not find statistically significant differences between immune infiltration in central regions of metastases with different HGP. In peripheral regions non-encapsulated metastases showed higher infiltration of $CD4^+$ positive lymphocyte subsets and $CD45R0^+$ cells.

3.2. Spatial Assessment of TILs in Liver Metastases

This initial analysis, however, did not take into account the differential histological characteristic represented by tumor encapsulation. Therefore, the analyzed peripheral regions in $_{d}$HGP were mainly represented by the capsule, which retained most of the immune infiltrates, while the peripheral regions in $_{nd}$HGP, selected for analysis, mostly consisted of tumor tissue, liver parenchyma and small areas of reactive stroma. Such a difference in histological composition makes the direct comparison of peripheral regions suboptimal and suggests establishment of more reliable methods with comparable reference elements in both HGPs. With these results, we set out to evaluate lymphocyte infiltration, considering spatial location of immune infiltrates in relation to tumor and host tissue. However, the relation between these tissue elements is not equivalent in $_{nd}$HGP and $_{d}$HGP. Thus, the interface between healthy and tumoral tissue is easy to identify and could serve as a reference for spatial analysis in $_{nd}$HGP metastases. However, in metastases with $_{d}$HGP the fibrotic rim constitutes a barrier between host liver parenchyma and tumor tissue, and it is not clear whether to consider the capsule as an element of the host or the tumor. Taking into account this histological characteristic, we considered two interface lines between different tissue types, to serve as references for spatial analysis of the immune infiltrates, allowing two measurement types: A and B, as illustrated in Figure 2. Measure A evaluates cell distance from the interface between liver parenchyma and either capsule (in $_{d}$HGP) or tumor (in $_{nd}$HGP) or small areas of reactive stroma (in $_{nd}$HGP). Measure A thus includes the cells, located in the capsule in $_{d}$HGP metastases, in reactive stroma in $_{nd}$HGP metastases, and in tumor tissue in both HGP. Measure B excludes cells from stroma between liver parenchyma and tumor and includes only the cells from tumor tissue, thus, strictly speaking that which corresponds to the invasive margin of the tumor.

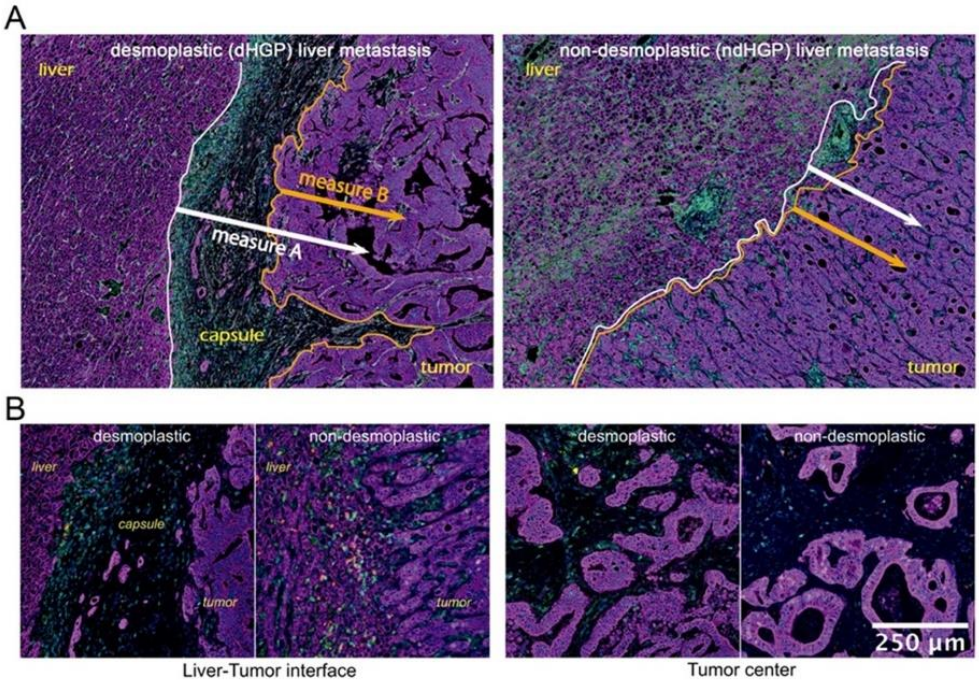

Figure 2. (**A**) Distances considered in relation to the tumor-host interface. Measure A, using as a reference the tumor-liver interface, including as part of the tumor, the fibrous capsule in case of $_{d}$HGP or any small stromal area in the case of $_{nd}$HGP; Measure B, using the tumor margin as a reference and then, not considering capsule or any peritumoral stromal. We use this measure throughout the manuscript to refer to the invasive margin. (**B**) Detailed magnification of the tumor/liver interface and central tumoral areas for both main histologic growth patterns.

Considering Measure A, desmoplastic $_{d}$HGP metastases displayed higher infiltration of $CD8^+$, $CD8^+$ single positive, and $CD20^+$ lymphocytes, particularly in areas close to the liver parenchyma (Figure 3A, left panel). This distance, in encapsulated metastases, corresponds mainly to the outer capsule fragment closest to the liver, where a large quantity of TILs is retained. However, when moving away from the parenchyma towards the tumor, the differences between HGP became less prominent and at 400 µm were completely lost. These, deeper regions most likely corresponded to invasive margin in $_{d}$HGP and deeper tumoral regions in $_{nd}$HGP.

On the other hand, the results were different when we used Measure B. In this case, $CD4^+$, $CD4^+$ single positive, $CD4^+$ memory, CD4_Treg ($CD4^+$ and $FoxP3^+$), and $CD45R0^+$ TILs were significantly more abundant in non-encapsulated metastases (Figure 3A, right panel), while no difference was seen for $CD8^+$ subsets.

Interestingly, the overall cell density for most of the immune subsets was lower when using Measure B not only in encapsulated metastases (which is because the majority of the immune cells in this HGP is retained in the capsule) but also in non-encapsulated metastases, probably, revealing the impact of the regions of reactive stroma, present on the tumor/liver border in non-encapsulated lesions (as an example, the infiltrates located between the white and orange lines in Figure 1B right image). This difference was especially prominent for all $CD4^+$ subsets, CD20 cells, and $CD45R0^+$ cells.

Even larger prevalence of $CD4^+$, $CD4^+$ single positive, $CD4^+$ memory, CD4_Treg, and $CD45R0^+$ cells in terms of statistical significance and absolute cell counts was demonstrated in non-encapsulated metastases. Additionally, $CD20^+$ B cells showed higher levels in non-encapsulated samples, thus, demonstrating cellular composition in the regions of reactive stroma.

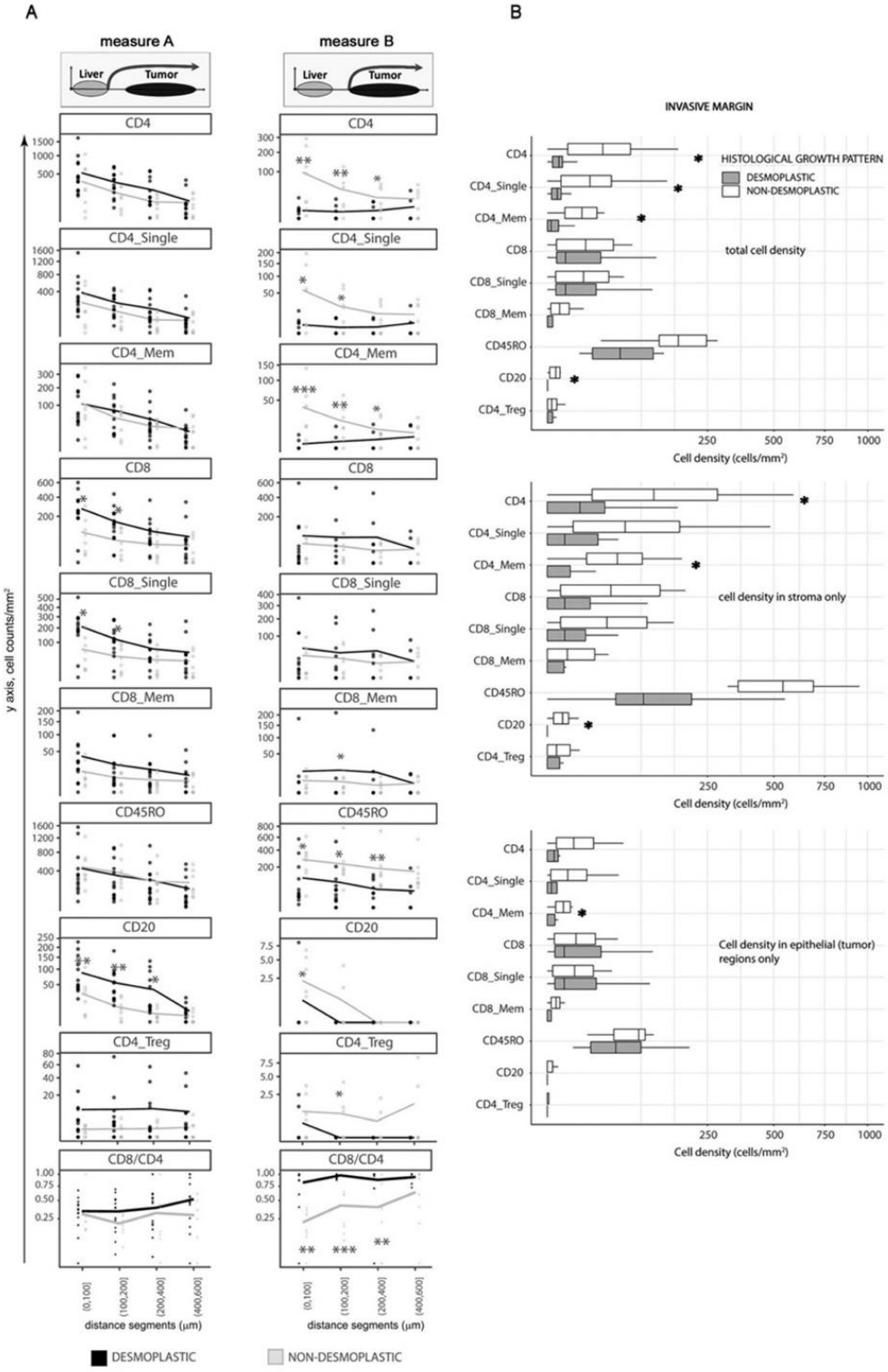

Figure 3. (**A**) Spatial assessment of lymphocyte subsets in $_{d}$HGP and $_{nd}$HGP CRC-LM according to two different measures, Measure A, from liver margin, Measure B, from the outer tumoral region (invasive margin). Lines show mean levels of cell densities. Dots show cell count/mm^2. *X*-axis is square-root transformed (distant segments, μm). Mann–Whitney U test was applied for statistical analysis. (**B**) Boxplots of cell densities (cells/mm^2) for each of the subsets were assessed and stratified by HGP according to the invasive margin. Asterisks illustrate p value < 0.05, Mann–Whitney U test comparing $_{d}$HGP vs. $_{nd}$HGP.

In conclusion, the fibrotic capsule in encapsulated metastases, especially the outer capsule part is characterized by increased quantity of $CD8^+$ positive lymphocyte subsets and B cells, in comparison to peripheral regions in $_{nd}$HGP metastases. However, the invasive margin of tumor tissue in encapsulated metastases did not demonstrate enrichment of these immune cell subsets, and conversely, showed a lower density of $CD4^+$ positive lymphocyte subsets and $CD45R0^+$ cells. The reactive stroma regions in non-encapsulated metastases are characterized by accumulation of $CD4^+$ positive lymphocyte subsets, $CD45R0^+$ cells, and $CD20^+$ cells.

3.3. The Comparison of Immune Cell Densities in the Invasive Margin of Liver Metastases

Spatial analysis revealed the importance of accurate assessment of the histological peculiarities of liver metastases with different HGP. Because we assumed that direct interaction between immune cells and malignant tissue is of major importance for immune surveillance in metastatic disease, we focused our next analyses on the metrics, derived using 'Measure B' approach and performed manual selection of the invasive margin regions (i.e., tumor regions, excluding capsule, liver parenchyma, and reactive stroma) in both HGP.

Non-encapsulated metastases displayed higher quantity of total $CD4^+$, $CD4^+$ single positive, $CD4^+$ memory cells, as well as $CD20^+$ B cells in the invasive margin (Figure 3B; $p = 0.011$, $p = 0.038$, $p = 0.008$ and $p = 0.032$ respectively). These differences corresponded mainly to inflammatory infiltrates circumscribed to the stromal compartment, which retained most of the identified infiltrates (Figure 3B, middle panel), with the exception of total $CD4^+$ memory cells that demonstrated greater infiltration also in the epithelial compartment in non-encapsulated metastases (Figure 3B, lower panel).

In conclusion, the analysis of the invasive margin confirmed the spatial analysis and demonstrated that non-encapsulated metastases have higher infiltration of several $CD4^+$ positive lymphocyte subsets.

3.4. The Comparison of Immune Cell Densities in the Invasive Margin and Tumor Center

Next, we compared the inflammatory infiltrates between the invasive margin and central areas of the tumor in each sample in a pairwise manner. $_{d}$HGP displayed higher infiltration by $CD4^+$ total, $CD4^+$ single positive, and CD4_Treg cells in central areas compared to the invasive margin while the trend was the opposite for these cell subtypes in $_{nd}$HGP (Supplementary Figure S1). Encapsulated metastases also showed more CD20 B cells in central areas than in the invasive margin.

Thus, summarizing the results from two HGPs and two locations (central and invasive margin) we can state that the poorest immune infiltration is observed in the invasive margin of encapsulated metastases, while their central parts as well as the invasive margin and central parts of non-encapsulated metastases demonstrated comparable quantities of TILs.

3.5. Anti-Tumoral Status of the Immune Infiltrates in the Invasive Margin and Tumor Center

Our results did not match the established paradigm of TIL infiltration in tumors. Thus, TIL infiltration is expected to be associated with improved survival. Encapsulated metastases are also known to have substantially better prognosis than non-encapsulated. However, in our study, we observed lower TIL levels in malignant tissues of encapsulated metastases. We hypothesized, that such results may be explained by the presence of TILs with immune-suppressive functions. In fact, while CD8 lymphocytes are considered to be main tumor cell killers [11], among the $CD4^+$ T helper subsets, the cells of type 2 (Th2) may dominate in tumors [12]. Th2 cells drive the polarization of macrophages towards M2-type and eventually create an immune-suppressive tumor microenvironment [13].

Thus, we sought to evaluate the overall anti-tumoral status of the TIL infiltrates, assuming that $CD8^+$ cells represent anti-tumor immunity while $CD4^+$ cell subsets may contain significant fraction of Th2 T cells and therefore reflect pro-tumor characteristics. To assess TIL antitumoral status we generated a metric : $\frac{CD8}{CD8+CD4}$, which is denoted further in the text as 'CD8/CD4 ratio'.

The CD8/CD4 ratio was higher in the invasive margin, than in the central areas in $_{d}$HGP samples, while in $_{nd}$HGP metastases the result was the opposite (Supplementary Figure S1). Further, when applying spatial analysis using Measure B, i.e., excluding any peritumoral stroma, encapsulated metastases demonstrated a higher CD8/CD4 ratio at the tumor margin and up to 400 μm towards the tumor center ($p < 0.05$) (Figure 3A, right panel). At the same time, no difference was seen in the CD8/CD4 ratio between the central areas of the two HGP (Figure 4, upper panel). Finally, analysis of invasive margin regions confirmed the observations of spatial distribution and demonstrated a greater CD8/CD4 ratio in encapsulated metastases (Figure 4, upper panel).

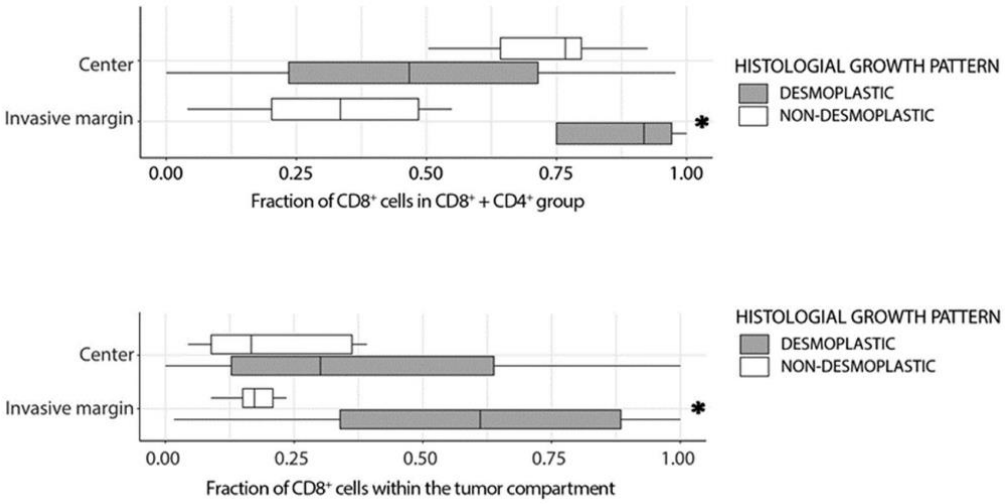

Figure 4. Top panel, boxplot for CD8/CD4 ratio comparing $_{d}$HGP and $_{nd}$HGP in central tumoral areas and at the invasive margin. Bottom panel, boxplot displaying the fraction of CD8^{+} cells within the epithelial compartment, both at the invasive margin and central tumor areas. Asterisks illustrate p value < 0.05, Mann–Whitney U test comparing $_{d}$HGP vs. $_{nd}$HGP.

The active anticancer response by cytotoxic cells requires their presence in the immediate vicinity of the malignant cells, enabling their direct contact and cytotoxic function. Thus, if the CD8/CD4 ratio reflects the antitumoral immune microenvironment in $_{d}$HGP metastases, one would expect a higher number of CD8 (cytotoxic) cells in the epithelial compartment in $_{d}$HGP in comparison to $_{nd}$HGP samples. Indeed, when we analyzed CD8^{+} infiltration in the invasive margin specifically in the epithelial compartment, in relation to the cytotoxic cells that remain limited in the stromal compartment, the encapsulated metastases demonstrated significantly higher levels (evaluated as $\frac{\text{CD8 epithelial}}{\text{CD8 epithelial+CD8 stromal}}$; Figure 4, lower panel; $p = 0.021$, Mann–Whitney U test).

Collectively, the CD8/CD4 ratio, which we consider as a surrogate metric of the antitumoral status of the TIL infiltrates, was significantly elevated in the invasive margin in encapsulated metastases, in comparison to central areas and to the invasive margin in non-encapsulated lesions, potentially reflecting an anti-tumoral immune microenvironment in $_{d}$HGP metastases. Moreover, the invasive margin in encapsulated metastases was characterized by higher prevalence of CD8^{+} cells in the epithelial compartment, suggesting the presence of an anti-tumoral microenvironment in $_{d}$HGP lesions and the presence of an immune-suppressive, pro-tumoral microenvironment in $_{nd}$HGP lesions.

4. Discussion

The present study aimed to characterize the spatial distribution of lymphocytic infiltrates in chemonaive CRC-LM in the context of the particular HGP. We analyzed the immune infiltrates in 22 untreated CRC-LM taking into account the characteristic HGP of metastases. We assessed the spatial distribution in the tissue on three different levels: (a) by distinguishing the tumor central and peripheral regions and the invasive margin,

(b) by accurate measurement of immune cell distribution in relation to different histological hallmarks and (c) by the analysis of the immune infiltration in stromal and epithelial compartments. To the best of our knowledge, this is the first study, providing a systematic and reproducible approach for the topographic distribution of lymphocytic infiltrates in CRC-LM in the context of the HGP.

There are many studies related to prognostic factors in CRC-LM, whether surgical parameters [2], histopathological [14], molecular [15] or immunological parameters [16]. However, the importance of immunological parameters, such as Immunoscore [17], has recently become evident, adding to the already known predictive value of Kras mutations [18].

On the other hand, the HGP have a deep impact on the survival of patients with CRC-LM [19–21]. Likewise, the tumor microenvironment (TME) is of paramount relevance in the formation of such growth patterns, since in the fibrotic rim and the lymphocytic belt there are contained demarcate histologic structures that might define the immune response against the tumor. However, the retention on the outer portion of the capsule of such a large number of infiltrates and the association with a better prognosis remains to be elucidated.

In addition, it has already been published that lymphocytic infiltrates are not uniformly distributed in CRC-LM [22], and quite often immune cells tend to be located in the peripheral areas of the tumor [23–25]. However, in the majority of these published studies neither the HGP nor the spatial distribution was taken into consideration. More recently, Berthel A et al. [26], reported distinct patterns of immune cell infiltration in CRC-LM, revealing a certain degree of infiltrate heterogeneity depending on the distance from the invasive margin. However, no mention was made of HGP. Hoppener D et al. [27] reported that encapsulating metastases are characterized by an increase in cell densities of different cytotoxic populations, and the authors attribute this fact to the better survival of patients with these metastases. Following this observation, some authors suggested that $_{nd}$HGP CRC-LM should be considered as *immune desert* tumors and $_{d}$HGP as *immune excluded* [28].

The main difference in our exploratory study compared to previously reported results is that we introduced a standardized reproducible approach for spatial analysis in three different locations, (i) in central areas of the tumor, where there is usually an enrichment in a mature stroma with low tumor cellularity, (ii) in the tumor invasive margin, that is, in the outermost area with the presence of malignant cells, either in contact with hepatocytes ($_{nd}$HGP), reactive stroma regions (n$_{d}$HGP), or with the fibrous capsule ($_{d}$HGP) and iii) in the peripheral area, also referred to as the outer invasive margin [29], which in CRC-LM includes the capsule ($_{d}$HGP), reactive stroma regions (n$_{d}$HGP), any small portions (100 µm) of peritumoral stroma, and normal liver parenchyma and small portions (100 µm) of tumor.

In our initial analysis we evaluated immune cells in peripheral areas, which were not stringently defined and observed the expected prevalence of cytotoxic cells in encapsulated metastases, thus, supporting the *immune excluded/immune desert* paradigm. However, we noticed that most of the immune cells of the peripheral regions in $_{d}$HGP are retained in the outer part of the desmoplastic capsule and thus, never establish contacts with cancer cells, while most of the immune cells in $_{nd}$HGP are localized in regions of reactive stroma. When we excluded these regions form the analysis, we observed higher immune cell densities in $_{nd}$HGP lesions. Thus, we doubt that the *immune excluded/immune desert* concept is applicable for CRC-LM.

Interesting, the higher immune cell densities in the invasive margin of $_{nd}$HGP lesions were represented by the subsets of CD4^{+} cells. Although we could not dissect the functional characteristic of these subsets, we hypothesize they may contain an increased fraction of Th2-type T helpers with immune-suppressive capacities.

This hypothesis is supported by the analysis of the CD8/CD4 ratio, which was significantly lower in non-desmoplastic tumors, and even further confirmed by the analysis of CD8^{+} cells, which were enriched in the epithelial compartment in the invasive margin in desmoplastic tumors, suggesting cytotoxic activity. Additionally, a higher CD8/CD4 ratio was measured in the central areas of $_{nd}$HGP compared to their matched invasive

margin, which could be closely related to the mechanism of CD8 siphoning described very recently [30].

Taken together, the quantity of cytotoxic $CD8^+$ cells is comparable in invasive margins in both HGP, but the immune microenvironment in $_{nd}$HGP seem to be immune-suppressive and blocks the cytotoxic activity of $CD8^+$ cells. One might therefore speculate that $_{nd}$HGP CRC-LM could benefit from immune-checkpoint therapy, which may help to re-activate pre-existing antitumoral lymphocytes. On the other hand, $_{d}$HGP CRC-LM could be suitable candidates for immunotherapy based on adoptive T cell transfer since small amounts of cytotoxic CD8 T cells reached the tumor nests.

5. Conclusions

As a summary, the present study provides a description of different patterns of lymphocyte infiltration depending on the HGP. The composition and the topographic demarcation in relation to the invasive margin depicted different immune scenarios according to the HGP in CRC-LM. Perhaps the most relevant finding was the presence of immune-suppressive microenvironment in metastases with $_{nd}$HGP, and antitumoral immune microenvironment in metastases with $_{d}$HGP, a fact that could explain the better prognosis of encapsulating metastases. Despite this difference, both HGP are characterized by low levels of cytotoxic lymphocytes and thus, could benefit from immune-therapies. Some aspects remain unresolved for now, such as understanding the reason for the retention of a large number of lymphocytic infiltrates in the external part of the capsule.

Supplementary Materials: The following supporting information can be downloaded at: https://www.mdpi.com/article/10.3390/cancers14030689/s1, Figure S1: Pairwise comparison of immune cell densities in the invasive margin (IM) and central areas of the tumor (CT). Wilcox-on signed-rank test with Pratt modification was used to look for statistically significant differences between the two different areas.

Author Contributions: J.C.R., K.M., F.L., L.L. and N.R. selected the cases, provided samples, and assessed the histologic growth pattern. G.G.-V. performed the laboratory procedures and contributed to the manuscript writing. N.M. and M.B. provided laboratory technical support. P.M. contributed with logistical support and authorization of the use of the facilities (Vectra Polaris) at Uppsala University. A.M. performed data analyses and manuscript writing. D.G.M. conceived and designed the study, provided funding support and manuscript writing. All authors have read and agreed to the published version of the manuscript.

Funding: This work was supported by grant PI18/1140 from the Fondo de Investigaciones Sanitarias of the Spanish Government, Fondo Europeo de Desarrollo Regional (FEDER) "Una manera de hacer Europa"/"A way of shaping Europe" and AGAUR grant number SGR771. In addition, GGV is recipient of the 2019 FI_B 00673 grant, funded by AGAUR the Department of Health of the Generalitat de Catalunya by the call "Ajuts per a la contractació de personal investigador novell FI 2019". We thank CERCA Programme/Generalitat de Catalunya for institutional support.

Institutional Review Board Statement: The study was conducted in accordance with the Declaration of Helsinki, and approved by the Institutional Review Board of IDIBELL (protocol code PR305/19).

Informed Consent Statement: Informed consent was obtained from all subjects involved in the study.

Data Availability Statement: The data presented in this study are available in this article (and Supplementary Material).

Conflicts of Interest: None of the authors have any conflict of interest to declare.

References

1. Tzeng, C.W.; Aloia, T.A. Colorectal liver metastases. *J. Gastrointest. Surg.* **2013**, *17*, 195–201. [CrossRef] [PubMed]
2. Adam, R.; De Gramont, A.; Figueras, J.; Guthrie, A.; Kokudo, N.; Kunstlinger, F.; Loyer, E.; Poston, G.; Rougier, P.; Rubbia-Brandt, L.; et al. The oncosurgery approach to managing liver metastases from colorectal cancer: A multidisciplinary international consensus. *Oncologist* **2012**, *17*, 1225–1239. [CrossRef] [PubMed]

3. Van Cutsem, E.; Tabernero, J.; Lakomy, R.; Prenen, H.; Prausová, J.; Macarulla, T.; Ruff, P.; Van Hazel, G.A.; Moiseyenko, V.; Ferry, D.; et al. Addition of aflibercept to fluorouracil, leucovorin, and irinotecan improves survival in a phase III randomized trial in patients with metastatic colorectal cancer previously treated with an oxaliplatin-based regimen. *J. Clin. Oncol.* **2012**, *30*, 3499–3506. [CrossRef] [PubMed]
4. Johnsson, A.; Hagman, H.; Frodin, J.E.; Berglund, Å.; Keldsen, N.; Fernebro, E.; Sundberg, J.; Christensen, R.D.P.; Spindler, K.L.G.; Bergström, D.; et al. A randomized phase III trial on maintenance treatment with bevacizumab alone or in combination with erlotinib after chemotherapy and bevacizumab in metastatic colorectal cancer: The Nordic ACT Trial. *Ann. Oncol.* **2013**, *24*, 2335–2341. [CrossRef] [PubMed]
5. Van den Eynden, G.G.; Bird, N.C.; Majeed, A.W.; Van Laere, S.; Dirix, L.Y.; Vermeulen, P.B. The histological growth pattern of colorectal cancer liver metastases has prognostic value. *Clin. Exp. Metastasis* **2012**, *29*, 541–549. [CrossRef]
6. Galjart, B.; Nierop, P.M.H.; van der Stok, E.P.; van den Braak, R.R.C.; Höppener, D.J.; Daelemans, S.; Dirix, L.Y.; Verhoef, C.; Vermeulen, P.B.; Grünhagen, D.J. Angiogenic desmoplastic histopathological growth pattern as a prognostic marker of good outcome in patients with colorectal liver metastases. *Angiogenesis* **2019**, *22*, 355–368. [CrossRef]
7. van Dam, P.J.; van der Stok, E.P.; Teuwen, L.A.; Van den Eynden, G.G.; Illemann, M.; Frentzas, S.; Majeed, A.W.; Eefsen, R.L.; Van Den Braak, R.R.; Lazaris, A.; et al. International consensus guidelines for scoring the histopathological growth patterns of liver metastasis. *Br. J. Cancer* **2017**, *117*, 1427–1441. [CrossRef]
8. Mezheyeuski, A.; Bergsland, C.H.; Backman, M.; Djureinovic, D.; Sjöblom, T.; Bruun, J.; Micke, P. Multispectral imaging for quantitative and compartment-specific immune infiltrates reveals distinct immune profiles that classify lung cancer patients. *J. Pathol.* **2018**, *244*, 421–431. [CrossRef]
9. Lundgren, S.; Elebro, J.; Heby, M.; Nodin, B.; Leandersson, K.; Micke, P.; Jirström, K.; Mezheyeuski, A. Quantitative, qualitative and spatial analysis of lymphocyte infiltration in periampullary and pancreatic adenocarcinoma. *Int. J. Cancer* **2020**, *146*, 3461–3473. [CrossRef]
10. Fu, T.; Dai, L.J.; Wu, S.Y.; Xiao, Y.; Ma, D.; Jiang, Y.Z.; Shao, Z.M. Spatial architecture of the immune microenvironment orchestrates tumor immunity and therapeutic response. *J. Hematol. Oncol.* **2021**, *14*, 98. [CrossRef]
11. Raskov, H.; Orhan, A.; Christensen, J.P.; Gögenur, I. Cytotoxic CD8(+) T cells in cancer and cancer immunotherapy. *Br. J. Cancer* **2021**, *124*, 359–367. [CrossRef] [PubMed]
12. Coussens, L.M.; Zitvogel, L.; Palucka, A.K. Neutralizing tumor-promoting chronic inflammation: A magic bullet? *Science* **2013**, *339*, 286–291. [CrossRef] [PubMed]
13. Pollard, J.W. Trophic macrophages in development and disease. *Nat. Rev. Immunol.* **2009**, *9*, 259–270. [CrossRef] [PubMed]
14. Hoppener, D.J.; Galjart, B.; Nierop, P.M.H.; Buisman, F.E.; van der Stok, E.P.; Coebergh van den Braak, R.R.; van Amerongen, M.J.; Balachandran, V.P.; Jarnagin, W.R.; Kingham, T.P.; et al. Histopathological Growth Patterns and Survival After Resection of Colorectal Liver Metastasis: An External Validation Study. *JNCI Cancer Spectr.* **2021**, *5*, pkab026. [CrossRef] [PubMed]
15. Schlicker, A.; Ellappalayam, A.; Beumer, I.J.; Snel, M.H.; Mittempergher, L.; Diosdado, B.; Dreezen, C.; Tian, S.; Salazar, R.; Loupakis, F.; et al. Investigating the concordance in molecular subtypes of primary colorectal tumors and their matched synchronous liver metastasis. *Int. J. Cancer* **2020**, *147*, 2303–2315. [CrossRef]
16. Tanis, E.; Julie, C.; Emile, J.F.; Mauer, M.; Nordlinger, B.; Aust, D.; Roth, A.; Lutz, M.P.; Gruenberger, T.; Wrba, F.; et al. Prognostic impact of immune response in resectable colorectal liver metastases treated by surgery alone or surgery with perioperative FOLFOX in the randomised EORTC study 40983. *Eur. J. Cancer* **2015**, *51*, 2708–2717. [CrossRef]
17. Pages, F.; Mlecnik, B.; Marliot, F.; Bindea, G.; Ou, F.S.; Bifulco, C.; Lugli, A.; Zlobec, I.; Rau, T.T.; Berger, M.D.; et al. International validation of the consensus Immunoscore for the classification of colon cancer: A prognostic and accuracy study. *Lancet* **2018**, *391*, 2128–2139. [CrossRef]
18. Van Cutsem, E.; Cervantes, A.; Adam, R.; Sobrero, A.; Van Krieken, J.H.; Aderka, D.; Aguilar, E.A.; Bardelli, A.; Benson, A.; Bodoky, G.; et al. ESMO consensus guidelines for the management of patients with metastatic colorectal cancer. *Ann. Oncol.* **2016**, *27*, 1386–1422. [CrossRef]
19. Nielsen, K.; Rolff, H.C.; Eefsen, R.L.; Vainer, B. The morphological growth patterns of colorectal liver metastases are prognostic for overall survival. *Mod. Pathol.* **2014**, *27*, 1641–1648. [CrossRef]
20. Fernandez Moro, C.; Bozoky, B.; Gerling, M. Growth patterns of colorectal cancer liver metastases and their impact on prognosis: A systematic review. *BMJ Open Gastroenterol.* **2018**, *5*, e000217. [CrossRef]
21. Falcao, D.; Alexandrino, H.; Caetano Oliveira, R.; Martins, J.; Ferreira, L.; Martins, R.; Serôdio, M.; Martins, M.; Tralhão, J.G.; Cipriano, M.A.; et al. Histopathologic patterns as markers of prognosis in patients undergoing hepatectomy for colorectal cancer liver metastases-Pushing growth as an independent risk factor for decreased survival. *Eur. J. Surg. Oncol.* **2018**, *44*, 1212–1219. [CrossRef] [PubMed]
22. Baldin, P.; Van den Eynde, M.; Mlecnik, B.; Bindea, G.; Beniuga, G.; Carrasco, J.; Haicheur, N.; Marliot, F.; Lafontaine, L.; Fredriksen, T.; et al. Prognostic assessment of resected colorectal liver metastases integrating pathological features, RAS mutation and Immunoscore. *J. Pathol. Clin. Res.* **2021**, *7*, 27–41. [CrossRef] [PubMed]
23. Van den Eynde, M.; Mlecnik, B.; Bindea, G.; Fredriksen, T.; Church, S.E.; Lafontaine, L.; Haicheur, N.; Marliot, F.; Angelova, M.; Vasaturo, A.; et al. The Link between the Multiverse of Immune Microenvironments in Metastases and the Survival of Colorectal Cancer Patients. *Cancer Cell* **2018**, *34*, 1012–1026.e1013. [CrossRef]

24. Mlecnik, B.; Van den Eynde, M.; Bindea, G.; Church, S.E.; Vasaturo, A.; Fredriksen, T.; Lafontaine, L.; Haicheur, N.; Marliot, F.; Debetancourt, D.; et al. Comprehensive Intrametastatic Immune Quantification and Major Impact of Immunoscore on Survival. *J. Natl. Cancer Inst.* **2018**, *110*, 97–108. [CrossRef]
25. Brunner, S.M.; Kesselring, R.; Rubner, C.; Martin, M.; Jeiter, T.; Boerner, T.; Ruemmele, P.; Schlitt, H.J.; Fichtner-Feigl, S. Prognosis according to histochemical analysis of liver metastases removed at liver resection. *Br. J. Surg.* **2014**, *101*, 1681–1691. [CrossRef] [PubMed]
26. Berthel, A.; Zoernig, I.; Valous, N.A.; Kahlert, C.; Klupp, F.; Ulrich, A.; Weitz, J.; Jaeger, D.; Halama, N. Detailed resolution analysis reveals spatial T cell heterogeneity in the invasive margin of colorectal cancer liver metastases associated with improved survival. *Oncoimmunology* **2017**, *6*, e1286436. [CrossRef]
27. Hoppener, D.J.; Nierop, P.M.H.; Hof, J.; Sideras, K.; Zhou, G.; Visser, L.; Gouw, A.S.; de Jong, K.P.; Sprengers, D.; Kwekkeboom, J.; et al. Enrichment of the tumour immune microenvironment in patients with desmoplastic colorectal liver metastasis. *Br. J. Cancer* **2020**, *123*, 196–206. [CrossRef]
28. van Dam, P.J.; Daelemans, S.; Ross, E.; Waumans, Y.; Van Laere, S.; Latacz, E.; Van Steen, R.; De Pooter, C.; Kockx, M.; Dirix, L.; et al. Histopathological growth patterns as a candidate biomarker for immunomodulatory therapy. *Semin. Cancer Biol.* **2018**, *52 Pt 2*, 86–93. [CrossRef]
29. Kather, J.N.; Suarez-Carmona, M.; Charoentong, P.; Weis, C.A.; Hirsch, D.; Bankhead, P.; Horning, M.; Ferber, D.; Kel, I.; Herpel, E.; et al. Topography of cancer-associated immune cells in human solid tumors. *eLife* **2018**, *7*, e36967. [CrossRef]
30. Yu, J.; Green, M.D.; Li, S.; Sun, Y.; Journey, S.N.; Choi, J.E.; Rizvi, S.M.; Qin, A.; Waninger, J.J.; Lang, X.; et al. Liver metastasis restrains immunotherapy efficacy via macrophage-mediated T cell elimination. *Nat. Med.* **2021**, *27*, 152–164. [CrossRef]